Design of experiments for optimizing NBR nanocomposite formulations

Meera Balachandran[1], Lisha P Stanly[2], R. Muraleekrishnan[3] and S.S. Bhagawan[1]
[1]Dept. of Chemical Engg. & Mat. Science, Amrita Vishwa Vidyapeetham, Coimbatore 641105
[2]High Energy Materials Research Laboratory, Pune
[3] Propellant Engineering Division, Vikram Sarabhai Space Centre, Thiruvananthapuram 695022

Email: ss_bhagawan@ettimadai.amrita.edu

ABSTRACT

Design of Experiments (DoE) is a structured statistical technique used for analyzing the behaviour of a product, process, or simulation by changing multiple design parameters in a specific manner and recording the response. Applications of DoE include choosing between alternatives, selecting the key factors affecting a response, response surface modelling, regression modeling, etc. The interpretation of results consists of determining the set of factors that are statistically significant for each response measured in the experiment, quantifying the relationship between each measured response and the statistically significant factors and determining the ranges of the statistically significant factors (or "process windows" or "process set points") that lead to certain optimal/desired ranges for the measured responses.

In the present work we used DoE to optimize the formulation of NBR [nitrile rubber] based nanocomposites. A Box-Benken Design with three factors and three levels was used to quantify the relationship between mechanical properties and levels of ingredients. The variables chosen are silica content, nanoclay loading and vulcanization system. A masterbatch of NBR and nanoclay was made in a Haake Rheocord followed by compounding on a two roll mill. The compounds were compression molded and evaluated for tensile strength, modulus, elongation at break and hardness. The effect of heat ageing on mechanical properties was also studied. Based on regression analysis, data from the experiments were used to fit mathematical models of the general form

$$Y = b_1 + b_2x_1 + b_3x_2 + b_4x_3 + b_5x_4 + b_6x_1^2 + b_7x_2^2 + b_8x_3^2 + b_9x_4^2 + b_{10}x_1x_2 + b_{11}x_1x_3 + b_{12}x_1x_4 + b_{13}x_2x_3 + b_{14}x_2x_4 + b_{15}\, x_3x_4$$

The sign and magnitude of the coefficients were different for different ingredients and properties. The predictions based on the design was confirmed by verification experiment. MINITAB was used for generating contour plots to study the interaction between the three factors. The contour plots were overlaid to find the optimal formulation.

INTRODUCTION

Reinforcing polymer with nanosized clay particles yields materials with enhanced performance without recourse to expensive synthesis procedures [1-3]. Among the various clays used, organoclays of montmorillonite family have been widely used in both thermoplastic and elastomeric systems [2,4,5]. These composites have comparatively much better mechanical properties, barrier properties and fire and ignition resistance than conventional microcomposites. The size of the nanoclay particles and the amount of filler used play a major role in the development of the properties of the rubber [6-10]. Acrylonitrile-butadiene rubber (NBR) is a special purpose, oil resistant rubber and hence can be used in applications where oil resistance is a must. The objectives of the work include varying the properties of the composite with nanoclay content, silica loading and sulphur-accelerator ratio. In the present work we used response surface methodology, a collection of mathematical and statistical techniques, to model the properties of NBR nanocomposites and to optimize the mechanical and heat ageing properties. A Box-Behnken design for three factors has been used for analysis.

EXPERIMENTAL

Materials

Nitrile rubber (JSR N230SL) with 35% Acrylonitrile content showing a Mooney viscosity of ML *(*1 + 4*)* at 100 ^{o}C = 42 was used. The nanoclay Cloisite 20A, a natural montmorillonite modified with

quaternary ammonium salt (organic modifier - dimethyl dehydrogenated tallow, quaternary ammonium, modifier concentration 95 meq/100g clay and d_{001} =24.2Å) was procured from Southern Clay Products, USA. Silica [Ultrasil], sulphur, dicumyl peroxide and other compounding ingredients, were obtained from standard suppliers.

Preparation of Nanocomposites

Cloisite 20A was mixed into NBR in the ratio 1:3 using an internal mixer type Fissions Haake Rheocord 90 at 60 rpm and at 50°C for 10 minutes. The internal mixer has an 8-shaped chamber in which two sigmoid, counter-rotating blades turn. The NBR – nanoclay masterbatch was later compounded with NBR and other compounding ingredients in laboratory size two roll mill (15cm x 33cm) with friction ratio 1 : 1.25 at room temperature using standard procedures. The rubber formulations were evaluated for cure characteristics on TechPro Rheotech ODR. (ASTM D-2084)). Curing was done at 150°C and 200 kg/cm² for the optimum cure time in a hydraulic press to make ~ 2mm thick rubber sheets.

Characterization of NBR Nanocomposites.

Dumbbell specimens were punched out from the molded sheets and stress-strain characteristics were evaluated as per ASTM D412 method on a UTM . The dumbbell specimens were subjected to heat ageing at 100°C for 48 hours.

Design Selection for Property Optimization

A Box-Benken design was chosen for the study considering its efficiency in the number of required runs. Also, this design does not contain any points at the vertices of the cubic region created by upper and lower limits for each variable and hence is advantageous when these points are impossible to be tested because of physical constraints. The three level three factor Box-Benken design employed in this study required 15 experiments. [11 -15] with silica content (X_1), Nanoclay loading (X_2) and sulphur / Accelerator ratio (X_3) as the independent variables. The compositions were optimized for mechanical properties and heat ageing properties. The coded and uncoded levels of the independent variables are given in Table 1.

RESULTS AND DISCUSSION

The mechanical properties of NBR nanocomposites before and after heat ageing are tabulated in Table 2. A wide range of values were observed for the different NBR compounds..

Statistical analysis

The experimental data obtained by following the above procedures were analyzed by the response surface regression procedure using the following second-order polynomial equation:

$$y = \beta_0 + \sum_{i=1}^{3} \beta_i x_i + \sum_{i=1}^{3} \beta_{ii} x_i^2 + \sum \sum_{i<j=1}^{3} \beta_{ij} x_i x_j$$

where y is the response x_i and x_j are the uncoded independent variables and β_0, β_i, β_{ii} and β_{ij} are intercept, linear, quadratic and interaction constant coefficients, respectively. MINITAB software package was used for regression analysis. The regression coefficients for the various parameters are tabulated in Table 3. The factors with positive coefficients have a positive effect on the property and vice versa. Using the regression equation, the contour diagrams and response surface plots were generated (fig 1 & 2).

Overlaying of Contour Plots

The contour plots for tensile strength, elongation at break, modulus at 100% elongation and changes in tensile strength and modulus after heat ageing were overlaid to find the feasible region (shown as white region) having desired properties [Fig 3 & 4]. The desired values of all these properties can be obtained at any given combination within the optimized region. For the purpose of overlaying, nanoclay and silica contents were chosen as variables keeping the value of sulphur/accelerator ratio constant at mid point.

Verification Experiments

Confirmatory experiments were carried out to validate the equations, using combinations of independent variables which were not part of the original experimental design but were within the experimental region.The values are listed in table 4. The predicted and experimental values were in good agreement. These validations confirmed the suitability of the design chosen, method of sample preparation and property evaluation.

CONCLUSION

Silica loading, nanoclay content and sulphur / accelerator ratio of NBR compounds were optimized using Design of Experiments approach. The nanocomposites were characterized for Tensile Strength, Modulus and Elongation at break, both before and after heat ageing. The data obtained were used to generate models by linear regression analysis using MINITAB package. Contour plots [a series of curves that identified different combinations of variables for which the response was constant] for tensile strength, elongation, modulus and change in tensile strength and modulus after heat ageing were overlaid to provide an optimum region for a desired set of specifications. Results from verification experiments were found to be within reasonable limits.

Table 1 Coded and Uncoded levels of Independent Variables – NBR –nanoclay systems

VARIABLE	LOW (-1)	MID (0)	HIGH (1)
Silica Loading (X1), phr	0	10	20
Nanoclay Content (X2), phr	0	5	10
Sulphur/Accelerator ratio (X3)	0.3	2	3.7

Table 2 Three variable Box – Behnken design in coded units and Mechanical properties NBR Nanocomposites

RO	Name	Coded Variable			Properties before Heat Ageing				Properties before Heat Ageing			
		Silica	Nano -clay	S/Accl Ratio	TS N/mm^2	Eb %	M100 N/mm^2	M300 N/mm^2	TS N/mm^2	Eb %	M100 N/mm^2	M300 N/mm^2
1	NBR201	-1	1	0	6.44	757	1.36	2.39	4.96	486	1.58	2.97
2	NBR202	0	0	0	7.89	1063	1.20	1.91	6.87	736	1.43	2.40
3	NBR203	0	1	-1	7.99	1279	1.13	1.62	6.81	919	1.21	1.81
4	NBR204	0	0	0	7.28	1013	1.06	1.81	7.76	797	1.53	2.55
5	NBR205	-1	0	1	5.07	556	1.35	2.57	4.49	400	1.55	3.23
6	NBR206	1	-1	0	11.14	1378	1.01	1.54	8.70	917	1.27	2.09
7	NBR207	0	-1	1	5.16	762	1.00	1.61	5.49	601	1.26	2.27
8	NBR208	0	-1	-1	4.76	1392	0.74	0.95	4.03	958	0.83	1.11
9	NBR209	1	0	-1	8.15	1488	0.90	1.36	7.81	1116	1.04	1.36
10	NBR210	-1	-1	0	2.77	720	0.78	1.18	2.43	536	0.92	1.37
11	NBR211	1	1	0	11.41	1129	1.37	2.46	11.46	870	1.72	3.21
12	NBR212	-1	0	-1	4.23	958	0.79	1.31	4.01	748	1.01	1.59
13	NBR213	1	0	1	12.90	944	1.54	2.98	11.37	644	2.05	4.30
14	NBR214	0	0	0	8.49	1079	1.09	1.93	7.94	771	1.47	2.56
15	NBR215	0	1	1	11.60	766	1.80	3.74	9.16	515	2.34	4.90

Table 3 Regression Coefficients for Properties of NBR Nanocomposites

Term		Before heat ageing			After Heat ageing		
		Tensile Strength N/mm2	Eb %	M100 N/mm2	Tensile Strength N/mm2	Eb %	M100 N/mm2
Constant	β0	7.89	1051.51	1.12	7.52	768.18	1.48
Silica	β1	3.13	243.30	0.07	2.93	172.23	0.13
Nanoclay	β2	1.70	-40.21	0.27	1.47	-27.68	0.32
S/Accl Ratio	β3	1.20	-261.21	0.27	0.98	-197.72	0.39
Silica*Silica	β12	0.13	-59.37	0.00	-0.05	-43.48	-0.05
Nanoclay*Nanoclay	β22	-0.08	3.84	0.02	-0.59	-22.19	-0.05
S/Accl Ratio*S/Accl Ratio	β32	-0.43	-5.62	0.03	-0.56	2.35	-0.02
Silica*Nanoclay	β1β2	-0.85	-71.57	-0.05	0.06	0.66	-0.05
Silica*S/Accl Ratio	β1β3	0.98	-35.55	0.02	0.77	-30.99	0.12
Nanoclay*S/Accl Ratio	β2β3	0.80	29.22	0.10	0.22	-11.78	0.18

Table 4 Comparison of the predicted and the observed values

Properties		Predicted	Experimental	% change from actual
Before heat Ageing	Tensile strength, N/mm2	7.40	7.68	3.7
	Elongation at Break , %	914	811	-12.6
	M100 , N/mm2	1.24	1.27	2.6
After heat Ageing	Tensile strength, N/mm2	6.62	7.53	12.1
	Elongation at Break , %	652	602	-8.2
	M100 , N/mm2	1.56	1.64	5.0

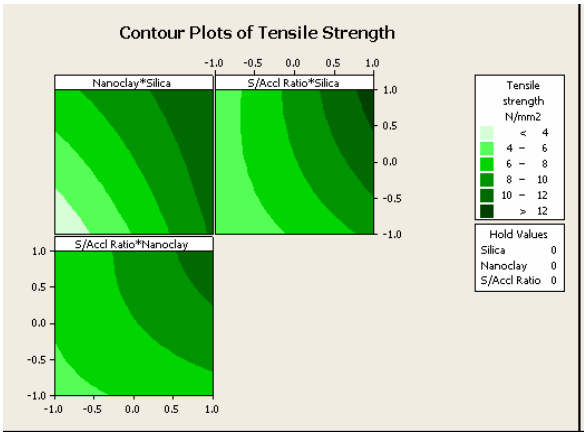

Fig 1. Contour Plots for Tensile Strength

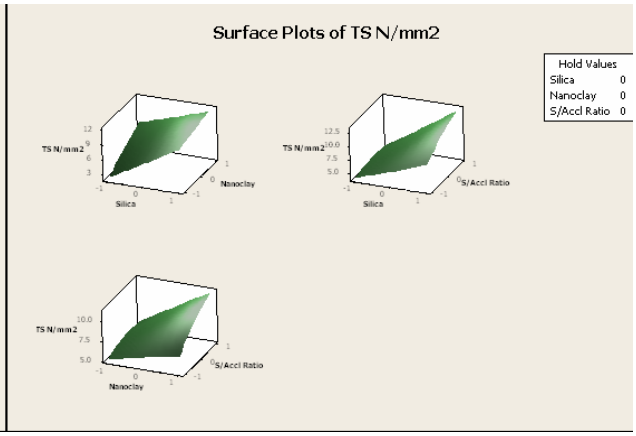

Fig 2. Response Surface Plots for Tensile strength

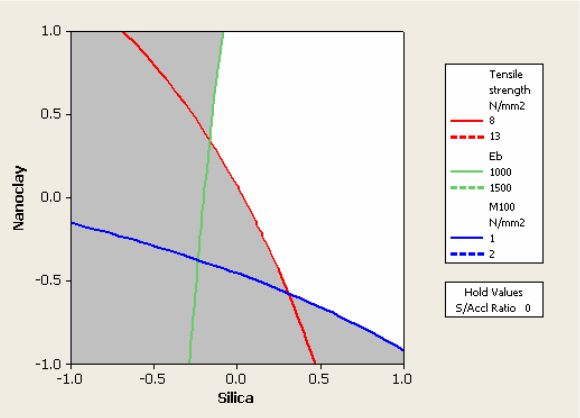

Fig 3 Overlaid contour plots for tensile strength, Elongation at break and M100

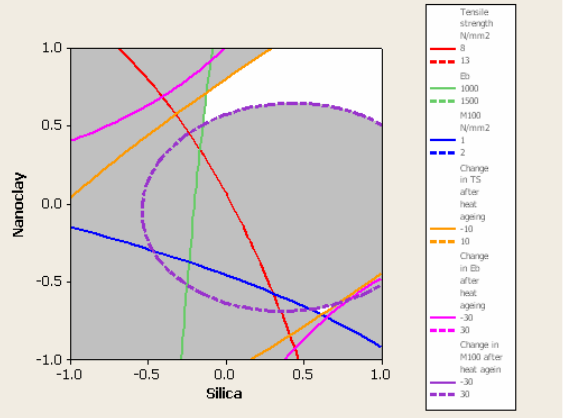

Fig 4 Overlaid contour plots for tensile strength, Elongation at break, M100 and change in these properties after

REFERENCES

1. T.V. Yen , James E.M., et al. (2001),. J Appl Polym Sci., 82, 1391-1403.
2. T.J. Pinnavaia and Beall G. W (Eds), "Polymer-Clay Nanocomposites", Wiley, New York, Ch 11 and 13 (2000)
3. A. Mousa & J. Karger-Kocsis (2001). Macromol .Mater. Eng, 286, 260-266.
4. Jin-tae Kim, Taeg-su Oh and Dong-ho Lee, Poly Intl, 52:1058–1063 (2003)
5. Yurong Liang, Yiqing Wang, et al., Poly Testing 24 (2005) 12-17
6. A. B. Morgan, W.G. Jeffrey, J App Poly Sci, 87 (2003) 1329-1338
7. S. Varghese, J. Karger-Kocsis, Polymer, 44 (2003) 4921-1927
8. S. Sadhu and A. K. Bhowmick, J Appl Poly Sci : Part B, Poly. Phy. 42, 1573 (2004)
9. A. M. Shanmugaraj, A. K. Bhowmick, J Appl Polym Sci, 88, 2992 (2003)
10. Wei-Gwo Hwang, Kung-Hwa Wei & Chang-Mon Wu, Polymer 45(2004) 5729-5734
11. D.C. Montgomery, Design and Analysis of Experiments, 4th Edn, John Wiley, 1996
12. Paritosh Jain, R.Muraleekrishnan, S.S. Bhagawan, M.S.Rao, "Response Surface Methodology: A tool for developing low SBR compounds", in Macromolecules : New Frontiers, Vol II, Ed. K.S.V.Srinivasan, John Wiley, New Delhi, 1998, 1058-61
13. E. Hajizadeh, and H. Garmabi, "Response Surface Based Optimization of Toughness of Hybrid Polyamide 6 Nanocomposites", Intl J Chem Biomol Engg, 2008, 1(1), 40-44.
14. V. Mittal, "Modeling the Behavior of Polymer-layered Silicate Nanocomposites using Factorial and Mixture Designs", Jl Thermoplastic Compos Matl, 2008, 21,9
15. S.S. Bhagawan, "Statistical Design in Polymer Processing" in 'Polymer Processing Technology', B.R. Gupta (Ed), Asian Books, New Delhi, 2008

Studies on pressure sensitive adhesives based on blends of natural rubber and polychloroprene rubber modified with phosphorylated cashew nut shell liquid prepolymer

A.R.R. Menon[#], J. Chameswary and J.D. Sudha

National Institute for Interdisciplinary Science and Technology (NIIST, CSIR)

Thiruvananthapuram – 695 019, Kerala, INDIA

Email : ravindranathamenon@yahoo.co.in

ABSTRACT

Effect of compositional and processing variations on the T-peel adhesion strength of rexin specimens bonded with phosphorylated cashew nut shell liquid prepolymer (PCNSL) based pressure sensitive adhesives (PSAs) containing natural rubber (NR) and polychloroprene rubber (CR) has been studied. Increase in adhesion strength above that of a commercial sample of PSA has been observed with the increase in solids content of the PCNSL based PSA from 15% to 25%. Also, considerable increase in adhesion strength has been obtained with the increase in storage time prior to testing of the specimens from 1 to 7 days which indicates the time dependent diffusion behavior of PCNSL based PSA facilitating wetting and bond formation with the substrates. Irrespective of the solids content and the type of PCNSL, a maximum in T-peel adhesion strength has been obtained at a CR dosage of 90 phr in the blend. Typical cohesive failure along-with high strength have been obtained with PSAs based on PCNSL having a higher degree of phosphorylation / oligomerization. Uniform and almost complete wetting of the substrate has been confirmed by the optical stereo micrographs of the failure surfaces of the test specimens and the results on viscosity obtained from rheometry.

INTRODUCTION

Pressure sensitive adhesives (PSAs) [1], popularly known as 'contact adhesives' hold a main stay in the present consumer and industrial market. A variety of PSAs based on natural rubber (NR) and polychloroprene rubber (CR) modified with tackifiers and other additives have been in use for various applications such as removable tapes / labels, upholstery, carpentry and footwears.[2-4] It has been established by the results of previous studies that Phosphorylated Cashew Nut Shell Liquid prepolymer (PCNSL) – an amphiphyllic derivative of cashew nut shell liquid (CNSL) could function as an excellent *multifunctional additive* for rubber compounding.[5-7] The chemical structure of PCNSL prepolymer is given in Fig. 1. The multifunctional role of PCNSL as a plasticizer, antioxidant and tackifier has been made use of in the design and development of a series of solvent based PSAs containing NR and CR. A preliminary study was made on the effect of different compositional and

processing variables on the adhesion strength of substrates bonded with these PSAs - the results of which are reported in this paper.

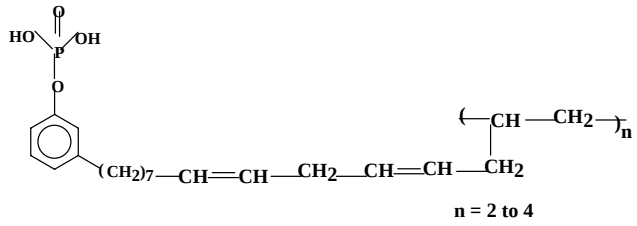

n = 2 to 4

(I) Prepolymer of PCNSL

Materials & Methods

Polychloroprene rubber (CR) (Skyprene Y-30H, Toyo Soda Co.) was supplied by M/s. Jeni Polyplast, Ahmedabad, Gujarat, India. CNSL conforming to Indian Standards IS: 840 - 1964 was supplied by M/s. Adarsh Industrial Chemicals, Sanoor, Mangalore, India. Commercial sample of PSA (Fevicol SR 998) was manufactured by M/s. Pidilite Industries Pvt. Ltd., Mumbai, India.

PCNSL was synthesized (at 20 kg level) by the simultaneous esterification and oligomerization of CNSL using o-phosphoric acid at controlled temperature, time and vacuum conditions in a Multi Purpose Reactor (*Pyrodevices*) supplied by M/s. Thermosystems, Veli, Thiruvananthapuram.

Blends of NR, CR and PCNSL (in various proportions) were prepared by mixing on an open two roll mill (6" X 12") for 5 minutes followed by homogenization and sheeting out. The sheets were cut to small pieces and weighed amounts of the same were kept immersed in requisite amount of dichloromethane for 24 h, stirred there-after for homogeneity and kept in air-tight containers.

The viscosity of the PSAs was measured on a rheometer (Anton Paar Physica, Austria, model MCR-150) by parallel plate method, at 28°C over the shear rate range from 0.1 s^1 to 100 s^1. T-peel test specimens were prepared from rexin sheet cut to size (75 mm X 25 mm). Two coats of the PSA were applied manually on an area of 50 mm X 25 mm from one end of the fabric surface, an open tack time of 2 minutes was given and bonded together under hand pressure. The test specimens were kept pressed between two flat sheets under a load of 10 kg, applied uniformly for a period of 24 h or 168 h. The T-peel adhesion strength of the specimens was measured on a Universal Tensile testing Machine (Hounsfield, H5KS) at a cross head speed of 100 mm/min. The optical micro photographs of the failure surfaces were obtained using a stereo microscope (Leica MZ 16A / DC Twain) at a magnification of X 11.

RESULTS AND DISCUSSION

Effect of type of PCNSL and storage time of bonded specimens on adhesion strength

The results on T-peel strength of rexin specimens bonded with the PCNSL based PSAs are given in Table 1. It shows a general increase in the T-peel strength with the change in type of PCNSL from

PCNSL-1 to PCNSL-3. This is expected to be due to the increase in cohesive strength of the PSA based on it due to the increase in molecular weight / viscosity up on changing from PCNSL-1 to PCNSL-3. Also, at higher solids contents the nature of failure changed from 'adhesive' to 'cohesive'

NR / CR / PCNSL (phr)		100 / 0 / 5		0 / 100 / 5	
Storage time (days)		1	7	1	7
	TSC (%)	Mean T-peel strength (N/25mm)			
PCNSL - 1	15	5.4	9.2	13.7	16.5
	20	8.8	10.4	21.5	33.7
	25	9.1	11.5	34.8	41
PCNSL - 2	15	5.3	7.3	14.6	18
	20	8.7	11	18.8	30
	25	9.3	12.1	33.3	45.3
PCNSL -3	15	6.3	7.4	15	16.9
	20	9.7	14.1	26	33.1
	25	13.4	17.1	32.6	43.9

Table 1. Variation in T-peel strength of rexin / rexin bonded with PCNSL based PSAs

type similar to that of the commercial sample. The adhesion strength of rexin specimens bonded with PCNSL based PSAs increase with storage time from 1 to 7 days. This is more prominent in the adhesive containing higher solids content, higher proportion of CR and PCNSL having a higher extent of oligomerization / phosphorylation. Time dependent diffusion of the PSA to the substrate matrix aiding 'wetting' may be one of the reasons for the increase in adhesion strength. A similar time dependent increase in self adhesion strength (tack) of PCNSL modified NR has been reported earlier[5] which was ascribed to higher molecular diffusion of NR assisted by the plasticizing effect of PCNSL. The T-peel strength of rexin bonded with Fevicol SR 998 showed a peak value (19N/25 mm) after storing for five days. This may probably be facilitated by its very low value of viscosity. However, it can be noted that the increase in adhesion strength is comparatively greater for the PCNSL modified CR based PSAs, particularly at the higher solids contents, as shown in Table 1. The progressively decreasing viscosity at higher shear rates of PCNSL – 1, PCNSL-2 and PCNSL-3 based PSAs may aid the flow of the adhesive and wetting of the substrates, facilitating development of a higher bond strength over a longer period of time. This increasing adhesion strength may also be due to possible physico-chemical interaction between CR and PCNSL as mentioned in an earlier work [7] where-in the polar phosphate group of PCNSL can interact with the chloro-group of CR. Polar – polar interaction between an additive and PSA has been reported as a factor responsible for a high value of T- peel strength.[8] Table 2 shows the mean T-peel strength of rexin bonded with PSAs based on unmodified blends of NR and CR, tested after 24 h. The lower values of adhesion strength here is in sharp contrast to the considerably higher values for the PCNSL based PSAs shown in Table 1.

NR / CR		100 / 0	75 / 25	50 / 50	25 / 75
	TSC (%)				
Mean T-peel strength (N/25mm)	15	2.4	3.3	4.9	3.7
	20	2.8	3.6	4.5	4.8

Table 2. T-peel strength of rexin / rexin bonded with unmodified NR/CR based PSAs

In the former, the lower segmental mobility of the elastomeric chains in the absence of PCNSL may reduce the flow and wetting of the substrates, essential for development of a high value of adhesion strength. It is expected that the plasticizing and softening effect of PCNSL in NR [5] and CR [6] as reported earlier facilitates the built up of adhesive tack in the PCNSL modified PSAs.

Effect of solids content of PSA on adhesion characteristics

The optical micro-photographs of the failure surfaces of rubber specimens bonded with Fevicol SR 998 and PCNSL based PSAs are given as Figure 2.

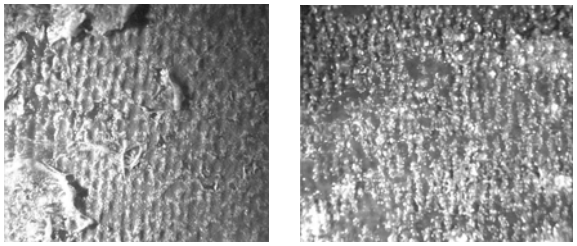

(a) (b)

Fig.2.T-peel failure surface of rubber / rubber bonded with (a) Fevicol and (b) PCNSL based PSA, (TSC – 30%)

Figure 2(a) shows almost uniform and complete wetting of the substrate with a layer of the adhesive. A similar morphology was observed for the PCNSL based adhesive at 30% solids content (Fig.2(b)). This was reflected in the increase in T-peel adhesion strength from 10% to 30% solids content, as given in Table 3. Also, the nature of adhesion failure changed from ‘adhesive’ to ‘cohesive’ type with

PSA	TSC (%)	Mean T-peel strength (N/25mm)
Fevicol SR 998	-	39.5
NR/CR/PCNSL	10	15.8
	20	25.9
	30	45.5

Table 3.T-peel strength of rubber / rubber bonded with Fevicol and PCNSL based PSA

the increase in solids content.

Effect of proportion of CR and type of PCNSL on adhesion strength

Table 2 gives the T- peel adhesion strength of rexin specimens bonded with PSAs based on blends of NR and CR at two different solids contents. It can be noted that irrespective of the content

of CR and solids content, all of the unmodified adhesives show low values of adhesion strength. The lower adhesion strength of the unmodified adhesives may be due to the absence of a plasticizer and / or tackifier which are known to be essential constituents of an elastomeric PSA.

Figure 3 shows that the PCNSL based PSAs show a maximum in the T-peel strength at a CR content of 90 phr. Also, at all the different proportions of NR and CR there is a gradual increase in T-peel strength (in the order PCNSL-1 < PCNSL-2 < PCNSL-3) with a change in the type of PCNSL.

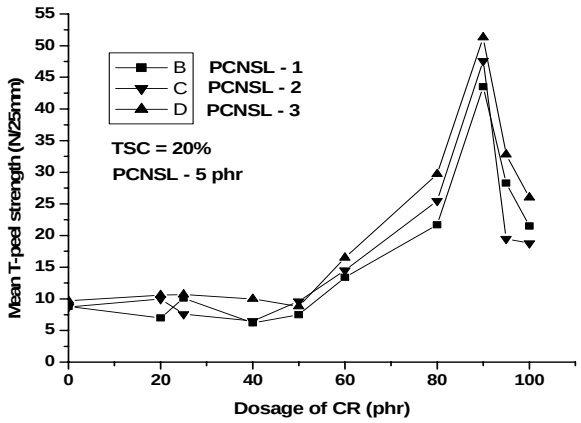

Fig.3. Variation in T-peel adhesion strength of rexin / rexin bonded specimens with dosage of CR in the NR/CR/PCNSL blend and at 20% TSC of adhesives.

This can be attributed to the increase in molecular weight of the resin in that order, contributing to the cohesive strength of the adhesive. Zosel has reported that above a minimum molecular weight of the modifier, tendency for fibrillation increases leading to an increase in cohesive strength of PSAs.[9] A similar mode of cohesive failure was observed for rexin specimens bonded with the PCNSL based PSA containing PCNSL-3. This indicates the possibility for entanglement of the pre-polymer chains of PCNSL with macromolecular chains of CR and NR with consequent increase in cohesive strength and T-peel adhesion strength. Also, the small proportion of NR (10 phr) may facilitate the visco-elastic deformation / flow characteristics of the adhesive facilitating quick and uniform wetting of the substrates and development of a high value of adhesion strength. The comparatively lower values of viscosity of Fevicol SR 998 at various shear rates may be one of the factors for its high value of adhesion strength. Thus, the low viscosity of this adhesive leads to almost complete wetting of the substrates as shown in the stereo optical micrograph of the failure surface, given as Fig.4 (a). The optical micrograph of the failure surface of rexin bonded with PCNSL based PSA having 25% solids content is given as Figures 4(b).This shows almost complete wetting of the substrate, accounting for

the observed high values of its T-peel strength (15.5 N/25mm as against 9.8 N/25mm for Fevicol SR 998).

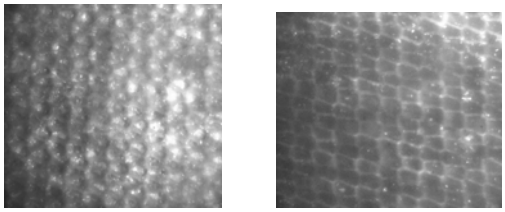

Fig.4.T-peel failure surface of rexin / rexin bonded with (a) Fevicol and (b) PCNSL based PSA

CONCLUSION

Adhesion strength higher than that of Fevicol SR 998 was obtained for PCNSL based PSAs with increases in solids content from 15% to 25% and storage time of test specimens prior to testing from 1 to 7 days which indicates time dependent diffusion characteristics of the latter causing a change in failure pattern from 'adhesive' to 'cohesive' type. Increase in the extent of phosphorylation / oligomerisation of CNSL during synthesis of PCNSL resulted in a resin having higher viscosity which enhanced the cohesive strength of the PSA and consequently the T-peel adhesion strength with flexible substrates. Rexin specimens bonded with the PCNSL based PSAs showed an optimum high value of T-peel adhesion strength at a CR dosage of 90 phr, irrespective of the type of PCNSL and solids content.

Acknowledgement: Thanks are due to the Kerala State Council for Science Technology & Environment

(KSCSTE), Thiruvanthapuram for sponsoring this work and to Prof. T.K. Chandrasekhar, Director, NIIST, Thiruvananthapuram for providing the necessary facilities.

REFERENCES

1. Wake, W.C. *Adhesion and the formulation of adhesives*; 2nd Edn., Appl Sci Pub., New York, 1982, Ch.10, pp. 220-223.

2. John, N.; Joseph, R. J Appl Polym Sci, 1998, 68, 1185.

3. Poh, B.T.; Kwo, H.K. J Appl Polym Sci, 2007,105 (2), 680.

4. Kozakiewicz, J.; Kujawa-Penczek, B.; Penczek, P.; Puton, K. J Appl Polym Sci, 1981, 26,

3699.

5. Menon, A.R.R.; Pillai, C.K.S. ; Nando, G.B. J Adhesion Sci Technol, 1995, 9(4), 443.

6. Menon, A.R.R.; Pillai, C.K.S.; Nando, G.B.; Bhattacharya, A.K.; Gupta, B.R. Kauts Gummi

Kunsts, 2000, 53(1-2), 35.

7. Menon, A.R.R.; Visconte, L.L.Y. J Appl Polym Sci, 2004, 91(3), 1619.

8. Taghizadeh, S.M.; Mirzadeh, H.; Barikani, M. ; Yousefi, M Iran Polym J, 2007, 16(4), 279.

9. Zosel, A. Int J Adhesion & Adhesives, 1998, 18, 265.

Nondestructive testing of defects in adhesive joints

P.N. Vinod, Reji John, Shiv Kumar, K. Shajahan, C.G. Padma Kumar and RMR Vishnubhatla
Naval Physical and Oceanographic Laboratory,
Defence Research and Development Organisation,
Thrikkakara P.O, Cochin-682 021

Email: tsonpol@vsnl.com

Abstract

Rubbers are generally used for encapsulating underwater components to prevent moisture ingress. Reliability aspects of these components are very important while considering the performance of the sensor. The sensor is deployed in underwater for quite long period of time and has no option for monitoring the structural health and functionality. The sub-surface defects such as micro-cracks, voids, porosity and delamination are generally introduced during the encapsulation or damage may create due to handling or when service stress exceeds design stresses. Nondestructive test (NDT) techniques such as infrared thermography (IRT) and micro-focal x-ray radiography techniques have been applied as an inspection methodology for detecting these defects in the encapsulants. The main advantage of the NDT techniques is that reliable and quantitative information about the hidden defects or flaws can be generated with high precision without sacrificing or damaging the entire structure of the device or its components. The bright spots and its dimensions observed on the IR images of the partially debonded samples correspond to the location as well as the relative size of the delamination presents in the sample. The x-ray image of the spiced cable joints shows that the internal structure with cracks or voids at the cable joints.

Keywords: encapsulants, NDT, infrared thermal imaging and microfocal x-ray radiography.

1. Introduction

Rubbers are generally used for encapsulating underwater components to prevent moisture ingress. The sensor is deployed in underwater for quite long period of time and has no option for monitoring the structural health and functionality on a regular basis. The generally observed defects of underwater components are delamination of adhesive joints or at the cable-spliced joints, cracks in ceramics, porosity and pin holes in transducer encapsulations and rubber moulded junction boxes, which are seriously affecting the reliability of the sonar systems. Hence, detection and localization of the above types of defects and monitoring the health of the components are the prime important factors to improve the reliability of the device and in predicting the life of the components, thereby eliminating the possibility of catastrophic failure of sonar. These defects are so tiny that visual inspection is not practically feasible. Consequently, there exists an increasing demand for reliable and effective non-destructive evaluation (NDE) for the wet-end components of the encapsulants. A number of different nondestructive test (NDT) techniques have also been developed as an inspection methodology and applied successfully to identify and characterize the defects [1-2]. No single method can detect all forms of flaws in all materials. Hence, suitable NDT inspection methods have to appropriately select for each case. In the present study, the delamination and cracks in the encapsulants of the wet-end components of the underwater sensors have been detected and characterized using the NDT technique such as micro-focal x-ray radiography and IR thermal imaging techniques. These techniques are applied due to their reliability and high sensitivity in detecting the defects [3].

1. (a) The principle of Infrared thermography

Infrared thermography is a non-contact sensing method concerned with the measurement of radiated thermal or infrared radiation from a surface in the infrared region. This involves the use of an IR camera to capture the evolution of surface temperature profiles of the test object after being

subjected to thermal perturbation from a high-energy uniform light source. It detects heat signatures via infrared imaging and uses this heat signature to detect leaks, cracks, debonding, corrosion etc. The spectrum and intensity of the radiation emitted by the object depends on its absolute temperature and emissivity of the surface [3]. The basic principle of this approach is that when a materials present defects; it introduces areas of locally high temperature because of the reduced heat flux in the areas immediately surrounding the defects. This results thermal gradients. This thermal transient flux can be picked up or recorded by an infrared camera operating in the infrared wavelength range 4 to 9μm. The analysis of the IR images provides qualitative information about the hidden defects or internal flaws in the material.

1. (b) The principle of X-ray radiography measurement

The radiography measurement is based on the differential absorption of x-ray radiation on its transmission through the structure of the tested specimen. This indicates that the intensity of the incident radiation on the tested structure is attenuated more or less due to the presence of any flaws or discontinuities in the specimen. Thickness alterations and the presence of discontinuities are visualized by differences in contrast (radiographic density) of the obtained images [3].

2. Experimental

For detecting the various defects-like thin line cracks, voids or sub-surface defects on the spliced neoprene cable, both IR thermal imaging and x-ray micro-focal radiography measurements were carried out. The tested samples were adhesively bonded aluminum disc with neoprene rubber used for encapsulating underwater acoustic sensors having delamination introduced deliberately. The Al disc had a thorough central hole to connect the rode for sensor assembling. The delamination was suitably created at the upper portion of the sample by not applying any adhesives and adhesive was applied at the lower portion of the samples. It serves as a delamination of one half of the 4” dia circular disc. The thermal imaging was carried out on adhesive joints to examine the delamination. The Thermovision 550 IR camera was used for the experimental works. The IR thermal imaging was performed in reflection mode in which both the heating source and the IR camera were positioned at the same side and infrared images were captured using the IR camera in the wavelength range 3-5μm. The test samples were heated using a hot air-gun for a few minutes. Then, the samples were allowed to cool for one minute. The IR thermal imaging system operated on the reflection mode in which both the heating source and the camera are positioned on the same side. The transient infrared images were acquired and analyzed. The micro-focal x-ray radiography measurements were carried out (using a Feinfocus FXE 225.20 unit which has a focal spot size of about 15μm with a geometric magnification of 3X) on the spliced cable joint to monitor the flaws/defects. Using this technique, the finer details of the cable joints such as delamination, voids, and quality of crimp, ingress of water, etc can be monitored. The radiography exposure parameters were suitably adjusted to obtain a radiographic density of about 2.0 to 2.5 at the region of interest (ROI). These films were processed manually under standard conditions to identify the fine-scale detailed of the damage or defects. A 3mm thick lead sheet was used at the entire area except the ROI for masking around the tube to control the scattering of the x-rays.

3. Results and Discussion

Fig 1 shows the IR thermal image of the tested structure consisting of neoprene rubber encapsulants glued to the Al housing of the sensor assemblies. Left side shows the schematic drawing of the 4” dia circular end cap of the sensor (test specimen) with upper portion is completely debonded and lower portion is completely bonded. From the thermal image given, a defect like non-bonded area can be detected with bright portion indicates the delamination. The presence of this bright area corresponds to the delamination indicating its shape and location of the delamination. The delamination of the encapsulants with the Al housing or ceramic rings is resulted due to the poor bonding practices employed or due to inadequate bonding of the adhesives [2]. For thin laminates, damage or defects is usually occurs at the subsurface and hence not readily detected visually (this is known as the barely

visible impact damage (BVID). The cracks, inclusions, void or delamination that transfers heat at different rates causes these thermal gradients. The temperature of the material changes rapidly after the initial thermal pulse because the thermal wave front propagates by diffusion process. The presence of delamination reduces the diffusion rate so that temperature gradient originates at or near around the defected area as the thermal wave propagates. Hence, it acts as an insulator and possesses a higher temperature with respect to the surrounding area. The large distribution of the temperature mapping at the non bonded area indicates that complete debonded condition of the encapsulants with the Al metal. The uniform distribution of temperature in the lower portion of the IR image shows that no delamination is present between the neoprene rubber encapsulants and Al housing of the sensor. Hence, it provides quantitative information about the hidden defects or internal flaws in the material.

A junction between two similar or dissimilar materials represents generally a weak structural joint and so it requires an appropriate choice of the most adequate joining technique to make good adhesion between the materials. An effective and reliable adhesive bond between dissimilar substrates is extremely important for transducer applications. Figure 2 shows the radiographic image of the spliced rubber cable. Fine details at the cable joints can be clearly seen in the image. Though there is contact at some locations (two strands), there was finite gap between the other strands. The gap is approximately 1 mm. The arrows indicate the transverse micro-cracks observed in the core strands. Figure 3(a) shows the photography of the tested cable splice. Fig 3(b-d) shows the micro-focal radiography images of the neoprene cable splice having a geometrical magnification of X3. In Fig 3b, the circled portion shows the large discontinuity in the copper conductor in the cable. The gap between the joints is indicated by a circle. Figure 4 shows the radiographic image of the spliced cable joints and it shows the splice in non-defective.

4. Conclusion

The sub-surface defects such as micro-cracks, voids, porosity and delamination are generally observed in the rubber encapsulants of the wet-end components. NDT tools like microfocal X ray radiography and IR thermal imaging techniques are useful to detect these defects. It was shown that with these techniques, finer details of the defects such as size and dimensions of delamination or cracks can be effectively detected and monitored. However, each of these NDT tools is sensitive to the type of defects present and hence can provide a quantitative account on the hidden flaws or faults in the encapsulants.

5. Acknowledgements

The authors thank Dr John Philip of IGCAR, Kalpakkam, Chennai, for the help rendered for characterizing samples for microfocal radiography and IR thermal imaging respectively. The encouragements and permission of the Director, NPOL to publish this work is greatly acknowledged.

6. References

1. C. Meola and G.M. Carlomagno, ‘Recent advances in the use of infrared thermography’, Measurement Science and Technology., 15, 27-58 (2004).
2. G. Busse, ‘Nondestructive evaluation of polymer materials,’ NDT & E Int’l, 27,253-262, (1994).
3. Bahman Zoofan, ‘Microradiography as a strong NDT tool’, ASNT handbook on Nondestructive test Series (http://www.asnt.org).

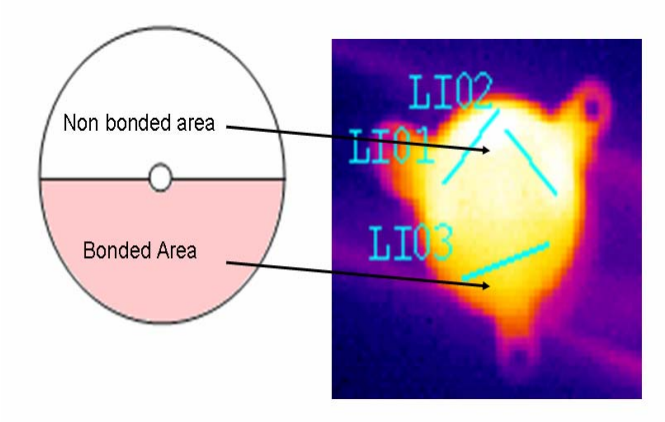

4. Fig 1. The IR image showing the delamination of the Al – Rubber joint.

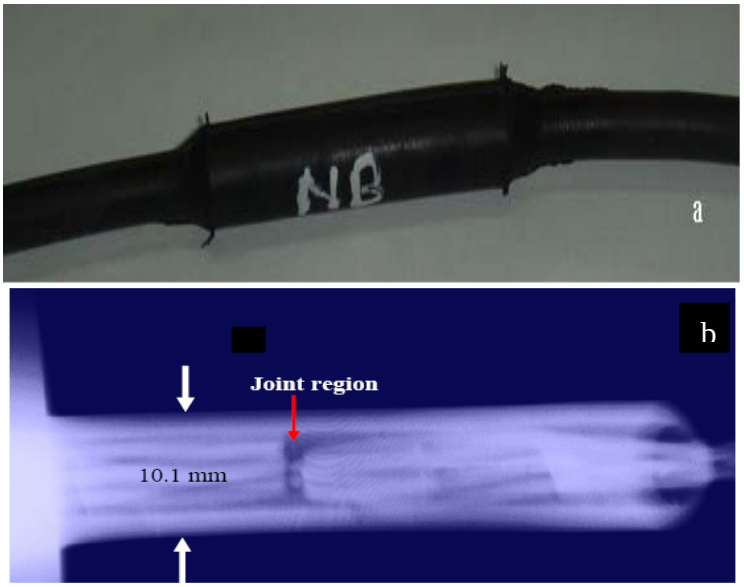

Fig 2. Photograph of the spliced neoprene cable and (b) Radiography image (3X) of the spliced cable.

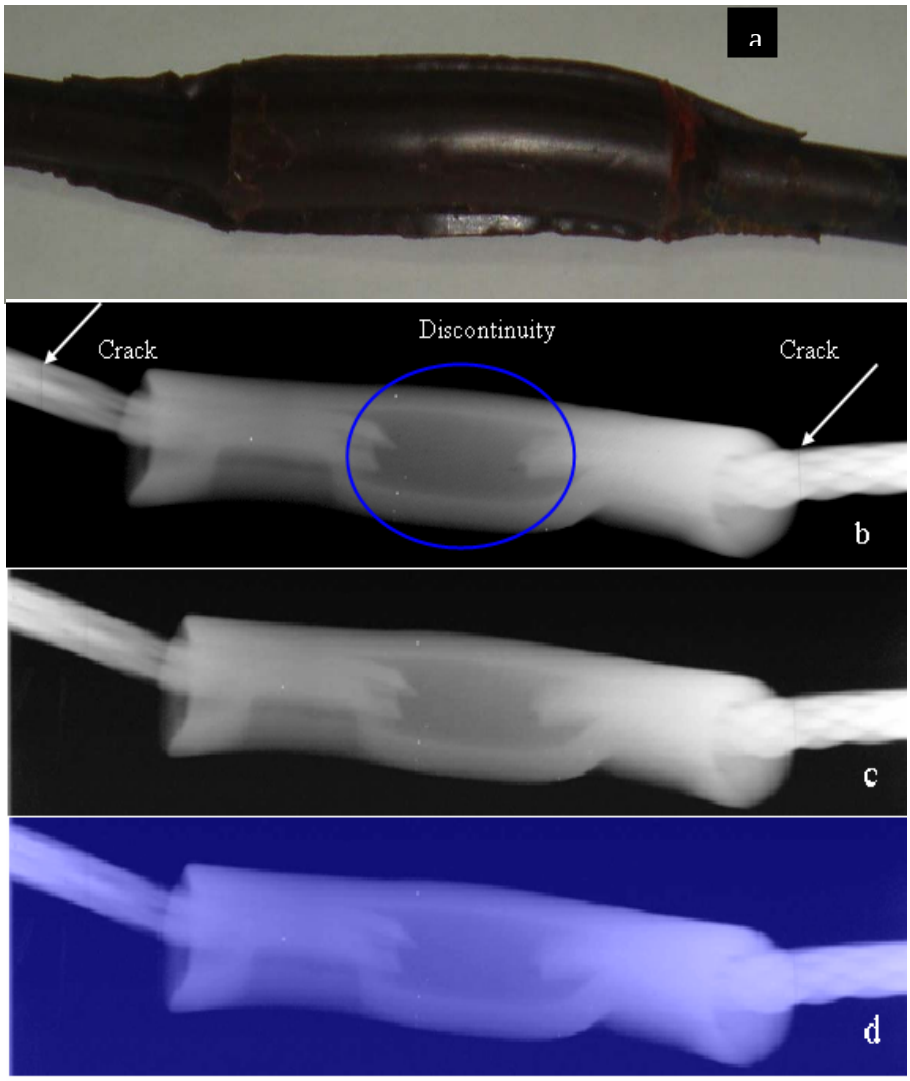

Fig 3(a) photograph of the tested cable and (b&d) represents radiography images.

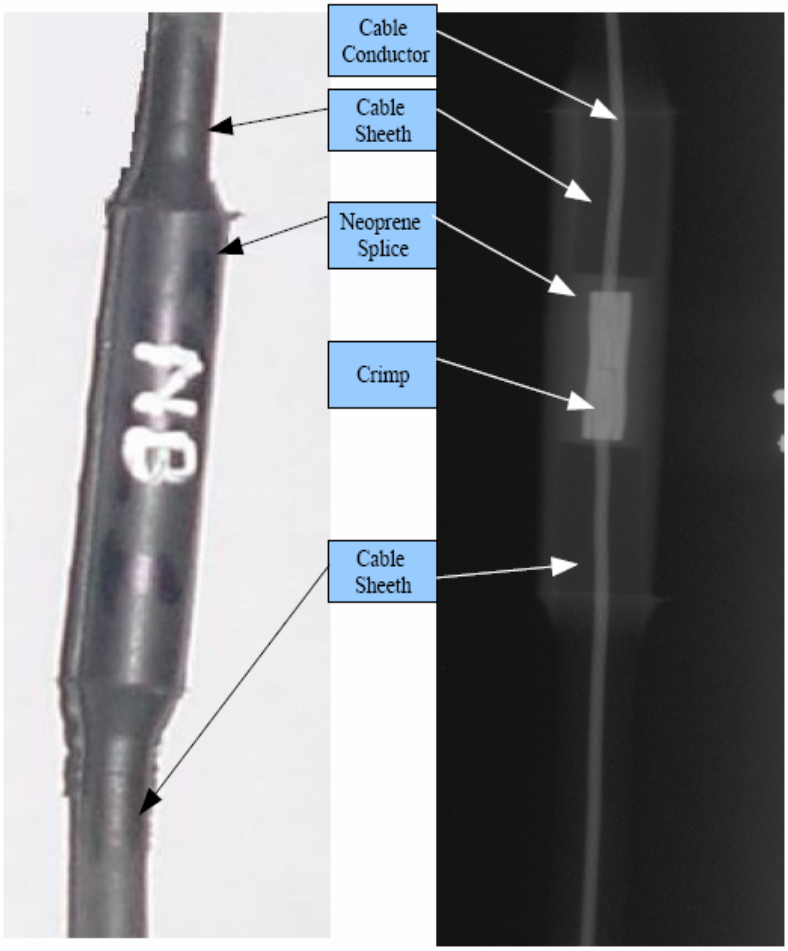

Fig 4. X-ray microfocal radiograph of spliced neoprene cable. The splice is no defective.

Electrical studies on silver subsurface particulate films on blends of polystyrene and poly (4-vinylpyridine)

Manjunatha Pattabi*#, Pratima Parashar and S C Gurumurthy

Department of Materials Science, Mangalore University, Mangalagangotri 574 199, INDIA

*E-mail: manjupattabi@yahoo.com

Abstract:

Vacuum deposition of metals on softened polymers offers a technique to prepare subsurface particulate films. Morphology of such films depends on deposition as well as thermodynamic parameters. In addition, the polymer metal interaction plays an important role in deciding the morphology. The electrical properties of particulate films are strongly dependent on their morphology. Blending of polymers can be used to control the morphology of such films and thereby, tailor their electrical properties. Blends of Polystyrene (PS) and Poly (4-vinylpyridine) (P4VP) prepared by mixing in common solvent, Di-methyl Formamide (DMF), are solution cast on to clean glass substrates. The substrates were held at 457 K, much above the glass transition temperature of both the polymers, to ensure sufficient polymer fluidity during deposition, to obtain a subsurface particulate film. A constant deposition rate of 0.4 nm/s was used throughout the study. The particle sizes were estimated from the line width broadening of the X-ray Diffraction (XRD) peaks and the mean particle sizes are in the range 30-50 nm. Films on softened PS give rise to a very high room temperature resistance due to the formation of a highly agglomerated structure. On the other hand, films on softened P4VP gives rise to a room temperature resistance in the range of a few tens to a few hundred MΩ/□, which is desirable for device applications. Blends of PS and P4VP show room temperature resistances in the desirable range, even at a PS/ P4VP ratio of 75:25. The film resistances in the desired range could be obtained on PS by blending it with P4VP.

Introduction

Organised small metal particles with an average inter-particle separation of a couple of nm would exhibit interesting optical and electrical properties which can be exploited for device applications. An interesting sub-surface particulate structure formation was reported when certain inorganic materials are vacuum deposited on to softened polymer substrates [1-4] and the morphology and formation of such structures depend on thermodynamic as well as deposition parameters [4, 3]. The morphology of sub-surface particulate structures also depends upon polymer metal interaction [5, 6].

Silver deposited on softened inert polymers like polystyrene (PS) substrates formed highly agglomerated structures with their room temperature resistances equalling that of the substrate, irrespective of the thickness deposited. On the other hand, silver deposited on an interacting polymers

like poly (2-vinylpyridine) (P2VP) or poly (4-vinylpyridine) (P4VP) resulted in the formation of smaller particles (~ a few tens of nm) with smaller inter-particle separations [6]. Such structures showed electrical resistance in the range desirable for device applications. However, P2VP and P4VP are hygroscopic while PS is a stable polymer. Therefore, it would be interesting to study the electrical properties of sub-surface particulate structures formed on PS/P4VP blends. This article reports the results of the studies taken up on the electrical properties of silver island films deposited on softened PS/P4VP blends.

Experimental technique

Poly (4-vinylpyridine) and silver (purity better than 99.99+ %) used in this study were procured from Sigma-Aldrich Chemicals Pvt. Ltd. Polystyrene was procured from Alfa-Aesar (A Johnson Mattey company). The molecular weight of P4VP and PS are 60,000 and 100,000, respectively. Polymer blends were prepared through solution blending by mixing in a common solvent, Die-methyl Formamide (DMF). 2 g of the total polymers at different ratios were dissolved in 20 ml of DMF at room temperature and solution cast on a glass slide pre-coated with silver contacts with a gap of 1 cm X 1 cm for electrical studies. Silver films of various thicknesses were deposited on these substrates held at 457 K in a vacuum better than 8×10^{-6} torr. A chromel-alumel thermocouple was used to measure the substrate temperature. A Telemark quartz crystal monitor (Model 850) was used to measure the deposition rate, as well as the overall film thickness. The deposition rate was 0.4 nm/s for all the films. Resistance measurements were carried out in-situ, using a Keithley electrometer model 617. The films were annealed at the deposition temperature for 1 hour before cooling them to room temperature. X-ray diffraction (XRD) studies were carried out for particle size measurements using a Bruker D8 Advance powder x-ray diffractometer with Cu K_{α} radiation.

Results and Discussion

Figure 1 shows the variation of the logarithm of resistance against inverse of temperature for silver films of different thicknesses deposited on polymers and blends at a temperature of 457 K, during cooling to room temperature. It is interesting to note that while some of the films show only negative temperature coefficient of resistance (TCR) some show almost zero TCR. Some of the films show negative TCR at higher temperatures and almost zero TCR at lower temperatures. The 50 nm thick silver films on pure PS and 75:25 blend of PS/P4VP show negative TCR. Silver on PS showed similar behaviour in our earlier studies resulting in room temperature resistance same as that of the substrate with the formation of large silver particles separated by large distances [7]. Blending the inert polymer PS with an interacting polymer like P4VP to the extent of 25% does not seem to alter the morphology of the particulate film as indicated by the electrical behaviour. When the P4VP content is increased to 50%, a negative TCR at high temperature followed by almost zero TCR at lower

temperatures exhibited by the 50 nm thick film is similar to the behaviour observed earlier for pure P4VP [8] indicating that the film consists of small particles separated by small distances. With further increase in P4VP content, the negative TCR part diminishes, giving rise to a near zero TCR.

It is also interesting to note that even at 50% P4VP, with an increase of silver deposited, films show electrical characteristics as that of the films on pure P4VP [8]. Further, when 150 nm thick silver is deposited on a polymer blend with only 25% of P4VP, the films show desirable electrical characteristics in contrast with the very high room temperature resistance observed for films on pure PS even at 300 nm of silver [7].This indicates blending has positive effect on electrical properties on silver films deposited on PS. It was shown through X-ray photoelectron spectroscopy (XPS) studies at various electron take off angles (ETOA) that silver clusters are formed at a depth of a couple of nm from the polymer surface [7,8]. It is known that the formation of subsurface particulate structure is subject to certain thermodynamic [4] and deposition conditions [3]. While the thermodynamic conditions are met for the deposition of metals on most of the polymer substrates, deposition conditions used in the present study are similar to those used in our earlier studies. Therefore, it is reasonable to assume that the particles are formed just a couple of nm below the polymer surface. Table 1 gives the resistance data and particle size estimated from the X-ray line width measurements for the silver films of different thicknesses deposited on the PS/P4VP blends of various compositions.

It is seen that the resistance of silver films at room temperature lie at a few tens of MΩ/□, at certain thicknesses even for the PS content of 50-75%, in contrast with the behaviour of silver on pure PS. The particle size increases with increase in PS content at a fixed silver thickness, as expected. It is seen that as the P4VP concentration increases there is a regular decrease of resistance at a fixed silver thickness. The plot of logarithm of these resistances with blend concentration gives linear fit as shown in figure 2. Through this fit, one can estimate the resistance of the film at a particular blend and for the given conditions and thickness.

Conclusions:

1. Deposition of silver on polymer blends coated substrate held at 457 K provides an approach to produce stable island films with reasonable control over their electrical resistance.
2. Higher thickness films show almost zero TCR near room temperature, a desirable property for most of the devices. Low thickness films show a negative TCR, characteristic of island films.
3. Silver particulate films deposited on PS/P4VP blends show better electrical properties compared to those on pure PS, even at a P4VP content of 25%. The blends PS/ P4VP (50:50, 25:75) seem to be better with regard to their electrical behaviour.

Acknowledgment:

One of the authors (PP) thanks Department of Science and Technology, Government of India, for financial assistance.

References

[1] Kovacs G J and Vincentt P S 1982 *J. Colloid. Interface. Sci*. **90** 335

[2] Kovacs G J and Vincentt P S 1983 *Thin Solid Films* **100** 341

[3] Kovacs G J, Vincentt P S, Trumblay C and Pundsak A L 1983 *Thin Solid Films* **101** 21

[4] Kovacs G J and Vincentt P S 1984 *Thin Solid Films* **111** 65

[5] Kunz M S, Shull K R and Kellock A J 1992 *J. Appl. Phys*. **72** 4458

[6] Mohan Rao K and Pattabi M 2001 *J. New Mat. Electrochem. Systems* **4** 11

[7] Mohan Rao K, Pattabi M, Mayya K S, Sainkar S R and Murali Sastry M S 1997 *Thin Solid Films* **310** 97

[8] Mohan Rao K, Manjunatha Pattabi, Sainkar S R, Arun Lobo, Kulkarni S K, Jayasheela Uchil and Murali Sastry M S 1999 *J. Phys. D: Appl.Phys*. **32** 2327

Table 1: Resistances at substrate temperature (R_{st}), after one hour of aging (R_{1hr}), at Room temperature (R_{rt}) and particle size for silver films deposited on PS/P4VP blends held at 457 K.

Polymer PS:P4VP	Silver film thickness	Resistances (MΩ/□)			Particle size XRD (nm)
		R_{st}	$R_{1\ hra}$	R_{rt}	
0:100	50 nm	1.9	26.8	27.1	30
25:75	50 nm	6.2	42.2	47.1	46.6
25:75	85 nm	3.2	14.7	14.2	53
50:50	50 nm	15.9	119.5	159.4	49.1
50:50	95 nm	2.9	29.9	30.1	47.5
75:25	50 nm	214	325	-	51.8
75:25	150 nm	14.8	98.2	248.9	46.4
100:0	50 nm	302	491	-	53.3

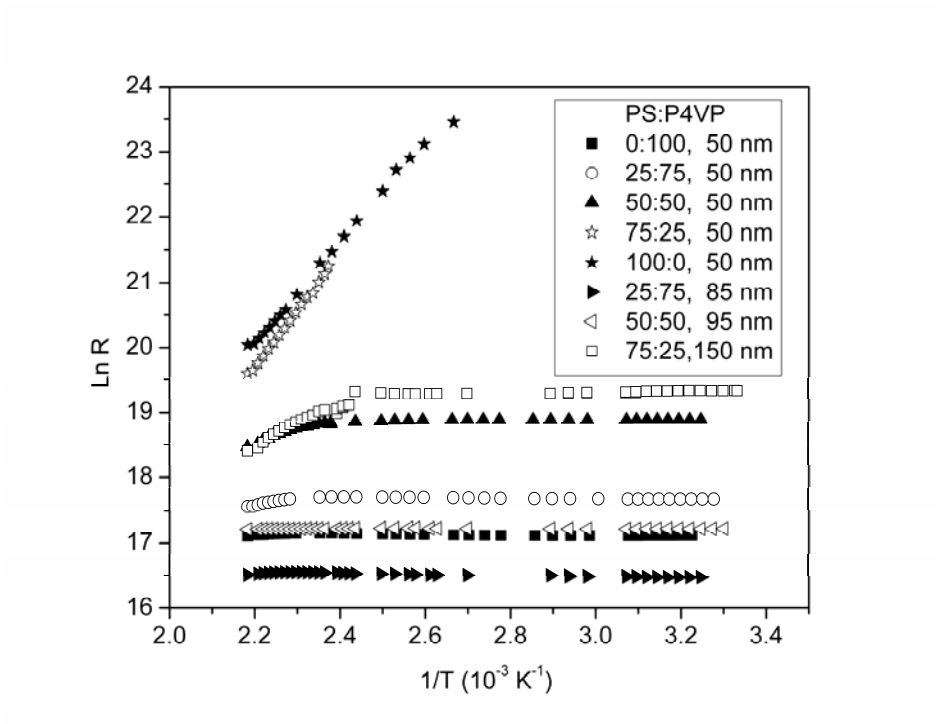

Figure 1: Variation of ln R with 1/T for silver films deposited on PS/P4VP blends held at 457 K

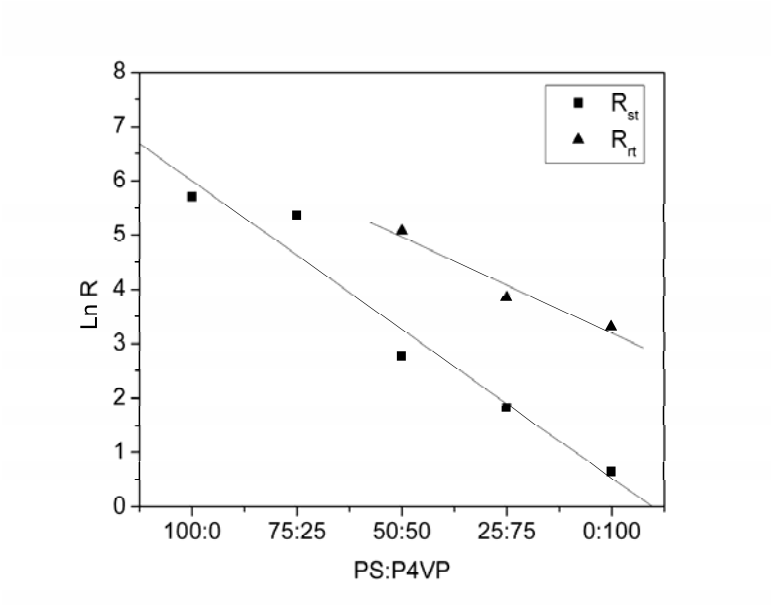

Figure 2: Variation of logarithm of resistances at 457 K and 300K with PS/P4VP blend composition for 50 nm silver films.

Uncompatibilized and reactively compatibilized ternary polymer blends of PA6/PP/ABS: Morphological investigation

Biswajit Panda *, Arup R. Bhattacharyya[#] and Ajit R. Kulkarni[#]

Department of Metallurgical Engineering and Materials Science, Indian Institute of Technology Bombay, Powai, Mumbai-400076, India

E-mail: arupranjan@iitb.ac.in ajit.kulkarni@iitb.ac.in

Abstract

Morphological investigation was carried out for melt mixed ternary polymer blends of polyamide 6(PA6)/ polypropylene (PP)/ acrylonitrile butadiene styrene (ABS) in order to understand the role of compatibilizer in morphological developments. Uncompatibilized 80/10/10 PA6/PP/ABS blends exhibited matrix- dispersed droplet type morphology in which the dispersed phases (PP & ABS) were found to exhibit core-shell type of morphology. The difference in morphology type may be due to the difference in surface free energy between the matrix and one of the dispersed phases. Eventually it was found that "core-shell" type of morphology changed to "co-continuous" type on increasing the concentration of PP and ABS in the ternary blends. In this context, styrene maleic anhydride co-polymer was found to act as a compatibilizer in PA6/PP/ABS ternary blends, manifesting in finer domain size of the dispersed phase.

Introduction

Multicomponent polymer blends consist of three or more immiscible polymers are a new interesting area in the field of polymer blends. A variety of phase morphology has been observed which directly influence the whole set of properties [1-2]. Three factors have been found to influence the morphological developments in immiscible multicomponent polymer blends viz. thermodynamic properties of the blends such as interfacial tensions of the constituent polymers [3], melt viscosity of the constituent polymers [4] and elasticity of the constituent polymers [5]. Hobbs et al. [6] explained the morphological phenomenon in ternary polymer blends on the basis of spreading co-efficient by modifying Harkin's equation, in which two dissimilar phases were dispersed in the third phase (matrix). If p, q and r are the three polymers of a ternary blend system and if p is the matrix, then the spreading co-efficient, λ_{rq} is given as

$$\lambda_{rq} = \sigma_{qp} - \sigma_{rp} - \sigma_{qr} \qquad (1)$$

where λ_{ij} is defined as the spreading co-efficient for i and j and σ_{ij} is the interfacial tension between i and j. If λ_{rq} is positive then q becomes the core encapsulated by r. Both r and q will disperse separately when both λ_{rq} and λ_{qr} are negative. Based on the spreading co-efficient sign four types of morphologies can be observed [7].

In the present work the morphological investigation has been carried out for PA6/PP/ABS blends and the influence of a reactive compatibilizer on the morphological developments has been investigated. Core-shell type of morphological observation in 80/10/10 PA6/PP/ABS has been analyzed with the help of spreading co-efficient and interfacial energy. 40/30/30 PA6/PP/ABS blends show co-continuous morphology. In this context morphological investigation has also been carried out for these blends in presence of styrene maleic anhydride copolymer (SMA) in order to understand the role of SMA as a compatibilizer.

Experimental

Polyamide6 (PA6 with zero shear viscosity = 180 Pa s at 260^{o}C) was obtained from GSFC, Gujarat, India (Gujlon M28RC, relative viscosity 2.8, Mv is 38642 in 85% formic acid). Polypropylene (H200MA) was obtained from Reliance Industries Ltd with melt flow index (MFI) of 23. Acrylonitrile-butadiene-styrene (ABS) copolymer (Absolac-120, with composition as: acrylonitrile 24 wt %, styrene 59.5 wt % and rubber content 16.5 wt %) was obtained from Bayer India Ltd. Styrene-maleic anhydride copolymer (SMA) with 8% MA content (Dylark 232) was supplied by Nova Chemicals, USA. The ternary blends of PA6/PP/ABS were prepared by melt mixing in a conical twin-screw microcompounder (Micro 5, DSM Research, Netherlands) at 260^{o}C with a rotational speed of 150 rpm for 15 min.

Morphological investigation was carried out by scanning electron microscopy (SEM, Hitachi S3400N).

Results and discussion

Depending on the composition two different types of morphologies have been observed in PA6/PP/ABS ternary blends viz. core-shell and co-continuous morphology for the compositions having 80/10/10 and 40/30/30 PA6/PP/ABS respectively.

The phase morphology of melt-mixed 80/10/10 PA6/PP/ABS blends has been investigated through SEM and can be found in Figure1. Core-shell type morphology has been observed in cryofractured etched surface of the extruded strands of the blends. By selective extraction of PP (by hot xylene) and ABS (by THF) it is revealed from the SEM micrographs that ABS is found to encapsulate the PP phase i.e. PP phase forming the core and ABS phase becomes the shell.

In case of 80/10/10 PA6/PP/ABS ternary blends system PA6 forms matrix and PP along with ABS form dispersed phases or more specifically core-shell type of morphology is observed from the SEM micrographs (Figure 1).The formation of this kind of morphology can better be understood from the spreading co-efficients of the respective polymer pairs [9]. The spreading coefficient $\lambda_{PP/ABS}$ of PP phase over ABS phase can be described as:

$$\lambda_{PP/ABS} = \sigma_{PA6/ABS} - \sigma_{PA6/PP} - \sigma_{ABS/PP} \quad \text{---------- (2)}$$

where σ_{ij} is the interfacial tension between i and j components.

If $\lambda_{PP/ABS}$ is >0 then PP phase becomes shell and ABS phase core. Similarly, if $\lambda_{ABS/PP}$ (Eq. 3) is >0 then ABS forms shell and PP core.

$$\lambda_{ABS/PP} = \sigma_{PA6/PP} - \sigma_{PA6/ABS} - \sigma_{PP/ABS} \quad \text{---------- (3)}$$

If both $\lambda_{PP/ABS}$ and $\lambda_{ABS/PP}$ are negative, the PP and the ABS phases will disperse separately in the PA6 matrix.

To determine the spreading co-efficient value, Interfacial tension (σ_{ij}) data were calculated for the three polymer-polymer interfaces present in the blends, i.e. PA6/ABS, PA6/PP and PPABS using the harmonic mean equation [8]:

$$\sigma_{12} = \sigma_1 + \sigma_2 - 4\sigma^{d}_{1}\sigma^{d}_{2} / \sigma^{d}_{1} + \sigma^{d}_{2} - 4\sigma^{p}_{1}\sigma^{p}_{2} / \sigma^{p}_{1} + \sigma^{p}_{2} \quad \text{----------(4)}$$

where σ_{ij} is the interfacial tension between the components i and j. σ_i is the surface tension of component i, σ^{d}_{i} is the dispersive fraction of the surface tension of component i and σ^{p}_{i} is the polar fraction of the surface tension of component i.

Incorporating the values in equation (3 and 4), it has been found that the spreading co-efficient values in all the cases were <0 manifesting the fact that both the minor phases (PP and ABS) will disperse separately in the PA6 matrix. But the observed phase morphology (Figure 1b) reveals that PP phase is encapsulated by ABS.

Figure2 shows the SEM micrograph for ternary polymer blends with varying concentration of SMA8 (2 to 6 wt %). It is well evident that from this micrograph that addition of compatibilizer has led to significant reduction in droplet size of the dispersed phase. Interestingly this reduction in the dispersed phase has been observed up to 2 wt % SMA8. Further it has been observed that with increase in concentration of SMA8, the domain size of the dispersed phase is found to be larger.

In case of 40/30/30 PA6/PP/ABS ternary blends, co-continuous morphology has been observed from the SEM micrograph (Figure3). This has been confirmed by selective extraction of the respective phases. In this context, it is worth pointing out that the extruded strand (after selective extraction of two phases viz. PP and ABS) has been found (Figure3d) to be self supporting, manifesting the co-continuous structure of the PA6 phase

Conclusions

Ternary polymer blends of PA6/PP/ABS without or with SMA8 have been successfully prepared by melt-mixing using a conical twin-screw microcompounder. The phase morphology was found to depend on the composition of the blends. 80/10/10 PA6/PP/ABS blends showed core-shell type morphology and 40/30/30 PA6/PP/ABS blends showed co-continuous type of morphology. Interestingly, on addition of SMA8 (up to 2 wt %) dispersed phase size was found to be finer indicating the compatibilizing action of SMA8 copolymer.

References

[1] Nemirovski N, Siegmann A, Narkis N. J Macromol Sci, Phys 1995; 34B:459.
[2] Horiuchi S, Matchariyakul N, Yase K, Kitano T, Choi HK, Lee YM. Polymer 1996; 37:3065.
[3] Hobbs SY, Dekkers MEJ, Watkins VH. *Polymer* **1998**; 29*:*1598-1602.
[4] Favis BD, Chalifoux JP, Polymers **1988**; 29: 1761-1767
[5] Reignier J, Favis BD, Heuzey MC. Polymer **2003**; 44: 49-59.
[6] Hobbs SY, Dekkers ME, Watkins VH. Polymer 1988; 29(9):1598–602.
[7] Reignier J and Favis BD. Macromolecules 2000; 33: 6998-7008
[8] Wu S. Polymer interface and adhesion. New York: Marcel Dekker; 1982, Chapter 3.
[9] Omonov T.S, Harrats C and Groeninckx G. Polymer 2005; 46:12322-12336

Table 1: Sample code and compositions of PA6/PP/ABS ternary blends

Sample code	PA6 (wt %)	PP (wt %)	ABS (wt %)	SMA8 (wt %)
8N1P1A	80	10	10	------
8N1P1A2S	78.4	9.8	9.8	2
8N1P1A4S	76.8	9.6	9.6	4
8N1P1A6S	75.2	9.4	9.4	6
4N3P3A	40	30	30	------

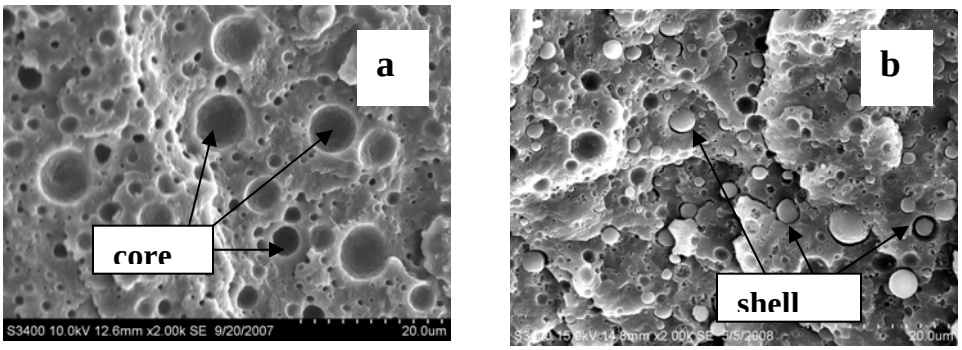

Figure 1: Core-shell morphology in 80/10/10 PA6/PP/ABS ternary blends in which (a) PP phase extracted by hot Xylene and (b) ABS phase extracted by THF

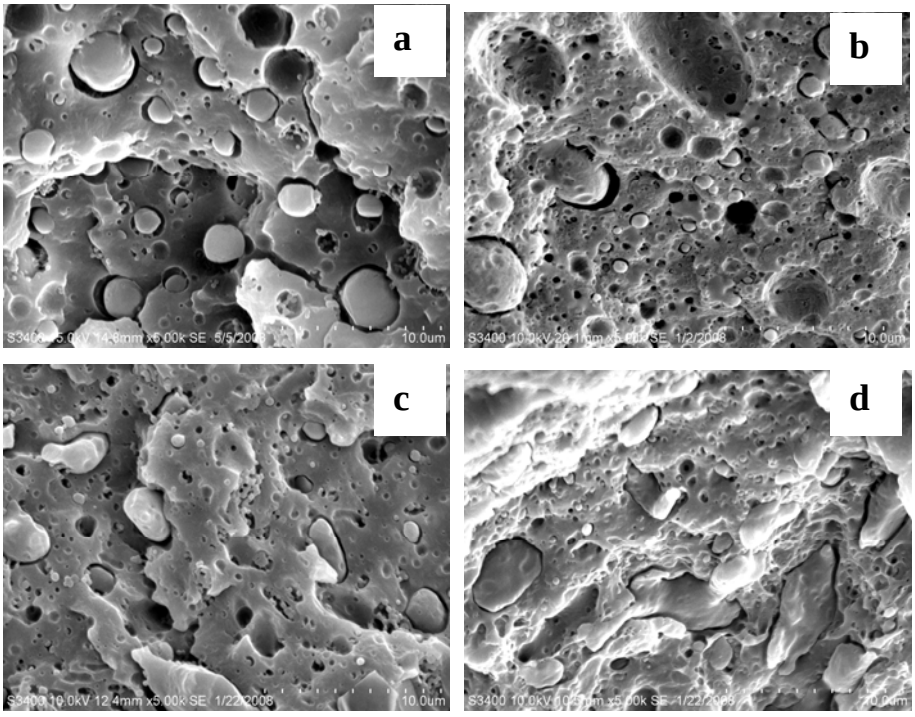

Figure2. 80/10/10 PA6/PP/ABS ternary phase morphology with (a) 0 wt%, (b) 2 wt%, (c) 4 wt% and (d) 6 wt% SMA8

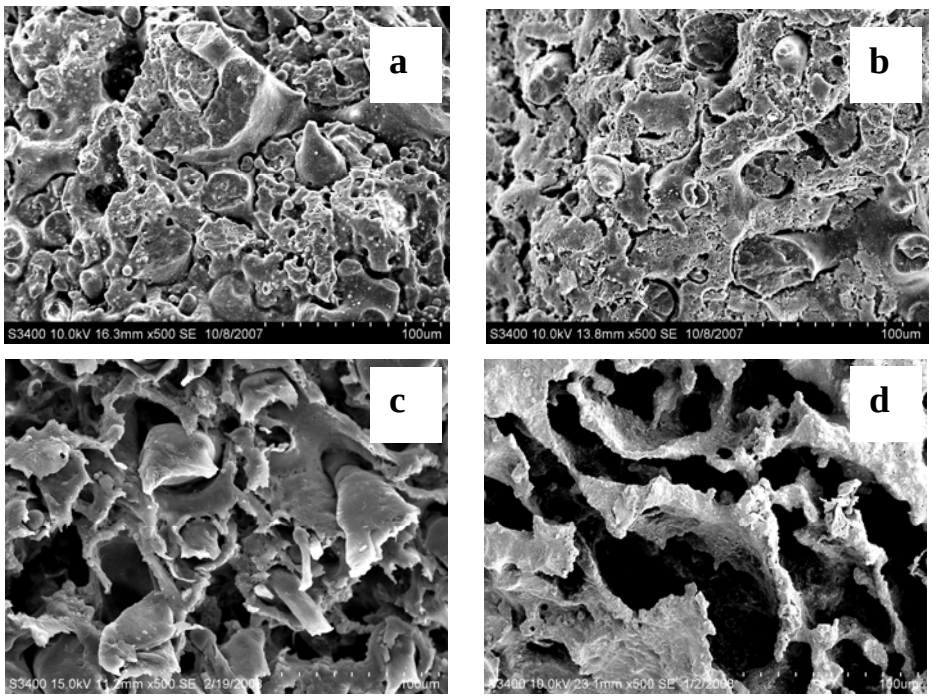

Fig.3 Co-continuous morphology of 40/30/30 PA6/PP/ABS ternary blends in which (a) ABS phase, (b) PP phase, (c) PA6 phase and (d) PP and ABS phases have been extracted

Blends of unsaturated polyester resin with maleated HTPB

Neethumol Varghese[1], Jenish Paul[2] and A. Benny Cherian[1]

1- Department of Chemistry, Union Christian College,Aluva
2- Polmer Science &Rubber Technology, CUSAT

Email: vavuty84@gmail.com

ABSTRACT

Unsaturated polyester resin is widely used in the fibre reinforced plastic industry. The fracture toughness and impact resistance of rigid unsaturated polyester can be improved by the incorporation of functional elastomers like hydroxy terminated polybutadiene (HTPB). HTPB is further funtionalised by maleic anhydride grafting. The maleated HTPB is then blended with polyester resin. Maleic anhydride graft HTPB is found to increase toughness substantially without seriously affecting tensile and flexural properties.

INTRODUCTION

Unsaturated polyester resin (UPR) is used extensively as a matrix for fibre- reinforced plastic (FRP). The wide spread use of the resin is due to its low cost, ease of processing, its ease of combination with reinforcements, rapid cure, excellent dimensional stability and ease of colouring and modification for special purpose. Carothers was the first to prepare UPR[1].

When cross-linking is initiated with the help of a catalyst and an accelerator styrene facilitates cross-linking at the sites of unsaturation in the polyester chains. The saturated acid reduces the number of cross-linking sites and consequently the cross-link density and brittleness of the cured resin. Since cross-linking occurs via free radical addition mechanism across the double bonds in the polyester chain and the reactive diluent, no volatiles are given off during cure. When cross-linking is initiated with the help of a catalyst and an accelerator, styrene forms polystyrene chains, which cross-link the polyester chains at the sites of unsaturation[2].

The broad objective of the work is (i) to study the effect of addition of hydroxy terminated polybutadiene (HTPB) and maleic anhydride graft hydroxy terminated polybutadiene (MA-g-HTPB) on the properties of polyester resin (ii) to investigate the optimum concentration of functional rubbers and (iii) to identify the functional rubber, which give optimum properties.

EXPERIMENTAL

Materials

GP grade UPR (Bakelite Hylam resin HSR 8113 M), styrene, methyl ethyl ketone peroxide (MEKP) and cobalt naphthenate were supplied by Sharon Engineering Enterprises, Cochin. HTPB (Mn=2620) was obtained from Vikram Sarabhai Space Centre, Thiruvananthapuram. MA and benzoyl peroxide were supplied by E. Merck India Ltd, Bombay.

Modification of UPR with HTPB

Unmodified resin was first cured at room temperature by the catalyst MEKP and by the accelerator cobalt naphthenate. These were used in concentrations of 0.5 % and 1 % of the

weight of the resin respectively to obtain a reasonable gel time. The resin was then poured into the tensile mould. Samples for impact test and flexural strength were cast separately in appropriate moulds. Curing was done at room temperature for 24 hrs, followed by post curing at 80^0C for 3 hrs

The blends were prepared by the following procedure. Varying amounts (0-5 wt %) of the HTPB were added to the resin. The mixture was stirred well using a mechanical stirrer to give a homogeneous liquid. Curing of the blend was done as per the procedure employed for UPR. Thereafter, post curing was done at 80^0C for 3 hrs.

The samples after post curing were tested for tensile strength, elongation at break, modulus, flexural strength and flexural modulus taking six trials in each case. The tensile and flexural properties were tested on a universal testing machine (ASTM D 638-89).

Modification of UPR with MA grafted HTPB

Maleated HTPB is prepared by mixing HTPB with 5% MA and 0.5% benzoyl peroxide in a Brabender at 100^0C and 50 RPM speed for 10 min. The reaction of MA with HTPB was confirmed by FTIR spectroscopy and titration. The amount of maleic anhydride reacted is determined by refluxing a solution of maleated HTPB in xylene saturated with water for 1 hr and then titrating with a solution of 0.05N ethanolic KOH using 1 % thymol blue as an indicator.

Varying amounts of MA modified HTPB containing 0-5 weight percentage of elastomers were blended and cast with the UPR by the same procedure adopted earlier. The tensile and flexural properties and water absorption were determined in accordance with ASTM standards.

Test methods

Tensile testing

Tensile tests were carried out according to ASTM D 638-89 using a universal testing machine.

Flexural properties (ASTM D 790-99*)*

Flexural strength is a measure of the load required to break a material when it is subjected to bending Flexural modulus is the ratio of stress to corresponding strain and is expressed in MPa. It is calculated by drawing a tangent to the steepest initial straight line portion of the load- deflection curve

Water absorption

Water absorption of the sample was measured according to ASTM 570-81.

RESULTS AND DISCUSSIONS

Mechanical Properties of UP resin modified by Functional elastomers

Tensile Properties

Referring to Fig.1, tensile strength values obtained by adding HTPB were significantly higher than that obtained by adding maleated HTPB. Tensile strength values reached a maximum on adding progressively larger amounts of HTPB, but addition of more rubber beyond this point resulted in a reduction of tensile strength. The improvement in tensile strength,

in comparison to that of the base resin was due to the high degree of compatibility arising from the polar groups of HTPB and UPR. The tensile strength of maleated HTPB blends gradually decreases on adding progressively larger amounts of rubber due to the higher flexibility of maleated HTPB.

The elongation at break increases with increase in elastomer concentration as shown in Fig.3. The addition of MA-g-HTPB produced the greatest increase in elongation at break compared to HTPB due to the higher flexibility and compatibility of maleated HTPB. The elongation at break of MA-g-HTPB/UPR is about 219 % of UPR

The energy absorption of the cured resin as a function of rubber concentration is shown in Fig.4. At 3-wt % MA-g-HTPB concentration, the energy absorption of the blend was at a maximum (about 305 % of the energy absorption of UPR). The energy absorption is related to the toughness of the sample. Higher elongation at break values increases the toughness of MA-g-HTPB. The performance of MA-g-HTPB was far superior to HTPB, due to better dispersion of the rubber phase as particles in the continuous polyester phase.

Flexural properties

Fig. 5 shows the variation of flexural strength with rubber content. The flexural strength of MA-g-HTPB/UPR blend decreases with elastomer concentration due to the higher flexibility and compatibility of maleated HTPB.

Water absorption

Water absorption of HTPB and maleated HTPB modified resins is shown by Fig.6. The maleated HTPB has slightly higher water absorption compared to HTPB due to the higher functionalisation.

CONCLUSIONS

The study reveals the effect of incorporating functional elastomers into UPR at low concentrations by a physical method. Toughness and tensile/flexural properties show maximum improvement at about 2-3 wt % HTPB concentrations. Interestingly, the increase in toughness (76 % of the energy absorption of UPR) has been observed with simultaneous increase in tensile and flexural properties for HTPB.

Maleation increases the toughness and elongation at break of HTPB. At 3-wt % MA-g-HTPB concentration, the energy absorption of the blend was at a maximum (about 305 % of the energy absorption of UPR) with marginal lowering of tensile and flexural properties.

REFERENCES

1. W. H. Carothers, *J. Am. Chem. Soc.1929*, 51, 2569,
2. Boeing, H.V., *Unsaturated polyester resin-structure and properties*, Elsevier Publishing Company, Amsterdam,1964.
3. F. J. McGarry, *Rubber in cross- linked Polymers*, Applied Science, London ,1983.
4. C. Fintemann., Polym. Plast. Tec.,1981, 17, 225.
5. A. Pavan, Reports of the 2nd Internat. Conf SIM-Plast. 79, Warsaw,1979, Vol.1, p.28.
6. C. Keith Riew and A.J. Kinloch, Rubber Toughened Plastics, American Chemical Society, Advances in chemistry series 233, Washington DC ,1993.
7. C. Keith Riew, Eds., in Rubber Toughened Plastics, Advances in chemistry series 222, American Chemical Society, Washington DC, 1989
8. G. A. Crosbie and M. G. Phillips, 37th Ann. Conf SPI, Sect. 8.C, 1982
9. Charles B. Arends, Eds., in Polymer Toughening, p-177, Marcel Dekker, Inc. New York, 1996.
10. C.Keith Riew, Rubber Toughened Plastics, American Chemical Society, Washington ,1989.
11. M .J. Owen and R. G. Rose, J. Mat. Sci.,1975, 10,1711.
12. A. Christiansen and J. B. Shortall, J. Mat. Sci.,1976,11,1113.
13. L. Leel, C. K. Riew, and A. R. Seeber, Polymer Mat. Sci. Eng.,1990, 63.
14. J. G. Park and C. E. Pohang, Chan. Eon.lnst. Sci. Tech.,1990, 1.4 (3), 266.
15. D.S. Kim, K. Cho, J.H. Park and C.E Pohang, J. Mat. Sci.,1992, 11(17).
16. Siebert Alan, R.Bertsch, and J. Robert, (B.F. Goodrich Co,), U.S.A,1992,17.
17. L.K. Kostanski, and W. Krolikowski, IPSAT,1985, 12(7).
18. E.H. Rowe, and F.J. McGarry, 35 th Ann. Tech. Conf. SPI, Sect. 18.E, 1980.
19. Yan-Jyi Huang and Chin-Cheng Su, *J. Appl. Polym. Sci.,1995,* 55, 305-342 .
20. A. A. Collyer, *Rubber Toughened Engineering Plastics,*1994,5.7, pp.160.
21. Korb, *J. Proc. Annu. Conf. SPE*,1984, 660.
22. Farmer, E.H. and Wheeler, J., U.S. Patent 2,1940, 227,777 (to British Rubber Producers Research Association), 1940, January 6.
23. Lawson D.F. Hergenrother, W. L. and Matlock M.G. *J. Appl. Polym. S.G.1990,* 39, 2331.
24. Trivedi, B.C. Culbertson, B.M. Maleic Anhydride, Plenum, New York ppt.,1982, 172-3.

Fig. 1 Tensile strength of rubber modified resin as a function of rubber concentration

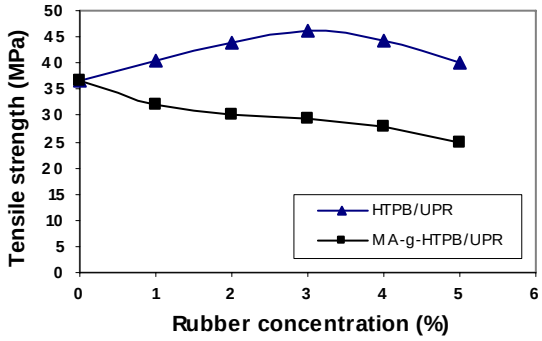

Fig. 2 Modulus of rubber modified resin as a function of rubber concentration

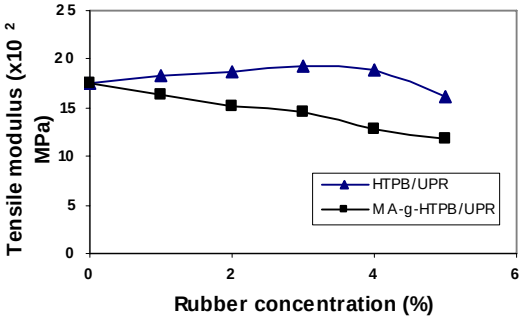

Fig. 3 Elongation at break of rubber modified resin as a function of rubber concentration

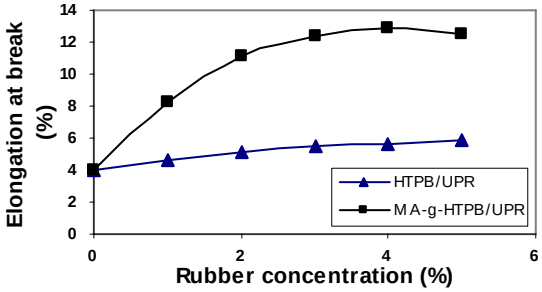

Fig. 4 Energy absorbed by rubber modified resin as a function of rubber concentration

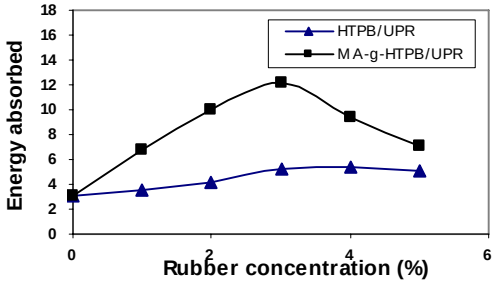

Fig. 5 Flexural strength of rubber modified resin as a function of rubber concentration

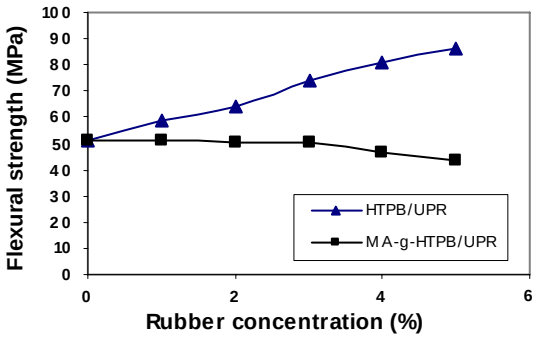

Fig. 6 Water absorption of rubber modified resin as a function of rubber concentration

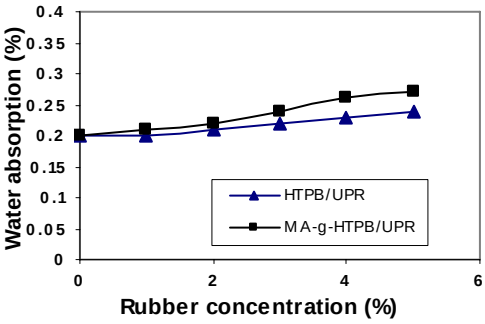

Effect of organic modification on the compatibilisation efficiency of Poly (trimethylene terephthalate) PTT/m-LLDPE blend nanocomposites

Kapil K. Gangele[1], S.Mohanty[2], S.K.Nayak[2*]
Laboratory for Advanced Research in Polymer Materials,
1. Central Institute of Plastics Engineering & Technology, Bhubaneswar-751024, India
2. Central Institute of Plastics Engineering & Technology, Chennai – 600 032, India

Email: drsknayak@yahoo.com

Abstract
Poly (Trimethylene Terephthalate)(PTT) and Metallocene Linear Low density Polyethylene (m-LLDPE) Blends and its Nanocomposites were prepared using melt blending technique in a batch mixer. Organically modified nanoclays; Cloisite 20A(C20A), Cloisite 30B(C30B) and Bentone 109(B109) have been used as nanoscale reinforcement to prepare blend nanocomposites. The blend composition of PTT/m-LLDPE of 70:30 has been optimized based on the mechanical performance. Further, characterization studies such as DMA, DSC/TGA, TEM and WAXD have been investigated to evaluate the effect of incorporation of nanoclays into the blend matrix. WAXD studies revealed a significant increase in of d_{001} spacing of clay galleries in the blend nanocomposites indicating intercalated morphology. From DSC, it was observed that Cloisite 30B with 5 wt. % shows higher crystallization temperature as compared with PTT Virgin and other modified clay systems. Further with the increase in the scanning rate, Crystallization temperature of PTT virgin polymer as well as Nanocomposites decreases. TGA thermograms indicated that the thermal stability of the blend increases with the incorporation of Cloisite 20A. DMA measurements reveal that the Cloisite 30B nanocomposite has maximum modulus as compared to other nanocomposites. It is interpreted from DMA results that PTT/m-LLDPE blend is immiscible blend due to observation of two peaks and shifting of Tg outward. Nanocomposites show higher tensile strength and modulus as well as flexural strength and modulus as compared to optimized blend. The Effect of m-LLDPE content on the mechanical properties of PTT has also been investigated. It is found that m-LLDPE functions as impact modifier to enhance the impact properties of neat PTT and prepare rubber-toughened blend.

Keywords-: Poly (Trimethylene Terephthalate), Polymer Blend and Nanocomposites

Introduction
Poly (Trimethylene Terephthalate) (PTT), aromatic polyester prepared by polycondensation reaction between propane 1, 3 diol and terephthalic acid or dimethyl Terephthalate, has gained commercialization over the last years. PTT has become a potential competitor of PET and PBT for various emerging applications in fibers, packaging, and films and as engineering thermoplastic [16]. PTT combines the mechanical properties of PET and processing characteristics of PBT, thus possessing the desired attributes of thermoplastic polyester, wherein the properties such as dimensional stability, solvent and abrasion resistance are pre-requisite. The polymer has very good tensile strength, elastic recovery and surface properties; together with relatively low melt temperature, good chemical resistance and rapid crystallization rate. However, certain impediments such as low toughness, low heat distortion temperature, low viscosity, poor optical properties and pronounced low temperature brittleness have restricted the optimum use of PTT, as engineering plastic in many applications. Several attempts have already been made by various researchers to increase the toughness of PTT by blending it with ABS [25], EPDM [26] and EOC [27]. In the present investigation, mechanical, thermal and morphological

characterization of PTT/m-LLDPE blend nanocomposites at variable weight percentages of organically modified nanoclay have been studied.

Experimental

Materials

PTT (Futura CPTT®) was purchased from M/s Futura Polymers Ltd., India, having density 1.3 g/cm^3 and intrinsic viscosity 0.915 dL/g (Phenol/Carbon Tetracholride, 60/40). m-LLDPE (Relene®) was obtained from M/s Reliance Industries Ltd., India having MFI 1.0 g/10 min. The clay minerals used were: Cloisite®20A (C20A) Cloisite®30B, (C30B), obtained from M/s Southern Clay Products Inc, USA, and Bentone®109 (B109) from M/s Elementis Ltd. UK. Prior to blending, PTT was dried at 110^{0}C for 24 hours and all the nanoclays were dried at 80^{0}C for 4 hrs.

Preparation of blend and blend nanocomposites

PTT/m-LLDPE blend of various composition (90/10, 80/20, 70/30, 50/50 by weight) were prepared using a Torque Rheocord-9000 (HAAKE®, Germany), at a screw speed of 70 rpm and temperature of 250 °C for a duration of 6 minutes. m-LLDPE was added to the molten PTT after 3 minutes. The blend composition was optimized at 70: 30 ratio of PTT : m-LLDPE. This blend composition was maintained for preparation of polymer blend nanocomposites using various nanoclays C20A, C30B and B109 at variable weight percent (1-5 wt. %). Specimens were prepared using mini Injection molding machine (HAAKE® Minijet) at 245^{0}C barrel temperature, 840-870 bar injection pressure and mold temperature of 110 ^{0}C as per ASTM standard.

X-ray Diffraction Analysis

The interlayer gallery spacing of nanoclays in the nanocomposites was studied by wide angle Philips X'Pert MPD (Japan)X-ray diffraction at ambient temperature.

Transmission Electron Microscopy (TEM)

For TEM observation, the samples were stained with OsO_4 vapor and microtomed at low temperature (-55^{0}C) and examined using a Transmission Electron Microscope (Philips CM12, The Netherlands) an acceleration voltage of 100 kv at 100nm scale.

Mechanical Properties

Tensile & Flexural Properties were determined using Universal Testing Machine (UTM), LR-100K (Lloyd Instruments Ltd. U.K as per ASTM-D 638 & ASTM-D 790. Izod impact strength was determined as per ASTM D 256.

Dynamic mechanical Analysis

The dynamic mechanical analysis of was investigated using DMA242 analyzer (NETZSCH, Germany). at fixed frequency of 1Hz, heating rate of 10K/min, under N2 atmosphere over a temperature range of -150^{o}C to 200^{0}C in three point bending mode.

Thermal analysis

DSC & TGA measurements were performed on a diamond DSC (Perkin Elmer Inc., USA) Pyris – 7 TGA equipment (Perkin Elmer Inc., USA).

Results and Discussion

X-Ray diffraction analysis

The state of dispersion of the silicate layers in the blend matrix have been investigated using X-ray diffraction patterns represented in the figure-1. The mean interlayer spacing of plane (d_{001}) of C30B was 4.01nm.In case of the 70PTT/30m-LLDPE/5C30B hybrid, the characteristic peak shifted to a smaller angle corresponding to d_{001} spacing of 4.01 nm, because of intercalation of both polymer chains into silicate galleries [37]. A similar shifting of angles was also observed in PTT/m-LLDPE/B109 to 4.02 nm and PTT/m-LLDPE/C20A to 4.06^0 nm nanocomposites system respectively revealing the formation of intercalated structure. Furthermore, it was also noticed that the X-ray diffractograms in all the blend nanocomposites system reveals diffraction peak in the similar range of 2.205^0. However, peak intensity of

original C30B, C20A increased significantly that probably due to more parallel stacking of the organoclays in the blend matrix**.**

Transmission electron microscopy (TEM)

To elucidate the dispersion of clay in the blend nanocomposites in detail, figure-2 illustrates the TEM micrographs of PTT/m-LLDPE/C20A, PTT/m-LLDPE/B109 and PTT/m-LLDPE/C30B. The dark lines represent the thickness of individual clay layers or agglomerates. Thick darker lines represent stacked silicate layers due to clustering or agglomeration. It was observed from the micrographs that clay particles preferentially resided in the PTT phase rather than m-LLDPE phase. In case C30B blend nanocomposites, it was found that stacked and intercalated silicate layers are well dispersed within the blend matrix especially in polar phase due to similar solubility parameter. It was interesting to note that the organoclay has a strong tendency to be located in the PTT phase and the domain size of dispersed particle effectively reduced, due to obstacle created by exfoliated clay, as shown in figure: 2(b) and(c). However, a mixed nanomorphology was obtained in both PTT/m-LLDPE/C20A as well as PTT/m-LLDPE/B109 nanocomposites due to presence of regions of ordered /disordered intercalation.

Mechanical Properties of Polymer Blend and Blend nanocomposites

The mechanical properties of PTT/m-LLDPE blend at variable weight percent (1-5 wt%) of m-LLDPE are depicted in table-1. It is evident that the tensile & flexural properties of PTT decreases with the increase in m-LLDPE content. This behavior is probably because m-LLDPE is inherently weak and soft with elastomeric properties due to linearity in its structure with 5-10% branching. Izod impact strength of PTT was observed to be 26.80 J/m. Incorporation of m-LLDPE to the tune of 10-30% results in an increase in the impact properties of PTT matrix in the blends. The blend prepared at PTT: m-LLDPE ratio of 70:30 exhibits maximum impact strength of 33.76 J/m, which subsequently reduces with the increase in PTT content to 50-wt%. This indicates that m-LLDPE acts as impact modifier due to presence of metallocene and butene in its structure, at lower concentrations. The blend prepared at 70:30 ratio of PTT: m-LLDPE has been optimized based on optimum impact performance and has been considered for fabrication of blend nanocomposites using various organically modified nanoclays.

The mechanical properties of PTT/m-LLDPE blend nanocomposites at various wt.% of organically modified is also depicted in table-1. It is evident that a tensile property of blend increases with addition of 5 wt% of C20A, B109 and C30B nanoclays. Tensile strength of blend matrix increases from 37.92 MPa to 50.86 MPa in PTT/m-LLDPE/C20A, 53.24 MPa in PTT/m-LLDPE/C30B and 51.36 MPa in PTT/m-LLDPE/B109 blend nanocomposites respectively at 5 wt. % of nanoclay loading, which indicates stiffening effect of nanoclay layers. A similar linear increase in tensile modulus to the tune of 52.1 % in C20A, 61.5 % in C30B and 57.4 % in B109 respectively was also obtained as compared with the blend matrix. According to Via and co-workers [38], the interlayer structure of the organically modified layered silicate should be optimized to attain maximum configurational freedom of the functionalzing chains upon layer separation and increase the potential reaction sites at the interlayer surface. In the present context, the methyl tallow bis-2 hydroxy ethyl quaternary ammonium intercalant in C30B has two –OH groups in its structure, which might have interacted with the carboxylic group of PTT resulting in enhanced polar-polar interactions of the silicate layer within PTT phase which further contributes to an increase in tensile properties. A similar increase in the flexural & impact strength of blend nanocomposites was also obtained. The mechanical performance of the blend matrix varies in the following order:

PTT/m-LLDPE/C30B > PTT/m-LLDPE/B109 > PTT/m-LLDPE/C20A > PTT/m-LLDPE.

This further indicates improved interactions in C30B system as compared with C20A and predominant role of PTT base matrix.

Dynamic mechanical properties (DMA)

The dynamic storage modulus (E') versus temperature of PTT, PTT /m-LLDPE blend and blend nanocomposites are shown in the figure-3. A gradual decrease in E' with increasing temperature from -150 to 200^0C was observed. It was noted that incorporation of m-LLDPE decreased the storage modulus of PTT matrix due to softening of diluting effect of the soft elastomeric phase. Conversely, addition of

organoclay into the blend matrix results in a remarkable increase in the storage modulus over the entire investigated temperature range. The blend nanocomposites prepared using C30B organoclay displays optimum E' as compared with the other blend nanocomposites

Differential Scanning Calorimetry (DSC)

The DSC thermogram of virgin PTT, virgin m-LLDPE, 70PTT/30m-LLDPE blend and the blend nanocomposites is depicted in figure-4. Virgin PTT depicts a melting transition around 247.59^{0}C with m-LLDPE at 127^{0}C.The DSC scan of the blend reveals two distinct T_m which indicates phase-separated morphology. Similar to the blend, the DSC curves of the blend nanocomposites also exhibited two distinct T_m's confirming presence of a phase-separated morphology. However, incorporation of organically modified nanoclays increases the Tm of the PTT phase in blend matrix, while reducing the Tm of the m-LLDPE phase. This indicates improved compatibility of nanoclay in the PTT matrix. The crystallization exotherms of virgin PTT, PTT/m-LLDPE blend and blend nanocomposite system is shown in figure-5. It is evident that the T_c of PTT matrix decreases from 175.47^{0}C to 170.40^{0}C with incorporation of m-LLDPE indicating elastomeric effect due to amorphous nature and low spherulitic growth of m-LLDPE. However incorporation of nanoclay increases the T_c of PTT phase in the blend matrix considerably indicating heterogeneous nucleating effect.

Thermo gravimetric analysis (TGA)

Virgin PTT exhibits an initial degradation temperature (T_{id}) of 352.12^{0}C with final degradation temperature (T_{fd}) 503.47 ^{0}C (Figure 6).Incorporation of m-LLDPE decreases T_{id} of matrix from 352.12^{0}C to 345.97 ^{0}C and Tfd of matrix from 503.47 ^{0}C to 495.90 ^{0}C.This is predominantly attributed to lower degradation temperature of ethylene linkage due to weak bonding between them and presence of side chain branching (5-10%) in m-LLDPE. Further addition of organoclays substantially increases the thermal stability (T_{id}, T_{fd}) of the blend matrix. Blend nanocomposites with C20A organoclay has highest thermal stability due to higher modifier concentration and gallery spacing.

Conclusion

The mechanical, thermal, crystallization and morphological characteristics of PTT/m-LLDPE blend and its nanocomposites prepared through batch mixing process were investigated. The impact strength of PTT increased up to 30 wt% loading of m-LLDPE. The blend nanocomposites prepared using C30B shown maximum mechanical performance. XRD results showed intercalated structure in the elastomer modified PTT organoclay nanocomposites DSC & DMA analysis revealed two phase morphology in the blend system. TGA thermograms indicated increased thermal stability of PTT matrix in the blends with the addition of nanoclays.

References

1. Mishra S.P.; Deopure L.; *Polym.Bull*; 1985:26:5.
2. Yu Y.; Choi K. ; *Polym. Eng. & Sci* 1997: 37: 91.
3. Nabisaheb D; Jog J.P., J. *Polym. Sci: part-B: Polym Phy*. 1999: 37: 2439.
4. Avramova N. *Polym* 1995: 36: 801.
5. Wfer J., M. US pat. 4,485,212 (1984)
6. Pratt C.F., Phadke S.V., Olivier E., U.S.Pat. 4,965,111 (1990)
7. Khatua B.B.; Lee D.J.; Kim H.Y.; Kim J.K.; *Macromolecules* 2004:37:2454-59.
8. Ray S.S.; Bousmina M.; *Macromol. Rapid Commun*., 2005:26:1639-46.
9. Lim J.W.; Hassan A.; Rahmat A.R.; Wahit M.U. *Polym Int* 2006:55:204-15.

Table 1: Mechanical properties of PPT/m-LLDPE blends and its Nanocomposites

Compositions	Tensile Strength (MPa)	Tensile Modulus (MPa)	Flexural Strength (MPa)	Flexural Modulus (MPa)	Impact Strength (J/m)
PTT Virgin	48.20	1420	58.80	2670	26.80
PTT/m-LLDPE (90/10)	45.32	1092.3	55.92	2342	31.22
PTT/m-LLDPE (80/20)	41.08	984.33	52.70	2180	31.22
PTT/m-LLDPE (70/30)	37.92	933.41	49.81	2028	33.76
PTT/m-LLDPE (50/50)	32.27	866.52	43.61	1816	31.11
PTT/m-LLDPE(70/30)/C20A5%	50.86	1422	61.73	2695	37.23
PTT/m-LLDPE 70/30)/C30B5%	53.24	1507	63.77	2810	39.88
PTT/m-LLDPE(70/30)/B109 5%	51.36	1470	62.12	2752	33.76

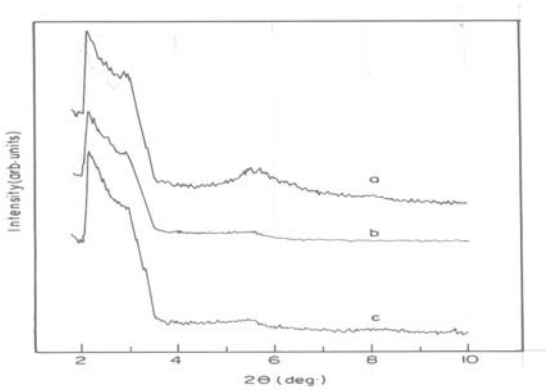

Figure: 1- XRD pattern of (a) PTT/m-LLDPE/C30B5 %(b) PTT/m-LLDPE/B109, 5 %(c) PTT/m-LLDPE/C20A5%

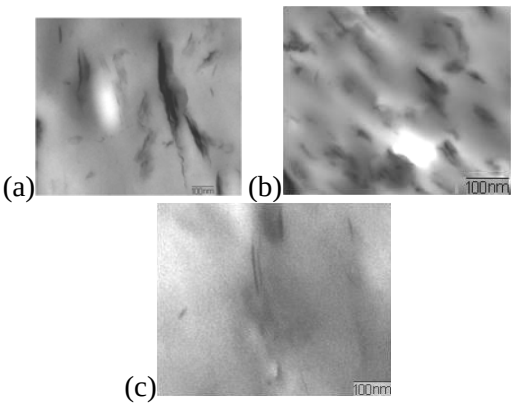

Figure: 2 TEM micrographs of (a) PTT/m-LLDPE/C30B 5% (b) PTT/m-LLDPE/C20A 5% (c) PTT/m-LLDPE/B109, 5%

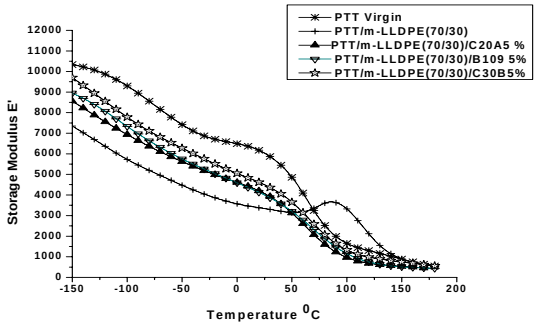

Figure 3: Temperature dependence of Storage modulus (E') blend and nanocomposites at 5% loading of nanoclay

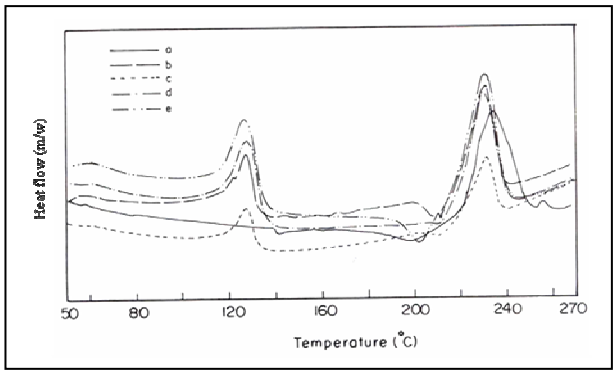

Figure: 4 - DSC thermogram of(a)PTT virgin (b) PTT/m-LLDPE(70/30) (c)) PTT/m-LLDPE(70/30)/C20A 5% (d) PTT/m-LLDPE(70/30)/B109 5% (e) PTT/m-LLDPE(70/30)/C30B 5%

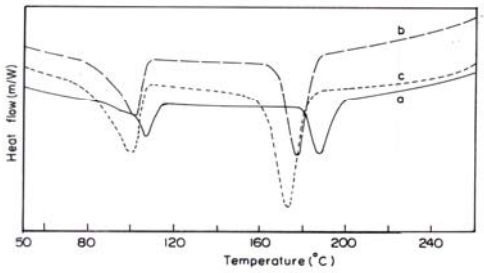

Figure: 5 - DSC cooling thermogram of (a) PTT/m-LLDPE(70/30)/C30B 5% (b)PTT/m-LLDPE(70/30)/B109 5% (c) PTT Virgin

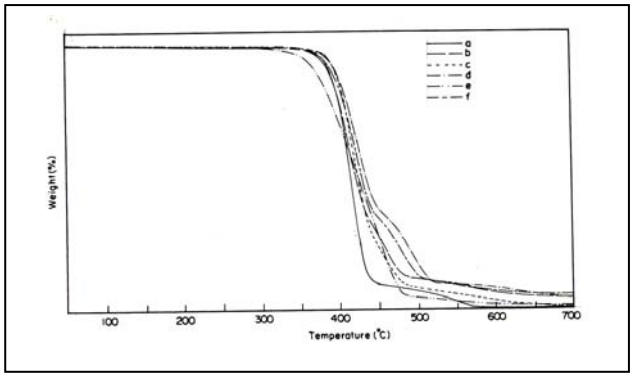

Figure: 6-TGA graph of (a) Virgin PT(b) m-LLDPE Virgin (c) PTT/m-LLDPE (70/30) (d) PTT/m-LLDPE (70/30)/C 20A5% (e) PTT/m-LLDPE (70/30)/B109,5% (f) PTT/m-LLDPE (70/30)/C 30B5%

Mechanical and rheological behavior of peroxide cured polypropylene (PP)/ethylene octene copolymer (EOC) thermoplastic vulcanizates (TPVS)

R.Rajesh Babu*, Nikhil K Singha and Kinsuk Naskar[#]
Rubber Technology Centre, Indian Institute of Technology,
Kharagapur -721302, India
E.mail: knaskar@rtc.iitkgp.ernet.in

Abstract

Technologically compatible binary blends of polypropylene (PP) and ethylene octene copolymer (EOC) were dynamically vulcanized by coagent assisted peroxide crosslinking system. Addition of peroxide in PP/EOC blend involves two major competing reactions: EOC cross-linking and PP degradation by β-scission. Final product properties are thus dependent on the balance among those two competing reactions. As the concentration of peroxide increases, particle size decreases. However, mechanical properties of these TPVs are not good enough, which is due to severe degradation in the PP phase in the presence of peroxide. Principally, coagent incorporation increases the crosslinking efficiency in the EOC phase and decreases the degradation in the PP phase. Present study focus on the influence of the three structurally different coagents namely triallyl cyanurate (TAC), trimethyol propane triacrylate(TMPTA) and N,N'-m-phenylene dimaleimide(HVA-2) on the mechanical and rheological properties of the PP/EOC thermoplastic vulcanizates (TPVs). Depending on the structure and reactivity, different coagents show different performance. All the compositions were prepared by melt mixing method in the Haake rheomix at 180°C and rheological properties also have been evaluated at the same temperature. Viscoelastic behaviors of the TPVs prepared were analyzed by a dynamic oscillatory rheometer in the melt state in Rubber Process Analyzer (RPA 2000). Morphologically TPVs consist of dense crosslinked rubber domains in the thermoplastic phase and their rheological behavior can be compared to that of highly filled polymers. The crosslinked particles tend to agglomerate and build local cluster which tends to disintegrate by shearing. A variety of rheological observations such as Payne effect, modulus recovery and shear rate sensitivity were studied by carrying frequency sweep and strain sweep.

Introduction

Thermoplastic vulcanizates (TPVs) are prepared by dynamic vulcanization process, where crosslinking of the elastomeric material takes place during its melt mixing with a thermoplastic material under high shear and temperature. Temperature should be high enough to activate and complete the process of vulcanization. The resulting morphology consists of micron sized finely dispersed cross-linked rubbery particles in a continuous thermoplastic matrix although the rubber content is higher than the thermoplastic component. The rheological behavior can be compared with that of highly filled polymers. TPVs have proven themselves to perform in a wide range of demanding engineering requirements mainly in automobile sectors. Several crosslinking agents are used in the preparation of TPVs such as phenolic resin, peroxide and silane crosslinking system. Phenolic resin gained considerable commercial importance but still the formation of black specks motivates the development of other potential crosslinking system. In this particular polypropylene (PP)/ ethylene octene copolymer (EOC) blend system; phenolic resin is ineffective, since the latter needs the presence of double bond to form a crosslinked network structure. Peroxides can crosslink both saturated and unsaturated polymers without any reversion characteristics. The formation of strong C-C bonds provides substantial heat resistance and good compression set property without any discoloration. It has been well established that

polypropylene exhibits β-chain scission reaction (degradation) with the addition of peroxide. Hence the use of only peroxide is limited to the preparation of PP based TPVs. An alternative approach is to use coagent together with peroxide curing system. Generally coagents are multifunctional vinyl monomers which are highly reactive towards free radicals either by addition reaction and/or by hydrogen abstraction. Chain scission also could be retarded by stabilizing the PP macroradicals by addition reaction across the double bond in the vinyl monomer (coagent). Hence addition of coagent in the PP/EOC blend increases the crosslinking efficiency in the EOC phase and decreases the extent of degradation in the PP phase. Different coagents have different reactivity and efficiency in terms of increasing the degree of crosslinking and decreasing the extent of degradation. The main objective of the present investigation is to study the influence of three structurally different coagents as a function of concentration on the dicumyl peroxide cured PP/EOC TPVs in terms of mechanical and rheological characteristics.

Experimental

Materials - The general purpose polyolefin elastomer Exact 5371 (specific gravity,0.870 g/cc at 23 °C; co-monomer octene content 13 %; melt flow index,5.0 @190 °C/2.16 Kg), was commercialized by Exxon Mobil Chemical company, USA. Polypropylene (Specific gravity, 0.9 g/cc at 23 °C; melt flow index, 3.0 @ 230 °C/2.16 Kg) was obtained from IPCL, India. Dicumyl peroxide (DCP) (Perkadox-BC-40B-PD) having active peroxide content of 40 %; temperature at which half life time ($t_{1/2}$) is 1 hour at 138°C; specific gravity of 1.53 g/cm^3 at 23 °C) was used as the crosslinking agent obtained from Akzo Nobel Chemical Company, The Netherlands. Three different types of coagents, Triallylcyanurate (TAC), Trimethylol propane triacrylate (TMPTA), N,N'-m-phenylene dimaleimide (HVA-2) were used as boosters for DCP-cured TPVs, were obtained from Sartomer Company, USA.

Preparation of PP/EOC TPVs - The TPV compositions employed are shown in Table 1. The experimental variables are the type and concentration of different coagents. All TPVs were mixed by a batch process in a Haake Rheomix 600 OS internal mixer, having a mixing chamber volume of 85 cm^3 with a rotor speed of 80 rpm at180°C. Immediately after mixing, passed once through a cold two-roll mill to achieve a sheet of about 2 mm thickness. The sheet was cut and pressed in a compression molding machine (Moore Press, Birmingham, UK) at 200°C, 4 min and 5 MPa pressure. The sheet was then cooled down to room temperature under pressure. Different coagents not only differ in molecular weight but they also have different relative functionality. Hence in order to compare different coagents, concentration employed should be in terms of milliequivalents.

Testing Procedure - Tensile tests were carried out according to ASTM D412-98 on dumb-bell shaped specimens using a universal tensile testing machine Hounsfield H10KS at a constant cross-head speed of 500 mm/min. Tear strength were carried out according to ASTM D-624-81 test method using un-nicked 90° angle test piece. Phase morphology of the cryo- fractured and etched samples was investigated by a JEOL JSM 5800 Digital Scanning Electron Microscope (SEM). Melt rheology of the blend components were studied in Rubber Process Analyzer (RPA 2000, USA). Each samples underwent the following test in sequence and in this order: frequency sweep (FS), strain sweep (SS) followed by relaxation period of 5 mins, frequency sweep, and strain amplitude sweep. Frequency sweep was logarithmically increased from 0.05 to 32 Hz at 6.95 % strain, which was selected to ensure that the dynamic moduli are measured in the linear viscoelastic region. For the strain sweep, amplitude ranges from 1 – 1250 % at 180°C with a constant frequency of 0.5 Hz. The sample relaxation was monitored by observing the decrease in shear rate with time.

Results and discussion

Mechanical properties

In order to understand the effectiveness of various coagents in the PP/EOC TPVs, it is necessary to understand the performance of different coagents only in the EOC compound (without PP). The reactivity and efficiency of different coagents were characterized by cure study on gum EOC vulcanizates. Figure 1 shows the rheographs of peroxide cured EOC vulcanizates containing various coagents at 20 meq concentration and compared with the control sample (without addition of any coagent). Irrespective of different coagents taken for the investigation, a considerable improvement in the maximum torque (Max S) and delta torque (Max S - Min S) values were inferred upon addition of coagent. This is mainly due to the improved crosslinking efficiency of DCP in presence of coagent. It is clear from the Figure-1 that, TAC shows the higher torque values followed by HVA-2 and TMPTA. Mechanical properties of the TPVs prepared by three different coagents with varying concentration were summarized in the Table 1. Mechanical properties are considerably improved by the dynamic vulcanization process. It is clear from the result that blend properties are sensitive to the type of coagents. Among the coagents used, HVA-2 shows the best overall balance of mechanical properties. TPVs prepared using HVA-2 as coagent, exhibit gradual increase and provide superior tensile strength, modulus, and tear strength values relative to the other coagents used. It is expected that HVA-2 can act as a reactive compatibiliser as well as crosslinking agent in this particular blend system. It has been previously reported that HVA-2 can act as a reactive compatibiliser in the NR-PP blend system. It generates a low degree of crosslinking in the NR phase and forms a block or graft copolymer in the NR-PP interface. It is clearly seen that, TMPTA shows lower delta torque value and there by exhibiting higher elongation at break. TAC shows the lowest value and HVA-2 shows the intermediate value of elongation in TPVs. It was generally accepted that a low crosslink density compound is indeed accompanied with the higher elongation at break. Since HVA-2 can act as a crosslinking agent as well as a compatibilising agent, where crosslinking decreases the elongation and compatibilisation increases the same. In this case both the effects are very sensitive in determining the final elongation at break.

Morphology

A SEM photomicrograph of the PP/EOC TPVs, in which PP phase was preferentially extracted by etching with hot xylene, is given in Figure 2. Qualitatively it shows crosslinked EOC particles are dispersed throughout the PP matrix (droplet and matrix morphology). Since EOC content is more than PP, the particle-particle association is strong to form aggregates and these aggregates can agglomerate. The crosslinked rubber aggregates are embedded in the PP macromolecules via joint shell mechanism and/or segmental interdiffusion mechanism.

Rheological properties

In the solid state, the properties of the TPVs are determined by the matrix molecular weight (which has a direct consequence on the percent crystallinity and entanglements density), extent of crosslinking, degree of dispersion, size and deformability of dispersed phase as well as morphology persist. In the melt state, changes in the morphology originating from matrix molecular weight (crystallinity) can be excluded and the influence of other factors can be studied. The rheological properties of 50/100 PP/EOC TPVs prepared by three different coagents are represented in Figures 3 to 6. Dynamic vulcanization blends show improved dynamic modulus and viscosity values (dynamic functions) than uncured blends. As expected, addition of coagent further improved the dynamic functions than the control one. Among the coagents, HVA-2 shows better dynamic functions and more nonlinear behavior followed by TAC and TMPTA. At equal formulation volume fraction, smaller particles can impart greater viscosity and more nonlinear

behavior. Here two possible effects can account: particle size reduction by improvement in interfacial tension cause rise in viscosity and these small particles have higher tendency to agglomerate or aggregate, which results in more nonlinear behavior. In other words, presence of secondary clusters increases the viscosity and enhances the viscoelastic nonlinearity.

Payne effect: For a constant frequency, with increasing the strain amplitude dynamic storage modulus decreases. In general, the decrease in dynamic functions (nonlinearity) is related to the disintegration of secondary structures. Indeed it may also relate to the bonding and debonding of dispersed phase from the matrix phase. TPVs show more progressive nonlinear behavior i.e, decrease of dynamic functions with increasing strain amplitude is observed (Figure 3). In TPVs the secondary structure corresponds to the agglomeration or aggregates of crosslinked EOC particles dispersed in PP matrix. In simple blends the nonlinearity at high strain is due to both the disintegration of entanglement network and debonding of molecules of PP anchored in EOC matrix phase.

Modulus recovery: Another important aspect in the mechanism of nonlinearity in TPVs is restoration of moduli following the large strain amplitude effects. Figure 4 shows the effect of complex modulus on the subsequent strain sweep experiment results. It is clear that only minor effects occurred in modulus values. Furthermore, the critical strain amplitude (where the nonlinearity effect occurs) is slightly moved towards lower amplitude region in the subsequent strain sweep test. It is anticipated that interfacial slippage between crosslinked EOC domains and PP matrix, cause to reduce the linear viscoelastic region.

Frequency dependence of viscoelastic behavior: Dynamic frequency sweep tests were conducted in linear viscoelastic region to further study on network formation and microstructural changes in detail. Figure 5 shows that the frequency (ω) depends of storage modulus (G') in unvulcanized and dynamically vulcanized blends. It is well established that dynamical vulcanization increase storage modulus values especially at low frequency region. As the frequency increases the curves become close to each other. HVA-2 based TPVs show higher values in the entire range of frequency studied. Low frequency improvement in G' indicates strong interaction between crosslinked EOC phase and PP matrix. Polymers are non Newtonian liquids and their viscosity decrease with increasing shear rate. Figure 6 shows the log complex viscosity ($\acute{\eta}^*$) vs log ω. It can be seen that the viscosity is highly sensitive with significant drop at higher shear rate, so the related structure are of pseudoplastic nature. Formation of agglomeration and aggregated structure of dispersed phase may be responsible for the high initial value of complex viscosity. The frequency dependence after the strain amplitude sweep was reproducible confirming that the strain sweep does not significantly deform microstructure and the deformation induced is reversible.

Conclusion

Comparative studies of the mechanical, microstructure and rheological properties were carried out in PP/EOC TPVs prepared by three different coagents. Among the various coagents taken for the investigation, most interesting properties were observed for HVA-2 containing TPVs. It is found to give better solid and melt state properties, which may be attributed to the strengthening of interfacial adhesion between blend components. HVA-2 is shown to effectively behave as a crosslinking agent and compatibilizer for the PP/EOC blend system and thereby improvement is significant.

References

1. Coran, A.Y. In: Thermoplastic Elastomers - A Comprehensive Review; Legge, N. R.; Holden, G. Eds.; Hanser Publisher: Munich, 1987.
2. Naskar, K. Rubber Chem. Technol 2007, 80, 504.
3. Henning, S. K.; Costin, R. Fundamentals of curing elastomer with peroxide and coagents. Paper presented in Spring 167 th ACS technical meeting.

4. Costin, R. Selection of coagents for use in peroxide cured elastomers. Application Bulletin 5519. Sartomer Company, USA.

Table-1 Comparitive physical properties of TPVs prepared by three different coagents

Compound Name	DC0	DC10	DC20	DC30	DA10	DA20	DA30	DM10	DM20	DM30
EOC	100	100	100	100	100	100	100	100	100	100
PP	50	50	50	50	50	50	50	50	50	50
DCP*	3.38	3.38	3.38	3.38	3.38	3.38	3.38	3.38	3.38	3.38
TAC/TMPTA/HVA-2[#]	-	10	20	30	10	20	30	10	20	30
Physical properties	DC0	DC10	DC20	DC30	DA10	DA20	DA30	DM10	DM20	DM30
Tensile strength (MPa)	7.6	9.7	9.3	8.2	10.5	10	11.2	10.6	10.9	11.4
Elongation at break (%)	258	244	180	142	300	300	277	280	254	234
100% Modulus (MPa)	6.6	7.3	7.7	7.5	7.2	7.2	7.7	7.5	7.9	8.4
Tear strength (N/mm)	65	68	72.2	63	80.5	82	64	76.3	87.2	88.1

*Peroxide concentration has been optimized in the previous work at 3.38 phr of DCP corresponds to 5 milliequivalent concentration.
[#]Coagent concentration are in milliequivalent

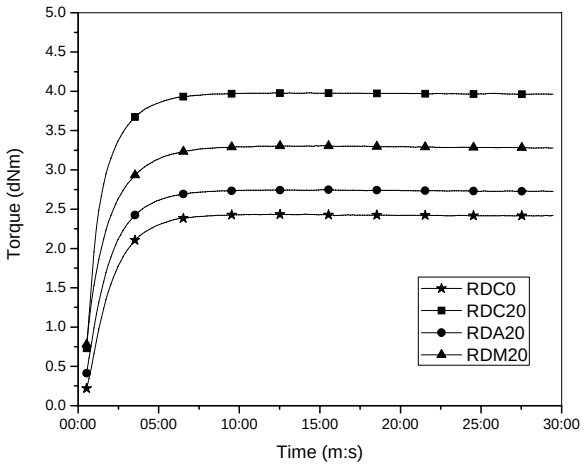

Figure -1: Rheograms of only EOC compound with 20 meq concentration of various coagents at 180°C

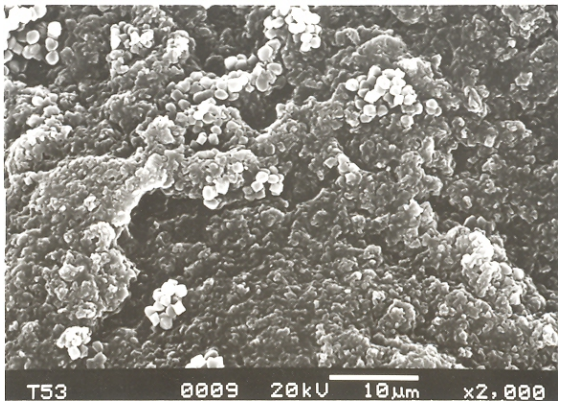

Figure -2: SEM photomicrograph of PP/EOC TPVs (PP phase is preferentially etched)

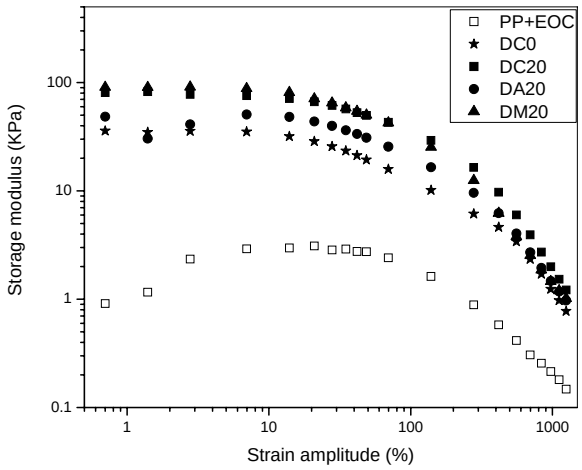

Figure -3: Dependence of G' on strain amplitude at a constant frequency of 1 Hz at 180°C

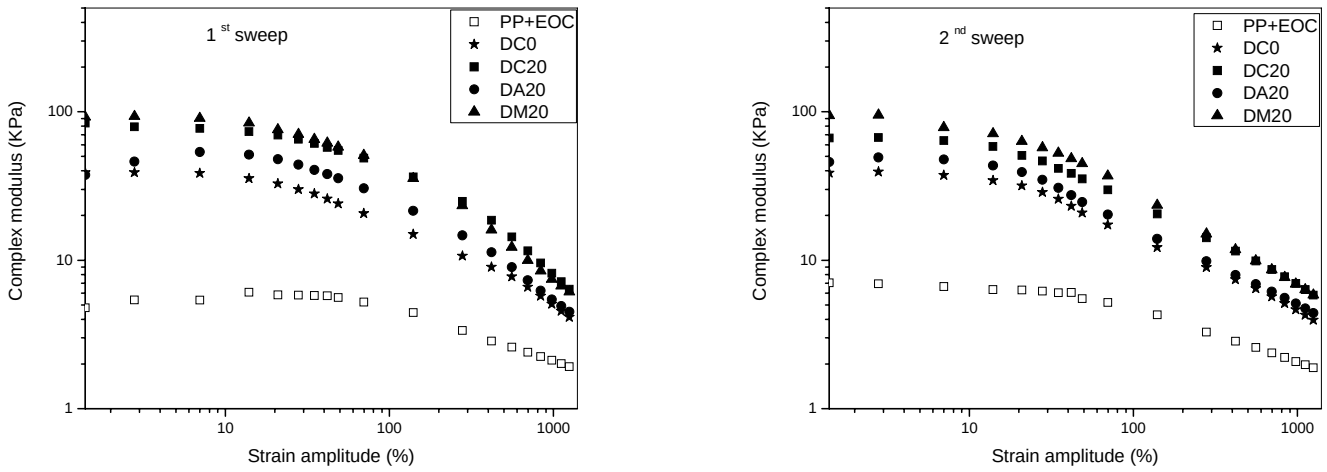

Figure -4: Complex modulus (G*) as a function of strain amplitude at a constant frequency of 1 Hz and 180°C with subsequent strain sweep (1 st seep followed by 2nd sweep after a relaxation time of 5 mins)

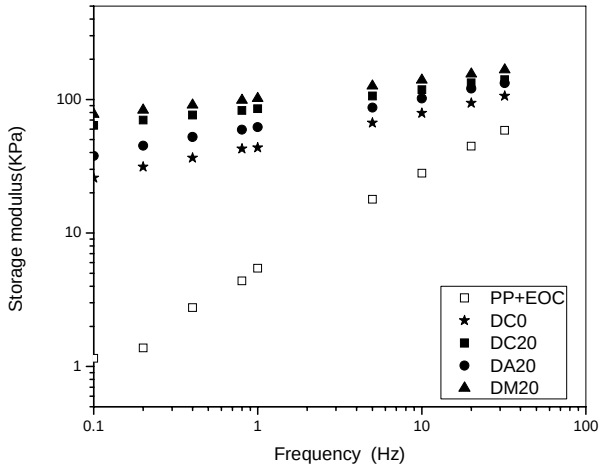

Figure -5: Storage modulus as a function of frequency at low strain amplitude and at 180°C

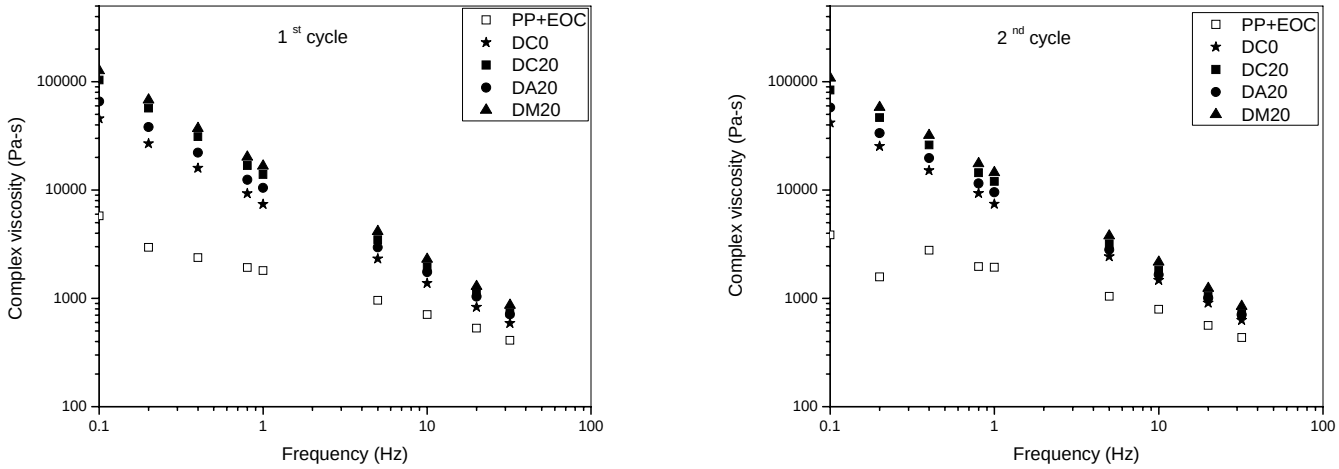

Figure -6: Dependence of complex viscosity (ή*) on frequency at a low strain amplitude and 180°C with subsequent frequency sweep (1 st sweep followed by 2nd sweep after an strain amplitude sweep and a relaxation time of 5 mins)

A comprehensive study on degradation of nano-silica filled model TPE blend systems

S. Chattopadhyay*, S. Hui and T.K. Chaki
Rubber Technology Centre
Indian Institute of Technology
Kharagpur-721302, India
Email: santanuchat71@yahoo.com, santanu@rtc.iitkgp.ernet.in

Abstract:
The effect of nano-silica on the thermal degradation behaviors of LDPE-EVA based thermoplastic elastomeric blends were monitored in nitrogen as well as in oxygen atmospheres using thermo gravimetric analyses (TGA). The pristine silica nano-particles were melt-blended with the LDPE-EVA system at 1.5, 3 and 5 wt% loadings, respectively, by varying the sequence of addition. In one of the compositions, coupling agent Bis-[3-(triethoxysilyl)propyl] tetrasulphide (Si-69) was used to improve the interaction of hydrophilic silica fillers with polymer matrices. In anaerobic condition, no significant changes were observed in terms of thermal stability of such blend systems. However, in oxygen atmosphere, the TGA plots reflected a dramatic change. A two staged degradation were observed for most of the filled samples but in some cases a three staged process were also followed. The changes in the decomposition onset (T_i) and maximum degradation temperatures (T_{max}) were correlated well with the morphology of the filled TPE systems as observed by transmission and scanning electron microscopes. The kinetic rate constants and activation energies were calculated using non-isothermal kinetic analysis. On the whole, it was observed that the thermal stability of TPE blends was a strong function of morphology which in turn was decided by the sequence of addition of ingredients during blend preparation, amount of silica nano-fillers addition and presence of coupling agent.

Introduction
Polymer characterization using the tools of thermal analysis is a useful method in analytical polymer laboratories. The study of degradation and stabilization of polymers is an extremely important area from the scientific and industrial view points. Thermo gravimetric analysis (TGA) is an excellent tool for studying the kinetics of thermal degradation. It is now widely used because of its experimental simplicity and the wealth of information obtained from a simple thermogram [1].

Low density polyethylene (LDPE) and poly (ethylene-co-vinyl acetate) (EVA) and their blends are widely used in the wire and cable industry as insulation sheath or jacket. Recently, several papers have been published dealing with the thermal analysis and thermo-oxidative degradation of different polymer, blends and polymer- nanocomposites. Early studies on the degradation of EVA [2] have been reported that the initial step in the degradation involves the formation of acetic acid and which is enhanced with increasing vinyl acetate content. The second step involves degradation of the main chains with little evidence of interaction between the ethylene and vinyl acetate units. Studies on thermal degradation behavior of EVA/LDPE blend has been studied by Ray et al [3] where pure EVA and its blends similarly show two staged decomposition and the blends exhibit better thermal stability compared to pristine polymers. The thermal degradation behavior of EVA has been studied by several researchers [4-6]. Marcilla [7] has reported that the oxidative pyrolysis of EVA involves four main decomposition steps, and each of them also involves different types of reactions. A study of the degradation of LDPE and an EVA copolymer under air atmosphere, in the presence and absence of mesoporous silicates (MCM-41),

has been carried out using thermogravimetric analysis (TGA) by Marcilla et al [8] focusing on the degradation behavior of EVA.
The thermal degradation mechanisms of poly(vinyl acetate) (PVAc) and EVA copolymers have been investigated by Rimez et al [9]. Thermal properties and flammability of EVA/LLDPE/montmorillonite nanocomposites have been studied by Chuang et al [10].
In this present investigation, an attempt has been made to study the thermal and thermo-oxidative degradation characteristics of this particular nano-silica filled blend system by thermal analysis and to correlate the thermal properties with nano- and micro-scale morphology.

Experimental

Materials
The plastic used for the present work was LDPE - Indothene MA 400 supplied by IPCL, Vadodera, India (0.918 g/cm^3 density, MFI as per ASTM D1238 @ 190^{o}C using 2.16 kg load 30 g/10min melt index). The elastomer used was EVA containing 40% vinyl acetate (EVA-40) (MFI: 3) purchased from Bayer Co., Ltd. (Leverkusen, Germany). Silicon dioxide nano-powder was procured from Aldrich Chemical Co. Ltd., USA. Bis-[3-(triethoxysilyl) propyl] tetrasulphide (Si- 69) was purchased from Degussa, Germany.

Sample Preparation
Melt blending was carried out with EVA and LDPE with various loading of silicon dioxide nano-powder (1.5, 3 and 5 wt%, respectively) in a Brabender Plasticorder (PLE-330) at 130^{0}C and 80 rpm rotor speed by varying two different sequence of additions of ingredients. The total mixing time was 10 minutes. Then they were remixed for another 2 minutes. The sheets were compression molded between two Teflon sheets for 3 minutes at 150^{0}C with a pre-heat time of 1 minute and with a load of 5 Tons in an electrically heated hydraulic press to obtain films of 0.03 ~ 0.04 cm thickness. The moldings were cooled under compression to maintain the overall dimensional stability. The details of the samples and their appropriate designations are given in Table-1.

Characterization
Thermogravimetric measurements of the composites were conducted using TGA Q50 of TA Instruments-Waters LLC, USA operated in the dynamic mode. The conversion values 5,8,11,4,17 and 20% were used for computing the non-isothermal kinetic parameters using the Flynn-Wall-Ozawa method.
For the transmission electron microscopic (TEM) observations, a high resolution transmission electron microscope (HRTEM) (JEOL JEM 2100, Japan) operated was used at an accelerating voltage of 200 kV.
The bulk morphology of the blends was observed with field emission scanning electron microscope (FESEM) (Leo 1530, Carl Zeiss, Oberkochen, Germany).

Results and discussion

Effect of pristine nano silica filler on thermal degradation characteristics of EVA/LDPE blends under N_2 atmosphere
All thermograms showed two-staged decomposition (not shown here) with well defined initial and final degradation temperatures. No drastic improvement in thermal stability was observed for the filled systems. A modest improvement in thermal stability was found only in case of ELS6/4/3-2. Thus in inert atmosphere, silica particles did not have a major role to influence the thermal stability of the blend systems.

Effect of pristine nano silica filler on oxidative degradation characteristics of EVA/LDPE blends

The control blend (EL6/4) exhibited greater thermal stability than the pure EVA and LDPE [Figure 1(a)]. Also, EVA was also found to be thermally more stable than LDPE. Thus in presence of EVA, LDPE was stabilized. In all silica filled blends there were two distinct and well separated steps in the thermogravimetric curves (TG) (corresponding weight loss peaks in derivative thermgravimetric, DTG) curves as represented in Figure 1 (b) and (c). The first step (309-315^{0}C) for all samples (unfilled and filled) was possibly due to de-acetylation of vinyl acetate group of EVA with the elimination of acetic acid. As a result, double bonds were formed [10] in the main chain. The second step (413-418^{0}C) might be assigned to the further degradation of polyacetylene-ethylene chains formed in the first step accompanied with the degradation of LDPE [10].

As compared to inert atmosphere, it was observed that the initial stages of degradation for all samples were accelerated in the presence of oxygen [Fig. 2(a)]. Thus the rate of reaction might be controlled by O_2 diffusion in the polymeric matrix. There was also an initial gain in weight prior to deacetylation in the presence of oxygen. This suggested a rapid initial oxidation of the blends. Due to the presence of SiO_2 particles, the onsets of degradation of filled blends were shifted towards higher temperatures as compared to the unfilled one. Therefore, the filled systems were thermally more stable than the pure blend. But interestingly, at very high temperature (~ above 425^{0}C) the presence of nano silica accelerated degradation of filled blends. This might be due to the fact that at these temperatures silica acted as an acid catalyst. The outcomes from TGA are represented in Table 2. As compared to samples prepared following sequence-2, ELS6/4/3-1 exhibited higher thermal stability at lower temperature ranges. This indicated the occurrence of intermixing of LDPE and EVA in ELS6/4/3-1. In TEM observations also silica particles were found to be dispersed in both phases as well as in the interface for this system. Si69 increased the compatibility between two phases (in ELS6/4/3-2-Si69) and made silica well dispersed in the polymeric matrix. Hence, ELS6/4/3-1 and ELS6/4/3-2-Si69 exhibited greater thermal stability than the rest of the samples. The degradation behavior was well correlated with the morphology analyzed by TEM and FESEM. The details of the analysis are not given in this brief article. It will be mentioned during the presentation.

The iso-conversional integral method named Flynn-Wall-Ozawa method suggested independently by Ozawa [11] and Flynn and Wall [12] uses Doyle's approximation [13] of the temperature integral. From Eq. (1) and using Doyle's approximation, the result of the integration after taking logarithms is:

$$\log \beta = \log (AE/g(\alpha)R) - 2.315 - 0.457\, E/RT \quad \text{.....(1)}$$

where β is the heating rate, A is the pre-exponential factor, E is the activation energy, α is the degree of conversion and T is the temperature. Thus, for α = constant, the plot of log β versus 1000/T obtained at several heating rates should yield a straight line whose slope can be used to evaluate the activation energy.

All the filled samples showed higher activation energy of degradation than the control sample. This implied that the thermal stability of the silica filled nanocomposites was higher than the neat control blend. From plots (not shown in text) it can be observed that the best fitted straight lines (with at least 90% correlation) were nearly parallel to each other and thus confirmed the applicability of this method with in the conversion range studied. Interestingly, mean activation energy of ELS6/4/3-2 was higher than that of ELS6/4/3-1. The kinetic analysis was performed by both dynamic and static methods and the results were well correlated. However, the details of kinetic analysis will be discussed during presentation.

Table 1. Sample designation

Sample ID*	LDPE (wt %)	EVA (wt%)	SiO_2 (wt %)	Sequence of addition
EL 6/4	40	60	0	-
ELS 6/4/1.5	40	60	1.5	2
ELS 6/4/3-1	40	60	3	1
ELS 6/4/3-2	40	60	3	2
ELS 6/4/3-2-Si69	40	60	3 +10% Si 69 w.r.t. silica	2
ELS 6/4/5	40	60	5	2

*E :- EVA, L:- LDPE, S:- Silica

Table 2. Percentage of degradation for various blend systems at a heating rate (q) of 10^0C/min.

Conversion (%)	EL6/4 (^{o}C)	ELS6/4/1.5 (^{o}C)	ELS6/4/3-1 (^{o}C)	ELS6/4/3-2 (^{o}C)	ELS6/4/3-2-Si69 (^{o}C)	ELS6/4/5 (^{o}C)
5	228	230	258	247	278	244
8	235	241	278	271	289	270
11	242	255	290	289	296	288
14	249	271	298	301	300	297
17	256	284	305	308	302	305
20	265	292	309	313	308	310

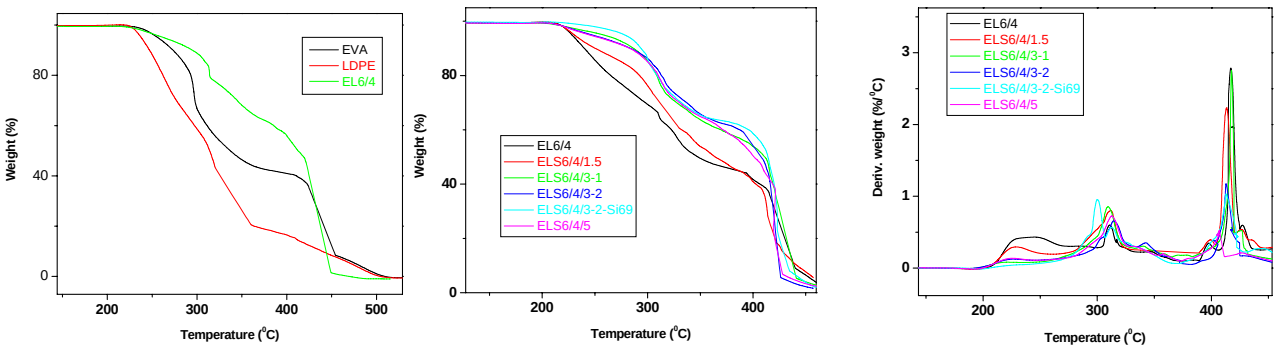

(a) **(b)** **(c)**

Figure 1. (a) TG curve of pure EVA, pure LDPE and EL6/4 in O_2 atmosphere at 10^{o}C per minute.
(b) TG curve of silica filled EVA/LDPE blends at different loadings in O_2 atmosphere at 5^{o}C per minute.
(c) DTG curve of silica filled EVA/LDPE blends at different loadings in O_2 atmosphere at 5^{o}C per minute.

Conclusions

In anaerobic condition, no significant changes were observed in terms of thermal stability of such blend systems. However, in oxygen atmosphere, the TGA plots reflected a dramatic change. The initial part of degradation was probably controlled by oxygen diffusion, decomposition of LDPE and acetic acid elimination from EVA. The next stage of degradation was found to be a strong function of mutual interactions between EVA and nano-silica. Si-69 provided a significant thermal stabilization. On the whole, it was observed that the thermal stability of TPE blends was a strong function of morphology which in turn was decided by the sequence of addition of ingredients during blend preparation, amount of silica nano-fillers addition and presence of coupling agent. The mutual interaction of the polymer matrices with nano-silica fillers strongly influenced the kinetic parameters.

Acknowledgements

The authors are grateful to the Department of Science and Technology (DST), New Delhi for funding the project (SR/FTP/ETA-15/2005 Dated 02.11.2005). One of the authors is highly grateful to CSIR, New Delhi for funding her fellowship to carry out this work. Authors are grateful to Mr. Sayed Mushtaq, RTC, IIT Kharagpur for helping with RPA measurements.

References

1. Wang XL, Yang KK, Wang YZ, Wu B, Liu Y, Yang B. Polym Degrad Stab 2003; 81:415-421.
2. McNeill, IC, Jamieson, A, Toshand, DJ, McClune, JJ. Eur. Polym. J. 1976; 12: 305.
3. Ray I, Roy S, Chaki TK, Khastgir D. Journal of Elastomers and Plastics 1994; 26(2), 168-182.
4. Kaczaj J, Trickey, R. Anal. Chem. 1969; 41(11): 1511.
5. Sultan BA, Sorvik, E. J. Appl. Polym. Sci. 1991; 43: 1737-1761.
6. Wang J, Tu H. Proceedings of the Second Beijing International Symposium/Exhibition on Flame Retardants, Beijing Institute of Technology Press, Beijing, 1993, p.272.
7. Marcilla A, Gómez-Siurana A, Menargues S. Thermochimica Acta 2005; 438: 155–163.
8. Marcilla A, Gómez -Siurana A, Menargues S, Ruiz-Femenia R, García-Quesada. JC . J. Anal. Appl. Pyrolysis 2006; 76: 138-143.
9. Rimez B, Rahier H, Van Assche G, Artoos T, Biesemans M, Van Mele B. Polymer Degradation and Stability 2008; 93: 800-810.
10. Chuang TH, Guo W, Cheng KC, Chen SW, Wang HT, Yen YY. Journal of Polymer Research 2004; 11:169-174.
11. Ozawa T. Bull Chem Soc Jpn 1965; 38(11): 1881-1886.
12. Flynn JH, Wall LA. Polym Lett 1966; 4(5): 323-328.
13. Doyle CD. J Appl Polym Sci 1962; 6(24):639-642.

.

Mechanical properties of natural rubber / poly butadiene rubber blends prepared using fatty acid incorporated natural rubber

R. Alex*, T.Cherian, S.Joseph, and K.T Thomas
Rubber Research Institute of India, Kottayam -9, Kerala
Email: rosammaalex2000@yahoo.com

ABSTRACT

Natural rubber(NR) can be sensitized for quick coagulation by addition of suitable fatty acid salts as stabilizers. A portion of the fatty acids formed remains on rubber after coagulation Fatty acids play a major role on cure characteristics and mechanical properties of recovered rubber. Use of this rubber in blends with polybutadiene rubber (BR) can alleviate some of the problems of rubber blends like cure mismatch and unequal filler distribution. In this paper an investigation on the preparation, cure characteristics and mechanical properties of NR/BR blends prepared using fatty acid incorporated NR is carried out.

Natural rubber latex is treated with a required quantity of fatty acid soap and then coagulated by addition of suitable acids. The coagulum is washed well to remove acids and then dried at 70 ^{0} C in an air oven to get dry rubber. Rubber compounds based on pure NR, 80/20 and 60/40 NR/BR blends are prepared using conventional mixing methods. The compounds are vulcanized and tested as per standard test methods. The fatty acid soaps added to latex get adsorbed or rubber particles and get converted to the corresponding fatty acids by reaction with acids during the process of coagulation. Due to presence of fatty acids, the pure and NR/BR blends show better cure characteristics as revealed from a higher level of vulcanization. Due to the higher level of crosslinking and better filler dispersion, pure and blend vulcanizates show a higher modulus, tensile strength, and hardness along with comparable dynamic properties like heat build-up and compression set in relation to conventional rubber vulcanizates. The presence of fatty acids also helps in a better dispersion of filler in pure rubbers as revealed from scanning electron microscopy (SEM) studies. A noticeably higher ageing resistance is also observed for NR/BR blends prepared by the new process due to the presence of better interaction of filler with rubber.

INTRODUCTION

Blends based on natural rubber and polybutadiene rubber are extensively used in tire sector due to the enhanced mechanical properties like low heat build-up, and abrasion resistance realized in the vulcanizates. The basic problems with such rubber blends are the inherent incompatibility, unequal filler distribution and uneven crossslinking. In general elaostomer blends are microheterogenious, the continuous phase being either the polymer in highest concentration or polymer of lowest viscosity. Filler distribution is influenced by the point of addition of filler, mixing method, surface polarity of filler and other factors like unsaturatiion , viscosity and polarity of blend components. The incorporation of 50/50 elastomer preblends indicated that black affinity decreased in the order, SBR, CR, NBR, NR, EPDM, IIR.[1,2] Curative distribution is influenced by the level of unsaturation , viscosity and polarity of blend constituents. The type and nature of colloidal stabilizers retained on rubber during the coagulation process also affect the cure characteristics and filler dispersion.

Both natural and synthetic rubber latices, (depending on the polymerization technique) have fatty acid salts as stabilizers. In the case of fresh NR latex the colloidal stability is afforded by protein anions and to a small extent by fatty acid anions. In NR latex , the sensitivity to coagulation by acids is controlled by the type of colloidal stabilizers and the fatty acid anions have more sensitivity to coagulation by acids. [3] By using suitable fatty acid soaps the coagulation characteristics and non rubber constituents retained in rubber can be adjusted. By this process the cure characteristics, along with filler dispersion can be controlled so as to have

enhancement in mechanical properties. There are no systematic reports on use of in situ formation of fatty acids that can affect cure characteristics, filler dispersion and hence mechanical properties of rubber blends.

In this paper an investigation on the preparation, cure characteristics and mechanical properties of NR/BR blends prepared using fatty acid incorporated NR is carried out.

EXPERIMENTAL

Fresh Natural rubber (NR) latex used in this study was obtained from Rubber Research Institute of India. Poly butadiene rubber (CISAMER) was obtained from Indian Petrochemicals Corporation Ltd, Vadodara , Other ingredients used were rubber grade chemicals .

Preparation of rubber by fatty acid sensitized coagulation of NR latex

NR latex was mixed with the quantity of fatty acid soap required for sensitization to quick coagulation as reported earlier [4]. The latex was then diluted to a dry rubber content of 20% and coagulated by addition of 10% acetic acid. The coagulum was washed free of acid and dried at 70ºC in a laboratory oven. The control NR was prepared as per the conventional method of sheet preparation. .The NR prepared by the two methods were blended with BR in 80/20 and 60/40 proportions by conventional mixing method as per formulation in Table 1.

Cure behaviour, mechanical properties and SEM evaluation

The vulcanization characteristics were determined using moving die rheometer (RheoTech MD) Test samples for determination of mechanical properties were vulcanized to optimum cure time in a hydraulic press at 150 ^{0} C. Filler dispersion in rubber was assessed using a JOEL model scanning electron microscope. Tensile fracture and abraded surfaces of vulcanizates were coated with gold to conduct SEM study

SEM was carried out using a scanning electron microscope model using sputter coated samples. Analysis was conducted on fractured surfaces and abraded surfaces.

The mechanical properties were determined from relevant ASTM standards.The ageing tests were carried out as per ASTM method after ageing the samples at 100 ^{0} C /3days.

RESULTS AND DISCUSSION

1. Effect of fatty acid soaps on coagulation of latex

Fatty acid sensitized fresh NR latex coagulated immediately on addition of acids. On addition of fatty acid soaps to latex they cause displacement of proteins and gets strongly absorbed on rubber particles. In this way the protein stabilized latex gets transformed into a soap stabilized system. On addition of acids to soap treated latex the adsorbed soap anions react with acid to form un-dissociated fatty acid, and deprive the latex particles of stabilizers. As a consequence, latex coagulates immediately. [3,5]

2. Vulcanization characteristics

The cure characteristics of the blend mixes along with pure NR mixes are given in Figure 1.The rubber recovered from soap-sensitized coagulation showed better overall cure characteristics as compared to conventional mix. It had a higher level of cross slinking and a faster onset of cure which is attributed to the fatty acids retained on rubber. There was enhancement of level of vulcanization in 80/20 and 60 /40 NR/BR blends.

As an activator of vulcanization ZnO requires sufficient amount of fatty acids which converte it into rubber soluble form . Though NR contains a certain amount of these acids it is usually insufficient. Therefore their contents are adjusted to the required level by addition of commercial stearic acid which can be replaced by lauric acid that is more soluble in rubber[6] Hence it is inferred that when fatty acid is added as soap to latex it disperses uniformly in latex

due to adsorption on rubber particles and convert into fatty acid during coagulation. This uniformly dispersed fatty acids help in activating cure characteristics of rubber.

3. **Mechanical properties** .

Soap coagulated rubber recorded a higher modulus, tensile strength, and hardness. Heat - build up and compression set were comparable to that of control (Table 2) .The NR/BR 80/20 and 60/40 blends also showed a higher modulus tear strength and hardness in comparison with blends prepared using conventionally obtained NR.

Improvement in mechanical properties is attributed to the formation of higher level of crosslinks and other interactions involving filler and rubber. Oxygen containing groups present in rubber have a considerable effect on vulcanization kinetics and have a role in interaction with rubbers. It is expected that there is better polymer filler interaction involving uniformly dispersed fatty acid soaps though the actual mechanism is not clear from this study. There are reports that use of higher dosage of stearic acid in tread formulation enhanced in abrasion resistance. In this study it is inferred that fatty acids soaps are formed during vulcanization from added surfactant and it acts as lubricant, reducing the abrasion loss [7]

SEM photographs of tensile fracture and abraded surfaces of NR vulcanizates are shown in Figures 2 and 3. The tensile fracture surface of NR prepared from soap sensitized coagulation has a more uniform surface and less matrix removal, as compared to conventional NR fillerwhich shows enhanced filler dispersion in presence of in situ formed fatty acids. The abraded surface of the sample from soap coagulation shows fine ridges while the conventional mix has bigger ridges and foldings. It is known that wear occurs as a result of two processes; local mechanical rupture (tearing) and general decomposition of the molecular network to a low molecular weight material (smearing). [8, 9] It is known that molecular rupture under frictional forces followed by stabilization of the newly formed polymeric radicles by reaction with oxygen or with other polymer molecules or with other macroradicals take place during the abrasion process. In rubber obtained by soap sensitized coagulation mainly due to higher levels of crosslinking there is lower crack growth and removal of the matrix The ageing characteristics are shown in Table 3. The blends prepared from in situ formed fatty acid has a higher retention of tensile strength and less variation in modulus and elongation at break as compared to blends prepared from conventional sheet rubber. The enhancement is attributed to higher level of vulcanization and better filer dispersion.

CONCLUSION

The carboxylic acid soaps added to latex get adsorbed on rubber particles and are retained in rubber after coagulation. The fatty acids retained on rubber activate the vulcanization and improve the mechanical and ageing characteristics of recovered rubber. NR/BR blends prepared from fatty acid incorporated rubber have higher level of vulcanization, and better mechanical and ageing properties as compared to blends prepared from conventional rubber.

REFERENCES

1. Corish PJ, Powell B.D.W. Rubber Chem. Technol. 1974:47:481-509
2. Gallen G.E, Hess W.M., Scott, C.E, Rubber Chem. Technol 1971:44: 814-837
3. Blackley, D.C. (1997). Polymer Latices, Science and Technology, Vol. 2. Types of lattices , Chapter 9.
4. Alex, R., Premalatha, C.K., Nair, R.B. and Kuriakose, B. (2003). Journal of Rubber Research, 6(**4**): 221-230.
5. Cockbain, E.G. (1952). Transactions, IRI, **28**: 297-302.
6. Franta, I. (1989). Elastomers and Rubber compounding materials manufacture properties and applications. Elsiever Publications, Chapter6.

7. Gelling, I.R. In: proceedings of the Workshop on the Development of natural rubber based truck tyre retreading compounds,Cane, M.E., Rashid, S.Z.M., Eds., Malaysian Rubber Research and Development Board, Kuala Lumpur, Malaysia, 1992, p. 49.
8. Gent A.N., Pulford C .T.R. J.Appl. Polym. Sci.:2003:28(3):943-960.
9. Bhowmick A.K., Sanjay Basu, De S.K. . J Material Sci. 1981:16(6): 1654-1660

Table 1 Formulation of NR/ BR mixes

Ingredients	**parts**		
Natural Rubber/BR	100/0	80/20	60/40
ZnO	5	5	5
Stearic acid	1	1.25	1.5
Antioxidant TDQ [1]	1	1	1
HAF black	40	40	40
Aromatic oil	2	2	2
CBS [2]	0.75	0.75	0.75
Sulphur	2.5	2.5	2.5

Table 2. Mechanical properties of carbon black filled pure and blend vulcanizates

Parameter	**NR**		**NR/BR 60/40**		**NR/BR 60/40**	
	Sample	**Control**	**Sample**	**Control**	**Sample**	**Control**
Modulus 100%, MPa	2.53	1.66	2.16	1.78	2.71	2.63
Modulus 200%, MPa	5.11	3.11	4.2	3.34	5.38	5.15
Modulus 300%, MPa	8.44	5.05	6.78	5.5	8.55	8.28
Tensile strength, MPa	24.27.	24.40	19.98	21.1	11.72	11.12
Elongation at break, %	670	690	690	700	400	390
Tear strength, kN/m	58	82	66	51	39	30
Hardness, Shore A	67	66	66	65	68	67
Heat build-up, ΔT,ºC	21	20	19	20	20	20
Din abrasion loss, cc	88	100	79	80	74	75

Table 3 Ageing resistance of carbon black filled pure and blend vulcanizates (aged at 100^0 C/3d).

Parameter	**NR**		**NR/BR 60/40**		**NR/BR 60/40**	
	Sample	**Control**	**Sample**	**Control**	**Sample**	**Control**
Modulus 100%, MPa	3.64	3.25	2.71	3.36	3.55	4.05
Modulus 200%, MPa	7.98	7.08	5.57	-	-	-
Tensile strength, MPa	8.82	8.87	6.78	5.47	6.82	5.69
Elongation at break, %	215	240	230	150	180	140
Percent change of modulus 100%,	43.87	95.78	25.46	88.76	30.99	53.99
Percent retention of tensile strength	36.34	36.35	33.93	25.92	58.19	51.16

Preparation and Characterization of ethylene co-vinyl acetate based drug delivery system for cardiovascular applications

V. D. Anumon*, Roy Joseph and C.V. Muraleedharan[#]

Biomedical Technology Wing, Sree Chitra Tirunal Institute for Medical Sciences and Technology, Thiruvananthapuram, Kerala – 695012, India, Contact (Off.) 0471-2520259

Email: muralicv@sctimst.ac.in

Abstract

Major complications of cardiovascular lesions are often accompanied by inflammatory reactions and smooth muscle cell proliferation. Curcumin has been shown to possess anti-inflammatory and anti-proliferative properties. As a solution to above cardiovascular problems, sustained drug delivery system releasing curcumin from ethylene-co-vinyl acetate (EVA) matrices is proposed. Various grades of EVA having 40%, 28%, 18% and 12% vinyl acetate content were evaluated for the selection of a suitable grade. The EVA grades were characterized by Fourier Transform Infrared (FT-IR) Spectroscopy, dynamic mechanical analysis (DMA), testing solubility in organic solvents and determining mechanical properties. Curcumin is incorporated into the matrices by dissolving both matrix and curcumin separately in solvents, mixing together and later evaporating the solvent from the system. Curcumin loaded systems were characterized by FT-IR, contact angle measurements, water absorption, mechanical testing and checking the drug release profile from the matrix. FT-IR data confirms that there was no chemical reaction between EVA and the drug. Increased drug content in the matrices results significant increase in tensile strength and modulus where as fracture strain records substantial decrease. The results of contact angle indicated that loading curcumin in EVA does not alter surface properties of the matrix significantly. DMA revealed that addition of curcumin does not alter glass transition temperature either. It also shows that when the vinyl acetate content increases the storage modulus decreases. Water absorption studies show an increase in water uptake by matrices with increase in drug loading. From the results obtained EVA with 40% vinyl acetate content was found to be the most suitable system as a matrix. The selection was based on the low modulus, high elongation, solubility in the organic solvents and film forming properties. Drug elution profiles up to a period 15 days were monitored. From the results it is expected that curcumin loaded EVA-40 system would be suitable for drug release applications in cardiovascular system.

1. Introduction

Cardiovascular disease (CVD) is not only the biggest cause of death worldwide, but also responsible for a significant proportion of health complications requiring long-term management. According to World Health Organization (WHO) estimates, in 2003, 16.7 million people around the globe die of CVD each year [1]. This is over 29% of all deaths globally. In India in the past five decades, rates of coronary disease among urban populations have risen from 4 % to 11% [2]. In 1998 the annual death rate for India was 840 per 100,000 populations. Cardiovascular diseases contribute to 27% of these deaths and its crude mortality rate was 227 per 100,000 [3]. The WHO estimates that 60% of the world's cardiac patients will be Indian by 2010 [2].

Literature reveals that major complications of cardiovascular lesions are often accompanied by inflammatory reactions and smooth muscle cell proliferation [4]. Curcumin (diferuloyl methane) possesses a wide range of pharmacological activities including low intrinsic toxicity, anti-thrombus, anti-oxidation and antiproliferation properties [5, 6] and may be suitable for treating above complications.

Sustained release of the above drugs to the affected area may be possible by loading these drugs into suitable matrices. Ethylene vinyl acetate (EVA) copolymer, a heat processable, flexible and stable material [7] is commercially available with vinyl acetate (VAc) content varying from 3 to 50%. The properties of EVA vary with VAc content. Vinyl acetate content up to 10% is more transparent, flexible and tougher than LDPE. Between 15 and 30% VAc content copolymers are soft and flexible. Compounds with 30–40% VAc are soft, elastic and their strength and adhesion properties are desirable for coatings and adhesives [8]. Between 40 and 50% VAc content in EVA produce rubber like properties [8]. In this study curcumin is incorporated in EVA copolymers by casting method and sustained release of curcumin is evaluated.

2. Experimental

2.1. Materials

Polymer matrices used for this study are: (a) EVA grades of vinyl acetate content 12% (NOCIL, India), 18% (Aldrich, USA), 28% (NOCIL, India) & 40% (Aldrich, USA). Curcumin (trade-named Biocurcumax) was obtained from M/s Arjuna natural extracts Ltd., Aluva, Kerala. Solvents used in the study were of 99.5% purity and were obtained from s.d. fine chemicals, Mumbai.

2.2. Differential scanning calorimetry

DSC analysis of curcumin was done based on the ASTM E 1356-03 standard using DSC 2920 by TA Instruments Inc., USA. The test was done in nitrogen atmosphere (99.99% N_2 and 1 ppm moisture, 1 ppm O_2) using an empty aluminum pan as the reference material. The scan temperature ranged from -50°C to 200°C at a heating rate of 10°C/min.

2.3. FT-IR analysis

FT-IR spectra of the curcumin were recorded on a Thermo Nicolet 5700 spectrometer with a diffused reflectance sample holder (Thermo Scientific, Germany).

2.4. Dynamic Mechanical Analysis

Dynamic Mechanical Analysis (DMA) was performed using a Tritec 2000B DMA (Triton Technology Limited, UK). Storage modulus and damping characteristics of EVA grades and curcumin loaded matrices were determined as a function of temperature. Temperature scan was done from (-) 150°C to (+) 100°C at a frequency of 1 Hz. The heating rate used was of 1°C/min.

2.5. Tensile properties

The tensile properties of EVA grades and curcumin loaded EVA were measured by using an Instron (model 3345) Universal Testing Machine equipped with a 100N load cell. Dumbbell shaped test samples were cut from cast films. The samples were conditioned at 23±1°C and at 50% relative humidity, and the test was performed at a crosshead speed of 100 mm/minute.

2.6. Solubility test

About 0.1 gm of polymer was taken in a 50ml beaker and 10ml solvent was added to it. This was kept on a hot plate stirrer (Schott Instrument, Germany) and slightly heated along with continuous stirring to dissolve the polymer.

2.7. Fabrication of curcumin eluting polymer films and its structure

Curcumin loading in EVA grades was achieved by preparing solutions of polymer and curcumin and cast on glass plates. Cast films were washed with de-ionized water and air-dried. FT-IR spectra of the curcumin loaded EVA grades were recorded on a Thermo Nicolet 5700 spectrometer (Thermo Scientific, Germany).

2.8. Contact angle measurement

Contact angle of the films are measured at room temperature (~23^{o}C) using the sessile drop method by a video based contact angle measuring device (Data Physics OCA 15 plus, Germany) and imaging software (SCA 20). Five independent measurements were performed on different region of the sample surface.

2.9. Curcumin release profile

Samples of 1 cm^2 surface area were cut from the curcumin loaded polymer films and suspended in 5ml phosphate buffered saline (PBS) at 37^{o}C and placed in a shaking water bath (Julabo, SW22, Germany) at 60rpm. At definite time intervals whole quantity of PBS was withdrawn and fresh PBS was added. Elution kinetics was monitored using UV spectroscopy at a wavelength of 420nm for a period of 15 days.

3. Results and discussion

3.1. Physico-chemical characterization of Curcumin, EVA grades and Curcumin loaded EVA

Solubility of EVA grades tends to increase with increase in vinyl acetate content in the polymer. EVA-40 was found to be soluble in a number of organic solvents such as tetrahydrofuran, toluene, dichloromethane, cyclohexane, etc. FTIR spectra of EVA, Curcumin and Curcumin-loaded EVA matrices are shown in the Figure 1. Spectra of EVA shows characteristic absorption peaks at 1735.9 cm^{-1} due to the stretching vibrations of C = O. A peak in the region 2872 and 2956 cm^{-1} corresponds to symmetric and asymmetric stretching vibration of C-H bond. A peak was observed in the region 1143cm-1 corresponding to C-O-C stretch. The spectrum of Curcumin shows characteristic aromatic absorption peaks in the range 1600.1 to 1504.9 cm^{-1}. A broad peak in the region from 3223.6 to 3508.6 cm^{-1} indicates the presence of OH. A feeble peak was observed at 1624.8cm^{-1} corresponding to C=O, C-O-C peak was obtained at 1272.7 cm^{-1}, benzoate trans-CH in CH=CH obtained at 959.2 cm^{-1}, cis CH in aromatic at 713 cm^{-1}. The spectra of polymer matrix incorporated with Curcumin (10wt%) does not exhibit any shift in peaks with respect to the characteristic peaks discussed above. From these results it is clear that curcumin incorporated in the EVA matrix does not undergo any reaction or complexation with the matrix.

The storage modulus and tan delta of EVA grades and curcumin loaded EVA are given as a function of temperature in figure 2. It may be seen that the two grades of EVA, i.e., EVA 12 and EVA 18 have higher modulus compared to EVA 28 and EVA 40. All the EVA grades show glass transition in the range -15°C to -19°C. EVA 40 shows lower modulus because it has maximum vinyl acetate content which increases the flexibility of the polymer and hence increased the damping. Incorporation of Curcumin on to EVA matrices does not alter the characteristic glass transition temperature of the matrices. However, substantial increase in storage modulus is evident.

Mechanical properties of EVA grades are given in Table 1. Depending upon the vinyl acetate content and source of EVA grades properties tends to vary. Effect of addition of curcumin in EVA-40

is shown in table 2. Curcumin addition substantially increased the tensile strength and modulus of the resultant system. A considerable decrease in the fracture strain is observed with curcumin loading. Results indicate that curcumin acts as a reinforcing agent in EVA matrix. Effect of tensile strength on short term ageing of EVA and curcumin loaded EVA in PBS is shown in figure 3. The system tends to be stable during ageing except for that containing 10wt% curcumin. Contact angle data obtained for EVA and curcumin loaded EVA shows no significant changes in contact angle data with curcumin loading (figure 4). Matrices exhibited increase in water uptake with higher curcumin loadings. Water uptake behavior is shown in figure 5 with respect to curcumin content in the EVA matrix. Increases in curcumin content increased water uptake by the polymer matrix.

3.2. Elution profile of curcumin

Cumulative release of curcumin from EVA40 is shown in figure 6. Different concentrations of curcumin were loaded in the matrix and release was monitored upto 15days. The quantity of curcumin released is a function of curcumin loaded in the matrix.

Conclusion

EVA copolymer is found to be a suitable system for the sustained release of curcumin. Curcumin released from the matrix depended on the quantity of curcumin loaded in it.

References

1. International Cardiovascular Disease Statistics, American Heart Association, 2007.
2. Express Healthcare Management, Indian Express Newspapers Ltd., India, 2001.
3. Gupta R, Misra A, Pais P, Rastogi P, Gupta VP. International Journal of Cardiology 2006; 108 (3): 291-300.
4. Boehm M and Nabel EG. Progress in Cell Cycle Research; 2003; 5; 19-30.
5. Pan CJ, Tang JJ, Shao ZY, Wang J and Huang N. Colloids and Surfaces B: Biointerfaces 2007; 59 (1):105-111.
6. Pan CJ, Tang JJ, Weng YJ, Wang J, Huang N. Journal of Controlled Release 2006; 116(1): 42-49.
7. Guo Q, Guo S, Wang Z. Journal of Controlled Release 2007:118(3):318-324.
8. Tambe S, Singh SK, Patri M, Kumar D. Progress in Organic Coatings 2008;62 (4):382-386.

Table 1. Mechanical Properties of EVA grades

Polymer grade	Tensile strength (MPa)	Elongation at break (%)	Modulus (MPa)
EVA -12	11.97 ± 0.99	2790 ± 207	5.28 ± 0.61
EVA -18	8.44 ± 0.54	1183 ± 92	19.97 ± 2.19
EVA -28	13.50 ± 1.19	1723 ±129	5.00 ± 1.37
EVA -40	8.81 ± 0.20	2610 ± 97	0.56 ± 0.05

Table 2. Effect of curcumin content on the mechanical properties of EVA-40

Curcumin content, (wt %)	Tensile strength (MPa)	Elongation at break (%)	Modulus (MPa)
0	06.73 ± 0.45	1450 ± 567	01.54 ± 0.32
1	11.17 ± 1.58	1130 ± 656	02.50 ± 0.33
2	12.56 ± 3.06	1429 ± 523	03.14 ± 0.64
5	12.58 ± 0.92	1094 ± 544	10.02 ± 1.79
10	15.09 ± 1.59	676 ± 360	26.11 ± 10.87

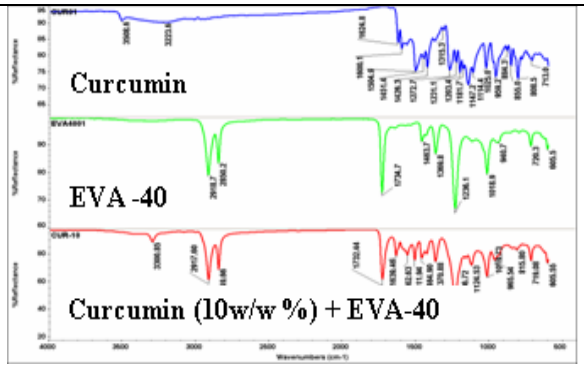

Figure 1. FTIR spectrum of Curcumin, EVA & Curcumin loaded (10wt %) EVA40

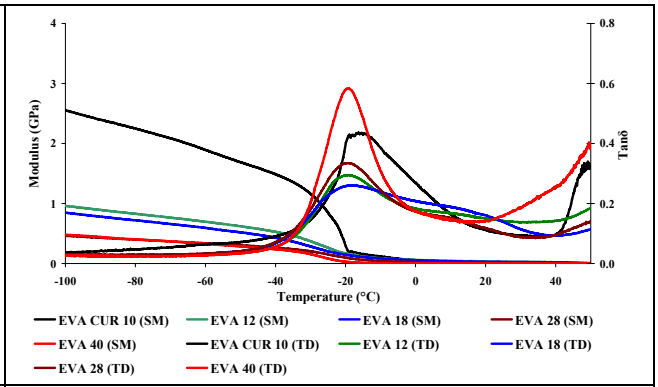

Figure 2. DMA traces of EVA grades and curcumin loaded (10%) EVA

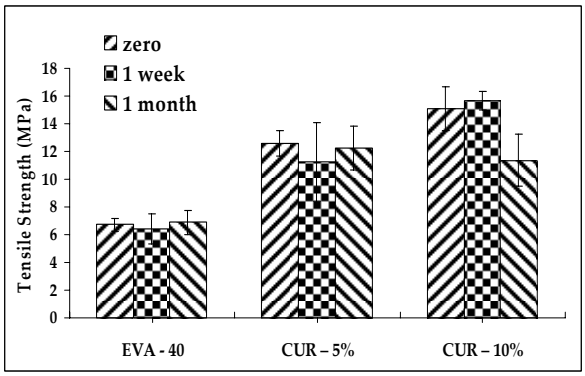

Figure 3. Tensile Properties of Curcumin-loaded EVA matrices

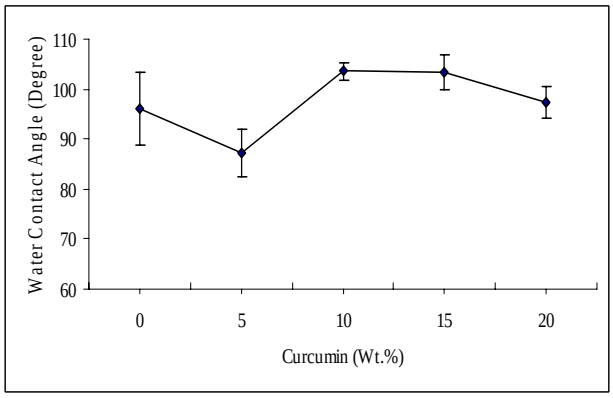

Figure 4. Contact Angle measurements of Curcumin - loaded EVA matrices

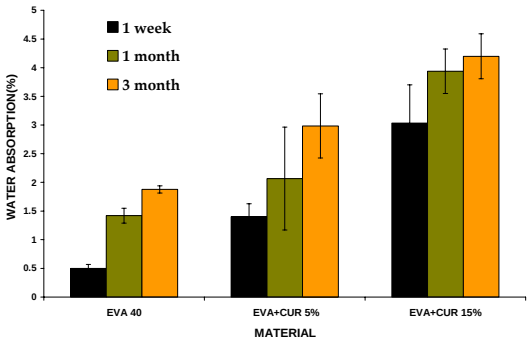

Figure 5. Water absorption of Curcumin-loaded EVA matrices

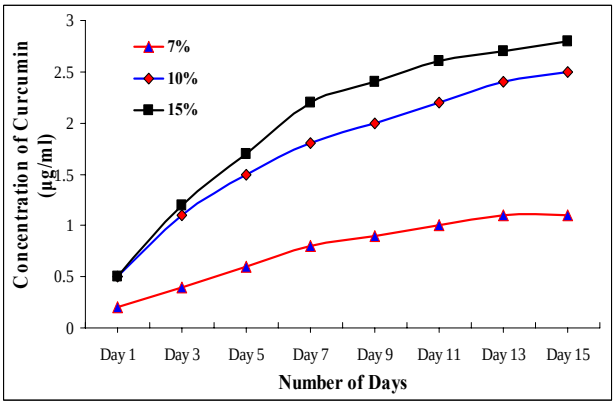

Figure 6. Cumulative elution profile of curcumin from EVA40 for different loadings

Aromatic-aliphatic co-polyester poly (butylene adipate-co-terephthalate) bio-nanocomposite: Influence of organic modification on structure and properties

B.P. Sahoo[1], G.Sornarajendran[2], S.Mohanty[2] and S.K.Nayak[2]

Laboratory for Advanced Research in Polymeric Materials

[1]Central Institute of Plastic Engineering and Technology, Bhubaneswar-751024,

[2]Central Institute of Plastic Engineering and Technology, Guindy, Chennai- 600032

Email: drsknayak@gmail.com

Abstract:

Bio-nanocomposite hybrids based on poly (butylene adipate-co-terephthalate) (PBAT) and layered silicates were prepared by melt interaction technique using co-rotating twin-screw extruder having blown film unit. Sodium montmorillonite (Na^+MMT) along with three different commercially available nanoclays i,e, Cloisite30B (C30B), Cloisite20A (C20A), Bentonite (B109) have been used. Wide Angle X-Ray Diffraction (WAXD) studies indicated an increase in d-spacing of the nanoclays in the bio-nanocomposite hybrids revealing formation of intercalated morphology. Morphological studies using Transmission electron microscopy (TEM) also confirmed that nanoclays were finely dispersed in the PBAT matrix and there was presence of partially exfoliated clay galleries along with intercalated structures in the bio-nanocomposite hybrids. Mechanical tests showed that the bio-nanocomposite hybrids prepared using Bentonite (B109) nanoclay exhibited higher tensile modulus. Functionalization of PBAT matrix upon grafting with maleic anhydride (MA) resulted in further improvement in mechanical properties. The existence of interfacial bonds in grafted bio-nanocomposite hybrids are substantiated using FTIR spectroscopy. Thermal properties of bio-nanocomposite hybrids employing DSC, TGA also revealed improved Tg, Tc and thermal stability over the virgin polymer. Dynamic Mechanical Analysis (DMA) indicated an increase of storage modulus(E') of PBAT biopolymer with incorporation of nanofiller. **Key words:** Poly(butylene adipate-co-terephthalate), TEM, DMA, MA-g-PBAT

Introduction

Polymer layered silicate nanocomposites have received considerable attention in the recent years. At minimal concentration of nanofiller to the tune of 1%, there has been a concurrent improvement of mechanical thermal, optical and physico chemical properties as compared with a conventional micro/macro composite [1]. The layered silicates with a thickness of 1 nm have a very high aspect ratio, ranging between 10 to 1000 that creates an effective surface area for polymer filler interaction leading to property enhancements in the virgin matrix [2]. Tailoring composites with a perspective of sustainable development and ecofriendly characteristics have resulted in renewed interest in natural renewable resource based and compostable materials. Research effects in the areas of natural fiber based plastics; biodegradable polymers, starch based plastics etc. have already been undertaken with a primary focus on development of biodegradable composites with environmentally safe characteristics and desired attributes. Despite several advantages in the development of biodegradable plastics, its introduction to the market as a viable alternative to petrochemical thermoplastics has been prevented. Some of the major impediments are fragility, thermal degradability at temperature not far above the melting point and high price [3]. However, incorporation of nanoscale fillers can significantly enhance the mechanical, thermal, dimensional and barrier performance in the biodegradable polymers [4].

Biodegradable nanocomposites can be prepared using various methods such as solution intercalation, melt intercalation, in-situ intercalative polymerization and template synthesis [5]. Polymer melt intercalation has been proved to be a versatile technique in the fabrication of biodegradable nanocomposites because of its environmental friendly characteristics and compatibility with the nanofillers [6].The present article summarizes an extensive investigation on physico-mechanical and thermal characterization of PBAT bio-nanocomposites.

Experimental

Materials

PBAT (Ecoflex) MFR (190^0C; 2.16 Kg)=3.3 to 6.6g/10min; Mass Density = 1.25 to 1.27g/cm3; Melting point = 110^0C to 115^0C was supplied by BASF Japan Ltd. Commercially available Cloisite 30B (C30B), Cloisite 20A (C20A), Bentone 109 (B109) have been used as nanoclays. The organoclays and PBAT pellets were dried under vacuum at 80^0C for 5hrs and 40^0C for 30minutes respectively.

Preparation of PBAT Nanocomposite

The bio-nanocomposite hybrids of PBAT with various organically modified nanoclays at different weight percentage (1, 3, 5 wt%) was prepared using melt blending technique in a co-rotating twin screw extruder (Haake Rheocord 9000, Germany) at a temperature difference from feed to die zone between 165° - 180°C and screw speed of 60-70 rpm. Maleic anhydride grafted PBAT (MA-g-PBAT) bio-nanocomposite hybrids were prepared through a two steps reactive extrusion process employing free radical grafting of PBAT using MA at a temperature of 165°C-180°C and screw speed of 60-80 rpm. In the second step, MA-g-PBAT was melt blended with various organically modified nanoclays using the same optimized temperature and speed. Subsequently the extrudate was pelletized to granules.

Wide Angle X-Ray Diffraction (WAXD): XRD Analysis was performed at ambient temperature using Phillips X'Pert MPD(JAPAN) at a scanning rate of 2^oC/min with CuK$\propto$ radiation(λ=0.154 nm) at 40KV and 14mA.

Mechanical Tests: Specimens of dimension 130mm x 25mm were prepared for Tensile testing as per ASTM D882 in Universal Testing Machine (UTM) at a gauge length of 50mm. Tear test for the prepared samples were performed as per ASTM D1922 in Pendulum Tear tester (ATSFAAR, VignateMI, Italy) with maximum load of 3920 grams. The samples were conditioned at 23 $\pm$ 5^0C and 55% RH prior to testing and five replicate were used for each test. The data reported are the averages from five tests.

Differential Scanning Calorimetry (DSC):DSC was performed on a Perkin-Elmer Pyris equipment (USA). 5-10mg samples were scanned at a heating rate of 10^0C/min from -80^0C to 200^0C in nitrogen atmosphere. The crystallization temperature (Tc), Glass transition Temperature (Tg) and Melting temperature(Tm) of the virgin PBAT, Nanocomposites and its blend were determined.

Thermo Gravimetric Analysis (TGA):TGA performed using Perkin-Elmer Pyris (USA). 5-10mg samples were heated at 20^0C/min from 50^0C to 600^0C. The degradation temperature was determined.

Dynamic Mechanical Analysis (DMA): The samples were studied using Dynamic Mechanical Thermal Analyzer (NETZSCH DMA 242, Germany), at fixed frequency of 1Hz and heating rate of 10°C/min.

Results & Discussion

The bio-nanocomposite structure characterized using WAXD patterns (Fig 1b) reveal characteristics peaks, shifted to smaller diffraction angles at 2.175, 2.145 and 2.03° respectively due to intercalation of PBAT chains into the silicate galleries. The interlamellar d_{001}-spacing follows the following order B109 (nm)> C20A (nm)> C30Bnm, confirming highly intercalated structure, due to strong interaction between carbonyl groups (>C=O) of PBAT with -OH groups of organoclay. In case of MA-g-samples absence of deflection peak within the experimental range, indicates exfoliation of clay galleries. Further, the TEM micrographs (Figure 2) confirm intercalated clay galleries as well as stacks of agglomerated clays galleries noticed within the PBAT matrix in case of PBAT/C20A, PBAT/B109 and PBAT/30B bio-

nanocomposites respectively. However, grafting of PBAT with MA results in improved dispersion characteristics of organically modified clays within MA-g-PBAT matrix with a smaller amount of stack platelets in broad and obscure regions & regions of exfoliated clay galleries along with intercalated stacks.

The mechanical properties of bio-nancomposite hybrid is depicted in Table-1 It is evident that incorporation of nanoclays results in an increase in the tensile modulus of matrix polymer in both transverse and as well as in machine direction respectively. In case of the nanocomposite prepared using C30B nanoclay an increase of Young's modulus to the tune of 30.59% and 31.99% respectively was observed. A similar increase in Young's modulus of PBAT/B109, PBAT/C20A nanocomposite hybrids was also noticed to the tune of 38.88% 46.94%, and 14.50% 7.22% in transverse and machine direction respectively as compared with the virgin matrix. The increase in Young's modulus of virgin PBAT matrix follows the following order PBAT/B109>PBAT/C30B>PBAT/C20A> PBAT/Na^{+}MMT. The nanocomposite hybrid with B109 exhibited optimum performance as compared with the other nanocomposite hybrids. This behavior is probably due to the homogeneous distribution and micro dispersion of nanoclay facilitating separation of tactoids and platelets in partial exfoliation and intercalations accomplished through shear stress during melt compounding. In all the cases, the nanocomposite hybrids exhibited higher performance in the machine direction, which is probably due to the uniform alignment and improved interfacial adhesion of the nanoscale reinforcement within the PBAT matrix. However, addition of nanoclays leads to a decrease in tensile strength as well as elongation at break. The MA-g-PBAT bio-nanocomposite hybrids exhibited improved tensile modulus as compared with the ungrafted bio-nanocomposite hybrids. This is probably due to the formation of inter molecular hydrogen bonding between hydrogenated tallow groups of B109 and C20A and MA-g-PBAT matrix. The bio-nanocomposite hybrid prepared using B109 clay exhibited maximum Young's modulus, which can be explained due to similar cause that B109 provides increased clay platelets per surface area of contact with virgin matrix.

The tear resistance of PBAT matrix and the bio-nanocomposite hybrids also exhibits a linear increase with the addition of nanoclays and MA. Nearly 19% increase in the tear strength of PBAT matrix was observed in PBAT/B109 bio-nanocomposite hybrid. PBAT/C30B as well as PBAT/C20A bio-nanocomposite hybrid also exhibited an increase in tear strength of PBAT from 335.3 g/mm to 343.17 g/mm and 283.00 g/mm respectively. Further, functionalization of PBAT matrix with MA through reactive extrusion results in modification of the interfacial region between PBAT and nanoclays through formation of covalent bonds/hydrogen bonds with suitable chemical/pendent groups [24]. The bio-nanocomposite hybrid of MA-g-PBAT/B109 exhibited a tear resistance of 445.39 g/mm where as MA-g-PBAT/C30B exhibited a tear resistance of 375.05 g/mm respectively.

The storage modulus verses temperature of the virgin matrix and nanocomposite hybrid is represented in fig 3. It is evident that storage modulus of PBAT biopolymer increases with incorporation of nanofiller which is probably due to the efficient stress transfer from the filler to matrix. Further the grafted sample exhibited improved modulus as compared with the ungrafted nanocomposite hybrids. This further confirms improved interface between the nanofiller and the biopolymer matrix upon functionalisation with MA. MA-g-PBAT/B109 sample exhibited optimum storage modulus as compared with MA-g-PBAT/C30B nanocomposite hybrid which is probably due to better exfoliated structure.

The melting temperature of PBAT matrix depicted in DSC Thermograms (fig.4)also showed a substantial increase from 109.2°C to 125°C in PBAT/C30B, 126.72°C in PBAT/B109, 138.25°C in MA-g-PBAT/C30B and 139.02°C in MA-g-PBAT/B109 nanocomposite hybrids respectively.

The variation of crystallization temperature (Tc) of virgin matrix and nanocomposite hybrids is presented fig 5. The virgin matrix exhibits a crystallization peak around 66.14°C which increased substantially with the incorporation of nanoclays as well as functionalization of PBAT with MA. PBAT/C30B bio-nanocomposite hybrid exhibits optimum crystallization peak around 96.45°C. This is primarily due to heterogeneous nucleation effect in presence of nanoclay which increase the nucleation sites in the polymer matrix. However, grafting of virgin matrix does not show any appreciable increase in the

crystallization temperature of PBAT in the bio-nanocomposites as compared with the ungrafted bio-nanocomposites.

The thermal stability of virgin PBAT, PBAT bio-nanocomposite hybrids and MA-g-PBAT bio-nanocomposites are assessed employing TGA showed that incorporation of organically modified nanoclays substantially increases the thermal stability of the biopolymer. PBAT/C30B nanocomposite hybrid exhibits the initial degradation temperature around 322.58°C and final degradation temperature around 469.58°C which is comparatively higher than that of virgin matrix. The grafted bio-nanocomposite hybrids exhibited a further increase in the degradation temperature. MA-g-PBAT/B109 showed maximum initial and final degradation temperature of 339.59°C and 505.82°C. The bio-nanocomoposite hybrid samples prepared using B109 nanoclay exhibited optimum thermal performance owing to its higher surface area and smaller platelets (fig 6).

Conclusion

Nanocomposites based on PBAT and layered silicate (C30B, C20A and B109) was prepared using melt intercalation and subsequently blown films were prepared. Morphological observation from TEM and WAXD revealed that PBAT/C30B and PBAT/B109 exhibits intercalated structure whereas MA-g-PBAT/B109 showed few layers of exfoliated clay galleries as well as intercalated structure. Mechanical tests showed an increase in the tensile modulus of PBAT nanocomposites hybrid in the grafted samples. Thermal stability of the virgin biopolymer also increased with the incorporation of organically modified nanoclays. Future research will be primarily focused in the development of nanocomposite hybrid with improved mechanical performance.

References

1. Alexander, M; Dubois,P; Mater Sci Eng 200,28,1.
2. Li,X; Kang,T; Cho,W,J; Lee,J,K; Ha,C,S; Macromol Rapid Commun 2001,22,1306.
3. Chang,J,H; An,X,U; Sur,G,S; J polym sci part B: polym Phys 2003,41,94.
4. Ray,S,S; Okamoto,M; Macromol Rapid Commun 2003,24,815.
5. Messermith,P,B; Giannelis; E.P.J.Polym Sci Part A: Polym Chem 1995, 33, 1047.
6. Di, Y.; Iannace, S.; Maio, E. D.; Nicolais, L. j Polym Sci Part B: Polym Phys 2003, 41 670.
7. Chen, G. X.; Hao, G. J.; Guo,T. Y; J Appl Polym Sci 2004, 93, 655.
8. Chen, G. X.; Hao, G. J.; Guo,T. Y.; Song, M. D.; Zhang,B. H. J Mater Sci Lett 2002, 21, 1587.
9. Ray, S. S.; Okamoto, K.; Maiti, P.; Okamoto, M. J Nanosci Nanotechnol 2002,2,1.
10. Ray, S. S.; Okamoto, K.; Okamoto, M. Macroolecules 2003, 36, 2355.

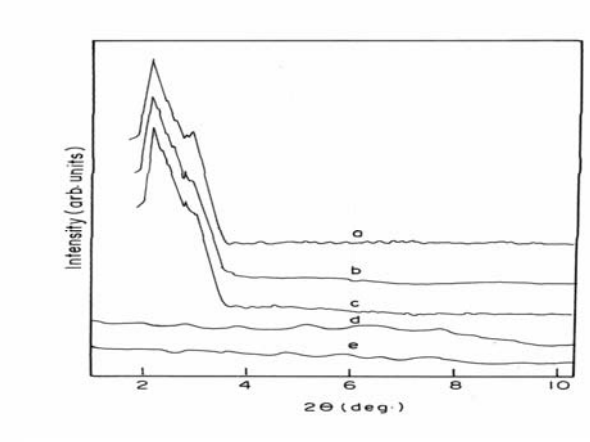

Fig 1: WAXD patterns for bio-nanocomposites; (a). PBAT/C20A,(b). PBAT/C30B, (c). PBAT/B109, (d). MA-g-PBAT-C30B, (e). MA-g-PBAT-B109

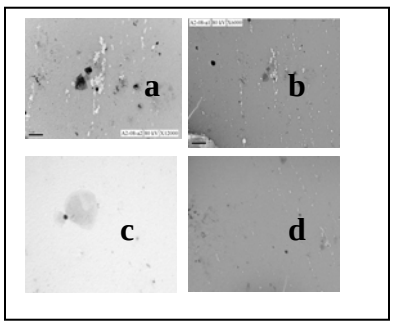

Fig 2: TEM Micrographs of bio-nanocomposites; (a) PBAT/C30B (b). PBAT/B109, (c). MA-g-PBAT-C30B, (d). MA-g-PBAT-B109

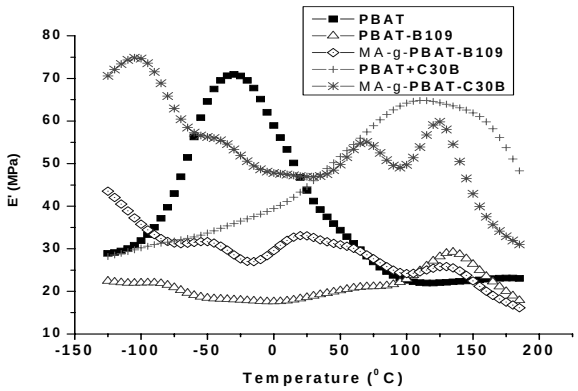

Fig 3: Storage Modulus of Virgin PBAT and bio-nanocomposites

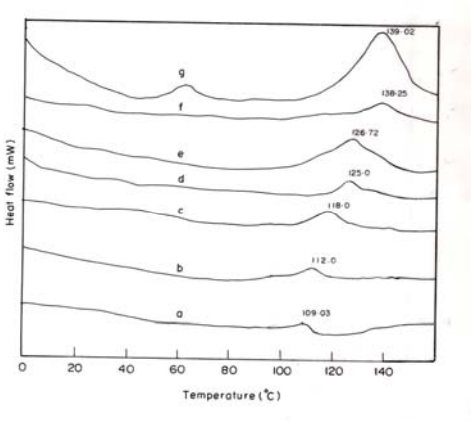

Fig 4: DSC Thermograms of Virgin PBAT and bio-nanocomposites

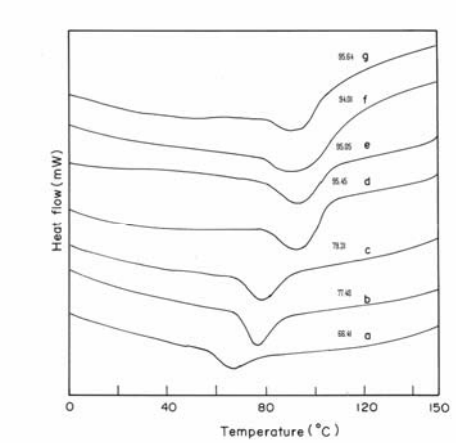

Fig 4: Crystallization temperature of Virgin PBAT and bio-nanocomposites

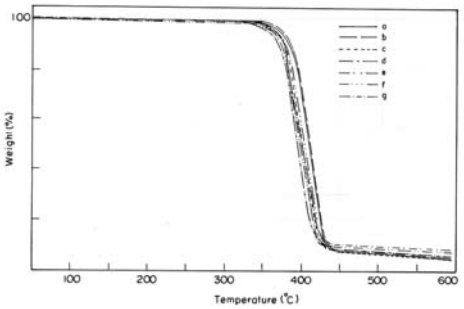

Fig 4: TGA of (a). PBAT, (b). PBAT-Na^{+}MMT, (c). PBAT-C20A, (d). PBAT-C30B, (e). PBAT-B109, (f). MA-g-PBAT-C30B, (g). MA-g-PBAT-B109 bio-nanocomposites

Table 1: Mechanical Properties of PBAT & bio-nanocomposites

Samples	Tensile Modulus (MPa)	Tensile Strength (N/mm^2)	Elongation at break (%)	Tear Strength g/mm
PBAT	26.20(T) 30.17(M)	20.814(T) 14.328(M)	602.33 (T) 766.44 (M)	335.3
PBAT/C30B3%	34.215(T) 39.824(M)	6.883(T) 10.78(M)	552.84 (T) 601.66 (M)	343.17
PBAT/C20A3%	30.03(T) 32.35M)	3.513(T) 4.193(M)	544.08 (T) 550.33 (M)	283.00
PBAT/B1093%	36.389(T) 44.333(M)	5.490(T) 17.370(M)	595.41 (T) 740.30 (M)	348.98
PBAT-g-MA/C30B	52.489(T) 56.213(M)	8.353(T) 12.314(M)	605.39(T) 684.32(M)	375.05
PBAT-g-MA/C20A	43.467(T) 52.597(M)	3.221(T) 6.391(M)	560.93(T) 590.39(M)	290.03
PBAT-g-MA/B109	73.123(T) 81.854(M)	7.7952(T) 8.627(M)	695.35(T) 760.39(M)	445.39

Biomimetic synthesis of nanohybrids based on calcium hydroxyapatite and carboxymethyl cellulose

Annamalai Pratheep Kumar[a*], Kamal Khaja Mohaideen[a, b] and Raj Pal Singh[a#]
[a] Division of Polymer Science and Engineering,
[b] Physical and Materials Chemistry Division
National Chemical Laboratory, Dr. Homi Bhaba Road, Pune - 411 008, India.
E-mail[#]: rp.singh@ncl.res.in

Abstract

In the present paper we report biomimetic synthesis of nanohybrids based on carboxymethyl cellulose (CMC) and hydroxyapatite (HA) nanoparticles by a co-precipitation method. The physico-chemical characterizations were done before and after calcination using Fourier transform infrared spectroscopy, solid state ^{31}P nuclear magnetic resonance (NMR) spectroscopy and thermogravimetric analysis (TGA). The formation of nanohybrid was observed by wide angle X-ray diffraction (WAXD), scanning electron microscopy (SEM) with energy dispersive X-ray analysis (EDX) and transmission electron microscopy (TEM). The nanohybrid was formed as aggregates of nanoparticles adsorbed on CMC. With increasing content of CMC, the crystallite size of hydroxyapatite particles decreased (with 2 wt. % 18±3 nm). The morphological aspects of calcined samples have shown the sintering ability of HA nanoparticles. The possible mechanism for interaction between CMC and HA, nucleation and growth of nanocrystals of HA is discussed. It is summarized that nanohybrids of hydroxyapatite nanoparticles can be prepared for mimicking the process of nucleation and growth in nature using biodegradable and biocompatible macromolecules like CMC.

1. Introduction

Over the past decade, the main goal of bone tissue engineering has been to develop biodegradable materials as bone graft substitutes for filling large bone defects. Bone and teeth consist of a small amount of organic matrix, which manipulates the formation of apatite into distinct microstructures suitable for the mechanical forces which they encounter *in-vivo* [1, 2]. There has been widespread use of calcium phosphate bioceramics, such as hydroxyapatite (HA) and tricalcium phosphate (TCP), for bone regeneration applications. Their biocompatibilities are thought to be due to their chemical and structural similarity to the mineral phase of native bone [3]. Biomineralized tissues are often found to contain polymorphs and individual minerals whose crystal morphology, size, and orientation are often controlled by local conditions and, in particular, by organic macromolecules such as proteins and polysaccharides [1, 4]. Owing to their small size and high surface area, HA nanoparticles, which are similar to that in bone tissue, can effectively interact with living cells [8, 9]. The drawbacks of HA nanoparticles are their instability, associated with migration of nanoparticles to surrounding tissues under the action of blood flow, and their low solubility [10]. To overcome these, a new development in this field is the biomimetic synthesis of nanosized calcium phosphates (mainly HA) in

polymer-matrices to produce composites that can initiate osteogenesis when implanted in bony sites [11]. In biomedical applications, cellulose, a polysaccharide, is used either as regenerated films, fibers or as derivatives (esters, ethers) [14-16]. Considering, the biodegradability, biocompatibility, non-toxicity, muco-adhesive nature and the carboxyl groups on structure of carboxymethyl cellulose, we expect that CMC can interact with precursors and direct the nucleation and growth of hydroxyapatite to produce bioactive ceramics. Thus, the present study is to prepare nanohybrids of carboxymethyl cellulose (CMC) and hydroxyapatite (HA) nanoparticles and to study the effect of CMC on size, structure and morphology of HA.

2. Experimental

Keeping the molar ratio of calcium / phosphate as constant ~1.67, the CMC content was varied from 0 to 2 wt. % of total weight formulations were calculated as represented in Table 1. The weighed amounts of polymer and calcium reagent ($CaCl_2$) were dissolved in aqueous ammonia at room temperature (~27 °C). After 15 min, the phosphate reagent, diammonium hydrogenphosphate ($(NH_4)_2HPO_4$) was added to this solution and stirred for 2 weeks at room temperature (~27 °C). During the reaction, the pH was monitored and adjusted at 10 by addition of ammonia solution. After reaction, precipitate was washed with deionized water and dried in a vacuum oven at 40 °C for 12 h. Portions of the prepared samples were calcined at 1000 °C for 1.5-2 h. The physico-chemical characterizations were done before and after calcination using Fourier transform infrared spectroscopy, solid state ^{31}P nuclear magnetic resonance (NMR) spectroscopy and thermogravimetric analysis (TGA). The formation of nanohybrid was observed by wide angle X-ray diffraction (WAXD), scanning electron microscopy (SEM) with energy dispersive X-ray analysis (EDX) and transmission electron microscopy (TEM).

3. Results and Discussion

3.1. FTIR spectroscopy

In Figure 1, the characteristic peaks at 2800-3000 cm $^{-1}$, 3100-3500 cm $^{-1}$, 1650-1700 cm^{-1}, and 1100 cm^{-1}, which are assignable for C-H, hydroxyl, carboxylate and C-O- group regions, respectively, indicate the presence of CMC. The absorption bands at 3571 $cm^{-1}$and 631 cm^{-1}, arise from stretching and bending modes of OH^- ions, respectively. The absorbance at 1040 and 1090cm^{-1} is attributed to (ν_3) phosphate PO_4^{3-}. The other bands at 962 cm^{-1} (for ν_1), 601 and 574 cm^{-1} (for ν_4), and 472 cm^{-1} (for ν_2) are also attributed to unique characteristic vibrations of PO_4. The weak intensity of bands in 2200 -1950 cm^{-1} region derives from overtones of bands and combinations of ν_3 and ν_1 phosphate modes. The sharpness of bands, especially at 631, 601 and 574 cm^{-1} indicate a well crystallized HA [22]. The 1037 cm^{-1} and 1096 cm^{-1} bands in Figure 1a and b are PO_4^{3-} ν_3 mode and asymmetric HA, respectively.

3.2. ^{31}P-NMR Spectroscopy

Figure 2 Shows the solid state ^{31}P NMR Spectra of as-synthesized and calcined calcium hydroxyapatite. The peak at 2.3 - 2.5 ppm, which is typical for hydroxyapatite, can be observed for all the samples. They, however, differ in the line width, and the broadening of peak at foot is also observed for the *as-synthesized* nanohybrids. The broadening of peak is attributed to nanoscale crystalline particles [25].

3.3. Thermogravimetric analysis (TGA)

In TGA thermograms of as-synthesized nanohybrids (Figure 3), The observed weight loss in the temperature range from 75 °C to 550 °C under nitrogen atmosphere can be attributed to dehydration of water molecules present / adsorbed in the crystals, carbon dioxide evolution from carbonate defects of calcium phosphates and decomposition of carboxymethyl cellulose. Since the nanohybrids were thoroughly washed with deionized water for several times while filtration, only the strongly adsorbed / bound CMC molecules can contribute to the additional weight loss.

3.4. Wide angle X-ray diffraction (WAXD)

Figure 4 shows the WAXD patterns of as-synthesized and calcined nanohybrids. The characteristic peaks at 2θ ~10.8, 18.8, 25.8, 31.7 (with maximum intensity), 32.9, 34.0, 39.8, 46.83, 49.4, and 53.1° are attributed to hydroxyapatite. The broadening at foot of peak at 2θ ~31.7° for as-synthesized samples can be correlated to nanocrystal formation. For the calcined samples, these peaks are narrow and sharp. The effect of CMC content on the crystallite size D (nm) of HA in both as-synthesized and calcined samples was calculated using Scherer formula. With increasing content of CMC, the crystallite size decreases. After calcination, regardless of CMC content the crystallite size is increased upto 48 ± 4nm, which can be attributed to the sintering and densification phenomena at a constant and higher temperature [31]. The consistency in crystallite size can be attributed to the constant calcination temperature and conditions in which the coalescence of finer particles is expected to be in similar rate [33, 34].

3.5. Scanning Electron Microscopy (SEM) and Energy Dispersive X-ray Analysis (EDX)

SEM images of the *as-synthesized* and calcined samples are shown in Figure 5 (HA-05 and Figure 5 (HA-1). In the *as-synthesized* samples, the nanoparticles are embedded / surrounded by CMC molecules, to form agglomerates whose size is about 100 – 300 nm. These agglomerates show rough and interconnected porous surface. As FTIR spectra results suggest the presence of CMC in as-synthesized nanohybrids, the agglomeration of nanoparticles might be due to CMC molecules. After calcination, particles are bigger in size and smoother on the surface than that of as-synthesized ones. As mentioned above, the increase in particle size can be attributed to the sintering of HA nanoparticles at higher temperature. Figure 7 shows the EDX graph of the as synthesized and calcined sample of HA-05. The Ca/P ratios for as-synthesized and calcined sample were about 1.45 and 1.67, respectively. This also confirms the formation of hydroxyapatite precipitates.

3.6. Transmission Electron Microscopy (TEM)

The bright field TEM images of as-synthesized and calcined samples are shown in Figure 6. The *as-synthesized* nanohybrids can be seen as agglomerates of nanoparticles grown on the CMC matrix. The size of agglomerates can be found about 100 to 300nm. After calcination, the HA particles are found to be bigger. In the as-synthesized samples, the agglomeration of HA nanoparticles can be explained by interactions between carboxymethyl cellulose, HA and its precursors with each other.

4. Conclusion

In the present study, we have prepared nanohybrids of carboxymethyl cellulose (CMC) and hydroxyapatite (HA) nanoparticle by co-precipitation method at room temperature. The FTIR, ^{31}P-NMR spectroscopy and wide-angle X-ray diffraction measurements have shown the formation CMC-nanohybrids. TG analysis revealed that content of CMC in nanohybrids is linear with initial input. The SEM and TEM images shown that nanohybrids are formed as aggregates of HA nanoparticles embedded in CMC matrix. The morphological aspects of calcined samples have shown the sintering capacity of HA nanoparticles. Possible mechanism for interaction between HA and CMC, nucleation and growth is discussed. Thus, we can summarize that the nanohybrids of hydroxyapatite nanoparticles can be prepared for mimicking the process of nucleation and growth in nature using biodegradable and biocompatible polymer like CMC.

Acknowledgement:

The authors are grateful to Dr. S. Sivaram, Director, National Chemical Laboratory (NCL), Pune, for providing the infrastructure and encouragement. Dr. P.A. Joy, Physical and Materials Chemistry Division, NCL, Pune is acknowledged for his fruitful discussions and valuable suggestions.

References

1. S.I. Stupp, P.V. Braun, Science 277 (1997) 1242.
2. T. Kokubo, H.-M. Kim, M. Kawashita, Biomaterials 24 (2003) 2161.
3. D. Skrtic, J.M Antonucci, E.D. Eanes, J. Res. Natl. Inst. Stand. Technol. 108 (2003) 167.
4. H.A. Lowenstam, S. Weiner, On Biomineralization, Oxford University Press, New York, 1989.
5. Y. Doi, T. Horiguchi, J. Biomed. Mater. Res. 31 (1996) 43.
6. T.J. Webster, R.W. Siegel, R. Bizios, Biomaterials 21 (2000) 1803.
7. Y. Miyamoto, K.I. Shikawa, Biomaterials 19 (1998) 707.
8. I. Lee, S.W. Han, H. J. Choi, K. Kim, Adv. Mater. 13 (2001) 1617.
9. T. Miyamoto, S. Takahashi, H. Ito, H. Inagaki, J. Biomater. Res. 23 (1989) 125.
10. A.G. Walton, J. Blackwell, Biopolymers, Academic Press, New York, 1973.
11. P.Y. Yang, S. Kokot, J. Appl. Polym. Sci. 60 (1998) 1137.
12. M. Markovic, B.O. Fowler, M.S. Tung, J. Res. Natl. Inst. Stand. Technol. 109 (2004) 553.
13. C. Jäger, T. Welzel, W. Meyer-Zaika, M. Epple, Magn. Reson. Chem. 44 (2006) 573.
14. A. Bigi, A. Incerti, N. Roveri, E. Foresti-Serantoni, R. Mongiorgi, L.R. di Sanseverino, A. Krajewski, A. Ravaglioli, Biomaterials 1 (1980) 140.
15. H. Y. Juang, M. H. Hon, Biomaterials 17 (1996) 2059
16. H.E.-Hosseini, M. R. Housaindokht, M. Chahkandi, Mater. Chem. Phys. 106 (2007) 310

Tables and Figure

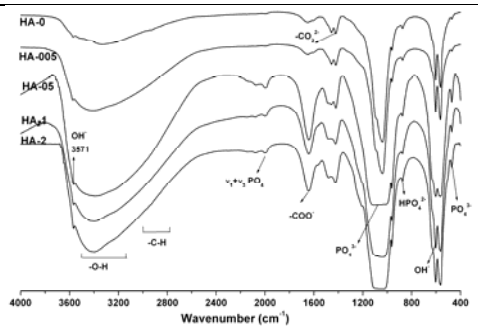

Fig1a: FTIR Spectra of as-synthesized samples

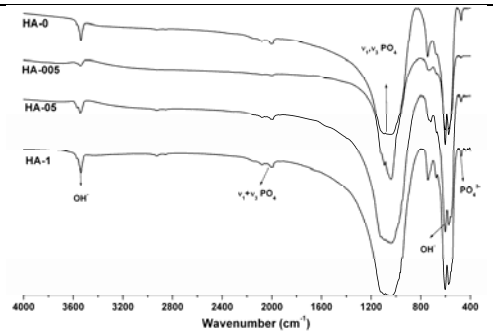

1b: FTIR Spectra of calcined samples

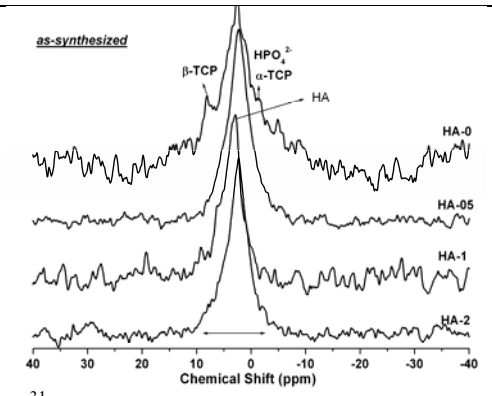

Fig 2: ^{31}P-NMR Spectra of as-synthesized samples

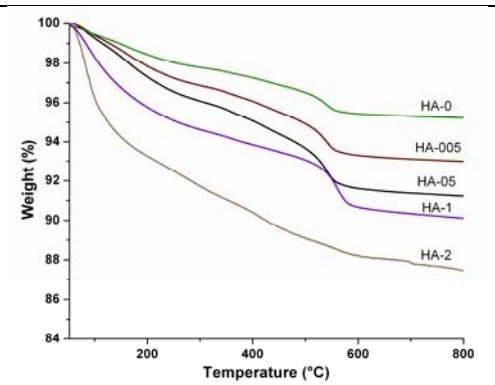

Fig 3:TGA of as-synthesized samples

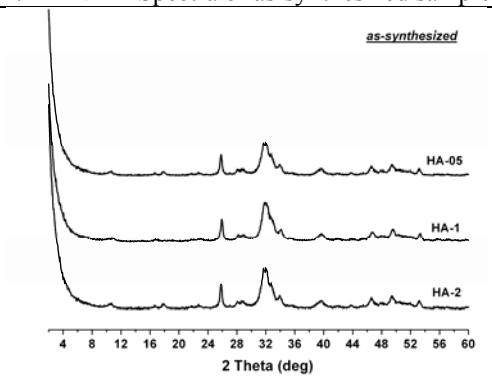

Fig 4a: WAXD patterns of as-synthesized samples

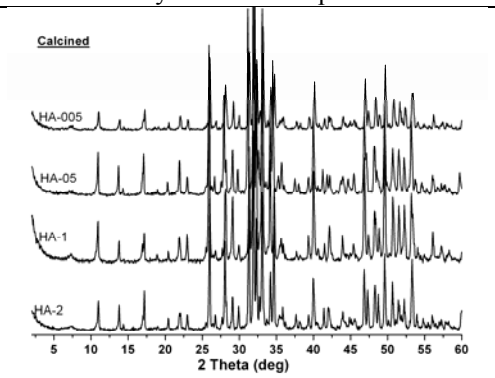

Fig 4b: WAXD patterns of calcined samples

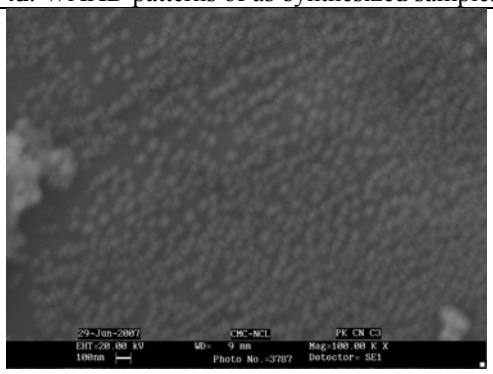

Fig 5a: SEM image of as-synthesized sample

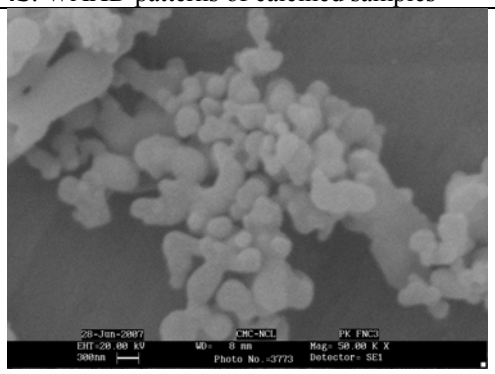

Fig 5b: SEM image of as-synthesized sample

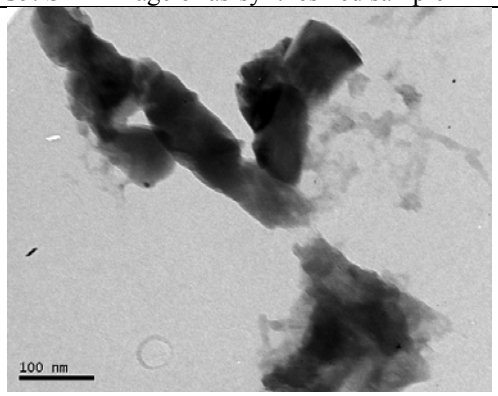

Fig. 6a: TEM image of as-synthesized sample

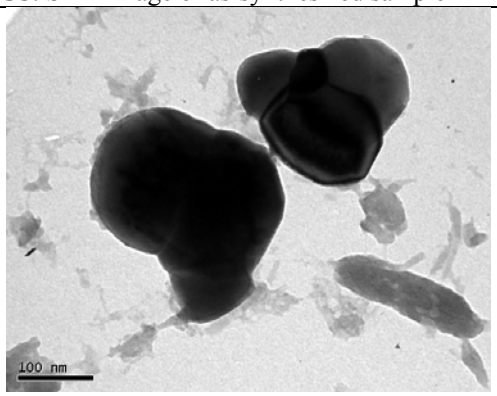

Fig.6b: TEM image of calcined sample

Use of deproteinized and normal skim rubbers for property improvement in natural rubber

K. Mariamma George*, Rosamma Alex, Salini K.S and K.T. Thomas

Rubber Research Institute of India, Rubber Board, Kottayam -9, India
Email: *mariamma@rubberboard.org.in, mgpattani@yahoo.co.in

Abstract

Skim rubber is the rubber recovered from skim latex, which is obtained as a by-product during the centrifugal concentration of natural rubber (NR) latex. Blending skim rubber with natural rubber is a method of taking advantage of the relatively low price of skim rubber while minimizing its disadvantages. In addition, it seems possible that in such blends the fast curing characteristics of the skim can be utilized. We have examined the cure behaviour and technological properties on adding 20 p.h.r (parts per hundred rubber) each of deproteinized skim rubber (DPSR) and normal skim rubber to ISNR 20 without further addition of curatives and comparing the properties to that of a similar ISNR 20 mix. Two cure systems, one which contain usual dosage of accelerator and antioxidant and the other system which contain comparatively lower level of accelerator without any antioxidant were studied. In the former case, the cure characteristics showed that there is attainment of good level of cure and cure rate even after addition of 20 p.h.r skim rubber or DPSR to ISNR 20 with no extra curatives, compared to the conventional ISNR 20 mix. Also the ISNR 20 vulcanizate and the vulcanizate containing additional 20 parts of skim rubber showed comparable values of moduli, tensile strength, tear strength and abrasion resistance and these values were higher than that observed for ISNR 20 vulcanizate containing 20 parts DPSR. Skim rubber incorporated mix showed a slightly higher resistance to crack initiation and crack failure when compared to ISNR 20 mix. Blend which contain 20 parts DPSR showed slightly better dynamic properties and improved air ageing characteristics as compared to normal skim rubber. For the mixes which contain lower level of curatives, cure characteristics were comparable but the values were lower than that which contain the usual dosage. Same trend was observed for the mechanical properties and ageing characteristics. The study has shown that incorporation of 20 parts skim rubber or deproteinized skim rubber to ISNR 20 imparts cure characteristics and mechanical properties similar to that attained by ISNR 20 without the incorporation of additional curatives.

Introduction

Skim rubber is obtained by the coagulation of skim latex, the secondary fraction of natural rubber latex, from the centrifugal concentration process. The processing of skim latex has many associated problems due to the peculiar physical and chemical characteristics of the same and is an issue of environmental concern. Skim latex has very low dry rubber content (4-8%) and rubber particles are smaller in size with high specific surface area [1, 2]. It has higher proportion of non-rubber solids which is mostly proteinaceous in nature. It is difficult to coagulate skim latex [3] and there is considerable loss in skim rubber during processing. Acid coagulation and auto coagulation are used to recover rubber from skim latex [4]. To improve the raw rubber properties of skim rubber, attempts have been made by deproteinization using certain enzymes [5] and subsequent creaming [6] of skim latex. The proteolytic enzyme stabilized liquid papain used for deproteinization followed by creaming results in quick and easy coagulation of skim latex [7]. The type and high level of non-rubbers present in the skim rubber give rise to scorchy cure and generally give vulcanizates of high modulus. The latter can be considered to arise at least in part due to the protein present in the rubber acting as a reinforcing filler and participation in the curing process. Despite these adverse features, skim rubber has low dirt content, often accompanied by light colour and relatively low cost. Blending skim rubber with natural rubber is a method of taking advantage of the relatively low price of skim rubber while minimizing its disadvantages. In addition, it seems possible that in such blends the fast curing characteristics of the skim can be utilized [8].

In this work we have examined the cure behaviour and technological properties on adding 20 phr (parts per hundred rubber) each of deproteinized skim rubber (DPSR) and skim rubber to ISNR 20 mix without further addition of curatives and comparing the properties to that of a similar ISNR 20 mix. Two cure systems, one which contain usual dosage of accelerator and antioxidant and the other system which contain comparatively lower level of accelerator without any antioxidant were studied.

Experimental

ISNR 20 - From the Pilot Crumb Rubber Factory, Rubber Board
DPSR - Prepared at the Rubber Technology Division, RRII
Skim rubber - From the Central Experiment Station, Chethackal, Rubber Board
The other ingredients used were of commercial grade

Preparation of deproteinized skim rubber

Liquid papain of 0.25 phr as 5% solution was initially treated with 0.5 phr potassium oleate. This was then mixed with the skim latex, stored for 48 h at room temperature, treated with potassium oleate (0.01% w/v on latex as 10% solution) and stored for further 24 h. It was then subjected to creaming with ammonium alginate (0.3% w/v on latex as 3% solution), coagulated the cream with 5% H_2SO_4, the coagulum soaked for 24 h in oxalic acid solution and dried [7]. The fatty acids present in both DPSR and skim rubber were determined using gel permeation chromatograph (GPC – Waters 510) attached to a 410 diffraction refractometer. The solvent used was THF/water/acetonitrile in the ratio 25/35/45 (v/v) at a flow rate of 2ml/min. Raw rubber properties of ISNR 20, DPSR and skim rubber were determined and are given in Table 1.

Preparation of mixes

In order to study the cure behaviour and technological properties, two cure systems were selected. Mixes were prepared as per the formulations given in Table 2 using a laboratory model two roll mixing mill. Cure characteristics of the samples were determined using Tech Pro Rheo Tech MD + at 150°C. Vucanizates were moulded using an electrically heated hydraulic press to their respective optimum cure. Properties of the vulcanizates were determined as per the relevant ASTM standards. Ageing of the vulcanizates was carried out at 70°C for 7 days in an air oven as per ASTM standards.

Results and discussion

Fatty acids

Fig.1 shows the chromatogram of the fatty acids present in the skim rubber prepared by conventional method and that obtained after deproteinization and creaming. The fatty acids present include linoleic, oleic, stearic, linolenic and lauric. There is a reduction in the quantity of fatty acids after deproteinization and creaming. Higher quantity of fatty acids retained in skim rubber adversely affects the ageing characteristics.

Raw rubber properties

Results in Table 1 show that ISNR 20 has nitrogen content of 0.37 % where as skim rubber has nitrogen content of 2.3 %. DPSR prepared by using the protelytic enzyme papain has reduced the nitrogen content to 0.62 %. Being a protease, this enzyme catalysis the hydrolysis of proteins which are bound to the latex particles in to water soluble polypeptides and amino acids, which get removed during the creaming process [9]. Ash content was more for the skim rubber than ISNR 20. During deproteinization and creaming some of these mineral materials were removed and hence the value for the ash content of DPSR was lower than skim rubber but higher than ISNR 20. Initial plasticity, Po for the three samples were within the limit specified by Bureau of Indian Standards (BIS). Comparatively low PRI was recorded by the skim rubber while DPSR recorded a PRI comparable to that of ISNR 20. The low PRI of skim rubber could be attributed to the presence of high proportion of copper and unsaturated fatty acids that accelerate the oxidation of rubber [10]. It is reported that the PRI can be improved by immersion of the coagulum in 1% oxalic acid solution and the improvement observed for the enzyme treated sample may be due to the extraction of free copper from the rubber

[11]. Skim rubber and DPSR differed most obviously from ISNR 20 in the high levels of fatty acid and protein content and hence the acetone extractable of skim rubber and DPSR were higher than that of ISNR 20. Mooney viscosity of the three samples was within the processable limit.

Cure characteristics and mechanical properties

Cure characteristics and mechanical properties of mixes 1, 2 and 3 are given in Table 3. The results showed that there is attainment of good level of cure and cure rate even after addition of 20 phr skim rubber or DPSR to ISNR 20 with no extra curatives, compared to the conventional ISNR 20 mix. This shows that both in skim rubber and DPSR there is sufficient quantity of amines and proteins that have an accelerating effect on vulcanization. ISNR 20 vulcanizate and the vulcanizate containing additional 20 parts of skim rubber showed comparable values of moduli, tensile strength, tear strength and abrasion resistance and these values were higher than that observed for ISNR 20 vulcanizate containing 20 parts DPSR. Skim rubber incorporated mix showed slightly higher resistance to crack initiation and crack failure when compared to ISNR 20 mix. However, comparable flex resistance was obtained for ISNR 20 mix and DPSR (20 parts) incorporated mix. It is reported that the proteins present in skim rubber can improve the modulus and resistance to flex cracking of rubber vulcanizate owing to its reinforcing characteristics[12]. Comparatively lower values of resilience, higher heat build-up and compression set were recorded for the mix containing 20 parts of skim rubber. The proteins present in skim rubber are known to adversely affect dynamic properties like compression set, resilience and heat build-up. Blend which contains 20 parts of DPSR showed slightly better dynamic properties compared to normal skim rubber. The improvement may be attributed to the reduction of protein content and partial removal of unsaturated fatty acids. The above results showed that incorporation of 20 parts of skim rubber or deproteinized skim rubber to ISNR 20 imparts cure characteristics and mechanical properties similar to that attained by ISNR 20 without the incorporation of additional curatives.

Cure characteristics and mechanical properties of mixes 4, 5 and 6 are also given in Table 3. Cure characteristics were comparable but the values were lower than that which contains the usual dosage, i.e. for mixes 1, 2 and 3. Same trend was observed for the mechanical properties.

The ageing resistance in modulus and tensile strength of the vulcanizates after ageing at 70°C for 7 days are given in Figs. 2 and 3. For mixes 1, 2 and 3, retention of modulus and strength for the blend which contain DPSR were better than ISNR 20 mix and the blend containing skim rubber. The improvement in ageing characteristics may be attributed to the partial removal of unsaturated fatty acids and metal ions that are pro-oxidants during deproteinization and creaming process. For mixes 4, 5 and 6 retention of modulus and strength were comparable but the values were lower than that obtained for the mixes 1, 2 and 3.

Conclusions

Incorporation of 20 parts of skim rubber or deproteinized skim rubber to ISNR 20 imparts cure characteristics and mechanical properties similar to that attained by ISNR 20 without the incorporation of additional curatives. Skim rubber incorporated mix showed a slightly higher resistance to crack initiation and crack failure when compared to ISNR 20 mix. Blend which contains 20 parts DPSR showed slightly better dynamic properties as compared to normal skim rubber. For the system which contains the normal dosage of curatives, retention of modulus and strength for the blend which contain DPSR were better than ISNR 20 mix and the blend containing skim rubber.

References

1. Subramanian, A.RRIM Technol Bulletin, 1980, 4, 1.
2. Yeang, H. Y, Eshah, Y, Samsidah, H. J Rubb Res, 1995, 10, 108.
3. Smith, M.G. J Rubb Res Malaya, 1969, 23, 1, 70.
4. John, C.K, Sin, S.W. J Rubb Res Inst Malaya, 1973, 23, 4, 257.
5. Morris, J. E. Proc 3rd Rubb Tech Conf, London, June 1954, 13.
6. Sakdapipanich, J.T, Nawamawati, K, Tanaka, Y. J Rubb Res, 2002, 5, 1, 1.

7. George, K.M, Alex, R, Joseph, S and Thomas, K.T. Proc Int Conf on Rubber and Rubber like materials, IIT, Kharagpur, Jan 2008,
8. Bristow, G.M. J Nat Rubb Res 1990, 5, 2,114.
9. George, K.M, Rajammal, G, Joseph, S, Varghese, T.C, Mathew, N.M. Proc 3rd Int Rubb Glove Conf & Exhi, Kuala Lumpur, Malaysia, September 2006, C4, 2.
10. Arnold, A.R, Evans, P. J Nat Rubb Res, 1991, 6, 2, 75.
11. Hasma, H, Othman, A.B. J Nat Rubb Res, 1990, 5, 1, 1.
12. Knight, G.T, Tan, A.S. Proc Int Rubb Conf, Kuala Lumpur, 1975, 4, 115.

Table 1. Raw rubber properties

Parameter	ISNR 20	DPSR	Skim rubber
Nitrogen content, %w/w	0.37	0.62	2.30
Ash content, % w/w	0.36	0.40	0.53
Initial plasticity, P_o	51	38	39
Plasticity retention index, PRI	49	56	17
Acetone extractable, %	2.64	6.78	6.24
Mooney viscosity, [ML(1+4)100°C]	86	76	70
Copper content, ppm	6.0	10.0	18.0

Table 2. Formulation of mixes

Ingredient	Mix Nos					
	1	2	3	4	5	6
ISNR 20	100	100	100	100	100	100
Deproteinized skim rubber	-	20	-	-	20	-
Skim rubber	-	-	20	-	-	20
Zinc oxide	5	5	5	5	5	5
Stearic acid	2	2	2	2	2	2
HAF black (N300)	30	30	30	30	30	30
Naphthenic oil	1.5	1.5	1.5	1.5	1.5	1.5
Antioxidant TDQ[1]	1	1	1	-	-	-
CBS[2]	0.7	0.7	0.7	0.5	0.5	0.5
Sulphur	2.5	2.5	2.5	2.5	2.5	2.5

[1]2,2,4-trimethyl 1,2-dihydroquinoline
[2]N-cyclohexyl-2-benzthiazil sulphenamide

Table 3. Cure characteristics and mechanical properties

Parameter	Mix Nos					
	1	2	3	4	5	6
Minimum torque, dN.m	0.39	0.35	0.40	0.24	0.40	0.37
Maximum torque, dN.m	9.43	8.09	8.81	5.97	5.07	5.25
Δ, Rheometric torque, dN.m	9.04	7.74	8.41	5.73	4.67	4.88
Optimum cure time (t_{90}) at 150ºC, min	7.33	8.88	7.08	9.17	10.58	9.54
Scorch time (t_{s2}) at 150ºC, min	2.17	3.09	2.35	3.07	4.91	4.07
Cure rate, dN.m/min	1.47	1.08	1.16	0.48	0.41	0.43
100 % Modulus, MPa	1.1	0.9	1.1	1.2	1.2	1.2
200 % Modulus, MPa	2.1	1.6	2.0	2.4	2.4	2.5
300 % Modulus, MPa	3.5	2.5	3.3	4.9	4.8	5.1
Tensile strength, MPa	28.1	25.1	27.0	23.6	24.7	24.9

Elongation at break, %	707	748	720	644	648	649
Tear strength, N/mm	71.2	67.3	70.5	57	50	52
Hardness, Shore A	50	49	50	41	41	41
Abrasion loss, mm^3	125	130	126	132	140	141
Rebound resilience, %	68.5	68.8	67.3	65.2	65.2	65.2
Heat build-up, ΔT ºC	11	11	12	12	12	12
Compression set, %	22.8	24.2	25.9	24.3	25.8	26.3
Dematttia flexing						
Crack initiation, K/cycles	74.4	74.4	86.9	22.4	19.4	28.1
Crack failure, K/cycles	132.5	135.9	181.6	36.0	35.1	40.8

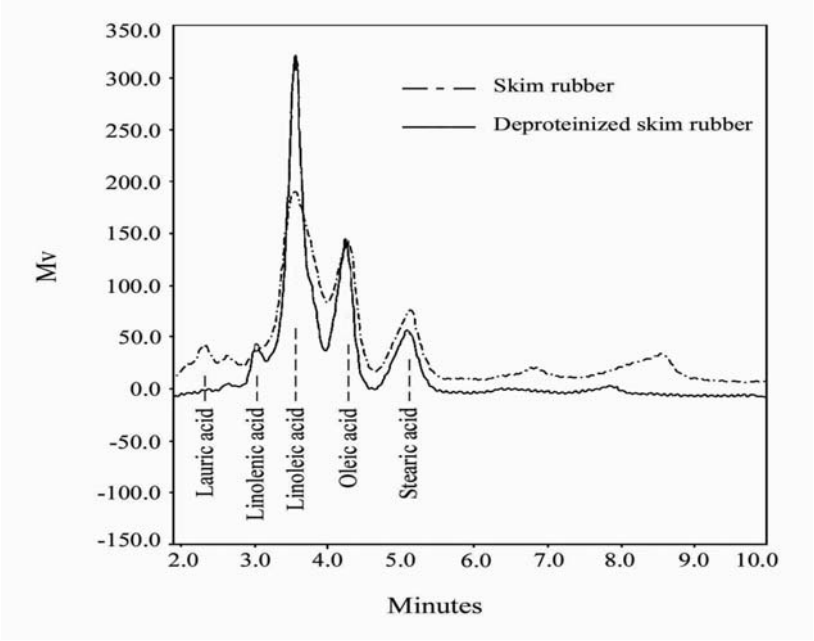

Fig.1. Chromatogram showing the fatty acids in skim rubbers

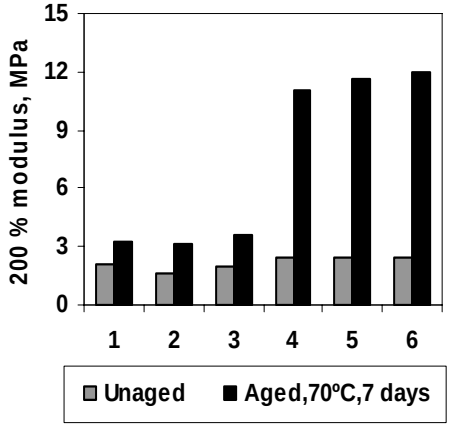

Fig.2 Effect of ageing on 200 % modulus

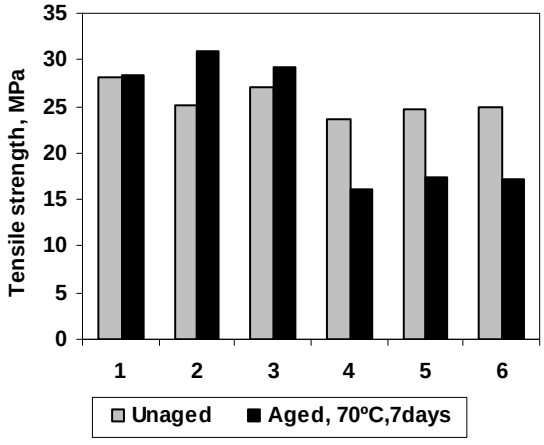

Fig.3 Effect of ageing on tensile strength

Reinforcement studies – Effect of thiophene-plasma coating of silica on the performance in EPDM, SBR and NBR

M. Tiwari, R. N. Datta, A. G. Talma, J. W. M. Noordermeer, W. K. Dierkes

Department of Elastomer Technology and Engineering, University of Twente,
7500 AE Enschede, The Netherlands
and
Wim J. Van Ooij
Department of Chemical and Materials Engineering, University of Cincinnati,
Cincinnati, OH 45221-0012, USA
Email: J.W.M.Noordermeer@utwente.nl

Abstract

The filler surface chemistry is a crucial factor for the level of dispersion and filler-polymer interaction in rubber, thus determining the vulcanizate properties. Plasma-polymerization allows tailoring the surface chemistry without influence on the bulk properties. Thiophene was used as monomer in this study for its sulfur moiety, and the plasma-thiophene (PTh) coated silica was blended with EPDM, SBR and NBR, as these polymers differ in polarity and unsaturation. As reference, untreated and silanized silica were used.

In EPDM, plasma-polymerization onto silica results in a lowering of the filler-filler interaction compared to untreated silica due to a better match of the surface energy between filler and polymer. The PTh-silica shows the best dispersion compared to untreated and silanized silica. The final properties of the PTh-silica reinforced material are improved compared to untreated silica reinforced EPDM.

In SBR and NBR, the plasma-treatment again results in a better dispersion as well as a higher bound rubber content. In terms of mechanical properties, the PTh-silica results in a better performance compared to untreated and even to silanized silica.

This study shows that thiophene plasma-polymerized silica can act as a replacement for the silica-silane system; and in some cases it performs even better than the silanized silica.

Introduction

The reinforcing effect of fillers depends on the nature of filler-rubber interactions as well as the filler dispersion in the elastomeric matrix. Both processes are linked and controlled by the primary particle size and its distribution, the shape, structure and site energy distribution as well as functional groups on the filler surface[1,2]. Silica has been recognized as an important filler for rubber reinforcement and is used as a partial or even complete replacement for carbon black. However, silica has a high density of hydrophilic silanol groups on its surface, resulting in a strong filler-filler interaction and a poor filler-polymer interaction. Therefore, silica tends to form agglomerates as a secondary structure by hydrogen bonds between silanol groups on the silica surface. To produce silica-filled rubber compounds with high performance, the compatibility between silica and rubber has to be enhanced. For this purpose, a silane coupling agent is

commonly used to chemically modify silica surfaces and promote interactions between hydrophilic silica surfaces and the hydrophobic rubber phase[3-5]. In the conventional technology, the reaction between silica and the silane coupling agent takes place in the rubber-filler blend during mixing. This in-situ modification requires a number of precautions regarding the mixing sequence and the mixing temperature, as well as careful adjustment of mixing conditions for every silane containing compound.

Recently, plasma polymerization has emerged as a surface modification technique for polymers, metals and powders. Van Ooij et al.[6] have reported plasma modification of silica, which changes the surface chemistry of the filler.

In the previous work[7,8], the effect of plasma-acetylene coated silica on the properties of S-SBR, EPDM, NBR compounds and their blends have been studied. In this study, the silica is modified with plasma-thiophene, which has a sulphur moiety in its cyclic structure. The effect on processing behavior and properties of EPDM, SBR and NBR compounds containing plasma-thiophene (PTh) coated silica will be evaluated.

Experimental

For the surface modification of silica powders, a radiofrequency (13.56 MHz) electrodeless tumbler plasma reactor is used, based on a horizontally mixing principle and with a capacity of 350 g/batch. The plasma polymerization was carried out after charging 100 g of dried silica (Ultrasil VN3) into the reactor, evacuating the reactor to 13 Pa and introducing thiophene gas. The operating pressure, which was determined by the thiophene vapour flow, was 20 Pa. The power and treatment time were 100 Watts and 90 minutes.

The general characterization techniques used for treated silica powders are an immersion test, water penetration measurements[9], Thermo-Gravimetric Analysis (TGA), Time-of-Flight Secondary Ion Mass Spectroscopy (ToF-SIMS) and Energy Dispersive X-ray Spectrometry (EDX).

Mixing of the filler-rubber compounds was done in an internal mixer; the curatives were added on a two roll mill. The compounds were characterized by measuring the Payne effect (RPA 2000) and bound rubber content[10,11]. The cure characteristics (RPA 2000) were measured, and the reinforcement parameter (α_F)[12] as well as the mechanical properties (ISO-37) were determined. As references, untreated and silane-treated silica were used.

Results and Discussion

Immersion and water penetration tests show a change in the surface energy after the plasma treatment of the silica filler: The polythiophene (PTh)-film coated aggregates are more hydrophobic and show a lower surface energy.

The weight-loss measured by TGA was higher for silica after plasma-thiophene treatment as shown in Fig. 1: this indicates film deposition on the surface of the silica.

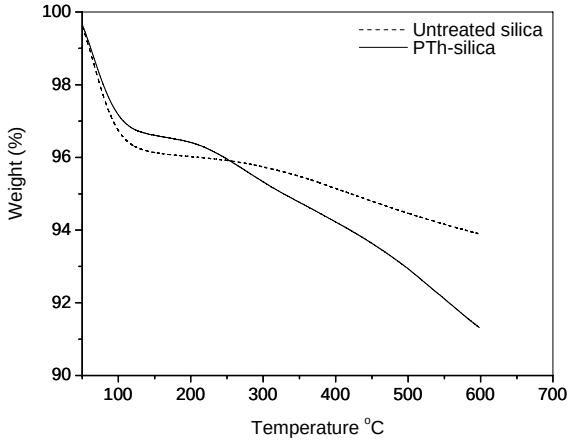

Fig. 1: *TGA analysis of untreated and plasma-polymerized-polythiphene coated silica*

Positive ToF-SIMS spectra of the untreated silica sample showed no specific peaks in the low mass region such as $C_2H_3^+$, $C_{10}H_{10}^+$ and no cluster peaks in the higher mass region. In the negative spectra, no specific peak of sulphur at 32 amu is found. However, the thiophene monomer treated sample (PTh) shows the specific plasma-polymerized hydrocarbon peaks in the low mass region and strong polythiophene cluster peaks in the higher mass region, indicating a good polythiophene surface coating on the silica powders. The presence of sulphur at 32 amu in the negative spectra also confirms the deposition of PTh-film on the surface of silica.

Elemental analysis by EDX also confirms the deposition of a PTh-film on the silica surface, as the elemental carbon and sulphur content increased.

The PTh- and silane-modified silica filled EPDM, SBR and NBR showed a lower Payne effect compared to the unmodified silica filled rubbers, indicating a lower filler-filler interaction.

The reinforcement parameter[12] was lowered for the PTh-silica filled matrices; this indicates a better dispersion compared to untreated as well as silane modified silica filled samples. The PTh-silica filled EPDM shows the lowest value of the reinforcement parameter compared to both other silica's. The PTh-silica filled SBR and NBR show a higher bound rubber

content due to higher filler-polymer interactions compared to untreated and silane-treated silica. PTh- and untreated-silica filled EPDM show similar levels of bound rubber content, lower than the silane-treated silica.

PTh-silica filled EPDM (EPTh), SBR (SPTh), and NBR (NPTh) show self-curing behavior as shown in Fig. 2. This self-curing behaviour is due to the presence of sulphur moieties in the deposited PTh-film on the silica surface.

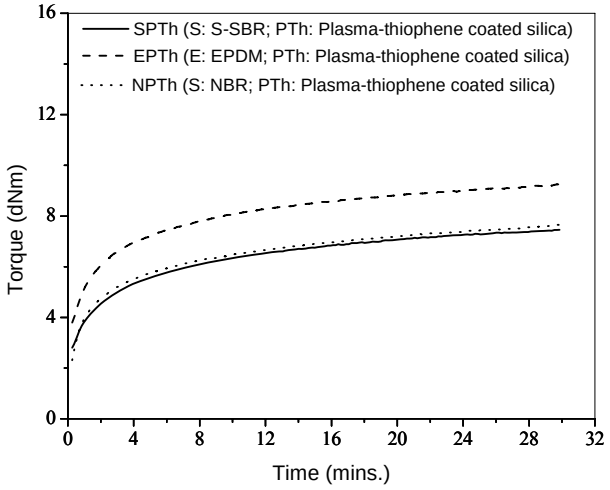

Fig. 2: *Self-curing behaviour of PTh-silica filled SBR, EPDM and NBR*

For all three polymers, tensile strength is increased significantly due to the PTh-treatment. However, for SBR (SPTh) the addition of PTh-coated silica results in higher tensile strength as well as a higher modulus at 300% elongation and lower elongation at break values as shown in Fig. 3. This can be explained by a better dispersion and filler-polymer interaction as well as a higher crosslink density.

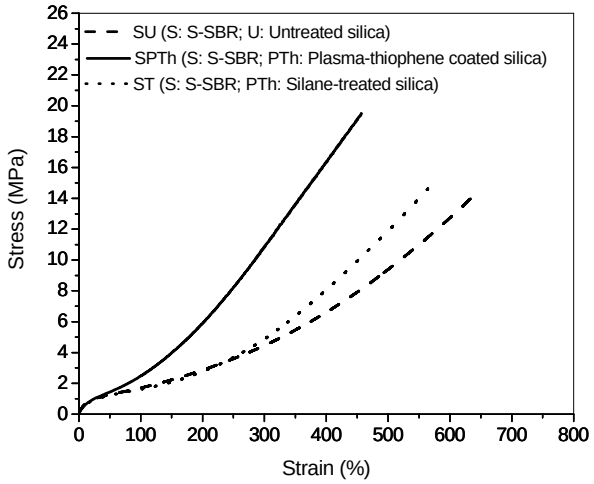

Fig. 3: *Tensile properties of untreated, PTh- and silane-treated silica filled SBR*

In a PTh-silica filled EPDM, the material shows higher tensile strength and elongation at break values due to a better dispersion and compatibilization with the polymer. However, lowering of the modulus in EPDM shows the formation of a less dense network due to a lower number of unsaturation sites in the polymer chain structure. In NBR, the PTh-treated silica showed improved tensile properties resulting from an improved morphology and stronger network compared to untreated and silane-treated silica.

Conclusions

Silica as reinforcing filler for elastomers can be plasma-coated under vacuum conditions. As a consequence, it shows a significant decrease in surface energy due to film deposition.

It is possible to improve the dispersion of the filler in different polymers by matching the surface energies. The properties of the silica surface can be tailored by depositing different functional groups by plasma-polymerization, which leads to an improvement of the final properties of filled polymers.

Acknowledgements

The support of STW, Hexagon Polymers and Timcal Graphite & Carbon is greatly acknowledged.

References

1. A. Schroeder; M. Klueppel; R. H. Schuster; J. Heidberg *Carbon* 2002, *40*, 207.
2. W. M. Hess; C. Herd; P. C. Vegvari *Rubber Chem. Technol.* 1993, *66*, 834.
3. L. A. E. M. Reuvekamp; J. W. ten Brinke; P. J. Van Swaaij; J. W. M. Noordermeer *Rubber Chem. Technol.* 2002, *75*, 187.
4. R. Alex; N. M. Mathew; P. P. De; S. K. De *Kautsch. Gummi Kunstst*. 1989, *42*, 674.
5. E. M. Dannerberg *Rubber Chem. Technol.* 1975, *48,* 410.
6. W. J. van Ooij; N. Zhang; S. Guo; S. Luo *Paper presented at Functional Fillers and Fibers for Plastics 98*, P. R. China 1998, June 15-17.
7. M. Tiwari; W. K. Dierkes; J. W. M. Noordermeer; W. J. van Ooij *Rubber Chem. Technol. 2008, 81*, 276.
8. M. Tiwari; W. K. Dierkes; J. W. M. Noordermeer; W. J. van Ooij *Polym. Adv. Technol.* 2008, *19*, 1-12.
9. N. Inagaki; S. Tasaka; H. Abe *J. Appl. Poly. Sci.* 1992, *46*, 595.
10. S. Wolff *Rubber Chem. Technol.* 1981, *55*, 967.
11. J. L. Leblanc; P. Hardy *Kautsch. Gummi Kunstst*. 991, *44*, 1119.
12. S. Wolff *Kautsch. Gummi. Kunststoffe* 1970, *23*, 7.

Effect of plasticizer, filler and solvent swell on polyurethane elastomers

Santosh K Gurunath[a]*, M. Rengasamy[b] and V. Sivasubramanian[a#]

[a] Department of Chemical Engineering, National Institute of Technology Calicut, Kerala – 673 601, India.
[b]Department of Petrochemical Technology, Bharathidasan Institute of Technology, Tiruchirappalli -620 024, India.
Email: siva@nitc.ac.in

Abstract

Polyurethane elastomers are developed using different types of isocyanate terminated polyether based prepolymers (A, B and C) with four types of multifunctional hydroxy derivated curatives (X1, X2, X3 and X4) and selected processing additives namely plasticizer and filler. The polyurethane elastomers are developed with a view to utilize them in high performance print roller applications, with improved strength and solvent resistant characteristics. The properties like pot life, hardness, tensile strength, modulus, tear strength, compression set, density and solvent resistance of these polyurethane elastomers are studied in the absence of additives and also in the presence of additives. Among the polyurethane elastomers prepared, the product obtained from prepolymer C with curative X3 exhibits better strength properties and solvent resistant characteristics than those from other products. Incorporation of additives (plasticizer and filler) improves the performance characteristics of polyurethane elastomers. However, the degree of improvement varies based on the nature of reactants involved.

Keywords : Polyurethane elastomers, Plasticizers and Solvent swell

Introduction

Polyurethanes are available as rigid, flexible and structural foams, elastomers, coatings, adhesives, casting resins and fibres[1]. These can be manufactured in the wide range of varying densities from 6 kg/m^3 to 1220 kg/m^3 and polymer stiffness from very flexible elastomers to rigid hard plastics. Polyurethane has high porosity, low weight to volume ratio, good thermal and acoustic properties, good resilience, abrasion resistance and oil resistance. This material finds wide industrial and engineering applications. Polyurethane is a product[2] of the poly addition of an isocynate and an alcohol. Reaction is an exothermic.

$$nR – NCO + n\ HO –R' \rightarrow R – [NHCOO]_n – R'$$

There are many kinds of poly isocynates and polyols of different molecular weights and functionalities are used and each one has its one particular property to give a different product for definite end use. Polyurethane elastomers are used in many fields like automobile, textile, oil, mining, electronic, and other engineering industries. There is a very good future of polyurethane elastomers. They are versatile engineering materials designed to provide properties that are not obtained from conventional rubbers, metals, and plastics. They have higher oil and solvent resistance and better aging properties than most general purpose rubbers and plastics. They have greater abrasion and tear resistance than neoprene or natural rubber, greater load bearing capacity; extensibility and impact character of polyurethane elastomer are also greater than those of most plastics. They have a wide range of hardness from soft rubbers to rigid plastics[3-10]. The objective of the present study is to prepare polyurethane elastomer and to study the performance characteristics.

Experimental Procedure

Liquid Castable Polyurethane Elastomer

Cast elastomers are usually slightly cross linked thermoset polymers. In the production of urethane elastomer the heated prepolymer is mixed with a selected curative in specific proportion. Prepolymers contain terminal isocyanate (NCO) groups, which react chemically with hydroxyl (OH) or amine (NH_2) groups in the curative. The mixture is poured into a heated mould where the components rapidly react to form a solid elastomeric article.

Reaction

$$\underset{\text{Polyol}}{HO - A - OH} + \underset{\text{Diisocyanate}}{OCN - R_1 - NCO}$$

$$\downarrow$$

$$OCN - R_1 - HNCOO - A - OCONH - R_1 - NCO + (n\text{-}1)HO - R_2 - OH$$

Prepolymer — Alcohol

$$\downarrow$$

$$-\left[-O - A - OCONH - R_1NHCO - (O - R_2 - OCONH - R_1 - NHCO-)_{n-1}\right]-$$

Polyurethane Elastomer

The flexibility is imparted by the long chain glycols, whereas the rigidity is obtained by short chain glycols. There are two types of polyurethane elastomers, depending upon the polyol used. These are called polyether based polyurethane elastomers and polyester based polyurethane elastomer. Polyether based polyurethane elastomers give lower densities and better hydrolytic stability, fungus resistance and electrical properties. Polyester based polyurethane elastomers result in higher densities – better tear and abrasion resistance and less oil and solvent absorption. Polyesters are also less easily oxidized and resist higher temperatures than polyethers.

PROCESSING

Process Conditions

Reaction Temperature	70 – 80°C
Stoichiometry	95%
Mixing Time	3 min
Oven Temperature	120°C
Cure Condition	16 hours at 120°C
Post-cure condition	Two weeks at room temperature

Procedure

The desired amount of prepolymer is weighed into a suitable container and the prepolymer is heated to 70 – 80°C. The over heating should be avoided. The required amount of plasticizer and filler are added in the case of filled products. The reaction is carried out in vacuum and with suitable amount of curatives. The mixed reactants are degassed and poured into a preheated (120°C) mould and is allowed for 16 hours to complete the reaction (curing). Further, the product is kept for two weeks time at room temperature for post curing before being tested.

Results and Discussion

Properties of Unplasticized and Unfilled Polyrethane Elastomer

The curing efficiency of four types (X1, X2, X3, and X4) of hydroxyl terminated curatives have been tested on three types of polyether based isocyanate terminated prepolymer (A,B and C) with different functional additives. Among the curatives, the curative X1 imparts highest pot life (working time) towards the polyether prepolymers (A, B and C) tested in this investigation, whereas the curative X4 imparts shortest pot life and other two curatives X2 and X3 lie between these two extremes. This behavior may be attributed to the reactive nature and the percentage of isocyanate groups and hydroxyl groups present in the polyether prepolymers and curatives respectively. The pot life for prepolymer A obtained, when mixed with curatives X1, X2, X3, and X4 are 75, 62, 47 and 29 minutes at 100°C respectively.

Hardness of the cured polyurethane elastomers is determined using the durometer and the results are obtained for different combinations of prepolymer and curatives. Hardness, shore A obtained for the polyurethane elastomer resulted from prepolymer A with curatives X1, X2, X3 and X4 are 57, 54, 53, and 45 respectively. Among the polyurethane elastomer obtained, the product from prepolymers A with curative X1 results in highest hardness (shore A57) which may be explained due to the influence of higher cross link density resulted from the molecular structure. Similarly, among the prepolymers A, B and C, the product polyurethane elastomer obtained from prepolymer C with corresponding curative imparts higher hardness, shore A69, than prepolymers A and B, due to higher percentage of isocyanate and hydroxyl groups, which in turn enhances the crosslink density.

Tensile strength determined using tensile tester for the different polyurethane elastomers are presented. Tensile strength results are merely reflections of hardness values, the product from prepolymer C with curative X1 possess higher tensile strength (42.7 kg/cm^2) than from other combinations of prepolymers A and B curatives X2, X3 and X4. Percentage elongation results obtained for different polyurethane elastomers are studied. The product resulted from prepolymer B with curative X4 exhibits highest elongation (500%), while for the product from prepolymer C with curative X1 gives lowest value (120%). The percentage elongation values are inversely proportional to the hardness and link density of the products.

Modulus, tear strength, and density for different combinations of elastomers are studied. All these values increase with increasing crosslink density and hardness due to higher percentage of reactive groups in the prepolymers. Compression set values for the polyurethane elastomers tested after 22 hours at 70°C are given. The elastomer from the prepolymer A with curative X1 exhibits lowest value of compression set 1.6%, while 3.19% is obtained for the product from prepolymer B with X1, these results reveals that the former AX1 imparts better dimensional stability than the latter BX1.

Solvent resistance characteristics of different combinations of elastomers are carried out by immersing them in different organic solvents for the period of 7 days. The solvent resistant characteristics are expressed in the form of percentage weight gain of the elastomer. In this respect, the product from CX1 gives the lowest value (135%) and the product from BX4 gives the highest value (505%), this is due to nature of molecular structure and types of secondary forces involved. Among the solvent system used, ethyl acetate influences more swelling of elastomers than others due to dipole-dipole attraction. The moisture absorption characteristics of different elastomer combinations are also studied. The product from CX4 absorbs lowest percentage (1.5%) of moisture; whereas the product from AX1 absorbs highest percentage (3.1%) of moisture. This behavior is due to the number of hydrogen bonds involved in the elastomer structure.

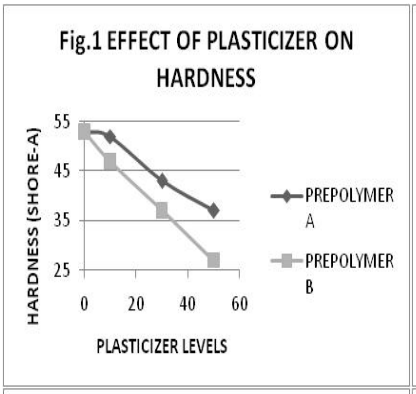
Fig.1 EFFECT OF PLASTICIZER ON HARDNESS
HARDNESS (SHORE-A)
55
45
35
25
0
20
40
60
PLASTICIZER LEVELS
PREPOLYMER A
PREPOLYMER B

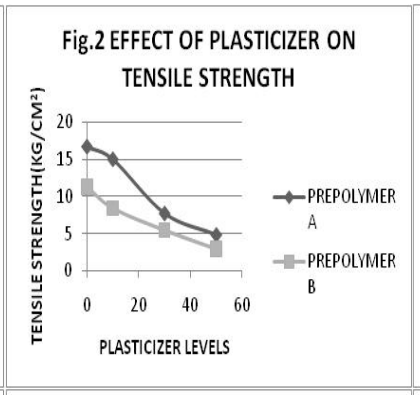
Fig.2 EFFECT OF PLASTICIZER ON TENSILE STRENGTH
TENSILE STRENGTH(KG/CM²)
20
15
10
5
0
0
20
40
60
PLASTICIZER LEVELS
PREPOLYMER A
PREPOLYMER B

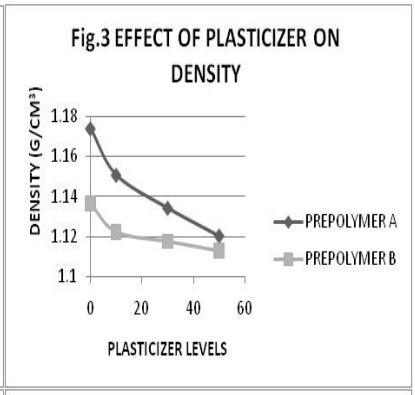
Fig.3 EFFECT OF PLASTICIZER ON DENSITY
DENSITY (G/CM³)
1.18
1.16
1.14
1.12
1.1
0
20
40
60
PLASTICIZER LEVELS
PREPOLYMER A
PREPOLYMER B

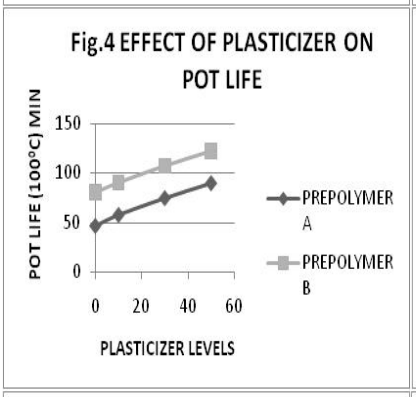
Fig.4 EFFECT OF PLASTICIZER ON POT LIFE
POT LIFE (100°C) MIN
150
100
50
0
0
20
40
60
PLASTICIZER LEVELS
PREPOLYMER A
PREPOLYMER B

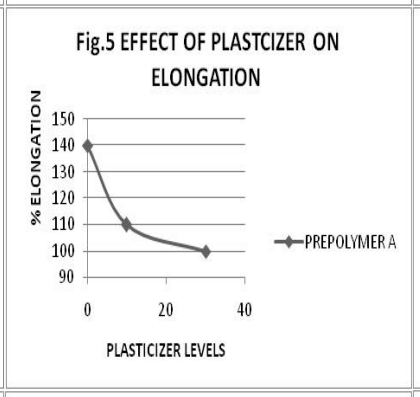
Fig.5 EFFECT OF PLASTCIZER ON ELONGATION
% ELONGATION
150
140
130
120
110
100
90
0
20
40
PLASTICIZER LEVELS
PREPOLYMER A

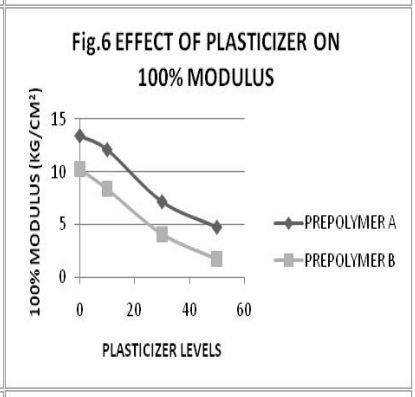
Fig.6 EFFECT OF PLASTICIZER ON 100% MODULUS
100% MODULUS (KG/CM²)
15
10
5
0
0
20
40
60
PLASTICIZER LEVELS
PREPOLYMER A
PREPOLYMER B

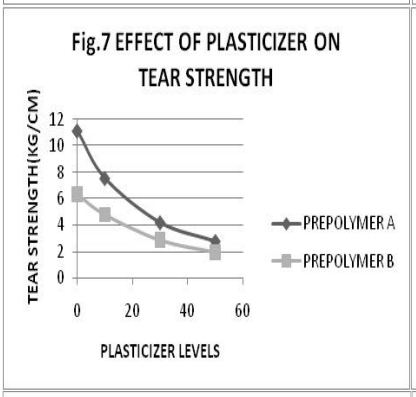
Fig.7 EFFECT OF PLASTICIZER ON TEAR STRENGTH
TEAR STRENGTH(KG/CM)
12
10
8
6
4
2
0
0
20
40
60
PLASTICIZER LEVELS
PREPOLYMER A
PREPOLYMER B

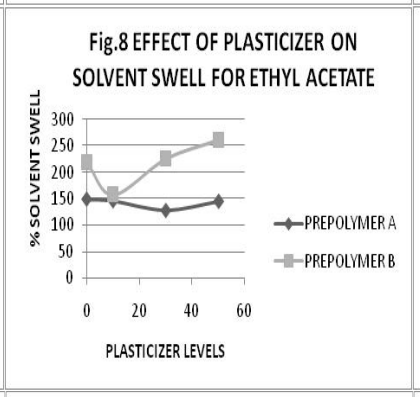
Fig.8 EFFECT OF PLASTICIZER ON SOLVENT SWELL FOR ETHYL ACETATE
% SOLVENT SWELL
300
250
200
150
100
50
0
0
20
40
60
PLASTICIZER LEVELS
PREPOLYMER A
PREPOLYMER B

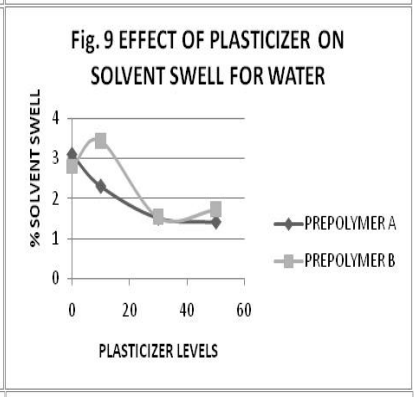
Fig. 9 EFFECT OF PLASTICIZER ON SOLVENT SWELL FOR WATER
% SOLVENT SWELL
4
3
2
1
0
0
20
40
60
PLASTICIZER LEVELS
PREPOLYMER A
PREPOLYMER B

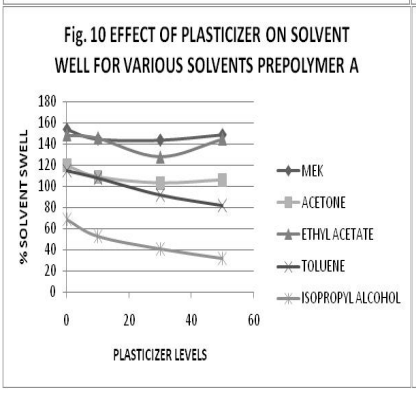
Fig. 10 EFFECT OF PLASTICIZER ON SOLVENT WELL FOR VARIOUS SOLVENTS PREPOLYMER A
% SOLVENT SWELL
180
160
140
120
100
80
60
40
20
0
0
20
40
60
PLASTICIZER LEVELS
MEK
ACETONE
ETHYL ACETATE
TOLUENE
ISOPROPYL ALCOHOL

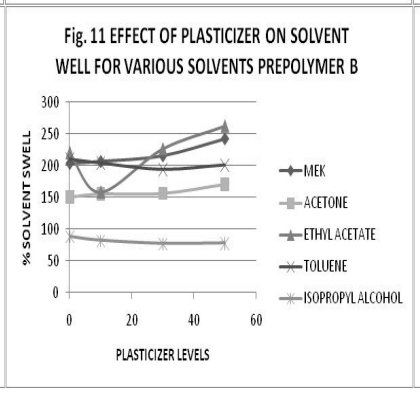
Fig. 11 EFFECT OF PLASTICIZER ON SOLVENT WELL FOR VARIOUS SOLVENTS PREPOLYMER B
% SOLVENT SWELL
300
250
200
150
100
50
0
0
20
40
60
PLASTICIZER LEVELS
MEK
ACETONE
ETHYL ACETATE
TOLUENE
ISOPROPYL ALCOHOL

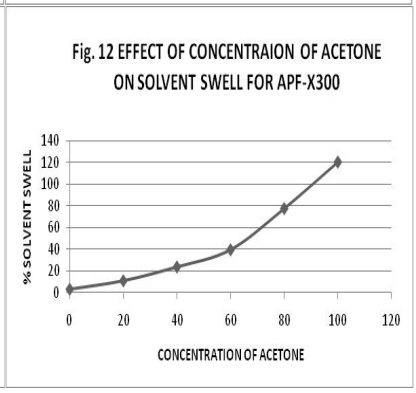
Fig. 12 EFFECT OF CONCENTRAION OF ACETONE ON SOLVENT SWELL FOR APF-X300
% SOLVENT SWELL
140
120
100
80
60
40
20
0
0
20
40
60
80
100
120
CONCENTRATION OF ACETONE

Effect of Plasticizer

The polyurethane elastomers resulted from prepolymers A and B with curative X3 are blended with varying levels (10phr, 30phr and 50phr) of plasticizer are studied. The incorporation of plasticizer influences the properties of elastomer. The increase in level of plasticizer decreases the mechanical characteristics of polyurethane elastomer. For example, the hardness of the elastomer product AX3 falls from 53 to 37 by increasing the concentration of plasticizer from 0% to 50%. Similarly the hardness of product BX3 falls from 53 to 27 for the same level of plasticizer concentration. The plot of varying concentration of plasticizer against hardness of the polyurethane elastomer (AX3 and BX3) is given in figure 1. The hardness decreases with increase in plasticizer level.

Tensile strength, density, modulus and tear strength are also in the same trend as shown in figures 2, 3, 6 and 7. The strength, modulus and density decreases with increase in plasticizer concentration. The increase in the plasticizer level influences the pot life of the products. The plot of varying level of plasticizer against pot life of the polyurethane elastomer (AX3 and BX3) is given in Figure 4. The pot life increases with increase in plasticizer concentration. The increase in plasticizer concentration influences the elongation for the product of BX3, but it is reversible for the product of AX3 (Figure 5). This is due to the nature of prepolymer A and this behavior may be explained due to the anti-plasticization effect observed with the reactants involved. Generally 30 phr plasticized polyurethane elastomer gives higher solvent resistance than 10phr and 50phr plasticizer concentration.

Properties of Filler on Plasticized Polyurethane Elastomer

Polyurethane elastomers resulted from prepolymers A, B, and C with curatives X3 are incorporated separately with 30phr and 50phr plasticizers and 60phr filler, in order to improve their performance characteristics. The hardness, tensile strength, tear strength, density, elongation and solvent resistant characteristics of additive blended polyurethane elastomers are studied. The incorporation of filler in the plasticized polyurethane enhances the hardness, tensile strength, modulus, density, tear strength and solvent resistance. For a particular level of prepolymer the pot life increases, when additives are added. For example the pot life for unfilled product from AX3 is 45 minutes. Whereas the same product filled with 60 phr filler and 50 phr plasticizer gives 85 minutes. The enhancement of pot life is due to retardation of reactive functional groups.

The addition of filler (60phr) to the product AX3 increases the hardness from 43 to 61, whereas the same product with 60 phr filler and 50 phr plasticizer enhances hardness from 37 to 52. The strength properties (tensile strength, modulus, tear strength) of plasticized (30 phr) elastomer, namely for the product from AX3, the tensile strength increases from 7.6 kg/cm^2 to 22.1 kg/cm^2, modulus increased from 7.2 kg/cm^2 to 18.2 kg/cm^2, and tear strength from 4.18 kg/cm to 8.41 kg/cm respectively.

The increase in strength properties is due to the reinforcement effect of filler and the formation of secondary bonding with polar groups of polyurethane elastomers. The results obtained from the solvent treatment reveals that the incorporation of filler improves the solvent resistant characteristics. For example 30phr plasticized product AX3, the swelling in ethyl acetate for 7 days gives 128% whereas the same product filled with 60phr filler in the same solvent for the same period gives swelling of 69%.

Conclusions

The different combinations of polyurethane elastomers are prepared using prepolymers A, B and C with curatives X1, X2, X3 and X4. In order to utilize the product for the print roller applications, the properties i.e., hardness, pot life, tensile strength, modulus, tear strength, elongation, density, compression set and solvent resistance are studied by standard methods. The polyurethane elastomer obtained from

prepolymers having higher percentage of reactive groups impart better mechanical properties and solvent resistant characteristics. The effect of plasticizer and filler addition on polyurethane elastomeric products is also studied. Both plasticizer and filler addition improved the performance characteristics of the products. The data resulted from various studies suggest that the product CX3 possess better characteristics than other products, required for print roller applications.

References

1. George Woods, The ICI Polyurethanes Book, John Wiley & Sons, Singapore, 1987, 10-12, 37-46, 50-52, 175-196.
2. Sayih, A.A.R. and Shah. T.M, Popular plastics, 1974, July, 17-21.
3. Buist. J.M. and Gudgeon.H, Advances in Polyurethane Technology, Elsevier Publishing Company, London, 1968, 25-62.
4. Hepburn.C, Polyurethane Elastomer, Second edition, Elsevier Applied Science, London, 1991, 122-123, 161-163, 405, 199-220.
5. Kirk and Othmer, Encylcopedia of Chemical Technology, Third Edition, Wiley and Inter Science Publication, 1984, 23, 576-608.
6. Kothandaraman.H. and Venkatarao.K, J. Applied Science, 1990, 39, 943-954.
7. Maurice.E, Bailey, J. of Chemical Education, 1971, 48, 12, 809-813.
8. Pegoraro.M, Landro, L.D, Severini. F,Cao.N and Donzelli. P, J. Polymer Science, Part B: Polymer Physics, 1991, 29, 365-370.
9. Reji John, E., Thachil, T., Racindran, P., Neelakantan, N.R. and Subramanian, N., 1991, Polymer Plastic Tech. Eng., 30, 2,3, 227-238.
10. Ullman's Encyclopedia of Industrial Chemistry, VCH Publication, 1986, A21, 665-716.

Effect of electron beam curing on mechanical and electrical properties of silica filled silicone and FKM rubber and its comparison with chemical curing

R.K. Ramamoorthy, K. Naskar, D Khastgir*
Rubber Technology centre, IIT Kharagpur-721302, INDIA

Email: dkhastgir@yahoo.co.uk, khasdi@rtc.iitkgp.ernet.in

Introduction:

The treatment of polymers by an electron beam has been reviewed different authors [11-14]. It is observed that , in general, rubbers can be cross-linked using an electron beam(EB) , where as some plastics like polypropylene and poly(vinyl chloride) have a tendency to degrade[13,14].

The effects of electron beam (EB) irradiation on mechanical and electrical properties of Silicone rubber (MQ), and Fluro rubber (FKM) compounds filled with Precipitated and Fumed Silica filler have been reported in the present paper. The effect of different degree of radiation dosage on both electrical and mechanical properties was investigated. Some comparison has been made between properties of EB cured vulanizates of theses two rubbers with Peroxide cured Silicon rubber and Calcium hydroxide cured FKM rubber. The type of silica filler used affects both electrical and mechanical properties of EB cured vulcanizates.

Experimental:

All mixing was carried out in laboratory size open mixing mill in accordance with the formulations given in table1-3 under identical condition of time, temperature and friction ratio. Some samples were subjected to electron beam curing with various dosage of radiation level and other samples are chemically cured up to optimum cure time using electrically heated press. Gel fraction and different mechanical and physical properties were measure in accordance with standard ASTM methods.

Table1.Formulation for Electron Beam Irradiation Cure

Ingredient	Q	Q	FKM	FKM
Precipitated Silica (phr)	20	-	20	-
Fumed silica (phr)	-	20	-	20
TQ (phr)	2	2	2	2
Sunpar Oil (phr)	2	2	2	2

Table2. Formulation for Peroxide cure

Ingredient	Q	Q
Precipitated Silica(phr)	20	-
Fumed silica (phr)	-	20
TQ (phr)	2	2
Sunpar Oil (phr)	2	2
DCP	5	5
Si-69	2	2

Table3.Formulation for Specific curing system

Ingredient	FKM	FKM
MgO (phr)	6	6
Precipitated Silica(phr)	20	-
Fumed silica (phr)	-	20
Sunpar Oil (phr)	2	2
Calcium hydroxide	3	3

Result and discussion;

Gel Fraction

The gel fraction is higher for silicone rubber compared to FKM rubber and change in gel fraction with radiation dosage is more pronounced in precipitated silica filled systems compared to fumed ones where changes are only marginal. The gel fraction level is almost same for chemical curing and EB curing methods for both the rubbers as presented in Figures 1(a)&1(b).

Mechanical Properties

Hardness

The hardness of both fluorocarbon and silicone rubber when reinforced by precipitated silica and EB cured increase with increasing irradiation dosage up to 15 MRads (figure 2(a)) followed by marginal reversion.

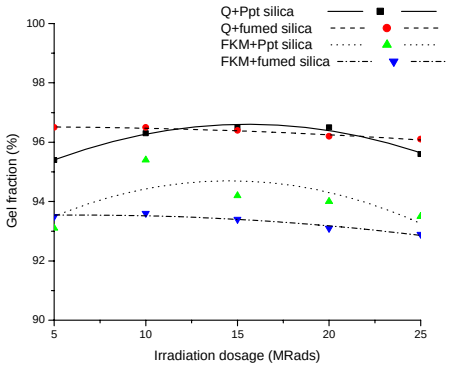

Figure 1 (a): Variation in Gel Fraction with increasing irradiation dosage

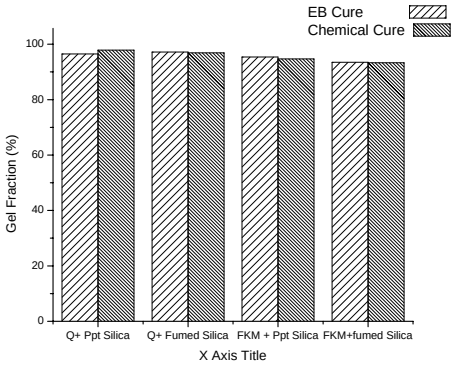

Figure 1 (b): Comparison of best Gel Fraction obtained of irradiated sample with chemical cure

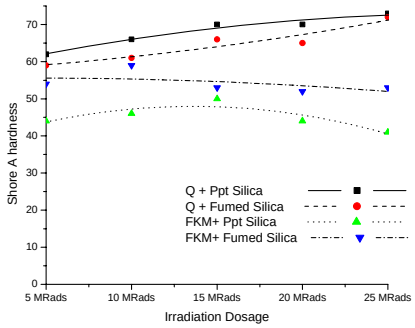

Figure 2 (a): Variation in Shore A Hardness with increasing irradiation dosage

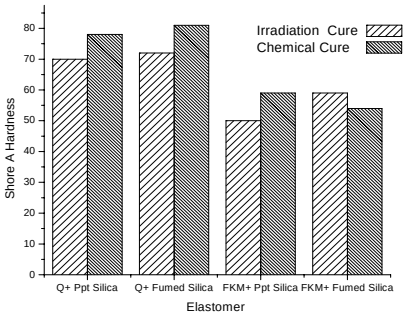

Figure 2 (b): Comparison of highest Shore A Hardness obtained of irradiated sample with chemical cure

The fumed silica filled silicone rubber shows a progressive increment of hardness with increased radiation dosage while slow but progressive decrement of hardness is observed in case of fluorocarbon rubber with same filler.

Generally the hardness of EB cured samples of both rubbers are comparatively lower than those of chemically cured ones (not shown).

Tensile Strength

The effect of EB on tensile strength of silicone rubber is relatively much less compared to that of FKM. Only slight improvement is observed with the increase in radiation dosage up to15Mrad there after some reversion is noted. The reinforcement effect of fumed silica is more than that of ppt silica in case of silicone rubber. However significant improvement of tensile strength is observed for FKM with the increase in radiation around15-20 MRad there after some reversion is noted. The effect ppt silica on reinforcement is more than fumed silica in case of FKM.

On comparison with type of cure the tensile strength for both rubbers is the best when reinforced by precipitated silica and chemically cured while it is the EB cure that gives best tensile strength when reinforced by fumed silica for both the rubbers figure 3(b)

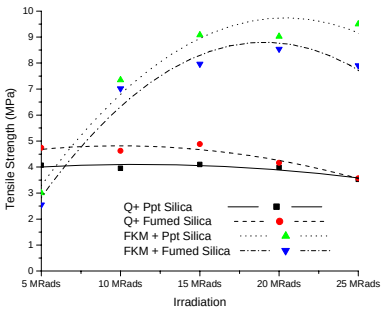

Figure 3 (a): Variation in Tensile strength (MPa) with increasing irradiation dosage

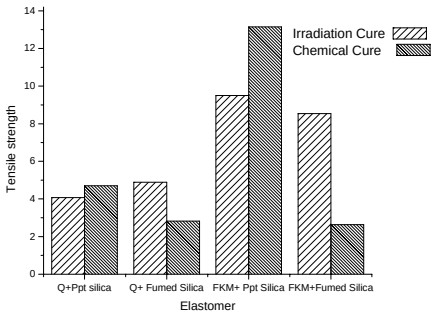

Figure 3 (b): Comparison of highest Tensile strength (MPa) obtained of irradiated sample with chemical cure

Elongation at Break

The elongation at break shows a decreasing trend with increasing irradiation dosage for both rubbers with either precipitated or fumed silica figure 5(a). The rate of decrease in elongation at break is higher in fluorocarbon when compared with silicone rubber. The most interesting observation here is that EB curing shows very high elongation at break for fluorocarbon and very low elongation at break of silicone rubber.

On comparison between types of cure the chemically cured silicone rubber shows higher elongation at break when reinforced with precipitated silica and lower elongation at

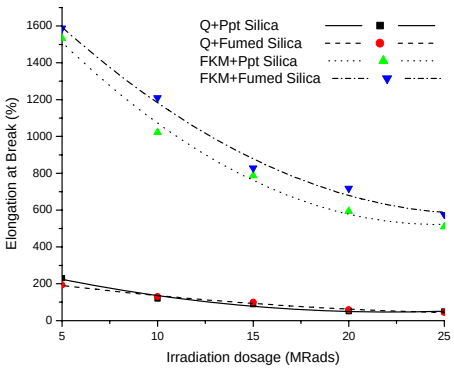

Figure 5 (a): Variation in Elongation at Break (%) with increasing irradiation dosage

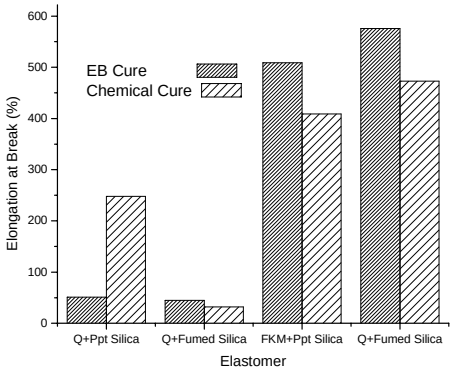

Figure 5 (b): Comparison of lowest Elongation at Break (%) obtained of irradiated sample with other types of cure

break when reinforced with fumed silica (figure 5(b)). The changes are more prominent with precipitated silica and only marginal with fumed silica. In the case of fluorocarbon the elongation at break is higher than chemical cure when EB cured irrespective of type of filler and the amount of increment also similar.

Electrical Properties

DC Volume Resistivity

The DC volume resistivity for all the rubbers shows marginal increase though not substantial with increasing irradiation dosages for both the rubbers with the two different fillers on EB cure. On chemical cure there is increase in resistivity only in the case of silicon rubber with precipitated silica reinforcement while in all other cases there is noticeable drop in resistivity by a small degree (figure 7).

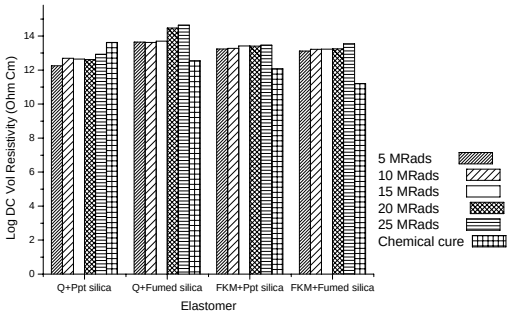

Figure 7: Comparison of Log DC Volume resistivity for different

dosage of Irradiated cure and other types of cure

Conclusion:

The mechanical properties of silicone rubber are not much affected by increasing irradiation dosage up to 15 MRads but any further increase in irradiation leads to marginal loss in properties. The fluorocarbon rubber responds with increasing properties with increasing irradiation dosage up to 20 MRads and any further increase leads to drop in mechanical properties.. The DC volume resistivity for both the rubbers shows marginal increase though not substantial with increasing irradiation dosage .

Reference:

[1] A. Charlesby, Radiat. Phys. Chem. 9 (1977) 17.
[2] N. Studer, IAEA TECDOC-454, 6–8 October 1986, p. 111
[3] Van Drumpt JD. Rubber World 1988; 33:33–41.
[4] Akiba M, Hashim AS. Prog Polym Sci 1997; 22:421–75.
[4] Ogunniyi DS. Progr Rubber Plast Technol 1999; 15(2):95–112.

All-PP composites based on β and α polymorphic forms: mechanical properties

T. N. Abraham and J. Karger-Kocsis

University of Kaiserslautern, D-67663 Kaiserslautern, Germany
Email: thomasnabraham@gmail.com

Abstract
All polypropylene (all-PP) composites were manufactured by exploiting the polymorphic forms of PP, in which alpha (α)-PP tapes worked as reinforcement and beta (β)-PP served as matrix. The mechanical performance of the composite was investigated in a range of frequencies and temperatures using dynamic mechanical thermal analysis (DMTA). The volume fractions of matrix and reinforcement were estimated using optical microscope images. Both the DMTA and the static flexural bending tests revealed that the α-PP tapes acts as an effective reinforcement for the β-PP matrix. Time temperature superposition (TTS) was applied to estimate the stiffness of the composites as a function of frequency ($f = 10^{-9\cdots10^{20}}$) in form of a master curve. The Williams-Landel-Ferry (WLF) model described properly change in the experimental shift factors used to create the storage modulus vs. frequency master curve. The activation energies for the α and β relaxations were also calculated by using the Arrhenius equation.
Key words: single polymer composites, dynamic mechanical thermal properties, polypropylene, all-polypropylene composite, β-modification, α-modification
E-mail: thomasnabraham@gmail.com

1. Introduction
Single thermoplastic composite (also termed thermoplastic homocomposites) have drawn research interest in recent years because of their environmental friendly character. All polypropylene (all-PP) is a single thermoplastic polymer composite which represents an effective alternative to the traditional fibre reinforced composites. Here the matrix and the reinforcement are from the same polymer, thereby supporting the ease of recyclability. Several techniques have been reported for the production of single thermoplastic polymer composite materials, such as film stacking followed by melting [1,2] hot compaction [3], powder and solution impregnation [4]. The basic principle behind all these techniques is to exploit the melt temperature difference between the oriented or highly stretched material (which should act as the reinforcement) and the same material without orientation (overtaking the role of the matrix). Beside recyclability, the interest for single polymer composites is based upon the expectation that a good interfacial bonding can be achieved if matrix and reinforcement are made from the same semi-crystalline polymer [5,6].
One of the promising approaches in the development of all-PP composites is to exploit the polymorphism-related difference in the melting range between the beta(β)- (matrix) and alpha(α)-phases (reinforcement) PPs [2,7]. An all-PP composite has been made in our laboratory with α-PP tapes as reinforcement and β-PP film as the matrix. However, the entirely thermoplastic nature of these composites raises important questions regarding the viscoelastic behaviour at elevated temperatures. To provide information about the viscoelastic properties, various experimental techniques can be used, among which the dynamic mechanical thermal analysis (DMTA) offer adaptable test procedures. Long-term viscoelastic properties of all-PP composite laminate have been investigated by using the time-temperature superposition principle [8,9]. Nevertheless, it is understood that these properties significantly govern the applicability of the material. The main aim of this paper is to investigate the response of a novel all-PP composite to mechanical loading in a broad range of temperature and frequencies. By using the DMTA responses, master curves

can be created to predict the performance of all-PP composites at much lower and higher frequencies than achievable in the laboratory.

2. Materials

The PP tapes used for the manufacture of laminates were produced in our laboratory using twin screw extruder. The temperature zones in the extruder were maintained at 190, 200, 210 and 220 °C from the feeder to nozzle. The die used had a dimension of 10 x 2 mm^2. Characteristics of PP tapes used for the preparation of the laminates are summarized in Table 1. Thin film of beta polymorph rich isotactic PP (β-PP) served as the matrix. The thin film (120μm thickness) were obtained by compression molding β- nucleated PP sheet of Tipplen H 483 F (melt flow index 6.5 g/10 min at 230 °C and 2.16 kg load) at 180 °C for 5 min. The manufacture of the PP laminates involved a two-stage process: winding of the PP tapes in a cross-ply manner (0/90°;CP), and consolidation of the related tape consisting fabric using hot compaction. The schematic of the tape winding process is shown in Figure 1. Before winding the PP tapes a thin β-PP film layer was placed on the surface of a thin steel plate. Using a typical winding machine, supplied by Bolenz & Schaefer Maschinenfabrik (Biedenkopf, Germany), PP tapes were wound from a bobbin onto the same steel plate rotating at a constant speed. After laying one layer of PP tape another layer of β-PP film was placed and the winding direction on the steel plate was changed. The same process continued and the total number of layers of PP tapes and β-PP film was kept four and five respectively. A similar winding process was already adopted for manufacturing CP type all-PP composite from coextruded Pure® tapes [10,11]. All-PP composite laminates were produced by the well known hot compaction method in a hot press (P/O/Weber GmbH, Remshalden, Germany) at a temperature of 160 °C and a holding time of 5 min under high pressure (7 MPa). The time temperature profile during the consolidation is shown schematically in Figure 2.

3. Experimental procedures

The presence of β-PP and the occurrence of β-α transformation were demonstrated by DSC using a Mettler-Toledo DSC821 instrument (Greifensee, Switzerland). In order to demonstrate the difference between the α and β modifications, the first heating scan (T=25 to 200 °C) was followed by a cooling one to T=100 °C, prior to a second heating cycle to T=200 °C. This heating cooling programme was selected based on the recommendation of Varga et al.[12] Microscopic images of the cross-section of the all-PP laminates were captured by a stereomicroscope (Leitz, Germany) equipped with a high resolution digital camera. The IMAGE-C analysis software was used to estimate the void content from the micrographs. DMTA of all-PP composite laminates was performed in dual cantilever flexural mode. Specimen were cut from the composite plates with dimensions of approximately 60mm × 15mm × 2mm (length × width × thickness) in the DMTA Q800 (TA Instruments, New Castle, USA) machine equipped with a data acquisition software. The specimens were cooled to -50 °C. The temperature was allowed to stabilize and then increased by 3 °C, kept 5 min isothermal, until 120 °C. The specimen was subjected to a sinusoidal flexural displacement applying a maximum tensile strain of 0.1% (which was well within the viscoelastic region) at frequencies 0.01 Hz, 0.1 Hz 1 Hz 5 Hz and 10 Hz at all isothermal temperatures. For each frequency, the complex dynamic modulus (E′) and loss factor (tanδ) were recorded. An attempt was made to apply the time temperature superposition (TTS) to the DMTA data measured as function of both temperature (T = -50 °C….+120 °C) and frequency (f = 0.01….10 Hz) using rheology advantage data analysis software provided by TA Instruments. Master curves in form of storage modulus (E′) vs frequency were produced by superimposing the storage modulus vs frequency traces using the TTS principle. A reference temperature (T_{ref} = 22 °C) was used for this superposition (shifting) process. The related shift factor a_T is given by equation (1):

$$a_T = \frac{E'(T)}{E'(T_{ref})} \qquad (1)$$

The shift factors of a master curve have some relationship with temperature. Fitting the experimentally determined shift factors to a mathematical model permits the creation of a master curve in form of storage modulus vs frequency. With a multi-frequency measurement, frequencies beyond the measurable range of the DMTA can be achieved by using the superposition method based on the Williams-Landel-Ferry (WLF) equation [13,14]. For the temperature range above the glass transition temperature, it is generally accepted that the shift factor-temperature relationship is best described by WLF equation:

$$\log a_T = \log\left(\frac{f}{f_0}\right) = \frac{-C_1(T - T_{ref})}{C_2 + (T - T_{ref})} \qquad (2)$$

where C_1 and C_2 are constants. The static flexural properties of the all-PP composites, such as modulus of elasticity and ultimate flexural strength were determined following the DIN EN ISO 178 standard on a Zwick 1445 test machine. Specimens of the same dimensions used for the DMTA test were employed for the three point bending measurement. A support span of 32.8 mm was used in the three point bending setup. The cross-head speed of 1mm/min was applied during the test and the elastic modulus was calculated in the strain range of 0.05-0.25%. Load was applied using a U2A type 10 kN load cell. A preload of 5 N was applied in the beginning of each test and the mean value of five specimens tested was reported.

4. Results and Discussion

DSC traces of all-PP composite and β PP film is represented in Figure 3. The melting temperature of the β modification of isotactic PP ($T_m \approx 154$ °C) homopolymer is lower than that of the reinforcing α-PP tape ($T_m \approx 165$ °C). The DSC trace of the all-PP composite also shows another interesting phenomenon of transformation of β-PP to α-form at temperatures above the melting point of the former. This phenomenon has already been observed by Padden and Keith [15]. Samuels and Yee [16], who have conducted extensive studies on the unit cell of β-polypropylene, have concluded that the transformation from the β to the α form must occur through a melt recrystallization process, since the two unit cells are very different.

A typical dynamic mechanical behaviour of PP tapes, β-PP matrix and all-PP composite laminates at 1 Hz frequency is represented in Figure 4. It shows that at subambient temperature (the glassy region of PP) the stiffness of PP tape is found to be fairly high. With increasing temperature the E′ decreases, as expected. Above 25 °C the stiffness of the tapes drops significantly. Although the tapes lost much of their elastic response above this temperature, their residual stiffness at 120 °C (end of the test) is still higher (E′ = 1 GPa) than that of an isotropic PP. The high stiffness is attributed to the highly oriented crystals and polymer chains in the stretching direction of the tape. This implies that the tape possesses a residual orientation even at this higher temperature. The results also indicates that stiffness of all-PP composite laminate is higher than the matrix (β-PP), confirms the reinforcement effect of α-PP tapes on β-PP matrix. At room temperature the E′ of PP tapes, all-PP composite laminates and β-PP matrix are 4.8, 2.9 and 2.2GPa respectively.

Figure 4 also exhibits the course of tanδ (ratio of E″/E′) with temperature, which shows a maximum at ≈ 80 °C. The maximum tanδ value recorded for the all-PP tape was 0.15. The tanδ peaks represent different relaxation transitions [12]. However, in Figure 3 PP tape does not

resolve any tanδ peak corresponding to the glass-transition of PP ($T_g \approx$ -10 °C – 0 °C), but a more definite tanδ peak is seen corresponding to the α-transition (T_α) at approximately 80°C. Since these tapes are produced by stretching, the amorphous phase becomes highly oriented between the crystalline regions and it has less freedom to be involved in segmental motions [17]. Therefore, in highly oriented PP systems, the magnitude of T_g peaks is greatly reduced compared to isotropic PP. While T_g reflects mobility within the amorphous regions, T_α dictates the onset of segmental motion within the crystalline regions[13,18,19]. The loss factor as a function of temperature for all-PP composite and β-PP matrix are also shown in Figure 4. The result shows a clear tanδ peak corresponding to β relaxation (T_g) near 0 °C for both the β-PP matrix and all-PP composite. The position of T_g remained nearly unchanged but the peak intensity and magnitude decreased significantly which indicates the increase in stiffness as result of reinforcement of β PP matrix.

It has been shown that a simple rule of mixtures can be very useful in helping to understand the in-plane properties of compacted single polymer composites. A model based on a parallel rule of mixtures and knowledge of the properties of the oriented and matrix phases and fraction of the two phases have been reported by Hine et al. [20].The compacted sheet modulus ($E_{\text{compacted sheet}}$) can then be shown simply to be given by equation 3

$$E_{compacted-sheet} = E_{tape}\frac{V_{tape}}{2} + E_{matrix/\,film}\left(\frac{1+V_{matrix/\,film}}{2}\right) \qquad (3)$$

where E_{tape} and $E_{matrix/film}$ are the modulus of the oriented and matrix phases respectively (assuming same chemical composition for both the matrix and reinforcement i.e. PP) and V is the appropriate fraction of each component. The volume fraction of each component is obtained from the optical micrographs shown in Figure 5. Using the IMAGE-C analysis software, the volume fraction of the reinforcing tapes was determined and found to be 50%. The storage modulus value obtained from DMTA for PP tape and β PP matrix at the same strain rate at room temperature were applied in equation for predicting the in-plane modulus of the compacted sheet using equation. The predicted modulus (3GPa) is comparable with the experimental measurements (2.9GPa), and indicates that this simple approach predicts the modulus quite satisfactorily.

Storage modulus for a wider range of frequencies can be obtained by TTS using the data from multi-frequency DMTA tests. Figure 6 show the variation of storage modulus for a range of temperature between -20 °C and 80 °C for the all-PP composites tested at 0.01 Hz, 0.1 Hz, 1 Hz, 5 Hz and 10 Hz, respectively. An increase in the storage modulus for all-PP composite laminates with increasing frequency and decreasing temperature, as expected. The variation of tanδ at different frequencies for the all-PP laminates are shown in Table 2. A remarkable influence of frequency was observed for both the α and β relaxations of the composites. The frequency increase shifted the position of the relaxation region to higher temperatures. The tanδ peaks corresponding to the β and α transitions of all-PP composite laminate were found to be at 4 °C and 97 °C, respectively, at 1 Hz frequency. The T_α peak became broader and less pronounced due to the additional melting region at higher temperatures. Master curves of the storage modulus against frequencies created at a reference temperature of 22 °C were shown in Figure 7 for the β-PP matrix and all-PP composite laminates. From the master curve data, the curve approach a similar plateau value at high frequency, but the terminal region at lower frequencies is more dependent on reinforcement effect of the composite compared with the β-PP matrix as expected. The storage modulus master curve provides a useful prediction of the modulus over loading frequencies from 10^{-9} to 10^{20} Hz. However, it must be emphasized that these master curves are quite reliable for short term, but significant deviation may occur at large time scales. Shift factor, a_T was obtained directly from the experimental storage modulus curves against time by measuring the amount of shift along the time scale necessary to superimpose the curves on the reference. The shift factors used for the generation of storage modulus master curve is shown in Figure 8.

We tried the classical WLF equation to describe the relation ship between a_T and temperature. It was found that the WLF equation is suitable to describe the temperature dependence.
Parallel to the dynamic flexural tests, short-term static flexural tests were also conducted. Table 3 shows a plot of the experimental results obtained from the flexural test of the all-PP composites. The result shows the average value of elastic modulus and maximum flexural strength of the β-PP matrix and all-PP composite laminates. The stiffness of the all-PP woven composites is to a great extent governed by the stiffness of the tapes in the longitudinal direction [23]. It shows that strength (36%) and stiffness (85%) of the β-PP matrix is improved significantly by reinforcing PP tapes. A detailed study on the flexural behaviour of all-PP composite (Pure®) was conducted in our laboratory and reported that the short-term as well as long-term viscoelastic behaviours are greatly influenced by the composite morphology, particularly the reinforcement architecture.

5. Conclusion

All-PP composite were produced from α-PP tapes and β-PP film/matrix by a hot consolidation method. This study has proved that extruded α-PP tapes (high melt temperature) can be used for reinforcing the β-PP matrix (low melt temperature). At room temperature the E′ of the β-PP matrix is increased by 0.7 GPa by the effective reinforcement of α-PP tape obtained by DMTA. Similarly there is an increase in the flexural strength and stiffness of the all-PP composite also observed. The tanδ peak was not discernable for the reinforcing α-PP tape, while it is clearly identified for the β-PP matrix and all-PP composite laminate. Though, the position of Tg remained nearly unchanged, the peak intensity and magnitude decreased significantly. The storage modulus master curve approach a similar plateau value at high frequency, but the terminal region at lower frequencies is more dependent on reinforcement effect of composite compared with the β-PP matrix. The experimental shift factors showed a good agreement with both WLF and Arrhenius models.

Acknowledgement

The authors thank the German Science Foundation for the financial support of this project (DFG Ka 1202/17)

References

1. Houshyar S, Shanks RA, Hodzic A Macromol Mater Eng. (2005) 290:45
2. Bárány T, Karger-Kocsis J, Czigány T Polym Adv Technol (2006) 17:818
3. Hine PJ, Ward IM, Jordan ND, Olley R, Bassett DC J Macromol Sci Phys (2001) 40B:959
4. Amornsakchal T, Bassett DC, Olley RH, Hine PJ, Ward IM J Appl Polym Sci (2000) 78:787
5. Capiati NJ, Porter RS J Mater Sci (1975) 10:1671
6. Mead WT, Porter RS J Appl Polym Sci (1978) 22:3249
7. Karger-Kocsis J. Patentschrift DE 10237803B4, Institut für Verbundwerkstoffe GmbH 2007.
8. Boiko YuM, Kovriga VV Intern J Polym Mater (1993) 22:209
9. Wortmann FJ, Schulz KV Polymer (1995) 36:315
10. Abraham T, Banik K, Karger-Kocsis J *eXPRESS Polymer Letters* (2007) 1:519
11. Banik K, Abraham T, Karger-Kocsis J Macromol Mater Eng (2007) 292:1280
12. Varga J J Macromol Science Part B-Physics (2002) 41: 1121
13. Williams ML, Landel RF, Ferry JD J Amer Chem Soc(1955) **77**: 3701
14. Ferry JD Viscoelastic properties of polymers, 2nd edition, Wiley, New York, (1970) 292
15. Padden FJ, Keith HD J Appl Phys (1959) 30:1479
16. Samuels RJ, Yee RY J Polym Phys Ed (1972) 10:385
17. Boyd RH Polymer (1985) 26:1123

18. Hu WG, Schmidt-Rohr K Acta Polymer (1999) 50:271
19. Roy SK, Kyu T, St. John Manley R Macromolecules (1988) 21:1741
20. Ward IM, Hine PJ Polymer (2004) 45(5):1423
21. Alcock B, Cabrera NO, Barkoula NM, Reynolds CT, Govaert LE, Peijs T Compos Sci Tech (2007) 67:2061
22. Amash A, Zugenmaier P J App Polym Sci(1997) 63:1143
23. Alcock B, Cabrera NO, Barkoula N-M, Loos J, Peijs T Composites: Part A (2006) 37:716

Tables

Table 1. Summary of	PP tape
Width	1.5 mm
Thickness	265μm
Density	901±9 Kg/m^3
Composition	homopolymer (Novolen 1104H melt flow index 2 g/10 min at 230 °C and 2.16 kg load)
Tensile modulus (ISO 527)	4±0.5 GPa

Table 2. T_g and T_α at different oscillating frequenies

	T_g(°C)	T_α(°C)
0.01Hz	0.99	55
0.1Hz	2.13	81
1Hz	3.89	97
10Hz	6.90	-

Table 3. Flexural properties of all-PP composite laminates

	Flexural properties		
Material	Modulus (GPa)	Strength (MPa)	Strain at max. load
β-PP film	1.2±0.17	44±5	5.6±0.2
all-PP composite	2.3±0.07	60±0.5	4.9±0.3

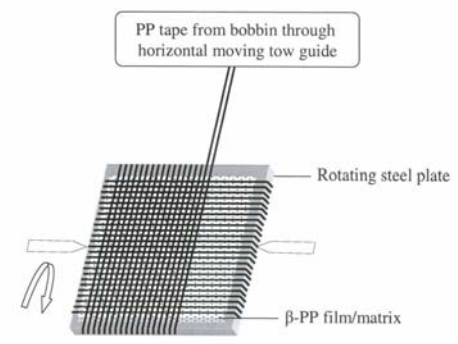

Figure 1. Scheme of the tape winding process for the fabrication of all-PP composites

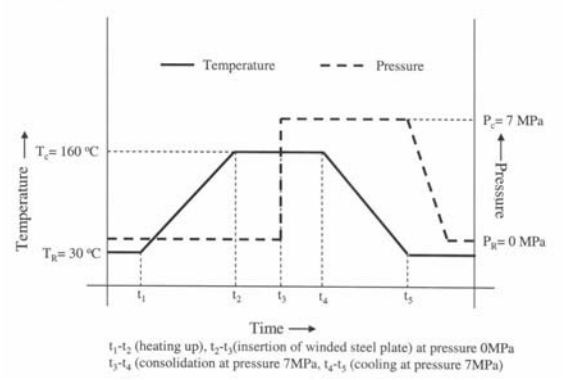

Figure 2. Schematic of time-temperature and time-pressure profile used for consolidation of all-PP by hot compaction (T_R and T_C are release and consolidation temperatures, P_R and P_C are release and consolidation temperatures)

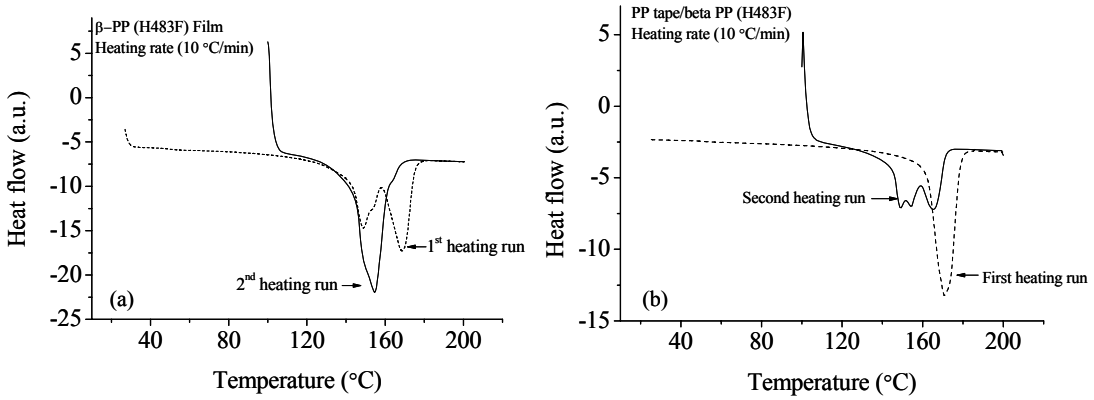

Figure 3. DSC traces of (a) β-PP matrix and (b) all-PP composite laminates (β-PP was cooled to T=100 °C prior to its second heating)

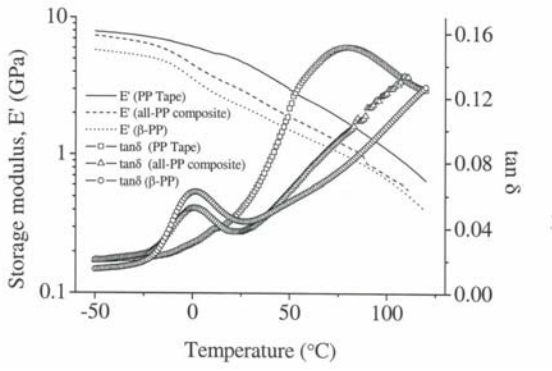

Figure 4. DMA plots of storage modulus and tanδ vs temperature for α-PP tape, all-PP composite laminates and β-PP matrix at frequency 1 Hz (note: log scale of E′)

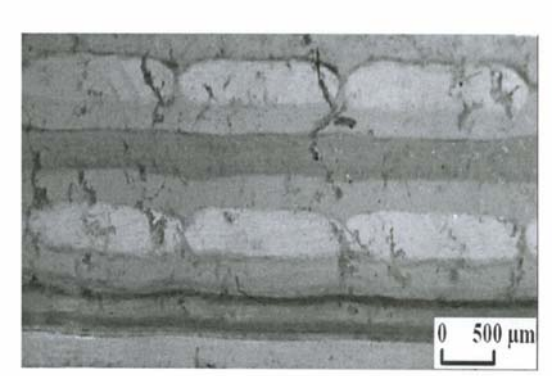

Figure 5. Optical micrograph from the cross-sections of all-PP composite laminates

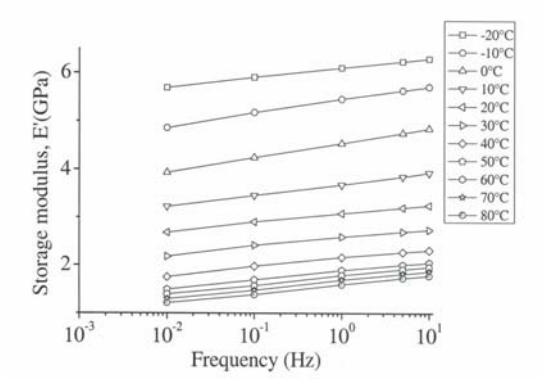

Figure 6. Storage modulus vs frequency for a range of temperatures for the all-PP composite

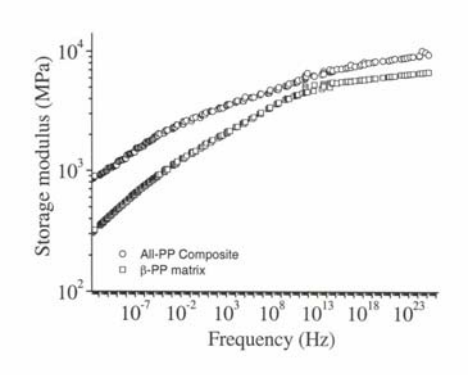

Figure 7. Storage modulus vs frequency master curves at a reference temperature of 22 °C for β-PP matrix and all-PP composite (note: log scale of y-axis)

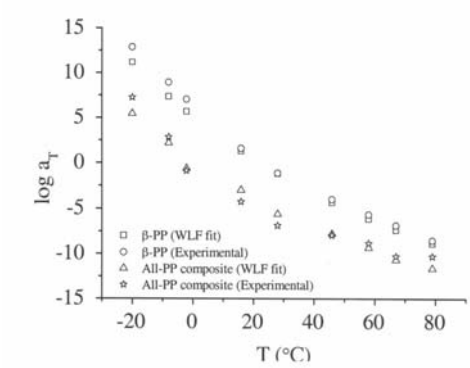

Figure 8. Experimentally determined shift factors and the WLF fits

Intercalated poly (methyl methacrylate) layered silicate nanocomposites: Effect of organoclay structure

M. Parua[1], S. Mohanty [2] and S.K. Nayak [2*]
Laboratory for Advanced Research in Polymeric Materials
1. Central Institute of Plastic Engineering and Technology, Bhubaneswar-751024, India.
2. Central Institute of Plastic Engineering and Technology, Chennai-600032, India
Email: drsknayak@gmail.com

Abstract
Poly (Methyl methacrylate)/layered silicate nanocomposites were prepared using melt intercalation technique. Commercially modified nanoclays such as Cloisite 30B, Cloisite 20A and Bentonite have been used as organoclays for the preparation of nanocomposites. Maleic anhydride (MA) has been used as a compatibilizing agent for improving the interfacial adhesion between organoclays and PMMA matrix. PMMA matrix with 5wt % of Cloisite 30B nanoclay exhibited optimum tensile properties. The tensile modulus of PMMA/Cloisite 30B 5% nanocomposite increases to about 35% as compared to virgin PMMA matrix. Thermal measurements employing differential scanning calorimetry (DSC), thermogravimetric analysis (TGA) also showed improved thermal stability and marginal increase in glass transition temperature of PMMA matrix with the incorporation of nanoclays. The morphological studies concerning wide-angle x-ray diffraction (WAXD) revealed an increase in d-spacing from 18.5 A^0 in C30B nanoclay to 39.4 A^0 in PMMA/C30B (5wt%) nanocomposites, thus confirming intercalated nanomorphology. The dispersion characteristics of organoclay with in PMMA matrix was also investigated using transmission electron microscopy (TEM). Further, dynamic mechanical analysis (DMA) shows a substantial increase in storage modulus of PMMA matrix with the incorporation of organoclays.
Key words: PMMA, Cloisite 30B, Bentonite, Nanocomposites, DMA

Introduction
Poly (methyl methacrylate) (PMMA) is an amorphous, atactic and optically transparent material with high technological importance because of its high weatherability, high optical clarity & gloss, high strength, low water absorption and stiffness. PMMA nanocomposites offer the potential to reduce gas permeability improve thermal, mechanical and flammability properties. PMMA is a highly combustible material and very difficult to impart flame retardancy even with the addition of larger amounts of conventional flame retardant agents. However, use of layer silicates as flame retardant additives is not only improves the flammability properties but also results in an increase in the physical properties of the nanocomposites relative to the polymer matrix. PMMA being semi-polar polymer, various attempts have been made by modifying the matrix polymer with numerous grafting agents to improve the interface with the layered silicate. Several reports on PMMA based nanocomposites synthesized using bulk polymerization of methyl methacrylate and also by melt compounding or extrusion of Poly (methyl methacrylate) has been studied. Free radical polymerization of methyl methacrylate using sodium montmorillonite has been used investigated by Blumstein et. al [1]. Similarly Wang et. al [2] have synthesized PMMA nanocomposites using bulk ,suspension, solution and emulsion polymerisation technique [3-5]. A detailed investigation on mechanical and thermal properties have been studied by Su and Wilkie et. al.[6] using N-methyl N,N divinyl benzyl octadecyl ammonium modified montmorillonite. Exfoliated PMMA nanocomposites were obtained at relatively lower clay loadings of < 5 wt. %, where as intercalated structure have been noticed at higher clay loading. Similar existence of intercalated and partially exfoliated structures have also been reported by Lee and Jang et. al. [7] and Brittain [8] where in PMMA/clay hybrids have been synthesised using emulsion & suspension polymerisation techniques respectively. In the present investigation PMMA based nanocomposites with different organically modified montmorillonites have been reported.

#Corresponding Author:- drsknayak@gmail.com
Fax-191-44-22254787

Experimental

Materials

PMMA (876 G) having MI: 6g/10min and density1.19g/cc, obtained from M/S GSFC Ltd., India, has been used as the base polymer matrix. Cloisite 30B (C30B, CEC of 90 meq / 100g clay), Cloisite 20A(C20A, CEC of 95 meq / 100g clay) and Bentone 109 (B109, CEC of 95 meq / 100g clay) procured from M/s Southern clay products, Inc. Gonzales, Texas and Elementis UK respectively has been used as organoclays. Maleic anhydride (MA) in presence of Benzoyl peroxide as initiator has been used as grafting agent for preparing grafted samples.

Preparation of PMMA Nanocomposites:

PMMA and nanoclays were dried at 65^0C in vaccum oven for a period of 12hrs prior to processing. PMMA nanocomposites were fabricated using different weight percentage of nanoclays (1, 3 and 5%) in Haake Rheocord at 180^0C , 50 rpm for a mixing time of 30 mins. Finally, these premixes were brought to room temperature and was injection molded using mini Injection molding machine (Haake^R Minijet 557-2270) (Thermoelectron corporation GMDH, Germany) with a barrel temperature of 200 ^{0}C and mold temperature of 140^0C with 700 bar injection pressure

Wide angle-X-Ray Diffraction: (WAXD):

Wide angle X-Ray diffraction (XRD) analysis was carried out using Philips X'Pert MPD (Japan), which had a graphite monochromator and a Cu Kα radiation source operated at 40kv and 30 mA. The basal spacing or d_{001} reflection of the samples was calculated from Bragg's equation by monitoring the diffraction angle, 2θ from $2\text{-}10^0$.

Transmission Electron Microscopy:

Samples for TEM imaging were sectioned using Lieca Ultracut UCT microtome and TEM of specimens were carried out using JEOL-1200 EX electron microscope at an accelerating voltage of 80 kV.

Thermal Characterization

The melting, glass transition temperature and thermal stability of virgin PMMA and the nanocomposite samples have been studied using DSC (Perkin-Elmer Diamond DSC, USA) and TGA (Perkin –Elmer Pyris-7 TGA, USA), respectively.

Mechanical Properties:

Tensile properties were measured as per ASTM-D 638 with gauge length of 25mm, and crosshead speed of 5 mm/min by using Universal Testing Machine (LR 100K Lloyds Instruments Ltd. UK). Tests were carried out taking five specimens for each set at a standard temperature 23 ± 2^0c and 50 ± 2% RH.

Dynamic mechanical properties:

The dynamic mechanical behaviour of the samples were carried out at fixed frequency of 1Hz and heating rate of 10^0C/min in a temperature range of –150 to 200^0C using DMTA (NETZSCH DMA 242).

Results & Discussion

Wide angle X-ray diffraction:

The WAXD patterns of PMMA/Na+ MMT, PMMA/C30B, PMMA/B109 and PMMA/C20A nanocomposites and grafted PMMA-g-MA/C30B and PMMA-g-MA/B109 nanocomposites is depicted in fig.1. The d_{001} peak in all the organically modified systems were observed within the range of 2θ =1 to 10^0 indicating intercalation of PMMA chains with in the clay galleries. Comparison of diffraction patterns of each nanocomposites systems with respective organoclays, C30B, B109 and C20A reveals that basal spacing increases from 18.5 A^0 to 39.4 A^0 in PMMA/ C30B, 30.0 A^0 to 35.3 A^0 in PMMA/ B109 and 24.2A^0 to 33 A ^{0} in PMMA/C20A nanocomposites respectively. However, in case of PMMA/ Na+ MMT nanocomposites agglomeration and intercalation was observed. Since there was no evidence of peak intensity within the investigated experimental range. Nevertheless, broadening of the peak was noticed which is probably due to macroscopic interaction between Na+ MMT & PMMA that might have resulted in dispersion of clay stacks with in the PMMA matrix. As reported by Sandeep Kumar et al. (9) some level of reduction in the no. of clay platelets per stacks in the polymer matrix might have resulted between Na+ MMT & PMMA from either the processing methods used in the fabrication of the nanocomposites or due to favourable interactions between

them. The nanocomposites prepared using C20A organoclay exhibited minimum intercalation of 33 A^0 as compared to the other two modified organoclays C30B and B109 respectively. The lower amount of intercalation possibly occurs due to less favourable intercalation between the ditallow intercalant in C20A containing more no. hydrophobic $–CH_2$ groups in the clay surface, with the polymer chain segments. In case of B109, a smectite organoclay, modified with hydrogenated tallow, provides more no. of clay platelets per surface area, which might have been the primary reason for enhancement of d spacing as compared with PMMA/C20A nanocomposites. However grafting of PMMA with MA could not show any appreciable increase in the d spacing as compared with the ungrafted nanocomposites .

Transmission Electron Microscopy: (TEM)

Bright field TEM images of PMMA with and without MA are represented in the fig.2. Dark lines represent silicate layers whereas bright region corresponds to PMMA matrix. This also indicated intercalated clay layers along with some individual clay layers for untreated PMMA/C30B nanocomposites. In case of grafted nanocomposites, PMMA-g-MA/C30B hybrid the smaller amount of stack plates appear in broad and obscure region. TEM results confirmed that PMMA based grafted and ungrafted nanocomposites mainly display an intercalated nanomorphology which is in agreement to the WAXD technique.

Thermal Analysis (DSC/TGA) :

Fig.3 shows the TGA curves of PMMA, PMMA/ Na+ MMT, PMMA/C20A, PMMA/C30B, PMMA/B109 nanocomposites and PMMA-g-MA/C30B and PMMA-g-MA/B109 grafted nanocomposites respectively. It is observed that onset of temperature increased in all the cases is around 25^0C for PMMA/C30B, 6^0C for PMMA/B109 and 24^0C for PMMA/C20A as compared with virgin PMMA. The temperature at 50% mass loss ($T_{0.5}$) also increases from 365^0C in case of PMMA to 412^0C in PMMA/C20A nanocomposites. This improvement in thermal stability of PMMA nanocomposites is mainly due to the intercalation of polymer matrix into the clay galleries, which act as a barrier for thermal degradation as well as nucleating effect of organoclays. The effect of maleic anhydride did not show a considerable improvement in thermal stability of nanocomposites. However in all the nanocomposite system the confinement of polymer chains into the clay galleries delayed the degradation process & diffusion of volatile products thereby increasing the flame retardancy.

The DSC thermograms of PMMA virgin and the nanocomposites systems are illustrated in fig .4. DSC thermograms represented the presence of second order transition corresponding to the Tg of the virgin PMMA matrix around 121.90^0C. Absence of 2^{nd} order transition or Tm indicated amorphous characteristics of the matrix polymer. DSC isotherms revealed marginal decrease in the Tg of PMMA in the nanocomposites system. PMMA/C30B nanocomposites exhibited Tg around 118.83^0C with PMMA/B109 at 120.01^0C and PMMA/C20A around 114.31^0C respectively .The grafted samples also exhibited glass transition in the similar range indicating no appreciable effect of grafting on the segmental mobility of the matrix polymer. The depression Tg is probably due to reduction in density, which caused chain end localization and reduced chain entanglements as compared with the bulk matrix. PMMA/C20A nanocomposites system exhibits maximum depression in Tg to the tune of 114.31^0C which reveals less compatibility of the ditallow organic modifier with the hydrophobic matrix.

Mechanical Properties:

Mechanical properties such as Young's modulus (E), stress at break and % strain at break and tensile strength is represented in the table1. It is evident that with the increase in clay loading from 1 to 5 wt %, there is a linear increase in the young's modulus of PMMA nanocomposites system. Incorporation of organically modified nanoclays to the tune of 5wt% increases (E) of PMMA from 1980 MPa to 2681 MPa in PMMA/C30B, 2469 MPa in PMMA/B109 and 2168 MPa in PMMA/C20A nanocomposites hybrid respectively. The nanocomposites prepared using C30B nanoclay exhibited an optimum increase in E as compared with virgin matrix which is probably due to polar interactions between ester groups of PMMA with the hydroxyl group of C30B. The grafted nanocomposites exhibited a higher modulus as compared with the ungrafted hybrids in all the cases PMMA-g-MA/C30B nanocomposites exhibited a maximum increase in Youngs modulus to the tune of 38.22 % as compared with the virgin matrix. This behaviour is probably due to formation of interfacial bonds between the anhydride groups of MA with the –OH groups in C30B as well as polar interactions of the ammonium cations with the MA. The tensile strength also increases with the increase in clay

loading. Na+MMT system shows a decrease in the tensile strength and stress at break indicating brittleness characteristics predominantly due to presence of clay agglomerates which leads to microcrack formation at the interface. The nanocomposites prepared using C30B &B109 shows an increase of 21.85 %and 20.91 % respectively as compared with the matrix polymer. PMMA/C20A nanocomposites exhibit less tensile strength of 67.94 MPa confirming comparatively less compatibility with the matrix polymer. Further grafted samples in all the systems exhibits lower tensile strength as compared with ungrafted nanocomposites system revealing brittleness characteristics of PMMA with interface modification in the nanocomposites system. Strain at break decreases with the incorporation of nanoclays, PMMA/C30B nanocomposites exhibited a decrease of 62.71% with PMMA/B109 to 54.1% and PMMA/C20A to 91.6 % respectively as compared with the matrix polymer. Grafting of PMMA with MA and influence of organic modifier /intercalant type had virtually no effect on the stress as well as strain at break of the nanocomposite hybrids.

Dynamic Mechanical Analysis:

The temperature dependence plots of storage modulus E' of PMMA and its nanocomposites as measured from –150 ^{0}C to 150 ^{0}C are depicted in fig.5. As observed in the figure, the glassy state storage modulus at 25 ^{0}C increases to the tune of 9.2% in PMMA/C30B, 15.5 % PMMA/B109 and 29.3% PMMA/C20A respectively as compared with the virgin matrix. The grafted nanocomposites also demonstrated moderate increase in E' of PMMA. PMMA-g-MA/C30B exhibits maximum increase in storage modulus Above 80 ^{0}C, the E' drops with considerable fall in matrix modulus observed in the vicinity of Tg indicating that the material undergoes a glass/ rubber transition. DMTA tests indicated remarkable increase in E' in the nanocomposites system as compared with virgin matrix. The E' values display improvement in glassy regions (except deviations in PMMA/B 109 system) confirming that incorporation of nanoclay induces reinforcing effect. At high temperature regions the nanocomposites system as well as PMMA displayed similar modulus and approaches constant level of temperature beyond 130 ^{0}C

Conclusion:

PMMA nanocomposities were prepared using melt blending technique. The effect of organic modifier on the mechanical, thermal and flammability properties of nanocomposites has been investigated. Mechanical properties indicated optimum tensile modulus is PMMA/C30B 5% as compared to virgin PMMA matrix and other nanocomposites. WAXD & TEM micrographs showed evidence of exfoliation and intercalation in PMMA/C30B nancomposites. Thermal study indicates an increase in onset of decomposition temperature and marginal increase in Tg of nanocomposites. DMA studies revealed substantial increase in the E' of the nanocomposites with the incorporation of C30B nanocomposites.

References

1. Blumstein, A.J Polym sci. part A: Gen pap 1965, 3, 2653
2. Wang, D.; Zhu, J.; Yao, Q.; Wilkie, C.A. Chem mater 2002,14,3837
3. Bandyopadhyay, S.; Giannelis, E. P.; Hsieh, A. J. Polym2000, 82, 208.
4. Hsieh, A. J.; Giannelis, E. P. Presented at the American Physical Society Symposia Presentation, Atlanta, GA, March 1999.
5. Salahuddin, N.; Shehata, M. Polymer 2001, 42, 8379.
6. S.u, S.; wilkie, C.A. J.Polym Sci. Part A: polym Chem 2003, 41, 1124
7. Lee, D.C.; Jang, L.W. J Appl Polym Sci., 1996,61,1117
8. Huang, X.; Brittain, W.J. Macromolecules, 2001,34,3255
9. S.Kumar, J.P. Jog, U.P, J. Appl. Polym. Sci. 2003, 89, 1186

Table 1: Mechanical Properties of PMMA & Nanocomposites at 5 wt% nanoclay loading

Sample ID	Tensile strength (MPa)	Tensile modulus (MPa)	Strain at break(%)
PMMA	56.4	1980	3.84
PMMA/C30B	68.81	2681	1.43
PMMA/B109	68.28	2469	1.76
PMMA/C20A	67.94	2168	0.32
PMMA-g-MA/C30B	65.29	2736	1.00
PMMA-g-MA/B109	59.40	2607	0.64

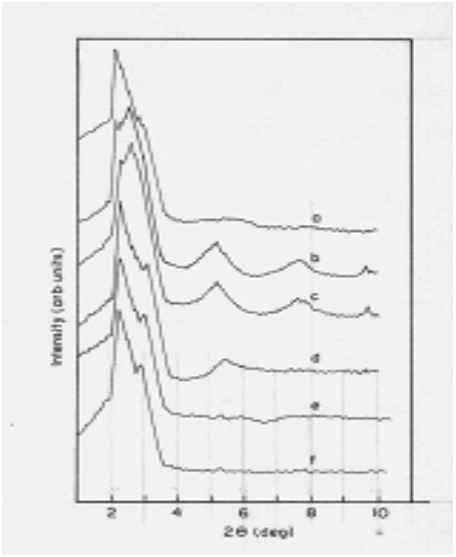

Figure.1 Wide angle X-ray Diffraction Pattern (a) PMMA/C30B, (b) PMMA/B109, (c) PMMA/C20A, (d) PMMA-g-MA/C30B, (e)PMMA-g-MA/B109,(f)PMMA-g-MA/C20A

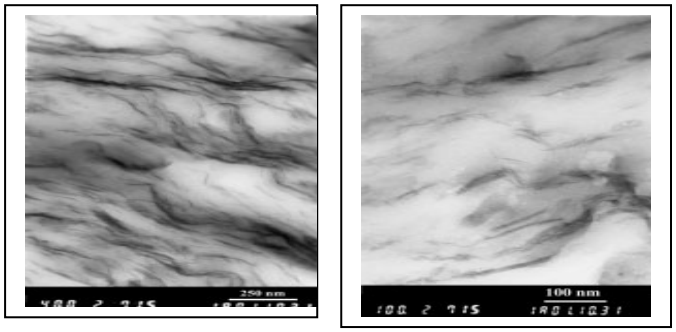

(a) (b)

Figure.2 .(a). PMMA/C30B (5%) without compatibiliser, (b), PMMA/C30B (5%) with compatibilizer

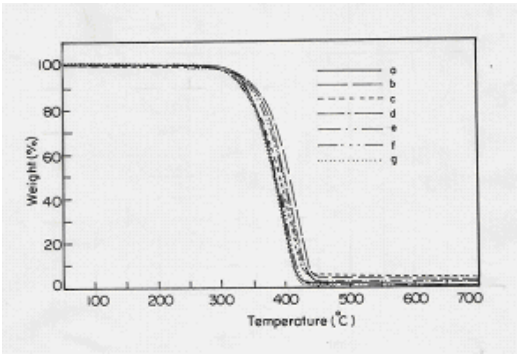

Figure.3 TGA of (a) PMMA (V), (b) PMMA/C30B, (c) PMMAB109 (d) PMMA/C20A, (e)PMMA-g-MA/C30B(f) PMMA-g-MA/B109 (g) PMMA-g-MA/C20A

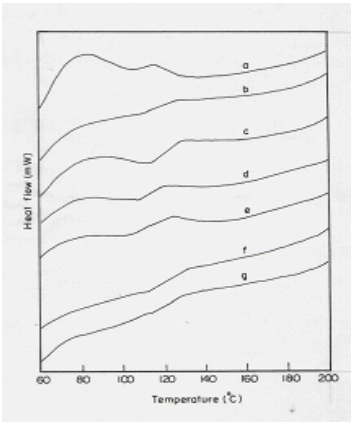

Figure.4 DSC of (a) PMMA (V), (b) PMMA/C30B (c) PMMAB109 (d) PMMA/C20A(e) PMMA-g-MA/C30B (f) PMMA-g-MA/B109 (g) PMMA-g-MA/C20A

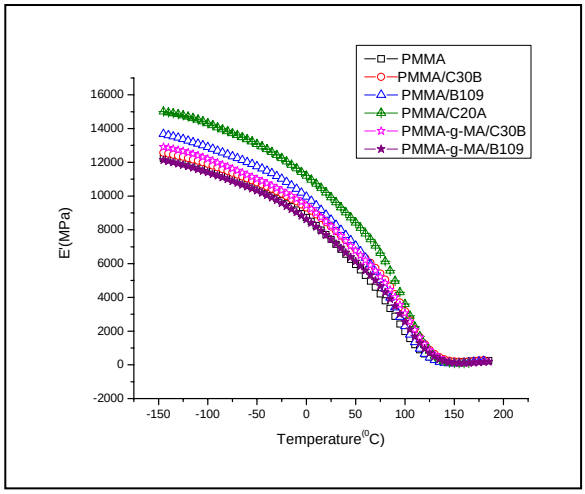

Figure.5 Variation of Storage Modulus with Temperature of PMMA and Nanocomposites

A Review on thermally stable organic modifiers for montmorillonite nanoclays

Reema Sinha* and Soumyadeb Ghosh
SABIC Innovative Plastics Program,
GE India Technology Centre – Bangalore, 560 066, India
Email: Sumanda.Bandyopadhyay@ge.com

Abstract

Among nanomaterials, polymeric nanocomposites have emerged as one of the most important class of materials and hence, a field of active research. One of the most important classes of nanocomposites is based on silicate nanoclays, modified with different ammonium cations, which have been studies most extensively for fundamental understanding as well as for commercial applications. However, the application space for polymer nanocomposites remained restricted to low temperature resins such as polyolefins and polyamides, due to relatively low thermal stability of the alkyl ammonium ions (below 250°C), used as modifiers. This restricts exploitation this technology in the arena of high performance polymers such as engineering thermoplastics, which are most often compounded at high temperatures. Hence, recently, a number of research groups have taken up the challenge of extending the applicability of nanoclays to high-temperature resins. In this presentation, recent efforts in compatibilization of nanoclays using thermally stable modifiers will be reviewed. The present status, with respect to the thermal stability reported in different classes of modified nanoclays, and the industry needs in terms of the temperature requirements for their melt-processing in different thermoplastic system, will be discussed.

Introduction

The field of nanotechnology is one of the most active areas of research in most of the technical disciplines. In recent years, polymer-layered silicate nanocomposites have attracted great interest in both in industry and in academia. This is because they show remarkable improvement in materials properties when compared with virgin polymer or conventional micro and macro-composites. These improvements include high moduli [1–3], increased strength and heat resistance [2], decreased gas permeability [4,5], flammability [6,7], and increased biodegradability of biodegradable polymers [8].

Toyota researchers [9,10] were first to show remarkable improvements in some physico-mechanical properties of polyamide-6 (PA-6) containing exfoliated organo-clay. They observed 100% improvement in modulus, 50% increase in strength and 80^{o}C enhancement in heat distortion temperature compared to neat PA-6. It is interesting that polymer-clay nanocomposites offer exceptional stiffness and strength at very low filler loading (e.g., 6.5 wt% clay), whereas ~20% of glass fibers is needed to achieve similar improvements [11]. Significant improvements in properties, albeit to lesser extent, were also demonstrated in nanocomposites based on polyolefins [12]. These advantages have benefits mainly in transportation and automotive industries, where lightweight structures and components are critical to improve the fuel economy.

The improvement in the properties are critically dependent on exfoliation of the layered silicate nanoclay particles in the nanocomposites, achieved by using appropriate modification of the negatively charged silicate layers with organic cations [12]. Nanoclay based composites of almost all classes of polymers have been evaluated for different applications and exfoliation of the

silicate layers leading to enhanced properties have been achieved in a number of systems. However, only handful of such systems has reached the market till date. One of the main reasons for this has been the thermal stability and compatibility of the organic modifier for the nanoclays. Most polymer-based products are manufactured by melt processing or require thermal treatments, whereas the commercially available nanoclays are organically modified using organic ammonium cations. Such cations are not stable at temperatures required for high rate production of nanocomposites of most polymeric systems. Hence, nanocomposites based on polyolefins and PA-6, which require comparatively lower processing temperatures, have found use in the market. In the present talk, the need for thermally stable nanoclay modifiers will be analyzed and various recent attempts for development of thermally stable modifiers for high temperature applications will be reviewed.

Thermally Stable Nanoclay Modifiers

Increasing the thermal stability of organoclay is one of the key needs in the successful industrial application of polymer-clay nanocomposites. This would enable the preparation of nanocomposites from thermoplastic polymers that require high melt-processing temperatures (PA-6,6, PC, PET, s-PS, PEI) or long residence times under high shear and from thermoset resins with high cure temperatures (cyanate esters, aromatic epoxies). To circumvent the detrimental effect of lower thermal stability of alkyl ammonium-treated montmorillonite (MMT), many cations, such as phosphonium, pyridinium, imidazolium etc. have been used to modifiy nanoclays because of their greater thermal stabilities [13,14]. Organoclays treated with these cations have thermal stability higher than 290 °C in inert atmosphere, based on the $Td_{5\%}$ data [12]. Studies on thermally stable modifiers and their application to different polymer systems have been reviewed earlier [12,15]. Here the efforts on application of different kinds of high-temperature modifiers in nanocomposites, is briefly summarized

Quaternary phosphonium modified nanoclays have been most extensively studied. Modifiers with phosphonium surfactants having either short alkyl chains, benzene ring, a long alkyl chain or a mixture of these groups have been tried. They are 50-80°C more stable than corresponding ammonium salts [16]. Besides improving mechanical properties, phosphonium clays also improves the flame retardancy and heat stabilization [17]. They have been incorporated in polymers like polyesters, syndiotactic polystyrene, epoxies, PMMA. Depending on the polymer, exfoliated, intercalated or mixed intercalated-exfoliated structures has been obtained [16,17]. Imidazolium modified nanoclay- such as trialkylimidazolium modified MMT give an organoclay, which is 100°C more stable than alkylammonium-modified MMT. The alkyl chain length affects the thermal stability of the salt, the stability decreases as the chain length is increased [18]. Studies with these clays have been done mainly in PA-6 and polystyrene to give an exfoliated PA-6 nanocomposite and a partially exfoliated polystyrene nanocomposite with improved thermal stability and reduced flammability [18,19]. Pyridinium cation modified nanoclay- Pyridinium treated nanoclays are 50-100°C more stable than ammonium modified clays. In PET, cetylpyridinium modified clay gave high level of dispersion and improved thermal stability of the nanocomposite [20].

The Need for Thermal Stability

Let us now consider the extent of thermal stability of the modified nanoclays required with respect to the present status of the technology. The typical temperature ranges required for melt-

processing of different commercial thermoplastic materials are given in figure 1 [21]. It may be observed that though many high-volume commodity thermoplastics can be processed at or below about 250°C, all the high-performance engineering thermoplastics need temperatures between 250°C – 350°C for processing, whereas some specialty polymers need up to 400°C.

To compare the state of art in nanoclay modification, some of the thermal stability indicators namely the temperature at initiation of thermal degradation and the temperatures at maximum rate of degradation, derived from the earlier works [17,22] are also presented in figure 1. It can be observed (Fig.1) that ammonium cation based modifiers, which are most commonly used for modification of nanoclays, have the lowest thermal stability among all the classes of modified presented above. While at about 250°C the phosphonium, cation based nanoclay just initiate to degrade and the other higher temperature nanoclays do not show any degradation, the ammonium based nanoclays reaches almost the point of maximum rate of degradation. According to the TGA data reported by Calderon et al., a typical ammonium nanoclay, with grade name Cloisite 10A, attains a weight-loss rate of 0.25 %/ °C. Taking the heating rate for the TGA experiment of 20°C /min [17], it can be inferred that the nanoclay degrades at a rate of about 5% per minute. For a more stable ammonium modified nanoclay, Closite 15A, the rate was about 1.5% per minute, which rapidly increases to 3.4% at 300°C and reaching the maximum of about 5.5% at 325°C.

Further, it should be noted that the TGA experiments were run under nitrogen atmosphere whereas thermoplastics are melt-processed in air and a typical thermoplastic itself may have functional groups that could be reactive to the organic modifier at the processing temperature, leading to rather severe degradation of the modifier groups on the nanoclays. This causes the loss of the alkyl long chains from the modifiers, which increases the interlayer interaction, preventing the exfoliation of nanoclays. In some cases, if the nanoclays are already exfoliated at lower temperatures (e.g. master-batching at lower temperatures using other processing methods), exposure to high temperatures in subsequent processing steps may cause collapse of the nanoclay layers on lager size particles.

In contrast to the ammonium based nanoclays, the nanoclays modified with higher temperature modifiers show negligible degradation up to 300°C. The phosphonium based nanoclay, which found to be least stable among the nanoclays studied, reaches a degradation rate of 0.15% per minute or 3% per minutes only above a temperature of 400°C, at the same experimental conditions. Similar observations may be made from figure 1 for the imidazolium and pyridinium based nanoclays too. Hence, development of organic modifiers based on these thermally stable cations should help in translating the technology to the systems of engineering thermoplastics. Since modified nanoclays has been successfully used in PA-6, which has processing temperature range that extends above 250°C, it may be hoped that some of the nanoclay modifier might survive the processing temperatures of specialty, high-temperature polymers such as Ultem*, PPS or PEEK.

* - Trademark of Sabic Innovative Plastics

Conclusion:

Though the technology of nanocomposites based on modified nanoclays has been demonstrated in a number of different polymers, it could reach the market only in cases of polymers having comparatively lower processing temperatures. Even in the market it is not very clear how well these new materials are performing. There may still be further need for the technology to achieve the right balance between the overall advantages in terms of property improvements and the cost. It may be a greater challenge to achieve this in commodity thermoplastics. On the other hand, there are strong market needs for special properties, such as thermo-mechanical stability, toughness, low flammability, chemical stability, high gas-barrier properties in polymeric materials. Nanocomposites of commodity plastics may match some of the properties (e.g. room

temperature mechanical properties, barrier properties) of the engineering polymers. However, a success in developing technology for true nanocomposites based on engineering thermoplastics would take polymers to new market arena, bettering metals with easier processibility, recyclability, design flexibility and lighter weight. Hence, development of a successful technology for exfoliation and dispersion of nanoclays in engineering or high-temperature thermoplastics, would bridge the gap between the technology and the market need with the right cost-benefit balance. In this presentation, the recent efforts in development of modified nanoclays for high temperature applications have been reviewed. A comparison of the thermal stability of the conventional, as well as, of the new high-temperature modifiers, have been made with respect to the processing temperature required for different common commercial polymers.

An effort is made to give a comprehensive picture of the field from the point of view of the present status, and the industry needs in terms temperature requirements for melt processing of different thermoplastics.

References

[1] Okada A, Kawasumi M, Usuki A, Kojima Y, Kurauchi T, Kamigaito O. Synthesis and properties of PA-6/clay hybrids. In: Schaefer DW, Mark JE, editors. Polymer based molecular composites. MRS Symposium Proceedings, Pittsburgh, vol. 171; 1990: p. 45–50.
[2] LeBaron PC, Wang Z, Pinnavaia TJ; Appl Clay Sci.1999;15: 11–29.
[3] Vaia RA, Price G, Ruth PN, Nguyen HT, Lichtenhan J.; Appl Clay Sci 1999;15:67–92.
[4] Bharadwaj RK; Macromolecules 2001; 34: 1989–92.
[5] Kojima Y, Usuki A, Kawasumi M, Fukushima Y, Okada A, Kurauchi T, Kamigaito O; J Mater Res 1993; 8:1179–84.
[6] Gilman JW; Appl Clay Sci 1999; 15:31–49.
[7] Gilman JW, Jackson CL, Morgan AB, Harris R, Manias E, Giannelis EP, Wuthenow M, Hilton D, Phillips SH; Chem Mater 2000; 12: 1866–73.
[8] Sinha Ray S, Yamada K, Okamoto M, Ueda K; Nano Lett 2002; 2:1093–6.
[9] Usuki A, Kawasumi M, Kojima Y, Okada A; J Mater Res 1993; 8:1174–8.
[10] Usuki A, Kojima Y, Kawasumi M, Ukada A, Fukushima Y, Kurauchi T, J Mater Res 1993;8:1179–84.
[11] Fornes TD, Paul DR; Polymer 2003; 44: 4993–5013.
[12] Leszczyńskaa A, Njugunab J, Pielichowskia K, Banerjee JR; Thermochim. Acta 2007; 453: 75-96.
[13] Xie W, Gao Z, Pan W, Hunte D, Singh A, Vaia R; Chem Mater 2001;13: 2979–2990.
[14] Takekoshi, T.; Khouri, F. F.; Campbell, J. R.; Jordan, T. C.; Dai, K. H. (General Electric Company). US Patent 5707439; 1998.
[15] Leszczyńskaa A, Njugunab J, Pielichowskia K, Banerjee JR; Thermochim. Acta 2007; 454: 1-22.
[16] Xie W, Xie R, Pan W, Hunter D, Koene B, Tan L, Vaia R; Chem. Mater 2002; 14: 4837–4845.
[17] Calderon JU, Lennox B, Kamal MR; Applied Clay Science 2008; 40: 90-98
[18] Awad W, Gilman J, Nyden M, Harris R, Sutto T, Callahan J, Trulove P, DeLong H, Fox D; Thermochimica Acta 2004; 409: 3–11.
[19] Gilman J, Awad W, Davis R, Shields J, Harris R, Davis C, Morgan A, Sutto T, Callahan J, Trulove P, DeLong H; Chem. Mater 2002; 14: 3776-3785.
[20] Fang Ou C, Ting Ho M, Rung Lin J; J Appl Polym Sci 2004; 91: 140–145.
[21] Injection Molding Reference Guide (4th edition), Publisher: Advanced Process Engineering, Cornvallis, Oregon; 1997: p35.
[22] Stoeffler K, Lafleur PG, Denault J; Polymer Degradation and Stability 2008; 93:1332–1350.

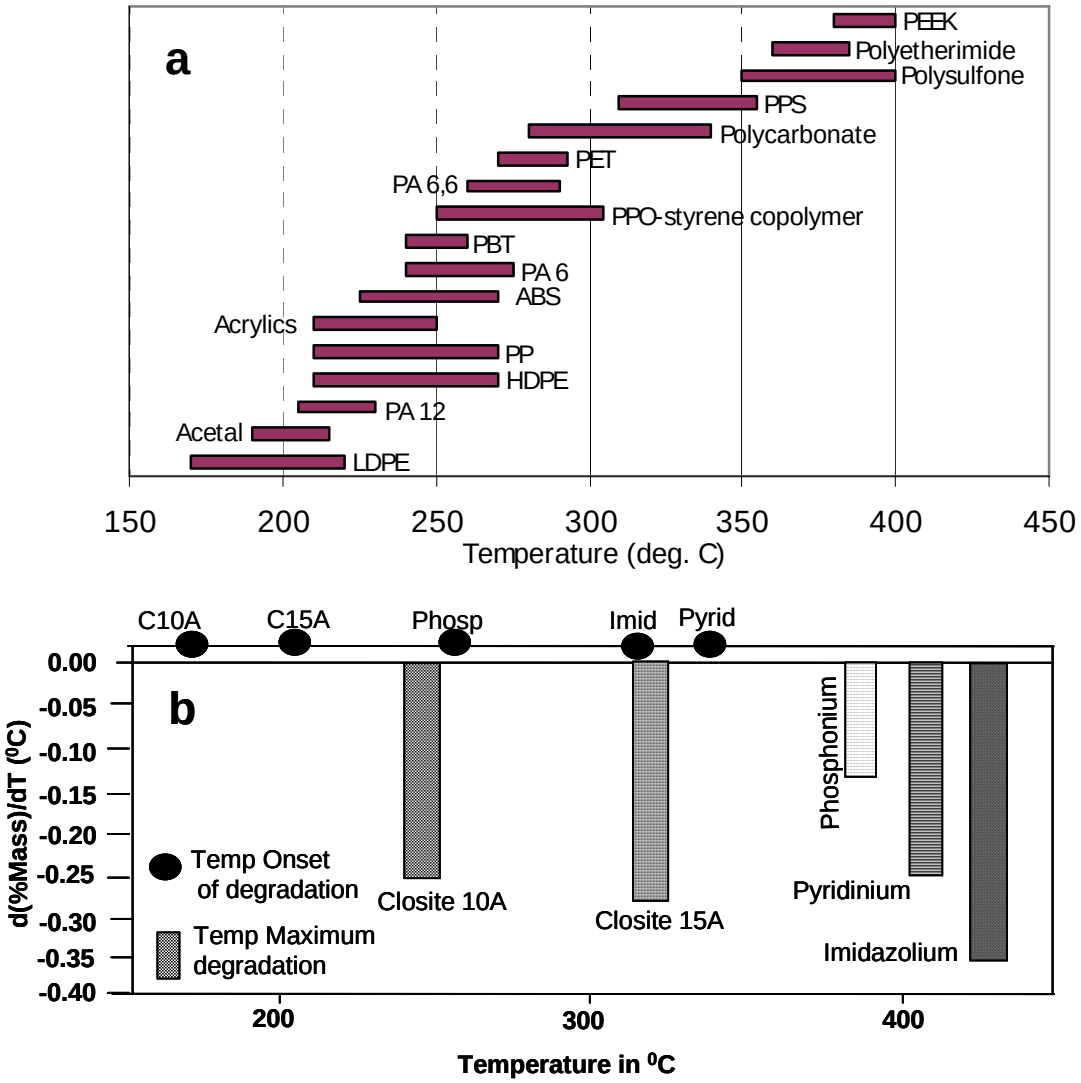

Figure 1. (a) Temperature ranges of different commercial thermoplastic polymers [21] (b) Onset temperatures and maxima of thermal degradation rates versus temperature for different nanoclays, modified different classes of organic cations (adapted from ref. 17, figure 3; ref. 22, figure 2)

Thermal and mechanical properties of poly (vinyl chloride)/ microscale and nanoscale calcium carbonate composites via melt intercalation

C. B. Patil, U. R. Kapadi, D. G. Hundiwale and P. P. Mahulikar*

School of Chemical Sciences, North Maharashtra University,
Jalgaon - 425 001 (M. S.) India
Email: mahulikarpp@rediffmail.com , dghundiwale@yahoo.com

Abstract

Calcium carbonate was synthesized by *in situ* deposition technique and its nano size (35 to 60 nm) was confirmed by Transmission Electron Microscopy (TEM). Composites of the filler $CaCO_3$ (micro and nano) and the matrix poly (vinyl chloride) (PVC) were prepared with different filler loading (0-5 wt. %) by melt intercalation. Brabender torque rheometer equipped with an internal mixer has been used for preparation of formulations for composites. The effect of filler content both nano and micro level on the nanostructure and properties is reported here. The nanostructures were studied by wide angle X-ray diffraction (WAXD). The mechanical, thermal and dynamic mechanical properties of PVC/ micro and nano $CaCO_3$ composites were characterized using Universal Testing Machine (UTM), Thermo Gravimetric Analyzer (TGA) and Dynamic Mechanical Analyzer (DMA). The results of thermal analysis indicated that the thermal stability of PVC/nano-$CaCO_3$ composites was improved as compared with corresponding microcomposites and that of pristine PVC and maximum improvement was obtained at 1 and 3 phr loadings. However, the tensile strength decreased significantly with increasing loading of both nano and micro $CaCO_3$ while storage modulus and glass transition temperature increased significantly.

Keywords: Nanoparticles, Transmission Electron Microscopy (TEM), Wide Angle X-ray Diffraction (WAXD), Tensile strength, Thermal stability.

1. Introduction:

Nanoscale calcium carbonate (nano $CaCO_3$) is one of the most common spherical nanoscale fillers used in the preparation of nanocomposites. $CaCO_3$ can be produced by a variety of methods, including precipitation, dry grinding, and wet grinding. The basic grades of $CaCO_3$ can be differentiated by changes in the size distribution, particle size, surface area, morphology, surface chemistry, and so forth [1-4].

This nanoconcept has been mostly focused on thermoplastic and thermosetting polymers including polyamides, polypropylene, epoxies and polyesters. The addition of nano-$CaCO_3$ to

composites has been reported to improve the strength, modulus, and toughness significantly. A study of polypropylene (PP)/nano-$CaCO_3$ composites revealed a dramatic toughening effect of nano-$CaCO_3$ on PP. However, the yield strength of PP slightly decreased because of the nucleating effect of nano-$CaCO_3$ [5, 6].

Relatively a little attention has been paid to polyvinyl chlorides (PVC) materials.The effects of inorganic fillers on the microstructure and mechanical properties of PVC composites depend strongly on the particle shape, particle size, aggregate size, surface characteristics, the fraction of fillers and their degree of dispersion [7-25].

2. Experimental Section:

2.1 Materials

Materials used for the synthesis of nanoparticles of calcium carbonate were $CaCl_2$, K_2CO_3 & PEG. Calcium chloride, potassium carbonate were of analytical grade and poly (ethylene glycol) (PEG; MW 6000 g) was procured from s. d. Fine Chem., Ltd. Mumbai, India. The polyvinyl chloride grade 57GERO68, was obtained from Reliance Industries Ltd., Mumbai, India.

2.2 Preparation of nanoparticles:

The nanosized calcium carbonate filler particles were synthesized using *in situ* deposition technique [7-8].

2.3 Preparation of Composites:

For preparation of composites, formulations were melt intercalated using a Brabender Plastograph EC equipped with an electrically heated mixing head (W 50 EHT mixer) having 55 cm^3 volume capacity and two non interchangeable rotors. The processing temperature, rotor speed and blending time were set at 170 ^{0}C, 60 rpm and 10 min, respectively. The sample volume of each blending was kept 90 % of the actual volume capacity of the mixer. The compounds of composites were obtained in the form of lumps. These lumps were then crushed to get the coarser particles/granules (approx. 3-4 mm size) suitable as feed for injection moulding to obtain tensile and impact specimens.

2.4 Characterization

The particle size of synthesized nano calcium carbonate particles were analysed using Transmission Electron Microscope (TEM, Philips Tecnai-20). The structure of PVC-$CaCO_3$ nanocomposites was characterized by WAXD.

A thermogravimetric analyzer was used to analyze thermal characteristics of the PVC/micro and nano $CaCO_3$ composites. The composites were heated from room temperature to 550 ^{O}C at the rate of 5 ^{O}C/min. under nitrogen stream. Tensile strength was determined by subjecting dumb-bell shaped specimens (in accordance with ASTM D – 412) to a Universal

Testing Machine. The dynamic mechanical analysis (DMA) was performed using a Gabo Eplexor dynamic mechanical analyzer at a fixed frequency rate 10 Hz in a temperature range from 30 to 120 ^{0}C, and the heating rate 2 ^{0}C/min.

3. Results and discussion

3.1 Particle Size Analysis

The particle size of the calcium carbonate was found to be in the range of 35 to 60 nm as verified from TEM micrograph of $CaCO_3$ nanoparticles [Fig.1]

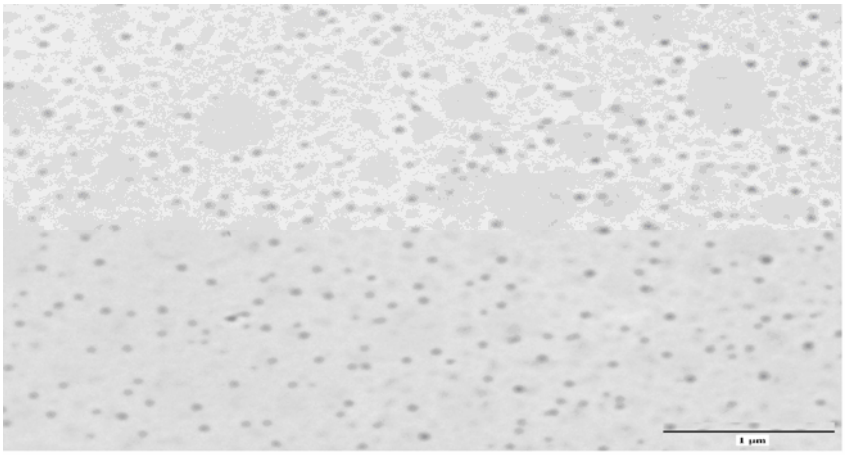

Figure 1: TEM micrograph of calcium carbonate nanoparticles prepared by *in situ* deposition technique.

3.2 Wide angle X-ray diffraction studies (WAXD)

The WAXD analysis is a very useful method to describe the extent of intercalation and exfoliation of inorganic nanofiller in the composites. Figure 2 (a) and (b) shows WAXD patterns of PVC/micro and nano-$CaCO_3$ composites of 1, 3 and 5 wt. % of filler. Figure 2 (a) shows minor peaks at 2 $\theta = 29.0^0$ while figure 2 (b) shows prominent sharp peaks at the same angle, obviously, these peaks are contributed by the filler nano-$CaCO_3$. The subsiding of peaks at 2 $\theta = 29.0^0$ in fig. 2 (a) in the case of micro-$CaCO_3$ filled composites at all wt. % (1, 3 & 5) indicates fairly good dispersion. While in the case of nano-$CaCO_3$ filled composites the peaks do not subside instead, they sharpen and the peak height at 2 $\theta = 29.0^0$ increases with increasing content of the filler (1-5 wt. %). Therefore it can be concluded that the structure of nanocomposites is intercalated and flocculated and not the exfoliated.

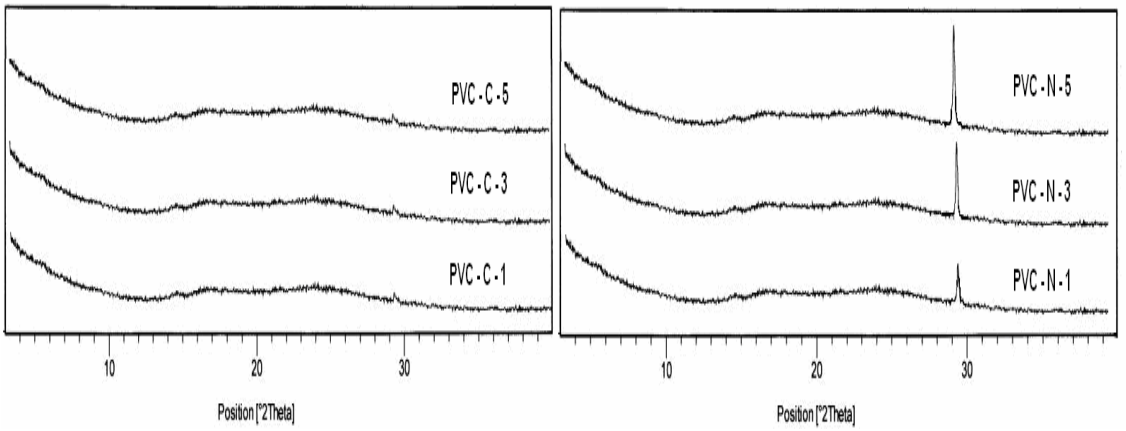

(a) **(b)**

Figure 2: WAXD of a) PVC/micro-$CaCO_3$ for composites of 1, 3 and 5 wt. % of filler and b) PVC/nano-$CaCO_3$

3.3 Tensile Behavior

Figure 4 shows the tensile behavior of PVC/micro and nano-$CaCO_3$ composites prepared by melt intercalation.

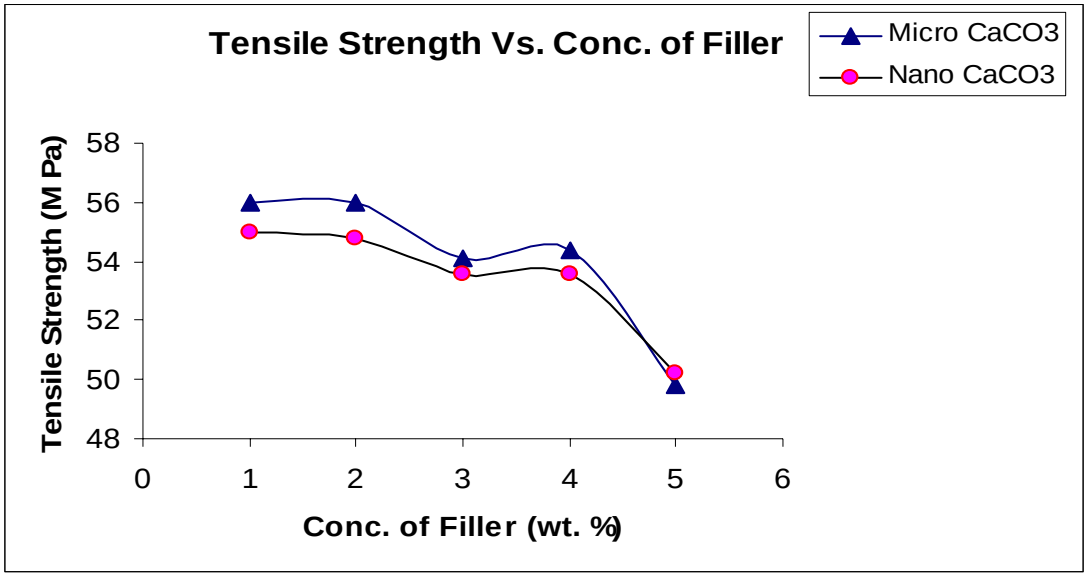

Figure 3: Tensile strength of composites (micro and nano) with the variation of filler content (1 to 5 wt. %)

With the increasing addition of the nano-$CaCO_3$ particles, due to the tendency of agglomeration of nanoparticles weak interfacial adhesion existed between the PVC matrix and the nanoparticles and hence the load bearing capacity of cross sectional area of composites decreased, and only a small amount of stress could be transferred from the matrix to inorganic particles hence tensile strength showed decrement in the magnitude; in this case agglomerated particles easily debonded from the matrix and could not bear any fraction of external load ultimately

decreasing the tensile strength. These results are inconsistent with the results of the research work carried out by Tianbin Ren et al. [16], Shuisheng Sun et al. [5], and Jie Ren et al [20].

3.4 Thermogravimetric Analysis (TGA)

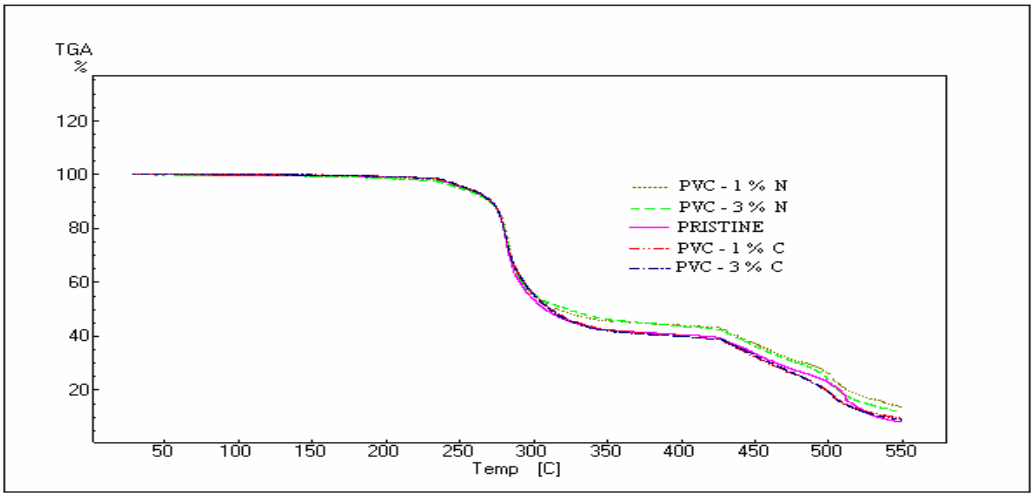

Figure 4: Representative TGA curves of PVC/micro and nano-$CaCO_3$ composites

Representative TGA curves of PVC/micro and nano-$CaCO_3$ composites are shown fig. 4 Looking at the values of T_{onset} from figure pristine PVC and PVC /micro-$CaCO_3$ composites did not show variation while those of PVC/nano-$CaCO_3$ composites showed marginal increase in the values of T_{onset}. Further, the weight residue of PVC/nano-$CaCO_3$ is higher than that of pristine PVC and their corresponding microcomposites of $CaCO_3$.

3.5 Dynamic Mechanical Analysis (DMA)

Dynamic storage modulus as a function of temperature for pristine PVC and PVC/micro and nano-$CaCO_3$ composites are ploted in fig. 5. It is observed that the storage modulus (E') of microcomposites is slightly higher than that of PVC/nanocomposites and pristine PVC in the glassy region. Moreover the magnitude of storage modulus is higher with the increasing content of micro $CaCO_3$ in the same (glassy region). A similar trend is observed in the case of glass transition temperature obtained from tan δ Vs. temperature curves. In general the nanocomposites did not show significant variation in storage modulus as well as in glass transition temperature, rather the trend is mediocre compared to pristine PVC and microcomposites this unexpected viscoelastic behavior again accounted for non uniform distribution of nanoparticles and the formation of agglomerates causing inhomogeneous interactions of organic matrix and the inorganic filler.

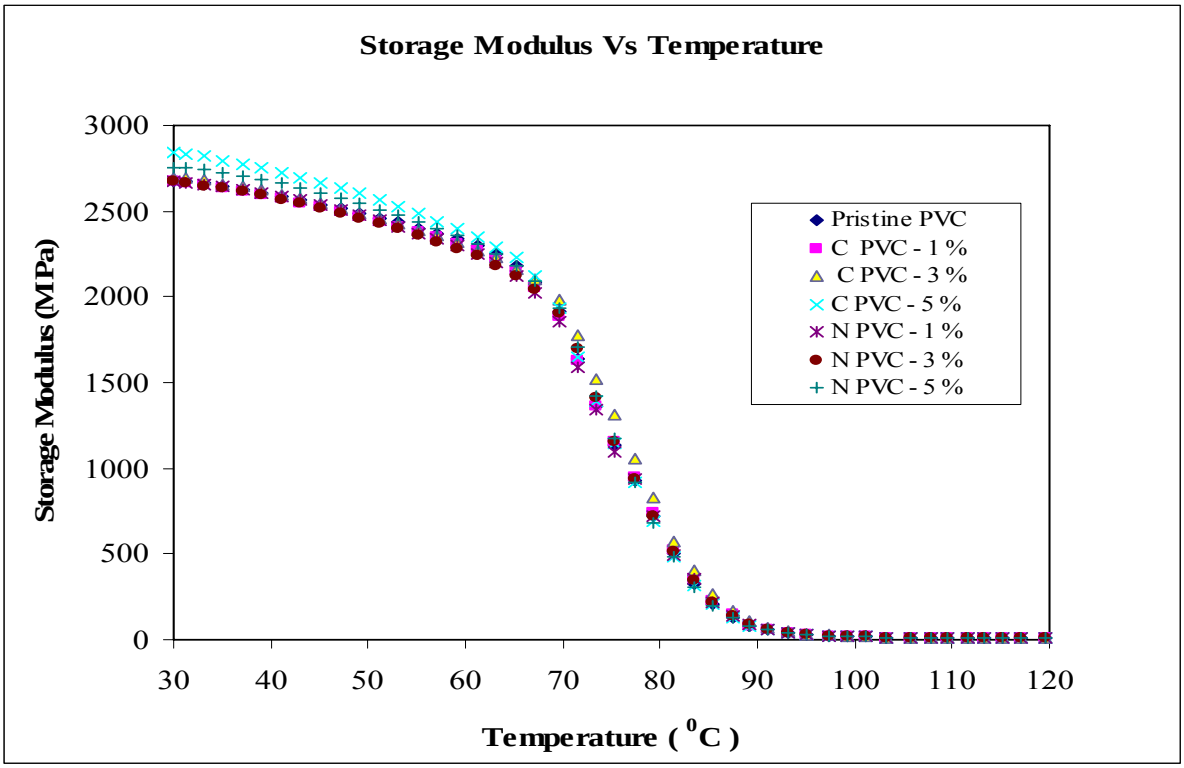

Figure 5: Variation of Storage Modulus with respect to temperature for Pristine PVC and PVC/micro and nano-$CaCO_3$ composites at 1, 3, and 5 wt. %

Table 1: T_g of PVC/ micro and nano $CaCO_3$ composites

% of Filler	T_g of PVC/micro -$CaCO_3$ composites (^{0}C)	T_g of PVC/nano-$CaCO_3$ composites (^{0}C)
0	91.2	91.2
1	91.6	92.0
3	93.3	91.4
5	93.3	91.1

Conclusions:

Nano $CaCO_3$ particles were successfully synthesized using *in situ* deposition technique and the particle size was obtained in the range of 35 to 60 nm confirmed by XRD and TEM techniques. The PVC/micro and nano-$CaCO_3$ composites were prepared by melt intercalation. The impact of nanoparticles on thermal, dynamic mechanical and tensile behavior was studied and compared with microcomposites. From the results of WAXD it was confirmed that dispersion of filler was not proper in PVC matrix and hence the structure of PVC nanocomposites was intercalated and flocculated. The tensile strength of both the micro and nanocomposites was decreased with the increasing $CaCO_3$ content. The storage modulus of both composites was found to be slightly

higher than that of pristine PVC. The glass transition temperature of both the composites was also slightly higher than pristine PVC. Further the onset degradation temperature of PVC/nano-$CaCO_3$ composites was marginally higher than microcomposites and pristine PVC. Thus this study shows that there is poor interaction between PVC and the nano-$CaCO_3$ filler. There is a need to modify interaction between PVC and nano-$CaCO_3$.

Acknowledgement

Authors thank the University Grants Commissions, New Delhi for providing financial assistance under grants of Special Assistance Programme (SAP) at Departmental Research Support (DRS) Level.

References:

1. Dezhen, W.; Xiaodong, W Yongzhi, S.; Riguang, J. J Appl Polymr Sci 2004, 92, 2714.
2. Cheng-Ho, C.; Chih-Chun, T.; Shun-Fua, S.; Wen-Chang, W.; Chien-Hsin, Y.; J Polym Sci Part B: Polym Phys 2006, 44, 451.
3. Sun, S.; Li, C.; Zhang L.; Du, HL.; Burnell- Gray, JS.; Polymer Int 2006, 55, 158.
4. Xiao-Lin, X.; Qing-Xi, L.; Robert Kwok-Yiu, L.; Xing-Ping, Z.; Qing-Xin, Z.; Zhong-Zhen, Y.; Yiu-Wing, M.; Polymer 2004, 45, 6665.
5. Ling, Z.; Xuehua, C.; Chunzhung, Li. J Mater Sci 2005, 40, 2097.
6. Chan, C.M.; Wu, J.; Li, J.X.; Cheung, Y. K.; Polymer 2002, 43, 2981.
7. Mishra, S.; Sonwane, S.H.; Singh, R.P. J Polym Sci Part B: Polym Phys 2005, 43, 107.
8. Saujanya, C.; Radhakrishan, S.; Polymer 2001, 42, 6723.
9. Cheng-Ho, C,; Chih-Chun, T,; Ming-Shyong, T,; Fu –Su, Y,; J Polym Sci Part B: Polym Phys 2006, 44, 2145.
10. Mingwang, P.; Xudong, S.; Xiucuo, L.; Haiyan, H.; Liucheng, Z. J Appl Polym Sci 2004, 94, 277.
11. Yong – Zhong, B.; Zhi-Miang, H.; Zhi-Xue, W.; J Appl Polym Sci 2006, 102, 1471.
12. Tianbin, R.; Jung, Y.; Yanxia H.; Jie, R.; Yan, L.; J Polym Comp 2006, 27, 55
13. Zhu-Mei, L.; Chao-Ying W.; Yong, Z.; Ping, W.; Jie, Y. J Appl Polym Sci 2004, 92, 567.
14. Chaoying, W.; Xiuying, Q.; Yong, Z.; Yinxi, Z. J Appl Polym Sci, 2003, 89, 2184.
15. Haiyan, Hu.; Mingwang, P.; Xiucuo Li.; Xudong, Shi.; Liucheng Z. Polymer Int 2004, 53, 225.
16. Jie, R.; Yanxia, H.; Yan, L,; Xiaozhen, T. Polym Test 2005, 24, 316.

17. Peprnicek, T.; Duchet, J.; Kovarova, L.; Malac, J.; Gerard, J. F.; Simonik, J. Polym Degrd Stab 2006, 91, 1855.
18. Gong, F. L.; Zhao, C. G.; Feng, M.; Qin, H.L.; Yang, M. S.; J Mate Sci 2004, 39, 293.
19. Peng, L.; Mingfei, Z.; Jinshan, G. J Macro Sci Part B: Phys 2006, 45, 1135.
20. Guangming, Chen. J Appl Polym Sci 2007, 106, 817.
21. Chaoying, W.; Xiuying, Q.; Yong Z.; Yinxi, Z. Polym Test 2003, 22, 453.
22. Chaoying, W.; Yong Z.; Yinxi, Z. Polym Test 2004, 23, 299.
23. Dongyan, W.; Daniel, P.; Qian, Y.; Charles A.W. J Vinyl Addit Tech 2001, 7 - 4, 203
24. Dongyan, W.; Charles, A. W, J Vinyl Addit Tech 2002, 8 - 4, 238.
25. Ismail, H.; Munusamy Y. J Rein Plast Comp 2007, 26, 1681.

In-situ generation of silica in epoxy matrix and modified epoxy matrix via sol-gel process

K.K.Iynesh Kumar and B.Kothandaraman
Department of Rubber and Plastics technology, Madras Institute of Technology, Anna University, Chennai, India.
Email: iyneshkumar@gmail.com bkraman@mitindia.edu

ABSTRACT

The precipitation of nanosilica was done through Sol-Gel process with Tetraethoxysilane (TEOS) as silica precursor at room temperature. The choice of epoxy as a matrix was made because of its polar nature which can interact with in-situ generated silica. The amine containing polydimethylsiloxane (PDMS) was used as liquid rubber modifier.

The precipitation was done directly on the organic matrix in the presence of Water, Tetraethoxysilane (TEOS) and Ethanol as mutual solvent. The nanocomposite was cured by triethylene tetramine at room temperature. To enhance bonding between organic and inorganic matrix Dichlorodimethylsilane (DDS) was used as a coupling agent.

Dispersion of silica particles was observed through Atomic force microscope (AFM). Infrared spectroscopic studies indicated the occurrence of chemical interaction within the epoxy/silica under ambient conditions. The glass transition temperature (T_g) was investigated through Differential scanning calorimeter (DSC). The thermal stability and filler content of the material were predicted through Thermogravimetricanalyser (TGA). The mechanical reinforcement within the material was demonstrated through flexural behavior of the material.

INTRODUCTION

The sol-gel process, which is mainly based on inorganic polymerization reactions, is a chemical synthesis method initially used for the preparation of inorganic materials such as glasses and ceramics. Its unique low-temperature processing characteristic also provides unique opportunities to make pure and well-controlled composition organic/inorganic hybrid materials through the incorporation of low molecular weight and oligomeric/polymeric organic molecules with appropriate inorganic moieties at temperatures under which the organics can survive. The organic/inorganic hybrid materials made in this way, which have been termed “creamers” by Wilkes [1] and “ormosils” or” ormocers” by Schmidt[2]., are normally nanocomposites and have the potential for providing unique combinations of properties which cannot be attained by other materials .

For the past decade, organic/inorganic nanocomposites prepared by the sol-gel process have attracted a great deal of attention, especially in the fields of ceramics, polymer chemistry, organic and inorganic chemistry, and physics. The preparation, characterization, and applications of organic/inorganic hybrid materials have become a fast expanding area of research in material science. The major driving forces behind the intense activities in this area are the new and different properties of the nanocomposites which the traditional macroscale composites and conventional materials don’t have. For example, unlike the traditional composite materials which have macroscale domain size of millimeter and even micrometer scale, most of the organic/inorganic hybrid materials are nanoscopic, with the physical

constraint of several nanometers, typically 1-100nm, as the minimum size of the components or phases. Therefore, they are often still optically transparent although microphase separation may exist. Through the combinations of inorganic and organic components in conjunction with appropriate processing methods, various types of primary and secondary bonding can be developed leading to materials with new properties for electrical, optical, structural, or related applications. [3]

EXPERIMENTAL

MATERIALS USED.

DGEBA liquid epoxy resin (LY556) with epoxy equivalent around 170 and viscosity of 8000 to 12000 cp at 25 degree Celsius was used as received from Araldite India Pvt. Ltd.The silicon alkoxide, TEOS was supplied by Aldrich, USA. Dimethyldichlorosilane was used as silane coupling agent supplied by M/s Merck .Organo modified polysiloxane with molecular weight around 5000 was used as liquid rubber modifier as received from Resil chemicals Pvt Ltd. Triethylene tetramine (HY 951-curing agent) was used as received from Araldite India Pvt.Ltd.

PREPARATION OF LIQUID RUBBER MODIFIED EPOXY MATRIX.

Amine containing polydimethylsiloxane was taken as liquid rubber modifier. Five phr of liquid rubber modifier was taken along with epoxy resin and the mixture was heated at 50 degree Celsius for 30 minutes with continuous stirring. Then the liquid rubber modified epoxy resin was allowed to cool in the room temperature.

PREPARATION OF SILANE COUPLING AGENT TREATED EPOXY RESIN.

Dichlorodimethylsilane was taken as silane coupling agent. The required amount of Dichlorodimethylsilane along with epoxy resin was heated at 60 degree Celsius with continuous stirring for 5 hours. The silane treated epoxy resin was left untouched for 4 to 5 hours. The same silane treatment procedure was carried out for Amine containing PDMS modified epoxy resin.

PREPARATION OF EPOXY AND MODIFIED EPOXY HYBRID MATERIALS.

The silica nano particles were prepared by hydrolysis of TEOS in ethanol medium. The reaction mixture (Water+TEOS+Ethanol) was stirred for 15 minutes in a glass beaker. Then the mixture was added to 50 ml epoxy resin and stirred continuously for 24 hours. The triethylene tetramine curing agent was added to in-situ silica precipitated epoxy resin at room temperature. Then the epoxy/silica hybrid material was cast between two polished mild steel plates and allowed to cure at room temperature for 24 hours. Then the cured material was post-cured at 150 degree Celsius for 3 hours. The above said procedure was repeated for Amine containing PDMS modified epoxy resin, silane treated epoxy resin, and silane treated Amine containing PDMS modified epoxy resin.

RESULTS AND DISCUSSIONS

FT-IR SPECTRUM STUDIES OF MODIFIED AND UNMODIFIED EPOXY –SILICA HYBRID MATERIALS

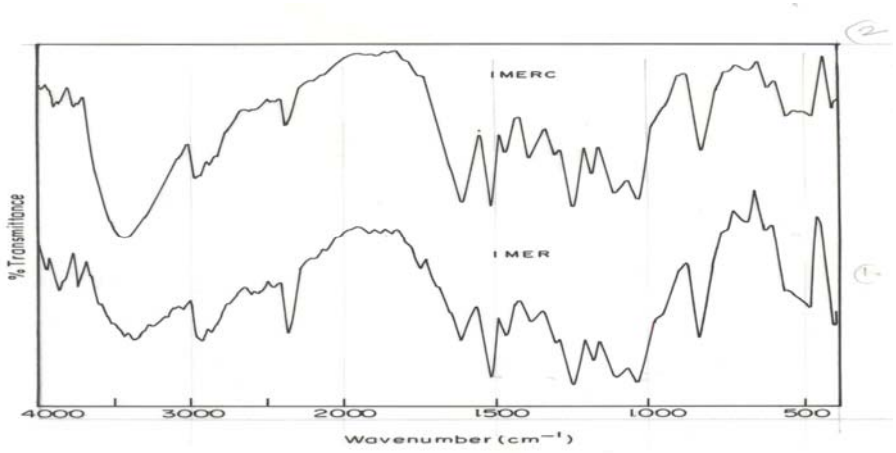

FT-IR spectrum. IMERC-in-situ silica precipitated modified epoxy resin treated with Dichlorodimethylsilane. IMER-in-situ silica precipitated modified epoxy resin.

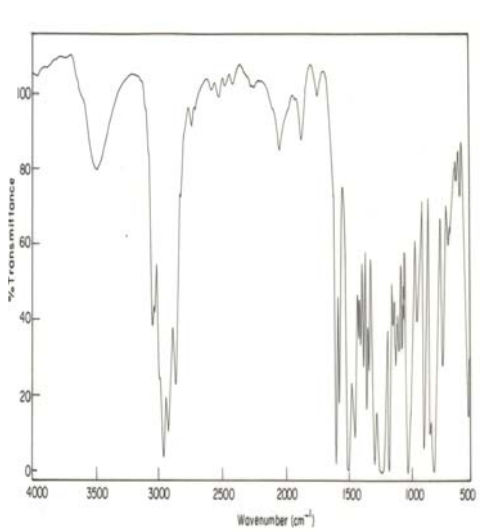

FT-IR spectrum of uncured epoxy

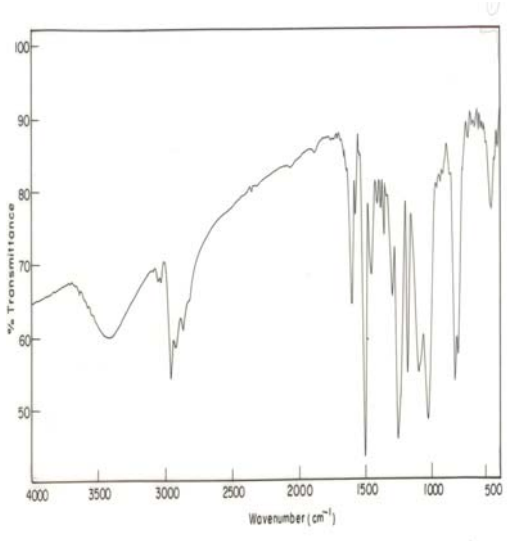

FT-IR spectrum of amine containing PDMS

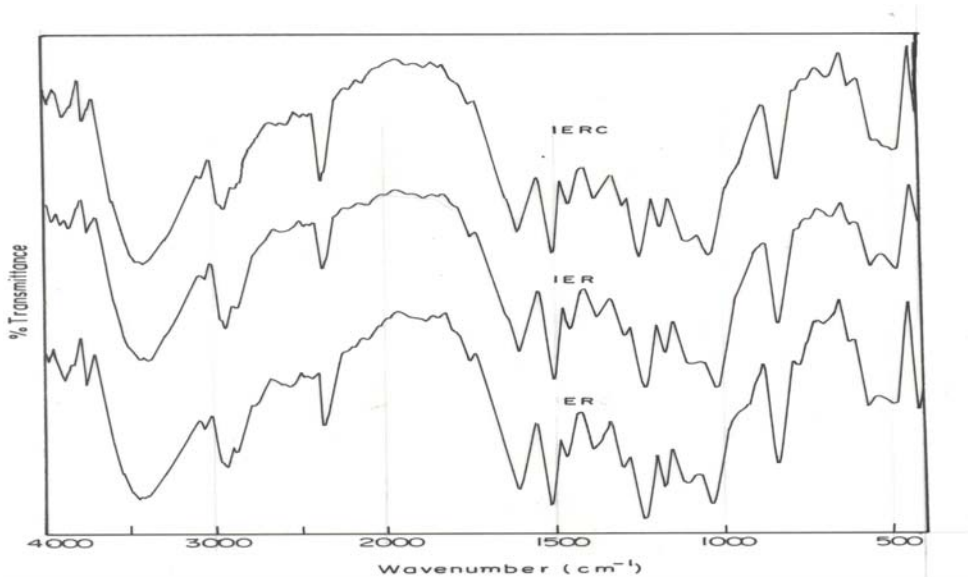

The FT-IR spectrum .ER-Epoxy resin, IER-in-situ silica precipitated epoxy resin.IERC-in-situ silica precipitated epoxy resin treated with Dichlorodimethylsilane.

The FTIR spectroscopy was done. The apparatus used was PERKIN-ELMER make.

Scanning Rate: 16 scans

Resolution: 4 cm^{-1}

IR spectroscopy is not helpful since the epoxy breathing bands as well as absorptions of the silanol groups were not clearly detected owing to a very broad band, involving the Si–O–Si network formation, ranging from 950 to 1250 cm-1[14].The Disappearance of epoxide peak at 915cm^{-1} indicates the complete curing of epoxy resin.

TGA STUDIES FOR MODIFIED AND UNMODIFIED EPOXY –SILICA HYBRID MATERIALS

TGA studies of Amine containing PDMS modified Epoxy-Silica hybrid materials

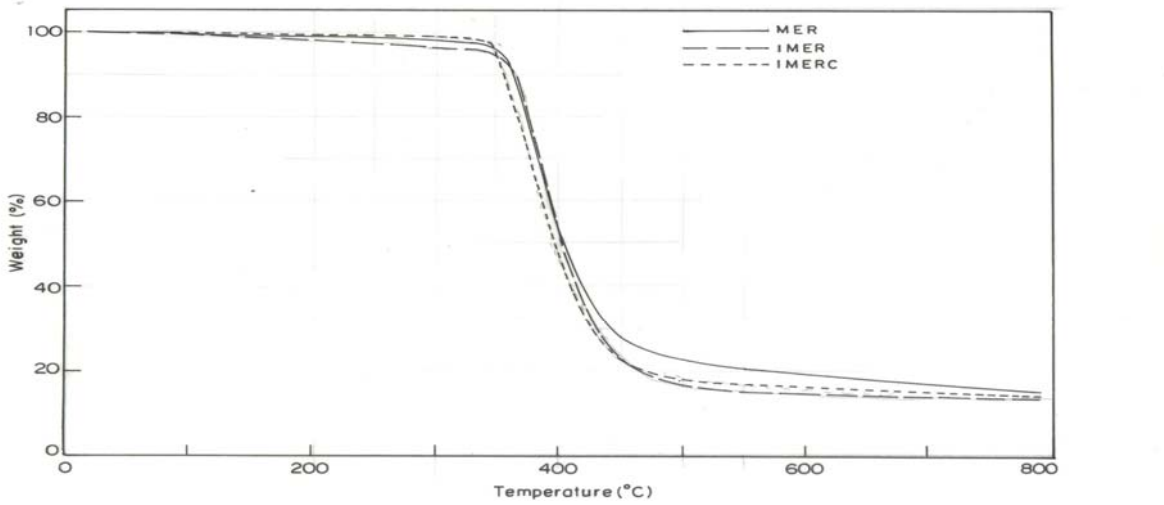

.MER-PDMS modified epoxy resin. IMER-in-situ silica precipitated PDMS modified epoxy resin. IMERC-in-situ silica precipitated PDMS modified epoxy resin.

TGA studies of Epoxy-Silica hybrid materials

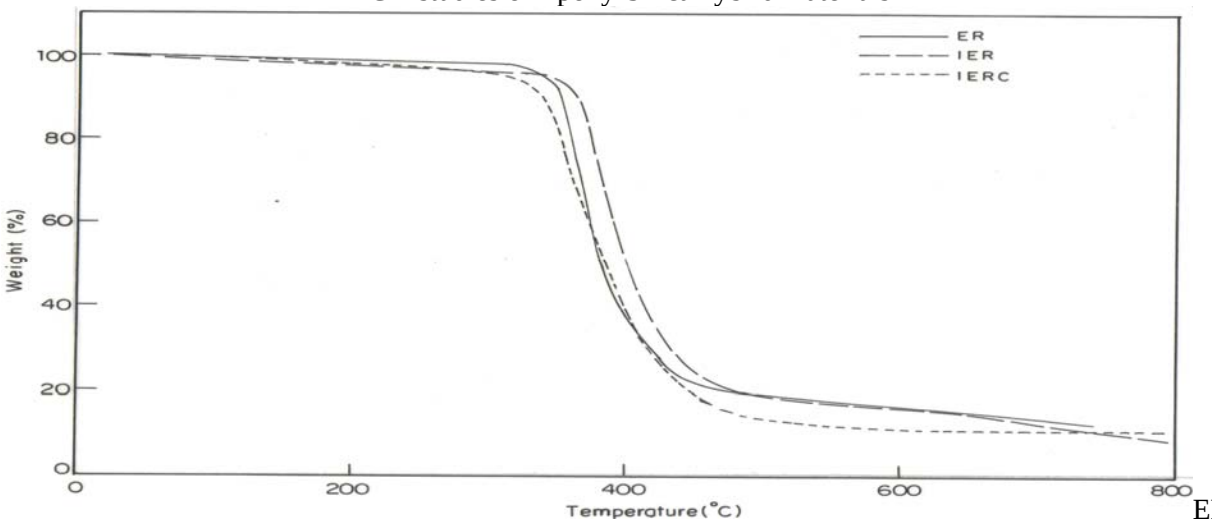

ER-ER-Epoxy resin.IER-in-situ silica precipitated epoxy resin. IERC-in-situ silica precipitated epoxy resin treated with Dichlorodimethylsilane.

The silica content and thermal stability of the materials were determined by using TA Qseries equipment at a heating rate of 20°C/min from 30°C to 800°C in the nitrogen atmosphere.

The drawback of using sol-gel process in preparing polymer-silica nanocomposites is its harm to the initial thermal stability of the resulting nanocomposites. This effect is mainly due to the residual of the silanoxy groups in the formed polymer-silica nanocomposites and the silanoxy group might perform dehydration reaction under high temperatures in the processing and the using period of nanocomposites [11]. Contradiction to this fact the initial thermal stability of the epoxy resin had improved with addition of TEOS. This shows the existence strong intermolecular hydrogen bonding between the organic and inorganic phase. The addition of DDS resulted in the decrease of initial decomposition temperature. At higher temperature Hcl liberated during the synthesize of hybrid materials resulted in the chain scission within the hybrid matrix.

The addition of Teos to Amine containing PDMS modified epoxy matrix showed improved initial decomposition temperature. The addition of Teos had reduced the free volume in the modified epoxy domains which have caused the restriction in the mobility of the chains resulted in higher initial decomposition temperature. The addition of DDS resulted in the decrease of initial decomposition temperature in the PDMS modified epoxy matrix. At higher temperature Hcl liberated during the synthesize of hybrid materials resulted in the chain scission within the hybrid matrix.

The char formation is of lesser importance as the percentage of silica loading is very low.

GLASS TRANSITION TEMPERATURE (T_g) VALUES OF MODIFIED AND UNMODIFIED EPOXY-SILICA HYBRID MATERIALS

Glass Transition temperature of Epoxy-Silica hybrid materials

S.No	Specimens	(T_g) deg Celsius
1	Neat(Without Siloxane)	106.92
2	TEOS	80
3	TEOS+DDS	106.09

Glass Transition temperature of Amine containing PDMS modified Epoxy-Silica hybrid materials

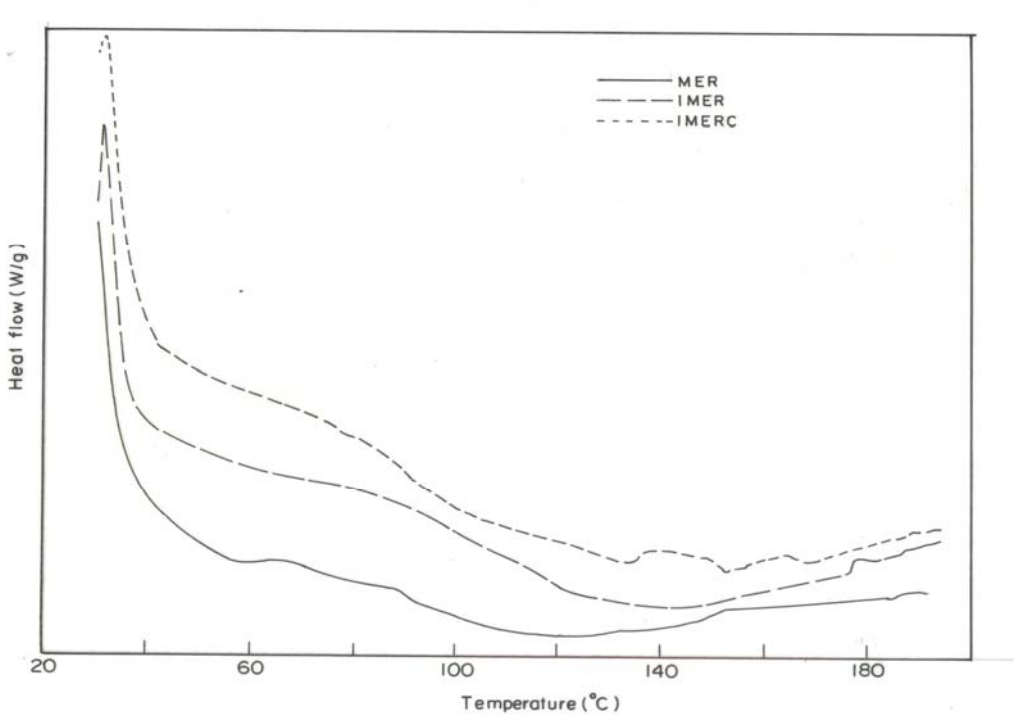

MER-PDMS modified epoxy resin. IMER-in-situ silica precipitated PDMS modified epoxy resin. IMERC-in-situ silica precipitated PDMS modified epoxy resin.

The glass transition temperature of the materials was studied by using Differential scanning calorimetry. TA Qseries equipment was used. The test was carried out with a heating rate of 20°C/min from 30°C to 200°C in the nitrogen atmosphere. The glass transition temperature

of epoxy resin was determined. It was found that, T_g of epoxy decrease with the addition of TEOS, the silica precursor. This shows the plastication effect of the silica. Introduction of silica particles might also increase the free volume of the resins to reduce their T_g. The addition of Dichlorodimethylsilane improves the additional cross-links in the organic and inorganic phase which resulted in similar T_g of neat epoxy resin.

The glass transition temperature of Amine containing PDMS modified epoxy phase was determined. The addition of Teos, the silica precursor did not decrease the T_g of epoxy phase this shows that there is limited compatibility between modified epoxy and inorganic phase. It was found that the addition of Dichlorodimethylsilane decreased the T_g of modified epoxy phase indicating the good compatibility that exists between modified epoxy and inorganic phase and the plastication effect of the silica. The Hcl liberated during the synthesize of hybrid material increases the rate of hydrolysis of TEOS.This suggest that less phase separation of PDMS and more will be incorporated in TEOS network hence good miscibility and lower T_g.

MORPHOLOGICAL PROPERTIES OF MODIFIED AND UNMODIFIED EPOXY-SILICA HYBRID MATERIALS

Here Veeco instruments AFM was used for the morphological studies of flexural fractured Modified and Unmodified Epoxy-Silica hybrid materials. Contact mode was used for morphology studies. The morphological analysis of the hybrid materials was investigated by Atomic Force Microscopy (AFM). The Atomic Force Microscopy images were taken for Modified and Unmodified Epoxy-Silica hybrid materials. The AFM images of unmodified Epoxy –Silica hybrid materials showed no phase separation and homogenous dispersion of silica particles without any aggregation. Optically transparent composite materials can be obtained if there is no macro- microphase separation during both the gel forming and drying process [3]. The resultant material was transparent. The AFM images of Amine containing PDMS modified Epoxy –Silica hybrid materials showed two phase morphology with rigid continuous phase and a dispersed rubbery phase with silica particles dispersed homogenously. The rubber particles are partly pulled out from the epoxy matrix and partially fractured. In this case, the crack developed through the rubbery particles and indicates that the interaction between the rubbery particles and matrix has occurred. The presence of cone shape in the afm images confirms the interaction of epoxy and rubbery phase.

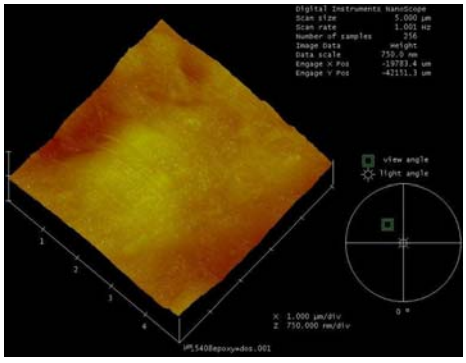

AFM image of epoxy matrix with TEOS and DDS

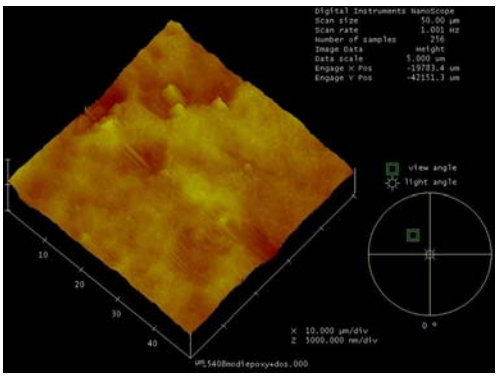

AFM image of Amine containing PDMS modified epoxy matrix with TEOS and DDS

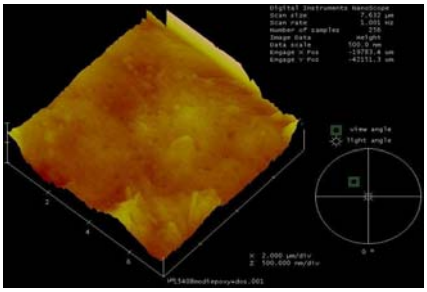

AFM image of Amine containing PDMS modified epoxy matrix with TEOS and DDS

MECHANICAL PROPERTIES OF MODIFIED AND UNMODIFIED EPOXY-SILICA HYBRID MATERIALS

The mechanical properties like flexural strength, flexural modulus and flexural strain to failure, of the modified and unmodified Epoxy-Silica hybrid materials were studied according to ASTM D790 standards. The flexural specimen dimension of 80mm × 25mm of 3mm was prepared. The flexural tests were carried at the crosshead speed of 3mm per minute. The results are tabulated below,

Flexural properties of Epoxy-silica Hybrid materials

S.No	Specimens	Flexural Strength (MPa)	Flexural Modulus (GPa)	Flexural Strain to Failure (%)
1	Neat(Without Siloxane)	97	3.8	2.5
2	TEOS	97.7	2.7	3.4
3	TEOS+DDS	122	2.8	3.9

Flexural properties of PDMS modified Epoxy-silica Hybrid materials

S.No	Specimens	Flexural Strength (MPa)	Flexural Modulus (GPa)	Flexural Strain to Failure (%)
1	Neat(With Siloxane)	75	2.6	2.8
2	TEOS	72	2.3	3.1
3	TEOS+DDS	95	2.6	3.7

The sol-gel processing of TEOS in epoxy resin decreased the flexural strength, modulus and increased the flexural strain to failure. At neutral condition, gel formation occurs at relatively low conversion and unhydrolysed TEOS can remain in the system [12, 13] those results in low modulus, and low flexural strength. The plasticizing effect of silica particles in the epoxy domains resulted in increase in the flexural strain to failure. The Dichlorodimethylsilane may act as coupling agent and it reduces gelation time. The gel formation occurs at relatively higher rate and there is a reduction in the amount of unhydrolysed TEOS in the system resulting in better flexural values.

There is a reduction in the flexural strength; modulus and increase in flexural strain to failure of Amine containing PDMS modified epoxy and TEOS system. The chemical link formation between inorganic and the amine group containing PDMS are poor, that results in incompatibility and reduction in properties. The addition of Dichlorodimethylsilane resulted with improvement in properties which are attributed to reduce in free volume which reduces chain mobility and the formation of additional cross links.

CONCLUSION

The TGA studies show the addition of Dichlorodimethylsilane decreased the thermal stability of the modified and unmodified epoxy composite and the nanosilica precipitated had not altered the thermal stability of the material. The DSC Studies showed T_g values decreased to greater extent indicating the plastication effect of silica within the matrix and slight decrease indicating the limited compatibility between organic and inorganic matrix. The AFM images confirmed no phase separation between organic and inorganic phase and fine dispersion of silica particles without any aggregation. The FT-IR spectroscopy confirmed the disappearance of epoxide peak. The flexural modulus decreased and flexural strain to failure increased indicating the plastication effect of silica .With the addition of Dichlorodimethylsilane which reduces gelation time. The gel formation occurs at relatively higher rate and there is a reduction in the amount of unhydrolysed TEOS in the system resulting in better flexural values.

REFERENCES

1. Wilkes,G.L.; Orler, B.;Huang, H.Polym.Prepr. 1985.26 pp300

2. Schmidt,H. J.Non- Cryst.Solids 1985,73,pp681.

3. Jianye Wen ., Garth L. Wilkes . Chem. Mater.1996.8,pp1667-1681

4. Sungtack Kang, Sung Il Hong, Chul Rim Choe, Min Park, Soonho Rim, JUnkyung Kim.Polymer. 2001.42, pp879

5. Suzanne Frings, Organic –inorganic coatings: based on polyester resins and in-situ formed silica,University of Eindhoven, 1999 [PhD Thesis]

6. Sanchez,C.; Ribot,F.New J. Chem. 1994, 18,1007.

7. Judeinstein,P.: Sanchez,C.J. Mater.Chem. 1996,6,511.

8. A.Al.Abrash, F.Al.Sagheer, A.A.m.Ali and Z.Ahmad, Thermal and mechanical properties of poly(hydroxyl-imide)-silica nanocomposites international journal of polymeric materials, 2006, vol.55, no-2, pp.103-120.

9. F.Al-Sagheer, A.A.M.Ali, S.Muslim, and Z.Ahmad, Thermal and mechanical properties of chemically bonded aramid-silica nanocomposite, science and technology of advanced materials, 2006, vol.7, no.1,pp.111-118

10. Gerhard Schottner, Chem.Mater.2001.13.3422-3435

11. Ying-Ling Liu, Chih-Yuan Hsu, Wen-Lung Wei, Ru-Jung Jeng, Polymer.2003.44.5159-5167

12. L.Matejka,O.Dukh and J.Kolarik,Polymer,41,(2000),1949.

13. L.Matejka.K.Dusek,J.Plestil.J.Kriz and F.Lednicky,Polymer 40(1998),171-181.

14. P. Cardianoa,*, P. Mineob, S. Sergia, R.C. Ponterioc, M. Triscari, P. Pirainoa Epoxy-silica polymers as restoration materials. Part II.Polymer 44 (2003) 4435-4441

Structure property relationship studies of melt spun carbon nanotubes filled polypropylene fiber

Pankaj B. Tambe[a*], Arup R. Bhattacharyya[a#], Srikanth Kamath[a], Ajit R. Kulkarni[a], T.V. Sreekumar[b], Kingsuk Mukhopadhyay[b] and Anurag Srivastav[b]

[a]Department of Metallurgical Engineering and Materials Science, Indian Institute of Technology Bombay, Powai, Mumbai 400076, India
[b]Defence Materials and Stores Research and Development Establishment (DMSRDE), DRDO, Kanpur 208013,India
Email: arupranjan@iitb.ac.in

Abstract

Two different types of multiwalled carbon nanotubes (MWNT) were utilized in order to understand the effect of different types of MWNT in enhancing mechanical properties of the melt spun MWNT filled polypropylene composite fibers. It was found that MWNT synthesized in DMSRDE were found to be superior over NC 3100 procured from Nanocyl, CA, Belgium in achieving high modulus and tenacity of PP/MWNT composite fibers. Herman's orientation factor of (110) PP plane and MWNT along the composite fiber axis were also calculated and it was found that MWNT prepared in DMSRDE found to exhibit higher orientation over NC 3100 MWNT.

1. Introduction

Polypropylene (PP) is one of the major polymeric fiber materials of future in view of its impressive consumption in the past decade. However, PP fiber needs reinforcement in order to achieve high stiffness and strength for engineering applications. Since the discovery of carbon nanotubes (CNT) by Iijima [1], CNT have emerged as a potential candidate as reinforcing filler in polymer based composites due to their unparallel mechanical, electrical and thermal properties. Melt spinning process is one of the most common and viable route to produce polymer fiber. The formation of fibers involves four stages: a) melting the polymer, b) extrusion of melt through spinneret, c) cooling along spin line and winding the resulting fiber on a roll and d) the resulting fiber post drawn to a maximum possible draw ratio.

Several studies have been carried out on crystallization, orientation and mechanical properties of melt-blended PP/single wall carbon nanotube (SWNT) [2] and PP/ multiwall carbon nanotube (MWNT) [3] composites fiber. In addition flourinated SWNT [4] and benzoyl per oxide initiated functionalization of SWNT [5] to PP chain were also utilized in order to improve the exfoliation and interfacial adhesion of SWNT with PP chain in order to improve the mechanical properties of composite fiber.

The aim of this work is to evaluate the effect of two different types of MWNT on the structure property of PP/MWNT composite fiber. Oriented structure of PP crystal plane and MWNT along the fiber axis are quantified as per Herman's orientation factor. The effect of orientation of PP crystal plane and MWNT are correlated with the mechanical properties of PP/MWNT composite fiber.

2. Experimental Details

Polypropylene was obtained from Reliance Industries Ltd, India (REPOL H200F, melt flow index of 20 g/10min). MWNT were obtained from Nanocyl CA Belgium (NC 3100, L/D=100-1000, purity=95%) and DMSRDE, Kanpur also subsequently utilized for our study. Various compositions of PP/MWNT composites using two different types of MWNT were prepared by melt mixing in a conical twin screw extruder (Micro 5, DSM Research, Netherlands) at optimized melt mixing condition of 260^0C with a rotational speed of 200 rpm for 15 min in which MWNT were varied from 0.5-3 wt%. Melt mixed PP/MWNT samples were dried at 80^0C under vacuum over night. PP/MWNT composite were melt-spun using a small scale spinning machine manufactured by the Bradford University Research Ltd. UK, using a single hole spinneret of 1 mm diameter. The fiber spinning was carried out at 200^0C with ram speed of 1.4 mm/min. The take up speed was kept at 20 m/min for all compositions. The melt spun fibers were further drawn at draw ratio of 8. The mechanical properties of drawn fiber were tested on a Favimat fiber tester (Textechno) with guage length of 20 mm and at a rate of 20 mm/min for 50 filaments. Raman spectroscopy was performed using Jobin Yovon (HR 800 micro-Raman) in the scanning range of 200–2000 cm^{-1} with incident laser excitation wavelength of 514 nm. Scanning electron microscopic (SEM) analysis was performed with Hitachi S3400, operated at 15 KV. Wide-angle X-ray diffraction (WAXD) studies were carried out on a Philips X-Pert Pro. The incident X-rays (λ=1.54 Å) from the Cu-target were monochromatized using a Ni filter.

3. Result and Discussion

3.1 Comparative study of Nanocyl NC 3100 and DMSRDE MWNT

TEM images of MWNT are shown in Figure (1a, 1b) shows a network of entangled MWNT. DMSRDE produced MWNT are found to be more straight, less coiled and less entangled as compared to NC 3100. Figure 1c shows the tangential Raman band for two types of MWNT. Raman peak at ~1347 cm^{-1} originates from disordered graphitic structure (D-band) and peak at ~1590 cm^{-1} originates from crystalline ordered structure of the graphene sheet (G-band); the intensity ratio, I_G/I_D provides a measure of crystalline structure in a given MWNT. The ratio of intensity of G-band and D-band (I_G/I_D) depict the order structure of MWNT. I_G/I_D value of DMSRDE MWNT (1.31) is found higher than NC 3100 MWNT (0.87) which manifests DMSRDE produced MWNT are more ordered as compared to NC 3100.

3.2 Orientation studies of PP crystal and MWNT along fiber axis

Figure 2a shows the Wide angle X-ray diffraction (WAXD) pattern for PP/MWNT composites containing 0.5 wt% MWNT. WAXD pattern of the composites show the typical α-form of PP crystals and exhibits complete absence of the β-crystal form [6, 7]. Quantification of average orientation of PP crystal plane has been carried out using WAXD by performing azimuthal scan along the specific (110) PP crystal plane (Representative Figure 2b). The detail procedure of quantification of crystal plane orientation is given below.

The crystalline orientation of the fibers has been determined quantitatively using Hermans orientation factor [8] as generalized to a set of three crystallographic axes by Stein [9]. This is defined as

$$f = \frac{3 < \cos^2 \phi > -1}{2} \qquad (1)$$

where $\left\langle \cos^2 \phi \right\rangle$ (is the averaged value of the square of the cosine of the angle ϕ between the reference direction of the sample (fiber axis) and the x-crystallographic axis. Assuming rotational symmetry about the fiber axis,

$$< \cos^2 \phi) >= \frac{\int_{-\pi/2}^{\pi/2} I(\phi) \cos^2 \phi \sin \phi d\phi}{\int_{-\pi/2}^{\pi/2} I(\phi) \sin \phi d\phi} \qquad (2)$$

where I(ϕ) is the intensity diffracted from the (hkl) planes which are normal to the x-crystallographic direction. Therefore f values can range from −0.5, when the chains are perpendicular to the x-crystallographic axis, to 1.0, when the chains are parallel to the x-crystallographic axis. When f equals zero there is random orientation in the sample.

From the X-ray diffraction pattern of drawn MWNT/P, the Herman's orientation factors for (110) PP planes are calculated, which are tabulate in Table 1. The (110) PP crystal orientation is found to be much higher in PP/MWNT composite fiber utilizing DMSRDE produced MWNT.

To calculate the Herman's orientation factor of MWNT along the fiber axis, Raman spectrum of each composition as a function of polarization angle 0, 30, 45, 60, 90^0C are considered (Representative Figure 3). From G band peak intensity at various angles, Herman's orientation factor are calculated as per equation 1 and 2. The calculated values of Herman's orientation factor are shown in Table 1, which indicates higher orientation of MWNT in PP/MWNT composite fiber while utilizing DMSRDE produced MWNT.

3.3 Mechanical Properties

Table 1 provides the details of mechanical properties data of the representative fiber compositions. Table 1 reveals composite fibers prepared by using DMSRDE MWNT show superior mechanical properties as compared to NC 3100. It is interesting to note that fiber tenacity and modulus of DMSRDE produced MWNT is higher. Fiber tenacity and modulus increases with an increase in concentration of MWNT up to 1 wt% and then decreases with an increase in MWNT concentration. The observation of superior mechanical properties in PP/MWNT composite fiber while utilizing DMSRDE produced MWNT may be related to less entangled, more straight MWNT of higher crystallinity.

3.4 Scanning electron microscopy (SEM) studies

Tensile fractured surface of PP/MWNT composite fiber are shown in Figure 4. Figure 4a shows the fibrillar structure of PP/MWNT composite fiber. The magnified micrograph of tip of fracture composite fiber (Figure 4b, c) shows that the fracture starts at PP/MWNT interface where the stress concentration was higher at the guage length of composite fiber.

4. Conclusion

Comparative study of DMSRDE produced MWNT and NC 3100 as reinforcing filler for PP/MWNT composite fiber reveal the superiority of DMSRDE produced MWNT as compared to NC 3100. The structure DMSRDE produced MWNT filled PP fiber exhibit superior orientation of PP crystal and MWNT along the fiber axis as compared to NC 3100.

5. Acknowlegements

We would like to acknowledge Microcompounder Central facility, CRNTS at IIT Bombay. We would also like to thank DMSRDE, Kanpur for financial assistance for the project.

6. References

[1] Iijima S, Nature 1991; 35:56.
[2] Bhattacharyya A R,, Sreekumar T.V, Liu T, Kumar S, Ericson L. M, Hauge R, Smalley R. E, Polymer 2003; 44:2373.
[3] Moncy V. J, Derrick D, James T, Gary P, Elijah N, Journal of Applied Polymer Science 2007; 103:3844.
[4] Daneesh M, Valery N. K, Enrique V. B, Chem. Mater., 2006; 18:4561.
[5] Daneesh M, Valery N. K, Enrique V. B, J. Phys. Chem. C 2007; 111:1592.
[6] Shaffer M. S. P., Fan X., Windle A. H., Carbon 1998; 36:1603.
[7] Kinloch I. A., Roberts S. A., Windle A. H., Polymer 2002; 43:7483.
[8] Hermans J J, Hermans P H, Vermeas D, Weidinger A. Rec Chim Trav 1946; 65:427.
[9] Stein RS. J Polym Sci, 1958; 31:327.

Table 1: Mechanical properties of melt-spun PP/MWNT composites fibers and Herman's orientation factor

Material	MWNT (wt%)	Tenacity (gpd)	Elongation (%)	Modulus (gpd)	Herman's orientation factor of (110) PP plane	Herman's orientation factor of MWNT along fiber axis
PP	------	10.02	17	114	0.6723	------
PP/MWNT DMSRDE	0.5	10.34	14	132	0.4193	0.8549
	1	11.5	14.11	153	0.4205	0.7726
	3	9.79	16	124	0.4652	0.7211
PP/MWNT Nanocyl (NC 3100)	0.5	8	21	87.5	0.3835	0.7243
	1	8.79	19.7	100	0.4246	0.7225
	3	7.2	14.8	94	0.5545	0.7181

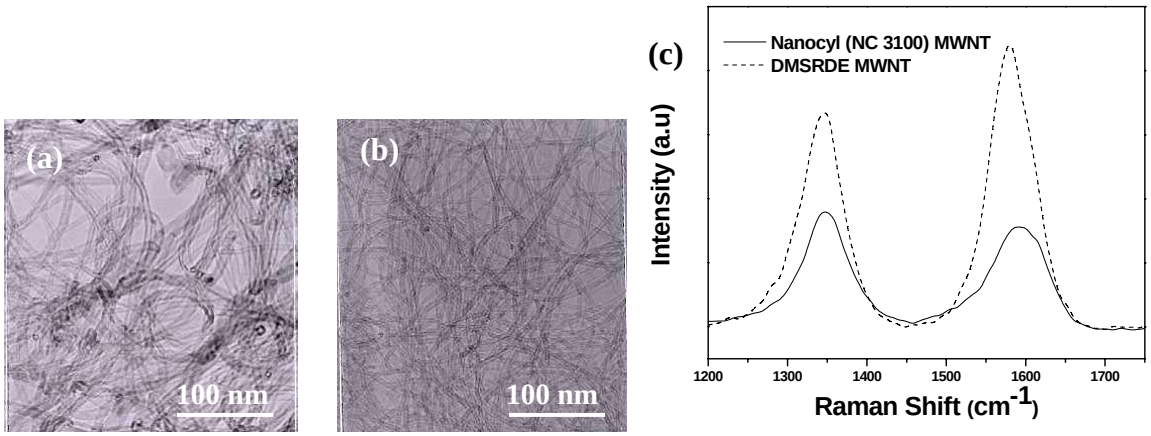

Figure 1: TEM images of MWNT (a) NC (3100) (b) DMSRDE (c) Raman spectra of DMSRE and Nanocyl (NC 3100) MWNT

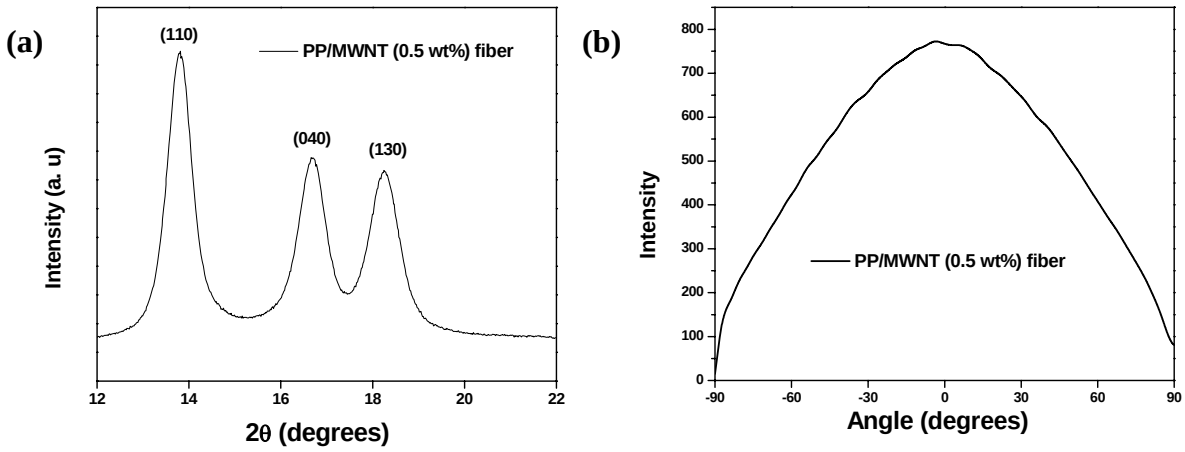

Figure 2: (a) Wide angle X-ray Diffraction (WAXD) spectra of PP/MWNT composites (b) Azimuthal scan of (110) PP plane

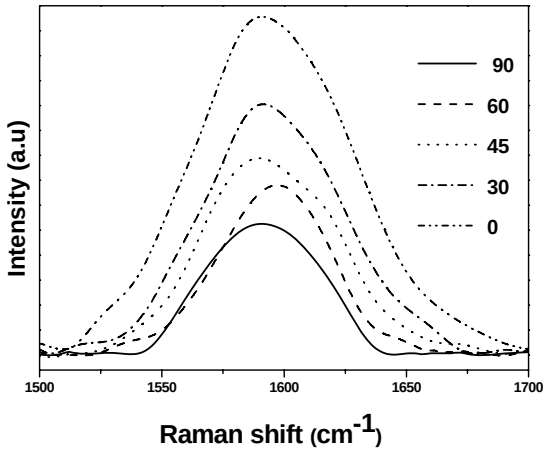

Figure 3: Tangential mode Raman spectra of PP/MWNT (0.5 wt% DMSRDE produced MWNT) composite fiber (draw ratio 8). From bottom to top, the angle between fiber axis and polarization direction is 0, 30, 45, 60, 90 degrees

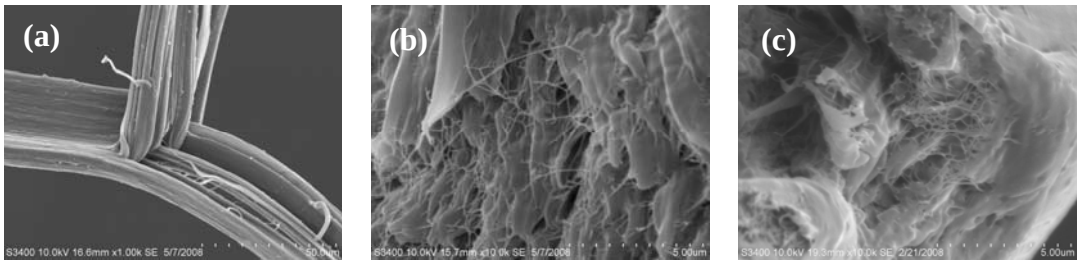

Figure 4: SEM images of PP/MWNT composite fiber

Synthesis and characterization of polypropylene/ionomer/ organoclay nanocomposites

S. R. Mallikarjuna, N. Ramesh, C. Ramesh and S. Sivaram
Divison of Polymer Science and Engineering, National Chemical Laboratory,
Pune-411 008, Maharashtra, India.
Email: c.ramesh@ncl.res.in

Abstract:
The compatibilization effects provided by ionomer-g-polypropylenes versus those of a maleated polypropylene, PPMA, for forming polypropylene-based nanocomposites were compared. We have prepared a novel compatibilizer by grafting ionic functional groups on to the PP and evaluated its efficiency as compatibilizer in the preparation of PP/clay nanocomposites. The PP/ionomer/organoclay nanocomposites were prepared by direct melt mixing and by masterbatch methods and the structure obtained were characterized by WAXD and TEM and were compared with nanocomposites prepared using PPMA as compatibilizer. Mechanical properties of the nanocomposites prepared were studied using INSTRON and the crystallization behavior was studied using Differential Scanning Calorimetry (DSC) and Polarized Optical Microscopy (POM). Thermal stabilities were characterized using TGA. The dispersion of clay was found to be dependent on the method of preparation, type of compatibilizer used and the amount of compatibilizer used. The dispersion of the organoclay was better with the ionomer than PPMA and the dispersion was better when the nanocomposites were prepared by two step masterbatch route than the single step direct mixing method. The dispersion of the organoclay improved with increase in the amount of compatibilizer. The nanocomposites obtained with ionomer as compatibilizer showed better enhancements in nucleation, thermal properties and mechanical properties as compared to the nanocomposites obtained using PPMA as compatibilizer.

Introduction:
Polypropylene (PP) is a fast growing thermoplastic and dominating the industrial applications due to its attractive combination of properties such as low density, high thermal stability, resistance to corrosion etc. and low cost. There is a strong need to improve their mechanical properties for its applications in automotive industry[1]. Researchers in the recent decade have shown that reinforcement with dispersed clay in the polymer matrix enhances the mechanical properties without much affecting the density of the polymer[2]. Therefore, various research efforts were made to disperse clay in the PP matrix. However it was very difficult to disperse clay in the PP matrix, as the polymer was highly non polar and there are no polar groups available to interact with the clay surface. The usual organo-modification of clay did not sufficiently lower the surface energy of the clay to interact with PP chains. Unmodified polyolefins lack the intrinsic thermodynamic affinity with currently available organoclays to form well dispersed nanocomposites[3]. The surface energy of PP chains was improved by introducing polar functionalities and used them for the preparation of nanocomposites[4-10]. To improve the surface energy of semi crystalline polymers in the preparation of nanocomposites, many researchers introduced ionic groups on to the polymer chains[11-19]. However compatibilizers such as amine and ammonium functionalized PP had failed to enhance the dispersion of clay in the PP matrix as compared to maleic anhydride grafted polypropylene via melt mixing[20].

Therefore in the present work, we have evaluated a novel metallic ionomer of PP as compatibilizer for preparing PP/organoclay nanocomposite by two different mixing routes. The properties of the obtained nanocomposites were compared with the nanocomposites, which are prepared using PPMA as compatibilizer.

Experimental:

The materials used in this study were polypropylene REPOL H034SG obtained from Reliance Industries (Pvt.) Ltd., maleated polypropylene (PPMA) selected for this work was FUSABOND M613-05, which contains 0.65 weight % maleic anhydride group. The organoclay, Cloisite20A provided by Southern Clay Products Inc. Potassium succinate grafted polypropylene ionomer (KPPSA) was prepared by simultaneous hydrolysis and neutralization of PPMA using methanolic KOH. All the nanocomposites were prepared by a melt mixing technique using a twin-screw extruder, DSM Micro 5 having a net barrel capacity of 5 CC with a screw speed of 100 rpm, the barrel temperature of 190 °C and a residence time of 10 min. Nanocomposites were prepared with different concentrations of compatibilizer keeping the organoclay concentration at 5 weight %. For comparison matrix polymer compositions without clay were also prepared. Nanocomposites were prepared in two different methods. In the first method, the PP, compatibilizer and the Cloisite 20A were all melt mixed directly in a single step. In the second method, the compatibilizer was mixed with the organoclay to form a masterbatch in the first step, which was then mixed with the PP in the second step. Various compositions prepared were coded in such a way that the number in the code after the compatibilizer name indicates the percentage of the respective compatibilizer, C for 5% organoclay, and the method of preparation indicated in the sample code by D for direct mixing and M for masterbatch route. Structure and morphology of all the nanocomposites prepared was studied using WAXD and TEM. Flexural moduli of the nanocomposites prepared were studied using INSTRON and the crystallization behavior was studied using Differential Scanning Calorimetry (DSC).

Results and Discussion:

Prior to evaluation of the new compatibilizer for dispersability of the organoclay in polypropylene, binary composites containing 95% compatibilizer and 5% C20A was prepared and characterized with WAXD. The WAXD pattern (figure 1a) of KPPSA/C20A showed no peak for the organoclay indicating that the organoclay was completely delaminated and exfoliated in the KPPSA matrix while PPMA/C20A showed a broad low intensity peak at a d-spacing of 38 Å indicating the presence of intercalated tactoids. The above result clearly indicates that the new compatibilizer, KPPSA containing more polar ionic functional group have better interaction with the organoclay than PPMA.

The nanocomposites were prepared by varying the concentration of the compatibilizer keeping the concentration of the organoclay, C20A, at a constant 5-wt %. Two different mixing routes such as direct mixing and masterbatch route were used to prepare the nanocomposites. The properties of the nanocomposites obtained were compared with the nanocomposites prepared using PPMA as compatibilizer under identical conditions. The WAXD patterns for the nanocomposites prepared were shown in figure1b-d. Nanocomposites prepared with KPPSA and masterbatch route showed higher d-spacing for the clay as compared the nanocomposites prepared with PPMA and direct mixing. At higher concentrations of KPPSA no peak for clay was observed indicating exfoliation. Typical TEM micrographs of the nanocomposites prepared by masterbatch route with 25% compatibilizer were shown in figure 2. It is clearly evident from the TEM pictures that the nanocomposites prepared with 25 wt % KPPSA as compatibilizer show completely exfoliated structures where the clay layers are completely delaminated and dispersed homogeneously in the polymer matrix while the nanocomposites prepared with 25% PPMA as compatibilizer showed intercalant clusters of clay layers suggesting intercalated structures.

Crystallization behaviors of various nanocomposites obtained were studied using DSC. Typical DSC thermogram curves obtained for various nanocomposites, the matrix polymers and the

pristine polypropylene during cooling from melt at 10 °C/min were shown in figure 3. Exfoliated clay nanocomposites obtained with 25 wt % KPPSA showed enhanced crystallization rates as compared to intercalated nanocomposites obtained with 25 wt % PPMA, which were evidenced with higher Tcc. In the exfoliated nanocomposite the clay layers are completely delaminated providing large surface for nucleation than the intercalated ones resulting in higher Tcc.

Flexural moduli of the nanocomposites measured were shown in Table 1. The flexural moduli of all the nanocomposites prepared showed improvements as compared to pristine PP. The improvements were highest in the case of KPPSA25C-M which contains 25% KPPSA, and was prepared by masterbatch.

Summary and Conclusions:

The nanocomposites were prepared by melt mixing of the organoclay with PP in presence of the compatibilizer in two different routes such as by single step direct mixing method and by two step method through masterbatch route. The dispersion of clay was found to be dependent on the method of preparation, type of compatibilizer used and the amount of compatibilizer used. The dispersion of the organoclay was better with KPPSA than PPMA and the dispersion was better when the nanocomposites were prepared by two step masterbatch route than the single step direct mixing method. The dispersion of the organoclay improved with increase in the amount of compatibilizer. The nanocomposites prepared using the KPPSA as compatibilizer at above critical concentrations resulted in exfoliated nanocomposites while only intercalated structures were obtained with PPMA as compatibilizer. This is further evidenced by higher crystallization rates for the exfoliated nanocomposites obtained with KPPSA than the intercalated nanocomposites obtained with PPMA as compatibilizer. The flexural modulus of the exfoliated nanocomposites prepared using novel metallic ionomer as compatibilizer showed improvements better than the intercalated nanocomposites prepared using conventional PPMA as compatibilizer. Thus we have shown that metallic ionomer such as KPPSA can act as better compatibilizer for the preparation of well-dispersed PP/organoclay nanocomposites.

References:

1. Usuki, A.; Hasegawa, N.; Koto, M. Adv. Polym. Sci. 2005, 179, 135.
2. Pinnavaia, T. J.; Beall, G. W. Polymer-Clay Nanocomposites, Wiley series in polymer science, 1997.
3. Manias, E.; Touny, A.; Wu, l.; Strawhecker, K.; Lu, B.; Chung, T. C. Chem. Mater. 2001, 13, 3516.
4. Kato, M.; Usuki, A.; Okada, A. J. Appl. Polym. Sci. 1997, 66, 1781.
5. Kawasumi, M.; Hasegawa, N.; Kato, M.; Usuki, A.; Okada, A. Macromolecules 1997, 30, 6333.
6. Hasegawa, N.; Kawasumi, M.; Kato, M.; Usuki, A.; Okada, A. J. Appl. Polym. Sci. 1998, 67, 87.
7. Reichert, P.; Nitz, H.; Klinke, S.; Brandsch, R.; Thomann, R.; Mulhaupt, R. Macromol. Mater. Engg. 2000, 275, 8.
8. Ishida, H.; Campbell, S.; Blackwell, J. Chem. Mater. 2000, 12, 1260.
9. Liu, X.; Wu, Q. Polymer 2001, 42,10013.
10. Zhang Y-Q, Lee J-H, Rhee J. M., Rhee K. Y. Composites Science and Technology 2004, 64, 1383.
11. Barber, G. D.; Calhoun, B. H.; Moore, R. B. Polymer 2005, 46, 6706.
12. Chisholm, B. J.; Moore, R. B.; Barber, G. D.; Khouri, F.; Hempstead, A.; Larsen, M.; Olson, E.; Kelley, J.; Balch, G.; Caraher, J. Macromolecules 2002, 35, 5508.

13. Wang, Z. M.; Nakajima, H.; Manias, E.; Chung, T. C. Macromolecules 2003, 36, 8919.
14. Shah, R. K.; Paul, D. R. Macromolecules 2006, 39, 3327.
15. Lee, J. A.; Kontopoulou, M.; Parent, J. S. Polymer 2005, 46, 5040.
16. Start, P. R.; Mauritz, K. A. J. Polym. Sci., Polym. Phys. 2003, 41,1563.
17. Kovarova, L.; Kalendova, A.; Malac, J.; Vaculik, J.; Malac, Z.; Simonic, J. Annu. Tech. Conf. Soc. Plast. Eng. 2002, 60, 2291.
18. Barber, G. D.; Carter, C. M.; Moore, R. B. Annu. Technol. Conf. Soc. Plast. Eng. 2000, 58, 3763.
19. Govindaiah, P.; Mallikarjuna, S. R.; and Ramesh, C. Macromolecules 2006, 39, 7199.
20. Lili C.; Paul, D. R. Polymer 2007, 48, 1632.

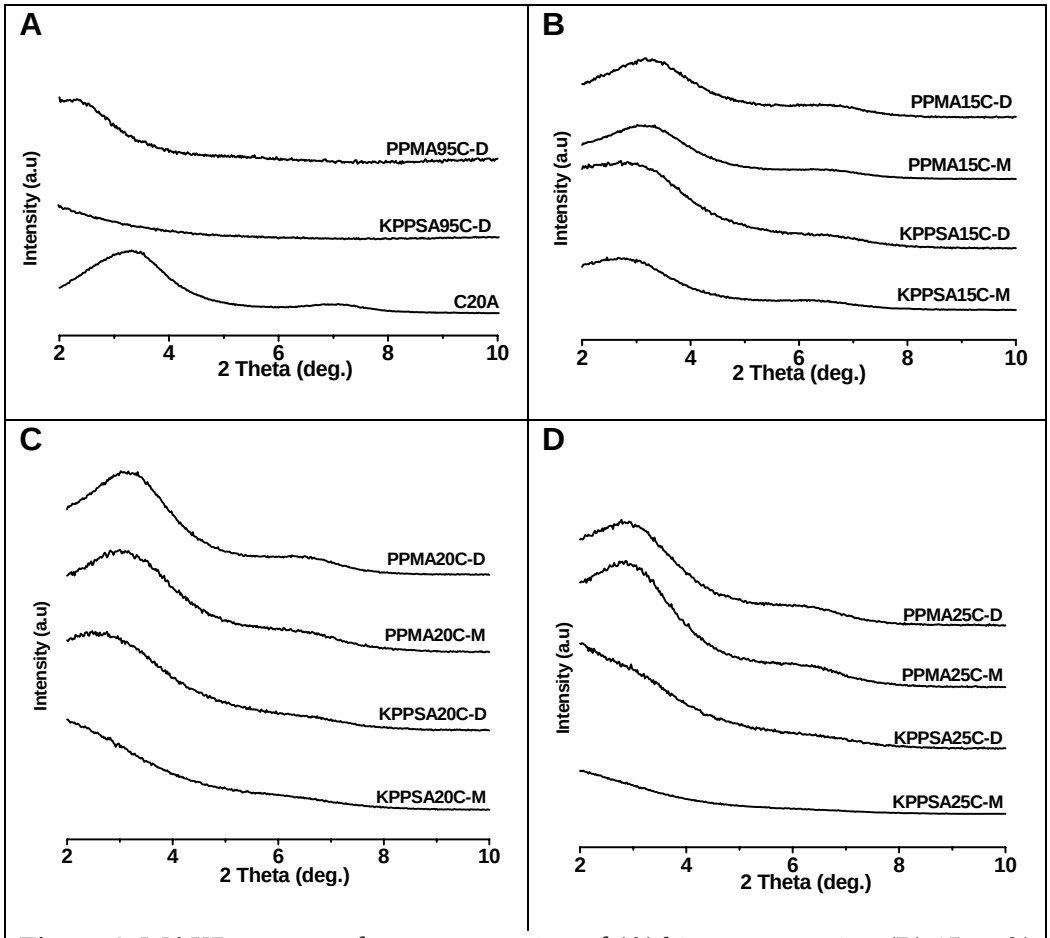

Figure 1: WAXD patterns of nanocomposites of (A) binary composites (B) 15 wt % of the compatibilizers (C) 20 wt % of the compatibilizers (D) 25 wt % of two compatibilizers; In the sample code, the number indicates wt % of the compatablizer, C indicates 5 wt % cloisite 20A, D for the samples prepared by direct mixing route and M for the samples prepared by masterbatch route.

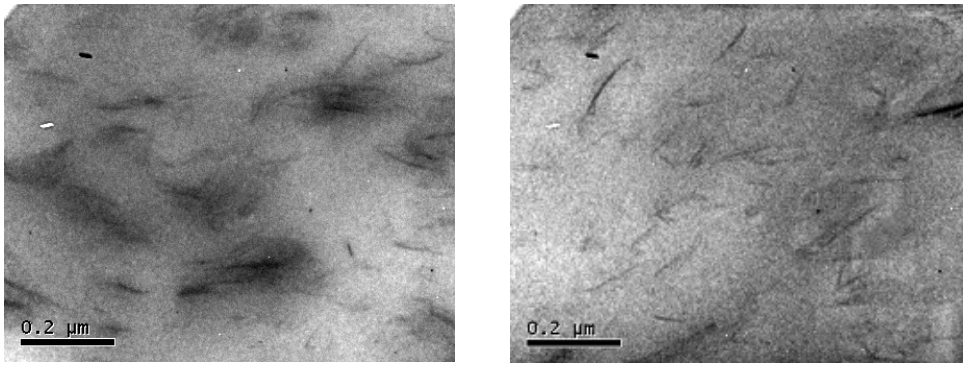

a **b**

Figure 2: Typical TEM micrographs of (a) PPMA25C-M (b) KPPSA25C-M

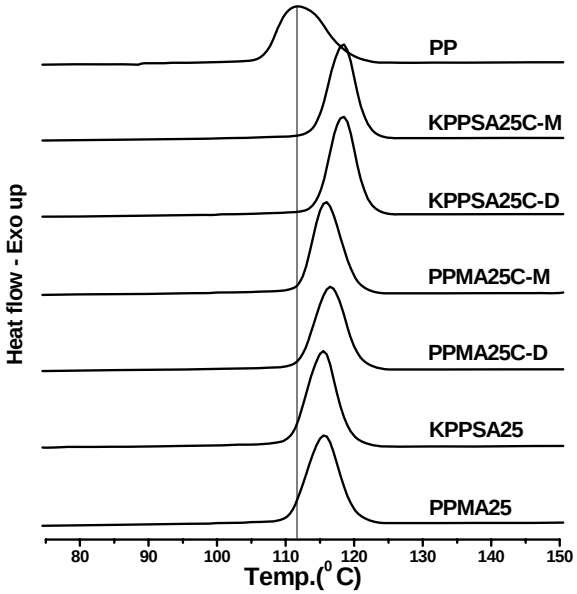

Figure 3: DSC thermogram curves of the matrix polymers and the nanocomposites during the cooling from melt at 10°C/min.

Table 1: Flexural modulus of the matrix polymer and the nanocomposites

Sample	Flexural modulus (MPa) with compatibilzer composition of		
	15 wt %	20 wt %	25 wt %
PPMA	747	710	691
KPPSA	738	759	788
PPMA-C-D	842	840	834
KPPSA-C-D	840	852	863
PPMA-C-M	862	852	845
KPPSA-C-M	888	895	937
Pristine PP	804		

A Study of mechanical properties of flax-g-poly(MA) reinforced phenol-formaldehyde composites

Susheel Kalia[1*], B.S. Kaith[2], Sanjeev Sharma[1], and Bandna Bhardwaj[1]

[1]Department of Chemistry, Singhania University, Pacheri Bari, Jhunjhunu – 333 515 (Rajasthan) India
[2]Department of Chemistry, Dr. B.R. Ambedkar National Institute of Technology (Deemed University), Jalandhar - 144 011, Panjab, India

[*]E-mail: susheel_kalia@yahoo.com, susheel.kalia@gmail.com

Abstract
In the present paper, we report the preparation of graft copolymers of flax fibers with methyl acrylate (MA) using Fenton's reagent (FAS-H_2O_2) as redox system. Synthesized flax-g-poly(MA) was characterized with FTIR, TGA/DTA, scanning electron microscopy (SEM), and X-ray diffraction (XRD) techniques. Composites were prepared using flax-g-poly(MA) as a reinforcement and phenol-formaldehyde (PF) as the binding material. Mechanical properties of phenol-formaldehyde composites were compared and it has been found that composites reinforced with flax-g-poly(MA) showed improvement in mechanical properties. Composites reinforced with flax-g-poly(MA) showed better tensile strength (235 N) and compressive strength (814 N) in comparison to composites reinforced with original flax fiber which showed lesser tensile strength (162 N) and compressive strength (372 N). Composites reinforced with flax-g-poly(MA) shows the improved MOR, MOE, and SP.

Key Words: Fiber, Flax-g-poly(MA), Composites, Mechanical Properties.

Introduction
The renewed interest in the natural fiber has resulted in a large number of modifications in order to bring it at par with and even superior to synthetic fibers. A rebirth in the application of natural fibers as reinforcing agent is occurring mainly in the automobile and packing industries. Advantage of indigenous natural fiber in their applications in the preparation of composites over synthetic fibers has been reported by Paramasivam and Kalam [1]. Flax fiber is a better reinforcing material for composites due to ecological and environmental merits and the attractive mechanical properties. Flax fiber is considered to be one of the strongest fibers among the natural fibers. Mechanical properties of polymers such as tensile strength, impact-strength, and extensibility have a direct correlation with the percentage grafting (P_g). On grafting crystal lattice of the polymer is disrupted but the strength of the material may act to reinforce the structure [2, 3]. However, if crystallinity is not disturbed on grafting, then continuous increase in strength can be obtained with increase in P_g [4]. Most of the cellulosic fibers possess both crystalline and amorphous regions. The X-ray pattern of crystalline polymers show both sharp features associated with regions of three-dimensional order and more diffused features characteristics of molecularly disordered substances like liquid. The occurrence of both types of features in the fibers indicates that ordered and disordered regions co-exist in crystalline polymers. Lower crystallinity means higher amorphous regions, which are more accessible to chemicals and water [5]. Methyl acrylate was graft copolymerized onto cellulose in alkaline aqueous solution using

potassium ditelluratoargentate (III) redox system. The evidence of grafting was obtained from IR spectra and gravimetric analysis. Thermal stability, crystallinity, and morphology of the graft copolymers were also studied [6].

Mwaikambo and Ansell [7] have prepared the hemp fiber reinforced cashew nut shell liquid composites and reported that tensile strength and modulus of untreated hemp fiber composites increase with increase in the molding pressure possibly due to reduced porosity. The properties of alkali treated hemp mat-cashew nut shell liquid composites decrease with increase in the molding pressure due to the breakage of entangled needle punched hemp fiber bundles, which have also become stiffer after alkali treatment and the hemp-cashew nut shell liquid interface is more coherent for the untreated than the alkali treated fiber. Schartel et al [8] have studied the thermal and fire behaviour of flax fiber reinforced PP composites containing ammonium polyphosphate and expandable graphite as fire retardants. The fire retardancy is a technical breakthrough for flax fiber reinforced PP composites.

Kaith et al [9-11] and Kalia et al [12-13] have reported the reinforcement of plastics with graft copolymers of flax fibers and it has been found that composites reinforced with graft copolymers of flax fibers showed better mechanical properties in comparison to original flax reinforcement. Mechanical properties of composites reinforced with acrylate grafted henequen cellulosics fibers were studied. They found that best results could be obtained with poly(MMA) grafted cellulose fibers because of better fiber-matrix adhesion [14]. Since the use of graft copolymers as reinforcing material in the preparation of composites is meagerly reported in literature, so in the present paper, we report the preparation of phenolic composites using flax-g-poly(MA) as reinforcing material.

Experimental

Materials

Natural flax fibers (*Linum usitatissimum*) were supplied by Department of Agronomy, CSK HP Agriculture University, Palampur (India). Phenolic resin (resole) was prepared by the reaction of phenol (S D Fine-Chem Ltd., India) and formaldehyde (CDH, India) in material science laboratory [11].

Flax fibers were Soxhlet extracted with acetone for 72 h. MA (Fluka) was washed with 5% sodium hydroxide followed by water and was dried over anhydrous sodium sulphate. The dried monomer was distilled and the middle fraction was used. Libror AEG-220 (Shimadzu make) electronic balance was used for weighing purpose. Graft Copolymerization of MA onto Flax was carried out as per method reported earlier [12-13]. IR spectra of the ungrafted and grafted flax fibers were taken with KBr pellets on PERKIN ELMER RXI Spectrophotometer. Scanning electron microscopic studies of flax and its graft copolymers were carried-out on Electron Microscopy Machine (LEO 435 VP). Thermogravimetric analysis and differential thermal analysis studies were carried-out in air at a heating rate of 10°C/min on a thermal analyzer (LINSEIS, L-81 11). X-ray diffraction studies were performed on X-ray diffractometer (Bruker AXS D8 Advance) as per reported methods [15-17].

Composites were prepared in Compression Molding Machine (SANTEC, India). Mechanical studies such as wear-resistance of the composites were carried-out on Wear & Friction Monitor (DUCOM, 20LE) and tensile strength, compressive strength, modulus of rupture (MOR), modulus of elasticity (MOE), and stress at the limit of proportionality (SP) of PF composites were carried on Universal Testing Machine (HOUNSFIELD, H25KS) [9-13].

Results and Discussion

C_2, C_3, and C_6 hydroxyls and the C-H groups are the active cites for grafting in cellulosics. The grafting onto flax fibers in presence of FAS-H_2O_2 as initiator is supposed to take place as per the mechanism proposed by various authors [18].

Optimization of Various Reaction Parameters

Optimized reaction conditions for getting maximum grafting were: MA (2.21 x 10^{-3} mol L^{-1}); FAS-H_2O_2 (molar ratio), 1:4; temperature (ºC), 50; time (min.), 90, and pH, 7.0.

Characterization of Graft Copolymers

FT-IR Spectra of Graft Copolymers

FT-IR spectrum of original flax showed a broad peak at 3422.8 cm^{-1} which was due to bonded –OH groups and at 2918.8, 1653.5 and 1058.7 cm^{-1} arising from –CH_2, C-C and C-O stretching, respectively. However, in case of graft copolymer, an additional peak at 1731.2 cm^{-1} because of >C=O group of MA has been observed. This suggests that MA has been graft copolymerized onto flax fiber through covalent linkages.

Thermal Analysis (TGA/DTA)

The results of TGA have been depicted in Table 1. It is shown that initial decomposition temperature (IDT) and final decomposition temperature (FDT) of original flax were 279.9 and 489.1 ºC, respectively, whereas, in case of flax-g-poly(MA), IDT and FDT were 313.7 and 478.4 ºC, respectively. Flax-g-poly(MA) showed the higher IDT than flax fiber. The results of TGA have been supported by DTA studies. DTA of original flax fiber shows the exothermic peaks at 325.3 ºC (13.8 µV) and there has been a continuous exothermic combustion of the sample at furnace temperature in presence of atmospheric oxygen. This peak shows the disturbance in H-bonded amorphous region. Another sharp exothermic peak has been observed at 455.3 ºC (38.9 µV), which indicates the complete break down of the crystalline region at this temperature. In case of flax-g-poly(MA), exothermic peaks at 322.5ºC (24.6 µV) and 380.4ºC (53.1 µV) have been observed. Thermal stability of flax-g-poly(MA) is not altered very much in comparison to original flax. This was due to undisturbed crystalline structure of the fiber. Thus, it has been found that there exists a direct correlation with percentage of grafting and crystallinity.

Table 1. TGA/DTA of flax and flax-g-poly(MA)

Sr. No.	Sample	Thermo-gravimetric analysis		Differential thermal analysis
		IDT (°C)	FDT (°C)	Exothermic peaks at temperature (μV)
1	Original flax	279.9	489.1	325.3 °C (13.8) 455.3 °C (38.9)
2	Flax-g-poly(MA)	313.7	478.4	322.5 °C (24.6) 380.4 °C (53.1)

Scanning Electron Microscopy (SEM)

A clear cut distinction between the scanning electron micrographs (SEM) of original flax and its graft copolymer reveals that there has been a sufficient deposition of poly(MA) onto flax fiber. The scans easily verify the fact that cellulosic fibers lying apart in original flax started forming bundles in the graft copolymers.

Percentage Crystallinity and Crystallinity index of Graft Copolymers

It has been observed that percentage crystallinity and crystallinity index of flax were decreased a little with grafting (Table 2). There was no comparable difference in the X-ray diffraction pattern of flax and flax-g-poly(MA). Percentage crystallinity of flax and flax-g-poly(MA) was

found to be 80.51 and 77.31, respectively. The crystalline material in the total cellulose was expressed by crystallinity index, which is an empirical measure of relative crystallinity. Crystallinity index of flax was found to be 0.7580 whereas, in case of flax-g-poly(MA), crystallinity index has been found to be 0.7065. The incorporation of monomer chains to the back-bone of flax had impaired the crystallinity of flax fiber. Therefore, grafting decreased the crystallinity of flax with reduction in its stiffness and hardness.

Table 2. Percentage crystallinity (%Cr) and crystallinity index (C.I.) of flax fiber and its graft copolymer

Sr. No.	Sample	P_g	at 2θ scale		%Cr	C.I.
			I_{22}	I_{18}		
1.	Flax fiber	–	1550	375	80.51	0.7580
2.	Flax-g-poly(MA)	86.24	3380	992	77.31	0.7065

Mechanical properties of Original flax and Graft Copolymers Reinforced Phenol-Formaldehyde Composites

Wear Test

In case of phenol-formaldehyde composites, material loss takes place by the mechanism of abrasion and frictional heat generated due to sliding. Moreover, reinforcement with graft copolymer improves the wear resistance as compared to reinforcement with original flax. Wear rate with original flax reinforced composites was much more at all loads. The wear rate was further enhanced with increase in load. In case of reinforcement of the phenol-formaldehyde matrix with graft copolymer, a reduced wear rate has been obtained. Maximum weight loss has been found in case of phenol-formaldehyde matrix followed by reinforcement with original flax. Graft copolymer reinforced PF composites showed better wear resistance in comparison to original flax reinforcement and PF matrix [9-13]. Results have been depicted in Table 3.

Tensile Strength

Composites reinforced with original flax can bear load upto 162 N and showed more extension (2.37 mm), whereas composites reinforced with graft copolymer showed 1.92 mm extension at load 235 N and PF matrix showed less extension (1.88 mm) and gets failure at load 125 N [9-13] (Table 3).

Compressive Strength

It is evident from Table 3 that pure phenol-formaldehyde matrix blocks have been observed with least compressive strength and could not withstand beyond 212 N with compression of 1.62 mm. Composites reinforced with graft copolymer showed less compression (0.78 mm) and can bear load upto 814 N, whereas composite reinforced with original flax showed 1.32 mm compression and gets failure at 372 N [9-13].

Table 3. Mechanical properties of original flax and flax-g-poly (MA) reinforced PF Composites

Sample	Tensile strength (N)	Compressive strength (N)	Wear rate (gm/m)×10^{-4}			
			1 kg	2 kg	3 kg	4 kg
PF matrix	125	212	18	34	56	77
Original flax reinforced PF composites	162	372	10	17	24	37
Flax-g-poly(MA) reinforced PF composites	235	814	09	14	19	32

Modulus of Rupture, Modulus of Elasticity and Stress at the limit of Proportionality

Table 4 shows the results of the MOR, MOE, and SP for flax fiber and its graft copolymer reinforced PF composites. MOR for phenol-formaldehyde and composites reinforced with flax fiber has been found to be 60.0 and 77.76 N/mm^2, respectively. Value of MOR was found to be 112.8 N/mm^2 for the composites reinforced with flax-g-poly(MA). Values of MOE were found to be 3404.8 N/mm^2 and 5248.0 N/mm^2 for the composites reinforced with original flax and flax-g-poly(MA), respectively. PF composites reinforced with flax-g-poly(MA) showed maximum value of SP (98.4 N/mm^2). The minimum value of SP was found in case of PF matrix [20]. Results showed that reinforcement of flax-g-poly(MA) increased the MOR. It was determined that reinforcement of PF composites with flax-g-poly(MA) increased the MOE and SP in comparison to flax fiber.

Table 4. Results of MOR, MOE, and SP for PF composites

Sr. No.	Sample	MOR (N/mm^2)	MOE (N/mm^2)	SP (N/mm^2)
1.	PF matrix	60.0	2611.2	48.9
2.	Original flax reinforcement	77.76	3404.8	63.84
3.	Flax-g-poly(MA) reinforcement	112.8	5248.0	98.4

Conclusion

Graft copolymerization is an effective method for modifying the properties of flax. Percentage crystallinity and thermal stability of flax-g-poly(MA) have been found close to that of flax fiber. Phenol-formaldehyde composites reinforced with flax-g-poly(MA) showed better mechanical properties in comparison to original flax fiber.

References

1. T. Paramasivam and A.P.J. Abdul Kalam, *Fibre. Sci. Technol.*, **7**, 85, (1974).
2. G.S. Patterson, A.S. Hoffmann, and E.W. Merill, *J. Appl. Polym. Sci.*, **4**, 159 (1960).
3. C. Sella, A. Chapiro, and A. Matsumoto, *J. Polym. Sci*., **57**, 529 (1962).
4. A. Chapiro, *J. Polym. Sci*., **23**, 377 (1957)**.**
5. S. Ishikawa, *J. Polym. Sci. Pol. Lett.*, **3**, 959 (1965).
6. Y. Liu, L. Yang, Z. Shi, and J. Li, *Polym. Int.*, **53,** 1561 (2004).
7. L.Y. Mwaikambo and M.P. Ansell, *Compos. Sci. Technol.*, **63**, 1297 (2003).
8. B. Schartel, U. Braun, U. Schwarz, and S. Reinemann, *Polymer*, **44**, 6241 (2003).
9. B.S. Kaith, Susheel Kalia, *Polym. Compos.*, **29**, 791 (2008).
10. D.K. Dwivedi, A.S. Singha, S. Kumar, and B.S. Kaith, *Int. J. Plast. Tech.*, **8**, 299 (2004).
11. A. S. Singha, Susheel Kumar, and B. S. Kaith, *Int. J. Plast. Tech*., **9**, 427 (2005).
12. B.S. Kaith, A.S. Singha, and Susheel Kalia, *Int. J. Plast. Tech*., **10**, 572 (2006).
13. B.S. Kaith, A.S. Singha, and Susheel Kalia, *Autex Res. J.*, **7**, 119 (2007).

14. G. Canche-Escamilla, J.I. Cauich-Cupul, E. Mendiza´bal, J.E. Puig, H. Va´zquez-Torres, and P. J. Herrera-Franco, *Composites: Part A*, **30**, 349 (1999).
15. N. Reddy and Y. Yang, *Polymer*, **46**, 5494 (2005).
16. A.M. Agrawal, R.V. Manek, W.M. Kolling, and S.H. Neau, *AAPS Pharm. Sci. Tech*., **4**, 1 (2003).
17. L.C. Segal, A.E. Martin, and C.M. Conrad, *Textile Res. J.*, **29**, 786 (1959).
18. A. Bhattacharya and B.N. Misra, *Prog. Polym. Sci*., **29**, 767, 2004.

Novel nanocomposite polymer electrolytes based on electrospun poly(vinylidene fluoride-co-hexafluoropropylene) for lithium batteries

Prasanth Raghavan, Xiaohui Zhao, James Manuel, Jou-Hyeon Ahn**

Department of Chemical and Biological Engineering and Engineering Research Institute, Gyeongsang National University, 900, Gajwa-dong, Jinju 660-701, Korea

Email: jhahn@gnu.ac.kr

Abstract

A series of nanocomposite polymer electrolytes (NCPE) based on poly(vinylidene fluoride-co-hexafluoropropylene) [P(VdF-HEP)] comprising nanoparticles of $BaTiO_3$, Al_2O_3 or SiO_2 were prepared by electrospinning technique. The presence of the ceramic nanoparticles has positive effect on the electrolyte uptake, relative absorption ratio and mechanical properties of the membranes. The ionic conductivity and the electrochemical stability window of the PEs were enhanced by the presence of the fillers. The prototype cell Li/$LiFePO_4$ based on the NCPE containing $BaTiO_3$ delivers a discharge capacity of 164 mAh/g, which corresponds to 96.5% utilization of the active material. In comparison, the performance of Li/$LiFePO_4$ cells with NCPEs containing Al_2O_3 and SiO_2 was observed to be lower with respective discharge capacities of 153 mAh/g and 156 mAh/g.

Keywords: Lithium batteries; Composite polymer electrolyte; Electrospinning; Fibrous membrane; Ceramic filler

1. Introduction

The high crystallinity of polymer membranes is one of the major factors of the low ionic conductivity of polymer electrolytes (PE), which limits their use in lithium batteries [1]. This problem can be addressed to a certain extent by the addition of nano-sized ceramic fillers to PEs. The addition of ceramic filler reduce the crystallinity of the host polymer. Even a small amount of these fillers can affect the mechanical strength and ionic conductivity of PEs. Apart from ionic conductivity, the ceramic filler nanoparticles also enhance interfacial stability between the PE and lithium electrode. The reduced capacity fading and improved cycling performance of the cell are other positive effects of the added nanoparticles [2].

Among many of polymers P(VdF-HFP) membranes prepared by electrospinning are suitable host polymers for preparing NCPEs due to the high affinity to the electrolyte, good electrochemical stability and desirable adhesion with the electrode.

In the present article, we report preparation, characterization and evaluation of the electrochemical properties of electrospun P(VdF-HFP) based NCPEs prepared with nanoparticles of three ceramic fillers, SiO_2, $BaTiO_3$ and Al_2O_3. The electrochemical properties of the NCPEs have been studied and the results have been compared with the PE prepared without the ceramic filler.

2. Experimental

2.1. Preparation of electrospun P(VdF-HFP) nanocomposite membranes

16% solution of P(VdF-HFP) (Kynar Flex 280) was prepared in a mixture of acetone/DMAc (7:3, w/w) at room temperature. To prepare the electrospun membranes with 6% ceramic fillers, 14% solution of P(VdF-HFP) was used. Al_2O_3, SiO_2 and $BaTiO_3$ (Aldrich), with a particle size range of 30-50 nm was used as nanoparticles. The resulting solutions were electrospun at 25 ºC as published elsewhere [3].

2.2. Characterization of electrospun P(VdF-HFP) nanocomposite membranes

The thermal properties of the membranes were evaluated by DSC (2010 TA Instruments) at a heating rate of 10 ºC/min under a nitrogen atmosphere from 50 to 200 ºC. The mechanical properties were evaluated following ASTM D638. The fiber morphology was recorded on field-emission SEM (FE-SEM: Hitachi S-4800), and the average fiber diameter (AFD) was estimated. The porosity (P) [4] and tortuosity [5] were determined as published elsewhere.

2.3. Electrochemical evaluation

PEs were prepared by soaking a circular piece of the membrane (diameter 2 cm) in the liquid electrolyte, 1 M $LiPF_6$ in EC/DMC (1:1 v/v) (Samsung Cheil Industries Inc.). The electrolyte uptake (δ) and the leakage properties of the PEs were measured following the procedure reported earlier [6].

The ionic conductivity of the PEs were measured by the AC impedance method using stainless steel (SS) Swagelok® cells with 1M6 frequency analyzer over the temperature range from 0 to 60 °C. The cell was kept at each measuring temperature for a minimum of 30 min to attain thermal equilibrium. The interfacial resistance R_f between the PE and lithium metal electrode was measured at room temperature by the impedance response of Li/PE/Li cells. Both the measurements were performed at an amplitude of 20 mV over the frequency range 10 mHz to 2 MHz. The electrochemical stability was determined by linear sweep voltammetry (LSV) of Li/PE/SS cells at a scan rate of 1 mV/s over the range of 2-5.5 V at 25 ºC. From the porosity and conductivity measurements, tortuosity of the membranes was calculated [5]:

Two-electrode lithium prototype coin cells were fabricated by placing the electrospun PE between lithium metal anode (300 μm thick, Cyprus Foote Mineral Co.) and carbon-coated lithium iron phosphate ($LiFePO_4$) cathode [7]. The electrochemical tests of the Li/PE/$LiFePO_4$ cells were conducted in an automatic galvanostatic charge-discharge unit, WBCS3000 battery cycler (WonA Tech. Co.), between 2.5 and 4.0 V at 25 ºC at a current density of 0.1 C.

3. Results and discussion

3.1. Membrane morphology

SEM images of P(VdF-HFP) membranes prepared without and with ceramic fillers reveal the presence of well interconnected interstices/pores between the fibers as shown in Fig. 1. The use of the solvent mixture of acetone/DMAc in the weight ratio of 7:3 results in membranes with lower AFD as compared to one component solvent or other solvent ratios and smaller pore size due to the formation of relatively large number of physical crosslinks. The membranes have fully interconnected pore structure. The ranges of fiber diameters obtained for different samples along with the AFDs are presented in Table 1. The membrane prepared without ceramic filler exhibits a comparatively uniform morphology with an AFD of 1.2 μm. The AFD is higher for the membranes that contain fillers. The membrane prepared with $BaTiO_3$ has more uniform fiber diameter and narrower distribution of the fiber diameters as compared to the other membranes. The larger diameter of the fiber in membranes with fillers can be attributed to the substantial increase in the viscosity that results from the blending of polymer solution with the filler particles.

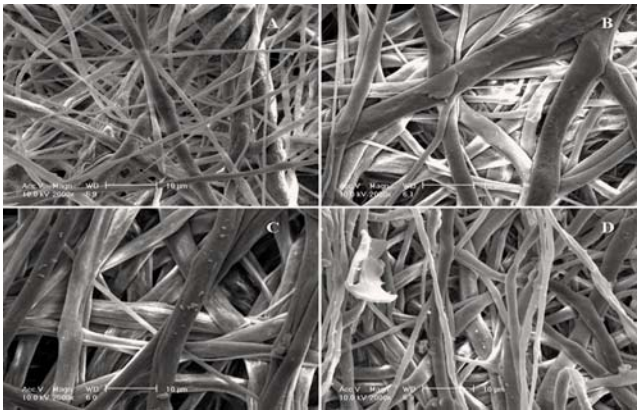

Fig. 1. SEM images of electrospun P(VdF-HFP) membranes with (A) no filler, (B) SiO_2, (C) Al_2O_3, and (D) $BaTiO_3$.

3.2. Thermal and mechanical properties

The effect of incorporation of 6% nano-sized ceramic fillers on the thermal properties of electrospun P(VdF-HFP) polymer is shown in Fig. 2. The melting temperature of pure P(VdF-HFP) is 159 ºC [8], while the electrospun

polymers with ceramic fillers have lower melting points in a close range of 153.4, 153.8 and 154.9 ºC for membranes with $BaTiO_3$, SiO_2 and Al_2O_3, respectively. The small change in the melting points of the composite membranes probably results from the orientation of the polymer chains along the fiber axis when drawn into the fibers rather than the interactions of the ceramic nanoparticles with the polymer. The % crystallinity values obtained from the DSC data follows the order $BaTiO_3$ (47.1%) < SiO_2 (47.9) < Al_2O_3 (49.2) < membrane without filler (74.5%) [8]. The mechanical properties of the membranes (based on the estimated values at the failure of the samples) are given in Table 1.

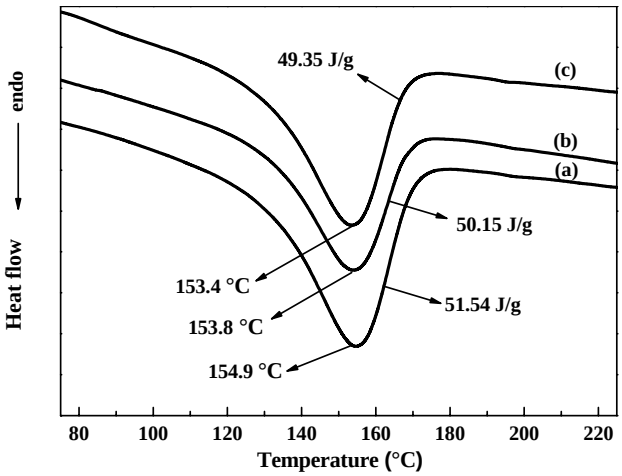

Fig. 2. Thermal properties (DSC) of electrospun P(VdF-HFP) membranes with 6% (a) Al_2O_3, (b) SiO_2 and (c) $BaTiO_3$.

3.3. Porosity, electrolyte uptake and electrolyte retention

The results of porosity determination by *n*-butanol uptake method are presented in Table 1. The porosity varies in the narrow range of 84-87% for the membranes, showing a slightly increasing trend with the filler content in the order $BaTiO_3$ > SiO_2 = Al_2O_3 > membrane without filler.

Fig. 3 presents a comparison of the electrolyte uptake (1M $LiPF_6$ in EC/DMC) of the membranes and the maximum uptake value of each membrane is also presented in Table 1. The fully interconnected pore structure of these membranes helps fast liquid penetration into the membrane, and hence the uptake process gets stabilized within a span of only 10 min. The relative absorption ratio (R) of the NCPEs and the PE without filler are presented in Fig. 3. It was seen that the electrolyte leakage reaches an equilibrium state within 1 h and all the PEs exhibit a high retention of the electrolyte with a cumulative leakage ~ 11% and ~ 14% after 1 h, respectively, in the case of the NCPEs and the PE without filler.

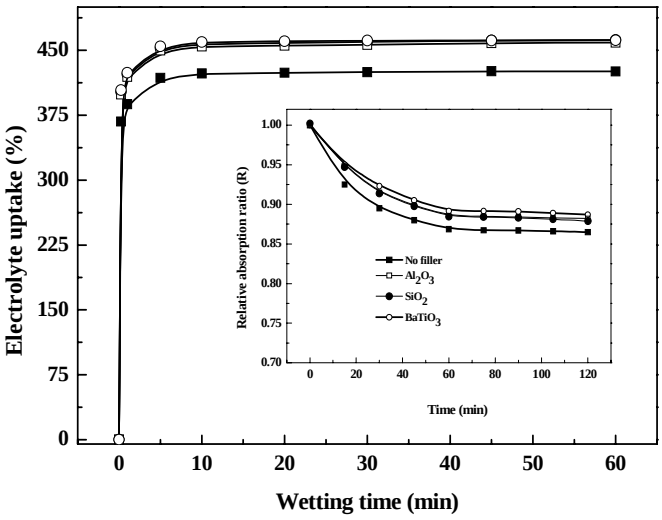

Fig. 3. Electrolyte uptake (%) of electrospun P(VdF-HFP) membranes with different ceramic fillers (liquid electrolyte: 1M $LiPF_6$ in EC/DMC).

3.4. Ionic transport properties

The ionic conductivity of the NCPEs at 25 ºC varies in the order $BaTiO_3$ > SiO_2 > Al_2O_3 > PE without filler. The higher ionic conductivity results from the interactions of O/OH groups on the filler surface and the large amorphous phase of the polymer [9]. And also the well knit porous structure of the membranes is one factor that facilitates the diffusion of the ions, hence high ionic conductivity was observed even for the PE without filler.

The tortuosity values calculated from the porosity and the ionic conductivity are listed in Table 1. As is evident from Table 1, the tortuosity of P(VdF-HFP) membranes with ceramic fillers decreases as a consequence of the nature of the filler, and follows the reverse order as is observed for the porosity of the membranes. These results are in agreement with those reported by Abraham et al. [6]. Song et al. also

reported that tortuosity decreases with the increase in the porosity of the membranes [10].

AC impedance of PEs based on electrospun P(VdF-HFP) membranes with different ceramic fillers at a temperature varies from 0 to 60 °C was determined. The bulk resistance R_b of the electrolyte at 25 °C varies between 1.6, 2.2, 3.8 and 4.8, respectively, for $BaTiO_3$, SiO_2, Al_2O_3 and PE without filler, thus, denoting a sufficiently high ionic conductivity. The temperature dependence of ionic conductivities of the NCPEs in the range of 0-60 ºC is presented in Figure 5. It can be observed that within the temperature range the Arrhenius plots are almost linear.

Properties		Filler		
		Al_2O_3	SiO_2	$BaTiO_3$
Fiber diameter range (μm)	0.4-2.2	1-4.9	0.7-4.5	0.9-3.3
Average fiber diameter (μm)	1.2	2.78	2.22	1.76
Porosity (%)	84	85	85	87
Electrolyte uptake (%)	425	459	459	462
Ionic conductivity at 25 °C (mS/cm)	4.21	5.92	6.45	7.21
Electrolyte retention ratio (R)	0.86	0.88	0.88	0.89
Tensile strength (MPa)	6.5	9.2	10.3	12.5
Modulus (MPa)	9.2	15.8	16.9	17.3
Elongation at break (%)	75	62	60	58
Tortuosity	14.81	12.56	12.04	11.52

Table 1. Properties of electrospun membranes and nanocomposite polymer electrolytes based on the membranes activated with 1M $LiPF_6$ in EC/DMC.

3.5. Electrochemical properties

The electrochemical stability window of electrospun P(VdF-HFP) based PE is shown in Fig. 6. The PE based on P(VdF-HFP) without ceramic filler exhibits an anodic stability up to 4.7 V. With the incorporation of filler particles in the polymer matrix, the electrochemical stability is enhanced. The stability order for the NCPEs follows as: 4.8 V (Al_2O_3) = 4.8 V (SiO_2) < 4.9 V ($BaTiO_3$). Thus, NCPEs have good anodic stability above 4.7 versus Li/Li^+, i.e., sufficient to be compatible with most of the common cathode materials used for lithium battery.

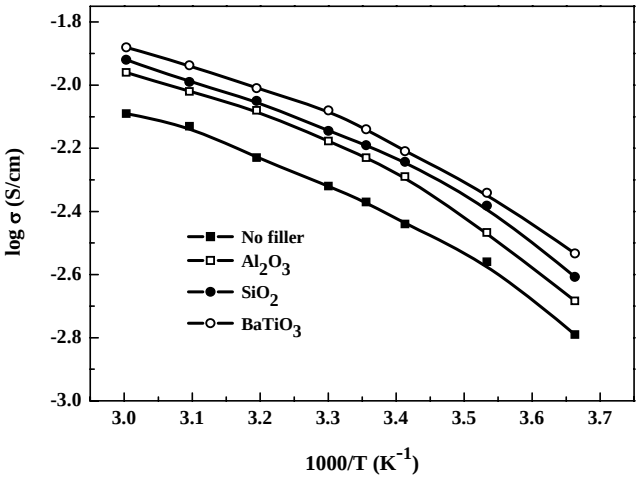

Fig. 5. Temperature effect of the ionic conductivity of PEs based on electrospun P(VdF-HFP) membranes with different ceramic fillers.

The impedance behavior of NCPEs with 1 M $LiPF_6$ in EC/DMC on lithium metal is presented in Fig. 7. R_f varies in the range 600-800 Ω with lower values recorded for the NCPEs. This indicates a good interface with the lithium electrode.

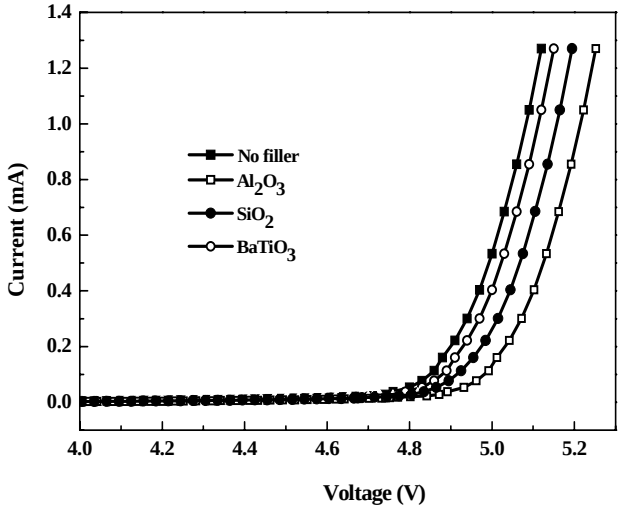

Fig. 6. Anodic stability by LSV of polymer electrolytes based on electrospun P(VdF-HFP) membranes with different ceramic fillers (Li/NCPE/SS cells, 1 mV/s, 2 to 5.5 V).

The PEs with and without filler have been evaluated for charge/discharge performance in $Li/LiFePO_4$ cells at room temperature. The first cycle charge-discharge properties at a current density corresponding to 0.1 C-rate are presented

in Fig. 8. The cell based on the PEs with $BaTiO_3$ delivers charge and discharge capacities of 164 mAh/g, which correspond to 96.5% utilization of the active material. The performance of the cell with PEs containing Al_2O_3 and SiO_2 is slightly lower as the discharge capacities of 153 and 156 mAh/g are obtained, respectively.

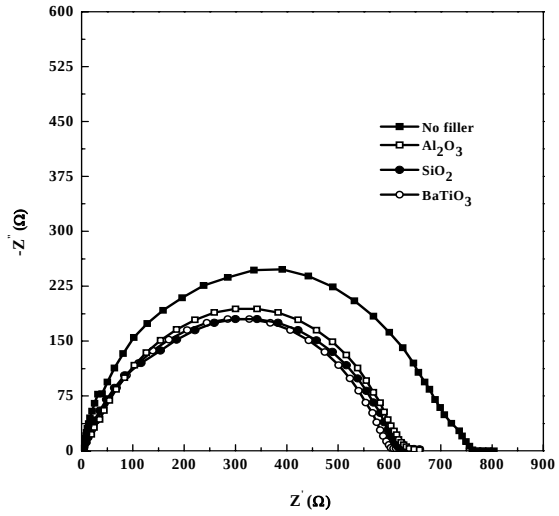

Fig. 7. AC impedance spectra of polymer electrolytes based on electrospun P(VdF-HFP) membranes with different ceramic fillers (Li/NCPE/Li cells, 10 mHz to 2 MHz).

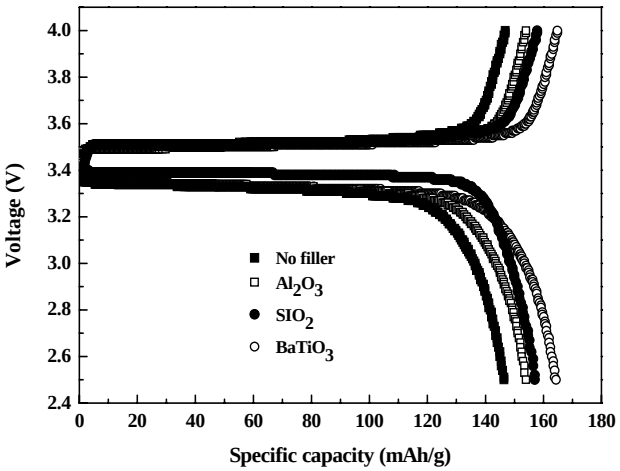

Fig. 8. Initial charge-discharge properties of Li/NCPE/$LiFePO_4$ cells with polymer electrolytes based on electrospun P(VdF-HFP) membrane containing 6% of ceramic fillers (25 °C, 0.1 C-rate, 2.5 to 4.0 V).

4. Conclusions

The nanocomposite PEs prepared by elctrospinning of P(VdF-HFP) show well interlaying of the fibers to generate a well interconnected porous membranes. The presence of the nano-scale ceramic fillers improves the mechanical properties of the membranes. The inclusion of fillers creates amorphous regions by way of the interactions between the filler surfaces and the polymer chains, which result in the reduced crystallinity of the polymer. The high electrolyte uptake by the NCPEs is attributed to the well interconnected pore structures and interactions of the fillers with the polymers as well as with the electrolyte. The nanocomposite PEs show minimum electrolyte leakage despite very high electrolyte uptake. Among the fillers $BaTiO_3$ has been observed to exhibit the highest electrolyte uptake, ionic conductivity, electrochemical stability and better compatibility with lithium metal. It also shows the maximum charge and discharge capacities. The reason for higher mechanical strength, electrolyte uptake and electrochemical performance of $BaTiO_3$ is attributed to the effective dispersion of its nanoparticles in the composite membranes during the electrospinning process that results in better interactions both with the polymer and the electrolyte.

Acknowledgements

This research was supported by Ministry of Knowledge Economy, Korea, under the Information Technology Research Center (ITRC) support program supervised by the Institute of Information Technology Assessment (IITA).

References

[1] F. Croce, S. Sacchetti, B. Scrosati, J. Power Sources 162 (2006) 685.

[2] G. Jiang, S. Maeda, H. Yang, Y. Saito, S. Tanase, T. Sakai, J. Power Sources 141 (2005) 143.

[3] X. Li, G. Cheruvally, J.K. Kim, J.W. Choi, J.H. Ahn, K.W. Kim, H.J. Ahn, J. Power Sources 167 (2007) 491.

[4] J.R. Kim, S.W. Choi, S.M. Jo, W.S. Lee, B.C. Kim, J. Electrochem. Soc. 152 (2005) A295.

[5] K.M. Abraham, M. Alamgir, D.K. Hoffman, J. Electrochem. Soc. 142 (1993) 683.

[6] J.R. Kim, S.W. Choi, S.M. Jo, W.S. Lee, B.C. Kim, Electrochim. Acta 50 (2004) 69.

[7] J.K. Kim, J.W. Choi, G. Cheruvally, J.U. Kim, J.H. Ahn, G.B. Cho, K.W. Kim, H.J. Ahn, Mater. Lett. 61 (2007) 3822.

[8] P. Raghavan, J.W. Choi, J.H. Ahn, G. Cheruvally, G.S. Chauhan, H.J. Ahn, C. Nah, J. Power Sources (doi:10.1016/j.jpowsour.2008.04.003).

[9] M.A.K.L. Dissanayake, P.A.R.D. Jayathilaka, R.S.P. Bokalawala, I. Albinsson, B.E. Mellander, J. Power Sources 119–121 (2003) 409.

[10] J.Y. Song, C.L. Cheng, Y.Y. Wang, C.C. Wan, J. Electrochem. Soc. 149 (2002) A1230.

Effect of nano TiO_2 in conducting polyaniline composites for smart corrosion prevention coatings

C.R.Siju*and S.Radhakrishnan[#]

Polymer Science and Engineering Division.
National Chemical Laboratory,
Pune 411 008, India

[#]Email: s.radhakrishnan@ncl.res.in

Abstract:

Coatings prepared from polyaniline- nanoTiO_2 particles synthesized by in situ polymerization were found to exhibit excellent corrosion resistance much superior to polyaniline in aggressive environments. The corrosion studies were carried out on steel plates coated with these formulations containing 10% polyaniline prepared with different concentrations of nanoTiO_2 by electrochemical impedance spectroscopy at periodic intervals during exposure to hot saline (65^o C) conditions for prolonged durations over a period of 90 hours. The open circuit potential (OCP) derived from Tafel plots was found to shift to more anodic side much above that of bare steel with time. The presence of nano-TiO_2 was found to be vital in prevention of corrosion and the shift of OCP to anodic side depended on the concentration of nano TiO_2 used. From these data, one could envisage more than 100 times improvement in the corrosion resistance especially for polyaniline prepared with 4.18% nano TiO_2. The exceptional improvement of performance of these coatings has been associated with the increase in barrier to diffusion as well as transport of charge by the nano sizeTiO_2, redox properties of polyaniline and very large surface area available for the liberation of dopant for the prevention of corrosion with self healing effect.

Key words: Conducting polymer, anti corrosion, nano-composite, titanium dioxide coating

1. Introduction:

Polyaniline (PANI) is one of the important conducting polymers which has been studied extensively for various applications such as sensors, transparent conductor, ESD and EMI protection, electrochromic displays etc. This polymer has been found to be an important constituent in coatings and recently that it has drawn attention as an effective material for corrosion protection. It has been reported that PANI based coatings can prevent corrosion even in scratched areas where bare steel surface is exposed to the aggressive environment. The anti corrosive coatings can be prepared from chemically synthesized PANI as dispersion coatings or PANI may be directly deposited on metal by electrochemical method as a first coat. Chemically synthesized PANI by conventional route does not dissolve in common organic solvents and hence it has to be blended with other polymers for its applicability in coatings.

The barrier properties can be enhanced if one uses appropriate fillers in the coatings. Further, it has been shown that nano-particulate fillers give much better barrier properties even at low concentrations than conventional micron size additives. As titanium dioxide (rutile or anatase) is commonly used as a pigment material for paints, it is thought worthwhile to use nano-particulate TiO_2 as a metal oxide additive in the composite which can give better dispersion of the formulation as well barrier properties in the coatings. In fact, it is anticipated that hybrid

composites containing nano additives as well as conducting PANI should improve tremendously the barrier properties of coatings as well as self healing effect giving large advantage in anticorrosion behaviour. Hence, the present studies were carried out on the preparation of nano TiO_2-PANI hybrid coating formulations using polyvinyl butyral (PVB) as the matrix and investigating their suitability for anticorrosive coatings.

2. Experimental:

2.1 Material

Aniline (ANI) (AR, Spectrochem Pvt. Ltd. India) was purified by distillation, 38% hydrochloric acid (AR,Ranbaxy), TiO_2 particles, ammonium peroxodisulphate (APS, AR, Spectrochem Pvt. Ltd, India) and methanol (E Merk) were used as such. Poly vinyl butyral (PVB) with M.W. 60,000 was obtained as granules from ABC Chemicals Exporter, Mumbai, India.

2.2 Preparation of PANI-TiO_2 composites of different PANI-TiO_2 ratio

To prepare PANI-TiO_2 composites of different ratios, the following steps were followed. 0, 0.1, 0.2, 0.3 and 0.5 g of TiO_2 nanoparticles (prepared according to procedure reported earlier) were added into a mixture of 1ml aniline and 90ml 1N HCl in a set of reaction vessels. The mixtures were stirred with magnetic stirrers in ice water baths for one hour to get a uniform suspension of TiO_2. To these mixtures, 100 ml pre-cooled 1N HCl solutions containing 2.5 g APS were added drop wise. The resulting mixtures were allowed to react in ice bath for about four hours. From these reactions we get pure PANI and TiO_2-PANI composites with compositions given in Table-1A. The products were washed with distilled water for several times and at last washed with methanol to remove low molecular weight oligomers along with other impurities. Then all samples were dried in an oven for 12 hours. These samples were characterized by UV, IR, XRD, SEM and TEM in the usual manner.

2.3 Preparation of PANI-TiO_2 dispersion formulations for coating

PVB (2g) was dissolved in methanol (20 ml) with continuous stirring for 6hr and then in a sonicator for few hours. The 10 wt % of PANI-TiO_2 powder having different compositions was crushed and slurry was made with small quantity of methanol. The slurry was added and mixed in the PVB solution and subjected to sonication for 24 Hrs. This yielded a uniform dispersion of PANI-TiO2 in the PVB solution with no settling. The stainless steel coupons (50mmx 10mmx 1mm) with rounded corners and edges were polished by C- 800 emery paper, washed with acetone and dried. The substrates were dip coated for 30 sec in PVB/PANI-TiO_2 dispersion and dried at room temperature for 30 min followed by baking in air circulating oven at 50^0 C for 4 hr. The samples were cooled and then subjected for measurement of corrosion inhibition properties..

2.4 Testing of corrosion resistance properties

Tafel plot and impedance measurements were carried out in 3.5 % NaCl solution as electrolyte. All measurements were performed on computerized electrochemical analyzer (supplied by CH instruments, USA). Stainless steel plates coated with the PANI-TiO_2 composites were used as working electrode while Pt and SCE were the counter and reference electrodes respectively. The voltammograms were measured between +1 to –1 V at a scan rate of 50 mV/s. Tafel plots was recorded at a scan rate of 10 mV/s. After initial measurements all the coupons were immersed in an external bath with hot 3.5 % NaCl solution (65 ^oC) for a period of 4 hrs so that accelerated testing could be carried out. The coupons were then again subjected to electrochemical measurements at an interval of 4 hours as described above [10, 19]. Micrographs of corroded samples were recorded on polarized optical microscope fitted with digital camera (model Leica Stereoscan 440, UK).

3. Results and Discussion :

The wide angle XRD of the PANI-nanoTiO2 powders is depicted in Figure-1 which indicates the typical PANI peaks with broad amorphous band for the samples with no TiO_2 and the characteristic reflections of anatase (JCPDS-21-1272) for the composite. The crystallite size determined from the FWHM of main 101 reflection of TiO_2 is 75 nm.

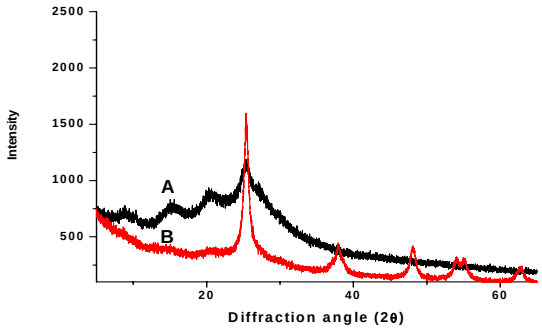

Figure:1. X-ray diffraction of (A) PANI and (B) PANI with nano-TiO_2

There is an increase in the particle size due to the formation of PANI around the particles. It is interesting to note that the polymerization yield is slightly increased for PANI-50 which indicates that polymerization is mainly initiated on the particle surface.

The PANI-nanoTiO_2 dispersed in PVB solution and studied for corrosion resistance by accelerated immersion test in 3.5% saline solution at 65^0C followed by Tafel tests. The Tafel plots of figure: 2 shows that corrosion protection of steel enhanced by the addition of increasing concentration of TiO_2.Because TiO_2 improves the barrier properties. Nano TiO_2 acts as noble metal and it may form a thin layer on the metal surface. The n-type nanoTiO_2 and p-type PANI forms p-n type junction which give potential barrier to charge transport. Also barrier to the diffusions of ions is improved due to nano-particles.

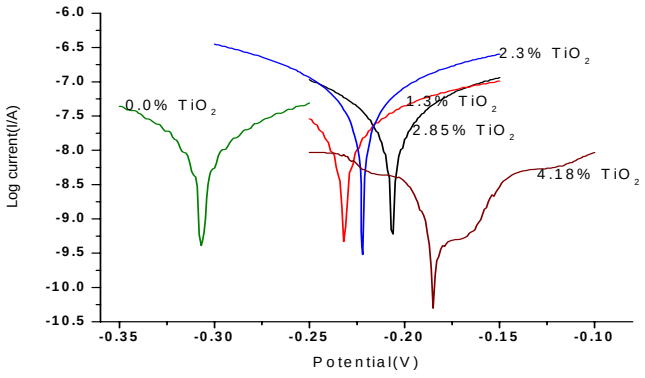

Figure:2. Tafel plots of accelerated PVB-PANI/TiO_2 coating after 40 hrs.

The open circuit potentials (OCP) determined from these plots recorded after different time of exposure to hot saline environment are indicated in Figure 3. The initial OCP of PVB is found to be on the cathodic side but more positive (-0.48) than that of bare steel (-0.6V SCE) [20] but after prolonged exposure to corrosive environment, the OCP shifts to more cathodic region. On the

other hand, the coatings containing PANI exhibit a self healing effect i.e. although there is a decrease in the OCP initially, it shifts to more anodic side after some time. This tendency to shift the OCP to potentials more nobel than the original bare steel increases with the increase in the TiO_2 content in the PANI-nano TiO_2 composite based coatings. In fact for PANI-TiO_2-4.18%, the OCP remains on the high anodic side of the other values even after 40 hr of exposure to hot saline atmosphere. High OCP value compared to that of bare substrate as well as plain PVB coated steel clearly indicates the high corrosion resistance provided by these coatings. It may also be noted that the breadth of the Tafel curve in the PANI-TiO_2-4.18% is much more than other composition.

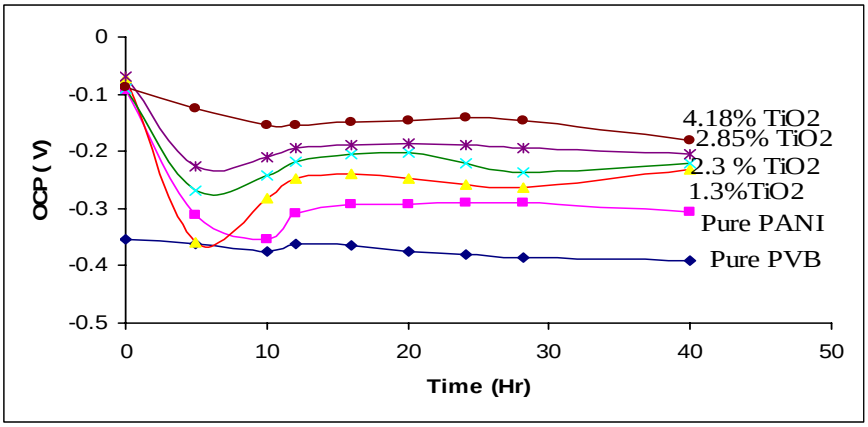

Figure: 3.OCP Vs Time graph of PVB-PANI containing different percentage of TiO_2

The corrosion rate (C_R) derived from the I_{corr} values using the equation

$$C_R = 0.129\ I_{corr}\,(EW) / (A.d)$$

Where EW is equivalent weight, A the area and d the density is shown in figure: 4 with the exposure time to hot saline conditions. It is interesting to observe that the corrosion rate initially increases but then tends to taper off above 10 hours to 20 hours. However, there is again a second region above 30 hours where the corrosion rate is seen to increase sharply. These changes can be attributed to the failure of the resin matrix, self healing due to PANI and then catastrophic failure above drastic conditions of corrosion testing. It can be noted that these changes are completely minimized in the coatings containing PANI-TiO_2-4.18% which withstand even the drastic conditions where other coatings are seen to completely give away.

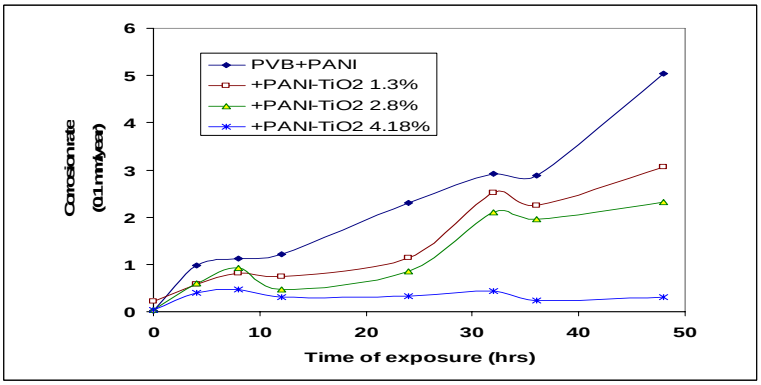

Figure: 4.Corrosion rate with respect to prolonged exposure of coatings to hot saline conditions.

This is further evidenced from the impedance plots (Bode) indicated in Figures 5 recorded after 40 hrs exposure to hot saline conditions. It can be seen from these figures that PANI-TiO_2-4.18% has higher resistance than the coatings without TiO_2 especially at low frequency which is associated with ionic transport through the film. This continues to remain high even after exposure to the corrosive environment. The accelerated testing conditions used in the present case are equivalent to testing for more than 800 hrs at room temperature which is derived using the reported logarithmic relations for corrosion rate of steel with temperature which gives about 10X as acceleration constant [21,22]. Thus, there is excellent corrosion protection obtained in these coatings especially when PANI-TiO_2 (4.18%) powder is used as an additive even at low level of loading (10wt %).

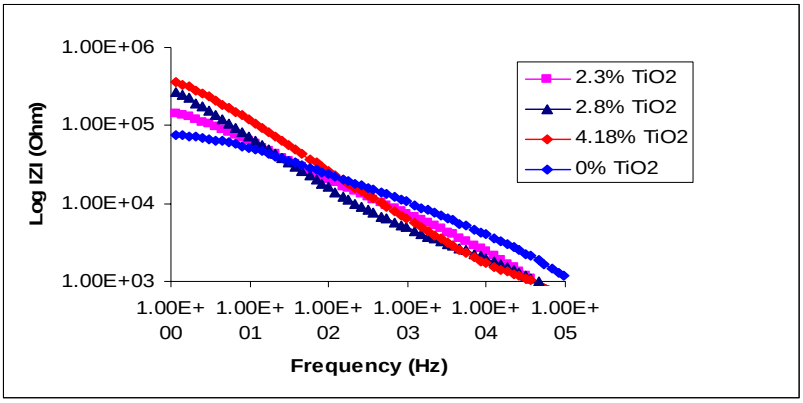

Figure: 5.Bode plots of PVB/PANI-NanoTiO_2 coatings after 40 hr immersion at 65^0C saline solution

The low frequency data in Bode plots has been associated with the diffusion processes and as mentioned above it indicates to some extent that nano-TiO_2 leads to such improvement. However, there is also an additional cause for further improvement of corrosion resistance especially when one considers that the total concentration of the additive in the formulation was same (10%) in all cases.

4. Conclusions:

The conducting PANI nano-particulate TiO_2 hybrid composites prepared by in situ polymerization were used for coating with PVB as the matrix. The effect of addition of nano TiO_2 on the improvement of has been clearly brought out The novelty of these coatings lies in generation of corrosion inhibition by three mechanisms operating simultaneously viz. improvement of barrier properties, redox behaviour of PANI and formation of p-n junctions preventing easy charge transport when coating is threatened to be destroyed due to scratch or scribble. Even if the main resin is damaged, the additives give a healing effect and prevent catastrophic failure. Apart from the prevention of corrosion, these coatings have good gloss and shiny surface, which is not easily obtained in conventional coating, prepared with commercial micron size particle additives. Such systems can be used as a primer coat or even as a single coating on steel where colour is not a very important criterion.

References :

1] L.Alcacer, Conducting Polymers, Riedel, Dordrecht, Holland, 1987

2] A.J.Dominis, G.M.Spinks, G.G.Wallace, Prog. Org. Coat. 48 (2003) 43.

3] P.J.Kinlen, J.Ding ,D.C.Silverman, Corrosion 58 (2002) 490

4] N. Ahmad, A.G. MacDiarmid, Synth. Met., 78 (1996) 103.

5] P.J.Kinlen, D.C.Silverman, C.R.Jeffreys, Synth. Met., 85 (1997) 1327.

6] T.Schauer, A.Joos, L.Dulog, C.D.Eisenbach, Prog.Org.Coat. 33 (1998) 20.

7] C.K.Tan, D.J.Blackwood, Corr. Sci., 45 (2003) 545.

8] P.Zarras, J.D.Stenge-Smith ,Y.Wei, Electroactive Polymers for Corrosion control, ACS Symposium Series 843, Washington DC,2003

9] G.G. Wallace, G.M.Spinks, L.A.P.Kane-Maguire, P.R. Teasdale, Conductive Electroactive Polymers: Intelligent Materials Systems, CRC press, New York, 2003, Chapter 1.

10] R.C.Patil , S.Radhakrishnan, Prog. Org. Coat. 57 (2006) 332

11] S.Sathiyanarayanan, S.S.Azim , G.Venkatachari, Synth.Metals 157(2007) 751

12] N.K.Lape, E.E.Nuxoll, E.L.Cussler, J.Membr.Sci. 236 (2004) 29

13] K.Yano,A.Usuki ,A.Okada, J.Polym.Sci. A: Polym.Chem. 35 (1997) 2289

14] M.Alexandre, P.Dubois, Mater.Sci.Eng. 28 (2000) 1-63

15] D.J.Chako, A.A.Leyva, Chem.Mater 17 (2005) 13

16] M.H.Priya and G.Madras J.Photochem. Photobiol. A: Chemistry 178 (2006) 1–7

17] S.Radhakrishnan , A.B.Mandale, Synth. Met. 62 (1994) 217

18] C.Saujanya ,S.Radhakrishnan , Polymer 42 (2001) 6723

19] R.G. Groseclose, C.M.Frey, F.L.Floyd, J.Coat.Technol. 56 (1984) 31

20] A.J.Bard , L.R.Faulkner, Electrochemical Methods: Fundamentals and Applications, Wiley, New York, 1980

21] J.C.Li, M.Zhao ,Q Jiang, Materials & Corrosion, 53 (2002) 269

22] P.Bruke, A.I.Sphahani ,B.S.Wright, Advances in CO2 Corrosion, Vol.2, NACE, Houston TX, 1985, p. 1-22; p.47-54

Transducer using Terfenol-D/epoxy composite

Reji John, Tusarkanta Sahoo, K A Thomas, Laly Joseph and K P B Moosad
Naval Physical and Oceanographic Laboratory
Defence Research and Development Organisation, Kochi-682021, India

Email: tsonpol@vsnl.com

Abstract:
Terfenol-D (alloy of iron, dysprosium and terbium rare-earth materials) has received considerable attention as a material for magnetostrictive transducers and actuators due to its giant magnetostriction. Nevertheless, device development using this material has always been hampered by problems related to eddy currents and high brittleness of the material. Both of these problems can be effectively addressed by developing composites of magnetostrictive materials in epoxy matrices. A study was carried out on a Terfenol-D /epoxy composite to assess its suitability as a transduction material for the application of low frequency underwater transducers. Composites with different percentages of volume filling of Terfenol-D powder having 0- 300 micron sizes were prepared and their magnetic and transduction properties were studied. The maximum attainable magnetostriction for a composite of 60% volume filling of Terfenol-D powder was found to be 450 ppm. In order to assess the suitability of the material for fabricating low frequency underwater transducer, the composite material was cast into rods (8 mm diameter X 28 mm length) and were employed in a Flextensional Transducer, as a transduction material . Underwater acoustic measurements were carried out and the results are compared with those of a similar transducer using monolithic Terfenol-D material, in the same geometries.

1.Introduction
Terfenol-D material has received considerable attention as magnetostrictive transducer and actuator material due to its giant magnetostriction. Nevertheless, device development on these materials has always been hampered by an eddy current induced bandwidth limitation to a few kilohertz and brittleness imposed challenges to produce complex shapes and designing of devices. By contrast, magnetostrictive polymer composite can be developed to alleviate the problems intrinsic in bulk material by incorporating magnetostrictive Terfenol-D particles into a passive polymer matrix. Recognizing the advantages of Terfenol-D composites, researchers began integrating these composites in sonar transducers. The motivation is partially explained from a preliminary study showing that monolithic Terfenol-D is superior to PZT in terms of power capability [1]. This idea was reinforced in a subsequent study suggesting that ‘‘composite Terfenol-D should be superior to both monolithic Terfenol-D and PZT in transducers for sonar arrays operating in the 20–30 kHz range’’ [2]. Of particular importance in sonar transducer design is the strain output and the modulus of the composite under different loading conditions. These properties dictate the work output delivered by the transducer. However, the unavailability of a comprehensive characterization of strain output, modulus, and coupling coefficient under different loading conditions and volume fractions limits the use of magnetostrictive composites. The intention of the study is to develop a Terfenol-D/ Epoxy composite having optimum modulus and large Magnetostriction to enhance the stress output for actuator applications. Also it is included in this paper, studies on the strain output of the magnetostrictive composites as a function of particulate volume fraction of Terfenol-D powder.

2. Experiments
2.1 Fabrication of magnetostrictive composite material The 1–3 composites are fabricated using a low viscosity epoxy (viscosity ~100 cps, Roto polymers, Chennai) as the matrix material and Terfenol-D powder (0-300microns, Etrema, USA) as the particulate filler. Low viscosity epoxy is

selected as matrix material due to the reason of easy removal of trapped air and wetting of the powder and further maximizing the filler loading . Composites are manufactured in an aluminum mold fabricated with a cavity of 8mm dia and 28 mm length. Appropriate volume fractions of Terfenol-D particles are mixed with epoxy resin in a beaker. The mixed slurry is placed in a vacuum for degassing. The degassed slurry is further poured into the mould just before the gelation time. The mold is then sealed and placed between two permanent magnets (field strength ~ 1000 gauss). The mould is further kept on rotation at room temperature during curing process to prevent the settling of dense Terfenol-D particles.

The magnets placed at the two ends of the mould, produce uniform horizontal magnetic field through the length of the cavity. This aligns the particulate into chains or pseudo fibers fashion, which when cured get locked in the epoxy matrix results in a 1–3 composite. A 1–3 composite produces a higher strain output than the particles are randomly aligned [3]. In addition to aligning the particles the magnetic field also further aligns the domains inside the particles, however, since Terfenol-D is a soft magnetic material the domains redistribute once the magnetic field is removed.

2.2. Magneto mechanical Characterisation

2.2 (a) compressive modulus.A universal testing machine (Zwick 1476) is employed to determine the compressive modulus of the composite.

2.2 (b) Magnetostriction The strain developed in the material is determined using a strain gauge and whetstone bridge setup.

2.2 (c) Magnetisation The saturation magnetization, remnant magnetic field and magnetic coercivity are determined using walker scientific magnetometer

2.3. Transducer Fabrication

2.3 (a) Approach: NPOL has designed and developed Flextensional Transducers (FT) using peizoceramic transduction material. The effort was to fabricate flextensional transducer using the fabricated magnetostricitve composite material. FT consists of an elliptical aluminium shell, encapsulated with neoprene rubber.

The main consideration for designing the driver using the GM material was the the space available in the shell. Composite rods of 8 mm diameter and 28 mm length were fabricated as described above. The conceptual sketch of the arrangement of the rods is shown in Fig. 1. The numbered items are (1) magentostricitve composite rods 8 mm dia, 28 mm long [6 Nos.] (2) Tablet-type 20 mm dia, 10 mm thick Samarium-Cobalt permanent magnets [12 Nos.] (3) 375 turns of 22 SWG Solenoids [6 Nos.] (4) 30 mm dia, 27.5 mm long aluminum bobbins [6 Nos.] (5) 8 mm thick brass magnetic de-coupler (6) I mm MS outer frame for magnetic flex return path (7) Aluminum shell [Elliptical cylinder]. The solenoids are connected in parallel and designed to be powered by AC current with a current limitation of 5 amp.). A compressive mechanical pre-stressing is given to the drive by elastic spring of the flextensional shell. For this the total length of the drive module taken is 0.5 mm more than the major axis of the shell. The drive module is inserted in the shell by mechanically pressing the shell in the minor axis. Once the drive module is inserted the pressing is removed and the shell is loaded against the drive and this will give sufficient pre-stress.

2.3(b) Design of magnetic circuit

Magnetic circuit was designed and analysed using a FE modeling software Vizimag^{R}. The input parameters are enlisted in table 1.On the basis of modeling a most suitable schemes is arrived at, and the plots of which is shown in Fig. 2 (a) and (b). Magnetostricitive composite material drive is shown in Fig. 3 and that of fabricated FT with is shown in Fig. 4.

2.3 (c) Transducer measurements

Measurements are made in the open water tank, keeping the transducer at a depth of 10 m. The sound projected by the transducer is picked up by a standard B& K hydrophone. A similar FT, with monolithic Terfenol-d rod drive was also subjected to measurements using the same set-up and the

results were compared. Measurements were repeated in two different methods, to confirm the results.

3. Results and discussion

The compressive modulus obtained was 1 GPa. The epoxy resin employed largely controls the modulus of the composite. Hence it is proposed to use resin having larger modulus. Upto a certain level of loading, magnetostriction of the composite increases as shown in Fig.5 with the volume fraction of the Terfenol-D powder added . The present composite having 60 % loading shows a magnetostriction of 450 ppm at a DC magnetic field of 2000 Oe. The remnant magnetic field present in the composite influences utilization of the devices for high frequency applications . As it is evident from the Fig. 6, the remnant magnetic field present in the composite is negligible. The composite exhibits saturation tendency above 4000 Oe. Fig. 3 shows a photograph of the realized drive as per the scheme in Fig.2 (a). The drive module was inserted into an elliptical Aluminum shell of a flex-tensional transducer (FT). Fig.4 shows a photograph of the assembled magnetostrictive transducer. End plates with O-rings were fastened to make the device water-worthy. As magnetostrictive transducers are current-driven devices, Transmitting Current Responses (TCRs) are used to characterize them, in place of the usual Transmitting Voltage Responses (TVRs) used in the case of transducers with piezoceramic drive.Fig. 7 shows the measured TCRs of the above FTs with monolithic Terfenol-D rods and composite rods respectively .The advantage of the composite is a slight lowering of the frequency at which the device shows peak performance. The peak performance is about 10 dB less for the FT with composite rods, compared FT with Terfenol-D rods.

5. Conclusion and suggestion for future work

Composite of Terfenol-D / epoxy resin exhibits magnetostriction. The magnetostiction values are largely depend on the percentage of Terfenol-D powder added. The magnetostrictive composite transduction material developed can drive elliptical aluminum shell. Magnetic circuit design play important role in the performance of the transducer. For improving the performance of the transducer, magneto-mechanical properties such as Young's modulus, magneto-mecahnical coupling factor etc has to be optimized.

Acknowledgement:
Authors would like to thank Prof. Markeyandalu, Dept. of physics, IIT-Madras, Chennai for the materials properties measurement. The encouragement and support of ASD(ME&MEMS) and the permission of the Director, NPOL to publish this work is greatly acknowledged.

6. Reference

[1] Moffett, M B, Porzio, R., Bernier, G L, "High Power Terfenol-D Flextensional Transducer – Revision A", NUWC Technical Document No. 10883A, 12 May 1995.
[2] M.B. Moffett, J.M. Powers, J.Acoust. Soc. Am. 90 (1991) 1184.
[3] J.H. Goldie, M.J. Gerver, J. Olesky, .P. Carman, T.A.Duenas, Proc. SPIE 3675 (1999),243.
[4] T.A. Duenas, G.P. Carman, Proc. ASME 291 (1998) 63.

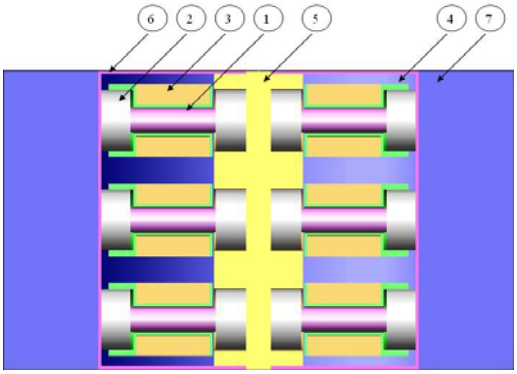

Fig.1 Conceptual sketch of Magnetostrictive composite material as driver in the aluminum shell of FT

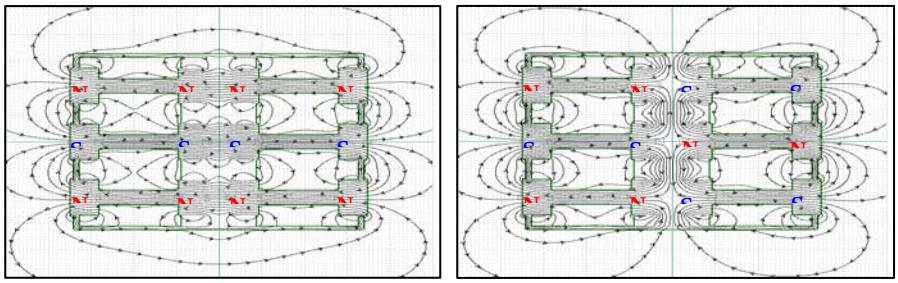

Fig. 2 (a) and (b) Field distributions in the two chosen schemes

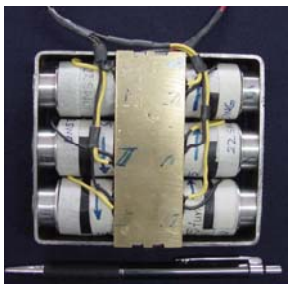

Figure 3 the Driver assembly

Fig. 4 Assembled Magnetstrictive FT

Table-1.Input parameters for modeling

Sl No.	Parameter	Value used
1	Current in the solenoid	4 Amps
2	No. of turns in the solenoid	300
3	Strength of the permanent magnets	1200 G
4	Permeability of the permanent magnets	1.2
5	Permeability of GM rod	7
6	Permeability of Mild steel frame	15
7	Permeability of Brass Magnetic decoupler	1

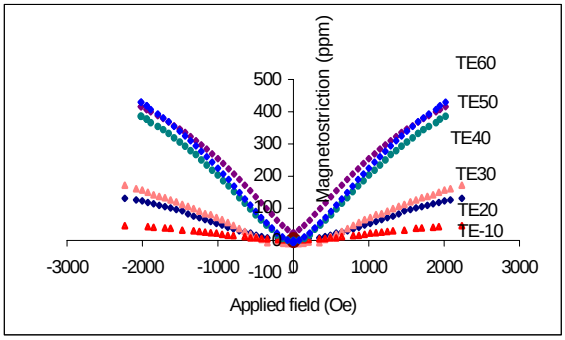

Fig.5.Magnetostriction of the composite at different volume fraction of Terfenol-D

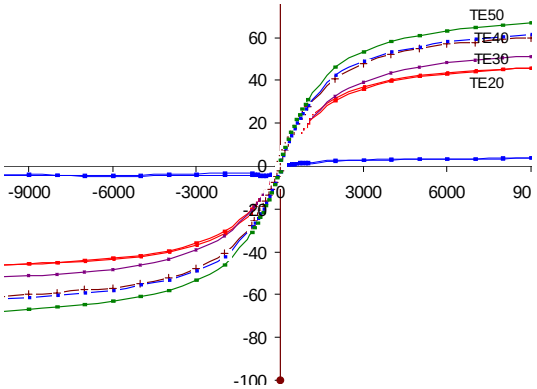

Fig. 6 Magnetisation curves of the composite for the different volume fraction

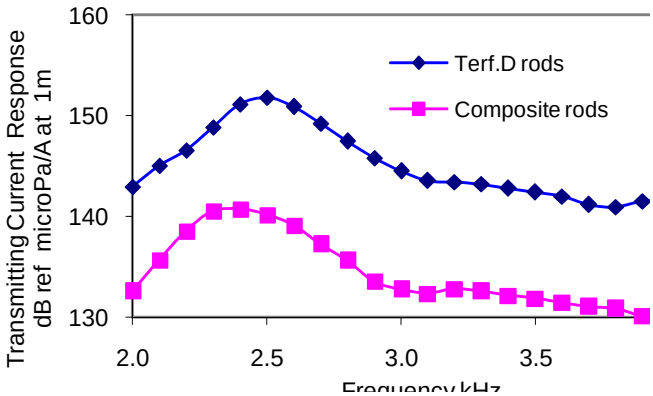

Fig. 7 TCR of a FT, driven by Terfenol D rods and Terfenol D composites

Competitive extraction of Na, K, Ba, Ca, Mg by NR/PEO-1000, NR/PEO-4000 block copolymers

Suryakala K. S. and M.R. Gopinathan Nair
School of Chemical Sciences, Mahatma Gandhi University, Kottayam 686560, Kerala, India.
Email: suryakutty@gmail.com

Abstract

A series of NR/PEO block copolymers were prepared from hydroxyl terminated liquid natural rubber and polyethylene oxide of $\bar{M}_n$=1000 (PEO-1000) and $\bar{M}_n$=4000 (PEO-4000). Complexation studies of these block copolymers with five different aqueous metal salt solutions were undertaken to find the order of competitive extraction. Selective complexation of metal cations was observed to occur with the following order of selectivity: $K^+ > Ba^{++} > Ca^{++} > Na^+ > Mg^{++}$; which parallels the results known for many crown ethers [1,2] and noncyclic polyethers [3] and is identified with the polyether portions of the block copolymers, which are thought to adopt helical conformation surrounding the complexed cation.

Introduction

In comparison with cyclic polyethers, noncyclic polyethers [3] seemed extraordinarily weak in ability of metal ion complexation [4]. A search of literature [5-7] showed that, before Pederson's discovery of macrocyclic polyethers [8], high molecular weight polyethylene oxide had been reported to form complexes with various metal salts especially alkali and alkaline earth metals [9-11].

In connection with the progress of the chemistry of macrocyclic polyethers, the interaction of open chain polyethylene oxide derivatives with metal ions has attracted special interest [12]. PEO has the structure $HO\text{-}[\text{-}CH_2\text{-}CH_2\text{-}O\text{-}]_n\text{-}H$. It differs from the crownether essentially in that the macrocyclic ring is opened and the molecule is laid out. X-ray diffraction [13,14] studies on PEO showed that the polymer in solid state is 7/2 helix. The structure is quite enough for some suggestion that every heptameric segment of PEO might behave as rudimentary crown ether. In solution, hydrodynamic evidence showed PEO chains change its helical structure into a new less ordered structure. In general the more flexible polyethylene oxide ligands are able to wrap the metal ions in a helical fashion while crown ethers, due to their rigid cavity size are found to co-ordinate in an out-of cavity fashion or are displaced to hydrogen bonded out of sphere locations if the metal cavity size fit was not compatible.

Recently, some researchers have thought that chemical modification may facilitate the enhancement of PEO complexation ability and selectivity, and have synthesized large number of PEO derivatives and related polyethers [15-25]. Based on the above reported works, it was decided to study the interaction of NR/PEO block copolymers, prepared in our laboratory with various metal salts. This was undertaken to explore the use of these block copolymers for metal ion extraction process, phase transfer catalysis, reverse osmosis and related purposes.

Experimental

Materials

Natural crumb rubber (ISNR-5): Weight average molecular weight = 8,20,000; Intrinsic viscosity in benzene at 30^0C= 4.45 dL/g; Wallace Plasticity, P_0=39 was supplied by Rubber Research Institute of India, Kottayam, Kerala.Toluene diisocyanate (TDI) (was 80/20 mixture of 2,4-and 2,6- isomers) was supplied by Aldrich, Germany and was used as received. Dibutyl tin dilaurate (DBTDL) supplied by Fluka, Switzerland, was used as catalyst without further purification. Hydrogen peroxide (30% w/v) supplied by E. Merck, India was used without further purification. Toluene (reagent grade) obtained from E. Merck; India was used as solvent without further purification. Methanol (reagent grade) supplied by E. Merck, India was used without further purification. Chloroform (laboratory reagent grade) was dried with anhydrous calcium oxide and then distilled before use. It was supplied by E. Merck, India.

Polyethylene oxide (PEO) of molecular weight ($\bar{M}_n$) 1000 and 4000 (PEO-1000 and PEO-4000 respectively) supplied by Aldrich, Germany were used as received. NaCl (Merck, India), KCl (Merck, India), $MgSO_4$ (Merck, India), $BaCl_2$ (Merck, India), $CaCl_2$ (Merck, India) were used as received. Double de-ionized water was used for the preparation of metal salt solutions.

Synthesis

Preparation of hydroxyl terminated liquid natural rubber (HTNR)

HTNR was prepared by the less vigorous but efficient method developed by Ravindran [26] et al using H_2O_2 and solar radiation.

Natural crumb rubber was masticated for 30 minutes at 40^0C, 500gm of it was dissolved in 10L toluene and the solution was charged into a flat bottomed flask made up of borosilicate glass and 500 ml of aqueous hydrogen peroxide (30%w/v) was added and thoroughly mixed with rubber solution. The mixture was then homogenized to a certain extent by the addition of 750 ml of methanol. The whole assembly with the material for irradiation was placed in sunlight under stirring. After an exposure of 60 hours a layer of water separated at the bottom with some white deposits. This was separated and the upper layer comprising liquid natural rubber in toluene was distilled to remove the toluene to recover the liquid natural rubber (HTNR). It was purified by precipitation by methanol twice from toluene solution and was dried in vacuum oven.

Synthesis of NR/PEO block copolymer

The second part of the experiment comprises the synthesis of NR/PEO block copolymer as given below [27].

HTNR (24gm) was dissolved in 68ml of chloroform (35%w/v) to get a solution. The whole solution was taken in a reaction vessel, dibutyl tin dilaurate catalyst (6% by weight of HTNR) was added and the solution brought to reflux with stirring. The stoichiometric amount of TDI (1:2.76:1 of HTNR) was added in drops, followed by the drop wise addition of 6gm of PEO-1000/24gm of PEO-4000 in chloroform (35%w/v) within a period of 1.5 hour. The reaction was allowed to continue for another 2 hours. Excess chloroform was then distilled off and the viscous polymer solution was cast in trays treated with silicone releasing agent. The sheet was removed from the tray after 24 hours, kept in a vacuum oven at 60^0C to remove traces of solvent and then cured at 70^0C for 24 hours, followed by one week ageing at room temperature in a moisture free atmosphere.

Complexation of metal ions: General procedure

A known mass of block copolymer (0.3g) was suspended in 50ml 2M metal salt solutions (NaCl, KCl, $MgSO_4$, $BaCl_2$, $CaCl_2$) at its natural pH, for 168 hours in a closed condition. The polymer was then taken out and washed the surface instantly but carefully with de-ionized water to remove any surface salt present. The metal ion intake of the block copolymer was obtained from the determination of the concentration of the metal salts solutions before and after complexation. From the decrease in concentration of metal ion solution, the amount of metal ion complexed by the polymer was calculated. The concentrations of the metal salt solutions were determined by volumetric methods-Na+ and K+ by Mohr's method [28], Mg++ and Ca++ by complexometric titrations [29], Ba++ by precipitation titration [30].

Results and discussion

Following the procedure under experimental part, sheets of polyether-natural rubber block copolymers were prepared. Polyether is hydrophilic in nature and natural rubber provides the nonpolar hydrophobic part. Series of NR/PEO-1000 and NR/PEO-4000 were synthesized by solution polymerization. The course of the reaction and the structure of the block copolymer are shown in Scheme I.

Interaction with metal salts

The interaction of NR/PEO block copolymers with various metal salts is due to the PEO content in the samples. The polyethylene oxide bearing $-[-CH_2-CH_2-O-]_n-$ units can exhibit crown ether or podand property by forming spiral or pseudo cavity of adequate size to accommodate the cations. The present study on the competitive extraction of different cations is originated from the above background. Even though the PEO part contains no crown ether like macrocycle, the long chain with $-[-CH_2-CH_2-O-]_n-$ units can adopt a ring like structure by taking a spiral shape. The salt solutions considered are NaCl, KCl, $MgSO_4$, $BaCl_2$, and $CaCl_2$.

The interaction of dried NR/PEO-1000 and NR/PEO-4000 with the above salt solutions were studied by estimating the cation impregnated in the polymer sample. The next step is to find the order of competitive extraction of these metal cations. The results have been analyzed by the overall metal complexation values [Table I]. The order of competitive extraction by these two block copolymers are the same as given below $K^+ > Ba^{++} > Ca^{++} > Na^+ > Mg^{++}$. The experiment was repeated with another concentration (0.2M) of the metal salt solutions. In that case too the extraction order was the same. From the above result it is clear that as the ionic radii increases ($Na^+=1.96A^0$, $K^+=2.66A^0$, $Ba^{++}=2.83A^0$, $Ca^{++}=2.12A^0$, $Mg^{++}=1.56A^0$) [31] complexation ability also increases, except for Ba^{++} as shown in Fig.1.

The HTNR and PEO used in the present study are made up of appreciably large number of respective monomer unit. The copolymerisation of these two using TDI makes the block copolymer system almost infinite size with alternate HTNR-PEO components. In this copolymer the NR part behaves as the soft segment and it is completely amorphous in nature. The PEO is the hard segment and in solution, not much ordering is expected from this fragment also. But when treated with metal salt solution the PEO fragments with $-[-CH_2-CH_2-O-]-$ units would tend to interact strongly with the metal ions, resulting in a high degree of ordering as shown in Fig 2. The corresponding situation with HTNR/PEO block copolymer is shown in Fig 3.

It is known that for alkali and alkaline earth metals, usually the co-ordination number is from 6-10 [32]. For the formation of a pseudohelical structure, the ligand should have 6 donor atoms. In our case, this structure is obtained using five -[-CH_2-CH_2-O-] groups along with a 6^{th} -CH_2-CH_2-O-group that forms the turn of the pseudohelix. The metal ion is accommodated in the cavity of the spiral structure, depending upon its size, i.e. either by size comparable to that of 15-crown-5 or 18-crown-6. Hence here the maximum extraction is for K^+, which shows the PEO chains prefer to take a pseudohelical structure similar to that of 18-crown-6. The cavity size of 18-crown-6 [1,2] is $2.6A^0$ which suits to K^+ ion and the extraction order is K^+>Rb^+>Cs^+>Na^+>Li^+. The situation can be diagrammatically represented in Fig 4.

The slight decrease in the affinity of block copolymer to form a strong complex with Ba^{++} can be explained as follows. Ba^{++} has a slightly greater ionic radius compared to the cavity size of 18-crown-6. Therefore the whole helical structure has to expand a little to accommodate this larger cation, which leads to lower absorption compared to K^+.

Conclusion

The work shows that NR/PEO block copolymers can be used to extract alkali and alkaline earth metals from aqueous media. The order of extractability is as follows: K^+>Ba^{++}>Ca^{++}>Na^+>Mg^{++}. The order of cation preference is nearly identical to that of 18-crown-6 derivatives and also of noncyclic polyethers. We thus believe that a helical arrangement of inwardly directed oxygen atoms forms the basis of complexation between cation and block copolymers.
Further investigation of NR/PEO extraction mechanisms is continuing in our laboratory. A number of analytical and other applications are being investigated and will be reported shortly.

References

1 Strzelbick J, Bartsch RA. Anal.Chem.1981; 53:1894-1899.
2 Strzelbick J, Bartsch RA. Anal.Chem.1981; 53: 2247-2250.
3 Awano H, Katsumichi O, Kenkichi M. Bull.Chem.Soc.Jpn. 1982; 55: 2525-2529.
4 Balasubramanian D, Chandani B. J.Chem.Educ. 1983; 60: 77-78.
5 Frensdorf HK. J.Am.Chem.Soc. 1971; 93: 600-606.
6 Timko JM, Helegeson RC, Newcomb M, Gokel GW, Cram DJ. J.Am.Chem.Soc. 1971; 96: 7097-7099.
7 Chaput G, Jeminet G, Juillard J. Can.J.Chem. 1975; 53: 2240-2246.
8 Pedersen CJ. J.Am.Chem.Soc. 1967; 89: 7017-7036.
9 Ono K, Konami H, Murakami K. Rep.Prog.Polym.Phys.Jpn. 1978; 21:17-21.
10 Barthelemy PP, Desreux JF, Marsaux J. J.Chem.Soc.Dalton.Trans. 1986; 6: 2497-2499.
11 Yanagida S, Takahshi K, Okahara M. Bull.Chem.Soc.Jpn. 1977; 50: 1386-1390.
12 Calzolari C, Favretto L, Marletta GP, Chem.Abstr. 1976; 84: 38132s.
13 Koenig JL, Angood AC. J.Polym.Sci.Part A: Polym.Chem. 1970; 8: 1787-1795.
14 Rogers RD, Bond AH, Aguinaga S, Reyes A. Pure and Appl.Chem. 1993; 65: 567-572.
15 Tummler B, Maass G, Vogtle F, Seiger H, Heimann U, Weber E. J.Am.Chem.Soc.1977; 99: 4683-4690.
16 Kang SI, Czech A, Czech BP, Stewart LE, Bartsch RA. Anal.Chem.1985; 57: 1713-1717.
17 Walkowiak W, Stewart E, Czech BP, Bartsch RA. Anal.Chem.1986; 58: 188-191.
18 McDowell WJ, Czech BP, Bartsch RA. Sovt. Extr.Ion Exch. 1986; 4: 411-419.
19 Walkowiak W, Desai DH, Lee HK, Bartsch RA. Anal.Chem.1992; 64: 1685-1690.
20 Hiratana K, Aiba S, Nakagawa T. Chem.Lett. 1980; 9: 477-480.
21 Hiratana K. Chem.Lett.1981; 1: 21-24.

22 Hiratana K. Chem.Lett.1982; 7: 1021-1024.
23 Hamon RF, Khan AS, Chow A.Talanta. 1982; 29: 313-326.
24 Okada T. Analyst. 1993; 118: 959-971.
25 Dale J, Frendrikson SB. Pur Appl.Chem.1989; 61: 1587-1592.
26 Ravindran T, Nair MRG, Francis DJ. J.Appl.Polym.Sci. 1988; 35: 1227-1239.
27 Nair, R.C., Block copolymers from liquid natural rubber and polyethers, Ph.D thesis 1998, pp 73-75.
28 Bassett J, Denney RC, Jeffery GH, Mendham J, editors, Vogel's Text book of quantitative inorganic analysis. 4th Ed.Longman group Ltd, 1978, pp-475
29 Bassett J, Denney RC, Jeffery GH, Mendham J, editors, Vogel's Text book of quantitative inorganic analysis. 4th Ed.Longman group Ltd, 1978, pp-257.
30 Bassett J, Denney RC, Jeffery GH, Mendham J, editors, Vogel's Text book of quantitative inorganic analysis. 4th Ed.Longman group Ltd, 1978, pp-452.
31 Ono K, Honda H, Murakami K. J.Macromol.Sci.Chem. 1989; A26: 567-582.
32 Truter MR, Nature 1970; 228: 648-651.

Scheme 1

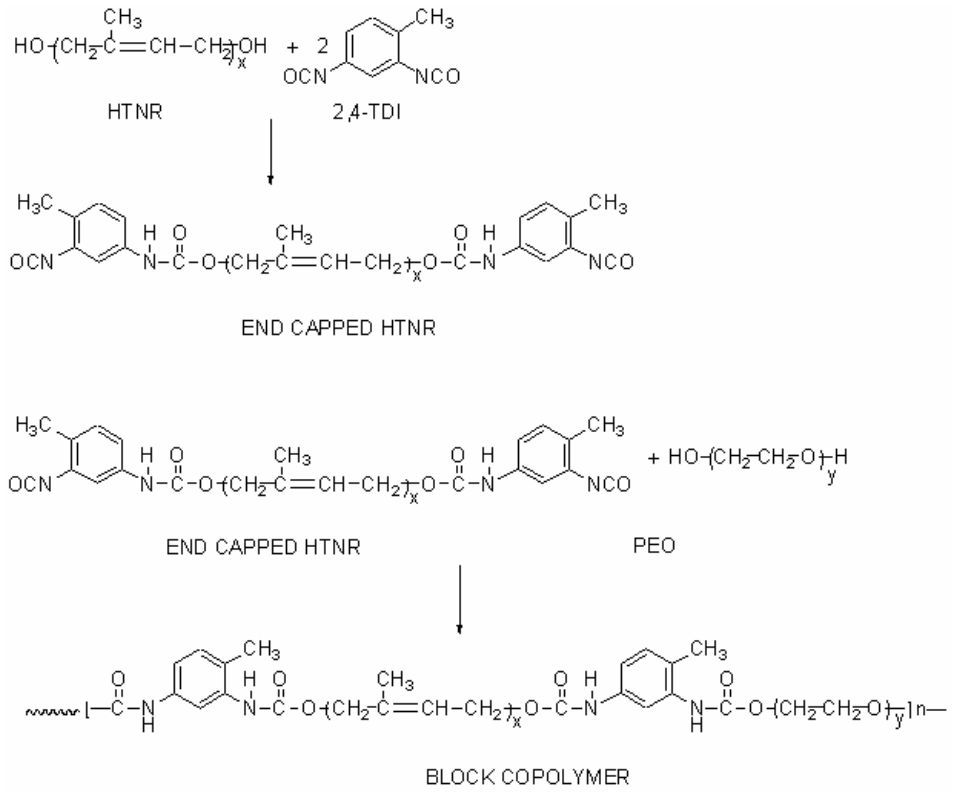

Table1. Ion uptake by the polymer samples

Polymer sample	Uptake of metal ions (mM/g)				
	Na^{+}	K^{+}	Ba^{++}	Ca^{++}	Mg^{++}
NR/PEO-1000	1.20	3.78	2.80	2.24	0.88
NR/PEO-4000	2.12	4.41	3.20	2.86	0.42

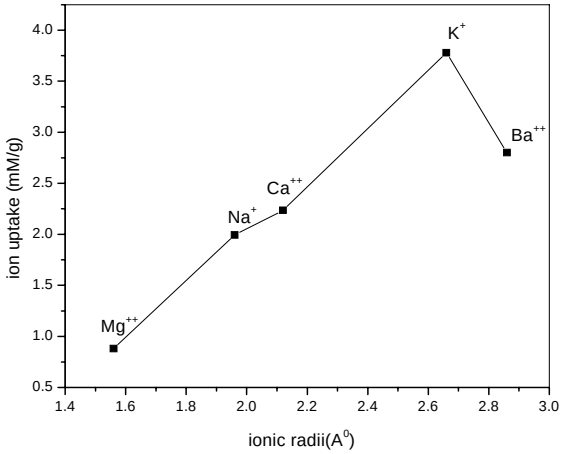

Figure 1. Plot of ion uptake versus ionic radii

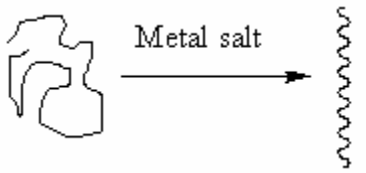

PEO before complexation

PEO after complexation

Fig.2. Complexation in polymers

Fig. 3 Complexation in NR/PEO block copolymer

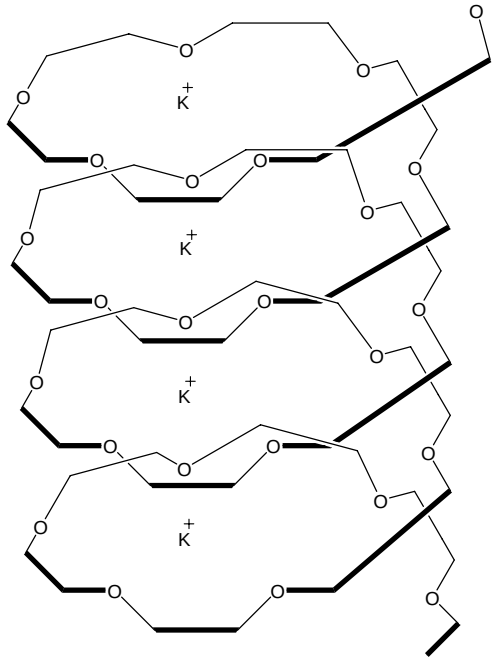

Fig. 4 Pseudocavity binding of K^+

Protein functionalized polysaccharide nano particles for novel applications

T.Emilia Abraham
Chemical Sciences & Technology Division,
National Institute for Interdisciplinary Science & Technology (NIIST), CSIR,
Thiruvananthapuram-695019
E-mail:emiliatea@gmail.com

Abstract

There has been growing interest in the use of natural polysaccharides for biomedical applications, drug delivery vehicles, as minimally invasive scaffolds for tissue engineering, because of their non toxicity, biocompatibility, biodegradability, low interfacial tension and high molecular and oxygen permeability. By exploiting these features it may be possible to mimic features of the natural extracellular matrix, and control tissue structure and cellular functions. Protein/peptide oral drug delivery is complicated process mainly due to poor intrinsic protein permeability as a result of large molecular weight, degradation by proteolytic enzymes in the stomach and in the small intestine, and chemical instability. Protein functionalized micro and nano particles are very versatile and were made to overcome this problem. Low molecular weight chitosan, guar gum, were used for the preparation of nano particles using precipitation and ionic cross linking method and was then linked to the enzyme (subtilisin) by glutaraldehyde coupling. Polysaccharides having a molecular mass of 8 to 36 KDa gave high-quality nano composite spherical particles of 100-500 nm size, with a good poly dispersity index of 0.1- 0.7. Poly saccharides having a molecular mass greater than 50 KDa gave micro particles and vesicles of more than 1 microns as indicated by Dynamic laser light scattering, SEM, and TEM studies. The optimum pH of the polysaccharide nanoparticle immobilized enzyme was shifted to 8.0 from 7.0, whereas there was no change in the optimum temperature. The immobilized enzyme shows better affinity to the substrate (casein) with a lower K_M value of 4.097×10^{-5} than the native subtilisin which is 3.30×10^{-4}. These composite catalytic nano particles are having excellent activity, pH sensitivity and stability which make them suitable for oral drug delivery, tissue scaffolds, microreactors or for cosmetic applications.

1. Introduction:

There is significant interest in the protein functionalized nanosized particles; with potential applications ranging from biosensors [1-3] enzymatic bioreactors [4] delivery of sensitive drugs [5] nano biochips and membranes for bioseparations [6], surface coatings,

adhesives, cosmetics, detergents, toothpaste, special food products and medical diagnostics. Polysaccharides possesses distinct chemical and biological properties that include biocompatibility, biodegradability to harmless products, nontoxicity, physiological inertness, remarkable affinity to proteins, hemostatic, fungistatic, antitumoral and anticholesteremic properties [19,20] Chitosan, a copolymer of β (1,4)-D-glucosamine and β(1-4)-N-acetyl-D-glucosamine, is a non toxic, biodegradable and positively charged polysaccharide widely used as a support for enzyme immobilization [8,9,10]. Galactomannas have a linear back bone of (1→4)-diequatorially linked β-D-mannose residues, some of which carry single- sugar side chains of α-L-galactose attached by (1→6) linkages. Guar gums normally have an M/G ratio of ~1.6. Low molecular weight, acid–free water-soluble polysaccharides (LMWPS), are made by depolymerization and from this nanoparticles can be made by ionic gelation technique[11, 12]. Important application of polysaccharide nanoparticles is in the controlled release of protein and peptide drugs, because they show excellent mucoadhesiveness and permeation enhancing effect across the biological surfaces. Protein/peptide oral drug delivery is complicated process mainly due to poor intrinsic protein permeability as a result of large molecular weight, degradation by proteolytic enzymes in the stomach and in the small intestine, and chemical instability [13,14]. Compared with conventional solid-phase supports, nano particulate matrices could have a higher catalyst loading capacity due to their very large surface areas [15]. Subtilisin is one of the major proteolytic enzymes having a neutral pH, which is used as a digestive aid in pancreatitis, and used for wound healing etc. The preparation and properties of subtilisin functionalized biocatalytic polysaccharide nano particles are reported here.

2. Experimental

2.1 Materials: Chitosan and Guar gum were produced from Sigma (St.Luis, USA). Subtilisin [Amano, Japan,], Gluteraldehyde and Aerosol-OT [Sigma, St.louis, USA], tripoly phosphate, solvents such as Isopropanol and all the other reagents are of analytical quality.

2.2 Preparation of polysaccharide nano particles; The polysaccharide nanoparticles were made by 3 methods such as nano precipitation and cross linking, dialysis and cross linking or by two phase separation.

2.3 Preparation of subtilisin functionalized polysaccharide nano particles(EFNP) : The sutilisin solution in phosphate buffer (pH 7.0, 0.1M) was added to a suspension having polysaccharide nano particles. The enzyme was immobilized by glutaraldehyde coupling and then glycine was added to remove any unreacted aldehyde groups. The particles were then dialyzed against fresh phosphate buffer (pH 7.0, 0.1M) for 4 hours to remove the excess cross linking agents.

2.4 Analysis of Particle size of ultra micro and nano particles of subtilisin functionalized nano particles: Particle size and polydispersity were determined by photon correlation spectroscopy (PCS) by using a Zetasizer 3000 (Malvern Instruments Ltd., UK). Mean size and polydispersity were measured three times for each batch.

2.5 Optimum pH, temperature & kinetic parameters of subtilisin functionalized chitosan nano particles : In order to determine the optimal pH of the enzyme, the enzyme assay was carried out at different pH values (6.0–10.5) at 50°C. Optimal temperature was determined by a standard activity assay in the temperature range from 30 to 80°C. The kinetic studies were done by changing the substrate (Casein) concentration from 0.25-2.5 (W/V %).

2.6 Nanoparticle morphology by Scanning Electron Microscopy; The shape and surface morphology of the subtilisin functionalized micro and nano particles were examined using electron microscope (JEOL make, model JSM 5600 LV, Tokyo, Japan). For SEM studies, lyophilized nanoparticle were mounted on metal stubs using double-sided adhesive tape and then sputtered with gold. The micrographs were taken at an accelerating voltage of 15 KV and at various magnifications.

2.7 TEM of subtilisin functionalized subtilisin functionalized chitosan nano particles: TEM pictures of polymeric nanoparticles were taken in a Hitachi H 7600 TEM instrument operating at magnification of 80 kv. A drop of aqueous solution of particle was placed on a carbon membrane coated grid surface and excess liquid was removed carefully with a filter paper (Whatman No.1). After 1 min the grid surface was dried under vacuum at room temperature before loading in the microscope.

3. Results and Discussion

Hydrogels, from naturally occurring polysaccharides which are highly stable organic compounds that swell when their environment becomes more acidic or slightly alkaline. All the methods are found to be suitable for the preparation of nano particles. The chitosans and galactomannans are essentially random coiled polysaccharides in solution. The enzyme used for the studies is a versatile serine protease, subtilisin which after purification had a specific activity of 0.012 U/mg protein**.**

3.1 Formation of chitosan nano particles: Nano composite particles were formed by the nanoprecipitation and ionic cross linking method. TPP, which is a poly anion to cross-link with the cationic amino group of chitosan through electrostatic interaction, avoiding possible toxicity. The particles are formed upon the addition of nonsolvent and tri polyphosphate and stabilized by anionic surfactant Aerosol OT. Size and size distribution of the chitosan –TPP nanoparticles

depend largely on concentration, molecular weight, additives and conditions of mixing ie, stirring or sonication. An average particle size of 310 to 490 nm was obtained with isopropanol and 347-438 nm with acetone, when chitosan of molecular mass of 8KDa was used Fig-1. The PKa of chitosan is 6.5 and below this pH, chitosan behaves as a poly cationic material, the phosphoric ions of TPP forms ionic cross linking with NH_3^+ groups of the chitosan and has a net positive charge on the surface (IEP-9.0) and the surface is comparatively hydrophobic [17].

3.2 Effect of cross linking agent on the size of nano particles of galactomannans: The cross linker used was either borate or sodium tripolyphosphate (TPP). Table 1. Two Guar gum chains cross links with borate ions -B (OH) $_4$ preferentially due to the cis diols present in the mannose ring. The reaction is favored at neutral pH conditions. TPP cross links with the hydroxyl groups of the polysaccharide forming phosphate bonds between the two polysaccharide chains

3.3 Effect of non solvent on the formation of nano particles: The production of nano particles dispersed in aqueous media by precipitation with non solvents involve the use of acetone, methanol, ethanol, isopropanol, amyl alcohol etc. The final mean particle size of NPs was clearly dependent on the nature of the non solvent used. The results showed that the use of isopropanol and acetone led to smaller particles, as measured by (DLS), where as other solvents gave larger particles (above 500 nm). Even though low log P values tend to give nano particles, there is not much correlation with the Log P values and nano particle formation. However the dielectric constants which are a measure of solvent polarity played a significant role. A slow reduction in the dielectric constant of the solution brings about nanoprecipitation. Acetone and isopropanol has similar medium dielectric constant value of 18-20, which favors the nano precipitation of chitosan molecules in water medium which is having a dielectric constant of 80

Table 1 Nano particle preparation of guar gum

Method	Z average particle size (nm)	PDI
Nano precipitation and cross linking		
Cross linker		
TPP	279.8	0.425
Boric acid	265.4	0.491
Dialysis and cross linking	128.6	0.756
Two phase separation		
Cross linker (boric acid)		
Organic	739.8	0.312
Aqueous	168	0.659
Cross linker (TPP)		
Organic	571.3	0.161
Aqueous	213.9	0.750

Table 2 Effect of non solvent on guar gum NPs

Non solvent	Dielectric Constant (ε)	log P	Zave	PI
Methanol	32.6	-0.764	300.3	0.3
Isopropanol	18.3	0.074	279.8	0.425
Acetone	20.7	-0.24	224.9	0.276
Ethanol	24.5	-0.30	320.1	0.491
Ethyl acetate	6.0	0.68	464.4	0.653

3.4 Effect of surfactants on the size of nano particles;

Nanoparticles were made using different surfactants like Triton x 100, Tween-20, Aerosol OT and Span-60. Anionic surfactant such as Aerosol OT and SPAN was useful for chitosan particle stabilization. A concentration 3mM of Aerosol OT was appropriate for the successful production of chitosan nano particles. The two non ionic surfactants found useful for the stability of the galactomannan nano particles are found to be Tween 20 and Triton X100 and the nano particle surface is thus surrounded by a thin layer of hydrated poly ethylene glycol chains. This hydrophilic shells forms a steric barrier which prevents close contact between particles and, hence, coagulation (“steric stabilization”)

(Fei Han et al.,2008) and in turn stabilizes the NPs Increase in surfactant concentration was not found suitable for nano particle preparation.

3.5 Immobilization of subtilisin on polysaccharide nano particles-EFNP

The enzyme immobilization efficiency of the nano particle was in the range of 45.38 to 70.10 % .b Immobilization of enzyme usually results in the conformational change in the enzyme resulting in a shift in the optimum pH. The effect of pH on the activity of free and immobilized protease preparations are given in (Figure 6). The optimum pH of the native enzyme was at 7.0 and was shifted to pH 8.0 after immobilization. This pH shift towards alkaline side is due to the secondary interactions between the coupling agent, enzyme and the polymeric gel matrix. The glutaraldehyde coupling of the matrix with the enzyme would have linked all the available amino groups on the surface of the enzyme, and hence the acidic groups on the enzyme surface gives a negative charge to the enzyme protein, ultimately shifting the optimum pH to the higher side. The protease activity of native enzyme increased gradually with temperature and a maximum activity was obtained at 55°C. The immobilized enzyme also showed the same temperature optima.

3.6 Reaction Kinetics of EFNPs compared with native subtilisin

The immobilized enzyme shows a lower K_m value than the native subtilisin. The higher affinity of the immobilized subtilisin towards the substrate may be due to the presence of a flexible glutaraldehyde arm, which in turn helps the enzyme to suitably orient its active site towards the substrate (casein). However the catalytic efficiency of the immobilized enzyme was found to be lower than that of the native enzyme (Table 4)

Table 4 Kinetic parameters of immobilized NPs and native subtilisin

Enzyme	K_m Moles/ml	V_{max} Moles/s/g	k_{cat} Moles/s/mole of enzyme	k_{cat}/K_m
Native	$1.07x10^{-5}$	$4.21x10^{-6}$	0.147	$1.4x10^{4}$
Immobilized	$4.097x10^{-5}$	$2.89x10^{-6}$	0.07611	$18x10^{2}$

Particle size of the nano - and micro particles is an important formulation property that influences other pharmaceutical and cellular uptake properties of the drugs.

As the particle size is reduced, surface area to volume ratio increases, resulting in a large surface area available for the buffer penetration into the particles and also for the faster escape of the polymer degradation products from the smaller sized nanoparticles. John Hopkins researchers have reported that nano particles of 200-500 nm having hydrophilic neutral polymers moves through mucus layer quickly than smaller ones which are less than 100 nm [16].

3.7 *SEM and TEM of subtilisin functionalized chitosan nano particles:* The morphological characterizations of the nanoparticles of chitosan, figure 3 and 4 shows nano particles prepared with chitosan and galactomannan functionalized with subtilisin in SEM. It was confirmed by a transmission electron microscope (Figure 5).

4. Conclusion : There is enormous interest in using ultra micro and nanoparticles for biomedical applications including enzyme encapsulation and drug delivery. Nanoparticles of chitosan and galactomannan functionalized with subtilisin in the presence of anionic surfactant, and a co solvent, with TPP and glutaraldehyde as cross linking agents was made having sizes ranging from 100 to 500 nm. The nano particles are biocompatible, non toxic and the production is cost effective and the scale-up will be easy. A therapeutic enzyme, subtilisin, a serine protease, was loaded without much inactivation. One can also load any other enzyme or any hydrophobic drug by this method and thereby the bioavailability of these drugs can be increased and more importantly may help treat previously untreatable conditions.

References

[1] G.A.Mun, Z.S.Nurkeeva, V.V.Khutoryanskiy, A.D.Sergaziyev, J.M Rosaik,. Radiat. Phys.Chem. 65 (2002) 67

[2] J.Wang, G.Liu, M.R. Jan, J.Am.Chem.Soc 126 (2004) 3010

[3]C.RMartin, P.Kohli, Nature Rev.Drug Discov 2 (2003) 29

[4] A.Star, J.C.P Gabriel, K.Bardley, G.Gruener, Nano Lett, 3 (2003) 459

[5] B.Lakshmi,C.R Martin, Nature 388 (1997)758

[6] E.S.Amalia, D.Yolanda, C. Margarita,G.Carmen, C.Sagrario,V.Ana, J.A.Maria, Invest Ophthalmol Vis Sci.,47 (2006)1416

[7] S.B.Lee, D.T.Mitchell, I.Trofin, T. K.Nevanen, H.Soderlund, C.R.Martin,,Science 296 (2002) 2198

[8] C.Walsh , Nature 409 (2001) 226

[9] F.Jinda, G.Yong, Journal of Experimental Nanoscience, 1 (2006)457

[10] R.S.Juang, F.C.Wu, R.L.Tseng, Bioresour Technol 80 (2001)187

[11] N.Duran, M.A.Rosa, A.D'Annibale, L.Gianfreda., Enzym Microb Technol 31 (2002)907

[12] R.S.Juang, F.C.Wu,Tseng, Adv. Environ. Res. 6 (2002)171

[13]. Dea, I.C.M., Morrison, A., (1975). Adv. Carbohydr.Chem. Biochem. 31, 241-312.

[14]. Doyle, J.P., Giannouli, P., Martin, E.J., Brooks, M., Morris, E.R., (2006). Carbohydr. Polym. 64, 391-401.

[15] A.P.Nicholas, J.K Nikhil, Eur J Pharm Sci.14 (2001) 201

[16] B.Savitha, F.Georg, S.Sheetal, R.Rajani, K.Collins, M.Amarnath, M.Anirba M, J Nano Biotech 5:3 (2007) 1

[17] D.R.Bhumkar, V.B.Pokharkar. AAPS PharmSci Tech. 7(2) (2006) E1-E6

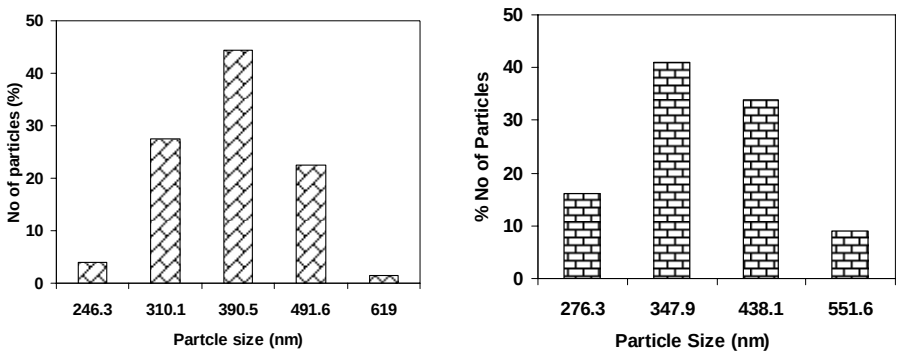

Figure 1 Nano particle distribution of chitosan enzyme composite (a, isopropanol, b acetone)

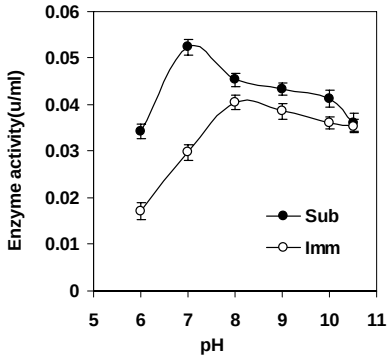

Figure 2 pH profile of immobilized & Native enzyme

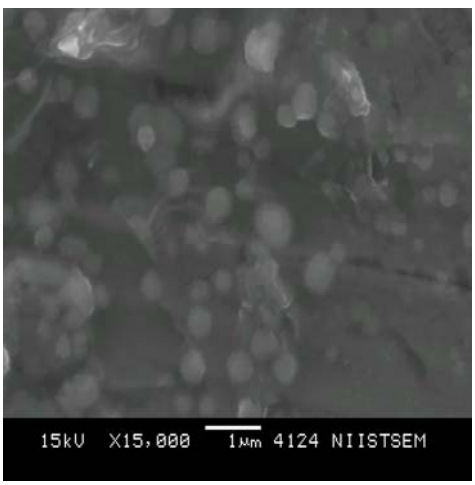

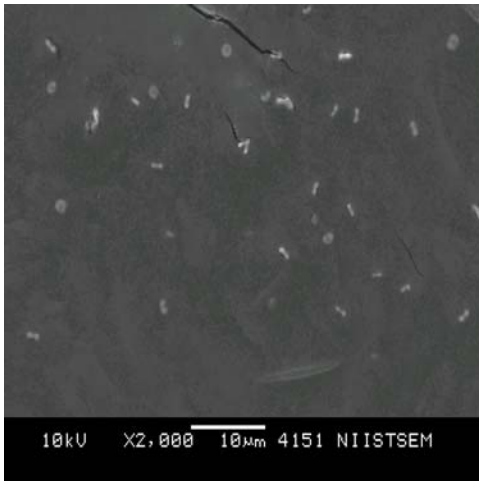

Figure- 3 SEM micrograph of EFNP of chitosan

.

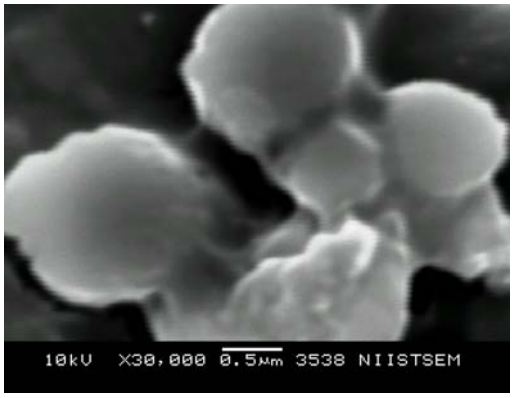

Fig-4 SEM image of EFNPs of galactomannan

Figure- 5 TEM micrograph of chitosan nano particles

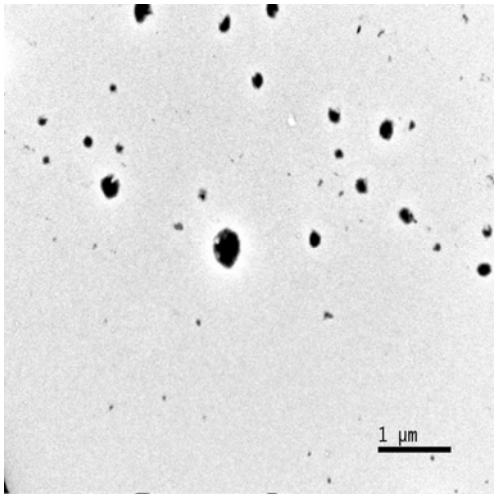

Preparation of polyvinylalcohol based thin film composite nanofiltration membranes: Application in the removal of hardness from brackish water

J.M.Gohil[*] and P.Ray[#]
Reverse Osmosis Discipline, Central Salt and Marine Chemicals Research Institute (CSIR), Bhavnagar, Gujarat, India.
E-mail: paramita022002@yahoo.co.in

Abstract
Polyvinyl alcohol (PVA) (degree of hydrolysis 86-87%), crosslinked with maleic acid (MA) has been used successfully as barrier layer of polysulphone (PSF) based thin film composite (TFC) membranes. The crosslinking of PVA and its presence in PSF matrix has been established by FTIR and contact angle study. PVA TFC membranes show dense phase morphology. The effect of variation of crosslinker (MA) dose, cure time and temperature on membrane performance (flux and rejection of inorganic salts) have been studied and the optimum membrane compositions were evaluated. Such membranes show differential rejection among the sulphate and chloride salts. On an average 65% difference exists between the rejection of $MgSO_4$ (70-90%) and NaCl (15-35%). The overall trend of rejection by such membranes is $R_{Na_2SO_4} > R_{MgSO_4} > R_{NaCl} > R_{MgCl_2} \cong R_{CaCl_2}$ (R = Rejection). The average molecular weight cutoff (MWCO) of such membranes varies between 250-450 Dalton. These membranes may be useful for the removal of dissolved sulphates (salts) and partial desalination of brackish water.

Introduction
Pressure driven membranes have acquired a significant position in the area of separation science and technology [1]. Nanofiltration (NF) membranes are relatively new class of charged pressure driven membranes. Due to preferential selectivity towards ions, lower operating pressure and higher flux, NF membranes have wide scope of applications in water and waste-water treatment [2, 3]. Hard water is probably the most common water problem found not only at home but also in the industries causing scaling in boilers, cooling towers, pipelines and other industrial equipments. Treatment of hard water with nanofiltration membranes may be a unique solution to produce soft water. Polyvinyl alcohol (PVA) being a water soluble biodegradable polymer has immense potential as a membrane material because of its high water permeation and film forming characteristics [4, 5]. Additionally presence of innumerable number of hydroxyl groups in this polymer may impart a charge effect in closer vicinity and make the membrane suitable to act as nanofiltration membranes with preferential rejection towards multivalent ions than the monovalent ones.
The main target of the work is to prepare polysulphone based thin film composite membranes with PVA as the selective barrier layer. The membrane composition has been optimized and the rejection trends of such membranes in different mono and bivalent salts have been evaluated.

Experimental
Materials:
Poly (vinyl alcohol) (PVA), with Mol. Wt. 1, 25,000, degree of hydrolysis 86-87%, Sodium chloride, Magnesium chloride, Calcium chloride, Magnesium sulfate, Sodium sulfate, Glycerol , all AR grade , supplied by SD Fine Chemicals, India.
D-Glucose Anhydride, LR grade, supplied by NICE Chemicals; Sucrose, LR grade, supplied by SRL; Raffinose pentahydrate, LR grade, supplied by Loba Chemie.

Membrane Preparation Method:
PVA solution 1% (w/w) (containing different dose of MA) was poured on PSF ultrafiltration membrane (prepared by phase inversion technique and acted as a porous support) mounted on a glass plate [6, 7].

Excess PVA solution was drained off and the membranes were dried at ambient temperature. The membranes were subsequently heated in oven at a temperature of 125±2 ºC for 30 minutes.

Characterization of Membranes:

FT-IR: The IR spectrum of PSF ultrafiltration and cross-linked PVA TFC membranes (of size 6 cm × 3 cm) were recorded in the middle infrared region using a Perkin Elmer 400 FT-IR spectrometer.

Contact angle (θ): Contact angle of resulting PVA TFC membranes was studied by Wilhelmy plate method using Dynamic Contact Angle Tensiometer (DCAT 21, Data Physics).

Scanning electron microscopy (SEM): Phase morphology (Cross-sectional and topography) of the membranes were studied using Leo microscope at 15 kV accelerating voltage.

Membranes performance testing: The salt rejection characteristics of membranes were studied in RO test cell by passing aqueous feed solutions of mono and bivalent salts separately through the membranes at different pressure (150-350 psi). Permeate flux was studied and solute rejection was calculated with the help of equation 1. The concentrations of inorganic salts in feed and permeate were determined by inductively coupled plasma spectrometry (ICP), chemical analysis and conductivity measurements.

$$Solute rejection(R)(\%) = \left[1 - \frac{Concentration\ of\ solute\ in\ permeate}{Concentration\ of\ solute\ in\ feed}\right] \times 100 \qquad (1)$$

Molecular weight cut-off (MWCO): A mixed solution containing glucose, sucrose, raffinose and glycerol each of 500 ppm was passed through the membranes. The percent organic solute in feed and permeate was analyzed by High performance liquid chromatography (HPLC) and Total organic carbon (TOC) analysis. The solute rejection was calculated by using the formula 1. The solute rejection above 85% was taken as MWCO of membranes.

Result and Discussion

The base PSF substrate was prepared from 17% PSF solution and PVA layer was coated with 1% PVA solution containing MA as curative in the concentration range from 2-50% (w/w with respect to PVA). The IR spectrum of PSF base substrate membrane is shown in figure 1(graph I). The existence of PVA at the surface of PSF TFC membranes is indicated by the peak at 3,200-3,400 cm^{-1} (Figure1, graph II), which is the characteristics of OH of PVA. The peak at 1,335 cm^{-1} is due to the ester linkages formed by the cross-linking of PVA with MA.

Contact angle reflects the hydrophilicity of any surface. PVA coating provides the hydrophilicity to hydrophobic PSF membranes. The hydrophilic nature of PVA TFC membranes are reflected by their average lower contact angle (81º) value compare to that of hydrophobic PSF membranes (89.5 º).

Cross sectional morphology of PSF membranes show a wide open pore structure (Figure 2A). However coating of PVA partially masks the polysulphone layer and overall reduction in the average pore size is observed (Figure 2B).

Effect of different process parameters on membranes performance:

Effect of variation of curative dose on membrane performance: To see the effect of MA concentration on stability of rejection layer, the flux (Figure 3) and rejection (Figure 4) profiles of the membranes (varying in the cross-link density of the rejection layer) were tested in continuous mode for a period of 24 hours using 500 ppm $MgSO_4$ solution. The membranes were cured at a temperature of 125±2 ºC for duration of 30 minutes. It is observed from Figure 3 that lowers the curative dose higher the membrane flux. However all the membranes show almost consistent flux over the studied period irrespective of the cross-linker dose. It is also observed (Figure 4) that in the rejection profiles there is a slight fall with time for membranes prepared with lower curative dose of 2 and 5% MA. However for MA dose >5% the rejection remains constant with time. Hence 5-10% concentration of MA may be considered as optimum for curing of such membranes.

Effect of cure time on membrane performance: Membranes were prepared from 17% PSF and 1% PVA-1 with MA concentration of 10% (w/w) cured by varying the cure time from 10-40 minutes at a temperature

of 125±2 ºC. Desalting performance of such membranes was studied in continuous mode for a period of 24 hours. It is observed (Figure 5) that membranes cured for all selected cure time except the lowest one (10 minutes) show almost constant flux and rejection with time. It is seen from Figure 5B that the rejection for membranes cured for 30 and 40 minutes are almost the same, whereas there is an average 15% rejection enhancement by varying the cure time from 20 to 30 minutes without much sacrifice in the flux. Hence 30 minutes cure time was selected as optimum.

Molecular weight cut off: The separation profile of different organic compounds (varying molecular weight from 90 to 600 gm/mole) with the variation of curative dose and cure time for different PVA TFC membranes are shown in Figure 6. It is seen that more the cross-link density of the barrier layer (due to higher cross-linker dose) higher the rejection of any selected organic compound. The lowest selected cross-linker dose of 2% produces membrane with no specific molecular weight cut off in the selected range i.e. 90-600 Dalton. The higher range of cross-linker doses i.e. 20-50% MA, produce membranes with MWCO in the range of 200-300 Dalton. For membranes with MA dose of 10%, MWCO values are between 350-450 Dalton.

Membranes performance with different inorganic salt solution: The desalting performances of the membranes were tested with different electrolyte solutions. The performances of the membranes (flux and rejection) varying in their curative dose are presented graphically in Figure 7. The % rejections of sulphate salts ($MgSO_4$ and Na_2SO_4) are almost same for all the selected membranes irrespective of their curative dose. The rejection of the chloride salts are much lesser than the sulfate salts, which may be due to higher repulsion of sulfate than chloride by the charged surface of the membranes. Although the variation of curative dose (2-50%) has negligible effect on the % rejection of sulphate salts but there is a gradual increase in rejection of chloride salts with increase in MA concentration which may be due to a synchronization of charge enhancement and membranes tightening.

Conclusions:

The overall trend of rejection by such membranes is $R_{Na_2SO_4} > R_{MgSO_4} > R_{NaCl} > R_{MgCl_2} \cong R_{CaCl_2}$ (R = Rejection). The average MWCO of the membranes varies between 350-450 Dalton. As for such membranes 65% difference is observed between the rejection of $MgSO_4$ (R 70-90%) and NaCl (R15-35%), hence, they may be useful for the removal of dissolved sulphate hardness and partial desalination of brackish water.

Acknowledgement: Financial assistance from CSIR, India is highly acknowledged.

References:

[1] Amjad Z. Ed.; Reverse Osmosis: Membrane Technology, Water Chemistry, and Industrial Applications, Van Nostrand Reinhold: New York, 1993.
[2] Ahn KH, Cha HY, Yeom IT, Song KG. Desalination 1998; 119(1-3):169-176.
[3] Ikeda K, Kimura S, Ueyama K. Maku 1998; 23:266-272.
[4] Krumova M, Lopez D, Benavente R, Mijangos C, Perena JM. Polymer 2000; 41(26):9265-9272.
[5] Suzuki M, Yoshida T, Koyama T, Kobayashi S, Kimura M, Hanabusa K, Shirai H. Polymer 2000; 41(12):4531-4536.
[6] Radovanovic P, Thiel SW, Hwang ST. Journal of Membrane Science 1992; 65(3):213-229.
[7] Kesting RE. A structure perspective' in: Synthetic Polymeric membranes, 2nd. ed. Wiley, 1985. Biomaterial membrane

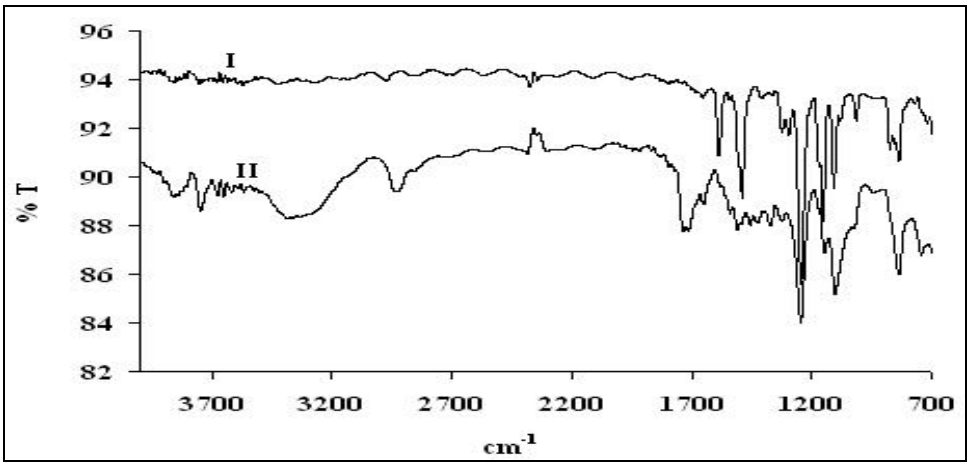

Figure 1. IR spectra of (I) PSF base membrane and (II) PVA TFC membrane

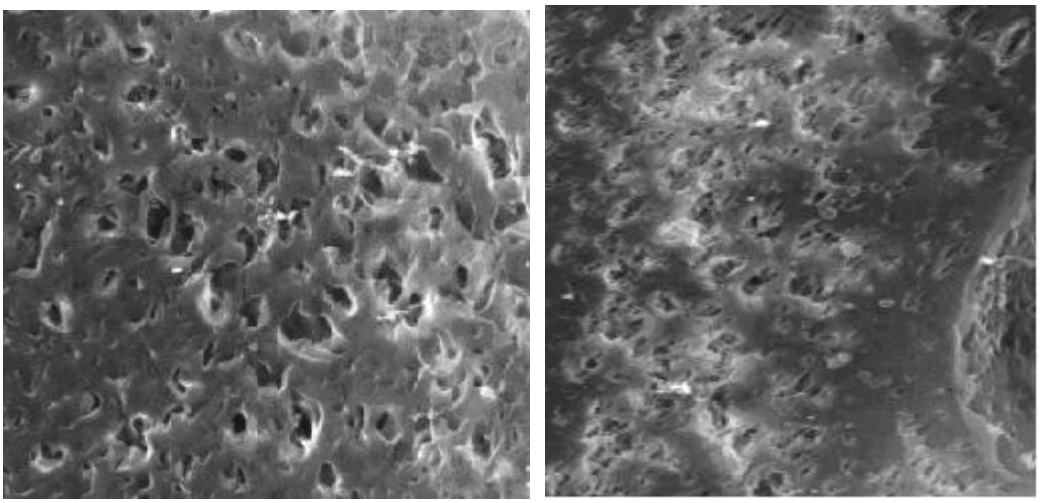

A **B**

Figure 2. SEM micrograph of A: PSF and B: PVA TFC membranes

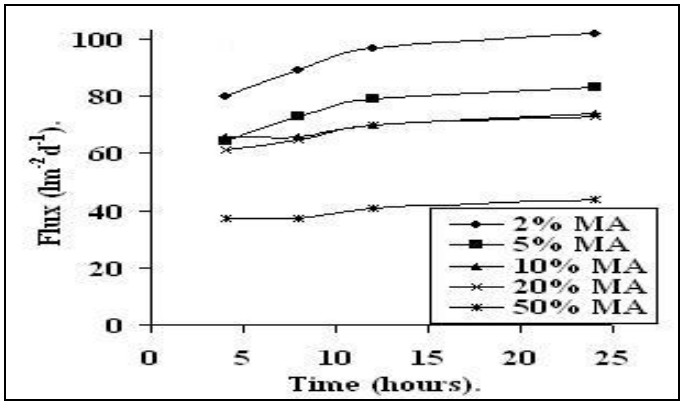

Figure 3. Time vs. Flux; for PVA TFC membranes with different cross-link densities, operating pressure 150 psi.

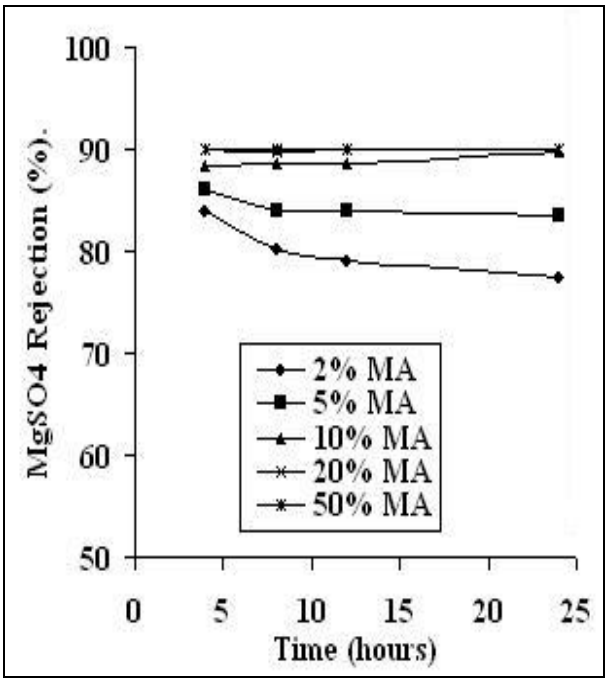

Figure 4. Time vs. % Rejection; for PVA TFC membranes with different cross-link densities, Operating pressure 150 psi.

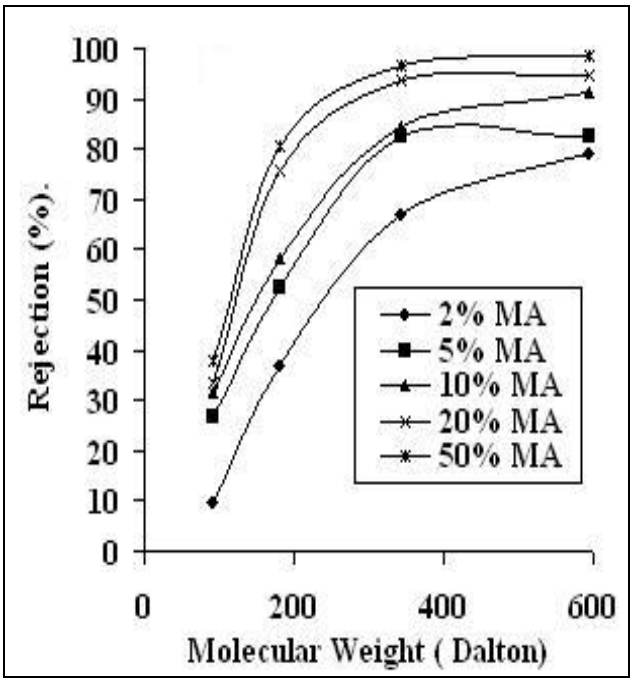

Figure 6. Molecular weight vs. % Rejection of TFC membranes with variable cross-link density of PVA layer. Operating pressure of 150 psi

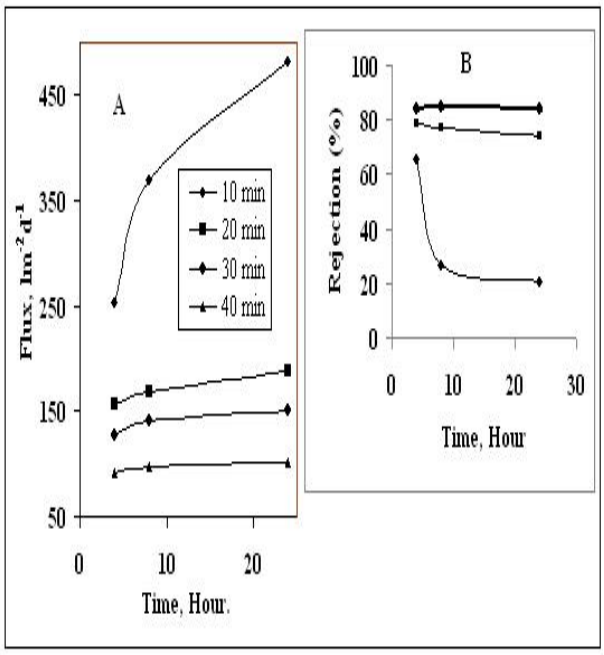

Figure 5. Variation of flux (A) and Rejection (B) with time for membranes cured for different time periods, at 125±2 ºC. MA 10%.

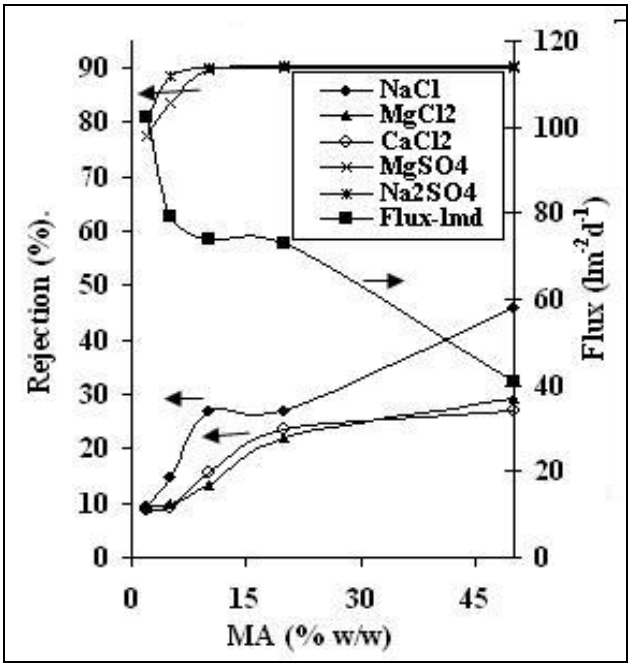

Figure 7. Variation of flux and rejection with MA concentration. Operating pressure of 150 psi

Photodegradable polypropylene film – Natural weathering studies

K. Rajakumar [a], V. Sarasvathy[a], A. Thamarai Chelvan [b], R. Chitra [c] and C. T. Vijayakumar [a,*]

[a] Department of Polymer Technology, Kamaraj College of Engineering and Technology, S. P. G. C. Nagar, K. Vellakulam Post – 625 701, Tamilnadu, India
[b] Post-graduate and Research Department of Chemistry, Thiagarajar College, P.O. Box 625 009, Madurai, India
[c] Centre for Fire, Explosive and Environment Safety, DRDO, P.O. Box 110 054, Timarpur, Delhi, India.

[*] E-mail: ctvijay22@yahoo.com

Abstract

Polypropylene (PP) is an attractive and dominating material for packaging due to its low cost, high tensile strength, gloss and versatility and hence, their consumption increases thereby littering, which leads to environmental pollution. To solve these problems, out of various technologies available, photodegradation seems to be a better choice due to the freely available sunlight. The polymers that degrade by peroxidation followed by bioassimilation of the oxidation products are more environmentally acceptable than the biodegradable polymers. In the present work, transition metal salt of stearic acid was synthesized as prodegradant (MF01) and incorporated in PP to enhance the photodegrdability. The virgin polypropylene and its blend with 0.2 % MF01 were extruded into films of 60 μm thickness. The films were naturally weathered from the period, December 2006 to March 2007 (winter season) and May 2007 to July 2007 (summer season). The photodegradation behavior was studied using Fourier Transform Infrared Spectrophotometry (FTIR), Universal Testing Machine (UTM) and Scanning Electron Microscope (SEM). A steep increase in the various indices like hydroperoxide, hydroxyl, carbonyl, lactone, ester, carboxylic acid, vinylidene and crystallinity were noted for virgin PP after 50 days of exposure whereas these values increased after 15 days of exposure for the prodegradant added PP. The sudden decrease in the elongation at break (%) for the materials signifies chain scission. PP films having higher carbonyl index values showed surface cracks in the scanning electron micrographs, indicating the degradation of the material.

Introduction

The synthetic polymers are used in vast areas based on their inertness towards outside factors like heat, radiation, chemicals and micro organism, but recently, this inertness has become a major contributor to the serious problem of solid waste disposal [1]. Increasing amounts of municipal solid waste (MSW), decreasing the landfill capacity for plastic disposal and slow degradation of plastic litter in the environment, which lead to generate intense interest in degradable plastics in the last quarter century.

According to estimates, plastic wastes represent 15-25% of municipal solid waste. To minimize this problem, there are three ways to utilize the plastic waste: landfilling, incineration with or without energy recovery and recycling. The largest amount of plastic waste is going for landfilling (65-70%), incineration and recycling amounts to about 20-25% and 10% respectively [2, 3]. Therefore, the environmental problem is still present. So, many researchers have intense interest to develop polymers that are more degradable in the natural environment after use, is desired for environmental conservation. Many authors have been investigating about degradable polymers which were reported in several research articles [4-7].

Now a days polypropylene has achieved in dominating position based on the excellent price/property relationship thereby it can be applied in various field. Also it is an attractive material

for packaging owing to their low cost of production, higher tensile strength, gloss and versatility [8]. Therefore, increase in its consumption leads to littering and causes environmental problem. So, polypropylene was taken as the material for investigation in the present study.

The degradation behaviour of PE using various photoinitiators under natural weathering condition was investigated [9, 10]. The photodegradation behaviour of polypropylene under natural weathering conditions using non-toxic transition metal carboxylate as prodegradant has not been pursued earlier. Iron stearate was taken as the prodegradant for polypropylene and the photo-degradability of polypropylene under natural weathering situations was investigated and the results are discussed.

Experimental

Materials

Stearic acid, potassium hydroxide, ferric sulphate monohydrate were used as received to synthesize ferric stearate. Iron salt of stearic acid (MF01) was synthesized by reacting ferric sulphate monohydrate with the potassium salt of the fatty acid. Polypropylene (Repol Grade H100EY) obtained from Reliance Industrial Limited, Jamnagar, India was chosen for the present study. The virgin polypropylene (4Kg) was blended with 0.2% of prepared prodegradant using a blender. The virgin PP and the prodegradant blended PP were blown into films using an extruder (Film width = 36cm and Film thickness = 60μm).

Methods

The films were naturally weathered on a suitably designed and fabricated outdoor exposure rack, which was located in the premises of Kamaraj College of Engineering and Technology, S.P.G.C. Nagar, K.Vellakulam Post - 625 701, Virudhunagar, India. The natural weathering of all PP films was carried out from December 2006 to March 2007 (winter season) and May 2007 to July 2007 (summer season). During the course of natural weathering the average temperature, pressure and humidity were about 34 °C, 748 mmHg and 40 % rel. respectively. The average visible and UV light intensity were 937 x 10^2 LUX and 998 uW/cm^2 respectively. The sampling was done at regular intervals to assess the changes occurring in the material during the natural weathering. Fourier Transform Infrared Spectrophotometry (FTIR), Universal Testing Machine (UTM) and Scanning Electron Microscopy (SEM) were utilized to follow the chemical and physical changes occurring in the material.

Results and Discussion

FTIR Studies

From the FTIR spectra of the weathered PP samples, hydroperoxide, hydroxyl, carbonyl, lactone, ester, carboxylic acid, vinylidene and crystallinity indices have been calculated. The characteristic infrared absorption frequencies for the different functional groups are listed in Table 1. In the present work, the band at 974 cm^{-1} (CH_3- rocking) was chosen as the reference peak, because it remains unchanged during photodegradation process.

Carbonyl index is the most used parameter to monitor the degree of degradation in polyolefins [11]. The carbonyl index was calculated as the ratio of the maximum absorbance at 1715 cm^{-1} to the absorbance at 974 cm^{-1}. The carbonyl index value increases with increasing exposure period only after certain days of exposure, which can be taken as the induction period for degradation. From Fig. 1, it is clear that PP weathered at winter season starts to degrade after 50 days of exposure whereas for PP weathered during summer season, the induction period for degradation was found to be 40 days. Incorporation of the prodegradant (iron stearate, MF01) in PP drastically reduces this induction period. These results confirm the fact that the added prodegradant plays an important role to induce photodegradation. Environmental conditions like temperature, UV intensity, visible light intensity, etc., also play a definite role in the photodegradation behaviour of PP. In general, carbonyl groups

were observed as a broad peak in the region of 1800 – 1700 cm^{-1} in the FTIR spectrum of weathered PP due to the overlap of different degradation products like lactone, ester, ketone, carboxylic acid, etc [12]. The carboxylic acid group concentration (Fig. 2) is higher while the lactone concentration is low because the carboxylic acid is the final stable product of degradation [13]. A similar trend was observed in the study of polypropylene natural weathering at Messina, Italy by Gallo et al.[14].

Hydroperoxide is the initial product of photooxidative degradation of PP and hence hydroperoxide group formation and its decomposition in the course of natural weathering is an important aspect, which may justify the faster degradation of materials. The hydroperoxide index was calculated as the ratio of the maximum absorbance at 3445 cm^{-1} to the absorbance at 974 cm^{-1}. From Figs. 1, 3a and 3b, the concomitant increase of the hydroperoxide groups and the carbonyl groups are explicit. It reveals that hydroperoxide formation and its decomposition take place simultaneously since the generated tertiary hydroperoxide is unstable. A similar trend has also been observed in the case of hydroxyl index variation.

In the case of photooxidation of PP, vinylidene group formation is the most probable one when compared to the vinyl group due to the presence of pendent methyl group. The vinylidene index was calculated as the ratio of absorbance at 888 cm^{-1} to the reference peak absorbance at 974 cm^{-1}. An irregular trend has been observed for this index. Certain environmental conditions lead to the consumption of this group to produce free radicals, whereas some environmental features favour the formation of this group.

In order to gather information regarding the variation of crystallinity as a function of outdoor exposure days, the ratio of absorbance at 998 cm^{-1} to the absorbance at 974 cm^{-1} was used to calculate the crystallinity index. The first band is regularity band characteristic of the crystalline PP, whereas the second band corresponds to both crystalline and amorphous phases of PP. In Figs. 1-3, it is clear that as the hydroperoxide, hydroxyl, carbonyl, lactone, ester, carboxylic acid, etc., indices increases, the crystallinity index is also increasing. This may be explained due to the formation of new low molecular weight photooxidation products capable of forming new crystalline domains.

Measurements of Tensile Properties

The elongation at break (%) can be frequently used to monitor the degradation of polymers. From Fig. 4, it is found that in the case of PP virgin, the elongation at break shows slight variation up to 45 days of exposure and then a sudden drop is seen. The value reaches near zero value soon indicating main chain scission in the polymer molecule. But, in the case of prodegradant added PP materials, the elongation properties are lost within 15 days of exposure, thereby rendering the film useless for practical applications.

Tensile strength is an important measure of product quality to certify the product and therefore its variation during weathering is one of the important parameter used to follow degradation. In almost all cases, PP films and PP containing prodegradant, tensile strength decreased considerably at the initial stages of weathering. Then a gradual decrease is noted and finally there is a sudden drop in the tensile strength values. This phenomenon may be attributed to chain reorganization and/or lower degree of orientation during natural weathering.

SEM studies

The scanning electron micrographs of weathered PP virgin (45 days) and its blend with MF01 (11 days) films are shown in Fig. 5. The SEM images clearly show the formation of cracks in the weathered material. The increase in carbonyl index, the decrease in elongation at break and the formation of cracks are enhanced at a much earlier stage when the prodegradant is added to PP.

Conclusion

A steep increase of carbonyl, hydroperoxide, hydroxyl, lactone, ester, carboxylic acid and crystallinity indices and a sudden decrease of elongation at break and tensile strength indicate the occurrence of main chain scissions in the materials investigated. Further, from the above results one can reasonably conclude that the added prodegradant (ferric stearate) plays an important role in initiating the photodegradation of polypropylene during weathering. Other weather parameters like temperature, UV intensity, visible light intensity, etc., are contribute substantially to the photooxidative degradation of the material.

References

1. Barenberg SA. In: Brash JL, Narayan R, Redpath AE, editors. Degradable Materials, Boston: CRC Press, 1990. pp. 559-583.
2. Misklczi N, Bartha L, Deak G, Jovev B. Polym Degrad Stab 2004; 86:357.
3. Aguado J, Serrano DP, Guillet JE. In: Clark JH, editor. Polymers and Ecological Problems, New York: Plenum Press, 1973.
4. Scott GJ. Polym Sci Symp 1976; 57:357.
5. Griffin JGL. In: Chemistry and technology of biodegradable polymers, London: Blackie Academic and Professional, 1994 (chapters 1-3).
6. Scott G. Degradable Polymers: Principles and Applications, London: Chapman & Hall, 1995 (chapter 9).
7. Scott G. Polymers and the Environment, Cambridge: Royal Society of Chemistry, 1999 (chapter 2).
8. Roder H, Vogl O. Prog Polym Sci 1999; 24:1205.
9. David C. Trojan M. Demarteau DA. Polym Degrad Stab 1992; 37:233.
10. Sheikh N, Akhavan A, Naiman F, Kholou F, Hasanpour S, Sohrabpour M. J Polym Env 2006; 14:103.
11. Carlsson DJ, Wiles DM. J Polym Rev 1976; 14:65.
12. Hamid SH, Prichard WH. Polym Plast Technol Eng 1988; 27:303.
13. Morlat S, Mailhot B, Gonzalez D, Gardette J. Chem Mater 2004; 16:377.
14. Gallo R, Severini F, Ipsale S, Fanti ND. Polym Degrad Stab 1997; 55:199.

Table 1. Characteristic infrared absorption frequencies

Functional Group	Frequency Range (cm^{-1})
Hydroxyl and Hydroperoxide	3600 - 3200
Carbonyl	1800 – 1700
Ketone	1725 – 1715
Carboxylic Acid	1712 – 1705
Ester	1750 – 1735
Lactone	1785 – 1760
Vinyl	909
Vinylidene	888

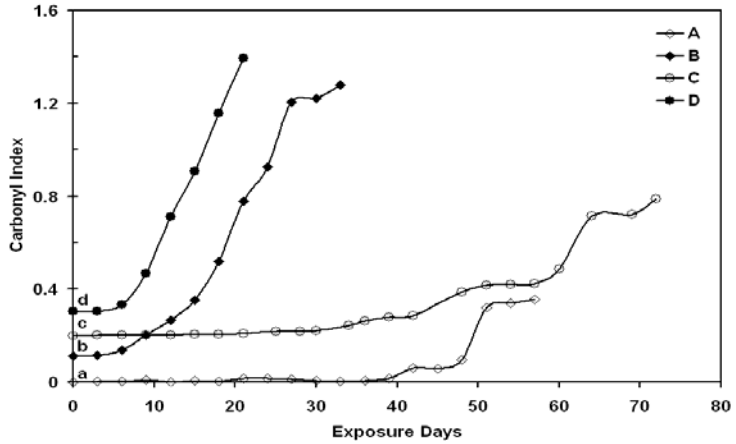

Fig. 1. Carbonyl index variation of weathered materials: Winter - (A) PP Virgin and (B) PP:MF01; Summer - (C) PP Virgin and (D) PP:MF01. The curves B, C and D are shifted along the ordinate by the distance ab, ac and ad respectively

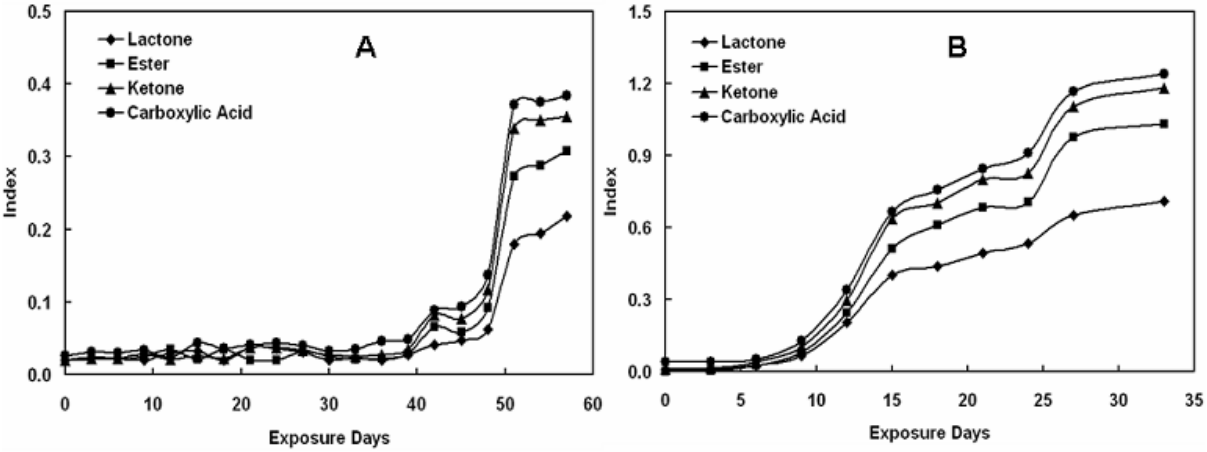

Fig. 2. Lactone, ester, ketone and carboxylic acid indices for weathered materials (A) PP Virgin; (B) PP:MF01 during winter

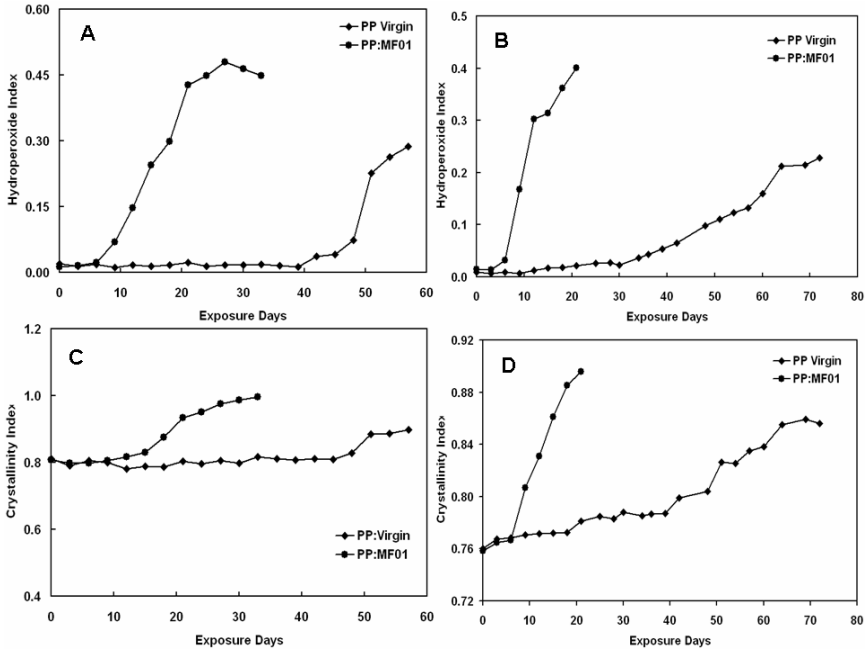

Fig. 3. Hydroperoxide and Crystallinity index variation: Winter - (A) and (C); Summer - (B) and (D)

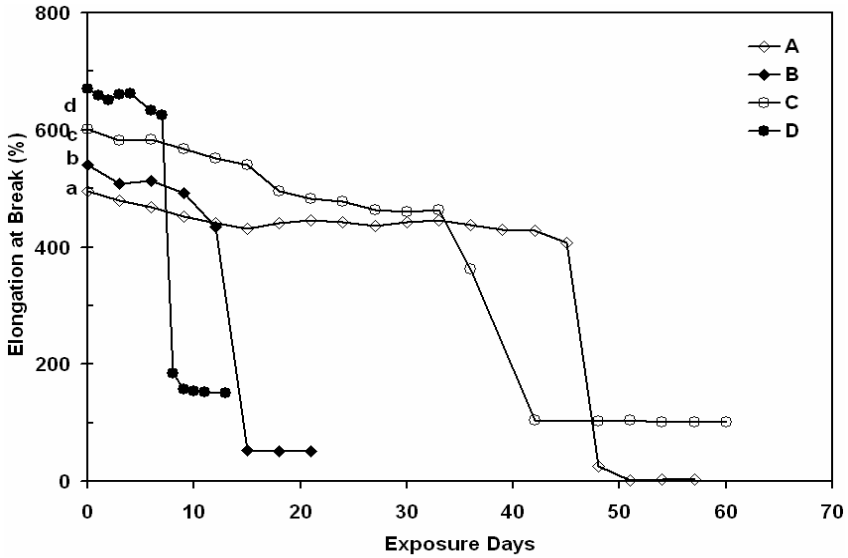

Fig. 4. Variation in the elongation at break (%) of weathered materials: Winter - (A) PP Virgin and (B) PP:MF01; Summer - (C) PP Virgin and (D) PP:MF01. The curves B, C and D are shifted along the ordinate by the distance ab, ac and ad respectively

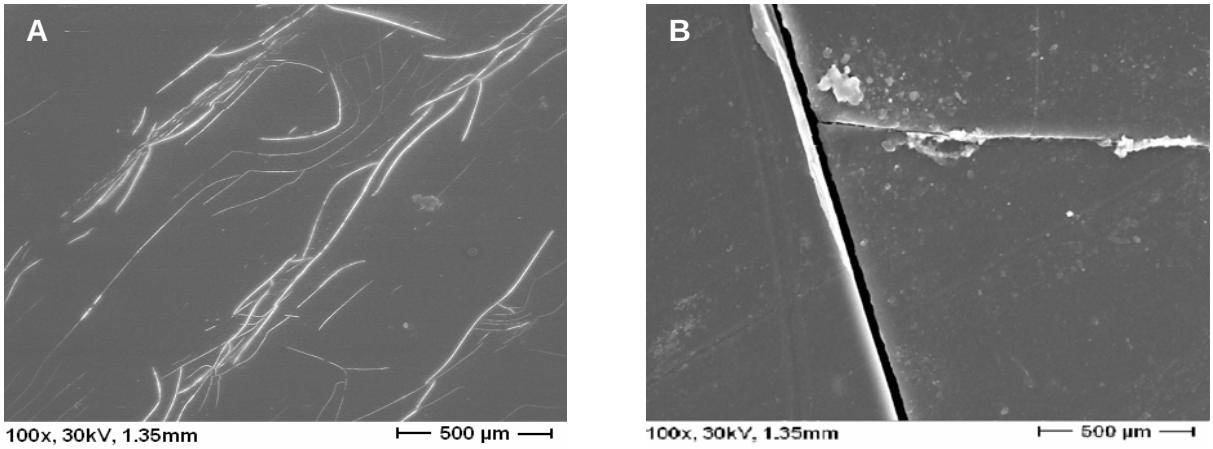

Fig. 5. SEM photographs of weathered materials: (A) PP virgin and (B) PP:MF01 blend

Swelling behaviour of hydrogels based on crosslinked NR/PEG block copolymers.

Christina George and M.R. Gopinathan Nair
School of Chemical Sciences, Mahatma Gandhi University, Priyadarshini Hills
Kottayam 686560, India.
E-mail: christeena.george@gmail.com

Abstract

A series of NR/PEG block copolymers were prepared from polyethylene glycol (PEG) and hydroxyl terminated liquid natural rubber (HTNR) by solution polymerization and dynamics of the water sorption process were studied. The effect of NCO/OH ratio and pH of the swelling medium were investigated with respect to the water sorption characteristics of the hydrogels. Results indicated that the hydrogels exhibited overshooting effect in their dynamic swelling behaviour. Mechanism of sorption, sorption kinetics and transport coefficients including diffusion coefficient, sorption coefficient and permeation coefficient were also determined. The sorption behaviour was found to vary with the variation in NCO/OH ratio of the block copolymers.

Introduction

Hydrogels are multi – component systems comprising of hydrophilic polymeric networks capable of absorbing enough water (> 20% of its dry weight) causing macroscopic changes in the sample dimension while maintaining its structural integrity. Due to the relatively high water content of these materials, they have found a plethora of applications in biomedical, pharmaceutical, food and environmental fields. Their high water content lends them high biocompatibility and makes them well tolerated when implanted in vivo. Consequently, they have emerged as promising candidates for a variety of biomedical applications such as drug delivery systems [1], wound dressings [2], contact lenses [3], artificial implants [4] etc. However, on increasing the water content, the mechanical strength of the hydrogel becomes lower and the gel transparency can decrease as a consequence of a macrophase separation between water and polymer. Hence to achieve a gel with high mechanical strength, transparency and water content, a composite molecular structure is needed. This structure will comprise of a hydrophilic component that absorbs large amounts of water and a hydrophobic component, which improves the mechanical strength [5]. It is according to this idea that for our study we synthesized amphiphilic NR/PEG block copolymers with hydrophobic natural rubber (NR) and hydrophilic polyethylene glycol (PEG).

The multitude of hydrogels available leaves numerous choices for polymeric formulations. The best approach for development of a hydrogel with desired characteristics is to correlate the macromolecular structure of the polymer with desired swelling characteristics. The swelling studies not only describes the amount of water contained within the hydrogel at equilibrium but also give ample insight into the network structure of the gels and the transport mechanisms of the water uptake process[4]. During these studies controllable volume change can be brought about in the hydrogels by changing the surrounding conditions such as pH [6], temperature [7], salt concentrations [8], chemistry [9], electric field [10], photo irradiation [11] and solvent composition [12].

Polyethylene glycol (PEG) with its desired set of properties has always been a front-runner among synthetic polymers used for designing hydrogels primarily because of its nontoxicity and biocompatibility [4]. The dynamic swelling behaviour of amphiphilic block copolymer based on polyethylene glycol (PEG) and polybutyl acrylate (PBA) was reported by Wang et al [13]. Bajpai

et al [4] reported the swelling behaviour of hydrogels prepared from polyethylene glycol (PEG) and poly (acrylamide-co-styrene) (PAMS). The water uptake of this hydrogel varied sensitively with the variation of the contents of hydrophilic polymer, crosslinking agent and temperature of the swelling medium. Karaky et al [14] synthesized a new type of pH switchable suparamolecular sliding gels based on polyrotaxanes of polyethyleneimine-block-poly (ethylene oxide)-block-polyethyleneimine block copolymer and α - cyclodextrin.

In the present work, transport behaviour of water through NR/PEG block copolymer with varying NCO/OH ratios has been investigated. The shape of diffusion profile, mechanism of sorption, sorption kinetics and the transport coefficients including diffusion coefficient, sorption coefficient and permeation coefficient are described here. Effect of NCO/OH ratio and pH on swelling behaviour of these block copolymers is also described.

Experimental

Materials

Natural crumb rubber (ISNR-5): Weight average molecular weight = 8,20,000; Intrinsic viscosity in benzene at 30^0C= 4.45 dL/g; Wallace Plasticity, P_0=39 was supplied by Rubber Research Institute of India, Kottayam, Kerala. Hydrogen peroxide (30% w/v) supplied by E. Merck, India was used without further purification. Toluene (reagent grade) obtained from E. Merck; India was used as solvent without further purification. Methanol (reagent grade) supplied by E. Merck, India was used without further purification. Toluene diisocyanate (TDI) (80/20 mixture of 2,4- and 2,6- isomers) was supplied by Aldrich, Germany and was used as received. Dibutyl tin dilaurate (DBTDL) supplied by Fluka, Switzerland, was used as catalyst without further purification. Chloroform (laboratory reagent grade) was dried with anhydrous calcium oxide and then distilled before use. It was supplied by E. Merck, India. Polyethylene glycol (PEG) of molecular weight 4000 supplied by Aldrich, Germany was used as received. Water used for the swelling studies was double distilled and deionized.

Hydroxyl terminated liquid natural rubber (HTNR) of number average molecular weight 4000 was prepared in the laboratory by the photochemical degradation of natural rubber as per reported procedure [15]. It was reprecipitated thrice from toluene using methanol and dried at 70^oC – 80^oC in vacuum.

Synthesis of the block copolymer

HTNR was dissolved in chloroform to get a 35% solution and taken in a flat-bottomed flask equipped with a magnetic stirrer, nitrogen inlet and outlet, water condenser and a dropping funnel. Dibutyl tin dilaurate (DBTDL) catalyst (6.1% by weight of HTNR) was added and the solution brought to reflux with vigorous stirring. Variation in crosslink density was brought about by varying the NCO/OH ratio. TDI was added drop wise over a period of 30 min followed by 2 h of the reaction to end cap HTNR. This was accompanied by the addition of the required amount of PEG as a solution in chloroform (35% w/v) drop wise during 1.5 h followed by 2 h of the reaction. The excess chloroform was distilled off and the viscous polymer was cast in tray treated with silicone release agent. The sheet removed from the tray after 24 h was kept in vacuum oven at 60^0C to remove traces of the solvent present and then cured at 70^0C for 24 h followed by one week ageing at room temperature in a moisture-free atmosphere [16].

Polymer designation

The block copolymer studied in this work is designated as NR/PEO (4000/4000)-1 which indicates that the sample contain HTNR and PEG where HTNR molecular weight is 4000 and PEG molecular weight is 4000. The number indicates the order of synthesis with the variation in NCO/OH ratio (Table I).

Swelling experiment

Circular shaped samples (diameter ~ 13 mm) were cut from the block copolymer sheet by means of a sharp edged steel die and thickness of the sample was measured with an accuracy of ± 0.01nm. Dry weight of the cut samples were taken before immersion into distilled water at room temperature. The samples were periodically removed from test bottles. Then the samples were weighed on an electronic balance (Shimadzu, Libor AEU-210, Japan) and immediately replaced into the test bottles. This procedure was continued until equilibrium swelling was attained in the case of each sample. The time taken for each weighing was kept constant to a minimum of 20-30s in order to avoid errors due to the escape of solvent from the samples. The results of these experiments were expressed as moles of solvent uptake by 100 g of polymer (Q_t mol %).

Results and Discussion

The swelling behaviour of the hydrogels depends on the nature of the polymer and the environmental conditions. The polymer's nature involves crosslink density, ionic content etc. The environmental conditions include pH and temperature [6,7]. A series of NR/PEG copolymeric hydrogels was investigated in terms of their swelling characteristics. The effect of NCO/OH ratio and pH on the swelling behaviour was studied.

Sorption dynamics and effect of NCO/OH ratio

The data from the sorption studies are plotted in Figure 1 with the percentage uptake of the penetrant against $t^{1/2}$, where t is the time taken to attain equilibrium. Since PEG is hydrophilic polymer and NR is hydrophobic in nature, the present block copolymer possesses these dual characteristics. In the case of a typical polar solvent like water, the interaction is restricted to only the matching hydrophilic domain in the block copolymer while the hydrophobic domain conveniently excludes it.

A remarkable feature that is observed in the sorption curves of the swelling ratio versus $t^{1/2}$ is that they are slightly sigmoidal initially and later level off. The sigmoidal shape is related to the time taken by the polymer chains to react to the swelling stress and realign themselves to accommodate the solvent molecules. Initially, due to the large concentration gradient, the swelling rate is too high. The end result of this behaviour is solvent induced stress in the polymer sample. However, as the concentration gradient decreases, the swelling ratio decreases and at equilibrium swelling the concentration differences almost vanishes [17].

In the NR/PEG hydrogels, Q_∞ mol% values varied with the variation in NCO/OH ratios (Table II). The maximum uptake was shown by the sample with NCO/OH ratio 1.1 followed by a decrease in the uptake values with the increase in NCO/OH ratios. This sort of behaviour maybe the outcome of increase in polymer mobility, free volume and better interactions existing in the sample with NCO/OH ratio 1.1.

Mechanism of sorption

The sorption data of the polymer – solvent systems for a circular geometry of the sample before the attainment of 55% equilibrium sorption have been fitted in the following empirical formula [18,19]

$$\frac{Q_t}{Q_\infty} = kt^n \qquad \text{.....(1)}$$

where Q_t and Q_∞ are the mol% increase in sorption at time t and equilibrium respectively. The type of diffusion mechanism has been analysed in terms of the empirical relation

$$\log \frac{Q_t}{Q_\infty} = \log k + n \log t \quad \ldots\ldots\ldots\ldots (2)$$

k and n have been determined from a least square fit of log Q_t / Q_∞ versus log T. Constant k depends on the structural features of the polymer system and its interaction with the solvent used [17]. The polarity and the size of the solvent along with the polar and non-polar segments in the block copolymer determine the value of k parameter. n is the diffusional exponent, which indicate the transport mechanism. If n =0.5, the mechanism of sorption is termed as Fickian, where the rate of polymer chain relaxation is higher than the diffusion rate of the penetrant. When n = 1, the mechanism is said to be non – Fickian where the chain relaxation is slower than the solvent diffusion. If the value lies between 0.5 and 1, then the mechanism follows anomalous transport where the polymer chain relaxation rates and the solvent diffusion rates are similar. By regression analysis, the values of n and k are obtained as slope and intercept and are consolidated in Table III. The correlation coefficient values are found to be 0.999. The values of n range from 0.42 to 0.61, which indicates that the mechanism of sorption follows Fickian mode in samples with lower NCO/OH ratios while the mechanism shifts to anomalous mode with a bias to non – Fickian mode in the samples with higher NCO/OH ratios. In the present study the k values do not show a regular trend.

Sorption kinetics

Sorption of liquid through polymer samples cause structural rearrangement, which induces kinetic behaviour that in turn are affected by the total free volume and its distribution in the polymer system. We have analysed the sorption data in terms of the first - order kinetic model. The first – order rate constant k_1 for the polymer – solvent system was obtained using the first – order equation [20]

$$dc/dt = k_1 (C_\infty - C_t) \quad \ldots\ldots\ldots\ldots\ldots\ldots (3)$$

where C_∞ and C_t are the concentration of the penetrant at equilibrium and time t respectively. C_∞ and C_t are equivalent to the equilibrium swelling Q_∞ and swelling at time t, which is Q_t. Integration of equation (3) gives

$$k_1 t = 2.303 \log [C_\infty / (C_\infty - C_t)] \quad \ldots\ldots\ldots (4)$$

Typical plots of log $(C_\infty - C_t)$ versus time is given in Figure 2 and the estimated rate constants for the penetrant are given in Table IV. A negative slope was observed and the values are found to range form 3.29×10^3 min^{-1} to 19.30×10^3 min^{-1}.

Transport coefficients

Diffusion in polymer is complex and depends strongly on the concentration, degree of swelling, solvent size and size of the voids in the polymer. From the slope θ of the linear portion of the sorption curve, the diffusion coefficient D has been calculated using [21]

$$D = \pi\left(\frac{h\theta}{4Q_\infty}\right)^2 \qquad \text{.....(5)}$$

where h is the thickness of the sample. Due to the swelling in a short period of time, swelling correction is necessary to get correct diffusion coefficient known as the intrinsic diffusion coefficient (D^*) [22]

$$D^* = \frac{D}{\varphi^{7/3}} \qquad \text{.....(6)}$$

where ϕ is the volume fraction of the polymer. The variation in D^* value depends on the nature of the crosslink, penetrant size and polarity. The values of D^* along with sorption and permeation coefficients are tabulated in Table V.

The D^* values varied with NCO/OH ratios, with the maximum value obtained in sample with NCO/OH ratio 1.1. With further increase in NCO/OH ratios, D^* values showed a steady decrease. This observation can be correlated to the equilibrium swelling uptake that was found to be maximum in sample with NCO/OH ratio 1.1. To sum up, D^* depends more on the molecular interaction between the penetrant and the polymer system. A better understanding of the interactions and their strengths can be obtained from the sorption coefficient S, which can be calculated as follows

$$S = \frac{M_S}{M_P} \qquad \text{.....(7)}$$

Where M_s is the mass of the solvent molecules at equilibrium swelling and M_p is the initial mass of the polymer sample [20]. The S value is high in sample showing high equilibrium swelling uptake values, i.e. the sample with NCO/OH ratio 1.1. The high S value in this system shows the better accommodation of the water molecules due to the favourable interactions with the polar region of the block copolymer. The permeability coefficient P depends on doth D and S, since permeation is a combined effect of diffusion and sorption [20].

$$P = D.S \qquad \text{.....(8)}$$

The permeation values are yet again high in sample with NCO/OH ratio 1.1. The P values reflect the net effect of diffusion and sorption. In the block copolymer studied, S values are higher compared to D^* and P, showing a larger tendency for the penetrant molecules to sorb rather than diffuse into the polymer. Thus sorption predominates over diffusion in the systems under study.

Effect of NCO/OH ratio and pH on overshooting effect

In Figure 1 and Figure 3, the dynamic swelling curves corresponding to copolymers swollen in water and at pH 9 respectively exhibit overshoot. Initially, the samples increase their swelling ratio, later on they reach a maximum and finally they deswell until an equilibrium value is reached. The sample with NCO/OH ratio 1.3, 1.4 and 1.5 exhibit overshoot in water while all the NR/PEG samples exhibit overshooting effect at pH 4, pH 7 and pH 9. We have attributed this feature to the anomalous transport with a bias to the non – Fickian mode (Table III). The primary factor contributing to overshooting effect is the difference existing between the relaxation and diffusion rates at experimental conditions. The stress generated due to the slow relaxation rate

compared to diffusion rate results in overshoot. Due to the thermodynamic interaction with macromolecular chains, water enters before these chains can relax or rearrange. Later the rearrangement of these chains result in partial exclusion of water leading to overshooting effect [23]. In short overshooting effect depends on the NCO/OH ratio and pH of the surrounding medium.

Conclusion

The water uptake of the hydrogel based on NR/PEG block copolymers varies sensitively with NCO/OH ratio. The maximum Q_∞ mol% uptake is shown by sample with NCO/OH ratio 1.1 followed by a decrease in the Q_∞ mol% values in heavily crosslinked samples. Increase in polymer mobility, free volume and better interactions existing in the sample with NCO/OH ratio 1.1 is the reason behind the high Q_∞ mol% uptake. The sorption kinetics has been studied and the experimental data suggests that the swelling process obeys first – order kinetics. Maximum D^* and S values are obtained in sample with NCO/OH ratio 1.1 which provide ample proof for the better molecular interactions existing between the polymer – water system in this sample. The S values of the block copolymers are higher compared to D^* and P values resulting in a precedence of sorption over both diffusion and permeation.
The entire block polymer samples exhibit remarkable overshoot at pH 4, pH 7 and pH 9 while in the case of samples swollen in water, the overshooting effect is limited to samples with higher NCO/OH ratios. The reason for the overshooting effect can be traced back to the swelling transport mechanism. The samples exhibiting overshooting effect follow anomalous transport with a bias to non – Fickian mode of transport. The experimental results reveal the influence of NCO/OH ratio and pH of the surrounding medium on the overshooting effect shown by the NR/PEG block copolymer samples.

References

1. Kim YH, Bae YH, Kim SW. J Control Release 1994; 28(2), 143-152.
2. Rosiak JM, Ulanski P, Pajewski LA, Yoshi F, Makuuchi K. Radiat Phys Chem 1995; 46(2): 161-168.
3. Kim J, Conway A, Chauhan A. Biomaterials 2008; 29(14): 2259-2269.
4. Bajpai AK, Shrivastava M. J Appl Polym Sci 2002; 85(7): 1419-1428.
5. Quintana JR, Valderruten NE, Katime I. Langmuir 1999; 15(14): 4728-4730.
6. Guan YL, Shao L, Liu J, Yao KD. J Appl Polym Sci 1996; 62(8): 1253-1258.
7. Hoffman AS. J Control Release 1987; 6(1): 297-305.
8. Park TG, Hoffman AS. Macromolecules 1993; 26(19): 5045-5048.
9. Ishihara K, Muramoto N, Shinohara I. J Appl Polym Sci 1984; 29(1): 211-217.
10. Eisenberg SR, Grodzinski AJ. J Membr Sci 1984; 19(2): 173-194.
11. Lee WF, Lin YH. J Appl Polym Sci 2001; 81(6): 1360-1371.
12. Katayama S, Hirokawa Y, Tanaka T. Macromolecules 1984; 17(12): 2641-2643.
13. Wang C, Zhang G, Dong Y, Chen X, Tan H. J Appl Polym Sci 2002; 86(12): 3120-3125.
14. Karaky K, Brochon C, Schlatter G, Hadziioannou G. Soft Matter 2008; 4(6): 1165-1168.
15. Ravindran T, Nayar MRG, Francis DJ. J Appl Polym Sci 1988; 35(5): 1227-1239.
16. Nair, R.C. Block copolymers from liquid natural rubber and polyethers, Ph.D thesis 1998, pp 73-75.
17. George SC, Thomas S. Polymer 1996; 37(26): 5839-5848.
18. Kim D, Caruthers JM, Peppas NA. Macromolecules 1993; 26(8): 1841-1847.
19. Johnson T, Thomas S. J Mater Sci 1999; 34(13): 3221-3239.
20. Harogoppad SB, Aminabhavi TM. Macromolecules 1991; 24(9): 2598-2605.

21. Bajsic G, Rek V. J Appl Polym Sci 2001; 79(5): 864-873.
22. Gopakumar S, Nair MRG. Polymer 2005; 46(23): 10419-10430.
23. Smith MJ, Peppas NA. Polymer 1985; 26(4): 569-574.

Table I (NR/PEG) block copolymer sample specifications

Block Copolymer	NCO/OH ratio	NR/PEG mole ratio
NR/PEG (4000/4000) – 1	1.0	1
NR/PEG (4000/4000) – 2	1.1	1
NR/PEG (4000/4000) – 3	1.2	1
NR/PEG (4000/4000) – 4	1.3	1
NR/PEG (4000/4000) – 5	1.4	1

Table II Equilibrium uptake values of the block copolymers in water

Block Copolymer	Equilibrium uptake (Q_∞ mol%) values
NR/PEG (4000/4000) – 1	9.45
NR/PEG (4000/4000) – 2	10.47
NR/PEG (4000/4000) – 3	7.78
NR/PEG (4000/4000) – 4	8.61
NR/PEG (4000/4000) – 5	4.72

Table III Swelling characteristics of NR/PEG block copolymers in water and at pH 4, pH 7 and pH 9.

Block Copolymer	Water		pH 4		pH 7		pH 9	
	n	k	n	k	n	k	n	k
NR/PEG (4000/4000) – 1	0.47	2.43	1.09	0.42	0.97	0.36	1.03	0.35
NR/PEG (4000/4000) – 2	0.42	6.63	0.74	2.78	0.74	2.43	0.60	4.79
NR/PEG (4000/4000) – 3	0.60	6.58	1.22	0.76	0.92	1.86	0.92	2.15
NR/PEG (4000/4000) – 4	0.59	4.38	0.88	1.90	0.73	3.01	0.70	3.28
NR/PEG (4000/4000) – 5	0.61	16.99	1.14	3.55	0.90	6.25	0.67	53.76

Unit: k x 10^2 gg^{-1} min^n.

Table IV Kinetic data on the solvent uptake by NR/PEG block copolymers in water.

Block Copolymer	k_1 x 10^3 (min^{-1})
NR/PEG (4000/4000) – 1	3.29
NR/PEG (4000/4000) – 2	6.33
NR/PEG (4000/4000) – 3	19.30
NR/PEG (4000/4000) – 4	33.12
NR/PEG (4000/4000) – 5	—[a]

-[a] – negative value was obtained

Table V Transport coefficients of block copolymers in water

Block Copolymer	D^* cm^2s^{-1}	S gg^{-1}	P cm^2s^{-1}
NR/PEG (4000/4000) – 1	0.96	1.70	1.63
NR/PEG (4000/4000) – 2	5.44	1.89	10.27
NR/PEG (4000/4000) – 3	0.58	1.40	0.81
NR/PEG (4000/4000) – 4	0.57	1.55	0.89
NR/PEG (4000/4000) – 5	0.43	0.85	0.37

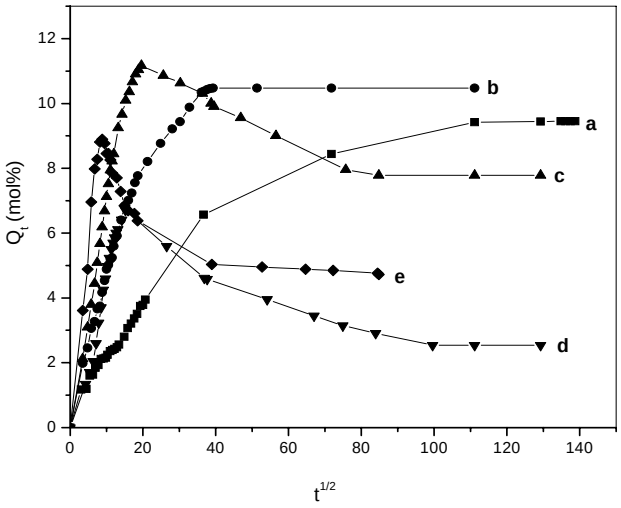

Fig.1. Percentage mass uptake for the block copolymers in water at room temperature: (a) NR/PEG (4000/4000)–1, (b) NR/PEG (4000/4000) – 2, (c) NR/PEG (4000/4000) – 3 (d) NR/PEG (4000/4000) – 4, (e) NR/PEG (4000/4000) – 5.

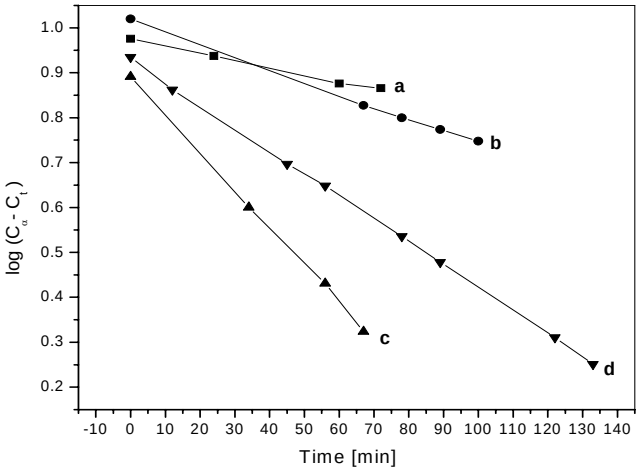

Fig.2. log (C_∞ - C_t) versus time for water uptake by block copolymers:
(a) NR/PEG (4000/4000) – 1, (b) NR/PEG (4000/4000) – 2, (c) NR/PEG (4000/4000) – 3
(d) NR/PEG (4000/4000) – 4.

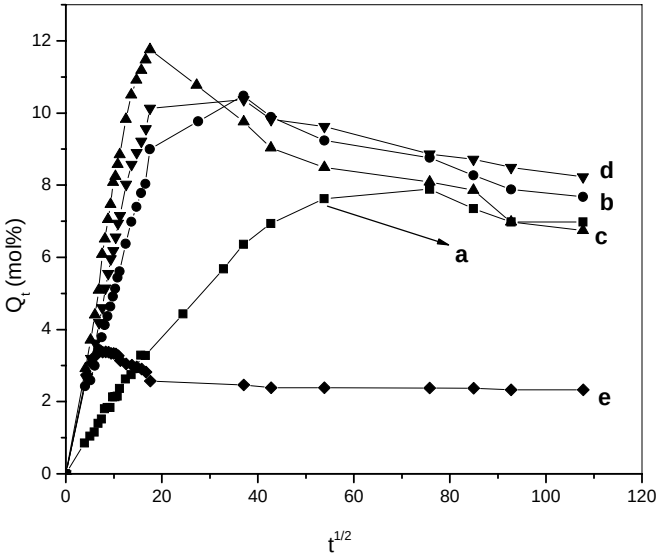

Fig.3. Percentage mass uptake for the block copolymers at pH 9:
(a) NR/PEG (4000/4000) – 1, (b) NR/PEG (4000/4000) – 2, (c) NR/PEG (4000/4000) – 3
(d) NR/PEG (4000/4000) – 4, (e) NR/PEG (4000/4000) – 5.

Studies on EPDM based compositions for underwater acoustic applications

Shajahan. K, Jayesh. P, Krishnaveni.K.P, Vasudevan.S and Reji John
Naval Physical & Oceanographic Laboratory
Defence Research & Development Organisation,
Kochi-682021
Email: tsonpol@vsnl.com

Abstract

Polymeric compositions are widely employed in various underwater acoustic applications. The major uses of these composites are for packaging underwater electronic gadgets, which cannot function if directly exposed to seawater environments. These composites have to function as acoustic windows, reflectors, absorbers or a combination of these, depending on the frequency of interest. In this paper, the acoustic properties of EPDM rubber formulations are studied for its window application. A series of compositions are made by incorporating different ingredients at various loading levels and evaluated for its acoustic parameters. All compositions are studied for its cure characteristics at various temperatures and time using MDR2000 rheometer. The compounds developed are found to be reversion resistant beyond its cure conditions. Compositions ranging from 150-250 pphr reinforcement loading are found to be transmitting acoustic energy with negligible loss. Circular discs of diameters 50mm and 200mm with 20mm thickness are used for acoustic studies. The insertion loss and echo reduction behaviour are studied in a vertical water filled pulse tube using standard acoustic projector cum receiver. Physical and mechanical properties are evaluated as per ASTM standards. Results showed that the material could be a good candidate for acoustic window application. The negligible water absorption and high underwater stability make this material suitable for sub-sea application. Studies showed that insertion loss of the material is 0.2dB in the range of 2 kHz to 15 kHz. The water absorption of the material is 0.002% when immersed in both fresh and saline for 24 hours at room temperature. The weight gain due to water absorption, when submerged in water for more than 260 days is negligible.

Keywords: encapsulants, EPDM, echo-reduction, insertion loss

Introduction

Polymeric compositions are widely employed in various underwater acoustic applications. The major uses of these composites are for packaging underwater electronic gadgets, which cannot function if directly exposed to seawater environments. These composites have to function as acoustic windows, reflectors, absorbers or a combination of these, depending on the frequency of interest [1]. In this paper, the acoustic properties of EPDM rubber formulations were studied for its window application.

Traditionally a number of polymers are used for underwater applications. Transducer encapsulation is the area where requires maximum acoustic energy transmission property , while an acoustic baffle or mount requires maximum sound energy absorption or isolation. Poly chloroprene, Halogenated Butyl, Nitrile, Styrene Butadiene rubbers and Thermoplastic elastomers are some of the candidates currently used for these applications. Each one has their merit and demerits but will operate moderately well in their functional parameters. One of the key concerns of these materials is their higher percentage of water absorption. With continuous exposure to sea environments, these materials can take considerable amount of water in and related changes in electro-acoustic parameters. These effects are become cumulative coupled with ageing factors.

In the present study, the one of the environmentally stable rubber viz. EPDM was studied for acoustic properties. EPDM has its inherent advantages of age resistance and superior water

resistance [2]. For converting it to an acoustic transparent material for using in encapsulation, we need to match the acoustic impedance (product of density and velocity of sound through the material) with seawater [3]. The present study focuses on effects of filler loading on acoustic parameters and its physico-mechanical properties.

Experimental

Materials

The materials used for this study are EPDM rubber-Nordel IP4520 procured from Dow Chemicals. Compounding ingredients like TMTD, MBT from ICI and ZnO, Stearic acid, sulphur, Silica, Precipitated $CaCO_3$, Talc, TiO_2, Naphthenic Oil etc are sourced from local market.

Compositions

To study the effect of filler loading on acoustic properties such as Insertion loss and Echo reduction, a series of compositions were made from EPDM rubber as given in Table-1. NORDEL™ IP 4520 Medium diene Hydrocarbon Rubber is an amorphous ethylene-propylene-diene terpolymer with Low molecular weight and Good low temperature properties [4]. This was selected with view to cater encapsulation by injection or transfer molding technique.
All compositions were made by mill mixing in a lab model two-roll mill. Cure characteristics were studied using rheometer MDR-2000 at 150^{o}C and 160^{o}C temperatures [5]. To study the reversion characteristics specimens were run for 60 minutes, 120 minutes and 180 minutes. The cure characteristics of optimized compositions were reported in Table-2.

Acoustic Measurements

Windows, reflectors, baffles and anechoic coatings constitute a complete set of materials insofar their function is concerned. Ideal specimens of the four materials will, respectively transmit 100%, reflect 100%, transmit 0% and reflect 0% of the sound incident on them [1]. Each of these four materials can be evaluated by measuring the percentage of sound transmitted through and reflected from the material when a sample is immersed in water. These two measurements are called “insertion loss” and “echo reduction,” are defined by

Insertion loss=20 log (Incident sound pressure / Transmitted sound pressure)

Echo reduction=20 log (Incident sound pressure/ Reflected sound pressure)

For studying Insertion loss and Echo reduction cylindrical specimens of 50mm diameter and 200mm diameter with a height of 20mm were made by compression moulding. Echo reduction behavior for 3 kHz to 15 kHz was studied using 50mm diameter specimen in vertical pulse tube with standard projectors and hydrophone at bottom. Echo reduction and Insertion loss behavior for the frequency range 1 kHz to 4 kHz was studied in vertical low frequency pulse tube using 200mm diameter specimen. For Insertion loss specimen was submerged in water in the pulse tube with projector and hydrophone located opposite sides of specimen. Mechanical properties were evaluated from standard specimens punched out from moulded test slabs of 150mm x 150mm x 2mm. For compression set study standard moulded cylinders were used. All properties were evaluated according to the relevant ASTM standards [6-7].

Short-term water absorption characteristics was studied for all specimens and reported in table-3. Long-term water absorption carried out for 260 days and the values obtained were plotted in Fig-1.

Results and Discussion

The cure characteristics of the optimised compositions are given in table-2. As filler loading increases scorch safety (ts2) decreases from 9 minutes to 2 minutes.
All the trends generally observed in the rubber compounds are also seen here. Energy dissipation capacity of the compound can alter by filler loading, as it is seen in the table. However, as the filler loading level increases the processability and mould flow characteristics seem to be decreased.

The physico-mechanical properties evaluated are presented in table-3. As observed generally with rubber compounds, higher the filler loading greater the density, hardness, compression set and tear strength etc with corresponding decrease in elongation at break. The maximum tensile strength in the talc alone series (E1-E5) was for E4 composition having 200phr filler loading. This may be due to the reinforcing effect of talc at that particular loading. For E6 the increased tensile strength was due to silica reinforcement. For E5 and E6, the elongation at break fall below 100% due excessive polymer matrix dilution. Water absorption for 24 hours was lowest for E4 (0.0247%) due to the highest level of exfoliation occurring because of optimum talc reinforcement.

Long-term water absorption characteristics of compositions are studied and plotted in figure-1. Compounds E3, E4 and E5 show the lower percentage of water absorption even after immersion for 259 days. The blank compound EB, shows a decreasing pattern due to the leaching of organic compounding ingredients [8]. Compound E6 is having higher percentage of water intake due to the presence of additional filler loading of precipitated $CaCO_3$ and Silica.

Generally all the EPDM compounds are acoustically transparent however, from the figure-2, it is seen that acoustic insertion loss of compound E4 and E5 are negligible to the extent of 0.02dB in the frequency range of 0.5 kHz to 4 kHz. These compounds can be good candidates for the developing acoustically transparent encapsulating material in the above frequency range.

The echo reduction behaviour of compounds in the frequency range of 3 kHz to 15 kHz evaluated using 50mm dia pulse tube specimens are plotted in figure-2. It is evident from the plot that all compounds except E3 and E4 are reflecting acoustic energy back to the source with almost negligible loss. This means that, compounds E2, E5 and E6 are acoustically transparent in this frequency range due to better acoustic impedance match. Compounds E3 and E4 can be used for anechoic liner application due increased echo reduction.

Echo reduction pattern of 200mm dia pulse tube specimens in the frequency range of 0.5 kHz to 4 kHz are shown in fig-4. Here similar behaviour as observed in fig-3 is obtained. Compounds E5 and E6 are less reflecting than E2, E3 and E4. Hence, E5 and E6 could be used for application where acoustic transparency is required.

Conclusions

Generally, all EPDM compositions are found to be acoustically transparent. Acoustic properties are found to be frequency dependent. However, for obtaining maximum underwater acoustic transparency, compounding with reinforcing filler like talc at 200-phr level could be a better choice with increased water resistance. The composition E4 and E5 can be used as an underwater encapsulant where acoustic transparency is required. The adhesion of EPDM compositions has to be studied and modified for better interfacing with metals and ceramics for device fabrication [9].

Acknowledgements

Authors wish to acknowledge the constant inspiration of Shri. Vishnubhatla RMR, Associate Director, NPOL. We gratefully acknowledge the Director, NPOL for granting permission to publish this work.

References

1. Bob RJ, Underwater Electro acoustic measurements, 1969
2. Blow C.M., Rubber Technology & Manufacture, Butterworth Scientific, UK
3. Thompson, Corley M, EPDM rubber as an underwater acoustic window, The Journal of the Acoustical Society of America, vol. 74, issue S1, pS50, 1983
4. Brydson J.A., Rubber Chemistry, Applied Science Publishers, UK
5. Annual Book of ASTM Standards, Section 9, Rubber, V.09.01, 1998
6. Annual Book of ASTM Standards, Section 9, Rubber, V.09.02, 1998
7. Brown, R.P, Physical Testing Rubbers,
8. Quinn, M. E. ; McGee,W. W, Analysis Technique for Determining the Levels of Organic Additives in an EPDM Rubber for Use in Underwater Acoustic Applications, Naval Research Lab, Washington DC, 1985
9. Beumel,Linda L. ; Thompson, Corley M, Development of an EPDM Elastomer with Improved Bondability for Use in Sonar Transducers, Naval Research Lab, Washington DC, 1987

Table-1. Compositions

Composition / Ingredient	**EB**	**E1**	**E2**	**E3**	**E4**	**E5**	**E6**
EPDM	100	100	100	100	100	100	100
ZnO	5	5	5	5	5	5	5
Stearic Acid	1	1	1	1	1	1	1
Sulphur	1.5	1.5	1.5	1.5	1.5	1.5	1.5
TMTD	1	1	1	1	1	1	1
MBT	0.5	0.5	0.5	0.5	0.5	0.5	0.5
Talc		50	100	150	200	250	250
TiO_2							10
Silica							75
Pptd $CaCO_3$							90
Naphthenic Oil	15	15	15	15	15	15	15
Batch weight	**124**	**174**	**224**	**274**	**324**	**374**	**549**

Table-2. Cure Characteristics @150^{o}C, 60minutes

Composition / Parameter	**EB**	**E1**	**E2**	**E3**	**E4**	**E5**	**E6**
ts1, min	7.87	7.50	5.53	4.21	3.48	2.75	2.02
ts2, min	9.29	8.88	6.47	4.89	3.98	3.13	2.37
t10, min	8.06	8.23	6.21	4.84	4.07	3.27	3.35
t50, min	12.70	14.14	10.58	9.30	8.74	8.42	17.07
t90, min	24.31	32.59	23.50	25.23	28.05	33.72	47.80
ML, dNm	0.18	0.32	0.31	0.34	0.57	0.77	21.50
mH, dNm	11.18	14.83	17.01	19.59	23.09	25.61	68.72
S”@ML	0.34	0.45	0.56	0.69	1.0	1.30	15.55
S”@MH	0.14	0.73	0.85	1.34	1.94	2.34	19.10
Tan delta @ML	1.944	1.394	1.781	2.0	1.772	1.684	0.724
Tan delta @MH	0.12	0.049	0.050	0.069	0.084	0.092	0.278

Table-3 Physico-mechanical properties

Composition / Property	EB	E1	E2	E3	E4	E5	E6
Density, g/cc	0.903	1.11	1.29	1.435	1.550	1.640	1.840
Hardness, Shore-A	45	56	65	70	75	80	92
Compression Set, %	9	11	13	14	16	19	21
Tensile Strength, MPa	1.17	2.54	3.94	4.01	4.24	3.92	6.23
M100, MPa	1.13	2.15	2.91	3.07	3.65	-	-
Elongation at Break %	108	160	214	217	174	68	32
Tear Strength, N/cm	62.83	77.40	109.43	151.80	244.66	251.70	212.17
Water absorption, (40^{o}C, 24 hrs, 3.5 % NaCl solution) %	0.1257	0.1160	0.0983	0.0270	0.0247	0.0280	0.1021

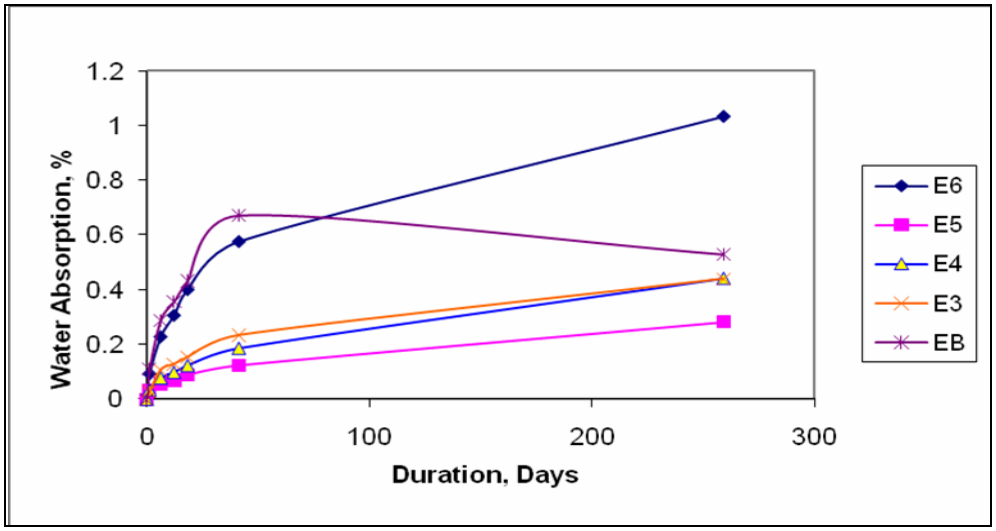

Figure-1 Long term water absorption characteristics

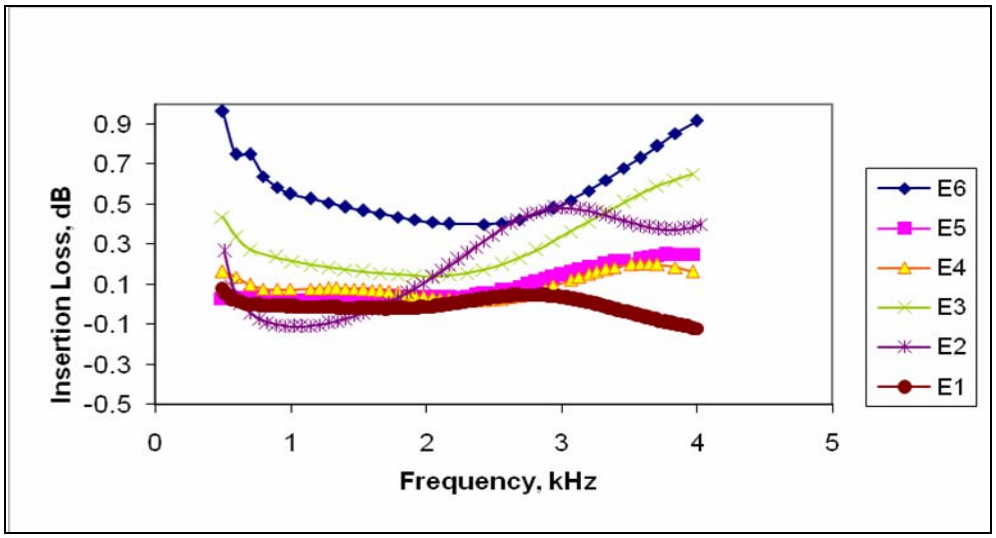

Figure-2 Insertion Loss behavior 0.5 kHz-4 kHz (200 mm dia pulse tube)

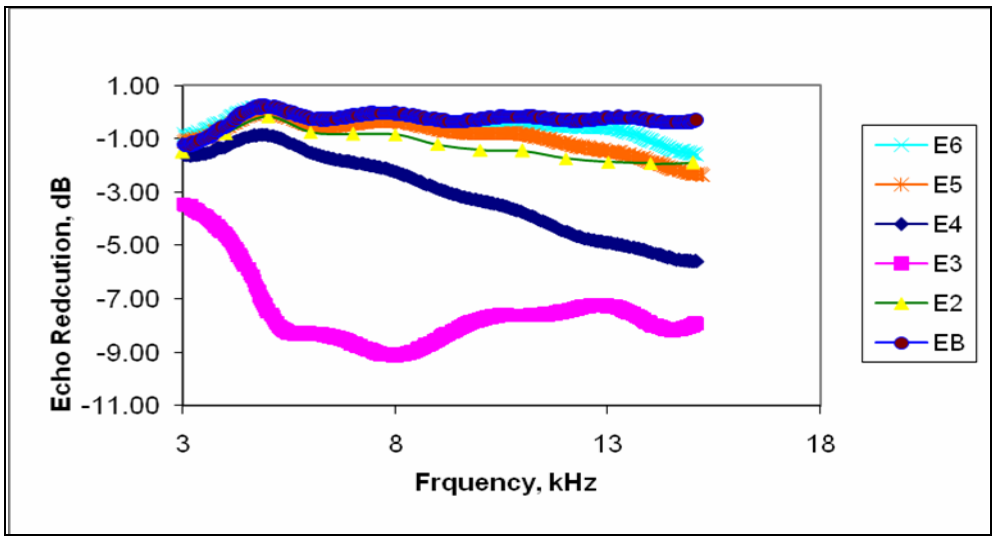

Figure-3 Echo Reduction 3kHz-15Hz (50mm dia pulse tube)

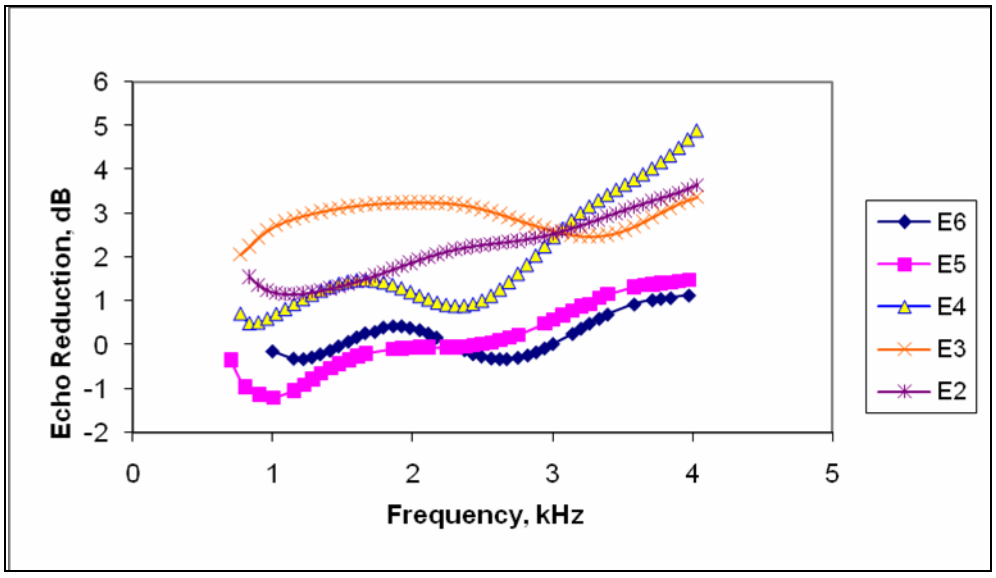

Fig-3 Echo Reduction 0.5 kHz-4 kHz (200 mm dia pulse tube)

Development of epoxy based material for rapid tooling applications

K.Elangovan*, B.Kothandaraman*, K.Kalaichelvan, Iynesh kumar***

*Department of Rubber and Plastic Technology, MIT Campus, Anna University, Chennai. India

**Department of Production Engg., MIT Campus, Anna University, Chennai,

India

Email: elango_k2000@yahoo.co.in

ABSTRACT

Development of new materials and new material processing techniques favors modern technological development. Among these composites occupy an important place in field of Aerospace, Defense, Automobiles and Biomaterials. Epoxy resin composites are frequently applied in moulds manufactured with rapid tooling technologies that are used for wax and polymer materials injection. Various percentages of Aluminum and spheriglass filled epoxy resin was prepared. Triethylene tetramine was used as room temperature curing agent. Amine containing polydimethylsiloxane was used as liquid rubber modifier. The micro structural analysis was done to examine the distribution of fillers in the matrix. The mechanical and thermal behavior of the materials was determined. Flexural, Tensile and Compressive behavior were determined by using universal testing machine. Thermal fatigue test was also done.

INTRODUCTION

Epoxy resin composites are frequently applied in moulds manufactured with rapid tooling technologies that are used for wax and polymer materials injection. With the propose of enlarging the application field of the polymer matrix systems, it is fundamental to select adequate dispersed phases and analyze their influence on the composite properties in order to reinforce the polymer matrix and tailor the properties according to the tools specifications.[1].Epoxy based sterolithography resins have been used successfully as tools for injection molding, Molds made out of these resins fail at distinct times:during the first injection of plastic; during the first part first ejection; during either injection or ejection,but after a certain number of parts have been produced.[4]

The various works was carried in this field around the world. Tri-phase materials composed by an epoxy resin, aluminum particle and milled fibers, were produced, with mechanical and thermal performances better than single materials, increasing the competitiveness of the epoxy rapid tooling process. The influence of the aluminum particles and carbon and glass fiber addition increases slightly the impact resistance of the aluminum filled composites. [2].The effects of particle size and silane treatment on the fracture toughness are experimentally evaluated for epoxy reinforced with nanometer and micrometer sized rigid particles. The fracture toughness if epoxy increases with the addition of aluminum

particles. Additionally, fractured surface are observed under an Optical metallurgical microscope to investigate both particle dispersion and evidence of extrinsic toughening mechanism. It is observed that the both improved particle dispersion and appropriated silane treatment lead to increase in toughness. [3].

Epoxy has excellent electrical, thermal and chemical resistance. Shrinkage during polymerization of epoxy resins is extremely low. Molded epoxy parts are hard, rigid, and relatively brittle and have excellent dimensional stability over a broad temperature range. Epoxy is readily machinable and can be employed over temperature range of 60 to 250° C. Aluminum has only one-third the weight of steel. Aluminium powder was used as filler material for epoxy resin to obtain good mechanical properties and high thermal capabilities and fatigue resistance.

Spheriglass solid glass spheres are microspheres with a density of 2.5g/cc. The addition of spheriglass to epoxy system does not alter viscosity of the epoxy system. These spheres are nonporous. They do not absorb resin in polymer system.

EXPERIMENTAL

MATERIALS USED.

DGEBA liquid epoxy resin (LY556) with epoxy equivalent around 170 and viscosity of 8000 to 12000 cp at 25 degree Celsius was used as received from Araldite India Pvt. Ltd.Organo modified polysiloxane with molecular weight around 5000 was used as liquid rubber modifier as received from Resil chemicals Pvt Ltd. Triethylene tetramine (HY 951-curing agent) was used as received from Araldite India Pvt.Ltd.Aluminium and spheiglass were received from Potter industries Inc.

PREPARATION OF LIQUID RUBBER MODIFIED EPOXY MATRIX.

Amine containing polydimethylsiloxane was taken as liquid rubber modifier. Five phr or ten phr of liquid rubber modifier was taken along with epoxy resin and the mixture was heated at 50 degree Celsius for 30 minutes with continuous stirring. Then the liquid rubber modified epoxy resin was allowed to cool in the room temperature.

PREPARATION OF ALUMINUM AND SPHERIGLASS FILLED EPOXY AND MODIFIED EPOXY MATRIX

The weighed amount of spheriglass was added to epoxy system and stirred for 15 min. Then weighed amount of aluminum was added to the spheriglass/epoxy system and stirred for 15 min. This tri-phase material was cured using triethylene tetramine at room temperature. The same procedure was carried out for Amine containing PDMS modified epoxy matrix. The material was cured at 100°C for 3 hrs.

Various percentages of Aluminum and spheriglass filled epoxy resin are as follows:

NOTATIONS USED

A→E-55, AL-45.S.g-27.5

B→E-50, AL-50, S.g-25

D→E-50, AL-50.S.g-50

E→E-55, Al-45, S.g-27.5, Si-10 phr

I→E-50, AL-50, S.g-50, Si-10phr

H→E-50.AL-50.S.g-50, Si-5phr

RESULTS AND DISCUSSIONS

MECHANICAL PROPERTIES OF ALUMINUM/SPHERIGLASS MATERIALS FILLED MODIFIED AND UNMODIFIED EPOXY MATRIX

The mechanical properties of the materials were studied using in SHIMAZDU universal testing machine.

The flexural specimen of dimension 80mm × 25mm with thickness of 3mm was prepared from each casting. Flexural strength, flexural modulus were studied in the universal testing machine. The flexural test was carried at the crosshead speed of 3mm/min. The flexural test was carried according to ASTM D 790 standards.

The Samples A, B, D and pure epoxy resin were prepared without post curing

S.No.	**Composition**	**Flexural strength MPa**	**Flexural Modulus GPa**
1	Pure Epoxy	53.15	3.638
2	A	46.7	6.0
3	B	36.95	6.0
4	D	37.75	6.0

The Samples E, I, H and pure epoxy resin were prepared with post curing

S.No.	Composition	Flexural strength MPa	Flexural Modulus GPa
1	Pure Epoxy	92.2	3.64
2	E	10.80	0.60
3	I	30.28	3.42
4	H	32.18	9.I5

The flexural strength reduced with addition of Amine containing PDMS which induced rubbery properties in epoxy matrix. The Modulus of the combination H increased indicating better dispersion supported by the spherical rubber precipitates and improved cross linking within the matrix.

TENSILE TEST

The flexural specimen of dimension 80mm × 10mm with thickness of 3mm was prepared from each casting. Tensile strength, Tensile modulus were studied in the universal testing machine. The tensile test was carried at the crosshead speed of 1mm/min. The flexural test was carried according to ASTM D 638 standards.

The Samples A, B, D and pure epoxy resin were prepared without post curing

S.No.	Composition	Tensile strength MPa	Tensile Modulus GPa
1	Pure Epoxy	35.32	0.947
2	A	19.26	1.343
3	B	15.76	1.212
4	D	10.51	1.659

The Samples E, I, H and pure epoxy resin were prepared with post curing

S.No.	**Composition**	**Tensile strength** **MPa**	**Tensile Modulus** **GPa**
1	Pure Epoxy	48.39	0.904
2	E	6.306	0.386
3	I	15.56	1.54
4	H	16.81	1.46

The higher phr of Amine containing PDMS reduced tensile strength to greater extent. The increase in modulus may correspond to reduce in free volume which restricts chain mobility.

COMPRESSION TESTING

Compression strength of the specimen was found out by using Universal Testing Machine (UTM). The test was carried at the crosshead speed of 1mm/min.

The Samples I, H and pure epoxy resin were prepared with post curing

S.No.	**Composition**	**Compressive strength** **MPa**	**Compressive Modulus** **GPa**
1	Pure Epoxy	115.16	1.18
3	I	124.14	1.94
4	H	124.06	2.0

The Toughening effect of Amine containing PDMS improved compressive strength and spheriglass contributed for higher modulus.

THERMAL FATIQUE TEST

The test was carried out at 250°C for measuring the thermal stability. The samples were tested for 30 cycles. Observations indicated that there is no change in dimension.

COMPOSITION	**NO.OF.CYCLES**	**TEMPERATURE AT 250°C**
Without Silicone A,B,D	30	Dimensionally stable
With Silicone E,I,H	30	Dimensionally Stable

MICROSTRUCTURAL ANALYSIS

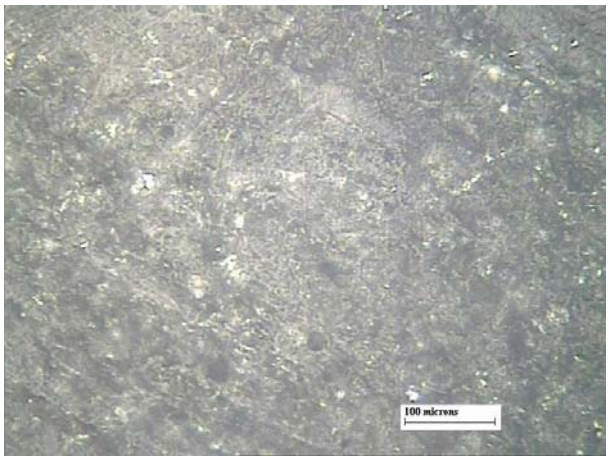

The combination A

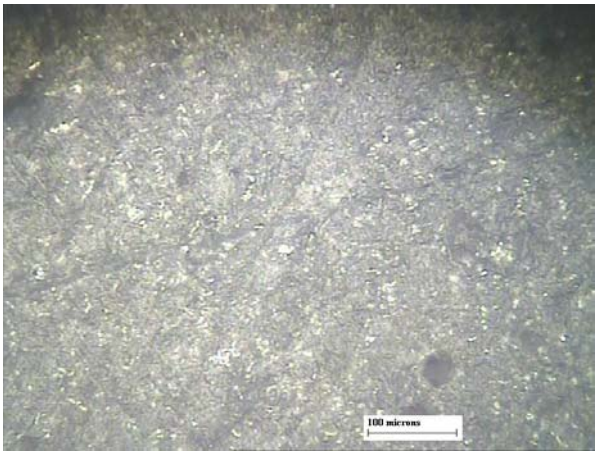

The combination E

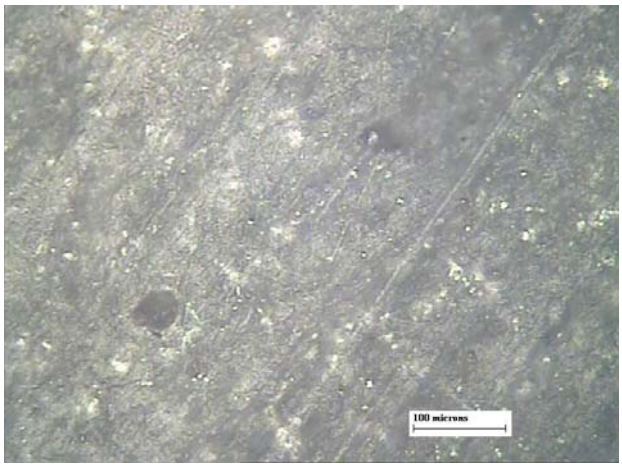

The combination B

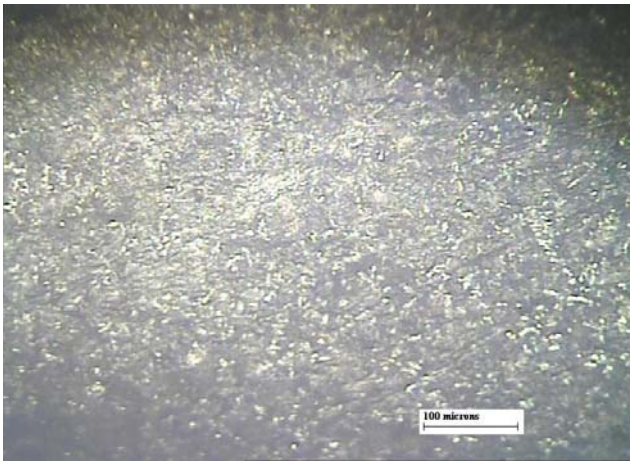

The combination I

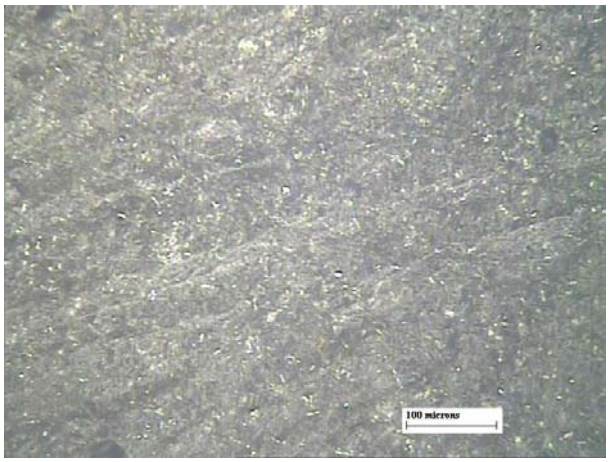

The combination D

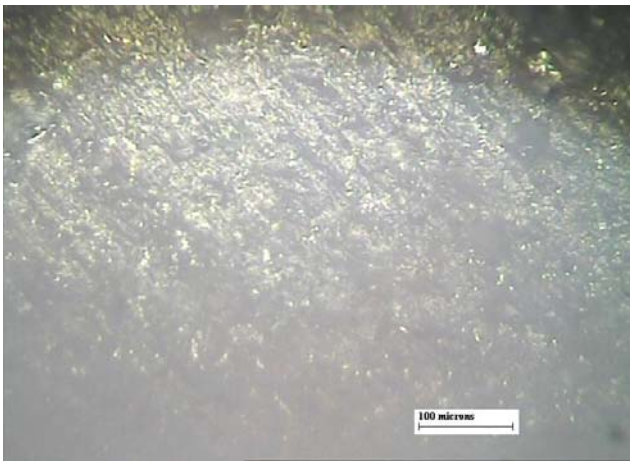

The combination H

The combination A, B, D and E shows filler aggregation with in the matrix .The combination I shows no aggregation and the combination H shows homogenous distribution of fillers without aggregation with in the Amine containing PDMS modified epoxy system. The lower phr addition of Amine containing PDMS supported homogenous distribution of fillers without any aggregation. The higher phr modification leads to decrease in free volume which resulted in agglomeration and reduced mechanical properties.

CONCLUSION

The lower phr of amine containing PDMS supported better dispersion of filler within the epoxy system. The modulus improved with addition of speriglass without changing viscosity of the material. The tri-phase composite was dimensionally stable at higher temperatures. The 5 phr of Amine containing PDMS modified epoxy resin, Aluminum, Speriglass in the ratio 1:1:1(The combination H) showed better

mechanical and thermal behaviors when compared with other materials. The combination H can be used as mould making material.

REFERENCES

1. F.Jorge lino and Co-authors Tribological behavior of epoxy based composite for rapid tooling.Wear 260(2006) 30-39
2. Vasconcelos,Lino,Magalhes,Neto Impact fracture study of epoxy-based composite with aluminum particles and milled fibers.Journal of material processing technology (2005) 277-283.
3. Suraj zunjarro, Raman singh. Characterization of the fracture behavior of epoxy reinforced with nanometer and micrometer sized aluminum particles.
4. Vincent rodet and Jonathan S.Colton ,Properties of rapid prototype injection mold tooling materials.Polymer engineering and science, January 2003,Vol.43,No.1

Graft-copolymerization of cellulose-based filter paper and its development as antibacterial food-packaging material

Rasika Tankhiwale* [#] **and S. K. Bajpai**

Polymer Research Laboratory, Dept. of Chemistry, Govt. Model Science College (Auto),

Jabalpur (M.P.)-482001, India

Email: rasika_81@rediffmail.com

Abstract

This work describes preparation of nano silver- loaded grafted filter paper. First, the filter paper was grafted with acrylamide by ceric ammonium nitrate induced free radical polymerization and then silver nanoparticles were loaded into grafted filter paper by equilibration in silver nitrate solution followed by citrate reduction. The formation of silver nanoparticles has been confirmed by TEM and SAED analysis. The particle size of nanoparticles has been determined by TEM analysis. The novel nano silver-loaded filter paper has been investigated for its antimicrobial properties against *E.coli*. This newly developed material shows strong antibacterial property and thus offers its candidature for possible use as antibacterial food- packaging material.

Keywords: grafting, hydrogel, silver nanoparticles, *E.coli*, TEM.

1. Introduction

With the growing public health awareness of disease transmissions and cross-infection caused by microorganisms, use of antimicrobial materials has increased in many application areas like protective clothing for medical and chemical works, other health related products [1-2], antibacterial packaging material that can improve product quality and keep it free from microbial adhesion [3], etc. Such antimicrobial packaging materials may be produced by introducing silver, gold or copper nanoparticles into polymer film. In particular, silver has been recognized for its broad –spectrum antimicrobial activities [4].Silver inactivates bacteria by interacting with the thiol groups of bacterial proteins and enzymes [5]. It is proposed that silver ions (Ag^{+}), released from silver nanoparticles (Ag^{o}), interact with phosphorous moieties in DNA, resulting in inactivation of DNA replication. In fact, silver nanoparticles are highly germicidal, quite harmless to humans and absolutely non-toxic. It has been reported that even the highest concentration of nano silver causes no side effects [6]. In a recent work by Wen et al [7], human fibroplasts were grown on various concentrations of silver nanoparticles during the period observation. The results of their study elucidated the non-toxicity of the interaction of nanometer- scale silver particles and the membrane surface.

Although synthetic polymeric films are frequently used as packaging material but their non-degradability has been a matter of great concern for environmentalists, and therefore attempts have been made to develop such materials which can undergo degradation and are ecofriendly. In our recent work [8], we have reported a unique approach for in situ formation of ZnO nanoparticles onto cotton fibers grafted with a copolymer. Now, utilizing this approach, we hereby report grafting of acrylamide onto filter paper, followed by incorporation of silver nanoparticles to yield antibacterial antibacterial filter paper. To the best of our belief, no such work has been reported earlier.

2. Experimental

2.1.Materials

The monomer acrylamide (AAm), crosslinker N,N'-methylene bisacrylamide (MB), and initiator ceric ammonium nitrate (CAN), nutrient broth and Nutrient m-Endo agars were obtained

from HiMedia Laboratories, Mumbai, India. The salts silver nitrate ($AgNO_3$) and tri-sodium citrate (TS) were obtained from E.Merck, Mumbai, India. Standard cultures of the organisms were provided by the department of Biotechnology, Govt. Model Science College, Jabalpur, India. The cellulose based filter paper (Whatman No.42) was received from Sameer Science Lab, Jabalpur, India. The double distilled water was used throughout the investigations.

2.2.Preparation of grafted filter paper (GFP)

The graft- co polymerization of monomer acrylamide onto filter paper was carried out using ceric ammonium nitrate as free radical initiator by following the same method as has been reported previously with cotton fabric as substrate [9].

2.3. Loading of silver nanoparticles into grafted filter paper (GFP)

The silver nanoparticles were loaded into the GFP by using a novel approach, developed in our laboratory [8]. The GFP was put in $AgNO_3$ solution (15 mg $AgNO_3$ in 40 ml distilled water) for 12 h, then was taken out and put in tri-sodium citrate solution (20 mg dissolved in 25 ml water) for next 12 h to reduce Ag^+ ions into silver nanoparticles. The material, so produced, was allowed to dry. In this way, silver nanoparticles-loaded GFP was prepared.

2.4. Water uptake analysis

Completely dry pre-weighed grafted filter paper was put in 200 ml of distilled water at 30ºC and then its mass was measured at different time- intervals. The percent mass swelling (% M_s) was calculated using the following expression [10]

$$\% M_s = \text{Swollen weight} - \text{Dry weight} \ / \ \text{Dry weight} \times 100 \qquad \ldots\ldots\ldots\ldots (5)$$

All the experiments (i.e. grafting and water uptake analysis) were done in triplicate and average values have been produced in the data.

2.4.Characterization of silver nanoparticles loaded paper

The silver nanoparticles were characterized by transmission electron microscopy (TEM). The TEM images were recorded using a Tecnai F 12 TEM instrument. X-ray photoelectron spectroscopy(XPS), Model ESCALAB Mg K α (hν = 1253.6 eV) with a resolution of 1.0×10^{-4} Pa was used to confirm formation of silver nanoparticles.

Microbial experimentation

For qualitative measurement of microbial activity, the filter paper was cut to make a circle of 7.4 cm diameter, and the antimicrobial activity was tested using modified agar diffusion assay (disc test). The plates were examined for possible clear zones after incubation at 37º C for 2 days. The presence of any clear zone that formed on the surface of the filter paper was recorded as an indication of inhibition against the microbial species.

3. Results and Discussion

Graft copolymerization of vinyl monomers onto cellulose has been studied extensively [11-15]. However, the substrates used in these studies were native cellulose, cellulose pulp or cotton linters. In our study, we have used filter paper as a substrate for graft- copolymerization. Indeed, the mechanism of grafting reaction is more or less the same and may briefly be given as below: In the presence of an acid used, HNO_3 (HA), primary radical species formation occurs as a result of the action of acid on Ce(IV):

$$Ce^{4+} + HA \rightarrow Ce^{3+} + H^+ + A^{\bullet} \qquad \ldots\ldots\ldots\ldots\ldots\ldots (1)$$

Once the free-radical species ($A^{\bullet}$) are formed, they produce cellulose macroradicals via direct abstraction of hydrogen atom cellulose molecules.

$$Cell-OH + A^{\bullet} \rightarrow Cell-O^{\bullet} + HA \quad \text{…..……..(2)}$$

where Cell – OH represents cellulose molecule. Cellulose macroradicals may also be formed by direct attack of Ce^{4+} ions on cellulose molecule via H abstraction.

$$Cell-OH + Ce^{4+} \rightarrow Cell-O^{\bullet} + Ce^{3+} + H^{+} \quad \text{……..(3)}$$

These cellulose macroradicals, so produced, combine with monomers AAm to induce graft-copolymerization.

3.1. Effect of reaction temperature

The temperature of the reaction system does influence the rate of graft polymerization and the grafting field. We varied the temperature of the monomer/crosslinker solution, in the range 10 to 15°C and determined the percent grafting. The results, as shown in the Fig.1 reveal that 30°C is the optimum reaction temperature for maximum grafting. Below 30°C, the percent grafting is poor due to insufficient formation of free radicals at lower temperatures which is commonly observed phenomenon [16-17]. However, when temperature is increased beyond 30°C, the percent grafting again shows decreasing trend. This may possibly be explained on the basis of the fact that at higher temperature, the acid catalyst may induce degradation of cellulose chains, thus lowering the number of grafting sites in substrate. It was also observed that when reaction temperature was 50°C, the filter paper became brittle and was torn to small pieces indicating enhanced breakdown of cellulose chains by HNO_3. In addition, the possibility of recombination of free of free radicals at higher temperature should also be not ruled out.

3.2. Water uptake analysis

Fig.2 depicts the water uptake behavior of grafted – filter paper (GFP) in distilled water at 30ºC. It is clear that when GFP is put in water, it begins to take up water as indicated by increasing percent mass swelling. This may simply be attributed to the fact that water enters into grafted polymer network of the filter paper, thus allowing it to absorb water which is retained within the network. After some time the water uptake attains maximum value.

3.3. Loading of Silver nanoparticles into GFP

As mentioned in the section introduction, the nano silver-loaded filter paper has been prepared by loading silver nanoparticles into the grafted filter paper, utilizing our newly developed approach [8]. The overall process of entrapment of nano silver may be explained as follows: when grafted filter paper is equilibrated in distilled water, the network swells due to hydrophilic nature of monomer and plasticization of macromolecular chains. On dipping swollen filter paper into aqueous solution of $AgNO_3$, Ag^{+} ions enter into the swollen grafted network. Later on when this Ag^{+} containing filter paper is put in the sodium citrate solution, a uniformly distributed array of Ag nanoparticles is obtained due to reduction of Ag^{+} ions. The crosslinked three dimensional network serves as stabilizer for silver nanoparticles and prevents them for aggregation.

Fig.3 clearly describes the color change observed due to reduction of Ag^{+} ions into silver nanoparticles. It is very clear that filter paper turns brown due to presence of silver nanoparticles.

3.4.Characterization

Fig.4 (A) shows the TEM image of the silver nanoparticles. The image indicates nearly uniform distribution of silver nanoparticles. In addition, a typical selected area electron diffraction (SAED) pattern of a collection of silver nanoparticles is also shown (see inset). The

pattern appears to be a little diffused due to smaller particle sizes, but three diffraction rings are clearly visible and they can be indexed to the face-centered cubic structure of silver as follows. The strongest ring and the one closest to the center is probably a combination of the (111) and (200) reflections. The second ring is likely the (222) reflection whereas the outermost and the weakest third ring are either the (420) and/or the (422) reflections. Almost similar results have also been reported elsewhere [18]. The size distributions were obtained by measuring the diameters of 35 particles in an arbitrarily chosen area of TEM image [see Fig. 4 (B)]. As can be seen, nearly 40% particles have an average diameter of 26 nm and moreover, the distribution curve appears to be almost symmetrical with all the nanoparticles falling within the narrow range of 12 to 42 nm.

Antibacterial property of nanosilver loaded GFP

Finally, we carried out antibacterial test for the prepared silver nanoparticles loaded GFP against *E.coli*. Fig.5 (A) clearly demonstrates dense population of bacterial colonies on the whole surface of the grafted filter paper which is simply due to absence of silver nanoparticles in the sample. However, in Fig 5 (B) a clear zone of inhibition can be seen on the whole surface of the nanosilver loaded grafted filter paper. This may simply be explained on the basis of the fact that as the filter paper contains silver nanoparticles, the colonization of bacteria is greatly inhibited on the nano Ag-loaded filter paper. Therefore it may be concluded that silver nanoparticles loaded grafted filter paper possesses strong antibacterial property.

4. Conclusion

From the above study it may be concluded that grafting of acrylamide onto filter paper, followed by incorporation of silver nanoparticles results in development of a novel biomaterial which demonstrates fair biocidal action against *E.coli*, and it can be used as an antibacterial packaging material to prevent food stuff from bacterial infection. As the proposed method does not involve use of toxic organic solvents or harsh conditions like high temperature, the strategy can be applied for the manufacture of antibacterial food packaging material.

Acknowledgement

I would like to owe my whole hearted gratitude to my supervisor Dr. S.K. Bajpai, Prof. of Chemistry, Govt. Model Science College, Jabalpur (M.P.) for his kind guidance.

References

1. Margaret I.P, Sau L.L, Vincent K.M.P, Ivan Lung, Andrew Bud. J.Med.Microbiology 2006;55; 59.
2. Duran N, Marcato P.D, De Souza G.I.H, Alves O.L, Esposito E. J.Biomed. Nanotech 2007;3; 203.
3. Park S.I, Zhao Y.J, Agric. Food Chem 2004 ;52 ;1933.
4. Galeano B, Korff E, Nicholson W.L. Appl.Environ.Microbial 2003;69;4329.
5. Lok C.N, Ho C.M, Chen R, He Q.Y, Yu W.Y, Sun H, Tam P.K, Chiu J.F, Che C.M. J. Proteome Res 2006;5;916.
6. Becker Robert O, Spardaro M.D, Joseph A. The Journal of Bone and Joint Surgery 1978; 60(A);871.
7. Wen Hua-Chiang Lin, Yao-Nan , Jian Sheng-Rui , Tseng Shih-Chun , Weng Ming-Xiang, Liu Yu-Pin , Lee Po-Te, Chen Pai-Yen , Hsu Ray-Quan, Wu Wen- Fa , Chou Chang-Pin. Journal of Physics: Conference Series 2007;61; 445.
8. Bajpai S.K, Mary G, Chand Navin, J. Macromol. Sci . Part. A (Pure and Appl.Chem.) 2008: 45(10).
9. Bajpai S.K, Bajpai M, Gupta Pamila. J. Macromol. Sci. Part. A (Pure and Appl.Chem.) 2008;45;1.
10. Okeowo, O.; Dorgan, J. R. Macromolecules. 2006, 39 (23), 8193.
11. Gupta, K.C.; Sahoo, S. J.Appl.Polym.Sci. 2001,79,767.
12. Zahran, M.K.; Mahmoud, R.I. J.Appl.Polym.Sci. 2003,87,1879.
13. Sabaa , M.W.; Mokhtar, S.M. Polym. Test. 2002, 71,337.
14. Salam. M.A.; J.Textile Apparel Technol. Management. 2005,4(4), 1.
15. Chen , H.; Hsieh, Y. Biotechnol. Bioeng. 2005,90(4), 405.
16. Martel,B.; Weltrowski,M.;Ruffin, D.; Morcellet, M.; J. Appl. Polym. Sci. 2002,83,1449.
17. Saihi, D.; El-Achari,A.; Vroman,I.; Caze,C.; J. Textile Apparel Technol. Management. 2004,4(1), 1
18. Andersson M, Alfredsson V, Kjellin P, Palmqvist A.E.C. Nano Lett 2002;12;1403.

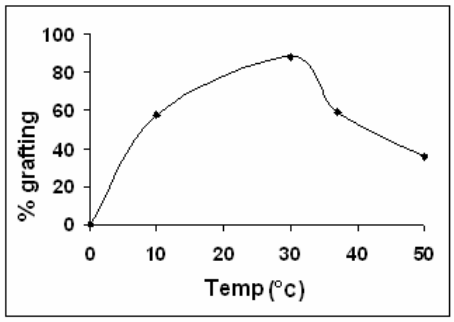

Fig.1. Effect of reaction temperature on percent grafting

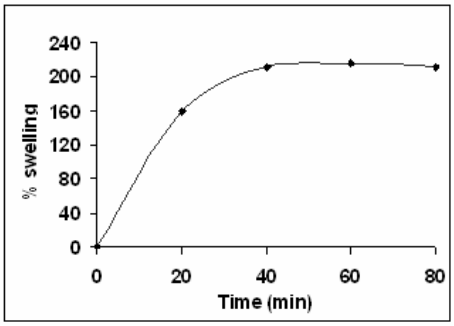

Fig.2. Dynamics of water uptake of grafted filter paper as a function of time at 30º C.

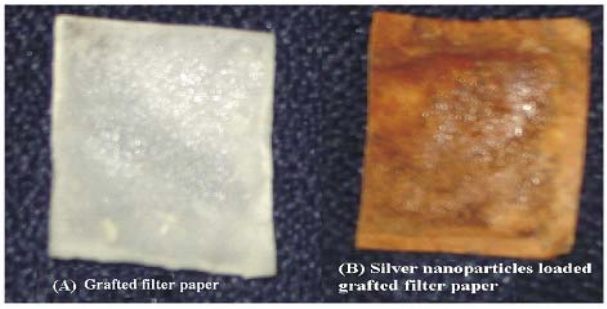

Fig 3. A comparative depiction of grafted and silver nanoparticles-loaded filter paper

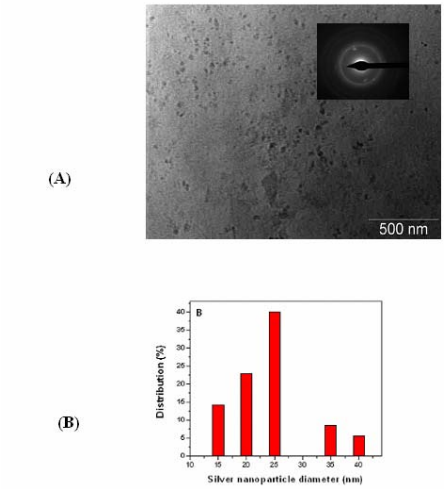

Fig.4. (A) TEM image of silver nanoparticles.
(B) Size distribution of silver nanoparticles

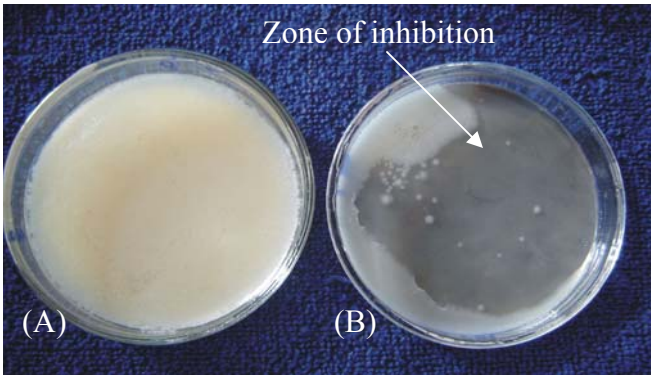

Fig.5. Photograph showing (A) growth of bacterial colonies around grafted filter paper. (B) Zone of inhibition around the silver nanoparticles loaded grafted filter paper.

Design of experiments for optimizing NBR nanocomposite formulations

Meera Balachandran[1], Lisha P Stanly[2], R. Muraleekrishnan[3] and S.S. Bhagawan[1]
[1]Dept. of Chemical Engg. & Mat. Science, Amrita Vishwa Vidyapeetham, Coimbatore 641105
[2]High Energy Materials Research Laboratory, Pune
[3] Propellant Engineering Division, Vikram Sarabhai Space Centre, Thiruvananthapuram 695022

Email: ss_bhagawan@ettimadai.amrita.edu

ABSTRACT

Design of Experiments (DoE) is a structured statistical technique used for analyzing the behaviour of a product, process, or simulation by changing multiple design parameters in a specific manner and recording the response. Applications of DoE include choosing between alternatives, selecting the key factors affecting a response, response surface modelling, regression modeling, etc. The interpretation of results consists of determining the set of factors that are statistically significant for each response measured in the experiment, quantifying the relationship between each measured response and the statistically significant factors and determining the ranges of the statistically significant factors (or "process windows" or "process set points") that lead to certain optimal/desired ranges for the measured responses.

In the present work we used DoE to optimize the formulation of NBR [nitrile rubber] based nanocomposites. A Box-Benken Design with three factors and three levels was used to quantify the relationship between mechanical properties and levels of ingredients. The variables chosen are silica content, nanoclay loading and vulcanization system. A masterbatch of NBR and nanoclay was made in a Haake Rheocord followed by compounding on a two roll mill. The compounds were compression molded and evaluated for tensile strength, modulus, elongation at break and hardness. The effect of heat ageing on mechanical properties was also studied. Based on regression analysis, data from the experiments were used to fit mathematical models of the general form

$$Y = b_1 + b_2x_1 + b_3x_2 + b_4x_3 + b_5x_4 + b_6x_1^2 + b_7x_2^2 + b_8x_3^2 + b_9x_4^2 + b_{10}x_1x_2 + b_{11}x_1x_3 + b_{12}x_1x_4 + b_{13}x_2x_3 + b_{14}x_2x_4 + b_{15}\, x_3x_4$$

The sign and magnitude of the coefficients were different for different ingredients and properties. The predictions based on the design was confirmed by verification experiment. MINITAB was used for generating contour plots to study the interaction between the three factors. The contour plots were overlaid to find the optimal formulation.

INTRODUCTION

Reinforcing polymer with nanosized clay particles yields materials with enhanced performance without recourse to expensive synthesis procedures [1-3]. Among the various clays used, organoclays of montmorillonite family have been widely used in both thermoplastic and elastomeric systems [2,4,5]. These composites have comparatively much better mechanical properties, barrier properties and fire and ignition resistance than conventional microcomposites. The size of the nanoclay particles and the amount of filler used play a major role in the development of the properties of the rubber [6-10]. Acrylonitrile-butadiene rubber (NBR) is a special purpose, oil resistant rubber and hence can be used in applications where oil resistance is a must. The objectives of the work include varying the properties of the composite with nanoclay content, silica loading and sulphur-accelerator ratio. In the present work we used response surface methodology, a collection of mathematical and statistical techniques, to model the properties of NBR nanocomposites and to optimize the mechanical and heat ageing properties. A Box-Behnken design for three factors has been used for analysis.

EXPERIMENTAL

Materials

Nitrile rubber (JSR N230SL) with 35% Acrylonitrile content showing a Mooney viscosity of ML *(*1 + 4*)* at 100 ^{o}C = 42 was used. The nanoclay Cloisite 20A, a natural montmorillonite modified with

quaternary ammonium salt (organic modifier - dimethyl dehydrogenated tallow, quaternary ammonium, modifier concentration 95 meq/100g clay and d_{001} =24.2Å) was procured from Southern Clay Products, USA. Silica [Ultrasil], sulphur, dicumyl peroxide and other compounding ingredients, were obtained from standard suppliers.

Preparation of Nanocomposites

Cloisite 20A was mixed into NBR in the ratio 1:3 using an internal mixer type Fissions Haake Rheocord 90 at 60 rpm and at 50°C for 10 minutes. The internal mixer has an 8-shaped chamber in which two sigmoid, counter-rotating blades turn. The NBR – nanoclay masterbatch was later compounded with NBR and other compounding ingredients in laboratory size two roll mill (15cm x 33cm) with friction ratio 1 : 1.25 at room temperature using standard procedures. The rubber formulations were evaluated for cure characteristics on TechPro Rheotech ODR. (ASTM D-2084)). Curing was done at 150°C and 200 kg/cm² for the optimum cure time in a hydraulic press to make ~ 2mm thick rubber sheets.

Characterization of NBR Nanocomposites.

Dumbbell specimens were punched out from the molded sheets and stress-strain characteristics were evaluated as per ASTM D412 method on a UTM . The dumbbell specimens were subjected to heat ageing at 100°C for 48 hours.

Design Selection for Property Optimization

A Box-Benken design was chosen for the study considering its efficiency in the number of required runs. Also, this design does not contain any points at the vertices of the cubic region created by upper and lower limits for each variable and hence is advantageous when these points are impossible to be tested because of physical constraints. The three level three factor Box-Benken design employed in this study required 15 experiments. [11 -15] with silica content (X_1), Nanoclay loading (X_2) and sulphur / Accelerator ratio (X_3) as the independent variables. The compositions were optimized for mechanical properties and heat ageing properties. The coded and uncoded levels of the independent variables are given in Table 1.

RESULTS AND DISCUSSION

The mechanical properties of NBR nanocomposites before and after heat ageing are tabulated in Table 2. A wide range of values were observed for the different NBR compounds..

Statistical analysis

The experimental data obtained by following the above procedures were analyzed by the response surface regression procedure using the following second-order polynomial equation:

$$y = \beta_0 + \sum_{i=1}^{3} \beta_i x_i + \sum_{i=1}^{3} \beta_{ii} x_i^2 + \sum \sum_{i<j=1}^{3} \beta_{ij} x_i x_j$$

where y is the response x_i and x_j are the uncoded independent variables and β_0, β_i, β_{ii} and β_{ij} are intercept, linear, quadratic and interaction constant coefficients, respectively. MINITAB software package was used for regression analysis. The regression coefficients for the various parameters are tabulated in Table 3. The factors with positive coefficients have a positive effect on the property and vice versa. Using the regression equation, the contour diagrams and response surface plots were generated (fig 1 & 2).

Overlaying of Contour Plots

The contour plots for tensile strength, elongation at break, modulus at 100% elongation and changes in tensile strength and modulus after heat ageing were overlaid to find the feasible region (shown as white region) having desired properties [Fig 3 & 4]. The desired values of all these properties can be obtained at any given combination within the optimized region. For the purpose of overlaying, nanoclay and silica contents were chosen as variables keeping the value of sulphur/accelerator ratio constant at mid point.

Verification Experiments

Confirmatory experiments were carried out to validate the equations, using combinations of independent variables which were not part of the original experimental design but were within the experimental region.The values are listed in table 4. The predicted and experimental values were in good agreement. These validations confirmed the suitability of the design chosen, method of sample preparation and property evaluation.

CONCLUSION

Silica loading, nanoclay content and sulphur / accelerator ratio of NBR compounds were optimized using Design of Experiments approach. The nanocomposites were characterized for Tensile Strength, Modulus and Elongation at break, both before and after heat ageing. The data obtained were used to generate models by linear regression analysis using MINITAB package. Contour plots [a series of curves that identified different combinations of variables for which the response was constant] for tensile strength, elongation, modulus and change in tensile strength and modulus after heat ageing were overlaid to provide an optimum region for a desired set of specifications. Results from verification experiments were found to be within reasonable limits.

Table 1 Coded and Uncoded levels of Independent Variables – NBR –nanoclay systems

VARIABLE	LOW (-1)	MID (0)	HIGH (1)
Silica Loading (X1), phr	0	10	20
Nanoclay Content (X2), phr	0	5	10
Sulphur/Accelerator ratio (X3)	0.3	2	3.7

Table 2 Three variable Box – Behnken design in coded units and Mechanical properties NBR Nanocomposites

RO	Name	Coded Variable			Properties before Heat Ageing				Properties before Heat Ageing			
		Silica	Nano -clay	S/Accl Ratio	TS N/mm^2	Eb %	M100 N/mm^2	M300 N/mm^2	TS N/mm^2	Eb %	M100 N/mm^2	M300 N/mm^2
1	NBR201	-1	1	0	6.44	757	1.36	2.39	4.96	486	1.58	2.97
2	NBR202	0	0	0	7.89	1063	1.20	1.91	6.87	736	1.43	2.40
3	NBR203	0	1	-1	7.99	1279	1.13	1.62	6.81	919	1.21	1.81
4	NBR204	0	0	0	7.28	1013	1.06	1.81	7.76	797	1.53	2.55
5	NBR205	-1	0	1	5.07	556	1.35	2.57	4.49	400	1.55	3.23
6	NBR206	1	-1	0	11.14	1378	1.01	1.54	8.70	917	1.27	2.09
7	NBR207	0	-1	1	5.16	762	1.00	1.61	5.49	601	1.26	2.27
8	NBR208	0	-1	-1	4.76	1392	0.74	0.95	4.03	958	0.83	1.11
9	NBR209	1	0	-1	8.15	1488	0.90	1.36	7.81	1116	1.04	1.36
10	NBR210	-1	-1	0	2.77	720	0.78	1.18	2.43	536	0.92	1.37
11	NBR211	1	1	0	11.41	1129	1.37	2.46	11.46	870	1.72	3.21
12	NBR212	-1	0	-1	4.23	958	0.79	1.31	4.01	748	1.01	1.59
13	NBR213	1	0	1	12.90	944	1.54	2.98	11.37	644	2.05	4.30
14	NBR214	0	0	0	8.49	1079	1.09	1.93	7.94	771	1.47	2.56
15	NBR215	0	1	1	11.60	766	1.80	3.74	9.16	515	2.34	4.90

Table 3 Regression Coefficients for Properties of NBR Nanocomposites

Term		Before heat ageing			After Heat ageing		
		Tensile Strength N/mm2	Eb %	M100 N/mm2	Tensile Strength N/mm2	Eb %	M100 N/mm2
Constant	β0	7.89	1051.51	1.12	7.52	768.18	1.48
Silica	β1	3.13	243.30	0.07	2.93	172.23	0.13
Nanoclay	β2	1.70	-40.21	0.27	1.47	-27.68	0.32
S/Accl Ratio	β3	1.20	-261.21	0.27	0.98	-197.72	0.39
Silica*Silica	β12	0.13	-59.37	0.00	-0.05	-43.48	-0.05
Nanoclay*Nanoclay	β22	-0.08	3.84	0.02	-0.59	-22.19	-0.05
S/Accl Ratio*S/Accl Ratio	β32	-0.43	-5.62	0.03	-0.56	2.35	-0.02
Silica*Nanoclay	β1β2	-0.85	-71.57	-0.05	0.06	0.66	-0.05
Silica*S/Accl Ratio	β1β3	0.98	-35.55	0.02	0.77	-30.99	0.12
Nanoclay*S/Accl Ratio	β2β3	0.80	29.22	0.10	0.22	-11.78	0.18

Table 4 Comparison of the predicted and the observed values

Properties		Predicted	Experimental	% change from actual
Before heat Ageing	Tensile strength, N/mm2	7.40	7.68	3.7
	Elongation at Break , %	914	811	-12.6
	M100 , N/mm2	1.24	1.27	2.6
After heat Ageing	Tensile strength, N/mm2	6.62	7.53	12.1
	Elongation at Break , %	652	602	-8.2
	M100 , N/mm2	1.56	1.64	5.0

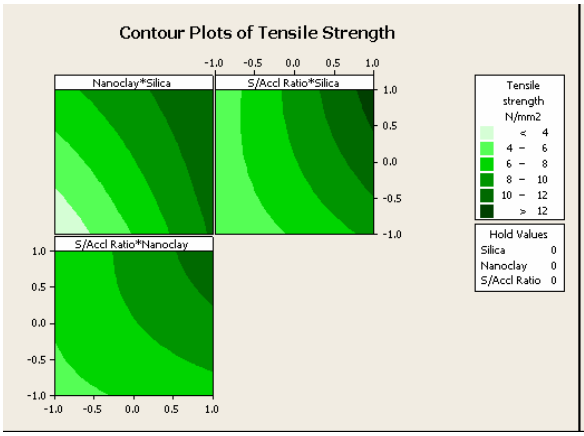

Fig 1. Contour Plots for Tensile Strength

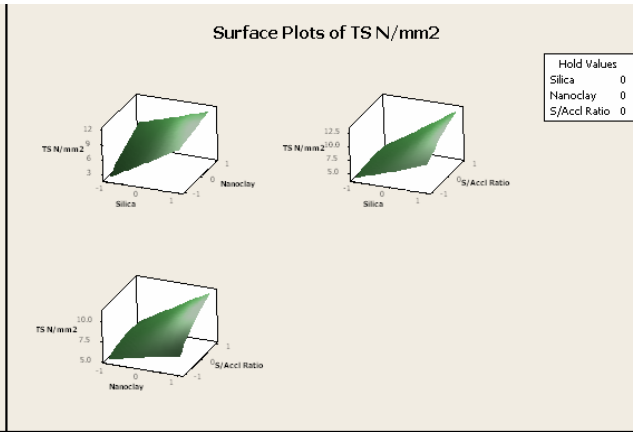

Fig 2. Response Surface Plots for Tensile strength

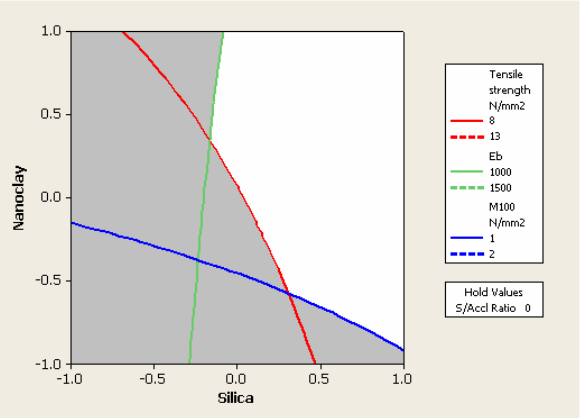

Fig 3 Overlaid contour plots for tensile strength, Elongation at break and M100

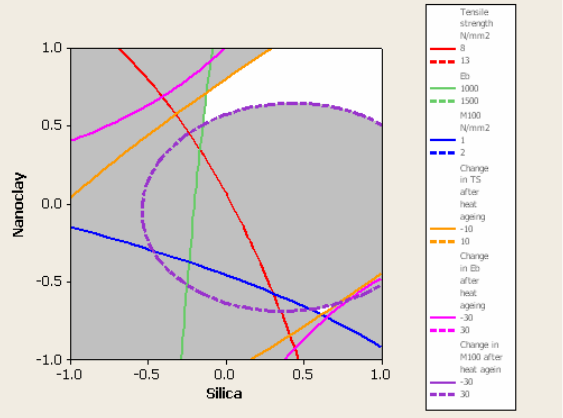

Fig 4 Overlaid contour plots for tensile strength, Elongation at break, M100 and change in these properties after

REFERENCES

1. T.V. Yen , James E.M., et al. (2001),. J Appl Polym Sci., 82, 1391-1403.
2. T.J. Pinnavaia and Beall G. W (Eds), "Polymer-Clay Nanocomposites", Wiley, New York, Ch 11 and 13 (2000)
3. A. Mousa & J. Karger-Kocsis (2001). Macromol .Mater. Eng, 286, 260-266.
4. Jin-tae Kim, Taeg-su Oh and Dong-ho Lee, Poly Intl, 52:1058–1063 (2003)
5. Yurong Liang, Yiqing Wang, et al., Poly Testing 24 (2005) 12-17
6. A. B. Morgan, W.G. Jeffrey, J App Poly Sci, 87 (2003) 1329-1338
7. S. Varghese, J. Karger-Kocsis, Polymer, 44 (2003) 4921-1927
8. S. Sadhu and A. K. Bhowmick, J Appl Poly Sci : Part B, Poly. Phy. 42, 1573 (2004)
9. A. M. Shanmugaraj, A. K. Bhowmick, J Appl Polym Sci, 88, 2992 (2003)
10. Wei-Gwo Hwang, Kung-Hwa Wei & Chang-Mon Wu, Polymer 45(2004) 5729-5734
11. D.C. Montgomery, Design and Analysis of Experiments, 4th Edn, John Wiley, 1996
12. Paritosh Jain, R.Muraleekrishnan, S.S. Bhagawan, M.S.Rao, "Response Surface Methodology: A tool for developing low SBR compounds", in Macromolecules : New Frontiers, Vol II, Ed. K.S.V.Srinivasan, John Wiley, New Delhi, 1998, 1058-61
13. E. Hajizadeh, and H. Garmabi, "Response Surface Based Optimization of Toughness of Hybrid Polyamide 6 Nanocomposites", Intl J Chem Biomol Engg, 2008, 1(1), 40-44.
14. V. Mittal, "Modeling the Behavior of Polymer-layered Silicate Nanocomposites using Factorial and Mixture Designs", Jl Thermoplastic Compos Matl, 2008, 21,9
15. S.S. Bhagawan, "Statistical Design in Polymer Processing" in 'Polymer Processing Technology', B.R. Gupta (Ed), Asian Books, New Delhi, 2008

Studies on pressure sensitive adhesives based on blends of natural rubber and polychloroprene rubber modified with phosphorylated cashew nut shell liquid prepolymer

A.R.R. Menon[#], J. Chameswary and J.D. Sudha

National Institute for Interdisciplinary Science and Technology (NIIST, CSIR)

Thiruvananthapuram – 695 019, Kerala, INDIA

Email : ravindranathamenon@yahoo.co.in

ABSTRACT

Effect of compositional and processing variations on the T-peel adhesion strength of rexin specimens bonded with phosphorylated cashew nut shell liquid prepolymer (PCNSL) based pressure sensitive adhesives (PSAs) containing natural rubber (NR) and polychloroprene rubber (CR) has been studied. Increase in adhesion strength above that of a commercial sample of PSA has been observed with the increase in solids content of the PCNSL based PSA from 15% to 25%. Also, considerable increase in adhesion strength has been obtained with the increase in storage time prior to testing of the specimens from 1 to 7 days which indicates the time dependent diffusion behavior of PCNSL based PSA facilitating wetting and bond formation with the substrates. Irrespective of the solids content and the type of PCNSL, a maximum in T-peel adhesion strength has been obtained at a CR dosage of 90 phr in the blend. Typical cohesive failure along-with high strength have been obtained with PSAs based on PCNSL having a higher degree of phosphorylation / oligomerization. Uniform and almost complete wetting of the substrate has been confirmed by the optical stereo micrographs of the failure surfaces of the test specimens and the results on viscosity obtained from rheometry.

INTRODUCTION

Pressure sensitive adhesives (PSAs) [1], popularly known as 'contact adhesives' hold a main stay in the present consumer and industrial market. A variety of PSAs based on natural rubber (NR) and polychloroprene rubber (CR) modified with tackifiers and other additives have been in use for various applications such as removable tapes / labels, upholstery, carpentry and footwears.[2-4] It has been established by the results of previous studies that Phosphorylated Cashew Nut Shell Liquid prepolymer (PCNSL) – an amphiphyllic derivative of cashew nut shell liquid (CNSL) could function as an excellent *multifunctional additive* for rubber compounding.[5-7] The chemical structure of PCNSL prepolymer is given in Fig. 1. The multifunctional role of PCNSL as a plasticizer, antioxidant and tackifier has been made use of in the design and development of a series of solvent based PSAs containing NR and CR. A preliminary study was made on the effect of different compositional and

processing variables on the adhesion strength of substrates bonded with these PSAs - the results of which are reported in this paper.

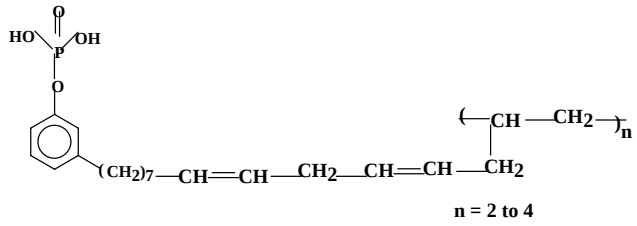

n = 2 to 4

(I) Prepolymer of PCNSL

Materials & Methods

Polychloroprene rubber (CR) (Skyprene Y-30H, Toyo Soda Co.) was supplied by M/s. Jeni Polyplast, Ahmedabad, Gujarat, India. CNSL conforming to Indian Standards IS: 840 - 1964 was supplied by M/s. Adarsh Industrial Chemicals, Sanoor, Mangalore, India. Commercial sample of PSA (Fevicol SR 998) was manufactured by M/s. Pidilite Industries Pvt. Ltd., Mumbai, India.

PCNSL was synthesized (at 20 kg level) by the simultaneous esterification and oligomerization of CNSL using o-phosphoric acid at controlled temperature, time and vacuum conditions in a Multi Purpose Reactor (*Pyrodevices*) supplied by M/s. Thermosystems, Veli, Thiruvananthapuram.

Blends of NR, CR and PCNSL (in various proportions) were prepared by mixing on an open two roll mill (6" X 12") for 5 minutes followed by homogenization and sheeting out. The sheets were cut to small pieces and weighed amounts of the same were kept immersed in requisite amount of dichloromethane for 24 h, stirred there-after for homogeneity and kept in air-tight containers.

The viscosity of the PSAs was measured on a rheometer (Anton Paar Physica, Austria, model MCR-150) by parallel plate method, at 28°C over the shear rate range from 0.1 s^1 to 100 s^1. T-peel test specimens were prepared from rexin sheet cut to size (75 mm X 25 mm). Two coats of the PSA were applied manually on an area of 50 mm X 25 mm from one end of the fabric surface, an open tack time of 2 minutes was given and bonded together under hand pressure. The test specimens were kept pressed between two flat sheets under a load of 10 kg, applied uniformly for a period of 24 h or 168 h. The T-peel adhesion strength of the specimens was measured on a Universal Tensile testing Machine (Hounsfield, H5KS) at a cross head speed of 100 mm/min. The optical micro photographs of the failure surfaces were obtained using a stereo microscope (Leica MZ 16A / DC Twain) at a magnification of X 11.

RESULTS AND DISCUSSION

Effect of type of PCNSL and storage time of bonded specimens on adhesion strength

The results on T-peel strength of rexin specimens bonded with the PCNSL based PSAs are given in Table 1. It shows a general increase in the T-peel strength with the change in type of PCNSL from

PCNSL-1 to PCNSL-3. This is expected to be due to the increase in cohesive strength of the PSA based on it due to the increase in molecular weight / viscosity up on changing from PCNSL-1 to PCNSL-3. Also, at higher solids contents the nature of failure changed from 'adhesive' to 'cohesive'

NR / CR / PCNSL (phr)		100 / 0 / 5		0 / 100 / 5	
Storage time (days)		1	7	1	7
	TSC (%)	Mean T-peel strength (N/25mm)			
PCNSL - 1	15	5.4	9.2	13.7	16.5
	20	8.8	10.4	21.5	33.7
	25	9.1	11.5	34.8	41
PCNSL - 2	15	5.3	7.3	14.6	18
	20	8.7	11	18.8	30
	25	9.3	12.1	33.3	45.3
PCNSL -3	15	6.3	7.4	15	16.9
	20	9.7	14.1	26	33.1
	25	13.4	17.1	32.6	43.9

Table 1. Variation in T-peel strength of rexin / rexin bonded with PCNSL based PSAs

type similar to that of the commercial sample. The adhesion strength of rexin specimens bonded with PCNSL based PSAs increase with storage time from 1 to 7 days. This is more prominent in the adhesive containing higher solids content, higher proportion of CR and PCNSL having a higher extent of oligomerization / phosphorylation. Time dependent diffusion of the PSA to the substrate matrix aiding 'wetting' may be one of the reasons for the increase in adhesion strength. A similar time dependent increase in self adhesion strength (tack) of PCNSL modified NR has been reported earlier[5] which was ascribed to higher molecular diffusion of NR assisted by the plasticizing effect of PCNSL. The T-peel strength of rexin bonded with Fevicol SR 998 showed a peak value (19N/25 mm) after storing for five days. This may probably be facilitated by its very low value of viscosity. However, it can be noted that the increase in adhesion strength is comparatively greater for the PCNSL modified CR based PSAs, particularly at the higher solids contents, as shown in Table 1. The progressively decreasing viscosity at higher shear rates of PCNSL – 1, PCNSL-2 and PCNSL-3 based PSAs may aid the flow of the adhesive and wetting of the substrates, facilitating development of a higher bond strength over a longer period of time. This increasing adhesion strength may also be due to possible physico-chemical interaction between CR and PCNSL as mentioned in an earlier work [7] where-in the polar phosphate group of PCNSL can interact with the chloro-group of CR. Polar – polar interaction between an additive and PSA has been reported as a factor responsible for a high value of T- peel strength.[8] Table 2 shows the mean T-peel strength of rexin bonded with PSAs based on unmodified blends of NR and CR, tested after 24 h. The lower values of adhesion strength here is in sharp contrast to the considerably higher values for the PCNSL based PSAs shown in Table 1.

NR / CR		100 / 0	75 / 25	50 / 50	25 / 75
	TSC (%)				
Mean T-peel strength (N/25mm)	15	2.4	3.3	4.9	3.7
	20	2.8	3.6	4.5	4.8

Table 2. T-peel strength of rexin / rexin bonded with unmodified NR/CR based PSAs

In the former, the lower segmental mobility of the elastomeric chains in the absence of PCNSL may reduce the flow and wetting of the substrates, essential for development of a high value of adhesion strength. It is expected that the plasticizing and softening effect of PCNSL in NR [5] and CR [6] as reported earlier facilitates the built up of adhesive tack in the PCNSL modified PSAs.

Effect of solids content of PSA on adhesion characteristics

The optical micro-photographs of the failure surfaces of rubber specimens bonded with Fevicol SR 998 and PCNSL based PSAs are given as Figure 2.

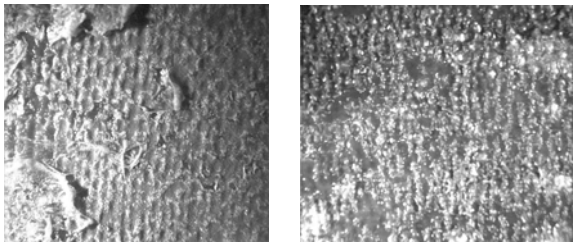

(a) (b)

Fig.2.T-peel failure surface of rubber / rubber bonded with (a) Fevicol and (b) PCNSL based PSA, (TSC – 30%)

Figure 2(a) shows almost uniform and complete wetting of the substrate with a layer of the adhesive. A similar morphology was observed for the PCNSL based adhesive at 30% solids content (Fig.2(b)). This was reflected in the increase in T-peel adhesion strength from 10% to 30% solids content, as given in Table 3. Also, the nature of adhesion failure changed from ‘adhesive’ to ‘cohesive’ type with

PSA	TSC (%)	Mean T-peel strength (N/25mm)
Fevicol SR 998	-	39.5
NR/CR/PCNSL	10	15.8
	20	25.9
	30	45.5

Table 3.T-peel strength of rubber / rubber bonded with Fevicol and PCNSL based PSA

the increase in solids content.

Effect of proportion of CR and type of PCNSL on adhesion strength

Table 2 gives the T- peel adhesion strength of rexin specimens bonded with PSAs based on blends of NR and CR at two different solids contents. It can be noted that irrespective of the content

of CR and solids content, all of the unmodified adhesives show low values of adhesion strength. The lower adhesion strength of the unmodified adhesives may be due to the absence of a plasticizer and / or tackifier which are known to be essential constituents of an elastomeric PSA.

Figure 3 shows that the PCNSL based PSAs show a maximum in the T-peel strength at a CR content of 90 phr. Also, at all the different proportions of NR and CR there is a gradual increase in T-peel strength (in the order PCNSL-1 < PCNSL-2 < PCNSL-3) with a change in the type of PCNSL.

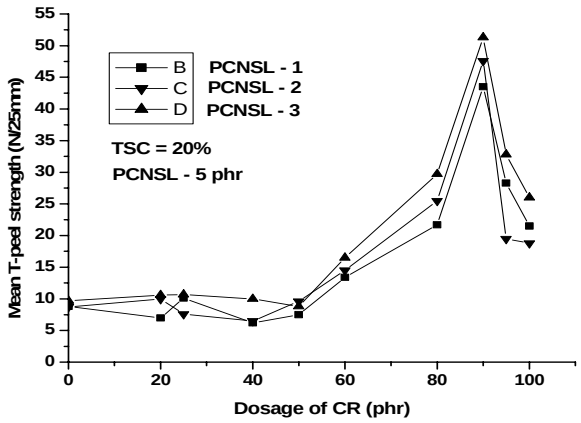

Fig.3. Variation in T-peel adhesion strength of rexin / rexin bonded specimens with dosage of CR in the NR/CR/PCNSL blend and at 20% TSC of adhesives.

This can be attributed to the increase in molecular weight of the resin in that order, contributing to the cohesive strength of the adhesive. Zosel has reported that above a minimum molecular weight of the modifier, tendency for fibrillation increases leading to an increase in cohesive strength of PSAs.[9] A similar mode of cohesive failure was observed for rexin specimens bonded with the PCNSL based PSA containing PCNSL-3. This indicates the possibility for entanglement of the pre-polymer chains of PCNSL with macromolecular chains of CR and NR with consequent increase in cohesive strength and T-peel adhesion strength. Also, the small proportion of NR (10 phr) may facilitate the visco-elastic deformation / flow characteristics of the adhesive facilitating quick and uniform wetting of the substrates and development of a high value of adhesion strength. The comparatively lower values of viscosity of Fevicol SR 998 at various shear rates may be one of the factors for its high value of adhesion strength. Thus, the low viscosity of this adhesive leads to almost complete wetting of the substrates as shown in the stereo optical micrograph of the failure surface, given as Fig.4 (a). The optical micrograph of the failure surface of rexin bonded with PCNSL based PSA having 25% solids content is given as Figures 4(b).This shows almost complete wetting of the substrate, accounting for

the observed high values of its T-peel strength (15.5 N/25mm as against 9.8 N/25mm for Fevicol SR 998).

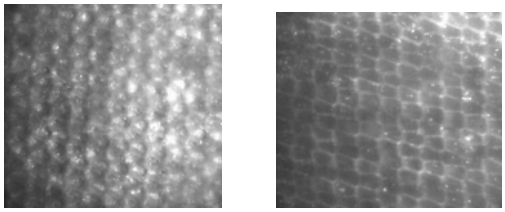

Fig.4.T-peel failure surface of rexin / rexin bonded with (a) Fevicol and (b) PCNSL based PSA

CONCLUSION

Adhesion strength higher than that of Fevicol SR 998 was obtained for PCNSL based PSAs with increases in solids content from 15% to 25% and storage time of test specimens prior to testing from 1 to 7 days which indicates time dependent diffusion characteristics of the latter causing a change in failure pattern from 'adhesive' to 'cohesive' type. Increase in the extent of phosphorylation / oligomerisation of CNSL during synthesis of PCNSL resulted in a resin having higher viscosity which enhanced the cohesive strength of the PSA and consequently the T-peel adhesion strength with flexible substrates. Rexin specimens bonded with the PCNSL based PSAs showed an optimum high value of T-peel adhesion strength at a CR dosage of 90 phr, irrespective of the type of PCNSL and solids content.

Acknowledgement: Thanks are due to the Kerala State Council for Science Technology & Environment

(KSCSTE), Thiruvanthapuram for sponsoring this work and to Prof. T.K. Chandrasekhar, Director, NIIST, Thiruvananthapuram for providing the necessary facilities.

REFERENCES

1. Wake, W.C. *Adhesion and the formulation of adhesives*; 2nd Edn., Appl Sci Pub., New York, 1982, Ch.10, pp. 220-223.

2. John, N.; Joseph, R. J Appl Polym Sci, 1998, 68, 1185.

3. Poh, B.T.; Kwo, H.K. J Appl Polym Sci, 2007,105 (2), 680.

4. Kozakiewicz, J.; Kujawa-Penczek, B.; Penczek, P.; Puton, K. J Appl Polym Sci, 1981, 26,

3699.

5. Menon, A.R.R.; Pillai, C.K.S. ; Nando, G.B. J Adhesion Sci Technol, 1995, 9(4), 443.

6. Menon, A.R.R.; Pillai, C.K.S.; Nando, G.B.; Bhattacharya, A.K.; Gupta, B.R. Kauts Gummi

Kunsts, 2000, 53(1-2), 35.

7. Menon, A.R.R.; Visconte, L.L.Y. J Appl Polym Sci, 2004, 91(3), 1619.

8. Taghizadeh, S.M.; Mirzadeh, H.; Barikani, M. ; Yousefi, M Iran Polym J, 2007, 16(4), 279.

9. Zosel, A. Int J Adhesion & Adhesives, 1998, 18, 265.

Nondestructive testing of defects in adhesive joints

P.N. Vinod, Reji John, Shiv Kumar, K. Shajahan, C.G. Padma Kumar and RMR Vishnubhatla
Naval Physical and Oceanographic Laboratory,
Defence Research and Development Organisation,
Thrikkakara P.O, Cochin-682 021

Email: tsonpol@vsnl.com

Abstract

Rubbers are generally used for encapsulating underwater components to prevent moisture ingress. Reliability aspects of these components are very important while considering the performance of the sensor. The sensor is deployed in underwater for quite long period of time and has no option for monitoring the structural health and functionality. The sub-surface defects such as micro-cracks, voids, porosity and delamination are generally introduced during the encapsulation or damage may create due to handling or when service stress exceeds design stresses. Nondestructive test (NDT) techniques such as infrared thermography (IRT) and micro-focal x-ray radiography techniques have been applied as an inspection methodology for detecting these defects in the encapsulants. The main advantage of the NDT techniques is that reliable and quantitative information about the hidden defects or flaws can be generated with high precision without sacrificing or damaging the entire structure of the device or its components. The bright spots and its dimensions observed on the IR images of the partially debonded samples correspond to the location as well as the relative size of the delamination presents in the sample. The x-ray image of the spiced cable joints shows that the internal structure with cracks or voids at the cable joints.

Keywords: encapsulants, NDT, infrared thermal imaging and microfocal x-ray radiography.

1. Introduction

Rubbers are generally used for encapsulating underwater components to prevent moisture ingress. The sensor is deployed in underwater for quite long period of time and has no option for monitoring the structural health and functionality on a regular basis. The generally observed defects of underwater components are delamination of adhesive joints or at the cable-spliced joints, cracks in ceramics, porosity and pin holes in transducer encapsulations and rubber moulded junction boxes, which are seriously affecting the reliability of the sonar systems. Hence, detection and localization of the above types of defects and monitoring the health of the components are the prime important factors to improve the reliability of the device and in predicting the life of the components, thereby eliminating the possibility of catastrophic failure of sonar. These defects are so tiny that visual inspection is not practically feasible. Consequently, there exists an increasing demand for reliable and effective non-destructive evaluation (NDE) for the wet-end components of the encapsulants. A number of different nondestructive test (NDT) techniques have also been developed as an inspection methodology and applied successfully to identify and characterize the defects [1-2]. No single method can detect all forms of flaws in all materials. Hence, suitable NDT inspection methods have to appropriately select for each case. In the present study, the delamination and cracks in the encapsulants of the wet-end components of the underwater sensors have been detected and characterized using the NDT technique such as micro-focal x-ray radiography and IR thermal imaging techniques. These techniques are applied due to their reliability and high sensitivity in detecting the defects [3].

1. (a) The principle of Infrared thermography

Infrared thermography is a non-contact sensing method concerned with the measurement of radiated thermal or infrared radiation from a surface in the infrared region. This involves the use of an IR camera to capture the evolution of surface temperature profiles of the test object after being

subjected to thermal perturbation from a high-energy uniform light source. It detects heat signatures via infrared imaging and uses this heat signature to detect leaks, cracks, debonding, corrosion etc. The spectrum and intensity of the radiation emitted by the object depends on its absolute temperature and emissivity of the surface [3]. The basic principle of this approach is that when a materials present defects; it introduces areas of locally high temperature because of the reduced heat flux in the areas immediately surrounding the defects. This results thermal gradients. This thermal transient flux can be picked up or recorded by an infrared camera operating in the infrared wavelength range 4 to 9μm. The analysis of the IR images provides qualitative information about the hidden defects or internal flaws in the material.

1. (b) The principle of X-ray radiography measurement

The radiography measurement is based on the differential absorption of x-ray radiation on its transmission through the structure of the tested specimen. This indicates that the intensity of the incident radiation on the tested structure is attenuated more or less due to the presence of any flaws or discontinuities in the specimen. Thickness alterations and the presence of discontinuities are visualized by differences in contrast (radiographic density) of the obtained images [3].

2. Experimental

For detecting the various defects-like thin line cracks, voids or sub-surface defects on the spliced neoprene cable, both IR thermal imaging and x-ray micro-focal radiography measurements were carried out. The tested samples were adhesively bonded aluminum disc with neoprene rubber used for encapsulating underwater acoustic sensors having delamination introduced deliberately. The Al disc had a thorough central hole to connect the rode for sensor assembling. The delamination was suitably created at the upper portion of the sample by not applying any adhesives and adhesive was applied at the lower portion of the samples. It serves as a delamination of one half of the 4” dia circular disc. The thermal imaging was carried out on adhesive joints to examine the delamination. The Thermovision 550 IR camera was used for the experimental works. The IR thermal imaging was performed in reflection mode in which both the heating source and the IR camera were positioned at the same side and infrared images were captured using the IR camera in the wavelength range 3-5μm. The test samples were heated using a hot air-gun for a few minutes. Then, the samples were allowed to cool for one minute. The IR thermal imaging system operated on the reflection mode in which both the heating source and the camera are positioned on the same side. The transient infrared images were acquired and analyzed. The micro-focal x-ray radiography measurements were carried out (using a Feinfocus FXE 225.20 unit which has a focal spot size of about 15μm with a geometric magnification of 3X) on the spliced cable joint to monitor the flaws/defects. Using this technique, the finer details of the cable joints such as delamination, voids, and quality of crimp, ingress of water, etc can be monitored. The radiography exposure parameters were suitably adjusted to obtain a radiographic density of about 2.0 to 2.5 at the region of interest (ROI). These films were processed manually under standard conditions to identify the fine-scale detailed of the damage or defects. A 3mm thick lead sheet was used at the entire area except the ROI for masking around the tube to control the scattering of the x-rays.

3. Results and Discussion

Fig 1 shows the IR thermal image of the tested structure consisting of neoprene rubber encapsulants glued to the Al housing of the sensor assemblies. Left side shows the schematic drawing of the 4” dia circular end cap of the sensor (test specimen) with upper portion is completely debonded and lower portion is completely bonded. From the thermal image given, a defect like non-bonded area can be detected with bright portion indicates the delamination. The presence of this bright area corresponds to the delamination indicating its shape and location of the delamination. The delamination of the encapsulants with the Al housing or ceramic rings is resulted due to the poor bonding practices employed or due to inadequate bonding of the adhesives [2]. For thin laminates, damage or defects is usually occurs at the subsurface and hence not readily detected visually (this is known as the barely

visible impact damage (BVID). The cracks, inclusions, void or delamination that transfers heat at different rates causes these thermal gradients. The temperature of the material changes rapidly after the initial thermal pulse because the thermal wave front propagates by diffusion process. The presence of delamination reduces the diffusion rate so that temperature gradient originates at or near around the defected area as the thermal wave propagates. Hence, it acts as an insulator and possesses a higher temperature with respect to the surrounding area. The large distribution of the temperature mapping at the non bonded area indicates that complete debonded condition of the encapsulants with the Al metal. The uniform distribution of temperature in the lower portion of the IR image shows that no delamination is present between the neoprene rubber encapsulants and Al housing of the sensor. Hence, it provides quantitative information about the hidden defects or internal flaws in the material.

A junction between two similar or dissimilar materials represents generally a weak structural joint and so it requires an appropriate choice of the most adequate joining technique to make good adhesion between the materials. An effective and reliable adhesive bond between dissimilar substrates is extremely important for transducer applications. Figure 2 shows the radiographic image of the spliced rubber cable. Fine details at the cable joints can be clearly seen in the image. Though there is contact at some locations (two strands), there was finite gap between the other strands. The gap is approximately 1 mm. The arrows indicate the transverse micro-cracks observed in the core strands. Figure 3(a) shows the photography of the tested cable splice. Fig 3(b-d) shows the micro-focal radiography images of the neoprene cable splice having a geometrical magnification of X3. In Fig 3b, the circled portion shows the large discontinuity in the copper conductor in the cable. The gap between the joints is indicated by a circle. Figure 4 shows the radiographic image of the spliced cable joints and it shows the splice in non-defective.

4. Conclusion

The sub-surface defects such as micro-cracks, voids, porosity and delamination are generally observed in the rubber encapsulants of the wet-end components. NDT tools like microfocal X ray radiography and IR thermal imaging techniques are useful to detect these defects. It was shown that with these techniques, finer details of the defects such as size and dimensions of delamination or cracks can be effectively detected and monitored. However, each of these NDT tools is sensitive to the type of defects present and hence can provide a quantitative account on the hidden flaws or faults in the encapsulants.

5. Acknowledgements

The authors thank Dr John Philip of IGCAR, Kalpakkam, Chennai, for the help rendered for characterizing samples for microfocal radiography and IR thermal imaging respectively. The encouragements and permission of the Director, NPOL to publish this work is greatly acknowledged.

6. References

1. C. Meola and G.M. Carlomagno, ‘Recent advances in the use of infrared thermography’, Measurement Science and Technology., 15, 27-58 (2004).
2. G. Busse, ‘Nondestructive evaluation of polymer materials,’ NDT & E Int’l, 27,253-262, (1994).
3. Bahman Zoofan, ‘Microradiography as a strong NDT tool’, ASNT handbook on Nondestructive test Series (http://www.asnt.org).

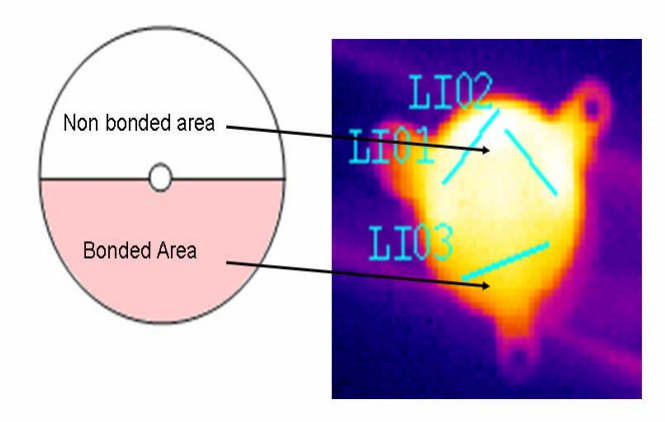

4. Fig 1. The IR image showing the delamination of the Al – Rubber joint.

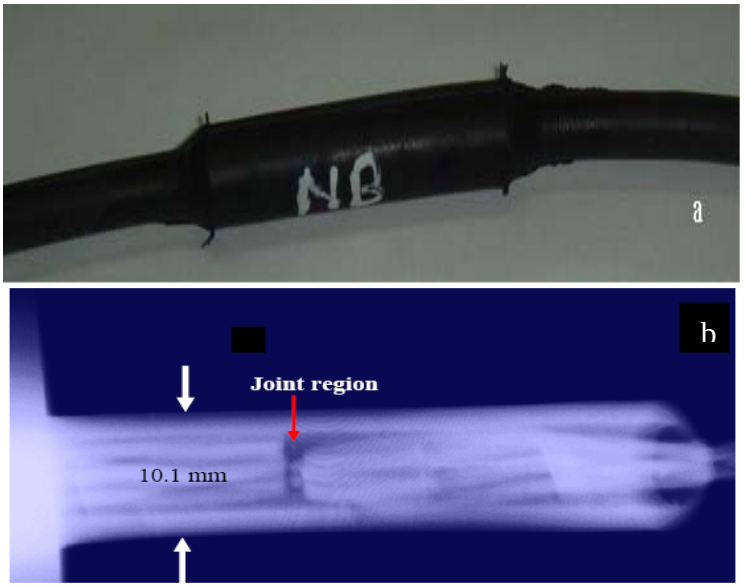

Fig 2. Photograph of the spliced neoprene cable and (b) Radiography image (3X) of the spliced cable.

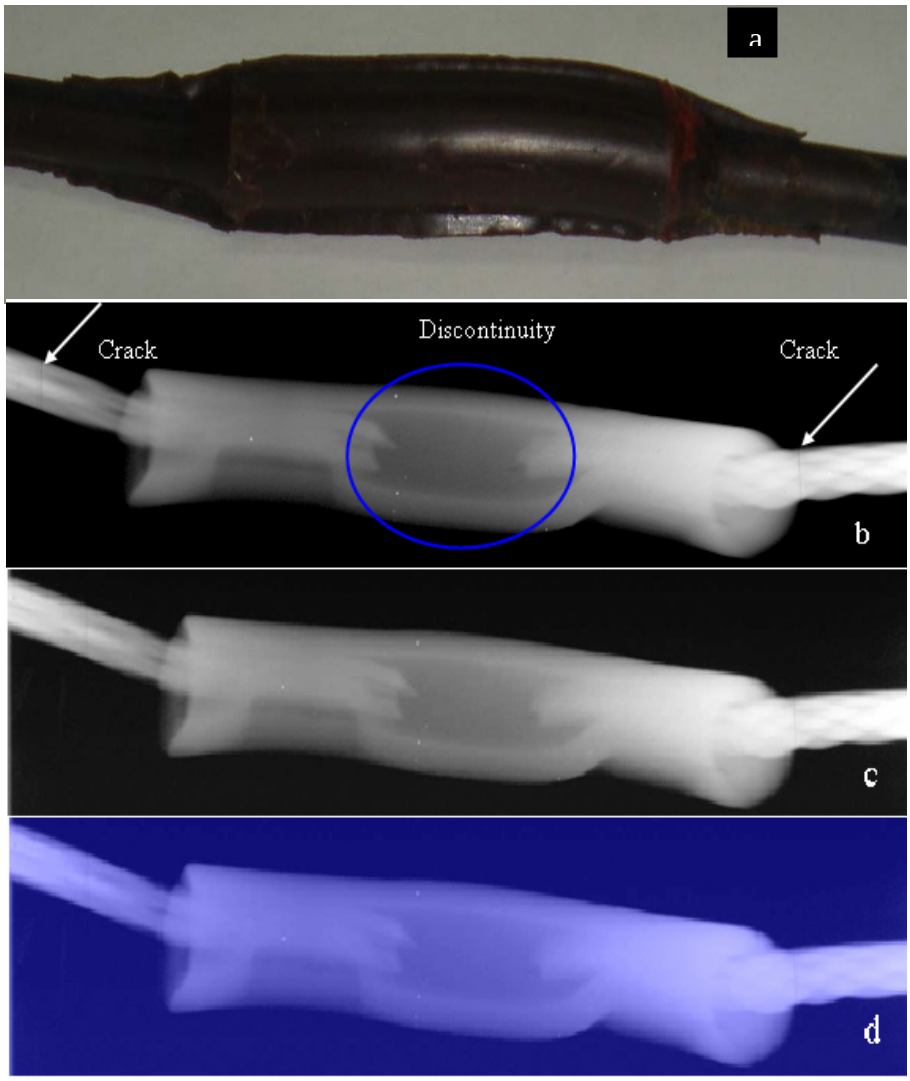

Fig 3(a) photograph of the tested cable and (b&d) represents radiography images.

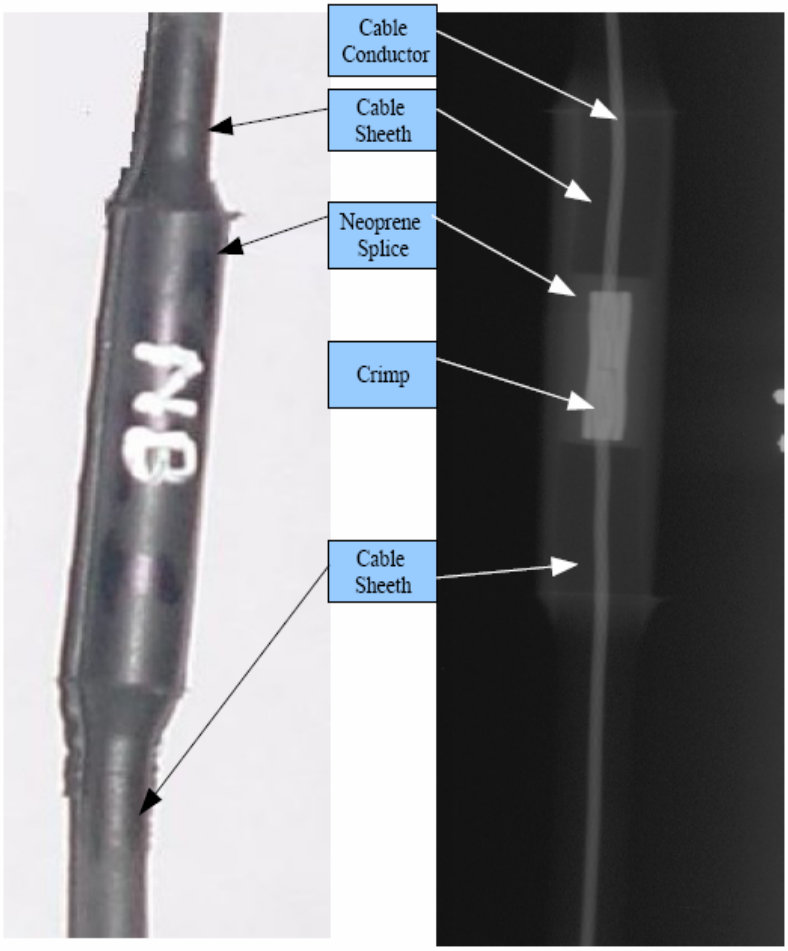

Fig 4. X-ray microfocal radiograph of spliced neoprene cable. The splice is no defective.

Electrical studies on silver subsurface particulate films on blends of polystyrene and poly (4-vinylpyridine)

Manjunatha Pattabi*#, Pratima Parashar and S C Gurumurthy

Department of Materials Science, Mangalore University, Mangalagangotri 574 199, INDIA

*E-mail: manjupattabi@yahoo.com

Abstract:

Vacuum deposition of metals on softened polymers offers a technique to prepare subsurface particulate films. Morphology of such films depends on deposition as well as thermodynamic parameters. In addition, the polymer metal interaction plays an important role in deciding the morphology. The electrical properties of particulate films are strongly dependent on their morphology. Blending of polymers can be used to control the morphology of such films and thereby, tailor their electrical properties. Blends of Polystyrene (PS) and Poly (4-vinylpyridine) (P4VP) prepared by mixing in common solvent, Di-methyl Formamide (DMF), are solution cast on to clean glass substrates. The substrates were held at 457 K, much above the glass transition temperature of both the polymers, to ensure sufficient polymer fluidity during deposition, to obtain a subsurface particulate film. A constant deposition rate of 0.4 nm/s was used throughout the study. The particle sizes were estimated from the line width broadening of the X-ray Diffraction (XRD) peaks and the mean particle sizes are in the range 30-50 nm. Films on softened PS give rise to a very high room temperature resistance due to the formation of a highly agglomerated structure. On the other hand, films on softened P4VP gives rise to a room temperature resistance in the range of a few tens to a few hundred MΩ/□, which is desirable for device applications. Blends of PS and P4VP show room temperature resistances in the desirable range, even at a PS/ P4VP ratio of 75:25. The film resistances in the desired range could be obtained on PS by blending it with P4VP.

Introduction

Organised small metal particles with an average inter-particle separation of a couple of nm would exhibit interesting optical and electrical properties which can be exploited for device applications. An interesting sub-surface particulate structure formation was reported when certain inorganic materials are vacuum deposited on to softened polymer substrates [1-4] and the morphology and formation of such structures depend on thermodynamic as well as deposition parameters [4, 3]. The morphology of sub-surface particulate structures also depends upon polymer metal interaction [5, 6].

Silver deposited on softened inert polymers like polystyrene (PS) substrates formed highly agglomerated structures with their room temperature resistances equalling that of the substrate, irrespective of the thickness deposited. On the other hand, silver deposited on an interacting polymers

like poly (2-vinylpyridine) (P2VP) or poly (4-vinylpyridine) (P4VP) resulted in the formation of smaller particles (~ a few tens of nm) with smaller inter-particle separations [6]. Such structures showed electrical resistance in the range desirable for device applications. However, P2VP and P4VP are hygroscopic while PS is a stable polymer. Therefore, it would be interesting to study the electrical properties of sub-surface particulate structures formed on PS/P4VP blends. This article reports the results of the studies taken up on the electrical properties of silver island films deposited on softened PS/P4VP blends.

Experimental technique

Poly (4-vinylpyridine) and silver (purity better than 99.99+ %) used in this study were procured from Sigma-Aldrich Chemicals Pvt. Ltd. Polystyrene was procured from Alfa-Aesar (A Johnson Mattey company). The molecular weight of P4VP and PS are 60,000 and 100,000, respectively. Polymer blends were prepared through solution blending by mixing in a common solvent, Die-methyl Formamide (DMF). 2 g of the total polymers at different ratios were dissolved in 20 ml of DMF at room temperature and solution cast on a glass slide pre-coated with silver contacts with a gap of 1 cm X 1 cm for electrical studies. Silver films of various thicknesses were deposited on these substrates held at 457 K in a vacuum better than 8×10^{-6} torr. A chromel-alumel thermocouple was used to measure the substrate temperature. A Telemark quartz crystal monitor (Model 850) was used to measure the deposition rate, as well as the overall film thickness. The deposition rate was 0.4 nm/s for all the films. Resistance measurements were carried out in-situ, using a Keithley electrometer model 617. The films were annealed at the deposition temperature for 1 hour before cooling them to room temperature. X-ray diffraction (XRD) studies were carried out for particle size measurements using a Bruker D8 Advance powder x-ray diffractometer with Cu K_{α} radiation.

Results and Discussion

Figure 1 shows the variation of the logarithm of resistance against inverse of temperature for silver films of different thicknesses deposited on polymers and blends at a temperature of 457 K, during cooling to room temperature. It is interesting to note that while some of the films show only negative temperature coefficient of resistance (TCR) some show almost zero TCR. Some of the films show negative TCR at higher temperatures and almost zero TCR at lower temperatures. The 50 nm thick silver films on pure PS and 75:25 blend of PS/P4VP show negative TCR. Silver on PS showed similar behaviour in our earlier studies resulting in room temperature resistance same as that of the substrate with the formation of large silver particles separated by large distances [7]. Blending the inert polymer PS with an interacting polymer like P4VP to the extent of 25% does not seem to alter the morphology of the particulate film as indicated by the electrical behaviour. When the P4VP content is increased to 50%, a negative TCR at high temperature followed by almost zero TCR at lower

temperatures exhibited by the 50 nm thick film is similar to the behaviour observed earlier for pure P4VP [8] indicating that the film consists of small particles separated by small distances. With further increase in P4VP content, the negative TCR part diminishes, giving rise to a near zero TCR.

It is also interesting to note that even at 50% P4VP, with an increase of silver deposited, films show electrical characteristics as that of the films on pure P4VP [8]. Further, when 150 nm thick silver is deposited on a polymer blend with only 25% of P4VP, the films show desirable electrical characteristics in contrast with the very high room temperature resistance observed for films on pure PS even at 300 nm of silver [7].This indicates blending has positive effect on electrical properties on silver films deposited on PS. It was shown through X-ray photoelectron spectroscopy (XPS) studies at various electron take off angles (ETOA) that silver clusters are formed at a depth of a couple of nm from the polymer surface [7,8]. It is known that the formation of subsurface particulate structure is subject to certain thermodynamic [4] and deposition conditions [3]. While the thermodynamic conditions are met for the deposition of metals on most of the polymer substrates, deposition conditions used in the present study are similar to those used in our earlier studies. Therefore, it is reasonable to assume that the particles are formed just a couple of nm below the polymer surface. Table 1 gives the resistance data and particle size estimated from the X-ray line width measurements for the silver films of different thicknesses deposited on the PS/P4VP blends of various compositions.

It is seen that the resistance of silver films at room temperature lie at a few tens of MΩ/□, at certain thicknesses even for the PS content of 50-75%, in contrast with the behaviour of silver on pure PS. The particle size increases with increase in PS content at a fixed silver thickness, as expected. It is seen that as the P4VP concentration increases there is a regular decrease of resistance at a fixed silver thickness. The plot of logarithm of these resistances with blend concentration gives linear fit as shown in figure 2. Through this fit, one can estimate the resistance of the film at a particular blend and for the given conditions and thickness.

Conclusions:

1. Deposition of silver on polymer blends coated substrate held at 457 K provides an approach to produce stable island films with reasonable control over their electrical resistance.
2. Higher thickness films show almost zero TCR near room temperature, a desirable property for most of the devices. Low thickness films show a negative TCR, characteristic of island films.
3. Silver particulate films deposited on PS/P4VP blends show better electrical properties compared to those on pure PS, even at a P4VP content of 25%. The blends PS/ P4VP (50:50, 25:75) seem to be better with regard to their electrical behaviour.

Acknowledgment:

One of the authors (PP) thanks Department of Science and Technology, Government of India, for financial assistance.

References

[1] Kovacs G J and Vincentt P S 1982 *J. Colloid. Interface. Sci*. **90** 335

[2] Kovacs G J and Vincentt P S 1983 *Thin Solid Films* **100** 341

[3] Kovacs G J, Vincentt P S, Trumblay C and Pundsak A L 1983 *Thin Solid Films* **101** 21

[4] Kovacs G J and Vincentt P S 1984 *Thin Solid Films* **111** 65

[5] Kunz M S, Shull K R and Kellock A J 1992 *J. Appl. Phys*. **72** 4458

[6] Mohan Rao K and Pattabi M 2001 *J. New Mat. Electrochem. Systems* **4** 11

[7] Mohan Rao K, Pattabi M, Mayya K S, Sainkar S R and Murali Sastry M S 1997 *Thin Solid Films* **310** 97

[8] Mohan Rao K, Manjunatha Pattabi, Sainkar S R, Arun Lobo, Kulkarni S K, Jayasheela Uchil and Murali Sastry M S 1999 *J. Phys. D: Appl.Phys*. **32** 2327

Table 1: Resistances at substrate temperature (R_{st}), after one hour of aging (R_{1hr}), at Room temperature (R_{rt}) and particle size for silver films deposited on PS/P4VP blends held at 457 K.

Polymer PS:P4VP	Silver film thickness	Resistances (MΩ/□)			Particle size XRD (nm)
		R_{st}	$R_{1\ hra}$	R_{rt}	
0:100	50 nm	1.9	26.8	27.1	30
25:75	50 nm	6.2	42.2	47.1	46.6
25:75	85 nm	3.2	14.7	14.2	53
50:50	50 nm	15.9	119.5	159.4	49.1
50:50	95 nm	2.9	29.9	30.1	47.5
75:25	50 nm	214	325	-	51.8
75:25	150 nm	14.8	98.2	248.9	46.4
100:0	50 nm	302	491	-	53.3

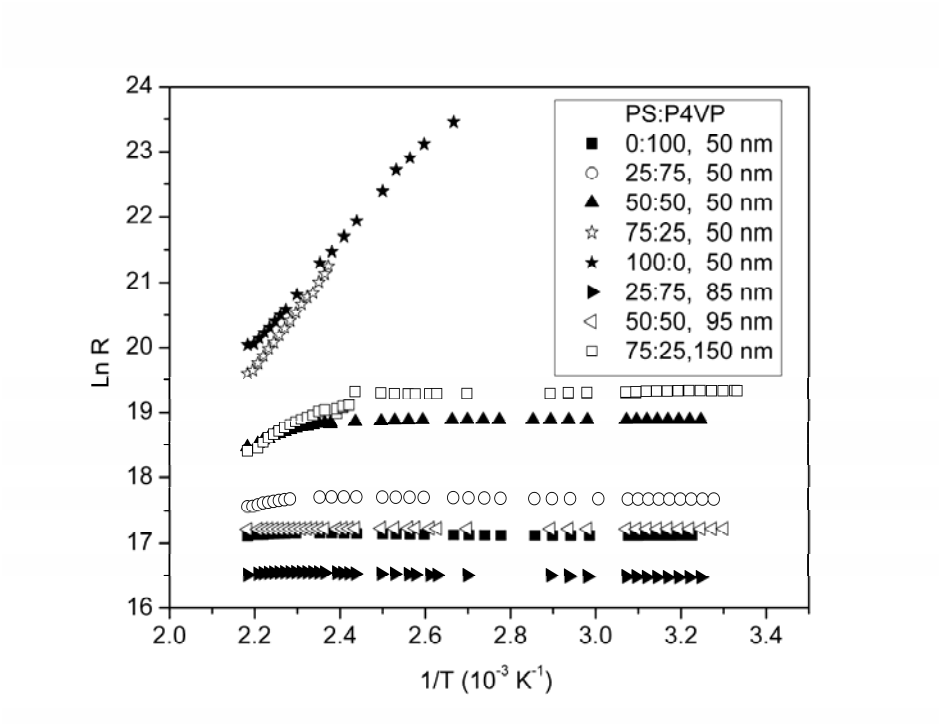

Figure 1: Variation of ln R with 1/T for silver films deposited on PS/P4VP blends held at 457 K

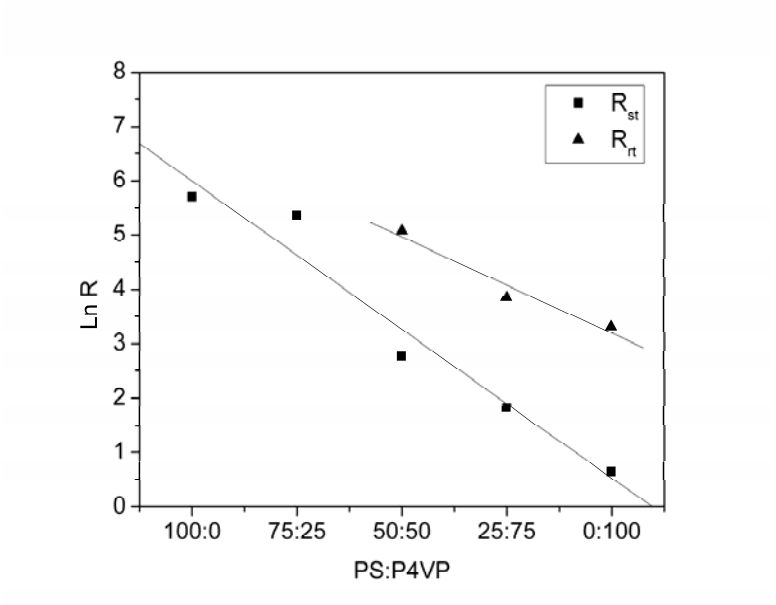

Figure 2: Variation of logarithm of resistances at 457 K and 300K with PS/P4VP blend composition for 50 nm silver films.

Uncompatibilized and reactively compatibilized ternary polymer blends of PA6/PP/ABS: Morphological investigation

Biswajit Panda *, Arup R. Bhattacharyya[#] and Ajit R. Kulkarni[#]

Department of Metallurgical Engineering and Materials Science, Indian Institute of Technology Bombay, Powai, Mumbai-400076, India

E-mail: arupranjan@iitb.ac.in ajit.kulkarni@iitb.ac.in

Abstract

Morphological investigation was carried out for melt mixed ternary polymer blends of polyamide 6(PA6)/ polypropylene (PP)/ acrylonitrile butadiene styrene (ABS) in order to understand the role of compatibilizer in morphological developments. Uncompatibilized 80/10/10 PA6/PP/ABS blends exhibited matrix- dispersed droplet type morphology in which the dispersed phases (PP & ABS) were found to exhibit core-shell type of morphology. The difference in morphology type may be due to the difference in surface free energy between the matrix and one of the dispersed phases. Eventually it was found that "core-shell" type of morphology changed to "co-continuous" type on increasing the concentration of PP and ABS in the ternary blends. In this context, styrene maleic anhydride co-polymer was found to act as a compatibilizer in PA6/PP/ABS ternary blends, manifesting in finer domain size of the dispersed phase.

Introduction

Multicomponent polymer blends consist of three or more immiscible polymers are a new interesting area in the field of polymer blends. A variety of phase morphology has been observed which directly influence the whole set of properties [1-2]. Three factors have been found to influence the morphological developments in immiscible multicomponent polymer blends viz. thermodynamic properties of the blends such as interfacial tensions of the constituent polymers [3], melt viscosity of the constituent polymers [4] and elasticity of the constituent polymers [5]. Hobbs et al. [6] explained the morphological phenomenon in ternary polymer blends on the basis of spreading co-efficient by modifying Harkin's equation, in which two dissimilar phases were dispersed in the third phase (matrix). If p, q and r are the three polymers of a ternary blend system and if p is the matrix, then the spreading co-efficient, λ_{rq} is given as

$$\lambda_{rq} = \sigma_{qp} - \sigma_{rp} - \sigma_{qr} \qquad (1)$$

where λ_{ij} is defined as the spreading co-efficient for i and j and σ_{ij} is the interfacial tension between i and j. If λ_{rq} is positive then q becomes the core encapsulated by r. Both r and q will disperse separately when both λ_{rq} and λ_{qr} are negative. Based on the spreading co-efficient sign four types of morphologies can be observed [7].

In the present work the morphological investigation has been carried out for PA6/PP/ABS blends and the influence of a reactive compatibilizer on the morphological developments has been investigated. Core-shell type of morphological observation in 80/10/10 PA6/PP/ABS has been analyzed with the help of spreading co-efficient and interfacial energy. 40/30/30 PA6/PP/ABS blends show co-continuous morphology. In this context morphological investigation has also been carried out for these blends in presence of styrene maleic anhydride copolymer (SMA) in order to understand the role of SMA as a compatibilizer.

Experimental

Polyamide6 (PA6 with zero shear viscosity = 180 Pa s at 260^{o}C) was obtained from GSFC, Gujarat, India (Gujlon M28RC, relative viscosity 2.8, Mv is 38642 in 85% formic acid). Polypropylene (H200MA) was obtained from Reliance Industries Ltd with melt flow index (MFI) of 23. Acrylonitrile-butadiene-styrene (ABS) copolymer (Absolac-120, with composition as: acrylonitrile 24 wt %, styrene 59.5 wt % and rubber content 16.5 wt %) was obtained from Bayer India Ltd. Styrene-maleic anhydride copolymer (SMA) with 8% MA content (Dylark 232) was supplied by Nova Chemicals, USA. The ternary blends of PA6/PP/ABS were prepared by melt mixing in a conical twin-screw microcompounder (Micro 5, DSM Research, Netherlands) at 260^{o}C with a rotational speed of 150 rpm for 15 min.

Morphological investigation was carried out by scanning electron microscopy (SEM, Hitachi S3400N).

Results and discussion

Depending on the composition two different types of morphologies have been observed in PA6/PP/ABS ternary blends viz. core-shell and co-continuous morphology for the compositions having 80/10/10 and 40/30/30 PA6/PP/ABS respectively.

The phase morphology of melt-mixed 80/10/10 PA6/PP/ABS blends has been investigated through SEM and can be found in Figure1. Core-shell type morphology has been observed in cryofractured etched surface of the extruded strands of the blends. By selective extraction of PP (by hot xylene) and ABS (by THF) it is revealed from the SEM micrographs that ABS is found to encapsulate the PP phase i.e. PP phase forming the core and ABS phase becomes the shell.

In case of 80/10/10 PA6/PP/ABS ternary blends system PA6 forms matrix and PP along with ABS form dispersed phases or more specifically core-shell type of morphology is observed from the SEM micrographs (Figure 1).The formation of this kind of morphology can better be understood from the spreading co-efficients of the respective polymer pairs [9]. The spreading coefficient $\lambda_{PP/ABS}$ of PP phase over ABS phase can be described as:

$$\lambda_{PP/ABS} = \sigma_{PA6/ABS} - \sigma_{PA6/PP} - \sigma_{ABS/PP} \quad \text{---------- (2)}$$

where σ_{ij} is the interfacial tension between i and j components.

If $\lambda_{PP/ABS}$ is >0 then PP phase becomes shell and ABS phase core. Similarly, if $\lambda_{ABS/PP}$ (Eq. 3) is >0 then ABS forms shell and PP core.

$$\lambda_{ABS/PP} = \sigma_{PA6/PP} - \sigma_{PA6/ABS} - \sigma_{PP/ABS} \quad \text{---------- (3)}$$

If both $\lambda_{PP/ABS}$ and $\lambda_{ABS/PP}$ are negative, the PP and the ABS phases will disperse separately in the PA6 matrix.

To determine the spreading co-efficient value, Interfacial tension (σ_{ij}) data were calculated for the three polymer-polymer interfaces present in the blends, i.e. PA6/ABS, PA6/PP and PPABS using the harmonic mean equation [8]:

$$\sigma_{12} = \sigma_1 + \sigma_2 - 4\sigma^{d}_{1}\sigma^{d}_{2} / \sigma^{d}_{1} + \sigma^{d}_{2} - 4\sigma^{p}_{1}\sigma^{p}_{2} / \sigma^{p}_{1} + \sigma^{p}_{2} \quad \text{----------(4)}$$

where σ_{ij} is the interfacial tension between the components i and j. σ_i is the surface tension of component i, σ^{d}_{i} is the dispersive fraction of the surface tension of component i and σ^{p}_{i} is the polar fraction of the surface tension of component i.

Incorporating the values in equation (3 and 4), it has been found that the spreading co-efficient values in all the cases were <0 manifesting the fact that both the minor phases (PP and ABS) will disperse separately in the PA6 matrix. But the observed phase morphology (Figure 1b) reveals that PP phase is encapsulated by ABS.

Figure2 shows the SEM micrograph for ternary polymer blends with varying concentration of SMA8 (2 to 6 wt %). It is well evident that from this micrograph that addition of compatibilizer has led to significant reduction in droplet size of the dispersed phase. Interestingly this reduction in the dispersed phase has been observed up to 2 wt % SMA8. Further it has been observed that with increase in concentration of SMA8, the domain size of the dispersed phase is found to be larger.

In case of 40/30/30 PA6/PP/ABS ternary blends, co-continuous morphology has been observed from the SEM micrograph (Figure3). This has been confirmed by selective extraction of the respective phases. In this context, it is worth pointing out that the extruded strand (after selective extraction of two phases viz. PP and ABS) has been found (Figure3d) to be self supporting, manifesting the co-continuous structure of the PA6 phase

Conclusions

Ternary polymer blends of PA6/PP/ABS without or with SMA8 have been successfully prepared by melt-mixing using a conical twin-screw microcompounder. The phase morphology was found to depend on the composition of the blends. 80/10/10 PA6/PP/ABS blends showed core-shell type morphology and 40/30/30 PA6/PP/ABS blends showed co-continuous type of morphology. Interestingly, on addition of SMA8 (up to 2 wt %) dispersed phase size was found to be finer indicating the compatibilizing action of SMA8 copolymer.

References

[1] Nemirovski N, Siegmann A, Narkis N. J Macromol Sci, Phys 1995; 34B:459.
[2] Horiuchi S, Matchariyakul N, Yase K, Kitano T, Choi HK, Lee YM. Polymer 1996; 37:3065.
[3] Hobbs SY, Dekkers MEJ, Watkins VH. *Polymer* **1998**; 29*:*1598-1602.
[4] Favis BD, Chalifoux JP, Polymers **1988**; 29: 1761-1767
[5] Reignier J, Favis BD, Heuzey MC. Polymer **2003**; 44: 49-59.
[6] Hobbs SY, Dekkers ME, Watkins VH. Polymer 1988; 29(9):1598–602.
[7] Reignier J and Favis BD. Macromolecules 2000; 33: 6998-7008
[8] Wu S. Polymer interface and adhesion. New York: Marcel Dekker; 1982, Chapter 3.
[9] Omonov T.S, Harrats C and Groeninckx G. Polymer 2005; 46:12322-12336

Table 1: Sample code and compositions of PA6/PP/ABS ternary blends

Sample code	PA6 (wt %)	PP (wt %)	ABS (wt %)	SMA8 (wt %)
8N1P1A	80	10	10	------
8N1P1A2S	78.4	9.8	9.8	2
8N1P1A4S	76.8	9.6	9.6	4
8N1P1A6S	75.2	9.4	9.4	6
4N3P3A	40	30	30	------

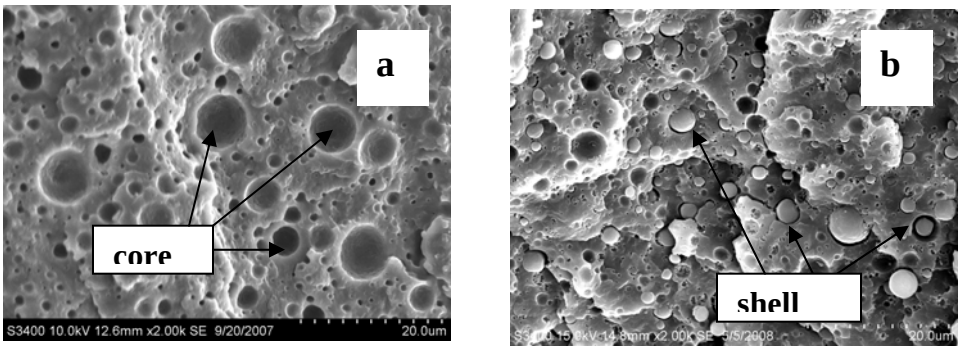

Figure 1: Core-shell morphology in 80/10/10 PA6/PP/ABS ternary blends in which (a) PP phase extracted by hot Xylene and (b) ABS phase extracted by THF

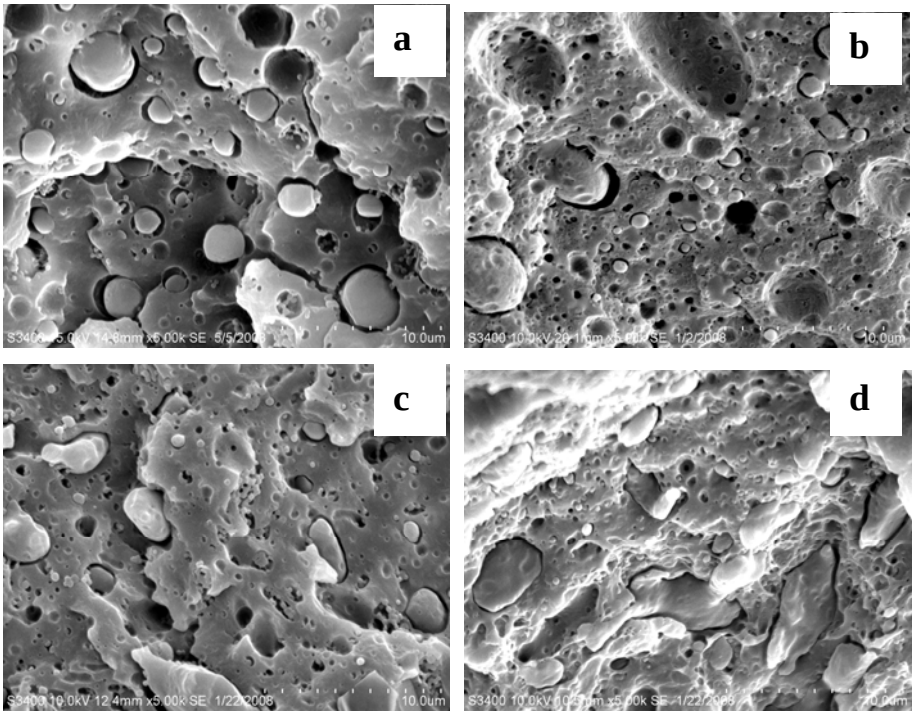

Figure2. 80/10/10 PA6/PP/ABS ternary phase morphology with (a) 0 wt%, (b) 2 wt%, (c) 4 wt% and (d) 6 wt% SMA8

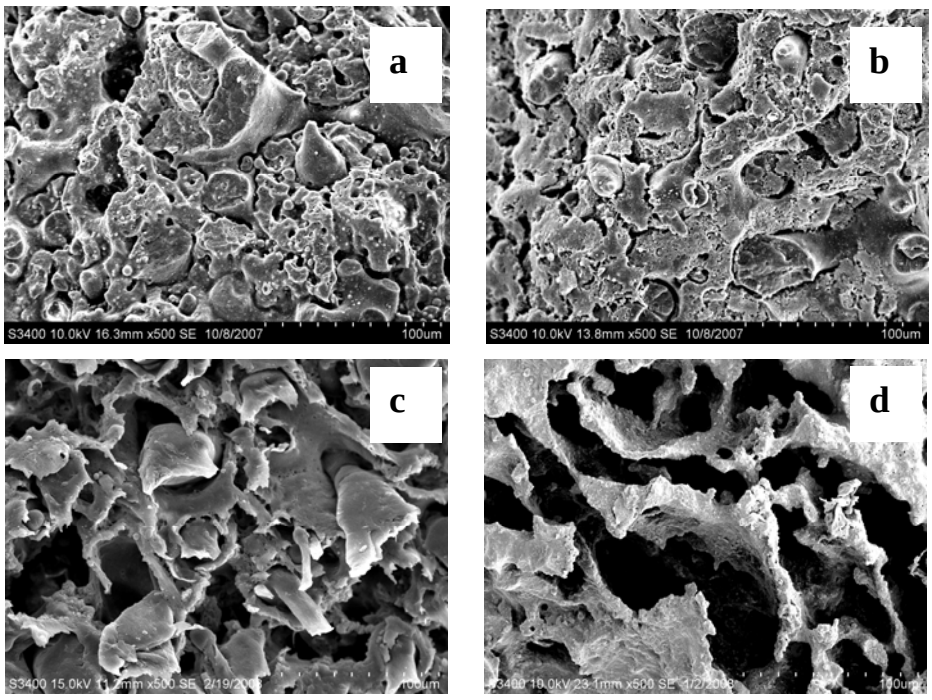

Fig.3 Co-continuous morphology of 40/30/30 PA6/PP/ABS ternary blends in which (a) ABS phase, (b) PP phase, (c) PA6 phase and (d) PP and ABS phases have been extracted

Blends of unsaturated polyester resin with maleated HTPB

Neethumol Varghese[1], Jenish Paul[2] and A. Benny Cherian[1]

1- Department of Chemistry, Union Christian College,Aluva
2- Polmer Science &Rubber Technology, CUSAT

Email: vavuty84@gmail.com

ABSTRACT

Unsaturated polyester resin is widely used in the fibre reinforced plastic industry. The fracture toughness and impact resistance of rigid unsaturated polyester can be improved by the incorporation of functional elastomers like hydroxy terminated polybutadiene (HTPB). HTPB is further funtionalised by maleic anhydride grafting. The maleated HTPB is then blended with polyester resin. Maleic anhydride graft HTPB is found to increase toughness substantially without seriously affecting tensile and flexural properties.

INTRODUCTION

Unsaturated polyester resin (UPR) is used extensively as a matrix for fibre- reinforced plastic (FRP). The wide spread use of the resin is due to its low cost, ease of processing, its ease of combination with reinforcements, rapid cure, excellent dimensional stability and ease of colouring and modification for special purpose. Carothers was the first to prepare UPR[1].

When cross-linking is initiated with the help of a catalyst and an accelerator styrene facilitates cross-linking at the sites of unsaturation in the polyester chains. The saturated acid reduces the number of cross-linking sites and consequently the cross-link density and brittleness of the cured resin. Since cross-linking occurs via free radical addition mechanism across the double bonds in the polyester chain and the reactive diluent, no volatiles are given off during cure. When cross-linking is initiated with the help of a catalyst and an accelerator, styrene forms polystyrene chains, which cross-link the polyester chains at the sites of unsaturation[2].

The broad objective of the work is (i) to study the effect of addition of hydroxy terminated polybutadiene (HTPB) and maleic anhydride graft hydroxy terminated polybutadiene (MA-g-HTPB) on the properties of polyester resin (ii) to investigate the optimum concentration of functional rubbers and (iii) to identify the functional rubber, which give optimum properties.

EXPERIMENTAL

Materials

GP grade UPR (Bakelite Hylam resin HSR 8113 M), styrene, methyl ethyl ketone peroxide (MEKP) and cobalt naphthenate were supplied by Sharon Engineering Enterprises, Cochin. HTPB (Mn=2620) was obtained from Vikram Sarabhai Space Centre, Thiruvananthapuram. MA and benzoyl peroxide were supplied by E. Merck India Ltd, Bombay.

Modification of UPR with HTPB

Unmodified resin was first cured at room temperature by the catalyst MEKP and by the accelerator cobalt naphthenate. These were used in concentrations of 0.5 % and 1 % of the

weight of the resin respectively to obtain a reasonable gel time. The resin was then poured into the tensile mould. Samples for impact test and flexural strength were cast separately in appropriate moulds. Curing was done at room temperature for 24 hrs, followed by post curing at 80^0C for 3 hrs

The blends were prepared by the following procedure. Varying amounts (0-5 wt %) of the HTPB were added to the resin. The mixture was stirred well using a mechanical stirrer to give a homogeneous liquid. Curing of the blend was done as per the procedure employed for UPR. Thereafter, post curing was done at 80^0C for 3 hrs.

The samples after post curing were tested for tensile strength, elongation at break, modulus, flexural strength and flexural modulus taking six trials in each case. The tensile and flexural properties were tested on a universal testing machine (ASTM D 638-89).

Modification of UPR with MA grafted HTPB

Maleated HTPB is prepared by mixing HTPB with 5% MA and 0.5% benzoyl peroxide in a Brabender at 100^0C and 50 RPM speed for 10 min. The reaction of MA with HTPB was confirmed by FTIR spectroscopy and titration. The amount of maleic anhydride reacted is determined by refluxing a solution of maleated HTPB in xylene saturated with water for 1 hr and then titrating with a solution of 0.05N ethanolic KOH using 1 % thymol blue as an indicator.

Varying amounts of MA modified HTPB containing 0-5 weight percentage of elastomers were blended and cast with the UPR by the same procedure adopted earlier. The tensile and flexural properties and water absorption were determined in accordance with ASTM standards.

Test methods

Tensile testing

Tensile tests were carried out according to ASTM D 638-89 using a universal testing machine.

Flexural properties (ASTM D 790-99*)*

Flexural strength is a measure of the load required to break a material when it is subjected to bending Flexural modulus is the ratio of stress to corresponding strain and is expressed in MPa. It is calculated by drawing a tangent to the steepest initial straight line portion of the load- deflection curve

Water absorption

Water absorption of the sample was measured according to ASTM 570-81.

RESULTS AND DISCUSSIONS

Mechanical Properties of UP resin modified by Functional elastomers

Tensile Properties

Referring to Fig.1, tensile strength values obtained by adding HTPB were significantly higher than that obtained by adding maleated HTPB. Tensile strength values reached a maximum on adding progressively larger amounts of HTPB, but addition of more rubber beyond this point resulted in a reduction of tensile strength. The improvement in tensile strength,

in comparison to that of the base resin was due to the high degree of compatibility arising from the polar groups of HTPB and UPR. The tensile strength of maleated HTPB blends gradually decreases on adding progressively larger amounts of rubber due to the higher flexibility of maleated HTPB.

The elongation at break increases with increase in elastomer concentration as shown in Fig.3. The addition of MA-g-HTPB produced the greatest increase in elongation at break compared to HTPB due to the higher flexibility and compatibility of maleated HTPB. The elongation at break of MA-g-HTPB/UPR is about 219 % of UPR

The energy absorption of the cured resin as a function of rubber concentration is shown in Fig.4. At 3-wt % MA-g-HTPB concentration, the energy absorption of the blend was at a maximum (about 305 % of the energy absorption of UPR). The energy absorption is related to the toughness of the sample. Higher elongation at break values increases the toughness of MA-g-HTPB. The performance of MA-g-HTPB was far superior to HTPB, due to better dispersion of the rubber phase as particles in the continuous polyester phase.

Flexural properties

Fig. 5 shows the variation of flexural strength with rubber content. The flexural strength of MA-g-HTPB/UPR blend decreases with elastomer concentration due to the higher flexibility and compatibility of maleated HTPB.

Water absorption

Water absorption of HTPB and maleated HTPB modified resins is shown by Fig.6. The maleated HTPB has slightly higher water absorption compared to HTPB due to the higher functionalisation.

CONCLUSIONS

The study reveals the effect of incorporating functional elastomers into UPR at low concentrations by a physical method. Toughness and tensile/flexural properties show maximum improvement at about 2-3 wt % HTPB concentrations. Interestingly, the increase in toughness (76 % of the energy absorption of UPR) has been observed with simultaneous increase in tensile and flexural properties for HTPB.

Maleation increases the toughness and elongation at break of HTPB. At 3-wt % MA-g-HTPB concentration, the energy absorption of the blend was at a maximum (about 305 % of the energy absorption of UPR) with marginal lowering of tensile and flexural properties.

REFERENCES

1. W. H. Carothers, *J. Am. Chem. Soc.1929*, 51, 2569,
2. Boeing, H.V., *Unsaturated polyester resin-structure and properties*, Elsevier Publishing Company, Amsterdam,1964.
3. F. J. McGarry, *Rubber in cross- linked Polymers*, Applied Science, London ,1983.
4. C. Fintemann., Polym. Plast. Tec.,1981, 17, 225.
5. A. Pavan, Reports of the 2nd Internat. Conf SIM-Plast. 79, Warsaw,1979, Vol.1, p.28.
6. C. Keith Riew and A.J. Kinloch, Rubber Toughened Plastics, American Chemical Society, Advances in chemistry series 233, Washington DC ,1993.
7. C. Keith Riew, Eds., in Rubber Toughened Plastics, Advances in chemistry series 222, American Chemical Society, Washington DC, 1989
8. G. A. Crosbie and M. G. Phillips, 37th Ann. Conf SPI, Sect. 8.C, 1982
9. Charles B. Arends, Eds., in Polymer Toughening, p-177, Marcel Dekker, Inc. New York, 1996.
10. C.Keith Riew, Rubber Toughened Plastics, American Chemical Society, Washington ,1989.
11. M .J. Owen and R. G. Rose, J. Mat. Sci.,1975, 10,1711.
12. A. Christiansen and J. B. Shortall, J. Mat. Sci.,1976,11,1113.
13. L. Leel, C. K. Riew, and A. R. Seeber, Polymer Mat. Sci. Eng.,1990, 63.
14. J. G. Park and C. E. Pohang, Chan. Eon.lnst. Sci. Tech.,1990, 1.4 (3), 266.
15. D.S. Kim, K. Cho, J.H. Park and C.E Pohang, J. Mat. Sci.,1992, 11(17).
16. Siebert Alan, R.Bertsch, and J. Robert, (B.F. Goodrich Co,), U.S.A,1992,17.
17. L.K. Kostanski, and W. Krolikowski, IPSAT,1985, 12(7).
18. E.H. Rowe, and F.J. McGarry, 35 th Ann. Tech. Conf. SPI, Sect. 18.E, 1980.
19. Yan-Jyi Huang and Chin-Cheng Su, *J. Appl. Polym. Sci.,1995,* 55, 305-342 .
20. A. A. Collyer, *Rubber Toughened Engineering Plastics,*1994,5.7, pp.160.
21. Korb, *J. Proc. Annu. Conf. SPE*,1984, 660.
22. Farmer, E.H. and Wheeler, J., U.S. Patent 2,1940, 227,777 (to British Rubber Producers Research Association), 1940, January 6.
23. Lawson D.F. Hergenrother, W. L. and Matlock M.G. *J. Appl. Polym. S.G.1990,* 39, 2331.
24. Trivedi, B.C. Culbertson, B.M. Maleic Anhydride, Plenum, New York ppt.,1982, 172-3.

Fig. 1 Tensile strength of rubber modified resin as a function of rubber concentration

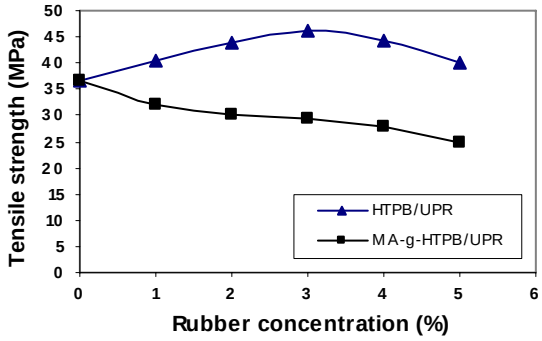

Fig. 2 Modulus of rubber modified resin as a function of rubber concentration

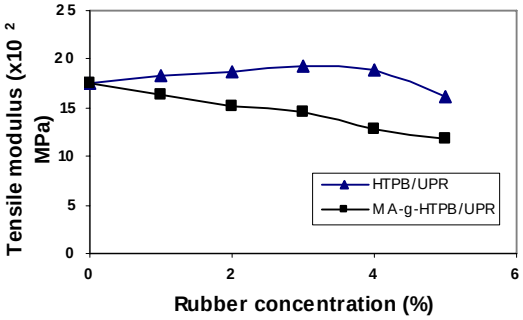

Fig. 3 Elongation at break of rubber modified resin as a function of rubber concentration

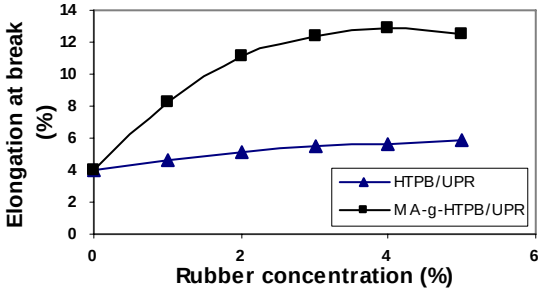

Fig. 4 Energy absorbed by rubber modified resin as a function of rubber concentration

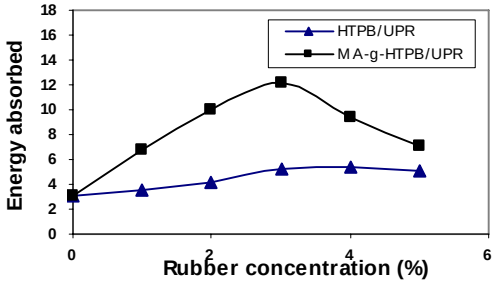

Fig. 5 Flexural strength of rubber modified resin as a function of rubber concentration

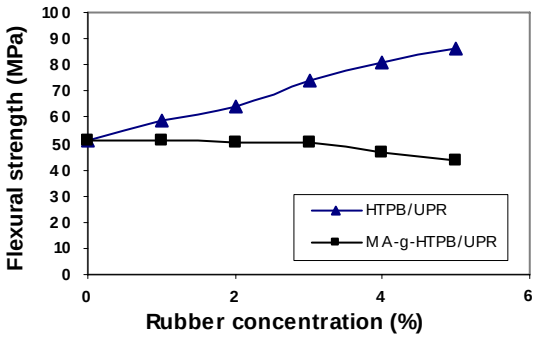

Fig. 6 Water absorption of rubber modified resin as a function of rubber concentration

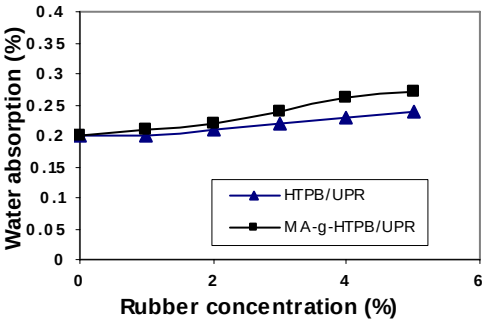

Effect of organic modification on the compatibilisation efficiency of Poly (trimethylene terephthalate) PTT/m-LLDPE blend nanocomposites

Kapil K. Gangele[1], S.Mohanty[2], S.K.Nayak[2*]
Laboratory for Advanced Research in Polymer Materials,
1. Central Institute of Plastics Engineering & Technology, Bhubaneswar-751024, India
2. Central Institute of Plastics Engineering & Technology, Chennai – 600 032, India

Email: drsknayak@yahoo.com

Abstract
Poly (Trimethylene Terephthalate)(PTT) and Metallocene Linear Low density Polyethylene (m-LLDPE) Blends and its Nanocomposites were prepared using melt blending technique in a batch mixer. Organically modified nanoclays; Cloisite 20A(C20A), Cloisite 30B(C30B) and Bentone 109(B109) have been used as nanoscale reinforcement to prepare blend nanocomposites. The blend composition of PTT/m-LLDPE of 70:30 has been optimized based on the mechanical performance. Further, characterization studies such as DMA, DSC/TGA, TEM and WAXD have been investigated to evaluate the effect of incorporation of nanoclays into the blend matrix. WAXD studies revealed a significant increase in of d_{001} spacing of clay galleries in the blend nanocomposites indicating intercalated morphology. From DSC, it was observed that Cloisite 30B with 5 wt. % shows higher crystallization temperature as compared with PTT Virgin and other modified clay systems. Further with the increase in the scanning rate, Crystallization temperature of PTT virgin polymer as well as Nanocomposites decreases. TGA thermograms indicated that the thermal stability of the blend increases with the incorporation of Cloisite 20A. DMA measurements reveal that the Cloisite 30B nanocomposite has maximum modulus as compared to other nanocomposites. It is interpreted from DMA results that PTT/m-LLDPE blend is immiscible blend due to observation of two peaks and shifting of Tg outward. Nanocomposites show higher tensile strength and modulus as well as flexural strength and modulus as compared to optimized blend. The Effect of m-LLDPE content on the mechanical properties of PTT has also been investigated. It is found that m-LLDPE functions as impact modifier to enhance the impact properties of neat PTT and prepare rubber-toughened blend.

Keywords-: Poly (Trimethylene Terephthalate), Polymer Blend and Nanocomposites

Introduction
Poly (Trimethylene Terephthalate) (PTT), aromatic polyester prepared by polycondensation reaction between propane 1, 3 diol and terephthalic acid or dimethyl Terephthalate, has gained commercialization over the last years. PTT has become a potential competitor of PET and PBT for various emerging applications in fibers, packaging, and films and as engineering thermoplastic [16]. PTT combines the mechanical properties of PET and processing characteristics of PBT, thus possessing the desired attributes of thermoplastic polyester, wherein the properties such as dimensional stability, solvent and abrasion resistance are pre-requisite. The polymer has very good tensile strength, elastic recovery and surface properties; together with relatively low melt temperature, good chemical resistance and rapid crystallization rate. However, certain impediments such as low toughness, low heat distortion temperature, low viscosity, poor optical properties and pronounced low temperature brittleness have restricted the optimum use of PTT, as engineering plastic in many applications. Several attempts have already been made by various researchers to increase the toughness of PTT by blending it with ABS [25], EPDM [26] and EOC [27]. In the present investigation, mechanical, thermal and morphological

characterization of PTT/m-LLDPE blend nanocomposites at variable weight percentages of organically modified nanoclay have been studied.

Experimental

Materials

PTT (Futura CPTT®) was purchased from M/s Futura Polymers Ltd., India, having density 1.3 g/cm^3 and intrinsic viscosity 0.915 dL/g (Phenol/Carbon Tetracholride, 60/40). m-LLDPE (Relene®) was obtained from M/s Reliance Industries Ltd., India having MFI 1.0 g/10 min. The clay minerals used were: Cloisite®20A (C20A) Cloisite®30B, (C30B), obtained from M/s Southern Clay Products Inc, USA, and Bentone®109 (B109) from M/s Elementis Ltd. UK. Prior to blending, PTT was dried at 110^{0}C for 24 hours and all the nanoclays were dried at 80^{0}C for 4 hrs.

Preparation of blend and blend nanocomposites

PTT/m-LLDPE blend of various composition (90/10, 80/20, 70/30, 50/50 by weight) were prepared using a Torque Rheocord-9000 (HAAKE®, Germany), at a screw speed of 70 rpm and temperature of 250 °C for a duration of 6 minutes. m-LLDPE was added to the molten PTT after 3 minutes. The blend composition was optimized at 70: 30 ratio of PTT : m-LLDPE. This blend composition was maintained for preparation of polymer blend nanocomposites using various nanoclays C20A, C30B and B109 at variable weight percent (1-5 wt. %). Specimens were prepared using mini Injection molding machine (HAAKE® Minijet) at 245^{0}C barrel temperature, 840-870 bar injection pressure and mold temperature of 110 ^{0}C as per ASTM standard.

X-ray Diffraction Analysis

The interlayer gallery spacing of nanoclays in the nanocomposites was studied by wide angle Philips X'Pert MPD (Japan)X-ray diffraction at ambient temperature.

Transmission Electron Microscopy (TEM)

For TEM observation, the samples were stained with OsO_4 vapor and microtomed at low temperature (-55^{0}C) and examined using a Transmission Electron Microscope (Philips CM12, The Netherlands) an acceleration voltage of 100 kv at 100nm scale.

Mechanical Properties

Tensile & Flexural Properties were determined using Universal Testing Machine (UTM), LR-100K (Lloyd Instruments Ltd. U.K as per ASTM-D 638 & ASTM-D 790. Izod impact strength was determined as per ASTM D 256.

Dynamic mechanical Analysis

The dynamic mechanical analysis of was investigated using DMA242 analyzer (NETZSCH, Germany). at fixed frequency of 1Hz, heating rate of 10K/min, under N2 atmosphere over a temperature range of -150^{o}C to 200^{0}C in three point bending mode.

Thermal analysis

DSC & TGA measurements were performed on a diamond DSC (Perkin Elmer Inc., USA) Pyris – 7 TGA equipment (Perkin Elmer Inc., USA).

Results and Discussion

X-Ray diffraction analysis

The state of dispersion of the silicate layers in the blend matrix have been investigated using X-ray diffraction patterns represented in the figure-1. The mean interlayer spacing of plane (d_{001}) of C30B was 4.01nm.In case of the 70PTT/30m-LLDPE/5C30B hybrid, the characteristic peak shifted to a smaller angle corresponding to d_{001} spacing of 4.01 nm, because of intercalation of both polymer chains into silicate galleries [37]. A similar shifting of angles was also observed in PTT/m-LLDPE/B109 to 4.02 nm and PTT/m-LLDPE/C20A to 4.06^0 nm nanocomposites system respectively revealing the formation of intercalated structure. Furthermore, it was also noticed that the X-ray diffractograms in all the blend nanocomposites system reveals diffraction peak in the similar range of 2.205^0. However, peak intensity of

original C30B, C20A increased significantly that probably due to more parallel stacking of the organoclays in the blend matrix**.**

Transmission electron microscopy (TEM)

To elucidate the dispersion of clay in the blend nanocomposites in detail, figure-2 illustrates the TEM micrographs of PTT/m-LLDPE/C20A, PTT/m-LLDPE/B109 and PTT/m-LLDPE/C30B. The dark lines represent the thickness of individual clay layers or agglomerates. Thick darker lines represent stacked silicate layers due to clustering or agglomeration. It was observed from the micrographs that clay particles preferentially resided in the PTT phase rather than m-LLDPE phase. In case C30B blend nanocomposites, it was found that stacked and intercalated silicate layers are well dispersed within the blend matrix especially in polar phase due to similar solubility parameter. It was interesting to note that the organoclay has a strong tendency to be located in the PTT phase and the domain size of dispersed particle effectively reduced, due to obstacle created by exfoliated clay, as shown in figure: 2(b) and(c). However, a mixed nanomorphology was obtained in both PTT/m-LLDPE/C20A as well as PTT/m-LLDPE/B109 nanocomposites due to presence of regions of ordered /disordered intercalation.

Mechanical Properties of Polymer Blend and Blend nanocomposites

The mechanical properties of PTT/m-LLDPE blend at variable weight percent (1-5 wt%) of m-LLDPE are depicted in table-1. It is evident that the tensile & flexural properties of PTT decreases with the increase in m-LLDPE content. This behavior is probably because m-LLDPE is inherently weak and soft with elastomeric properties due to linearity in its structure with 5-10% branching. Izod impact strength of PTT was observed to be 26.80 J/m. Incorporation of m-LLDPE to the tune of 10-30% results in an increase in the impact properties of PTT matrix in the blends. The blend prepared at PTT: m-LLDPE ratio of 70:30 exhibits maximum impact strength of 33.76 J/m, which subsequently reduces with the increase in PTT content to 50-wt%. This indicates that m-LLDPE acts as impact modifier due to presence of metallocene and butene in its structure, at lower concentrations. The blend prepared at 70:30 ratio of PTT: m-LLDPE has been optimized based on optimum impact performance and has been considered for fabrication of blend nanocomposites using various organically modified nanoclays.

The mechanical properties of PTT/m-LLDPE blend nanocomposites at various wt.% of organically modified is also depicted in table-1. It is evident that a tensile property of blend increases with addition of 5 wt% of C20A, B109 and C30B nanoclays. Tensile strength of blend matrix increases from 37.92 MPa to 50.86 MPa in PTT/m-LLDPE/C20A, 53.24 MPa in PTT/m-LLDPE/C30B and 51.36 MPa in PTT/m-LLDPE/B109 blend nanocomposites respectively at 5 wt. % of nanoclay loading, which indicates stiffening effect of nanoclay layers. A similar linear increase in tensile modulus to the tune of 52.1 % in C20A, 61.5 % in C30B and 57.4 % in B109 respectively was also obtained as compared with the blend matrix. According to Via and co-workers [38], the interlayer structure of the organically modified layered silicate should be optimized to attain maximum configurational freedom of the functionalzing chains upon layer separation and increase the potential reaction sites at the interlayer surface. In the present context, the methyl tallow bis-2 hydroxy ethyl quaternary ammonium intercalant in C30B has two –OH groups in its structure, which might have interacted with the carboxylic group of PTT resulting in enhanced polar-polar interactions of the silicate layer within PTT phase which further contributes to an increase in tensile properties. A similar increase in the flexural & impact strength of blend nanocomposites was also obtained. The mechanical performance of the blend matrix varies in the following order:

PTT/m-LLDPE/C30B > PTT/m-LLDPE/B109 > PTT/m-LLDPE/C20A > PTT/m-LLDPE.

This further indicates improved interactions in C30B system as compared with C20A and predominant role of PTT base matrix.

Dynamic mechanical properties (DMA)

The dynamic storage modulus (E') versus temperature of PTT, PTT /m-LLDPE blend and blend nanocomposites are shown in the figure-3. A gradual decrease in E' with increasing temperature from -150 to 200^0C was observed. It was noted that incorporation of m-LLDPE decreased the storage modulus of PTT matrix due to softening of diluting effect of the soft elastomeric phase. Conversely, addition of

organoclay into the blend matrix results in a remarkable increase in the storage modulus over the entire investigated temperature range. The blend nanocomposites prepared using C30B organoclay displays optimum E' as compared with the other blend nanocomposites

Differential Scanning Calorimetry (DSC)

The DSC thermogram of virgin PTT, virgin m-LLDPE, 70PTT/30m-LLDPE blend and the blend nanocomposites is depicted in figure-4. Virgin PTT depicts a melting transition around 247.59^{0}C with m-LLDPE at 127^{0}C.The DSC scan of the blend reveals two distinct T_m which indicates phase-separated morphology. Similar to the blend, the DSC curves of the blend nanocomposites also exhibited two distinct T_m's confirming presence of a phase-separated morphology. However, incorporation of organically modified nanoclays increases the Tm of the PTT phase in blend matrix, while reducing the Tm of the m-LLDPE phase. This indicates improved compatibility of nanoclay in the PTT matrix. The crystallization exotherms of virgin PTT, PTT/m-LLDPE blend and blend nanocomposite system is shown in figure-5. It is evident that the T_c of PTT matrix decreases from 175.47^{0}C to 170.40^{0}C with incorporation of m-LLDPE indicating elastomeric effect due to amorphous nature and low spherulitic growth of m-LLDPE. However incorporation of nanoclay increases the T_c of PTT phase in the blend matrix considerably indicating heterogeneous nucleating effect.

Thermo gravimetric analysis (TGA)

Virgin PTT exhibits an initial degradation temperature (T_{id}) of 352.12^{0}C with final degradation temperature (T_{fd}) 503.47 ^{0}C (Figure 6).Incorporation of m-LLDPE decreases T_{id} of matrix from 352.12^{0}C to 345.97 ^{0}C and Tfd of matrix from 503.47 ^{0}C to 495.90 ^{0}C.This is predominantly attributed to lower degradation temperature of ethylene linkage due to weak bonding between them and presence of side chain branching (5-10%) in m-LLDPE. Further addition of organoclays substantially increases the thermal stability (T_{id}, T_{fd}) of the blend matrix. Blend nanocomposites with C20A organoclay has highest thermal stability due to higher modifier concentration and gallery spacing.

Conclusion

The mechanical, thermal, crystallization and morphological characteristics of PTT/m-LLDPE blend and its nanocomposites prepared through batch mixing process were investigated. The impact strength of PTT increased up to 30 wt% loading of m-LLDPE. The blend nanocomposites prepared using C30B shown maximum mechanical performance. XRD results showed intercalated structure in the elastomer modified PTT organoclay nanocomposites DSC & DMA analysis revealed two phase morphology in the blend system. TGA thermograms indicated increased thermal stability of PTT matrix in the blends with the addition of nanoclays.

References

1. Mishra S.P.; Deopure L.; *Polym.Bull*; 1985:26:5.
2. Yu Y.; Choi K. ; *Polym. Eng. & Sci* 1997: 37: 91.
3. Nabisaheb D; Jog J.P., J. *Polym. Sci: part-B: Polym Phy*. 1999: 37: 2439.
4. Avramova N. *Polym* 1995: 36: 801.
5. Wfer J., M. US pat. 4,485,212 (1984)
6. Pratt C.F., Phadke S.V., Olivier E., U.S.Pat. 4,965,111 (1990)
7. Khatua B.B.; Lee D.J.; Kim H.Y.; Kim J.K.; *Macromolecules* 2004:37:2454-59.
8. Ray S.S.; Bousmina M.; *Macromol. Rapid Commun*., 2005:26:1639-46.
9. Lim J.W.; Hassan A.; Rahmat A.R.; Wahit M.U. *Polym Int* 2006:55:204-15.

Table 1: Mechanical properties of PPT/m-LLDPE blends and its Nanocomposites

Compositions	Tensile Strength (MPa)	Tensile Modulus (MPa)	Flexural Strength (MPa)	Flexural Modulus (MPa)	Impact Strength (J/m)
PTT Virgin	48.20	1420	58.80	2670	26.80
PTT/m-LLDPE (90/10)	45.32	1092.3	55.92	2342	31.22
PTT/m-LLDPE (80/20)	41.08	984.33	52.70	2180	31.22
PTT/m-LLDPE (70/30)	37.92	933.41	49.81	2028	33.76
PTT/m-LLDPE (50/50)	32.27	866.52	43.61	1816	31.11
PTT/m-LLDPE(70/30)/C20A5%	50.86	1422	61.73	2695	37.23
PTT/m-LLDPE 70/30)/C30B5%	53.24	1507	63.77	2810	39.88
PTT/m-LLDPE(70/30)/B109 5%	51.36	1470	62.12	2752	33.76

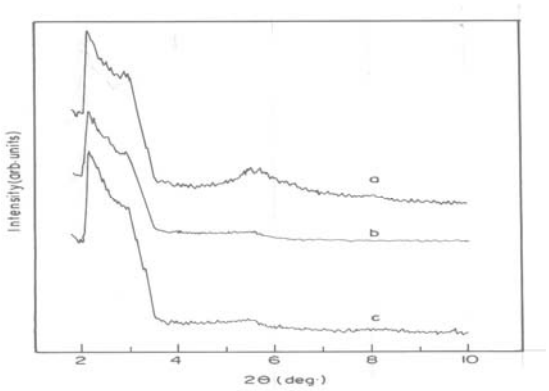

Figure: 1- XRD pattern of (a) PTT/m-LLDPE/C30B5 %(b) PTT/m-LLDPE/B109, 5 %(c) PTT/m-LLDPE/C20A5%

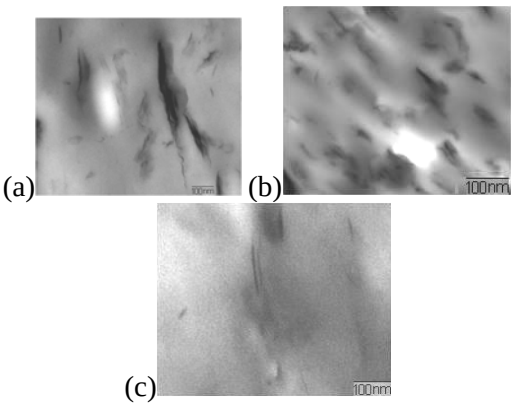

Figure: 2 TEM micrographs of (a) PTT/m-LLDPE/C30B 5% (b) PTT/m-LLDPE/C20A 5% (c) PTT/m-LLDPE/B109, 5%

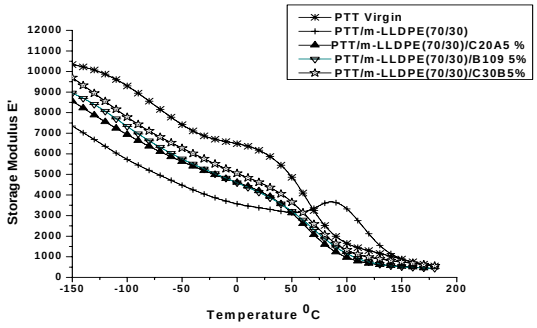

Figure 3: Temperature dependence of Storage modulus (E') blend and nanocomposites at 5% loading of nanoclay

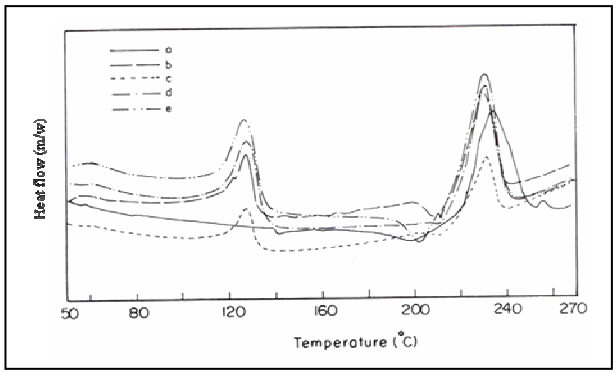

Figure: 4 - DSC thermogram of(a)PTT virgin (b) PTT/m-LLDPE(70/30) (c)) PTT/m-LLDPE(70/30)/C20A 5% (d) PTT/m-LLDPE(70/30)/B109 5% (e) PTT/m-LLDPE(70/30)/C30B 5%

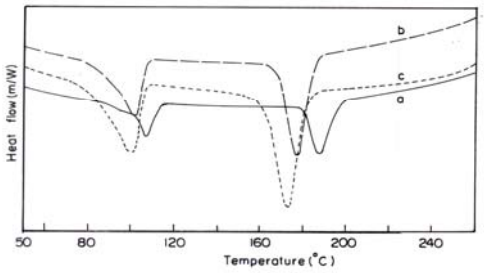

Figure: 5 - DSC cooling thermogram of (a) PTT/m-LLDPE(70/30)/C30B 5% (b)PTT/m-LLDPE(70/30)/B109 5% (c) PTT Virgin

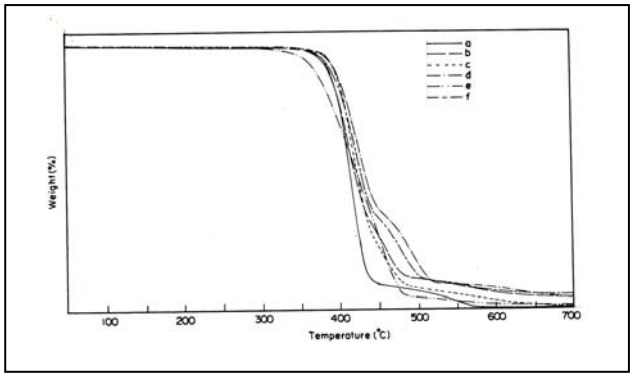

Figure: 6-TGA graph of (a) Virgin PT(b) m-LLDPE Virgin (c) PTT/m-LLDPE (70/30) (d) PTT/m-LLDPE (70/30)/C 20A5% (e) PTT/m-LLDPE (70/30)/B109,5% (f) PTT/m-LLDPE (70/30)/C 30B5%

Mechanical and rheological behavior of peroxide cured polypropylene (PP)/ethylene octene copolymer (EOC) thermoplastic vulcanizates (TPVS)

R.Rajesh Babu*, Nikhil K Singha and Kinsuk Naskar[#]
Rubber Technology Centre, Indian Institute of Technology,
Kharagapur -721302, India
E.mail: knaskar@rtc.iitkgp.ernet.in

Abstract

Technologically compatible binary blends of polypropylene (PP) and ethylene octene copolymer (EOC) were dynamically vulcanized by coagent assisted peroxide crosslinking system. Addition of peroxide in PP/EOC blend involves two major competing reactions: EOC cross-linking and PP degradation by β-scission. Final product properties are thus dependent on the balance among those two competing reactions. As the concentration of peroxide increases, particle size decreases. However, mechanical properties of these TPVs are not good enough, which is due to severe degradation in the PP phase in the presence of peroxide. Principally, coagent incorporation increases the crosslinking efficiency in the EOC phase and decreases the degradation in the PP phase. Present study focus on the influence of the three structurally different coagents namely triallyl cyanurate (TAC), trimethyol propane triacrylate(TMPTA) and N,N'-m-phenylene dimaleimide(HVA-2) on the mechanical and rheological properties of the PP/EOC thermoplastic vulcanizates (TPVs). Depending on the structure and reactivity, different coagents show different performance. All the compositions were prepared by melt mixing method in the Haake rheomix at 180°C and rheological properties also have been evaluated at the same temperature. Viscoelastic behaviors of the TPVs prepared were analyzed by a dynamic oscillatory rheometer in the melt state in Rubber Process Analyzer (RPA 2000). Morphologically TPVs consist of dense crosslinked rubber domains in the thermoplastic phase and their rheological behavior can be compared to that of highly filled polymers. The crosslinked particles tend to agglomerate and build local cluster which tends to disintegrate by shearing. A variety of rheological observations such as Payne effect, modulus recovery and shear rate sensitivity were studied by carrying frequency sweep and strain sweep.

Introduction

Thermoplastic vulcanizates (TPVs) are prepared by dynamic vulcanization process, where crosslinking of the elastomeric material takes place during its melt mixing with a thermoplastic material under high shear and temperature. Temperature should be high enough to activate and complete the process of vulcanization. The resulting morphology consists of micron sized finely dispersed cross-linked rubbery particles in a continuous thermoplastic matrix although the rubber content is higher than the thermoplastic component. The rheological behavior can be compared with that of highly filled polymers. TPVs have proven themselves to perform in a wide range of demanding engineering requirements mainly in automobile sectors. Several crosslinking agents are used in the preparation of TPVs such as phenolic resin, peroxide and silane crosslinking system. Phenolic resin gained considerable commercial importance but still the formation of black specks motivates the development of other potential crosslinking system. In this particular polypropylene (PP)/ ethylene octene copolymer (EOC) blend system; phenolic resin is ineffective, since the latter needs the presence of double bond to form a crosslinked network structure. Peroxides can crosslink both saturated and unsaturated polymers without any reversion characteristics. The formation of strong C-C bonds provides substantial heat resistance and good compression set property without any discoloration. It has been well established that

polypropylene exhibits β-chain scission reaction (degradation) with the addition of peroxide. Hence the use of only peroxide is limited to the preparation of PP based TPVs. An alternative approach is to use coagent together with peroxide curing system. Generally coagents are multifunctional vinyl monomers which are highly reactive towards free radicals either by addition reaction and/or by hydrogen abstraction. Chain scission also could be retarded by stabilizing the PP macroradicals by addition reaction across the double bond in the vinyl monomer (coagent). Hence addition of coagent in the PP/EOC blend increases the crosslinking efficiency in the EOC phase and decreases the extent of degradation in the PP phase. Different coagents have different reactivity and efficiency in terms of increasing the degree of crosslinking and decreasing the extent of degradation. The main objective of the present investigation is to study the influence of three structurally different coagents as a function of concentration on the dicumyl peroxide cured PP/EOC TPVs in terms of mechanical and rheological characteristics.

Experimental

Materials - The general purpose polyolefin elastomer Exact 5371 (specific gravity,0.870 g/cc at 23 °C; co-monomer octene content 13 %; melt flow index,5.0 @190 °C/2.16 Kg), was commercialized by Exxon Mobil Chemical company, USA. Polypropylene (Specific gravity, 0.9 g/cc at 23 °C; melt flow index, 3.0 @ 230 °C/2.16 Kg) was obtained from IPCL, India. Dicumyl peroxide (DCP) (Perkadox-BC-40B-PD) having active peroxide content of 40 %; temperature at which half life time ($t_{1/2}$) is 1 hour at 138°C; specific gravity of 1.53 g/cm^3 at 23 °C) was used as the crosslinking agent obtained from Akzo Nobel Chemical Company, The Netherlands. Three different types of coagents, Triallylcyanurate (TAC), Trimethylol propane triacrylate (TMPTA), N,N'-m-phenylene dimaleimide (HVA-2) were used as boosters for DCP-cured TPVs, were obtained from Sartomer Company, USA.

Preparation of PP/EOC TPVs - The TPV compositions employed are shown in Table 1. The experimental variables are the type and concentration of different coagents. All TPVs were mixed by a batch process in a Haake Rheomix 600 OS internal mixer, having a mixing chamber volume of 85 cm^3 with a rotor speed of 80 rpm at180°C. Immediately after mixing, passed once through a cold two-roll mill to achieve a sheet of about 2 mm thickness. The sheet was cut and pressed in a compression molding machine (Moore Press, Birmingham, UK) at 200°C, 4 min and 5 MPa pressure. The sheet was then cooled down to room temperature under pressure. Different coagents not only differ in molecular weight but they also have different relative functionality. Hence in order to compare different coagents, concentration employed should be in terms of milliequivalents.

Testing Procedure - Tensile tests were carried out according to ASTM D412-98 on dumb-bell shaped specimens using a universal tensile testing machine Hounsfield H10KS at a constant cross-head speed of 500 mm/min. Tear strength were carried out according to ASTM D-624-81 test method using un-nicked 90° angle test piece. Phase morphology of the cryo- fractured and etched samples was investigated by a JEOL JSM 5800 Digital Scanning Electron Microscope (SEM). Melt rheology of the blend components were studied in Rubber Process Analyzer (RPA 2000, USA). Each samples underwent the following test in sequence and in this order: frequency sweep (FS), strain sweep (SS) followed by relaxation period of 5 mins, frequency sweep, and strain amplitude sweep. Frequency sweep was logarithmically increased from 0.05 to 32 Hz at 6.95 % strain, which was selected to ensure that the dynamic moduli are measured in the linear viscoelastic region. For the strain sweep, amplitude ranges from 1 – 1250 % at 180°C with a constant frequency of 0.5 Hz. The sample relaxation was monitored by observing the decrease in shear rate with time.

Results and discussion

Mechanical properties

In order to understand the effectiveness of various coagents in the PP/EOC TPVs, it is necessary to understand the performance of different coagents only in the EOC compound (without PP). The reactivity and efficiency of different coagents were characterized by cure study on gum EOC vulcanizates. Figure 1 shows the rheographs of peroxide cured EOC vulcanizates containing various coagents at 20 meq concentration and compared with the control sample (without addition of any coagent). Irrespective of different coagents taken for the investigation, a considerable improvement in the maximum torque (Max S) and delta torque (Max S - Min S) values were inferred upon addition of coagent. This is mainly due to the improved crosslinking efficiency of DCP in presence of coagent. It is clear from the Figure-1 that, TAC shows the higher torque values followed by HVA-2 and TMPTA. Mechanical properties of the TPVs prepared by three different coagents with varying concentration were summarized in the Table 1. Mechanical properties are considerably improved by the dynamic vulcanization process. It is clear from the result that blend properties are sensitive to the type of coagents. Among the coagents used, HVA-2 shows the best overall balance of mechanical properties. TPVs prepared using HVA-2 as coagent, exhibit gradual increase and provide superior tensile strength, modulus, and tear strength values relative to the other coagents used. It is expected that HVA-2 can act as a reactive compatibiliser as well as crosslinking agent in this particular blend system. It has been previously reported that HVA-2 can act as a reactive compatibiliser in the NR-PP blend system. It generates a low degree of crosslinking in the NR phase and forms a block or graft copolymer in the NR-PP interface. It is clearly seen that, TMPTA shows lower delta torque value and there by exhibiting higher elongation at break. TAC shows the lowest value and HVA-2 shows the intermediate value of elongation in TPVs. It was generally accepted that a low crosslink density compound is indeed accompanied with the higher elongation at break. Since HVA-2 can act as a crosslinking agent as well as a compatibilising agent, where crosslinking decreases the elongation and compatibilisation increases the same. In this case both the effects are very sensitive in determining the final elongation at break.

Morphology

A SEM photomicrograph of the PP/EOC TPVs, in which PP phase was preferentially extracted by etching with hot xylene, is given in Figure 2. Qualitatively it shows crosslinked EOC particles are dispersed throughout the PP matrix (droplet and matrix morphology). Since EOC content is more than PP, the particle-particle association is strong to form aggregates and these aggregates can agglomerate. The crosslinked rubber aggregates are embedded in the PP macromolecules via joint shell mechanism and/or segmental interdiffusion mechanism.

Rheological properties

In the solid state, the properties of the TPVs are determined by the matrix molecular weight (which has a direct consequence on the percent crystallinity and entanglements density), extent of crosslinking, degree of dispersion, size and deformability of dispersed phase as well as morphology persist. In the melt state, changes in the morphology originating from matrix molecular weight (crystallinity) can be excluded and the influence of other factors can be studied. The rheological properties of 50/100 PP/EOC TPVs prepared by three different coagents are represented in Figures 3 to 6. Dynamic vulcanization blends show improved dynamic modulus and viscosity values (dynamic functions) than uncured blends. As expected, addition of coagent further improved the dynamic functions than the control one. Among the coagents, HVA-2 shows better dynamic functions and more nonlinear behavior followed by TAC and TMPTA. At equal formulation volume fraction, smaller particles can impart greater viscosity and more nonlinear

behavior. Here two possible effects can account: particle size reduction by improvement in interfacial tension cause rise in viscosity and these small particles have higher tendency to agglomerate or aggregate, which results in more nonlinear behavior. In other words, presence of secondary clusters increases the viscosity and enhances the viscoelastic nonlinearity.

Payne effect: For a constant frequency, with increasing the strain amplitude dynamic storage modulus decreases. In general, the decrease in dynamic functions (nonlinearity) is related to the disintegration of secondary structures. Indeed it may also relate to the bonding and debonding of dispersed phase from the matrix phase. TPVs show more progressive nonlinear behavior i.e, decrease of dynamic functions with increasing strain amplitude is observed (Figure 3). In TPVs the secondary structure corresponds to the agglomeration or aggregates of crosslinked EOC particles dispersed in PP matrix. In simple blends the nonlinearity at high strain is due to both the disintegration of entanglement network and debonding of molecules of PP anchored in EOC matrix phase.

Modulus recovery: Another important aspect in the mechanism of nonlinearity in TPVs is restoration of moduli following the large strain amplitude effects. Figure 4 shows the effect of complex modulus on the subsequent strain sweep experiment results. It is clear that only minor effects occurred in modulus values. Furthermore, the critical strain amplitude (where the nonlinearity effect occurs) is slightly moved towards lower amplitude region in the subsequent strain sweep test. It is anticipated that interfacial slippage between crosslinked EOC domains and PP matrix, cause to reduce the linear viscoelastic region.

Frequency dependence of viscoelastic behavior: Dynamic frequency sweep tests were conducted in linear viscoelastic region to further study on network formation and microstructural changes in detail. Figure 5 shows that the frequency (ω) depends of storage modulus (G') in unvulcanized and dynamically vulcanized blends. It is well established that dynamical vulcanization increase storage modulus values especially at low frequency region. As the frequency increases the curves become close to each other. HVA-2 based TPVs show higher values in the entire range of frequency studied. Low frequency improvement in G' indicates strong interaction between crosslinked EOC phase and PP matrix. Polymers are non Newtonian liquids and their viscosity decrease with increasing shear rate. Figure 6 shows the log complex viscosity ($\acute{\eta}^*$) vs log ω. It can be seen that the viscosity is highly sensitive with significant drop at higher shear rate, so the related structure are of pseudoplastic nature. Formation of agglomeration and aggregated structure of dispersed phase may be responsible for the high initial value of complex viscosity. The frequency dependence after the strain amplitude sweep was reproducible confirming that the strain sweep does not significantly deform microstructure and the deformation induced is reversible.

Conclusion

Comparative studies of the mechanical, microstructure and rheological properties were carried out in PP/EOC TPVs prepared by three different coagents. Among the various coagents taken for the investigation, most interesting properties were observed for HVA-2 containing TPVs. It is found to give better solid and melt state properties, which may be attributed to the strengthening of interfacial adhesion between blend components. HVA-2 is shown to effectively behave as a crosslinking agent and compatibilizer for the PP/EOC blend system and thereby improvement is significant.

References

1. Coran, A.Y. In: Thermoplastic Elastomers - A Comprehensive Review; Legge, N. R.; Holden, G. Eds.; Hanser Publisher: Munich, 1987.
2. Naskar, K. Rubber Chem. Technol 2007, 80, 504.
3. Henning, S. K.; Costin, R. Fundamentals of curing elastomer with peroxide and coagents. Paper presented in Spring 167 th ACS technical meeting.

4. Costin, R. Selection of coagents for use in peroxide cured elastomers. Application Bulletin 5519. Sartomer Company, USA.

Table-1 Comparitive physical properties of TPVs prepared by three different coagents

Compound Name	DC0	DC10	DC20	DC30	DA10	DA20	DA30	DM10	DM20	DM30
EOC	100	100	100	100	100	100	100	100	100	100
PP	50	50	50	50	50	50	50	50	50	50
DCP*	3.38	3.38	3.38	3.38	3.38	3.38	3.38	3.38	3.38	3.38
TAC/TMPTA/HVA-2[#]	-	10	20	30	10	20	30	10	20	30
Physical properties	DC0	DC10	DC20	DC30	DA10	DA20	DA30	DM10	DM20	DM30
Tensile strength (MPa)	7.6	9.7	9.3	8.2	10.5	10	11.2	10.6	10.9	11.4
Elongation at break (%)	258	244	180	142	300	300	277	280	254	234
100% Modulus (MPa)	6.6	7.3	7.7	7.5	7.2	7.2	7.7	7.5	7.9	8.4
Tear strength (N/mm)	65	68	72.2	63	80.5	82	64	76.3	87.2	88.1

*Peroxide concentration has been optimized in the previous work at 3.38 phr of DCP corresponds to 5 milliequivalent concentration.
[#]Coagent concentration are in milliequivalent

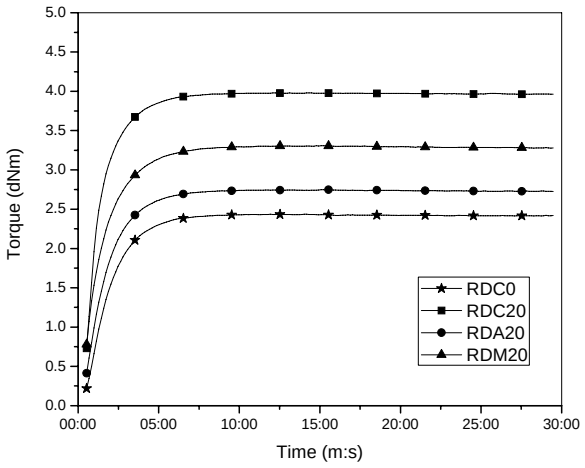

Figure -1: Rheograms of only EOC compound with 20 meq concentration of various coagents at 180°C

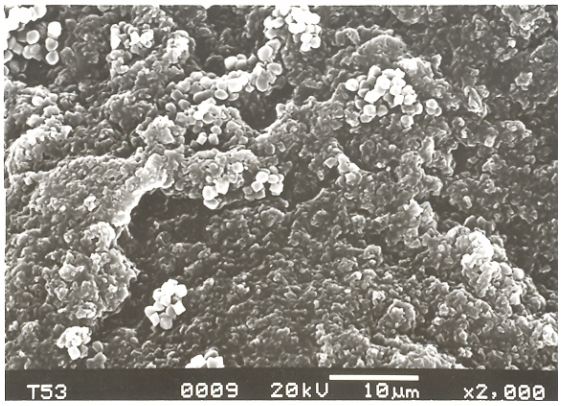

Figure -2: SEM photomicrograph of PP/EOC TPVs (PP phase is preferentially etched)

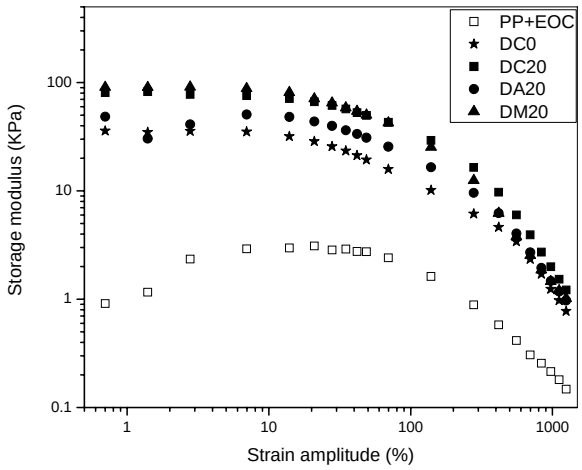

Figure -3: Dependence of G' on strain amplitude at a constant frequency of 1 Hz at 180°C

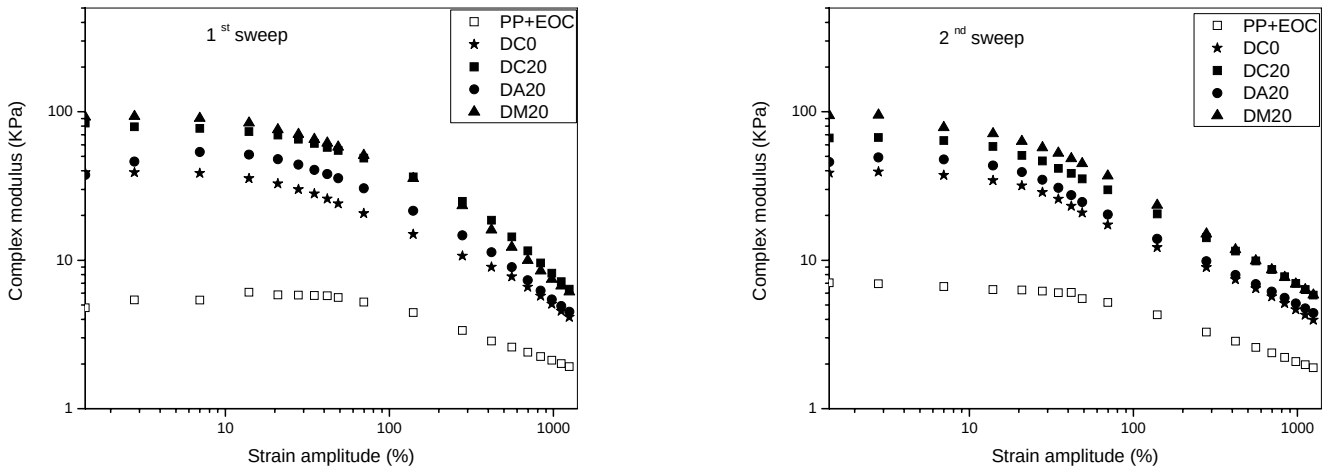

Figure -4: Complex modulus (G*) as a function of strain amplitude at a constant frequency of 1 Hz and 180°C with subsequent strain sweep (1 st seep followed by 2nd sweep after a relaxation time of 5 mins)

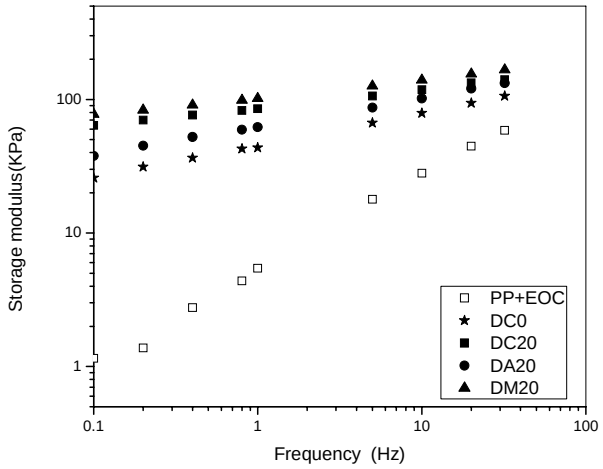

Figure -5: Storage modulus as a function of frequency at low strain amplitude and at 180°C

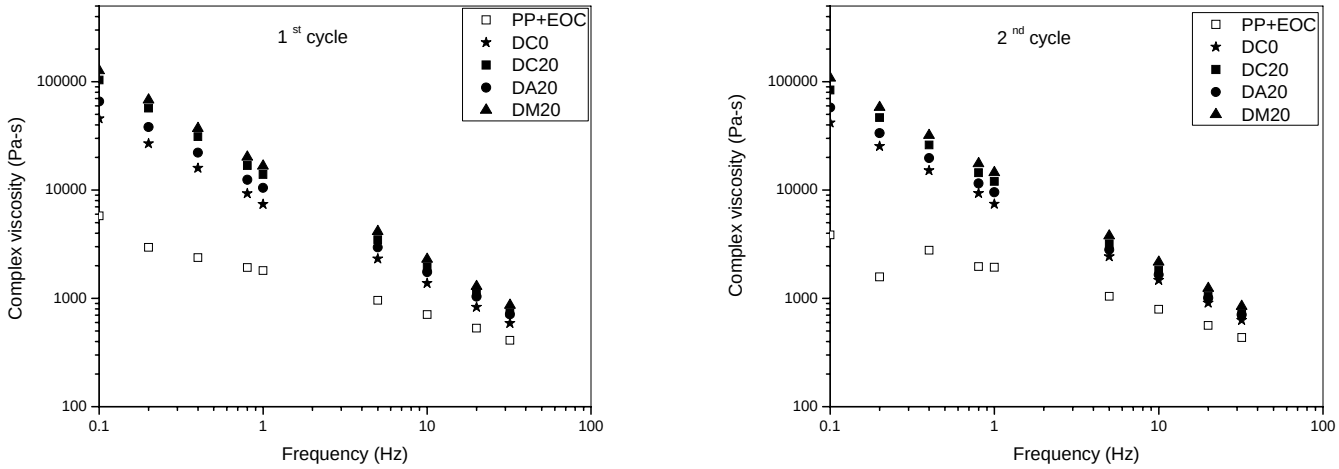

Figure -6: Dependence of complex viscosity (ή*) on frequency at a low strain amplitude and 180°C with subsequent frequency sweep (1 st sweep followed by 2nd sweep after an strain amplitude sweep and a relaxation time of 5 mins)

A comprehensive study on degradation of nano-silica filled model TPE blend systems

S. Chattopadhyay*, S. Hui and T.K. Chaki
Rubber Technology Centre
Indian Institute of Technology
Kharagpur-721302, India
Email: santanuchat71@yahoo.com, santanu@rtc.iitkgp.ernet.in

Abstract:
The effect of nano-silica on the thermal degradation behaviors of LDPE-EVA based thermoplastic elastomeric blends were monitored in nitrogen as well as in oxygen atmospheres using thermo gravimetric analyses (TGA). The pristine silica nano-particles were melt-blended with the LDPE-EVA system at 1.5, 3 and 5 wt% loadings, respectively, by varying the sequence of addition. In one of the compositions, coupling agent Bis-[3-(triethoxysilyl)propyl] tetrasulphide (Si-69) was used to improve the interaction of hydrophilic silica fillers with polymer matrices. In anaerobic condition, no significant changes were observed in terms of thermal stability of such blend systems. However, in oxygen atmosphere, the TGA plots reflected a dramatic change. A two staged degradation were observed for most of the filled samples but in some cases a three staged process were also followed. The changes in the decomposition onset (T_i) and maximum degradation temperatures (T_{max}) were correlated well with the morphology of the filled TPE systems as observed by transmission and scanning electron microscopes. The kinetic rate constants and activation energies were calculated using non-isothermal kinetic analysis. On the whole, it was observed that the thermal stability of TPE blends was a strong function of morphology which in turn was decided by the sequence of addition of ingredients during blend preparation, amount of silica nano-fillers addition and presence of coupling agent.

Introduction
Polymer characterization using the tools of thermal analysis is a useful method in analytical polymer laboratories. The study of degradation and stabilization of polymers is an extremely important area from the scientific and industrial view points. Thermo gravimetric analysis (TGA) is an excellent tool for studying the kinetics of thermal degradation. It is now widely used because of its experimental simplicity and the wealth of information obtained from a simple thermogram [1].

Low density polyethylene (LDPE) and poly (ethylene-co-vinyl acetate) (EVA) and their blends are widely used in the wire and cable industry as insulation sheath or jacket. Recently, several papers have been published dealing with the thermal analysis and thermo-oxidative degradation of different polymer, blends and polymer- nanocomposites. Early studies on the degradation of EVA [2] have been reported that the initial step in the degradation involves the formation of acetic acid and which is enhanced with increasing vinyl acetate content. The second step involves degradation of the main chains with little evidence of interaction between the ethylene and vinyl acetate units. Studies on thermal degradation behavior of EVA/LDPE blend has been studied by Ray et al [3] where pure EVA and its blends similarly show two staged decomposition and the blends exhibit better thermal stability compared to pristine polymers. The thermal degradation behavior of EVA has been studied by several researchers [4-6]. Marcilla [7] has reported that the oxidative pyrolysis of EVA involves four main decomposition steps, and each of them also involves different types of reactions. A study of the degradation of LDPE and an EVA copolymer under air atmosphere, in the presence and absence of mesoporous silicates (MCM-41),

has been carried out using thermogravimetric analysis (TGA) by Marcilla et al [8] focusing on the degradation behavior of EVA.
The thermal degradation mechanisms of poly(vinyl acetate) (PVAc) and EVA copolymers have been investigated by Rimez et al [9]. Thermal properties and flammability of EVA/LLDPE/montmorillonite nanocomposites have been studied by Chuang et al [10].
In this present investigation, an attempt has been made to study the thermal and thermo-oxidative degradation characteristics of this particular nano-silica filled blend system by thermal analysis and to correlate the thermal properties with nano- and micro-scale morphology.

Experimental

Materials
The plastic used for the present work was LDPE - Indothene MA 400 supplied by IPCL, Vadodera, India (0.918 g/cm^3 density, MFI as per ASTM D1238 @ 190^{o}C using 2.16 kg load 30 g/10min melt index). The elastomer used was EVA containing 40% vinyl acetate (EVA-40) (MFI: 3) purchased from Bayer Co., Ltd. (Leverkusen, Germany). Silicon dioxide nano-powder was procured from Aldrich Chemical Co. Ltd., USA. Bis-[3-(triethoxysilyl) propyl] tetrasulphide (Si- 69) was purchased from Degussa, Germany.

Sample Preparation
Melt blending was carried out with EVA and LDPE with various loading of silicon dioxide nano-powder (1.5, 3 and 5 wt%, respectively) in a Brabender Plasticorder (PLE-330) at 130^{0}C and 80 rpm rotor speed by varying two different sequence of additions of ingredients. The total mixing time was 10 minutes. Then they were remixed for another 2 minutes. The sheets were compression molded between two Teflon sheets for 3 minutes at 150^{0}C with a pre-heat time of 1 minute and with a load of 5 Tons in an electrically heated hydraulic press to obtain films of 0.03 ~ 0.04 cm thickness. The moldings were cooled under compression to maintain the overall dimensional stability. The details of the samples and their appropriate designations are given in Table-1.

Characterization
Thermogravimetric measurements of the composites were conducted using TGA Q50 of TA Instruments-Waters LLC, USA operated in the dynamic mode. The conversion values 5,8,11,4,17 and 20% were used for computing the non-isothermal kinetic parameters using the Flynn-Wall-Ozawa method.
For the transmission electron microscopic (TEM) observations, a high resolution transmission electron microscope (HRTEM) (JEOL JEM 2100, Japan) operated was used at an accelerating voltage of 200 kV.
The bulk morphology of the blends was observed with field emission scanning electron microscope (FESEM) (Leo 1530, Carl Zeiss, Oberkochen, Germany).

Results and discussion

Effect of pristine nano silica filler on thermal degradation characteristics of EVA/LDPE blends under N_2 atmosphere
All thermograms showed two-staged decomposition (not shown here) with well defined initial and final degradation temperatures. No drastic improvement in thermal stability was observed for the filled systems. A modest improvement in thermal stability was found only in case of ELS6/4/3-2. Thus in inert atmosphere, silica particles did not have a major role to influence the thermal stability of the blend systems.

Effect of pristine nano silica filler on oxidative degradation characteristics of EVA/LDPE blends

The control blend (EL6/4) exhibited greater thermal stability than the pure EVA and LDPE [Figure 1(a)]. Also, EVA was also found to be thermally more stable than LDPE. Thus in presence of EVA, LDPE was stabilized. In all silica filled blends there were two distinct and well separated steps in the thermogravimetric curves (TG) (corresponding weight loss peaks in derivative thermgravimetric, DTG) curves as represented in Figure 1 (b) and (c). The first step (309-315^{0}C) for all samples (unfilled and filled) was possibly due to de-acetylation of vinyl acetate group of EVA with the elimination of acetic acid. As a result, double bonds were formed [10] in the main chain. The second step (413-418^{0}C) might be assigned to the further degradation of polyacetylene-ethylene chains formed in the first step accompanied with the degradation of LDPE [10].

As compared to inert atmosphere, it was observed that the initial stages of degradation for all samples were accelerated in the presence of oxygen [Fig. 2(a)]. Thus the rate of reaction might be controlled by O_2 diffusion in the polymeric matrix. There was also an initial gain in weight prior to deacetylation in the presence of oxygen. This suggested a rapid initial oxidation of the blends. Due to the presence of SiO_2 particles, the onsets of degradation of filled blends were shifted towards higher temperatures as compared to the unfilled one. Therefore, the filled systems were thermally more stable than the pure blend. But interestingly, at very high temperature (~ above 425^{0}C) the presence of nano silica accelerated degradation of filled blends. This might be due to the fact that at these temperatures silica acted as an acid catalyst. The outcomes from TGA are represented in Table 2. As compared to samples prepared following sequence-2, ELS6/4/3-1 exhibited higher thermal stability at lower temperature ranges. This indicated the occurrence of intermixing of LDPE and EVA in ELS6/4/3-1. In TEM observations also silica particles were found to be dispersed in both phases as well as in the interface for this system. Si69 increased the compatibility between two phases (in ELS6/4/3-2-Si69) and made silica well dispersed in the polymeric matrix. Hence, ELS6/4/3-1 and ELS6/4/3-2-Si69 exhibited greater thermal stability than the rest of the samples. The degradation behavior was well correlated with the morphology analyzed by TEM and FESEM. The details of the analysis are not given in this brief article. It will be mentioned during the presentation.

The iso-conversional integral method named Flynn-Wall-Ozawa method suggested independently by Ozawa [11] and Flynn and Wall [12] uses Doyle's approximation [13] of the temperature integral. From Eq. (1) and using Doyle's approximation, the result of the integration after taking logarithms is:

$$\log \beta = \log (AE/g(\alpha)R) - 2.315 - 0.457\, E/RT \quad \text{.....(1)}$$

where β is the heating rate, A is the pre-exponential factor, E is the activation energy, α is the degree of conversion and T is the temperature. Thus, for α = constant, the plot of log β versus 1000/T obtained at several heating rates should yield a straight line whose slope can be used to evaluate the activation energy.

All the filled samples showed higher activation energy of degradation than the control sample. This implied that the thermal stability of the silica filled nanocomposites was higher than the neat control blend. From plots (not shown in text) it can be observed that the best fitted straight lines (with at least 90% correlation) were nearly parallel to each other and thus confirmed the applicability of this method with in the conversion range studied. Interestingly, mean activation energy of ELS6/4/3-2 was higher than that of ELS6/4/3-1. The kinetic analysis was performed by both dynamic and static methods and the results were well correlated. However, the details of kinetic analysis will be discussed during presentation.

Table 1. Sample designation

Sample ID*	LDPE (wt %)	EVA (wt%)	SiO_2 (wt %)	Sequence of addition
EL 6/4	40	60	0	-
ELS 6/4/1.5	40	60	1.5	2
ELS 6/4/3-1	40	60	3	1
ELS 6/4/3-2	40	60	3	2
ELS 6/4/3-2-Si69	40	60	3 +10% Si 69 w.r.t. silica	2
ELS 6/4/5	40	60	5	2

*E :- EVA, L:- LDPE, S:- Silica

Table 2. Percentage of degradation for various blend systems at a heating rate (q) of 10^0C/min.

Conversion (%)	EL6/4 (^{o}C)	ELS6/4/1.5 (^{o}C)	ELS6/4/3-1 (^{o}C)	ELS6/4/3-2 (^{o}C)	ELS6/4/3-2-Si69 (^{o}C)	ELS6/4/5 (^{o}C)
5	228	230	258	247	278	244
8	235	241	278	271	289	270
11	242	255	290	289	296	288
14	249	271	298	301	300	297
17	256	284	305	308	302	305
20	265	292	309	313	308	310

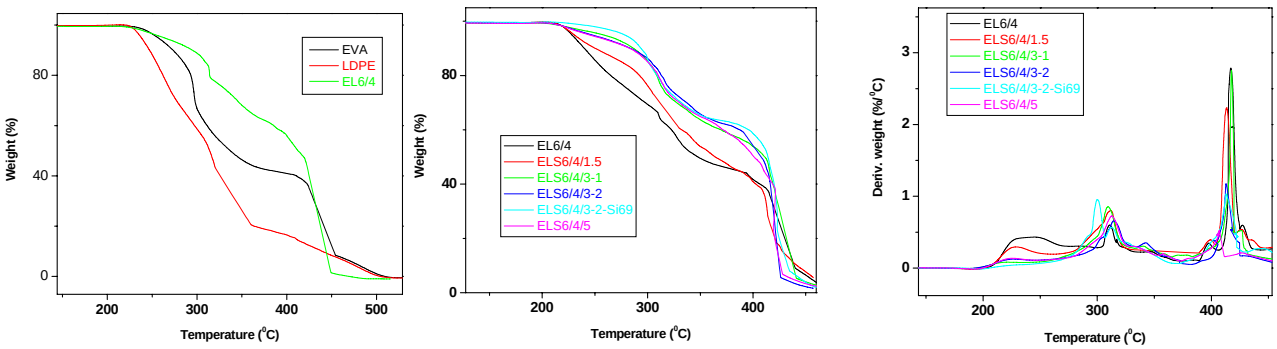

(a) **(b)** **(c)**

Figure 1. (a) TG curve of pure EVA, pure LDPE and EL6/4 in O_2 atmosphere at 10^{o}C per minute.
(b) TG curve of silica filled EVA/LDPE blends at different loadings in O_2 atmosphere at 5^{o}C per minute.
(c) DTG curve of silica filled EVA/LDPE blends at different loadings in O_2 atmosphere at 5^{o}C per minute.

Conclusions

In anaerobic condition, no significant changes were observed in terms of thermal stability of such blend systems. However, in oxygen atmosphere, the TGA plots reflected a dramatic change. The initial part of degradation was probably controlled by oxygen diffusion, decomposition of LDPE and acetic acid elimination from EVA. The next stage of degradation was found to be a strong function of mutual interactions between EVA and nano-silica. Si-69 provided a significant thermal stabilization. On the whole, it was observed that the thermal stability of TPE blends was a strong function of morphology which in turn was decided by the sequence of addition of ingredients during blend preparation, amount of silica nano-fillers addition and presence of coupling agent. The mutual interaction of the polymer matrices with nano-silica fillers strongly influenced the kinetic parameters.

Acknowledgements

The authors are grateful to the Department of Science and Technology (DST), New Delhi for funding the project (SR/FTP/ETA-15/2005 Dated 02.11.2005). One of the authors is highly grateful to CSIR, New Delhi for funding her fellowship to carry out this work. Authors are grateful to Mr. Sayed Mushtaq, RTC, IIT Kharagpur for helping with RPA measurements.

References

1. Wang XL, Yang KK, Wang YZ, Wu B, Liu Y, Yang B. Polym Degrad Stab 2003; 81:415-421.
2. McNeill, IC, Jamieson, A, Toshand, DJ, McClune, JJ. Eur. Polym. J. 1976; 12: 305.
3. Ray I, Roy S, Chaki TK, Khastgir D. Journal of Elastomers and Plastics 1994; 26(2), 168-182.
4. Kaczaj J, Trickey, R. Anal. Chem. 1969; 41(11): 1511.
5. Sultan BA, Sorvik, E. J. Appl. Polym. Sci. 1991; 43: 1737-1761.
6. Wang J, Tu H. Proceedings of the Second Beijing International Symposium/Exhibition on Flame Retardants, Beijing Institute of Technology Press, Beijing, 1993, p.272.
7. Marcilla A, Gómez-Siurana A, Menargues S. Thermochimica Acta 2005; 438: 155–163.
8. Marcilla A, Gómez -Siurana A, Menargues S, Ruiz-Femenia R, García-Quesada. JC . J. Anal. Appl. Pyrolysis 2006; 76: 138-143.
9. Rimez B, Rahier H, Van Assche G, Artoos T, Biesemans M, Van Mele B. Polymer Degradation and Stability 2008; 93: 800-810.
10. Chuang TH, Guo W, Cheng KC, Chen SW, Wang HT, Yen YY. Journal of Polymer Research 2004; 11:169-174.
11. Ozawa T. Bull Chem Soc Jpn 1965; 38(11): 1881-1886.
12. Flynn JH, Wall LA. Polym Lett 1966; 4(5): 323-328.
13. Doyle CD. J Appl Polym Sci 1962; 6(24):639-642.

.

Mechanical properties of natural rubber / poly butadiene rubber blends prepared using fatty acid incorporated natural rubber

R. Alex*, T.Cherian, S.Joseph, and K.T Thomas
Rubber Research Institute of India, Kottayam -9, Kerala
Email: rosammaalex2000@yahoo.com

ABSTRACT

Natural rubber(NR) can be sensitized for quick coagulation by addition of suitable fatty acid salts as stabilizers. A portion of the fatty acids formed remains on rubber after coagulation Fatty acids play a major role on cure characteristics and mechanical properties of recovered rubber. Use of this rubber in blends with polybutadiene rubber (BR) can alleviate some of the problems of rubber blends like cure mismatch and unequal filler distribution. In this paper an investigation on the preparation, cure characteristics and mechanical properties of NR/BR blends prepared using fatty acid incorporated NR is carried out.

Natural rubber latex is treated with a required quantity of fatty acid soap and then coagulated by addition of suitable acids. The coagulum is washed well to remove acids and then dried at 70 ^{0} C in an air oven to get dry rubber. Rubber compounds based on pure NR, 80/20 and 60/40 NR/BR blends are prepared using conventional mixing methods. The compounds are vulcanized and tested as per standard test methods. The fatty acid soaps added to latex get adsorbed or rubber particles and get converted to the corresponding fatty acids by reaction with acids during the process of coagulation. Due to presence of fatty acids, the pure and NR/BR blends show better cure characteristics as revealed from a higher level of vulcanization. Due to the higher level of crosslinking and better filler dispersion, pure and blend vulcanizates show a higher modulus, tensile strength, and hardness along with comparable dynamic properties like heat build-up and compression set in relation to conventional rubber vulcanizates. The presence of fatty acids also helps in a better dispersion of filler in pure rubbers as revealed from scanning electron microscopy (SEM) studies. A noticeably higher ageing resistance is also observed for NR/BR blends prepared by the new process due to the presence of better interaction of filler with rubber.

INTRODUCTION

Blends based on natural rubber and polybutadiene rubber are extensively used in tire sector due to the enhanced mechanical properties like low heat build-up, and abrasion resistance realized in the vulcanizates. The basic problems with such rubber blends are the inherent incompatibility, unequal filler distribution and uneven crossslinking. In general elaostomer blends are microheterogenious, the continuous phase being either the polymer in highest concentration or polymer of lowest viscosity. Filler distribution is influenced by the point of addition of filler, mixing method, surface polarity of filler and other factors like unsaturatiion , viscosity and polarity of blend components. The incorporation of 50/50 elastomer preblends indicated that black affinity decreased in the order, SBR, CR, NBR, NR, EPDM, IIR.[1,2] Curative distribution is influenced by the level of unsaturation , viscosity and polarity of blend constituents. The type and nature of colloidal stabilizers retained on rubber during the coagulation process also affect the cure characteristics and filler dispersion.

Both natural and synthetic rubber latices, (depending on the polymerization technique) have fatty acid salts as stabilizers. In the case of fresh NR latex the colloidal stability is afforded by protein anions and to a small extent by fatty acid anions. In NR latex , the sensitivity to coagulation by acids is controlled by the type of colloidal stabilizers and the fatty acid anions have more sensitivity to coagulation by acids. [3] By using suitable fatty acid soaps the coagulation characteristics and non rubber constituents retained in rubber can be adjusted. By this process the cure characteristics, along with filler dispersion can be controlled so as to have

enhancement in mechanical properties. There are no systematic reports on use of in situ formation of fatty acids that can affect cure characteristics, filler dispersion and hence mechanical properties of rubber blends.

In this paper an investigation on the preparation, cure characteristics and mechanical properties of NR/BR blends prepared using fatty acid incorporated NR is carried out.

EXPERIMENTAL

Fresh Natural rubber (NR) latex used in this study was obtained from Rubber Research Institute of India. Poly butadiene rubber (CISAMER) was obtained from Indian Petrochemicals Corporation Ltd, Vadodara , Other ingredients used were rubber grade chemicals .

Preparation of rubber by fatty acid sensitized coagulation of NR latex

NR latex was mixed with the quantity of fatty acid soap required for sensitization to quick coagulation as reported earlier [4]. The latex was then diluted to a dry rubber content of 20% and coagulated by addition of 10% acetic acid. The coagulum was washed free of acid and dried at 70ºC in a laboratory oven. The control NR was prepared as per the conventional method of sheet preparation. .The NR prepared by the two methods were blended with BR in 80/20 and 60/40 proportions by conventional mixing method as per formulation in Table 1.

Cure behaviour, mechanical properties and SEM evaluation

The vulcanization characteristics were determined using moving die rheometer (RheoTech MD) Test samples for determination of mechanical properties were vulcanized to optimum cure time in a hydraulic press at 150 ^{0} C. Filler dispersion in rubber was assessed using a JOEL model scanning electron microscope. Tensile fracture and abraded surfaces of vulcanizates were coated with gold to conduct SEM study

SEM was carried out using a scanning electron microscope model using sputter coated samples. Analysis was conducted on fractured surfaces and abraded surfaces.

The mechanical properties were determined from relevant ASTM standards.The ageing tests were carried out as per ASTM method after ageing the samples at 100 ^{0} C /3days.

RESULTS AND DISCUSSION

1. Effect of fatty acid soaps on coagulation of latex

Fatty acid sensitized fresh NR latex coagulated immediately on addition of acids. On addition of fatty acid soaps to latex they cause displacement of proteins and gets strongly absorbed on rubber particles. In this way the protein stabilized latex gets transformed into a soap stabilized system. On addition of acids to soap treated latex the adsorbed soap anions react with acid to form un-dissociated fatty acid, and deprive the latex particles of stabilizers. As a consequence, latex coagulates immediately. [3,5]

2. Vulcanization characteristics

The cure characteristics of the blend mixes along with pure NR mixes are given in Figure 1.The rubber recovered from soap-sensitized coagulation showed better overall cure characteristics as compared to conventional mix. It had a higher level of cross slinking and a faster onset of cure which is attributed to the fatty acids retained on rubber. There was enhancement of level of vulcanization in 80/20 and 60 /40 NR/BR blends.

As an activator of vulcanization ZnO requires sufficient amount of fatty acids which converte it into rubber soluble form . Though NR contains a certain amount of these acids it is usually insufficient. Therefore their contents are adjusted to the required level by addition of commercial stearic acid which can be replaced by lauric acid that is more soluble in rubber[6] Hence it is inferred that when fatty acid is added as soap to latex it disperses uniformly in latex

due to adsorption on rubber particles and convert into fatty acid during coagulation. This uniformly dispersed fatty acids help in activating cure characteristics of rubber.

3. **Mechanical properties** .

Soap coagulated rubber recorded a higher modulus, tensile strength, and hardness. Heat - build up and compression set were comparable to that of control (Table 2) .The NR/BR 80/20 and 60/40 blends also showed a higher modulus tear strength and hardness in comparison with blends prepared using conventionally obtained NR.

Improvement in mechanical properties is attributed to the formation of higher level of crosslinks and other interactions involving filler and rubber. Oxygen containing groups present in rubber have a considerable effect on vulcanization kinetics and have a role in interaction with rubbers. It is expected that there is better polymer filler interaction involving uniformly dispersed fatty acid soaps though the actual mechanism is not clear from this study. There are reports that use of higher dosage of stearic acid in tread formulation enhanced in abrasion resistance. In this study it is inferred that fatty acids soaps are formed during vulcanization from added surfactant and it acts as lubricant, reducing the abrasion loss [7]

SEM photographs of tensile fracture and abraded surfaces of NR vulcanizates are shown in Figures 2 and 3. The tensile fracture surface of NR prepared from soap sensitized coagulation has a more uniform surface and less matrix removal, as compared to conventional NR fillerwhich shows enhanced filler dispersion in presence of in situ formed fatty acids. The abraded surface of the sample from soap coagulation shows fine ridges while the conventional mix has bigger ridges and foldings. It is known that wear occurs as a result of two processes; local mechanical rupture (tearing) and general decomposition of the molecular network to a low molecular weight material (smearing). [8, 9] It is known that molecular rupture under frictional forces followed by stabilization of the newly formed polymeric radicles by reaction with oxygen or with other polymer molecules or with other macroradicals take place during the abrasion process. In rubber obtained by soap sensitized coagulation mainly due to higher levels of crosslinking there is lower crack growth and removal of the matrix The ageing characteristics are shown in Table 3. The blends prepared from in situ formed fatty acid has a higher retention of tensile strength and less variation in modulus and elongation at break as compared to blends prepared from conventional sheet rubber. The enhancement is attributed to higher level of vulcanization and better filer dispersion.

CONCLUSION

The carboxylic acid soaps added to latex get adsorbed on rubber particles and are retained in rubber after coagulation. The fatty acids retained on rubber activate the vulcanization and improve the mechanical and ageing characteristics of recovered rubber. NR/BR blends prepared from fatty acid incorporated rubber have higher level of vulcanization, and better mechanical and ageing properties as compared to blends prepared from conventional rubber.

REFERENCES

1. Corish PJ, Powell B.D.W. Rubber Chem. Technol. 1974:47:481-509
2. Gallen G.E, Hess W.M., Scott, C.E, Rubber Chem. Technol 1971:44: 814-837
3. Blackley, D.C. (1997). Polymer Latices, Science and Technology, Vol. 2. Types of lattices , Chapter 9.
4. Alex, R., Premalatha, C.K., Nair, R.B. and Kuriakose, B. (2003). Journal of Rubber Research, 6(**4**): 221-230.
5. Cockbain, E.G. (1952). Transactions, IRI, **28**: 297-302.
6. Franta, I. (1989). Elastomers and Rubber compounding materials manufacture properties and applications. Elsiever Publications, Chapter6.

7. Gelling, I.R. In: proceedings of the Workshop on the Development of natural rubber based truck tyre retreading compounds,Cane, M.E., Rashid, S.Z.M., Eds., Malaysian Rubber Research and Development Board, Kuala Lumpur, Malaysia, 1992, p. 49.
8. Gent A.N., Pulford C .T.R. J.Appl. Polym. Sci.:2003:28(3):943-960.
9. Bhowmick A.K., Sanjay Basu, De S.K. . J Material Sci. 1981:16(6): 1654-1660

Table 1 Formulation of NR/ BR mixes

Ingredients	**parts**		
Natural Rubber/BR	100/0	80/20	60/40
ZnO	5	5	5
Stearic acid	1	1.25	1.5
Antioxidant TDQ [1]	1	1	1
HAF black	40	40	40
Aromatic oil	2	2	2
CBS [2]	0.75	0.75	0.75
Sulphur	2.5	2.5	2.5

Table 2. Mechanical properties of carbon black filled pure and blend vulcanizates

Parameter	**NR**		**NR/BR 60/40**		**NR/BR 60/40**	
	Sample	**Control**	**Sample**	**Control**	**Sample**	**Control**
Modulus 100%, MPa	2.53	1.66	2.16	1.78	2.71	2.63
Modulus 200%, MPa	5.11	3.11	4.2	3.34	5.38	5.15
Modulus 300%, MPa	8.44	5.05	6.78	5.5	8.55	8.28
Tensile strength, MPa	24.27.	24.40	19.98	21.1	11.72	11.12
Elongation at break, %	670	690	690	700	400	390
Tear strength, kN/m	58	82	66	51	39	30
Hardness, Shore A	67	66	66	65	68	67
Heat build-up, ΔT,ºC	21	20	19	20	20	20
Din abrasion loss, cc	88	100	79	80	74	75

Table 3 Ageing resistance of carbon black filled pure and blend vulcanizates (aged at 100^0 C/3d).

Parameter	**NR**		**NR/BR 60/40**		**NR/BR 60/40**	
	Sample	**Control**	**Sample**	**Control**	**Sample**	**Control**
Modulus 100%, MPa	3.64	3.25	2.71	3.36	3.55	4.05
Modulus 200%, MPa	7.98	7.08	5.57	-	-	-
Tensile strength, MPa	8.82	8.87	6.78	5.47	6.82	5.69
Elongation at break, %	215	240	230	150	180	140
Percent change of modulus 100%,	43.87	95.78	25.46	88.76	30.99	53.99
Percent retention of tensile strength	36.34	36.35	33.93	25.92	58.19	51.16

Preparation and Characterization of ethylene co-vinyl acetate based drug delivery system for cardiovascular applications

V. D. Anumon*, Roy Joseph and C.V. Muraleedharan[#]

Biomedical Technology Wing, Sree Chitra Tirunal Institute for Medical Sciences and Technology, Thiruvananthapuram, Kerala – 695012, India, Contact (Off.) 0471-2520259

Email: muralicv@sctimst.ac.in

Abstract

Major complications of cardiovascular lesions are often accompanied by inflammatory reactions and smooth muscle cell proliferation. Curcumin has been shown to possess anti-inflammatory and anti-proliferative properties. As a solution to above cardiovascular problems, sustained drug delivery system releasing curcumin from ethylene-co-vinyl acetate (EVA) matrices is proposed. Various grades of EVA having 40%, 28%, 18% and 12% vinyl acetate content were evaluated for the selection of a suitable grade. The EVA grades were characterized by Fourier Transform Infrared (FT-IR) Spectroscopy, dynamic mechanical analysis (DMA), testing solubility in organic solvents and determining mechanical properties. Curcumin is incorporated into the matrices by dissolving both matrix and curcumin separately in solvents, mixing together and later evaporating the solvent from the system. Curcumin loaded systems were characterized by FT-IR, contact angle measurements, water absorption, mechanical testing and checking the drug release profile from the matrix. FT-IR data confirms that there was no chemical reaction between EVA and the drug. Increased drug content in the matrices results significant increase in tensile strength and modulus where as fracture strain records substantial decrease. The results of contact angle indicated that loading curcumin in EVA does not alter surface properties of the matrix significantly. DMA revealed that addition of curcumin does not alter glass transition temperature either. It also shows that when the vinyl acetate content increases the storage modulus decreases. Water absorption studies show an increase in water uptake by matrices with increase in drug loading. From the results obtained EVA with 40% vinyl acetate content was found to be the most suitable system as a matrix. The selection was based on the low modulus, high elongation, solubility in the organic solvents and film forming properties. Drug elution profiles up to a period 15 days were monitored. From the results it is expected that curcumin loaded EVA-40 system would be suitable for drug release applications in cardiovascular system.

1. Introduction

Cardiovascular disease (CVD) is not only the biggest cause of death worldwide, but also responsible for a significant proportion of health complications requiring long-term management. According to World Health Organization (WHO) estimates, in 2003, 16.7 million people around the globe die of CVD each year [1]. This is over 29% of all deaths globally. In India in the past five decades, rates of coronary disease among urban populations have risen from 4 % to 11% [2]. In 1998 the annual death rate for India was 840 per 100,000 populations. Cardiovascular diseases contribute to 27% of these deaths and its crude mortality rate was 227 per 100,000 [3]. The WHO estimates that 60% of the world's cardiac patients will be Indian by 2010 [2].

Literature reveals that major complications of cardiovascular lesions are often accompanied by inflammatory reactions and smooth muscle cell proliferation [4]. Curcumin (diferuloyl methane) possesses a wide range of pharmacological activities including low intrinsic toxicity, anti-thrombus, anti-oxidation and antiproliferation properties [5, 6] and may be suitable for treating above complications.

Sustained release of the above drugs to the affected area may be possible by loading these drugs into suitable matrices. Ethylene vinyl acetate (EVA) copolymer, a heat processable, flexible and stable material [7] is commercially available with vinyl acetate (VAc) content varying from 3 to 50%. The properties of EVA vary with VAc content. Vinyl acetate content up to 10% is more transparent, flexible and tougher than LDPE. Between 15 and 30% VAc content copolymers are soft and flexible. Compounds with 30–40% VAc are soft, elastic and their strength and adhesion properties are desirable for coatings and adhesives [8]. Between 40 and 50% VAc content in EVA produce rubber like properties [8]. In this study curcumin is incorporated in EVA copolymers by casting method and sustained release of curcumin is evaluated.

2. Experimental

2.1. Materials

Polymer matrices used for this study are: (a) EVA grades of vinyl acetate content 12% (NOCIL, India), 18% (Aldrich, USA), 28% (NOCIL, India) & 40% (Aldrich, USA). Curcumin (trade-named Biocurcumax) was obtained from M/s Arjuna natural extracts Ltd., Aluva, Kerala. Solvents used in the study were of 99.5% purity and were obtained from s.d. fine chemicals, Mumbai.

2.2. Differential scanning calorimetry

DSC analysis of curcumin was done based on the ASTM E 1356-03 standard using DSC 2920 by TA Instruments Inc., USA. The test was done in nitrogen atmosphere (99.99% N_2 and 1 ppm moisture, 1 ppm O_2) using an empty aluminum pan as the reference material. The scan temperature ranged from -50°C to 200°C at a heating rate of 10°C/min.

2.3. FT-IR analysis

FT-IR spectra of the curcumin were recorded on a Thermo Nicolet 5700 spectrometer with a diffused reflectance sample holder (Thermo Scientific, Germany).

2.4. Dynamic Mechanical Analysis

Dynamic Mechanical Analysis (DMA) was performed using a Tritec 2000B DMA (Triton Technology Limited, UK). Storage modulus and damping characteristics of EVA grades and curcumin loaded matrices were determined as a function of temperature. Temperature scan was done from (-) 150°C to (+) 100°C at a frequency of 1 Hz. The heating rate used was of 1°C/min.

2.5. Tensile properties

The tensile properties of EVA grades and curcumin loaded EVA were measured by using an Instron (model 3345) Universal Testing Machine equipped with a 100N load cell. Dumbbell shaped test samples were cut from cast films. The samples were conditioned at 23±1°C and at 50% relative humidity, and the test was performed at a crosshead speed of 100 mm/minute.

2.6. Solubility test

About 0.1 gm of polymer was taken in a 50ml beaker and 10ml solvent was added to it. This was kept on a hot plate stirrer (Schott Instrument, Germany) and slightly heated along with continuous stirring to dissolve the polymer.

2.7. Fabrication of curcumin eluting polymer films and its structure

Curcumin loading in EVA grades was achieved by preparing solutions of polymer and curcumin and cast on glass plates. Cast films were washed with de-ionized water and air-dried. FT-IR spectra of the curcumin loaded EVA grades were recorded on a Thermo Nicolet 5700 spectrometer (Thermo Scientific, Germany).

2.8. Contact angle measurement

Contact angle of the films are measured at room temperature (~23^{o}C) using the sessile drop method by a video based contact angle measuring device (Data Physics OCA 15 plus, Germany) and imaging software (SCA 20). Five independent measurements were performed on different region of the sample surface.

2.9. Curcumin release profile

Samples of 1 cm^2 surface area were cut from the curcumin loaded polymer films and suspended in 5ml phosphate buffered saline (PBS) at 37^{o}C and placed in a shaking water bath (Julabo, SW22, Germany) at 60rpm. At definite time intervals whole quantity of PBS was withdrawn and fresh PBS was added. Elution kinetics was monitored using UV spectroscopy at a wavelength of 420nm for a period of 15 days.

3. Results and discussion

3.1. Physico-chemical characterization of Curcumin, EVA grades and Curcumin loaded EVA

Solubility of EVA grades tends to increase with increase in vinyl acetate content in the polymer. EVA-40 was found to be soluble in a number of organic solvents such as tetrahydrofuran, toluene, dichloromethane, cyclohexane, etc. FTIR spectra of EVA, Curcumin and Curcumin-loaded EVA matrices are shown in the Figure 1. Spectra of EVA shows characteristic absorption peaks at 1735.9 cm^{-1} due to the stretching vibrations of C = O. A peak in the region 2872 and 2956 cm^{-1} corresponds to symmetric and asymmetric stretching vibration of C-H bond. A peak was observed in the region 1143cm-1 corresponding to C-O-C stretch. The spectrum of Curcumin shows characteristic aromatic absorption peaks in the range 1600.1 to 1504.9 cm^{-1}. A broad peak in the region from 3223.6 to 3508.6 cm^{-1} indicates the presence of OH. A feeble peak was observed at 1624.8cm^{-1} corresponding to C=O, C-O-C peak was obtained at 1272.7 cm^{-1}, benzoate trans-CH in CH=CH obtained at 959.2 cm^{-1}, cis CH in aromatic at 713 cm^{-1}. The spectra of polymer matrix incorporated with Curcumin (10wt%) does not exhibit any shift in peaks with respect to the characteristic peaks discussed above. From these results it is clear that curcumin incorporated in the EVA matrix does not undergo any reaction or complexation with the matrix.

The storage modulus and tan delta of EVA grades and curcumin loaded EVA are given as a function of temperature in figure 2. It may be seen that the two grades of EVA, i.e., EVA 12 and EVA 18 have higher modulus compared to EVA 28 and EVA 40. All the EVA grades show glass transition in the range -15°C to -19°C. EVA 40 shows lower modulus because it has maximum vinyl acetate content which increases the flexibility of the polymer and hence increased the damping. Incorporation of Curcumin on to EVA matrices does not alter the characteristic glass transition temperature of the matrices. However, substantial increase in storage modulus is evident.

Mechanical properties of EVA grades are given in Table 1. Depending upon the vinyl acetate content and source of EVA grades properties tends to vary. Effect of addition of curcumin in EVA-40

is shown in table 2. Curcumin addition substantially increased the tensile strength and modulus of the resultant system. A considerable decrease in the fracture strain is observed with curcumin loading. Results indicate that curcumin acts as a reinforcing agent in EVA matrix. Effect of tensile strength on short term ageing of EVA and curcumin loaded EVA in PBS is shown in figure 3. The system tends to be stable during ageing except for that containing 10wt% curcumin. Contact angle data obtained for EVA and curcumin loaded EVA shows no significant changes in contact angle data with curcumin loading (figure 4). Matrices exhibited increase in water uptake with higher curcumin loadings. Water uptake behavior is shown in figure 5 with respect to curcumin content in the EVA matrix. Increases in curcumin content increased water uptake by the polymer matrix.

3.2. Elution profile of curcumin

Cumulative release of curcumin from EVA40 is shown in figure 6. Different concentrations of curcumin were loaded in the matrix and release was monitored upto 15days. The quantity of curcumin released is a function of curcumin loaded in the matrix.

Conclusion

EVA copolymer is found to be a suitable system for the sustained release of curcumin. Curcumin released from the matrix depended on the quantity of curcumin loaded in it.

References

1. International Cardiovascular Disease Statistics, American Heart Association, 2007.
2. Express Healthcare Management, Indian Express Newspapers Ltd., India, 2001.
3. Gupta R, Misra A, Pais P, Rastogi P, Gupta VP. International Journal of Cardiology 2006; 108 (3): 291-300.
4. Boehm M and Nabel EG. Progress in Cell Cycle Research; 2003; 5; 19-30.
5. Pan CJ, Tang JJ, Shao ZY, Wang J and Huang N. Colloids and Surfaces B: Biointerfaces 2007; 59 (1):105-111.
6. Pan CJ, Tang JJ, Weng YJ, Wang J, Huang N. Journal of Controlled Release 2006; 116(1): 42-49.
7. Guo Q, Guo S, Wang Z. Journal of Controlled Release 2007:118(3):318-324.
8. Tambe S, Singh SK, Patri M, Kumar D. Progress in Organic Coatings 2008;62 (4):382-386.

Table 1. Mechanical Properties of EVA grades

Polymer grade	Tensile strength (MPa)	Elongation at break (%)	Modulus (MPa)
EVA -12	11.97 ± 0.99	2790 ± 207	5.28 ± 0.61
EVA -18	8.44 ± 0.54	1183 ± 92	19.97 ± 2.19
EVA -28	13.50 ± 1.19	1723 ±129	5.00 ± 1.37
EVA -40	8.81 ± 0.20	2610 ± 97	0.56 ± 0.05

Table 2. Effect of curcumin content on the mechanical properties of EVA-40

Curcumin content, (wt %)	Tensile strength (MPa)	Elongation at break (%)	Modulus (MPa)
0	06.73 ± 0.45	1450 ± 567	01.54 ± 0.32
1	11.17 ± 1.58	1130 ± 656	02.50 ± 0.33
2	12.56 ± 3.06	1429 ± 523	03.14 ± 0.64
5	12.58 ± 0.92	1094 ± 544	10.02 ± 1.79
10	15.09 ± 1.59	676 ± 360	26.11 ± 10.87

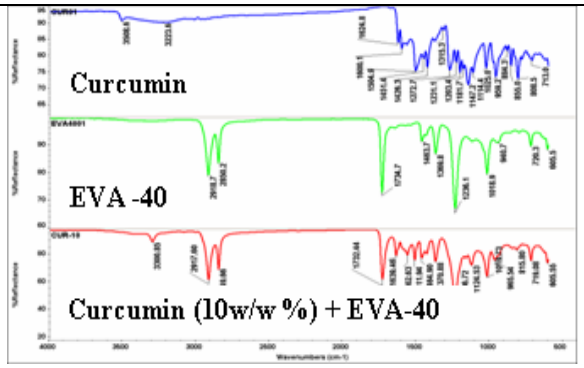

Figure 1. FTIR spectrum of Curcumin, EVA & Curcumin loaded (10wt %) EVA40

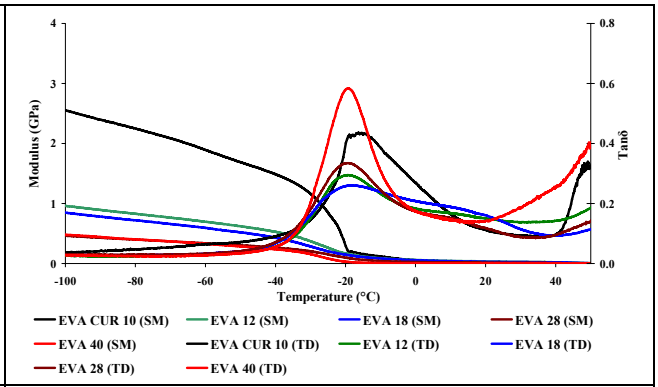

Figure 2. DMA traces of EVA grades and curcumin loaded (10%) EVA

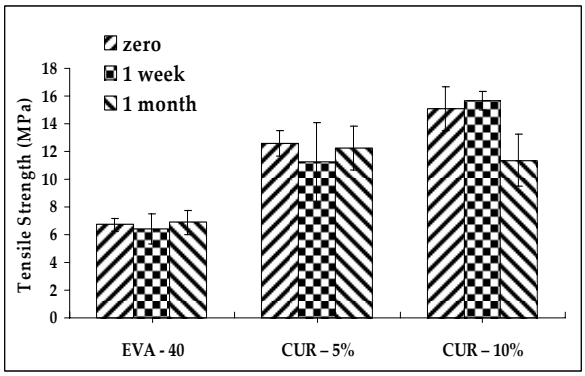

Figure 3. Tensile Properties of Curcumin-loaded EVA matrices

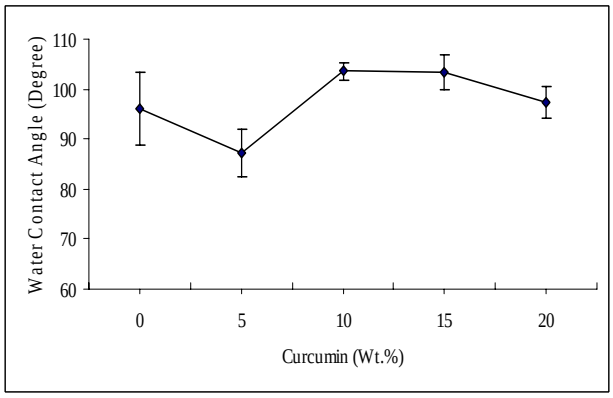

Figure 4. Contact Angle measurements of Curcumin - loaded EVA matrices

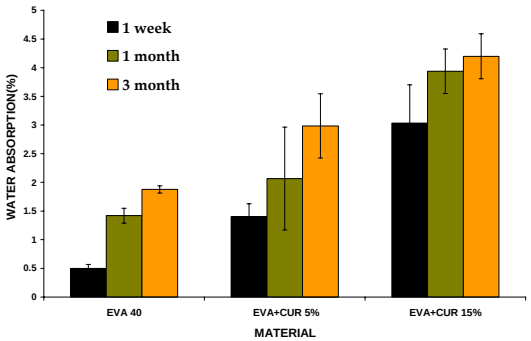

Figure 5. Water absorption of Curcumin-loaded EVA matrices

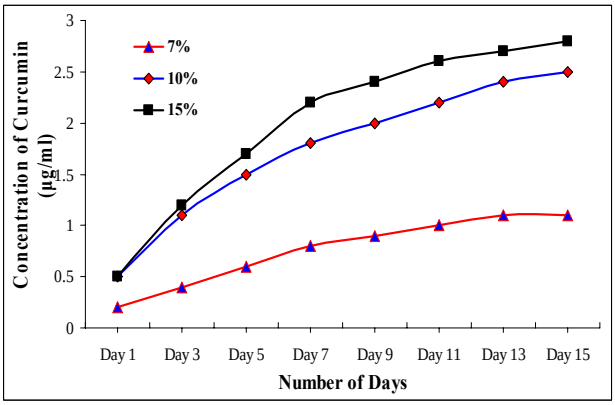

Figure 6. Cumulative elution profile of curcumin from EVA40 for different loadings

Aromatic-aliphatic co-polyester poly (butylene adipate-co-terephthalate) bio-nanocomposite: Influence of organic modification on structure and properties

B.P. Sahoo[1], G.Sornarajendran[2], S.Mohanty[2] and S.K.Nayak[2]

Laboratory for Advanced Research in Polymeric Materials

[1]Central Institute of Plastic Engineering and Technology, Bhubaneswar-751024,

[2]Central Institute of Plastic Engineering and Technology, Guindy, Chennai- 600032

Email: drsknayak@gmail.com

Abstract:

Bio-nanocomposite hybrids based on poly (butylene adipate-co-terephthalate) (PBAT) and layered silicates were prepared by melt interaction technique using co-rotating twin-screw extruder having blown film unit. Sodium montmorillonite (Na^+MMT) along with three different commercially available nanoclays i,e, Cloisite30B (C30B), Cloisite20A (C20A), Bentonite (B109) have been used. Wide Angle X-Ray Diffraction (WAXD) studies indicated an increase in d-spacing of the nanoclays in the bio-nanocomposite hybrids revealing formation of intercalated morphology. Morphological studies using Transmission electron microscopy (TEM) also confirmed that nanoclays were finely dispersed in the PBAT matrix and there was presence of partially exfoliated clay galleries along with intercalated structures in the bio-nanocomposite hybrids. Mechanical tests showed that the bio-nanocomposite hybrids prepared using Bentonite (B109) nanoclay exhibited higher tensile modulus. Functionalization of PBAT matrix upon grafting with maleic anhydride (MA) resulted in further improvement in mechanical properties. The existence of interfacial bonds in grafted bio-nanocomposite hybrids are substantiated using FTIR spectroscopy. Thermal properties of bio-nanocomposite hybrids employing DSC, TGA also revealed improved Tg, Tc and thermal stability over the virgin polymer. Dynamic Mechanical Analysis (DMA) indicated an increase of storage modulus(E') of PBAT biopolymer with incorporation of nanofiller. **Key words:** Poly(butylene adipate-co-terephthalate), TEM, DMA, MA-g-PBAT

Introduction

Polymer layered silicate nanocomposites have received considerable attention in the recent years. At minimal concentration of nanofiller to the tune of 1%, there has been a concurrent improvement of mechanical thermal, optical and physico chemical properties as compared with a conventional micro/macro composite [1]. The layered silicates with a thickness of 1 nm have a very high aspect ratio, ranging between 10 to 1000 that creates an effective surface area for polymer filler interaction leading to property enhancements in the virgin matrix [2]. Tailoring composites with a perspective of sustainable development and ecofriendly characteristics have resulted in renewed interest in natural renewable resource based and compostable materials. Research effects in the areas of natural fiber based plastics; biodegradable polymers, starch based plastics etc. have already been undertaken with a primary focus on development of biodegradable composites with environmentally safe characteristics and desired attributes. Despite several advantages in the development of biodegradable plastics, its introduction to the market as a viable alternative to petrochemical thermoplastics has been prevented. Some of the major impediments are fragility, thermal degradability at temperature not far above the melting point and high price [3]. However, incorporation of nanoscale fillers can significantly enhance the mechanical, thermal, dimensional and barrier performance in the biodegradable polymers [4].

Biodegradable nanocomposites can be prepared using various methods such as solution intercalation, melt intercalation, in-situ intercalative polymerization and template synthesis [5]. Polymer melt intercalation has been proved to be a versatile technique in the fabrication of biodegradable nanocomposites because of its environmental friendly characteristics and compatibility with the nanofillers [6].The present article summarizes an extensive investigation on physico-mechanical and thermal characterization of PBAT bio-nanocomposites.

Experimental

Materials

PBAT (Ecoflex) MFR (190^0C; 2.16 Kg)=3.3 to 6.6g/10min; Mass Density = 1.25 to 1.27g/cm3; Melting point = 110^0C to 115^0C was supplied by BASF Japan Ltd. Commercially available Cloisite 30B (C30B), Cloisite 20A (C20A), Bentone 109 (B109) have been used as nanoclays. The organoclays and PBAT pellets were dried under vacuum at 80^0C for 5hrs and 40^0C for 30minutes respectively.

Preparation of PBAT Nanocomposite

The bio-nanocomposite hybrids of PBAT with various organically modified nanoclays at different weight percentage (1, 3, 5 wt%) was prepared using melt blending technique in a co-rotating twin screw extruder (Haake Rheocord 9000, Germany) at a temperature difference from feed to die zone between 165° - 180°C and screw speed of 60-70 rpm. Maleic anhydride grafted PBAT (MA-g-PBAT) bio-nanocomposite hybrids were prepared through a two steps reactive extrusion process employing free radical grafting of PBAT using MA at a temperature of 165°C-180°C and screw speed of 60-80 rpm. In the second step, MA-g-PBAT was melt blended with various organically modified nanoclays using the same optimized temperature and speed. Subsequently the extrudate was pelletized to granules.

Wide Angle X-Ray Diffraction (WAXD): XRD Analysis was performed at ambient temperature using Phillips X'Pert MPD(JAPAN) at a scanning rate of 2^oC/min with CuK$\propto$ radiation(λ=0.154 nm) at 40KV and 14mA.

Mechanical Tests: Specimens of dimension 130mm x 25mm were prepared for Tensile testing as per ASTM D882 in Universal Testing Machine (UTM) at a gauge length of 50mm. Tear test for the prepared samples were performed as per ASTM D1922 in Pendulum Tear tester (ATSFAAR, VignateMI, Italy) with maximum load of 3920 grams. The samples were conditioned at 23 $\pm$ 5^0C and 55% RH prior to testing and five replicate were used for each test. The data reported are the averages from five tests.

Differential Scanning Calorimetry (DSC):DSC was performed on a Perkin-Elmer Pyris equipment (USA). 5-10mg samples were scanned at a heating rate of 10^0C/min from -80^0C to 200^0C in nitrogen atmosphere. The crystallization temperature (Tc), Glass transition Temperature (Tg) and Melting temperature(Tm) of the virgin PBAT, Nanocomposites and its blend were determined.

Thermo Gravimetric Analysis (TGA):TGA performed using Perkin-Elmer Pyris (USA). 5-10mg samples were heated at 20^0C/min from 50^0C to 600^0C. The degradation temperature was determined.

Dynamic Mechanical Analysis (DMA): The samples were studied using Dynamic Mechanical Thermal Analyzer (NETZSCH DMA 242, Germany), at fixed frequency of 1Hz and heating rate of 10°C/min.

Results & Discussion

The bio-nanocomposite structure characterized using WAXD patterns (Fig 1b) reveal characteristics peaks, shifted to smaller diffraction angles at 2.175, 2.145 and 2.03° respectively due to intercalation of PBAT chains into the silicate galleries. The interlamellar d_{001}-spacing follows the following order B109 (nm)> C20A (nm)> C30Bnm, confirming highly intercalated structure, due to strong interaction between carbonyl groups (>C=O) of PBAT with -OH groups of organoclay. In case of MA-g-samples absence of deflection peak within the experimental range, indicates exfoliation of clay galleries. Further, the TEM micrographs (Figure 2) confirm intercalated clay galleries as well as stacks of agglomerated clays galleries noticed within the PBAT matrix in case of PBAT/C20A, PBAT/B109 and PBAT/30B bio-

nanocomposites respectively. However, grafting of PBAT with MA results in improved dispersion characteristics of organically modified clays within MA-g-PBAT matrix with a smaller amount of stack platelets in broad and obscure regions & regions of exfoliated clay galleries along with intercalated stacks.

The mechanical properties of bio-nancomposite hybrid is depicted in Table-1 It is evident that incorporation of nanoclays results in an increase in the tensile modulus of matrix polymer in both transverse and as well as in machine direction respectively. In case of the nanocomposite prepared using C30B nanoclay an increase of Young's modulus to the tune of 30.59% and 31.99% respectively was observed. A similar increase in Young's modulus of PBAT/B109, PBAT/C20A nanocomposite hybrids was also noticed to the tune of 38.88% 46.94%, and 14.50% 7.22% in transverse and machine direction respectively as compared with the virgin matrix. The increase in Young's modulus of virgin PBAT matrix follows the following order PBAT/B109>PBAT/C30B>PBAT/C20A> PBAT/Na^{+}MMT. The nanocomposite hybrid with B109 exhibited optimum performance as compared with the other nanocomposite hybrids. This behavior is probably due to the homogeneous distribution and micro dispersion of nanoclay facilitating separation of tactoids and platelets in partial exfoliation and intercalations accomplished through shear stress during melt compounding. In all the cases, the nanocomposite hybrids exhibited higher performance in the machine direction, which is probably due to the uniform alignment and improved interfacial adhesion of the nanoscale reinforcement within the PBAT matrix. However, addition of nanoclays leads to a decrease in tensile strength as well as elongation at break. The MA-g-PBAT bio-nanocomposite hybrids exhibited improved tensile modulus as compared with the ungrafted bio-nanocomposite hybrids. This is probably due to the formation of inter molecular hydrogen bonding between hydrogenated tallow groups of B109 and C20A and MA-g-PBAT matrix. The bio-nanocomposite hybrid prepared using B109 clay exhibited maximum Young's modulus, which can be explained due to similar cause that B109 provides increased clay platelets per surface area of contact with virgin matrix.

The tear resistance of PBAT matrix and the bio-nanocomposite hybrids also exhibits a linear increase with the addition of nanoclays and MA. Nearly 19% increase in the tear strength of PBAT matrix was observed in PBAT/B109 bio-nanocomposite hybrid. PBAT/C30B as well as PBAT/C20A bio-nanocomposite hybrid also exhibited an increase in tear strength of PBAT from 335.3 g/mm to 343.17 g/mm and 283.00 g/mm respectively. Further, functionalization of PBAT matrix with MA through reactive extrusion results in modification of the interfacial region between PBAT and nanoclays through formation of covalent bonds/hydrogen bonds with suitable chemical/pendent groups [24]. The bio-nanocomposite hybrid of MA-g-PBAT/B109 exhibited a tear resistance of 445.39 g/mm where as MA-g-PBAT/C30B exhibited a tear resistance of 375.05 g/mm respectively.

The storage modulus verses temperature of the virgin matrix and nanocomposite hybrid is represented in fig 3. It is evident that storage modulus of PBAT biopolymer increases with incorporation of nanofiller which is probably due to the efficient stress transfer from the filler to matrix. Further the grafted sample exhibited improved modulus as compared with the ungrafted nanocomposite hybrids. This further confirms improved interface between the nanofiller and the biopolymer matrix upon functionalisation with MA. MA-g-PBAT/B109 sample exhibited optimum storage modulus as compared with MA-g-PBAT/C30B nanocomposite hybrid which is probably due to better exfoliated structure.

The melting temperature of PBAT matrix depicted in DSC Thermograms (fig.4)also showed a substantial increase from 109.2°C to 125°C in PBAT/C30B, 126.72°C in PBAT/B109, 138.25°C in MA-g-PBAT/C30B and 139.02°C in MA-g-PBAT/B109 nanocomposite hybrids respectively.

The variation of crystallization temperature (Tc) of virgin matrix and nanocomposite hybrids is presented fig 5. The virgin matrix exhibits a crystallization peak around 66.14°C which increased substantially with the incorporation of nanoclays as well as functionalization of PBAT with MA. PBAT/C30B bio-nanocomposite hybrid exhibits optimum crystallization peak around 96.45°C. This is primarily due to heterogeneous nucleation effect in presence of nanoclay which increase the nucleation sites in the polymer matrix. However, grafting of virgin matrix does not show any appreciable increase in the

crystallization temperature of PBAT in the bio-nanocomposites as compared with the ungrafted bio-nanocomposites.

The thermal stability of virgin PBAT, PBAT bio-nanocomposite hybrids and MA-g-PBAT bio-nanocomposites are assessed employing TGA showed that incorporation of organically modified nanoclays substantially increases the thermal stability of the biopolymer. PBAT/C30B nanocomposite hybrid exhibits the initial degradation temperature around 322.58°C and final degradation temperature around 469.58°C which is comparatively higher than that of virgin matrix. The grafted bio-nanocomposite hybrids exhibited a further increase in the degradation temperature. MA-g-PBAT/B109 showed maximum initial and final degradation temperature of 339.59°C and 505.82°C. The bio-nanocomoposite hybrid samples prepared using B109 nanoclay exhibited optimum thermal performance owing to its higher surface area and smaller platelets (fig 6).

Conclusion

Nanocomposites based on PBAT and layered silicate (C30B, C20A and B109) was prepared using melt intercalation and subsequently blown films were prepared. Morphological observation from TEM and WAXD revealed that PBAT/C30B and PBAT/B109 exhibits intercalated structure whereas MA-g-PBAT/B109 showed few layers of exfoliated clay galleries as well as intercalated structure. Mechanical tests showed an increase in the tensile modulus of PBAT nanocomposites hybrid in the grafted samples. Thermal stability of the virgin biopolymer also increased with the incorporation of organically modified nanoclays. Future research will be primarily focused in the development of nanocomposite hybrid with improved mechanical performance.

References

1. Alexander, M; Dubois,P; Mater Sci Eng 200,28,1.
2. Li,X; Kang,T; Cho,W,J; Lee,J,K; Ha,C,S; Macromol Rapid Commun 2001,22,1306.
3. Chang,J,H; An,X,U; Sur,G,S; J polym sci part B: polym Phys 2003,41,94.
4. Ray,S,S; Okamoto,M; Macromol Rapid Commun 2003,24,815.
5. Messermith,P,B; Giannelis; E.P.J.Polym Sci Part A: Polym Chem 1995, 33, 1047.
6. Di, Y.; Iannace, S.; Maio, E. D.; Nicolais, L. j Polym Sci Part B: Polym Phys 2003, 41 670.
7. Chen, G. X.; Hao, G. J.; Guo,T. Y; J Appl Polym Sci 2004, 93, 655.
8. Chen, G. X.; Hao, G. J.; Guo,T. Y.; Song, M. D.; Zhang,B. H. J Mater Sci Lett 2002, 21, 1587.
9. Ray, S. S.; Okamoto, K.; Maiti, P.; Okamoto, M. J Nanosci Nanotechnol 2002,2,1.
10. Ray, S. S.; Okamoto, K.; Okamoto, M. Macroolecules 2003, 36, 2355.

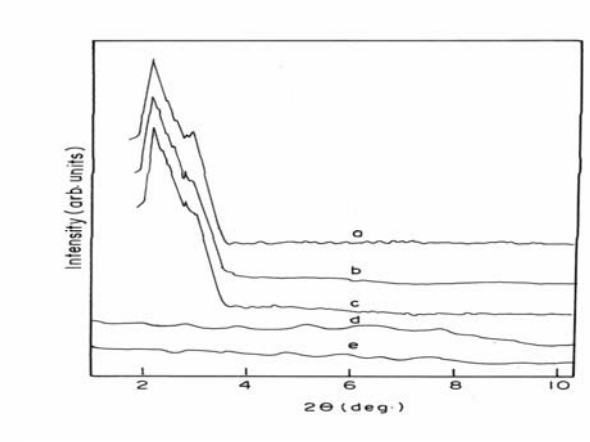

Fig 1: WAXD patterns for bio-nanocomposites; (a). PBAT/C20A,(b). PBAT/C30B, (c). PBAT/B109, (d). MA-g-PBAT-C30B, (e). MA-g-PBAT-B109

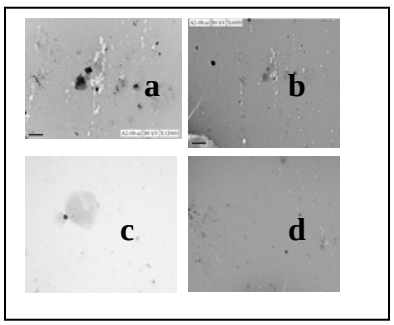

Fig 2: TEM Micrographs of bio-nanocomposites; (a) PBAT/C30B (b). PBAT/B109, (c). MA-g-PBAT-C30B, (d). MA-g-PBAT-B109

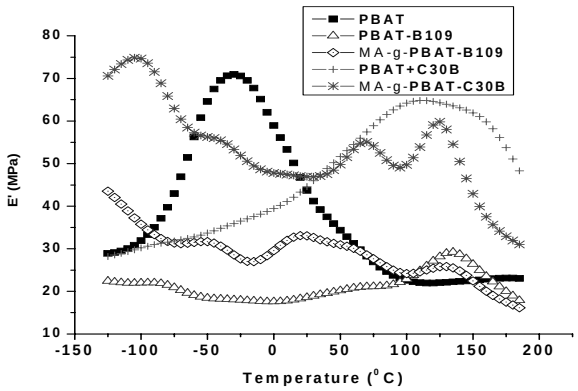

Fig 3: Storage Modulus of Virgin PBAT and bio-nanocomposites

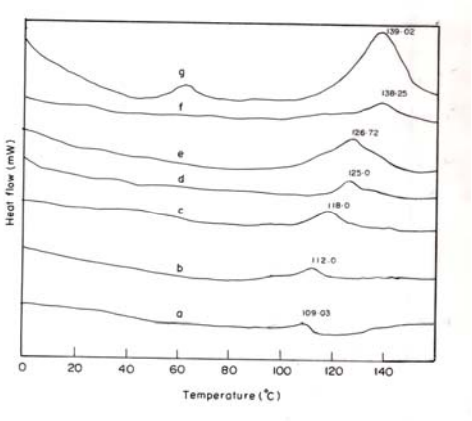

Fig 4: DSC Thermograms of Virgin PBAT and bio-nanocomposites

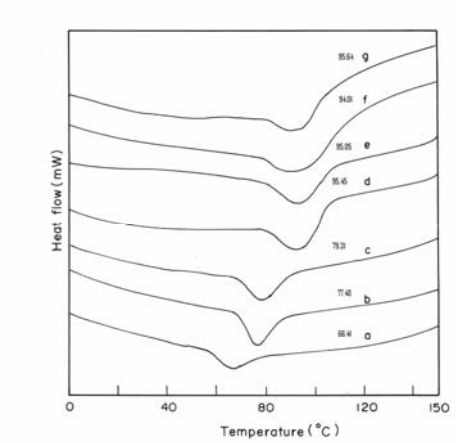

Fig 4: Crystallization temperature of Virgin PBAT and bio-nanocomposites

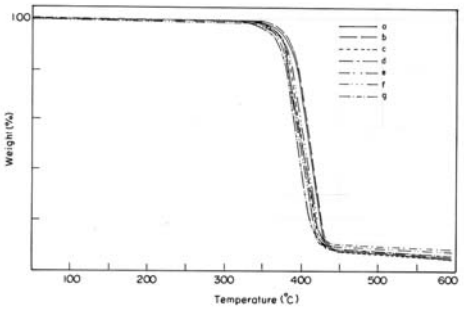

Fig 4: TGA of (a). PBAT, (b). PBAT-Na^{+}MMT, (c). PBAT-C20A, (d). PBAT-C30B, (e). PBAT-B109, (f). MA-g-PBAT-C30B, (g). MA-g-PBAT-B109 bio-nanocomposites

Table 1: Mechanical Properties of PBAT & bio-nanocomposites

Samples	Tensile Modulus (MPa)	Tensile Strength (N/mm^2)	Elongation at break (%)	Tear Strength g/mm
PBAT	26.20(T) 30.17(M)	20.814(T) 14.328(M)	602.33 (T) 766.44 (M)	335.3
PBAT/C30B3%	34.215(T) 39.824(M)	6.883(T) 10.78(M)	552.84 (T) 601.66 (M)	343.17
PBAT/C20A3%	30.03(T) 32.35M)	3.513(T) 4.193(M)	544.08 (T) 550.33 (M)	283.00
PBAT/B1093%	36.389(T) 44.333(M)	5.490(T) 17.370(M)	595.41 (T) 740.30 (M)	348.98
PBAT-g-MA/C30B	52.489(T) 56.213(M)	8.353(T) 12.314(M)	605.39(T) 684.32(M)	375.05
PBAT-g-MA/C20A	43.467(T) 52.597(M)	3.221(T) 6.391(M)	560.93(T) 590.39(M)	290.03
PBAT-g-MA/B109	73.123(T) 81.854(M)	7.7952(T) 8.627(M)	695.35(T) 760.39(M)	445.39

Biomimetic synthesis of nanohybrids based on calcium hydroxyapatite and carboxymethyl cellulose

Annamalai Pratheep Kumar[a*], Kamal Khaja Mohaideen[a, b] and Raj Pal Singh[a#]
[a] Division of Polymer Science and Engineering,
[b] Physical and Materials Chemistry Division
National Chemical Laboratory, Dr. Homi Bhaba Road, Pune - 411 008, India.
E-mail[#]: rp.singh@ncl.res.in

Abstract

In the present paper we report biomimetic synthesis of nanohybrids based on carboxymethyl cellulose (CMC) and hydroxyapatite (HA) nanoparticles by a co-precipitation method. The physico-chemical characterizations were done before and after calcination using Fourier transform infrared spectroscopy, solid state ^{31}P nuclear magnetic resonance (NMR) spectroscopy and thermogravimetric analysis (TGA). The formation of nanohybrid was observed by wide angle X-ray diffraction (WAXD), scanning electron microscopy (SEM) with energy dispersive X-ray analysis (EDX) and transmission electron microscopy (TEM). The nanohybrid was formed as aggregates of nanoparticles adsorbed on CMC. With increasing content of CMC, the crystallite size of hydroxyapatite particles decreased (with 2 wt. % 18±3 nm). The morphological aspects of calcined samples have shown the sintering ability of HA nanoparticles. The possible mechanism for interaction between CMC and HA, nucleation and growth of nanocrystals of HA is discussed. It is summarized that nanohybrids of hydroxyapatite nanoparticles can be prepared for mimicking the process of nucleation and growth in nature using biodegradable and biocompatible macromolecules like CMC.

1. Introduction

Over the past decade, the main goal of bone tissue engineering has been to develop biodegradable materials as bone graft substitutes for filling large bone defects. Bone and teeth consist of a small amount of organic matrix, which manipulates the formation of apatite into distinct microstructures suitable for the mechanical forces which they encounter *in-vivo* [1, 2]. There has been widespread use of calcium phosphate bioceramics, such as hydroxyapatite (HA) and tricalcium phosphate (TCP), for bone regeneration applications. Their biocompatibilities are thought to be due to their chemical and structural similarity to the mineral phase of native bone [3]. Biomineralized tissues are often found to contain polymorphs and individual minerals whose crystal morphology, size, and orientation are often controlled by local conditions and, in particular, by organic macromolecules such as proteins and polysaccharides [1, 4]. Owing to their small size and high surface area, HA nanoparticles, which are similar to that in bone tissue, can effectively interact with living cells [8, 9]. The drawbacks of HA nanoparticles are their instability, associated with migration of nanoparticles to surrounding tissues under the action of blood flow, and their low solubility [10]. To overcome these, a new development in this field is the biomimetic synthesis of nanosized calcium phosphates (mainly HA) in

polymer-matrices to produce composites that can initiate osteogenesis when implanted in bony sites [11]. In biomedical applications, cellulose, a polysaccharide, is used either as regenerated films, fibers or as derivatives (esters, ethers) [14-16]. Considering, the biodegradability, biocompatibility, non-toxicity, muco-adhesive nature and the carboxyl groups on structure of carboxymethyl cellulose, we expect that CMC can interact with precursors and direct the nucleation and growth of hydroxyapatite to produce bioactive ceramics. Thus, the present study is to prepare nanohybrids of carboxymethyl cellulose (CMC) and hydroxyapatite (HA) nanoparticles and to study the effect of CMC on size, structure and morphology of HA.

2. Experimental

Keeping the molar ratio of calcium / phosphate as constant ~1.67, the CMC content was varied from 0 to 2 wt. % of total weight formulations were calculated as represented in Table 1. The weighed amounts of polymer and calcium reagent ($CaCl_2$) were dissolved in aqueous ammonia at room temperature (~27 °C). After 15 min, the phosphate reagent, diammonium hydrogenphosphate ($(NH_4)_2HPO_4$) was added to this solution and stirred for 2 weeks at room temperature (~27 °C). During the reaction, the pH was monitored and adjusted at 10 by addition of ammonia solution. After reaction, precipitate was washed with deionized water and dried in a vacuum oven at 40 °C for 12 h. Portions of the prepared samples were calcined at 1000 °C for 1.5-2 h. The physico-chemical characterizations were done before and after calcination using Fourier transform infrared spectroscopy, solid state ^{31}P nuclear magnetic resonance (NMR) spectroscopy and thermogravimetric analysis (TGA). The formation of nanohybrid was observed by wide angle X-ray diffraction (WAXD), scanning electron microscopy (SEM) with energy dispersive X-ray analysis (EDX) and transmission electron microscopy (TEM).

3. Results and Discussion

3.1. FTIR spectroscopy

In Figure 1, the characteristic peaks at 2800-3000 cm $^{-1}$, 3100-3500 cm $^{-1}$, 1650-1700 cm^{-1}, and 1100 cm^{-1}, which are assignable for C-H, hydroxyl, carboxylate and C-O- group regions, respectively, indicate the presence of CMC. The absorption bands at 3571 $cm^{-1}$and 631 cm^{-1}, arise from stretching and bending modes of OH^- ions, respectively. The absorbance at 1040 and 1090cm^{-1} is attributed to (ν_3) phosphate PO_4^{3-}. The other bands at 962 cm^{-1} (for ν_1), 601 and 574 cm^{-1} (for ν_4), and 472 cm^{-1} (for ν_2) are also attributed to unique characteristic vibrations of PO_4. The weak intensity of bands in 2200 -1950 cm^{-1} region derives from overtones of bands and combinations of ν_3 and ν_1 phosphate modes. The sharpness of bands, especially at 631, 601 and 574 cm^{-1} indicate a well crystallized HA [22]. The 1037 cm^{-1} and 1096 cm^{-1} bands in Figure 1a and b are PO_4^{3-} ν_3 mode and asymmetric HA, respectively.

3.2. ^{31}P-NMR Spectroscopy

Figure 2 Shows the solid state ^{31}P NMR Spectra of as-synthesized and calcined calcium hydroxyapatite. The peak at 2.3 - 2.5 ppm, which is typical for hydroxyapatite, can be observed for all the samples. They, however, differ in the line width, and the broadening of peak at foot is also observed for the *as-synthesized* nanohybrids. The broadening of peak is attributed to nanoscale crystalline particles [25].

3.3. Thermogravimetric analysis (TGA)

In TGA thermograms of as-synthesized nanohybrids (Figure 3), The observed weight loss in the temperature range from 75 °C to 550 °C under nitrogen atmosphere can be attributed to dehydration of water molecules present / adsorbed in the crystals, carbon dioxide evolution from carbonate defects of calcium phosphates and decomposition of carboxymethyl cellulose. Since the nanohybrids were thoroughly washed with deionized water for several times while filtration, only the strongly adsorbed / bound CMC molecules can contribute to the additional weight loss.

3.4. Wide angle X-ray diffraction (WAXD)

Figure 4 shows the WAXD patterns of as-synthesized and calcined nanohybrids. The characteristic peaks at 2θ ~10.8, 18.8, 25.8, 31.7 (with maximum intensity), 32.9, 34.0, 39.8, 46.83, 49.4, and 53.1° are attributed to hydroxyapatite. The broadening at foot of peak at 2θ ~31.7° for as-synthesized samples can be correlated to nanocrystal formation. For the calcined samples, these peaks are narrow and sharp. The effect of CMC content on the crystallite size D (nm) of HA in both as-synthesized and calcined samples was calculated using Scherer formula. With increasing content of CMC, the crystallite size decreases. After calcination, regardless of CMC content the crystallite size is increased upto 48 ± 4nm, which can be attributed to the sintering and densification phenomena at a constant and higher temperature [31]. The consistency in crystallite size can be attributed to the constant calcination temperature and conditions in which the coalescence of finer particles is expected to be in similar rate [33, 34].

3.5. Scanning Electron Microscopy (SEM) and Energy Dispersive X-ray Analysis (EDX)

SEM images of the *as-synthesized* and calcined samples are shown in Figure 5 (HA-05 and Figure 5 (HA-1). In the *as-synthesized* samples, the nanoparticles are embedded / surrounded by CMC molecules, to form agglomerates whose size is about 100 – 300 nm. These agglomerates show rough and interconnected porous surface. As FTIR spectra results suggest the presence of CMC in as-synthesized nanohybrids, the agglomeration of nanoparticles might be due to CMC molecules. After calcination, particles are bigger in size and smoother on the surface than that of as-synthesized ones. As mentioned above, the increase in particle size can be attributed to the sintering of HA nanoparticles at higher temperature. Figure 7 shows the EDX graph of the as synthesized and calcined sample of HA-05. The Ca/P ratios for as-synthesized and calcined sample were about 1.45 and 1.67, respectively. This also confirms the formation of hydroxyapatite precipitates.

3.6. Transmission Electron Microscopy (TEM)

The bright field TEM images of as-synthesized and calcined samples are shown in Figure 6. The *as-synthesized* nanohybrids can be seen as agglomerates of nanoparticles grown on the CMC matrix. The size of agglomerates can be found about 100 to 300nm. After calcination, the HA particles are found to be bigger. In the as-synthesized samples, the agglomeration of HA nanoparticles can be explained by interactions between carboxymethyl cellulose, HA and its precursors with each other.

4. Conclusion

In the present study, we have prepared nanohybrids of carboxymethyl cellulose (CMC) and hydroxyapatite (HA) nanoparticle by co-precipitation method at room temperature. The FTIR, ^{31}P-NMR spectroscopy and wide-angle X-ray diffraction measurements have shown the formation CMC-nanohybrids. TG analysis revealed that content of CMC in nanohybrids is linear with initial input. The SEM and TEM images shown that nanohybrids are formed as aggregates of HA nanoparticles embedded in CMC matrix. The morphological aspects of calcined samples have shown the sintering capacity of HA nanoparticles. Possible mechanism for interaction between HA and CMC, nucleation and growth is discussed. Thus, we can summarize that the nanohybrids of hydroxyapatite nanoparticles can be prepared for mimicking the process of nucleation and growth in nature using biodegradable and biocompatible polymer like CMC.

Acknowledgement:

The authors are grateful to Dr. S. Sivaram, Director, National Chemical Laboratory (NCL), Pune, for providing the infrastructure and encouragement. Dr. P.A. Joy, Physical and Materials Chemistry Division, NCL, Pune is acknowledged for his fruitful discussions and valuable suggestions.

References

1. S.I. Stupp, P.V. Braun, Science 277 (1997) 1242.
2. T. Kokubo, H.-M. Kim, M. Kawashita, Biomaterials 24 (2003) 2161.
3. D. Skrtic, J.M Antonucci, E.D. Eanes, J. Res. Natl. Inst. Stand. Technol. 108 (2003) 167.
4. H.A. Lowenstam, S. Weiner, On Biomineralization, Oxford University Press, New York, 1989.
5. Y. Doi, T. Horiguchi, J. Biomed. Mater. Res. 31 (1996) 43.
6. T.J. Webster, R.W. Siegel, R. Bizios, Biomaterials 21 (2000) 1803.
7. Y. Miyamoto, K.I. Shikawa, Biomaterials 19 (1998) 707.
8. I. Lee, S.W. Han, H. J. Choi, K. Kim, Adv. Mater. 13 (2001) 1617.
9. T. Miyamoto, S. Takahashi, H. Ito, H. Inagaki, J. Biomater. Res. 23 (1989) 125.
10. A.G. Walton, J. Blackwell, Biopolymers, Academic Press, New York, 1973.
11. P.Y. Yang, S. Kokot, J. Appl. Polym. Sci. 60 (1998) 1137.
12. M. Markovic, B.O. Fowler, M.S. Tung, J. Res. Natl. Inst. Stand. Technol. 109 (2004) 553.
13. C. Jäger, T. Welzel, W. Meyer-Zaika, M. Epple, Magn. Reson. Chem. 44 (2006) 573.
14. A. Bigi, A. Incerti, N. Roveri, E. Foresti-Serantoni, R. Mongiorgi, L.R. di Sanseverino, A. Krajewski, A. Ravaglioli, Biomaterials 1 (1980) 140.
15. H. Y. Juang, M. H. Hon, Biomaterials 17 (1996) 2059
16. H.E.-Hosseini, M. R. Housaindokht, M. Chahkandi, Mater. Chem. Phys. 106 (2007) 310

Tables and Figure

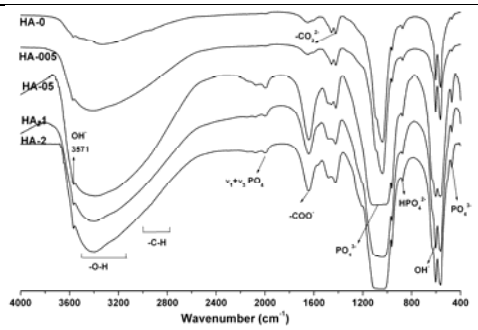

Fig1a: FTIR Spectra of as-synthesized samples

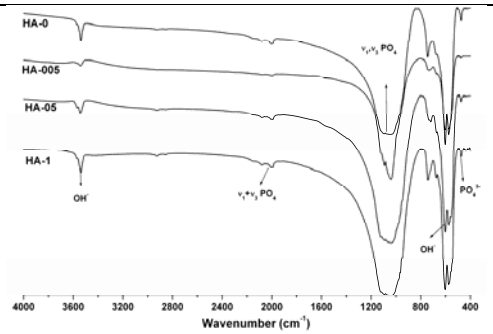

1b: FTIR Spectra of calcined samples

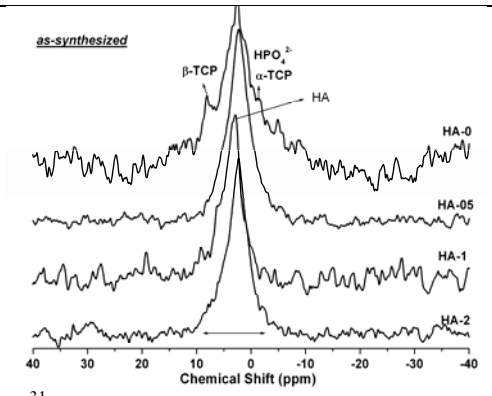

Fig 2: ^{31}P-NMR Spectra of as-synthesized samples

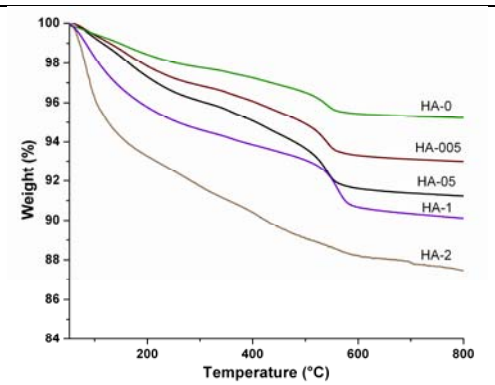

Fig 3:TGA of as-synthesized samples

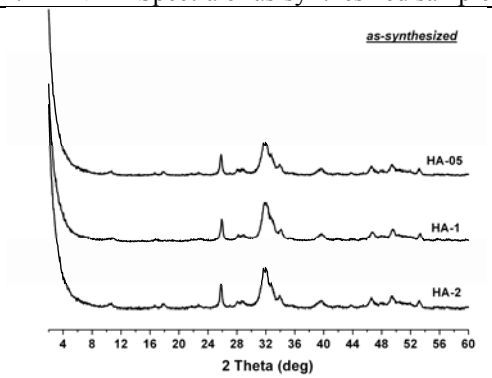

Fig 4a: WAXD patterns of as-synthesized samples

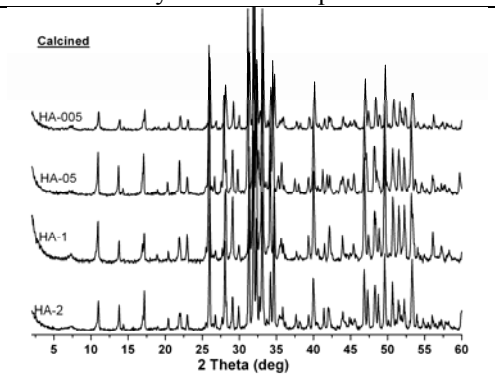

Fig 4b: WAXD patterns of calcined samples

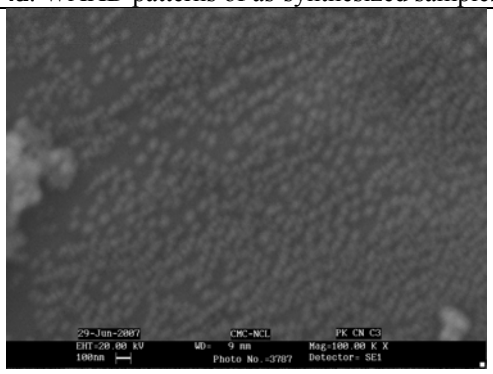

Fig 5a: SEM image of as-synthesized sample

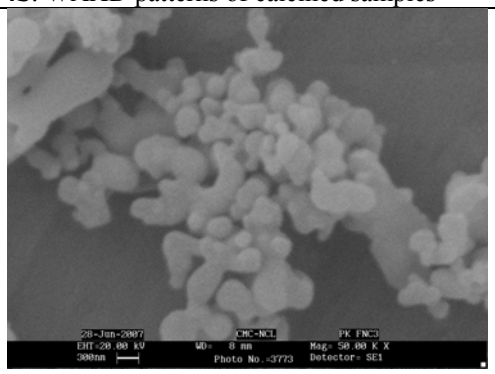

Fig 5b: SEM image of as-synthesized sample

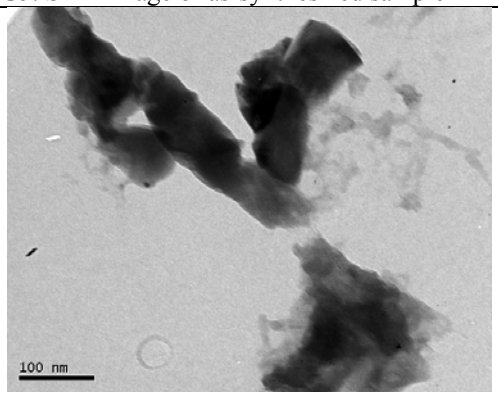

Fig. 6a: TEM image of as-synthesized sample

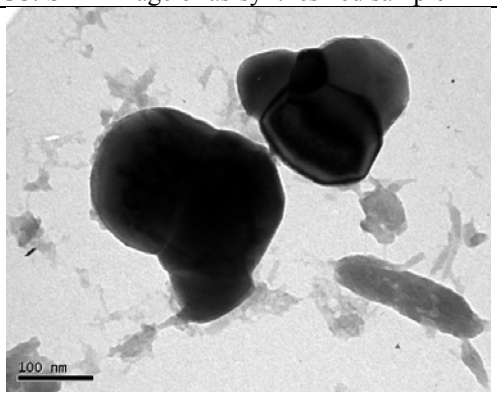

Fig.6b: TEM image of calcined sample

Use of deproteinized and normal skim rubbers for property improvement in natural rubber

K. Mariamma George*, Rosamma Alex, Salini K.S and K.T. Thomas

Rubber Research Institute of India, Rubber Board, Kottayam -9, India
Email: *mariamma@rubberboard.org.in, mgpattani@yahoo.co.in

Abstract

Skim rubber is the rubber recovered from skim latex, which is obtained as a by-product during the centrifugal concentration of natural rubber (NR) latex. Blending skim rubber with natural rubber is a method of taking advantage of the relatively low price of skim rubber while minimizing its disadvantages. In addition, it seems possible that in such blends the fast curing characteristics of the skim can be utilized. We have examined the cure behaviour and technological properties on adding 20 p.h.r (parts per hundred rubber) each of deproteinized skim rubber (DPSR) and normal skim rubber to ISNR 20 without further addition of curatives and comparing the properties to that of a similar ISNR 20 mix. Two cure systems, one which contain usual dosage of accelerator and antioxidant and the other system which contain comparatively lower level of accelerator without any antioxidant were studied. In the former case, the cure characteristics showed that there is attainment of good level of cure and cure rate even after addition of 20 p.h.r skim rubber or DPSR to ISNR 20 with no extra curatives, compared to the conventional ISNR 20 mix. Also the ISNR 20 vulcanizate and the vulcanizate containing additional 20 parts of skim rubber showed comparable values of moduli, tensile strength, tear strength and abrasion resistance and these values were higher than that observed for ISNR 20 vulcanizate containing 20 parts DPSR. Skim rubber incorporated mix showed a slightly higher resistance to crack initiation and crack failure when compared to ISNR 20 mix. Blend which contain 20 parts DPSR showed slightly better dynamic properties and improved air ageing characteristics as compared to normal skim rubber. For the mixes which contain lower level of curatives, cure characteristics were comparable but the values were lower than that which contain the usual dosage. Same trend was observed for the mechanical properties and ageing characteristics. The study has shown that incorporation of 20 parts skim rubber or deproteinized skim rubber to ISNR 20 imparts cure characteristics and mechanical properties similar to that attained by ISNR 20 without the incorporation of additional curatives.

Introduction

Skim rubber is obtained by the coagulation of skim latex, the secondary fraction of natural rubber latex, from the centrifugal concentration process. The processing of skim latex has many associated problems due to the peculiar physical and chemical characteristics of the same and is an issue of environmental concern. Skim latex has very low dry rubber content (4-8%) and rubber particles are smaller in size with high specific surface area [1, 2]. It has higher proportion of non-rubber solids which is mostly proteinaceous in nature. It is difficult to coagulate skim latex [3] and there is considerable loss in skim rubber during processing. Acid coagulation and auto coagulation are used to recover rubber from skim latex [4]. To improve the raw rubber properties of skim rubber, attempts have been made by deproteinization using certain enzymes [5] and subsequent creaming [6] of skim latex. The proteolytic enzyme stabilized liquid papain used for deproteinization followed by creaming results in quick and easy coagulation of skim latex [7]. The type and high level of non-rubbers present in the skim rubber give rise to scorchy cure and generally give vulcanizates of high modulus. The latter can be considered to arise at least in part due to the protein present in the rubber acting as a reinforcing filler and participation in the curing process. Despite these adverse features, skim rubber has low dirt content, often accompanied by light colour and relatively low cost. Blending skim rubber with natural rubber is a method of taking advantage of the relatively low price of skim rubber while minimizing its disadvantages. In addition, it seems possible that in such blends the fast curing characteristics of the skim can be utilized [8].

In this work we have examined the cure behaviour and technological properties on adding 20 phr (parts per hundred rubber) each of deproteinized skim rubber (DPSR) and skim rubber to ISNR 20 mix without further addition of curatives and comparing the properties to that of a similar ISNR 20 mix. Two cure systems, one which contain usual dosage of accelerator and antioxidant and the other system which contain comparatively lower level of accelerator without any antioxidant were studied.

Experimental

ISNR 20 - From the Pilot Crumb Rubber Factory, Rubber Board
DPSR - Prepared at the Rubber Technology Division, RRII
Skim rubber - From the Central Experiment Station, Chethackal, Rubber Board
The other ingredients used were of commercial grade

Preparation of deproteinized skim rubber

Liquid papain of 0.25 phr as 5% solution was initially treated with 0.5 phr potassium oleate. This was then mixed with the skim latex, stored for 48 h at room temperature, treated with potassium oleate (0.01% w/v on latex as 10% solution) and stored for further 24 h. It was then subjected to creaming with ammonium alginate (0.3% w/v on latex as 3% solution), coagulated the cream with 5% H_2SO_4, the coagulum soaked for 24 h in oxalic acid solution and dried [7]. The fatty acids present in both DPSR and skim rubber were determined using gel permeation chromatograph (GPC – Waters 510) attached to a 410 diffraction refractometer. The solvent used was THF/water/acetonitrile in the ratio 25/35/45 (v/v) at a flow rate of 2ml/min. Raw rubber properties of ISNR 20, DPSR and skim rubber were determined and are given in Table 1.

Preparation of mixes

In order to study the cure behaviour and technological properties, two cure systems were selected. Mixes were prepared as per the formulations given in Table 2 using a laboratory model two roll mixing mill. Cure characteristics of the samples were determined using Tech Pro Rheo Tech MD + at 150°C. Vucanizates were moulded using an electrically heated hydraulic press to their respective optimum cure. Properties of the vulcanizates were determined as per the relevant ASTM standards. Ageing of the vulcanizates was carried out at 70°C for 7 days in an air oven as per ASTM standards.

Results and discussion

Fatty acids

Fig.1 shows the chromatogram of the fatty acids present in the skim rubber prepared by conventional method and that obtained after deproteinization and creaming. The fatty acids present include linoleic, oleic, stearic, linolenic and lauric. There is a reduction in the quantity of fatty acids after deproteinization and creaming. Higher quantity of fatty acids retained in skim rubber adversely affects the ageing characteristics.

Raw rubber properties

Results in Table 1 show that ISNR 20 has nitrogen content of 0.37 % where as skim rubber has nitrogen content of 2.3 %. DPSR prepared by using the protelytic enzyme papain has reduced the nitrogen content to 0.62 %. Being a protease, this enzyme catalysis the hydrolysis of proteins which are bound to the latex particles in to water soluble polypeptides and amino acids, which get removed during the creaming process [9]. Ash content was more for the skim rubber than ISNR 20. During deproteinization and creaming some of these mineral materials were removed and hence the value for the ash content of DPSR was lower than skim rubber but higher than ISNR 20. Initial plasticity, Po for the three samples were within the limit specified by Bureau of Indian Standards (BIS). Comparatively low PRI was recorded by the skim rubber while DPSR recorded a PRI comparable to that of ISNR 20. The low PRI of skim rubber could be attributed to the presence of high proportion of copper and unsaturated fatty acids that accelerate the oxidation of rubber [10]. It is reported that the PRI can be improved by immersion of the coagulum in 1% oxalic acid solution and the improvement observed for the enzyme treated sample may be due to the extraction of free copper from the rubber

[11]. Skim rubber and DPSR differed most obviously from ISNR 20 in the high levels of fatty acid and protein content and hence the acetone extractable of skim rubber and DPSR were higher than that of ISNR 20. Mooney viscosity of the three samples was within the processable limit.

Cure characteristics and mechanical properties

Cure characteristics and mechanical properties of mixes 1, 2 and 3 are given in Table 3. The results showed that there is attainment of good level of cure and cure rate even after addition of 20 phr skim rubber or DPSR to ISNR 20 with no extra curatives, compared to the conventional ISNR 20 mix. This shows that both in skim rubber and DPSR there is sufficient quantity of amines and proteins that have an accelerating effect on vulcanization. ISNR 20 vulcanizate and the vulcanizate containing additional 20 parts of skim rubber showed comparable values of moduli, tensile strength, tear strength and abrasion resistance and these values were higher than that observed for ISNR 20 vulcanizate containing 20 parts DPSR. Skim rubber incorporated mix showed slightly higher resistance to crack initiation and crack failure when compared to ISNR 20 mix. However, comparable flex resistance was obtained for ISNR 20 mix and DPSR (20 parts) incorporated mix. It is reported that the proteins present in skim rubber can improve the modulus and resistance to flex cracking of rubber vulcanizate owing to its reinforcing characteristics[12]. Comparatively lower values of resilience, higher heat build-up and compression set were recorded for the mix containing 20 parts of skim rubber. The proteins present in skim rubber are known to adversely affect dynamic properties like compression set, resilience and heat build-up. Blend which contains 20 parts of DPSR showed slightly better dynamic properties compared to normal skim rubber. The improvement may be attributed to the reduction of protein content and partial removal of unsaturated fatty acids. The above results showed that incorporation of 20 parts of skim rubber or deproteinized skim rubber to ISNR 20 imparts cure characteristics and mechanical properties similar to that attained by ISNR 20 without the incorporation of additional curatives.

Cure characteristics and mechanical properties of mixes 4, 5 and 6 are also given in Table 3. Cure characteristics were comparable but the values were lower than that which contains the usual dosage, i.e. for mixes 1, 2 and 3. Same trend was observed for the mechanical properties.

The ageing resistance in modulus and tensile strength of the vulcanizates after ageing at 70°C for 7 days are given in Figs. 2 and 3. For mixes 1, 2 and 3, retention of modulus and strength for the blend which contain DPSR were better than ISNR 20 mix and the blend containing skim rubber. The improvement in ageing characteristics may be attributed to the partial removal of unsaturated fatty acids and metal ions that are pro-oxidants during deproteinization and creaming process. For mixes 4, 5 and 6 retention of modulus and strength were comparable but the values were lower than that obtained for the mixes 1, 2 and 3.

Conclusions

Incorporation of 20 parts of skim rubber or deproteinized skim rubber to ISNR 20 imparts cure characteristics and mechanical properties similar to that attained by ISNR 20 without the incorporation of additional curatives. Skim rubber incorporated mix showed a slightly higher resistance to crack initiation and crack failure when compared to ISNR 20 mix. Blend which contains 20 parts DPSR showed slightly better dynamic properties as compared to normal skim rubber. For the system which contains the normal dosage of curatives, retention of modulus and strength for the blend which contain DPSR were better than ISNR 20 mix and the blend containing skim rubber.

References

1. Subramanian, A.RRIM Technol Bulletin, 1980, 4, 1.
2. Yeang, H. Y, Eshah, Y, Samsidah, H. J Rubb Res, 1995, 10, 108.
3. Smith, M.G. J Rubb Res Malaya, 1969, 23, 1, 70.
4. John, C.K, Sin, S.W. J Rubb Res Inst Malaya, 1973, 23, 4, 257.
5. Morris, J. E. Proc 3rd Rubb Tech Conf, London, June 1954, 13.
6. Sakdapipanich, J.T, Nawamawati, K, Tanaka, Y. J Rubb Res, 2002, 5, 1, 1.

7. George, K.M, Alex, R, Joseph, S and Thomas, K.T. Proc Int Conf on Rubber and Rubber like materials, IIT, Kharagpur, Jan 2008,
8. Bristow, G.M. J Nat Rubb Res 1990, 5, 2,114.
9. George, K.M, Rajammal, G, Joseph, S, Varghese, T.C, Mathew, N.M. Proc 3rd Int Rubb Glove Conf & Exhi, Kuala Lumpur, Malaysia, September 2006, C4, 2.
10. Arnold, A.R, Evans, P. J Nat Rubb Res, 1991, 6, 2, 75.
11. Hasma, H, Othman, A.B. J Nat Rubb Res, 1990, 5, 1, 1.
12. Knight, G.T, Tan, A.S. Proc Int Rubb Conf, Kuala Lumpur, 1975, 4, 115.

Table 1. Raw rubber properties

Parameter	ISNR 20	DPSR	Skim rubber
Nitrogen content, %w/w	0.37	0.62	2.30
Ash content, % w/w	0.36	0.40	0.53
Initial plasticity, P_o	51	38	39
Plasticity retention index, PRI	49	56	17
Acetone extractable, %	2.64	6.78	6.24
Mooney viscosity, [ML(1+4)100°C]	86	76	70
Copper content, ppm	6.0	10.0	18.0

Table 2. Formulation of mixes

Ingredient	Mix Nos					
	1	2	3	4	5	6
ISNR 20	100	100	100	100	100	100
Deproteinized skim rubber	-	20	-	-	20	-
Skim rubber	-	-	20	-	-	20
Zinc oxide	5	5	5	5	5	5
Stearic acid	2	2	2	2	2	2
HAF black (N300)	30	30	30	30	30	30
Naphthenic oil	1.5	1.5	1.5	1.5	1.5	1.5
Antioxidant TDQ[1]	1	1	1	-	-	-
CBS[2]	0.7	0.7	0.7	0.5	0.5	0.5
Sulphur	2.5	2.5	2.5	2.5	2.5	2.5

[1]2,2,4-trimethyl 1,2-dihydroquinoline
[2]N-cyclohexyl-2-benzthiazil sulphenamide

Table 3. Cure characteristics and mechanical properties

Parameter	Mix Nos					
	1	2	3	4	5	6
Minimum torque, dN.m	0.39	0.35	0.40	0.24	0.40	0.37
Maximum torque, dN.m	9.43	8.09	8.81	5.97	5.07	5.25
Δ, Rheometric torque, dN.m	9.04	7.74	8.41	5.73	4.67	4.88
Optimum cure time (t_{90}) at 150ºC, min	7.33	8.88	7.08	9.17	10.58	9.54
Scorch time (t_{s2}) at 150ºC, min	2.17	3.09	2.35	3.07	4.91	4.07
Cure rate, dN.m/min	1.47	1.08	1.16	0.48	0.41	0.43
100 % Modulus, MPa	1.1	0.9	1.1	1.2	1.2	1.2
200 % Modulus, MPa	2.1	1.6	2.0	2.4	2.4	2.5
300 % Modulus, MPa	3.5	2.5	3.3	4.9	4.8	5.1
Tensile strength, MPa	28.1	25.1	27.0	23.6	24.7	24.9

Elongation at break, %	707	748	720	644	648	649
Tear strength, N/mm	71.2	67.3	70.5	57	50	52
Hardness, Shore A	50	49	50	41	41	41
Abrasion loss, mm^3	125	130	126	132	140	141
Rebound resilience, %	68.5	68.8	67.3	65.2	65.2	65.2
Heat build-up, ΔT ºC	11	11	12	12	12	12
Compression set, %	22.8	24.2	25.9	24.3	25.8	26.3
Dematttia flexing						
Crack initiation, K/cycles	74.4	74.4	86.9	22.4	19.4	28.1
Crack failure, K/cycles	132.5	135.9	181.6	36.0	35.1	40.8

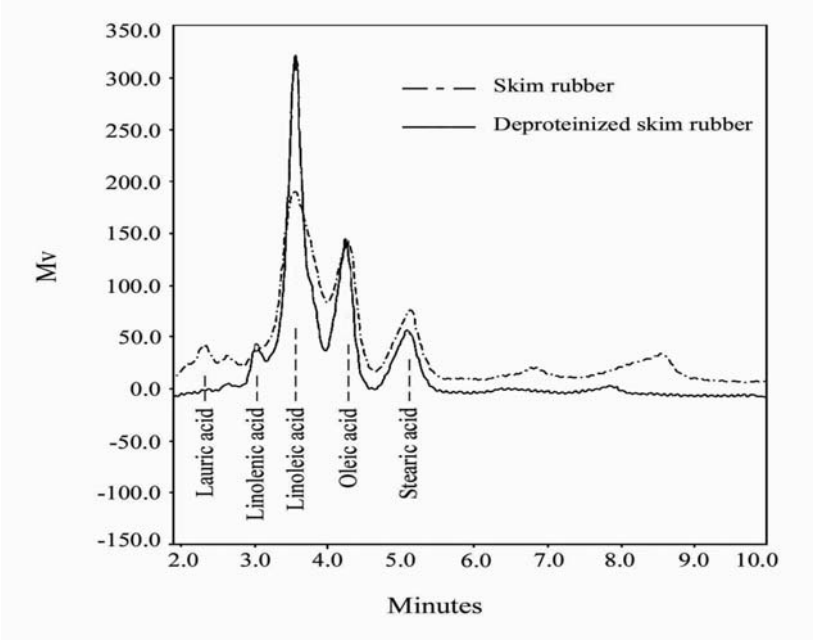

Fig.1. Chromatogram showing the fatty acids in skim rubbers

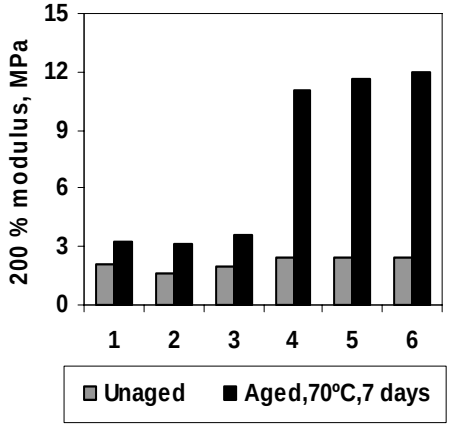

Fig.2 Effect of ageing on 200 % modulus

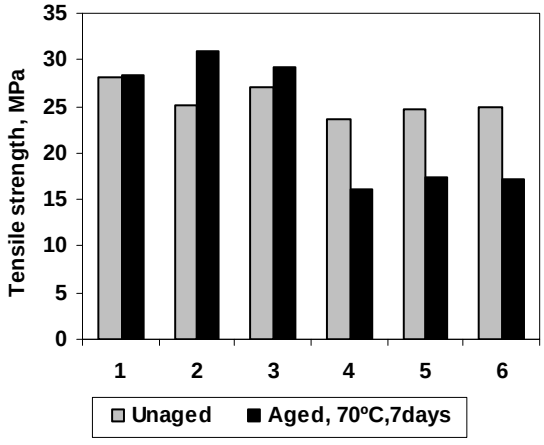

Fig.3 Effect of ageing on tensile strength

Reinforcement studies – Effect of thiophene-plasma coating of silica on the performance in EPDM, SBR and NBR

M. Tiwari, R. N. Datta, A. G. Talma, J. W. M. Noordermeer, W. K. Dierkes

Department of Elastomer Technology and Engineering, University of Twente,
7500 AE Enschede, The Netherlands
and
Wim J. Van Ooij
Department of Chemical and Materials Engineering, University of Cincinnati,
Cincinnati, OH 45221-0012, USA
Email: J.W.M.Noordermeer@utwente.nl

Abstract

The filler surface chemistry is a crucial factor for the level of dispersion and filler-polymer interaction in rubber, thus determining the vulcanizate properties. Plasma-polymerization allows tailoring the surface chemistry without influence on the bulk properties. Thiophene was used as monomer in this study for its sulfur moiety, and the plasma-thiophene (PTh) coated silica was blended with EPDM, SBR and NBR, as these polymers differ in polarity and unsaturation. As reference, untreated and silanized silica were used.

In EPDM, plasma-polymerization onto silica results in a lowering of the filler-filler interaction compared to untreated silica due to a better match of the surface energy between filler and polymer. The PTh-silica shows the best dispersion compared to untreated and silanized silica. The final properties of the PTh-silica reinforced material are improved compared to untreated silica reinforced EPDM.

In SBR and NBR, the plasma-treatment again results in a better dispersion as well as a higher bound rubber content. In terms of mechanical properties, the PTh-silica results in a better performance compared to untreated and even to silanized silica.

This study shows that thiophene plasma-polymerized silica can act as a replacement for the silica-silane system; and in some cases it performs even better than the silanized silica.

Introduction

The reinforcing effect of fillers depends on the nature of filler-rubber interactions as well as the filler dispersion in the elastomeric matrix. Both processes are linked and controlled by the primary particle size and its distribution, the shape, structure and site energy distribution as well as functional groups on the filler surface[1,2]. Silica has been recognized as an important filler for rubber reinforcement and is used as a partial or even complete replacement for carbon black. However, silica has a high density of hydrophilic silanol groups on its surface, resulting in a strong filler-filler interaction and a poor filler-polymer interaction. Therefore, silica tends to form agglomerates as a secondary structure by hydrogen bonds between silanol groups on the silica surface. To produce silica-filled rubber compounds with high performance, the compatibility between silica and rubber has to be enhanced. For this purpose, a silane coupling agent is

commonly used to chemically modify silica surfaces and promote interactions between hydrophilic silica surfaces and the hydrophobic rubber phase[3-5]. In the conventional technology, the reaction between silica and the silane coupling agent takes place in the rubber-filler blend during mixing. This in-situ modification requires a number of precautions regarding the mixing sequence and the mixing temperature, as well as careful adjustment of mixing conditions for every silane containing compound.

Recently, plasma polymerization has emerged as a surface modification technique for polymers, metals and powders. Van Ooij et al.[6] have reported plasma modification of silica, which changes the surface chemistry of the filler.

In the previous work[7,8], the effect of plasma-acetylene coated silica on the properties of S-SBR, EPDM, NBR compounds and their blends have been studied. In this study, the silica is modified with plasma-thiophene, which has a sulphur moiety in its cyclic structure. The effect on processing behavior and properties of EPDM, SBR and NBR compounds containing plasma-thiophene (PTh) coated silica will be evaluated.

Experimental

For the surface modification of silica powders, a radiofrequency (13.56 MHz) electrodeless tumbler plasma reactor is used, based on a horizontally mixing principle and with a capacity of 350 g/batch. The plasma polymerization was carried out after charging 100 g of dried silica (Ultrasil VN3) into the reactor, evacuating the reactor to 13 Pa and introducing thiophene gas. The operating pressure, which was determined by the thiophene vapour flow, was 20 Pa. The power and treatment time were 100 Watts and 90 minutes.

The general characterization techniques used for treated silica powders are an immersion test, water penetration measurements[9], Thermo-Gravimetric Analysis (TGA), Time-of-Flight Secondary Ion Mass Spectroscopy (ToF-SIMS) and Energy Dispersive X-ray Spectrometry (EDX).

Mixing of the filler-rubber compounds was done in an internal mixer; the curatives were added on a two roll mill. The compounds were characterized by measuring the Payne effect (RPA 2000) and bound rubber content[10,11]. The cure characteristics (RPA 2000) were measured, and the reinforcement parameter (α_F)[12] as well as the mechanical properties (ISO-37) were determined. As references, untreated and silane-treated silica were used.

Results and Discussion

Immersion and water penetration tests show a change in the surface energy after the plasma treatment of the silica filler: The polythiophene (PTh)-film coated aggregates are more hydrophobic and show a lower surface energy.

The weight-loss measured by TGA was higher for silica after plasma-thiophene treatment as shown in Fig. 1: this indicates film deposition on the surface of the silica.

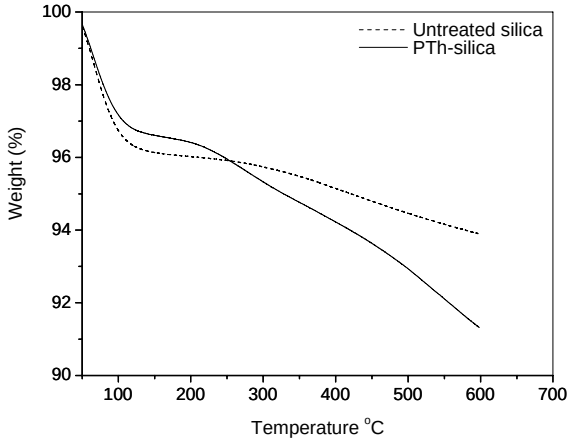

Fig. 1: *TGA analysis of untreated and plasma-polymerized-polythiphene coated silica*

Positive ToF-SIMS spectra of the untreated silica sample showed no specific peaks in the low mass region such as $C_2H_3^+$, $C_{10}H_{10}^+$ and no cluster peaks in the higher mass region. In the negative spectra, no specific peak of sulphur at 32 amu is found. However, the thiophene monomer treated sample (PTh) shows the specific plasma-polymerized hydrocarbon peaks in the low mass region and strong polythiophene cluster peaks in the higher mass region, indicating a good polythiophene surface coating on the silica powders. The presence of sulphur at 32 amu in the negative spectra also confirms the deposition of PTh-film on the surface of silica.

Elemental analysis by EDX also confirms the deposition of a PTh-film on the silica surface, as the elemental carbon and sulphur content increased.

The PTh- and silane-modified silica filled EPDM, SBR and NBR showed a lower Payne effect compared to the unmodified silica filled rubbers, indicating a lower filler-filler interaction.

The reinforcement parameter[12] was lowered for the PTh-silica filled matrices; this indicates a better dispersion compared to untreated as well as silane modified silica filled samples. The PTh-silica filled EPDM shows the lowest value of the reinforcement parameter compared to both other silica's. The PTh-silica filled SBR and NBR show a higher bound rubber

content due to higher filler-polymer interactions compared to untreated and silane-treated silica. PTh- and untreated-silica filled EPDM show similar levels of bound rubber content, lower than the silane-treated silica.

PTh-silica filled EPDM (EPTh), SBR (SPTh), and NBR (NPTh) show self-curing behavior as shown in Fig. 2. This self-curing behaviour is due to the presence of sulphur moieties in the deposited PTh-film on the silica surface.

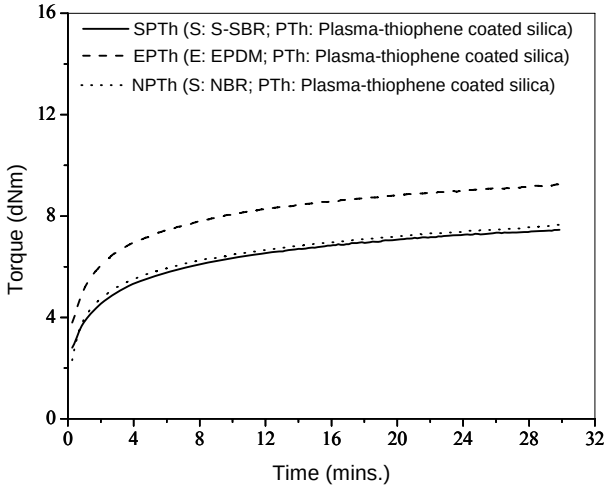

Fig. 2: *Self-curing behaviour of PTh-silica filled SBR, EPDM and NBR*

For all three polymers, tensile strength is increased significantly due to the PTh-treatment. However, for SBR (SPTh) the addition of PTh-coated silica results in higher tensile strength as well as a higher modulus at 300% elongation and lower elongation at break values as shown in Fig. 3. This can be explained by a better dispersion and filler-polymer interaction as well as a higher crosslink density.

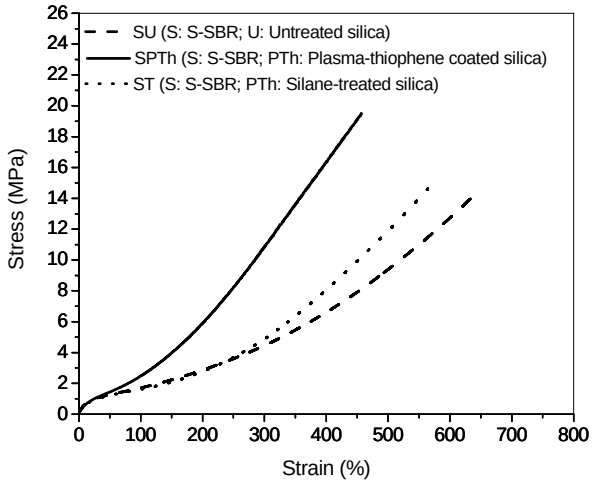

Fig. 3: *Tensile properties of untreated, PTh- and silane-treated silica filled SBR*

In a PTh-silica filled EPDM, the material shows higher tensile strength and elongation at break values due to a better dispersion and compatibilization with the polymer. However, lowering of the modulus in EPDM shows the formation of a less dense network due to a lower number of unsaturation sites in the polymer chain structure. In NBR, the PTh-treated silica showed improved tensile properties resulting from an improved morphology and stronger network compared to untreated and silane-treated silica.

Conclusions

Silica as reinforcing filler for elastomers can be plasma-coated under vacuum conditions. As a consequence, it shows a significant decrease in surface energy due to film deposition.

It is possible to improve the dispersion of the filler in different polymers by matching the surface energies. The properties of the silica surface can be tailored by depositing different functional groups by plasma-polymerization, which leads to an improvement of the final properties of filled polymers.

Acknowledgements

The support of STW, Hexagon Polymers and Timcal Graphite & Carbon is greatly acknowledged.

References

1. A. Schroeder; M. Klueppel; R. H. Schuster; J. Heidberg *Carbon* 2002, *40*, 207.
2. W. M. Hess; C. Herd; P. C. Vegvari *Rubber Chem. Technol.* 1993, *66*, 834.
3. L. A. E. M. Reuvekamp; J. W. ten Brinke; P. J. Van Swaaij; J. W. M. Noordermeer *Rubber Chem. Technol.* 2002, *75*, 187.
4. R. Alex; N. M. Mathew; P. P. De; S. K. De *Kautsch. Gummi Kunstst*. 1989, *42*, 674.
5. E. M. Dannerberg *Rubber Chem. Technol.* 1975, *48,* 410.
6. W. J. van Ooij; N. Zhang; S. Guo; S. Luo *Paper presented at Functional Fillers and Fibers for Plastics 98*, P. R. China 1998, June 15-17.
7. M. Tiwari; W. K. Dierkes; J. W. M. Noordermeer; W. J. van Ooij *Rubber Chem. Technol. 2008, 81*, 276.
8. M. Tiwari; W. K. Dierkes; J. W. M. Noordermeer; W. J. van Ooij *Polym. Adv. Technol.* 2008, *19*, 1-12.
9. N. Inagaki; S. Tasaka; H. Abe *J. Appl. Poly. Sci.* 1992, *46*, 595.
10. S. Wolff *Rubber Chem. Technol.* 1981, *55*, 967.
11. J. L. Leblanc; P. Hardy *Kautsch. Gummi Kunstst*. 991, *44*, 1119.
12. S. Wolff *Kautsch. Gummi. Kunststoffe* 1970, *23*, 7.

Effect of plasticizer, filler and solvent swell on polyurethane elastomers

Santosh K Gurunath[a]*, M. Rengasamy[b] and V. Sivasubramanian[a#]

[a] Department of Chemical Engineering, National Institute of Technology Calicut, Kerala – 673 601, India.
[b]Department of Petrochemical Technology, Bharathidasan Institute of Technology, Tiruchirappalli -620 024, India.
Email: siva@nitc.ac.in

Abstract

Polyurethane elastomers are developed using different types of isocyanate terminated polyether based prepolymers (A, B and C) with four types of multifunctional hydroxy derivated curatives (X1, X2, X3 and X4) and selected processing additives namely plasticizer and filler. The polyurethane elastomers are developed with a view to utilize them in high performance print roller applications, with improved strength and solvent resistant characteristics. The properties like pot life, hardness, tensile strength, modulus, tear strength, compression set, density and solvent resistance of these polyurethane elastomers are studied in the absence of additives and also in the presence of additives. Among the polyurethane elastomers prepared, the product obtained from prepolymer C with curative X3 exhibits better strength properties and solvent resistant characteristics than those from other products. Incorporation of additives (plasticizer and filler) improves the performance characteristics of polyurethane elastomers. However, the degree of improvement varies based on the nature of reactants involved.

Keywords : Polyurethane elastomers, Plasticizers and Solvent swell

Introduction

Polyurethanes are available as rigid, flexible and structural foams, elastomers, coatings, adhesives, casting resins and fibres[1]. These can be manufactured in the wide range of varying densities from 6 kg/m^3 to 1220 kg/m^3 and polymer stiffness from very flexible elastomers to rigid hard plastics. Polyurethane has high porosity, low weight to volume ratio, good thermal and acoustic properties, good resilience, abrasion resistance and oil resistance. This material finds wide industrial and engineering applications. Polyurethane is a product[2] of the poly addition of an isocynate and an alcohol. Reaction is an exothermic.

$$nR – NCO + n\ HO –R' \rightarrow R – [NHCOO]_n – R'$$

There are many kinds of poly isocynates and polyols of different molecular weights and functionalities are used and each one has its one particular property to give a different product for definite end use. Polyurethane elastomers are used in many fields like automobile, textile, oil, mining, electronic, and other engineering industries. There is a very good future of polyurethane elastomers. They are versatile engineering materials designed to provide properties that are not obtained from conventional rubbers, metals, and plastics. They have higher oil and solvent resistance and better aging properties than most general purpose rubbers and plastics. They have greater abrasion and tear resistance than neoprene or natural rubber, greater load bearing capacity; extensibility and impact character of polyurethane elastomer are also greater than those of most plastics. They have a wide range of hardness from soft rubbers to rigid plastics[3-10]. The objective of the present study is to prepare polyurethane elastomer and to study the performance characteristics.

Experimental Procedure

Liquid Castable Polyurethane Elastomer

Cast elastomers are usually slightly cross linked thermoset polymers. In the production of urethane elastomer the heated prepolymer is mixed with a selected curative in specific proportion. Prepolymers contain terminal isocyanate (NCO) groups, which react chemically with hydroxyl (OH) or amine (NH_2) groups in the curative. The mixture is poured into a heated mould where the components rapidly react to form a solid elastomeric article.

Reaction

$$\underset{\text{Polyol}}{HO - A - OH} + \underset{\text{Diisocyanate}}{OCN - R_1 - NCO}$$

$$\downarrow$$

$$OCN - R_1 - HNCOO - A - OCONH - R_1 - NCO + (n\text{-}1)HO - R_2 - OH$$

Prepolymer — Alcohol

$$\downarrow$$

$$-\left[-O - A - OCONH - R_1NHCO - (O - R_2 - OCONH - R_1 - NHCO-)_{n-1}\right]-$$

Polyurethane Elastomer

The flexibility is imparted by the long chain glycols, whereas the rigidity is obtained by short chain glycols. There are two types of polyurethane elastomers, depending upon the polyol used. These are called polyether based polyurethane elastomers and polyester based polyurethane elastomer. Polyether based polyurethane elastomers give lower densities and better hydrolytic stability, fungus resistance and electrical properties. Polyester based polyurethane elastomers result in higher densities – better tear and abrasion resistance and less oil and solvent absorption. Polyesters are also less easily oxidized and resist higher temperatures than polyethers.

PROCESSING

Process Conditions

Reaction Temperature	70 – 80°C
Stoichiometry	95%
Mixing Time	3 min
Oven Temperature	120°C
Cure Condition	16 hours at 120°C
Post-cure condition	Two weeks at room temperature

Procedure

The desired amount of prepolymer is weighed into a suitable container and the prepolymer is heated to 70 – 80°C. The over heating should be avoided. The required amount of plasticizer and filler are added in the case of filled products. The reaction is carried out in vacuum and with suitable amount of curatives. The mixed reactants are degassed and poured into a preheated (120°C) mould and is allowed for 16 hours to complete the reaction (curing). Further, the product is kept for two weeks time at room temperature for post curing before being tested.

Results and Discussion

Properties of Unplasticized and Unfilled Polyrethane Elastomer

The curing efficiency of four types (X1, X2, X3, and X4) of hydroxyl terminated curatives have been tested on three types of polyether based isocyanate terminated prepolymer (A,B and C) with different functional additives. Among the curatives, the curative X1 imparts highest pot life (working time) towards the polyether prepolymers (A, B and C) tested in this investigation, whereas the curative X4 imparts shortest pot life and other two curatives X2 and X3 lie between these two extremes. This behavior may be attributed to the reactive nature and the percentage of isocyanate groups and hydroxyl groups present in the polyether prepolymers and curatives respectively. The pot life for prepolymer A obtained, when mixed with curatives X1, X2, X3, and X4 are 75, 62, 47 and 29 minutes at 100°C respectively.

Hardness of the cured polyurethane elastomers is determined using the durometer and the results are obtained for different combinations of prepolymer and curatives. Hardness, shore A obtained for the polyurethane elastomer resulted from prepolymer A with curatives X1, X2, X3 and X4 are 57, 54, 53, and 45 respectively. Among the polyurethane elastomer obtained, the product from prepolymers A with curative X1 results in highest hardness (shore A57) which may be explained due to the influence of higher cross link density resulted from the molecular structure. Similarly, among the prepolymers A, B and C, the product polyurethane elastomer obtained from prepolymer C with corresponding curative imparts higher hardness, shore A69, than prepolymers A and B, due to higher percentage of isocyanate and hydroxyl groups, which in turn enhances the crosslink density.

Tensile strength determined using tensile tester for the different polyurethane elastomers are presented. Tensile strength results are merely reflections of hardness values, the product from prepolymer C with curative X1 possess higher tensile strength (42.7 kg/cm^2) than from other combinations of prepolymers A and B curatives X2, X3 and X4. Percentage elongation results obtained for different polyurethane elastomers are studied. The product resulted from prepolymer B with curative X4 exhibits highest elongation (500%), while for the product from prepolymer C with curative X1 gives lowest value (120%). The percentage elongation values are inversely proportional to the hardness and link density of the products.

Modulus, tear strength, and density for different combinations of elastomers are studied. All these values increase with increasing crosslink density and hardness due to higher percentage of reactive groups in the prepolymers. Compression set values for the polyurethane elastomers tested after 22 hours at 70°C are given. The elastomer from the prepolymer A with curative X1 exhibits lowest value of compression set 1.6%, while 3.19% is obtained for the product from prepolymer B with X1, these results reveals that the former AX1 imparts better dimensional stability than the latter BX1.

Solvent resistance characteristics of different combinations of elastomers are carried out by immersing them in different organic solvents for the period of 7 days. The solvent resistant characteristics are expressed in the form of percentage weight gain of the elastomer. In this respect, the product from CX1 gives the lowest value (135%) and the product from BX4 gives the highest value (505%), this is due to nature of molecular structure and types of secondary forces involved. Among the solvent system used, ethyl acetate influences more swelling of elastomers than others due to dipole-dipole attraction. The moisture absorption characteristics of different elastomer combinations are also studied. The product from CX4 absorbs lowest percentage (1.5%) of moisture; whereas the product from AX1 absorbs highest percentage (3.1%) of moisture. This behavior is due to the number of hydrogen bonds involved in the elastomer structure.

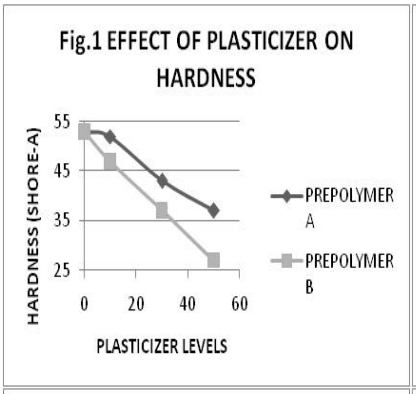
Fig.1 EFFECT OF PLASTICIZER ON HARDNESS
HARDNESS (SHORE-A)
55
45
35
25
0
20
40
60
PLASTICIZER LEVELS
PREPOLYMER A
PREPOLYMER B

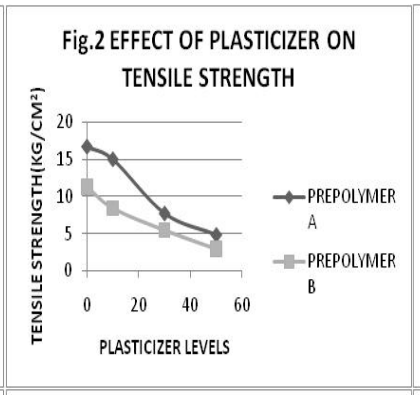
Fig.2 EFFECT OF PLASTICIZER ON TENSILE STRENGTH
TENSILE STRENGTH(KG/CM²)
20
15
10
5
0
0
20
40
60
PLASTICIZER LEVELS
PREPOLYMER A
PREPOLYMER B

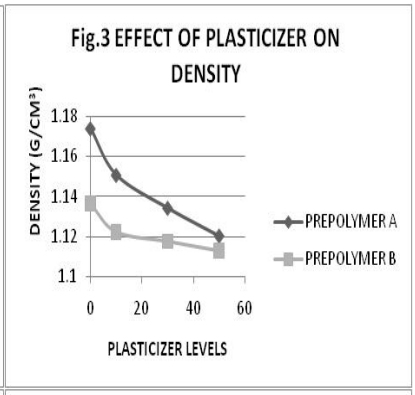
Fig.3 EFFECT OF PLASTICIZER ON DENSITY
DENSITY (G/CM³)
1.18
1.16
1.14
1.12
1.1
0
20
40
60
PLASTICIZER LEVELS
PREPOLYMER A
PREPOLYMER B

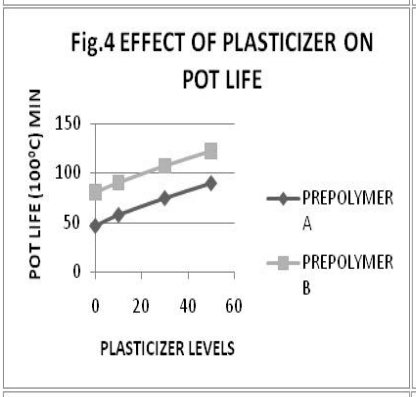
Fig.4 EFFECT OF PLASTICIZER ON POT LIFE
POT LIFE (100°C) MIN
150
100
50
0
0
20
40
60
PLASTICIZER LEVELS
PREPOLYMER A
PREPOLYMER B

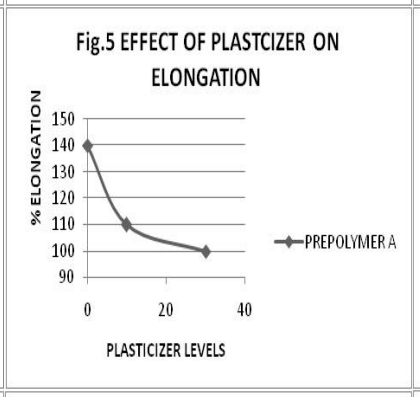
Fig.5 EFFECT OF PLASTCIZER ON ELONGATION
% ELONGATION
150
140
130
120
110
100
90
0
20
40
PLASTICIZER LEVELS
PREPOLYMER A

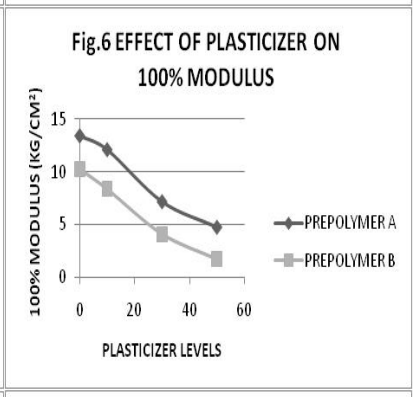
Fig.6 EFFECT OF PLASTICIZER ON 100% MODULUS
100% MODULUS (KG/CM²)
15
10
5
0
0
20
40
60
PLASTICIZER LEVELS
PREPOLYMER A
PREPOLYMER B

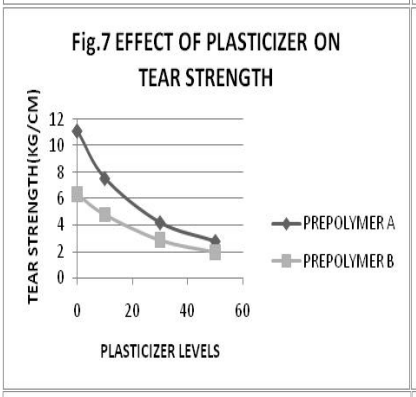
Fig.7 EFFECT OF PLASTICIZER ON TEAR STRENGTH
TEAR STRENGTH(KG/CM)
12
10
8
6
4
2
0
0
20
40
60
PLASTICIZER LEVELS
PREPOLYMER A
PREPOLYMER B

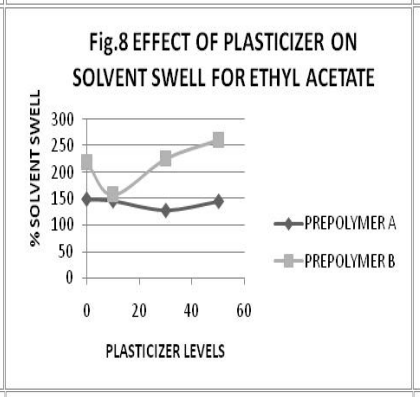
Fig.8 EFFECT OF PLASTICIZER ON SOLVENT SWELL FOR ETHYL ACETATE
% SOLVENT SWELL
300
250
200
150
100
50
0
0
20
40
60
PLASTICIZER LEVELS
PREPOLYMER A
PREPOLYMER B

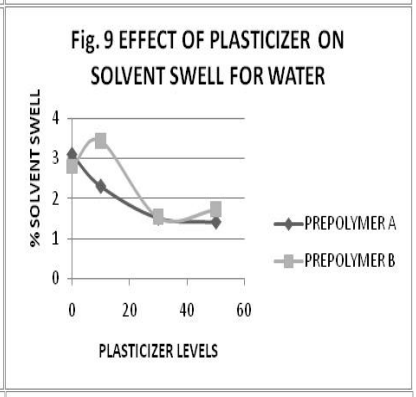
Fig. 9 EFFECT OF PLASTICIZER ON SOLVENT SWELL FOR WATER
% SOLVENT SWELL
4
3
2
1
0
0
20
40
60
PLASTICIZER LEVELS
PREPOLYMER A
PREPOLYMER B

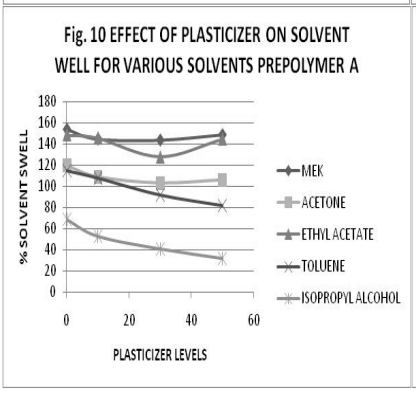
Fig. 10 EFFECT OF PLASTICIZER ON SOLVENT WELL FOR VARIOUS SOLVENTS PREPOLYMER A
% SOLVENT SWELL
180
160
140
120
100
80
60
40
20
0
0
20
40
60
PLASTICIZER LEVELS
MEK
ACETONE
ETHYL ACETATE
TOLUENE
ISOPROPYL ALCOHOL

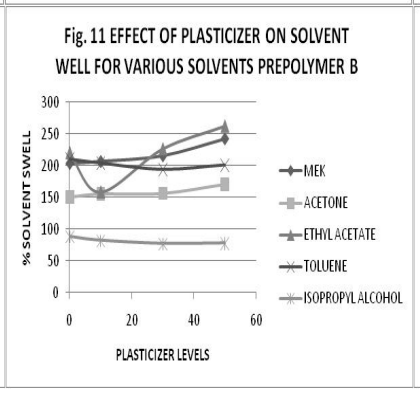
Fig. 11 EFFECT OF PLASTICIZER ON SOLVENT WELL FOR VARIOUS SOLVENTS PREPOLYMER B
% SOLVENT SWELL
300
250
200
150
100
50
0
0
20
40
60
PLASTICIZER LEVELS
MEK
ACETONE
ETHYL ACETATE
TOLUENE
ISOPROPYL ALCOHOL

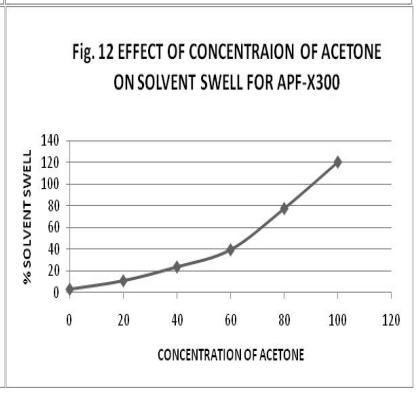
Fig. 12 EFFECT OF CONCENTRAION OF ACETONE ON SOLVENT SWELL FOR APF-X300
% SOLVENT SWELL
140
120
100
80
60
40
20
0
0
20
40
60
80
100
120
CONCENTRATION OF ACETONE

Effect of Plasticizer

The polyurethane elastomers resulted from prepolymers A and B with curative X3 are blended with varying levels (10phr, 30phr and 50phr) of plasticizer are studied. The incorporation of plasticizer influences the properties of elastomer. The increase in level of plasticizer decreases the mechanical characteristics of polyurethane elastomer. For example, the hardness of the elastomer product AX3 falls from 53 to 37 by increasing the concentration of plasticizer from 0% to 50%. Similarly the hardness of product BX3 falls from 53 to 27 for the same level of plasticizer concentration. The plot of varying concentration of plasticizer against hardness of the polyurethane elastomer (AX3 and BX3) is given in figure 1. The hardness decreases with increase in plasticizer level.

Tensile strength, density, modulus and tear strength are also in the same trend as shown in figures 2, 3, 6 and 7. The strength, modulus and density decreases with increase in plasticizer concentration. The increase in the plasticizer level influences the pot life of the products. The plot of varying level of plasticizer against pot life of the polyurethane elastomer (AX3 and BX3) is given in Figure 4. The pot life increases with increase in plasticizer concentration. The increase in plasticizer concentration influences the elongation for the product of BX3, but it is reversible for the product of AX3 (Figure 5). This is due to the nature of prepolymer A and this behavior may be explained due to the anti-plasticization effect observed with the reactants involved. Generally 30 phr plasticized polyurethane elastomer gives higher solvent resistance than 10phr and 50phr plasticizer concentration.

Properties of Filler on Plasticized Polyurethane Elastomer

Polyurethane elastomers resulted from prepolymers A, B, and C with curatives X3 are incorporated separately with 30phr and 50phr plasticizers and 60phr filler, in order to improve their performance characteristics. The hardness, tensile strength, tear strength, density, elongation and solvent resistant characteristics of additive blended polyurethane elastomers are studied. The incorporation of filler in the plasticized polyurethane enhances the hardness, tensile strength, modulus, density, tear strength and solvent resistance. For a particular level of prepolymer the pot life increases, when additives are added. For example the pot life for unfilled product from AX3 is 45 minutes. Whereas the same product filled with 60 phr filler and 50 phr plasticizer gives 85 minutes. The enhancement of pot life is due to retardation of reactive functional groups.

The addition of filler (60phr) to the product AX3 increases the hardness from 43 to 61, whereas the same product with 60 phr filler and 50 phr plasticizer enhances hardness from 37 to 52. The strength properties (tensile strength, modulus, tear strength) of plasticized (30 phr) elastomer, namely for the product from AX3, the tensile strength increases from 7.6 kg/cm^2 to 22.1 kg/cm^2, modulus increased from 7.2 kg/cm^2 to 18.2 kg/cm^2, and tear strength from 4.18 kg/cm to 8.41 kg/cm respectively.

The increase in strength properties is due to the reinforcement effect of filler and the formation of secondary bonding with polar groups of polyurethane elastomers. The results obtained from the solvent treatment reveals that the incorporation of filler improves the solvent resistant characteristics. For example 30phr plasticized product AX3, the swelling in ethyl acetate for 7 days gives 128% whereas the same product filled with 60phr filler in the same solvent for the same period gives swelling of 69%.

Conclusions

The different combinations of polyurethane elastomers are prepared using prepolymers A, B and C with curatives X1, X2, X3 and X4. In order to utilize the product for the print roller applications, the properties i.e., hardness, pot life, tensile strength, modulus, tear strength, elongation, density, compression set and solvent resistance are studied by standard methods. The polyurethane elastomer obtained from

prepolymers having higher percentage of reactive groups impart better mechanical properties and solvent resistant characteristics. The effect of plasticizer and filler addition on polyurethane elastomeric products is also studied. Both plasticizer and filler addition improved the performance characteristics of the products. The data resulted from various studies suggest that the product CX3 possess better characteristics than other products, required for print roller applications.

References

1. George Woods, The ICI Polyurethanes Book, John Wiley & Sons, Singapore, 1987, 10-12, 37-46, 50-52, 175-196.
2. Sayih, A.A.R. and Shah. T.M, Popular plastics, 1974, July, 17-21.
3. Buist. J.M. and Gudgeon.H, Advances in Polyurethane Technology, Elsevier Publishing Company, London, 1968, 25-62.
4. Hepburn.C, Polyurethane Elastomer, Second edition, Elsevier Applied Science, London, 1991, 122-123, 161-163, 405, 199-220.
5. Kirk and Othmer, Encylcopedia of Chemical Technology, Third Edition, Wiley and Inter Science Publication, 1984, 23, 576-608.
6. Kothandaraman.H. and Venkatarao.K, J. Applied Science, 1990, 39, 943-954.
7. Maurice.E, Bailey, J. of Chemical Education, 1971, 48, 12, 809-813.
8. Pegoraro.M, Landro, L.D, Severini. F,Cao.N and Donzelli. P, J. Polymer Science, Part B: Polymer Physics, 1991, 29, 365-370.
9. Reji John, E., Thachil, T., Racindran, P., Neelakantan, N.R. and Subramanian, N., 1991, Polymer Plastic Tech. Eng., 30, 2,3, 227-238.
10. Ullman's Encyclopedia of Industrial Chemistry, VCH Publication, 1986, A21, 665-716.

Effect of electron beam curing on mechanical and electrical properties of silica filled silicone and FKM rubber and its comparison with chemical curing

R.K. Ramamoorthy, K. Naskar, D Khastgir*
Rubber Technology centre, IIT Kharagpur-721302, INDIA

Email: dkhastgir@yahoo.co.uk, khasdi@rtc.iitkgp.ernet.in

Introduction:

The treatment of polymers by an electron beam has been reviewed different authors [11-14]. It is observed that , in general, rubbers can be cross-linked using an electron beam(EB) , where as some plastics like polypropylene and poly(vinyl chloride) have a tendency to degrade[13,14].

The effects of electron beam (EB) irradiation on mechanical and electrical properties of Silicone rubber (MQ), and Fluro rubber (FKM) compounds filled with Precipitated and Fumed Silica filler have been reported in the present paper. The effect of different degree of radiation dosage on both electrical and mechanical properties was investigated. Some comparison has been made between properties of EB cured vulanizates of theses two rubbers with Peroxide cured Silicon rubber and Calcium hydroxide cured FKM rubber. The type of silica filler used affects both electrical and mechanical properties of EB cured vulcanizates.

Experimental:

All mixing was carried out in laboratory size open mixing mill in accordance with the formulations given in table1-3 under identical condition of time, temperature and friction ratio. Some samples were subjected to electron beam curing with various dosage of radiation level and other samples are chemically cured up to optimum cure time using electrically heated press. Gel fraction and different mechanical and physical properties were measure in accordance with standard ASTM methods.

Table1.Formulation for Electron Beam Irradiation Cure

Ingredient	Q	Q	FKM	FKM
Precipitated Silica (phr)	20	-	20	-
Fumed silica (phr)	-	20	-	20
TQ (phr)	2	2	2	2
Sunpar Oil (phr)	2	2	2	2

Table2. Formulation for Peroxide cure

Ingredient	Q	Q
Precipitated Silica(phr)	20	-
Fumed silica (phr)	-	20
TQ (phr)	2	2
Sunpar Oil (phr)	2	2
DCP	5	5
Si-69	2	2

Table3.Formulation for Specific curing system

Ingredient	FKM	FKM
MgO (phr)	6	6
Precipitated Silica(phr)	20	-
Fumed silica (phr)	-	20
Sunpar Oil (phr)	2	2
Calcium hydroxide	3	3

Result and discussion;

Gel Fraction

The gel fraction is higher for silicone rubber compared to FKM rubber and change in gel fraction with radiation dosage is more pronounced in precipitated silica filled systems compared to fumed ones where changes are only marginal. The gel fraction level is almost same for chemical curing and EB curing methods for both the rubbers as presented in Figures 1(a)&1(b).

Mechanical Properties

Hardness

The hardness of both fluorocarbon and silicone rubber when reinforced by precipitated silica and EB cured increase with increasing irradiation dosage up to 15 MRads (figure 2(a)) followed by marginal reversion.

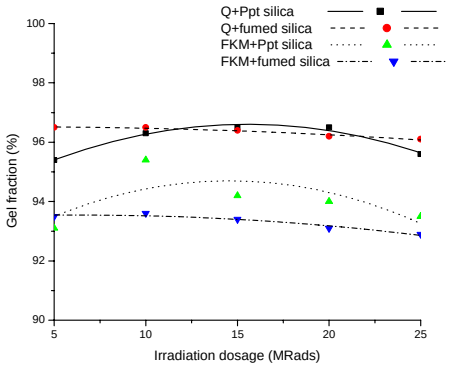

Figure 1 (a): Variation in Gel Fraction with increasing irradiation dosage

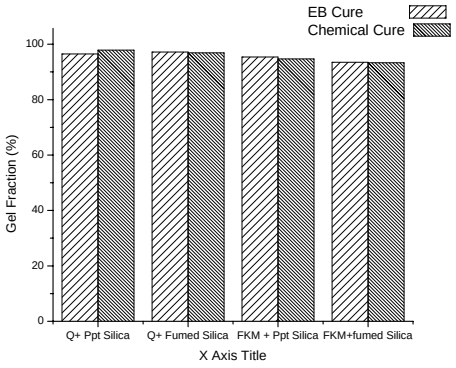

Figure 1 (b): Comparison of best Gel Fraction obtained of irradiated sample with chemical cure

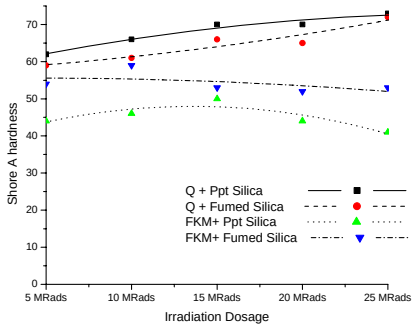

Figure 2 (a): Variation in Shore A Hardness with increasing irradiation dosage

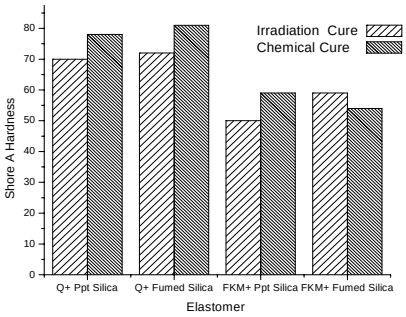

Figure 2 (b): Comparison of highest Shore A Hardness obtained of irradiated sample with chemical cure

The fumed silica filled silicone rubber shows a progressive increment of hardness with increased radiation dosage while slow but progressive decrement of hardness is observed in case of fluorocarbon rubber with same filler.

Generally the hardness of EB cured samples of both rubbers are comparatively lower than those of chemically cured ones (not shown).

Tensile Strength

The effect of EB on tensile strength of silicone rubber is relatively much less compared to that of FKM. Only slight improvement is observed with the increase in radiation dosage up to15Mrad there after some reversion is noted. The reinforcement effect of fumed silica is more than that of ppt silica in case of silicone rubber. However significant improvement of tensile strength is observed for FKM with the increase in radiation around15-20 MRad there after some reversion is noted. The effect ppt silica on reinforcement is more than fumed silica in case of FKM.

On comparison with type of cure the tensile strength for both rubbers is the best when reinforced by precipitated silica and chemically cured while it is the EB cure that gives best tensile strength when reinforced by fumed silica for both the rubbers figure 3(b)

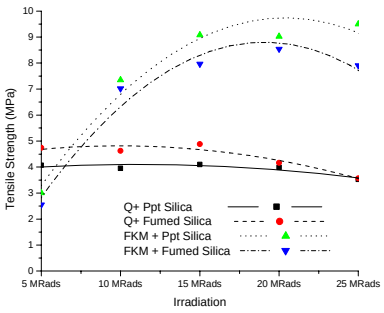

Figure 3 (a): Variation in Tensile strength (MPa) with increasing irradiation dosage

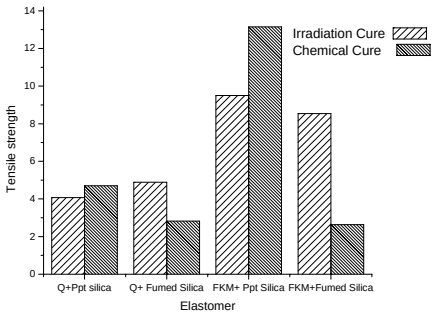

Figure 3 (b): Comparison of highest Tensile strength (MPa) obtained of irradiated sample with chemical cure

Elongation at Break

The elongation at break shows a decreasing trend with increasing irradiation dosage for both rubbers with either precipitated or fumed silica figure 5(a). The rate of decrease in elongation at break is higher in fluorocarbon when compared with silicone rubber. The most interesting observation here is that EB curing shows very high elongation at break for fluorocarbon and very low elongation at break of silicone rubber.

On comparison between types of cure the chemically cured silicone rubber shows higher elongation at break when reinforced with precipitated silica and lower elongation at

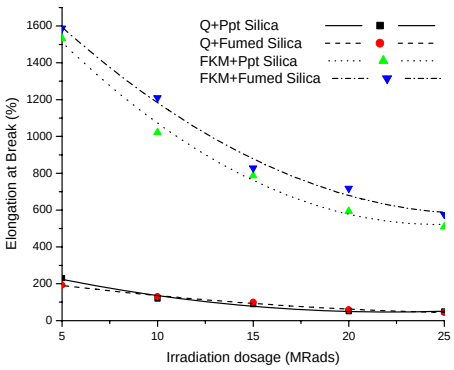

Figure 5 (a): Variation in Elongation at Break (%) with increasing irradiation dosage

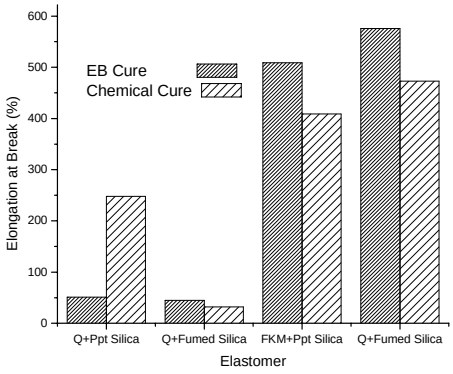

Figure 5 (b): Comparison of lowest Elongation at Break (%) obtained of irradiated sample with other types of cure

break when reinforced with fumed silica (figure 5(b)). The changes are more prominent with precipitated silica and only marginal with fumed silica. In the case of fluorocarbon the elongation at break is higher than chemical cure when EB cured irrespective of type of filler and the amount of increment also similar.

Electrical Properties

DC Volume Resistivity

The DC volume resistivity for all the rubbers shows marginal increase though not substantial with increasing irradiation dosages for both the rubbers with the two different fillers on EB cure. On chemical cure there is increase in resistivity only in the case of silicon rubber with precipitated silica reinforcement while in all other cases there is noticeable drop in resistivity by a small degree (figure 7).

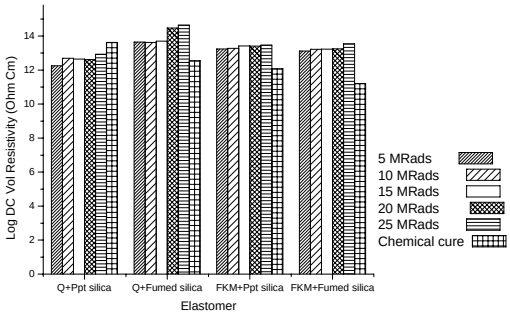

Figure 7: Comparison of Log DC Volume resistivity for different

dosage of Irradiated cure and other types of cure

Conclusion:

The mechanical properties of silicone rubber are not much affected by increasing irradiation dosage up to 15 MRads but any further increase in irradiation leads to marginal loss in properties. The fluorocarbon rubber responds with increasing properties with increasing irradiation dosage up to 20 MRads and any further increase leads to drop in mechanical properties.. The DC volume resistivity for both the rubbers shows marginal increase though not substantial with increasing irradiation dosage .

Reference:

[1] A. Charlesby, Radiat. Phys. Chem. 9 (1977) 17.
[2] N. Studer, IAEA TECDOC-454, 6–8 October 1986, p. 111
[3] Van Drumpt JD. Rubber World 1988; 33:33–41.
[4] Akiba M, Hashim AS. Prog Polym Sci 1997; 22:421–75.
[4] Ogunniyi DS. Progr Rubber Plast Technol 1999; 15(2):95–112.

All-PP composites based on β and α polymorphic forms: mechanical properties

T. N. Abraham and J. Karger-Kocsis

University of Kaiserslautern, D-67663 Kaiserslautern, Germany
Email: thomasnabraham@gmail.com

Abstract
All polypropylene (all-PP) composites were manufactured by exploiting the polymorphic forms of PP, in which alpha (α)-PP tapes worked as reinforcement and beta (β)-PP served as matrix. The mechanical performance of the composite was investigated in a range of frequencies and temperatures using dynamic mechanical thermal analysis (DMTA). The volume fractions of matrix and reinforcement were estimated using optical microscope images. Both the DMTA and the static flexural bending tests revealed that the α-PP tapes acts as an effective reinforcement for the β-PP matrix. Time temperature superposition (TTS) was applied to estimate the stiffness of the composites as a function of frequency ($f = 10^{-9\cdots10^{20}}$) in form of a master curve. The Williams-Landel-Ferry (WLF) model described properly change in the experimental shift factors used to create the storage modulus vs. frequency master curve. The activation energies for the α and β relaxations were also calculated by using the Arrhenius equation.
Key words: single polymer composites, dynamic mechanical thermal properties, polypropylene, all-polypropylene composite, β-modification, α-modification
E-mail: thomasnabraham@gmail.com

1. Introduction
Single thermoplastic composite (also termed thermoplastic homocomposites) have drawn research interest in recent years because of their environmental friendly character. All polypropylene (all-PP) is a single thermoplastic polymer composite which represents an effective alternative to the traditional fibre reinforced composites. Here the matrix and the reinforcement are from the same polymer, thereby supporting the ease of recyclability. Several techniques have been reported for the production of single thermoplastic polymer composite materials, such as film stacking followed by melting [1,2] hot compaction [3], powder and solution impregnation [4]. The basic principle behind all these techniques is to exploit the melt temperature difference between the oriented or highly stretched material (which should act as the reinforcement) and the same material without orientation (overtaking the role of the matrix). Beside recyclability, the interest for single polymer composites is based upon the expectation that a good interfacial bonding can be achieved if matrix and reinforcement are made from the same semi-crystalline polymer [5,6].
One of the promising approaches in the development of all-PP composites is to exploit the polymorphism-related difference in the melting range between the beta(β)- (matrix) and alpha(α)-phases (reinforcement) PPs [2,7]. An all-PP composite has been made in our laboratory with α-PP tapes as reinforcement and β-PP film as the matrix. However, the entirely thermoplastic nature of these composites raises important questions regarding the viscoelastic behaviour at elevated temperatures. To provide information about the viscoelastic properties, various experimental techniques can be used, among which the dynamic mechanical thermal analysis (DMTA) offer adaptable test procedures. Long-term viscoelastic properties of all-PP composite laminate have been investigated by using the time-temperature superposition principle [8,9]. Nevertheless, it is understood that these properties significantly govern the applicability of the material. The main aim of this paper is to investigate the response of a novel all-PP composite to mechanical loading in a broad range of temperature and frequencies. By using the DMTA responses, master curves

can be created to predict the performance of all-PP composites at much lower and higher frequencies than achievable in the laboratory.

2. Materials

The PP tapes used for the manufacture of laminates were produced in our laboratory using twin screw extruder. The temperature zones in the extruder were maintained at 190, 200, 210 and 220 °C from the feeder to nozzle. The die used had a dimension of 10 x 2 mm^2. Characteristics of PP tapes used for the preparation of the laminates are summarized in Table 1. Thin film of beta polymorph rich isotactic PP (β-PP) served as the matrix. The thin film (120μm thickness) were obtained by compression molding β- nucleated PP sheet of Tipplen H 483 F (melt flow index 6.5 g/10 min at 230 °C and 2.16 kg load) at 180 °C for 5 min. The manufacture of the PP laminates involved a two-stage process: winding of the PP tapes in a cross-ply manner (0/90°;CP), and consolidation of the related tape consisting fabric using hot compaction. The schematic of the tape winding process is shown in Figure 1. Before winding the PP tapes a thin β-PP film layer was placed on the surface of a thin steel plate. Using a typical winding machine, supplied by Bolenz & Schaefer Maschinenfabrik (Biedenkopf, Germany), PP tapes were wound from a bobbin onto the same steel plate rotating at a constant speed. After laying one layer of PP tape another layer of β-PP film was placed and the winding direction on the steel plate was changed. The same process continued and the total number of layers of PP tapes and β-PP film was kept four and five respectively. A similar winding process was already adopted for manufacturing CP type all-PP composite from coextruded Pure® tapes [10,11]. All-PP composite laminates were produced by the well known hot compaction method in a hot press (P/O/Weber GmbH, Remshalden, Germany) at a temperature of 160 °C and a holding time of 5 min under high pressure (7 MPa). The time temperature profile during the consolidation is shown schematically in Figure 2.

3. Experimental procedures

The presence of β-PP and the occurrence of β-α transformation were demonstrated by DSC using a Mettler-Toledo DSC821 instrument (Greifensee, Switzerland). In order to demonstrate the difference between the α and β modifications, the first heating scan (T=25 to 200 °C) was followed by a cooling one to T=100 °C, prior to a second heating cycle to T=200 °C. This heating cooling programme was selected based on the recommendation of Varga et al.[12] Microscopic images of the cross-section of the all-PP laminates were captured by a stereomicroscope (Leitz, Germany) equipped with a high resolution digital camera. The IMAGE-C analysis software was used to estimate the void content from the micrographs. DMTA of all-PP composite laminates was performed in dual cantilever flexural mode. Specimen were cut from the composite plates with dimensions of approximately 60mm × 15mm × 2mm (length × width × thickness) in the DMTA Q800 (TA Instruments, New Castle, USA) machine equipped with a data acquisition software. The specimens were cooled to -50 °C. The temperature was allowed to stabilize and then increased by 3 °C, kept 5 min isothermal, until 120 °C. The specimen was subjected to a sinusoidal flexural displacement applying a maximum tensile strain of 0.1% (which was well within the viscoelastic region) at frequencies 0.01 Hz, 0.1 Hz 1 Hz 5 Hz and 10 Hz at all isothermal temperatures. For each frequency, the complex dynamic modulus (E′) and loss factor (tanδ) were recorded. An attempt was made to apply the time temperature superposition (TTS) to the DMTA data measured as function of both temperature (T = -50 °C….+120 °C) and frequency (f = 0.01….10 Hz) using rheology advantage data analysis software provided by TA Instruments. Master curves in form of storage modulus (E′) vs frequency were produced by superimposing the storage modulus vs frequency traces using the TTS principle. A reference temperature (T_{ref} = 22 °C) was used for this superposition (shifting) process. The related shift factor a_T is given by equation (1):

$$a_T = \frac{E'(T)}{E'(T_{ref})} \qquad (1)$$

The shift factors of a master curve have some relationship with temperature. Fitting the experimentally determined shift factors to a mathematical model permits the creation of a master curve in form of storage modulus vs frequency. With a multi-frequency measurement, frequencies beyond the measurable range of the DMTA can be achieved by using the superposition method based on the Williams-Landel-Ferry (WLF) equation [13,14]. For the temperature range above the glass transition temperature, it is generally accepted that the shift factor-temperature relationship is best described by WLF equation:

$$\log a_T = \log\left(\frac{f}{f_0}\right) = \frac{-C_1(T - T_{ref})}{C_2 + (T - T_{ref})} \qquad (2)$$

where C_1 and C_2 are constants. The static flexural properties of the all-PP composites, such as modulus of elasticity and ultimate flexural strength were determined following the DIN EN ISO 178 standard on a Zwick 1445 test machine. Specimens of the same dimensions used for the DMTA test were employed for the three point bending measurement. A support span of 32.8 mm was used in the three point bending setup. The cross-head speed of 1mm/min was applied during the test and the elastic modulus was calculated in the strain range of 0.05-0.25%. Load was applied using a U2A type 10 kN load cell. A preload of 5 N was applied in the beginning of each test and the mean value of five specimens tested was reported.

4. Results and Discussion

DSC traces of all-PP composite and β PP film is represented in Figure 3. The melting temperature of the β modification of isotactic PP ($T_m \approx 154$ °C) homopolymer is lower than that of the reinforcing α-PP tape ($T_m \approx 165$ °C). The DSC trace of the all-PP composite also shows another interesting phenomenon of transformation of β-PP to α-form at temperatures above the melting point of the former. This phenomenon has already been observed by Padden and Keith [15]. Samuels and Yee [16], who have conducted extensive studies on the unit cell of β-polypropylene, have concluded that the transformation from the β to the α form must occur through a melt recrystallization process, since the two unit cells are very different.

A typical dynamic mechanical behaviour of PP tapes, β-PP matrix and all-PP composite laminates at 1 Hz frequency is represented in Figure 4. It shows that at subambient temperature (the glassy region of PP) the stiffness of PP tape is found to be fairly high. With increasing temperature the E′ decreases, as expected. Above 25 °C the stiffness of the tapes drops significantly. Although the tapes lost much of their elastic response above this temperature, their residual stiffness at 120 °C (end of the test) is still higher (E′ = 1 GPa) than that of an isotropic PP. The high stiffness is attributed to the highly oriented crystals and polymer chains in the stretching direction of the tape. This implies that the tape possesses a residual orientation even at this higher temperature. The results also indicates that stiffness of all-PP composite laminate is higher than the matrix (β-PP), confirms the reinforcement effect of α-PP tapes on β-PP matrix. At room temperature the E′ of PP tapes, all-PP composite laminates and β-PP matrix are 4.8, 2.9 and 2.2GPa respectively.

Figure 4 also exhibits the course of tanδ (ratio of E″/E′) with temperature, which shows a maximum at ≈ 80 °C. The maximum tanδ value recorded for the all-PP tape was 0.15. The tanδ peaks represent different relaxation transitions [12]. However, in Figure 3 PP tape does not

resolve any tanδ peak corresponding to the glass-transition of PP ($T_g \approx$ -10 °C – 0 °C), but a more definite tanδ peak is seen corresponding to the α-transition (T_α) at approximately 80°C. Since these tapes are produced by stretching, the amorphous phase becomes highly oriented between the crystalline regions and it has less freedom to be involved in segmental motions [17]. Therefore, in highly oriented PP systems, the magnitude of T_g peaks is greatly reduced compared to isotropic PP. While T_g reflects mobility within the amorphous regions, T_α dictates the onset of segmental motion within the crystalline regions[13,18,19]. The loss factor as a function of temperature for all-PP composite and β-PP matrix are also shown in Figure 4. The result shows a clear tanδ peak corresponding to β relaxation (T_g) near 0 °C for both the β-PP matrix and all-PP composite. The position of T_g remained nearly unchanged but the peak intensity and magnitude decreased significantly which indicates the increase in stiffness as result of reinforcement of β PP matrix.

It has been shown that a simple rule of mixtures can be very useful in helping to understand the in-plane properties of compacted single polymer composites. A model based on a parallel rule of mixtures and knowledge of the properties of the oriented and matrix phases and fraction of the two phases have been reported by Hine et al. [20].The compacted sheet modulus ($E_{\text{compacted sheet}}$) can then be shown simply to be given by equation 3

$$E_{compacted-sheet} = E_{tape}\frac{V_{tape}}{2} + E_{matrix/\,film}\left(\frac{1+V_{matrix/\,film}}{2}\right) \qquad (3)$$

where E_{tape} and $E_{matrix/film}$ are the modulus of the oriented and matrix phases respectively (assuming same chemical composition for both the matrix and reinforcement i.e. PP) and V is the appropriate fraction of each component. The volume fraction of each component is obtained from the optical micrographs shown in Figure 5. Using the IMAGE-C analysis software, the volume fraction of the reinforcing tapes was determined and found to be 50%. The storage modulus value obtained from DMTA for PP tape and β PP matrix at the same strain rate at room temperature were applied in equation for predicting the in-plane modulus of the compacted sheet using equation. The predicted modulus (3GPa) is comparable with the experimental measurements (2.9GPa), and indicates that this simple approach predicts the modulus quite satisfactorily.

Storage modulus for a wider range of frequencies can be obtained by TTS using the data from multi-frequency DMTA tests. Figure 6 show the variation of storage modulus for a range of temperature between -20 °C and 80 °C for the all-PP composites tested at 0.01 Hz, 0.1 Hz, 1 Hz, 5 Hz and 10 Hz, respectively. An increase in the storage modulus for all-PP composite laminates with increasing frequency and decreasing temperature, as expected. The variation of tanδ at different frequencies for the all-PP laminates are shown in Table 2. A remarkable influence of frequency was observed for both the α and β relaxations of the composites. The frequency increase shifted the position of the relaxation region to higher temperatures. The tanδ peaks corresponding to the β and α transitions of all-PP composite laminate were found to be at 4 °C and 97 °C, respectively, at 1 Hz frequency. The T_α peak became broader and less pronounced due to the additional melting region at higher temperatures. Master curves of the storage modulus against frequencies created at a reference temperature of 22 °C were shown in Figure 7 for the β-PP matrix and all-PP composite laminates. From the master curve data, the curve approach a similar plateau value at high frequency, but the terminal region at lower frequencies is more dependent on reinforcement effect of the composite compared with the β-PP matrix as expected. The storage modulus master curve provides a useful prediction of the modulus over loading frequencies from 10^{-9} to 10^{20} Hz. However, it must be emphasized that these master curves are quite reliable for short term, but significant deviation may occur at large time scales. Shift factor, a_T was obtained directly from the experimental storage modulus curves against time by measuring the amount of shift along the time scale necessary to superimpose the curves on the reference. The shift factors used for the generation of storage modulus master curve is shown in Figure 8.

We tried the classical WLF equation to describe the relation ship between a_T and temperature. It was found that the WLF equation is suitable to describe the temperature dependence.
Parallel to the dynamic flexural tests, short-term static flexural tests were also conducted. Table 3 shows a plot of the experimental results obtained from the flexural test of the all-PP composites. The result shows the average value of elastic modulus and maximum flexural strength of the β-PP matrix and all-PP composite laminates. The stiffness of the all-PP woven composites is to a great extent governed by the stiffness of the tapes in the longitudinal direction [23]. It shows that strength (36%) and stiffness (85%) of the β-PP matrix is improved significantly by reinforcing PP tapes. A detailed study on the flexural behaviour of all-PP composite (Pure®) was conducted in our laboratory and reported that the short-term as well as long-term viscoelastic behaviours are greatly influenced by the composite morphology, particularly the reinforcement architecture.

5. Conclusion

All-PP composite were produced from α-PP tapes and β-PP film/matrix by a hot consolidation method. This study has proved that extruded α-PP tapes (high melt temperature) can be used for reinforcing the β-PP matrix (low melt temperature). At room temperature the E′ of the β-PP matrix is increased by 0.7 GPa by the effective reinforcement of α-PP tape obtained by DMTA. Similarly there is an increase in the flexural strength and stiffness of the all-PP composite also observed. The tanδ peak was not discernable for the reinforcing α-PP tape, while it is clearly identified for the β-PP matrix and all-PP composite laminate. Though, the position of Tg remained nearly unchanged, the peak intensity and magnitude decreased significantly. The storage modulus master curve approach a similar plateau value at high frequency, but the terminal region at lower frequencies is more dependent on reinforcement effect of composite compared with the β-PP matrix. The experimental shift factors showed a good agreement with both WLF and Arrhenius models.

Acknowledgement

The authors thank the German Science Foundation for the financial support of this project (DFG Ka 1202/17)

References

1. Houshyar S, Shanks RA, Hodzic A Macromol Mater Eng. (2005) 290:45
2. Bárány T, Karger-Kocsis J, Czigány T Polym Adv Technol (2006) 17:818
3. Hine PJ, Ward IM, Jordan ND, Olley R, Bassett DC J Macromol Sci Phys (2001) 40B:959
4. Amornsakchal T, Bassett DC, Olley RH, Hine PJ, Ward IM J Appl Polym Sci (2000) 78:787
5. Capiati NJ, Porter RS J Mater Sci (1975) 10:1671
6. Mead WT, Porter RS J Appl Polym Sci (1978) 22:3249
7. Karger-Kocsis J. Patentschrift DE 10237803B4, Institut für Verbundwerkstoffe GmbH 2007.
8. Boiko YuM, Kovriga VV Intern J Polym Mater (1993) 22:209
9. Wortmann FJ, Schulz KV Polymer (1995) 36:315
10. Abraham T, Banik K, Karger-Kocsis J *eXPRESS Polymer Letters* (2007) 1:519
11. Banik K, Abraham T, Karger-Kocsis J Macromol Mater Eng (2007) 292:1280
12. Varga J J Macromol Science Part B-Physics (2002) 41: 1121
13. Williams ML, Landel RF, Ferry JD J Amer Chem Soc(1955) **77**: 3701
14. Ferry JD Viscoelastic properties of polymers, 2nd edition, Wiley, New York, (1970) 292
15. Padden FJ, Keith HD J Appl Phys (1959) 30:1479
16. Samuels RJ, Yee RY J Polym Phys Ed (1972) 10:385
17. Boyd RH Polymer (1985) 26:1123

18. Hu WG, Schmidt-Rohr K Acta Polymer (1999) 50:271
19. Roy SK, Kyu T, St. John Manley R Macromolecules (1988) 21:1741
20. Ward IM, Hine PJ Polymer (2004) 45(5):1423
21. Alcock B, Cabrera NO, Barkoula NM, Reynolds CT, Govaert LE, Peijs T Compos Sci Tech (2007) 67:2061
22. Amash A, Zugenmaier P J App Polym Sci(1997) 63:1143
23. Alcock B, Cabrera NO, Barkoula N-M, Loos J, Peijs T Composites: Part A (2006) 37:716

Tables

Table 1. Summary of	PP tape
Width	1.5 mm
Thickness	265μm
Density	901±9 Kg/m^3
Composition	homopolymer (Novolen 1104H melt flow index 2 g/10 min at 230 °C and 2.16 kg load)
Tensile modulus (ISO 527)	4±0.5 GPa

Table 2. T_g and T_α at different oscillating frequenies

	T_g(°C)	T_α(°C)
0.01Hz	0.99	55
0.1Hz	2.13	81
1Hz	3.89	97
10Hz	6.90	-

Table 3. Flexural properties of all-PP composite laminates

	Flexural properties		
Material	Modulus (GPa)	Strength (MPa)	Strain at max. load
β-PP film	1.2±0.17	44±5	5.6±0.2
all-PP composite	2.3±0.07	60±0.5	4.9±0.3

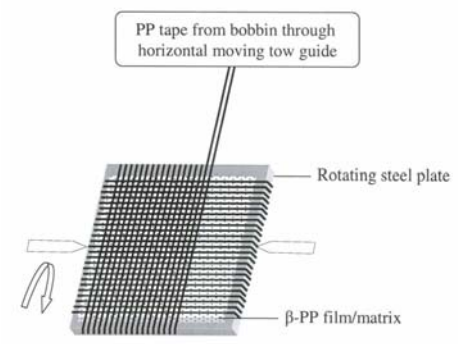

Figure 1. Scheme of the tape winding process for the fabrication of all-PP composites

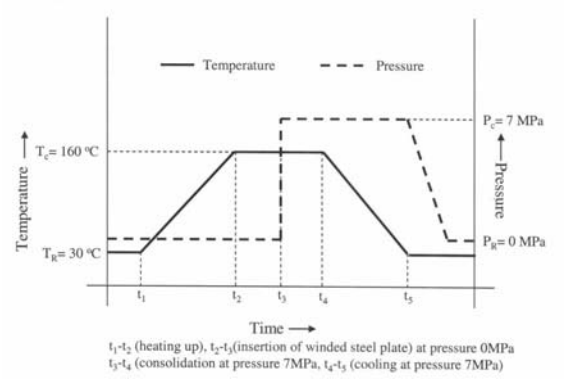

Figure 2. Schematic of time-temperature and time-pressure profile used for consolidation of all-PP by hot compaction (T_R and T_C are release and consolidation temperatures, P_R and P_C are release and consolidation temperatures)

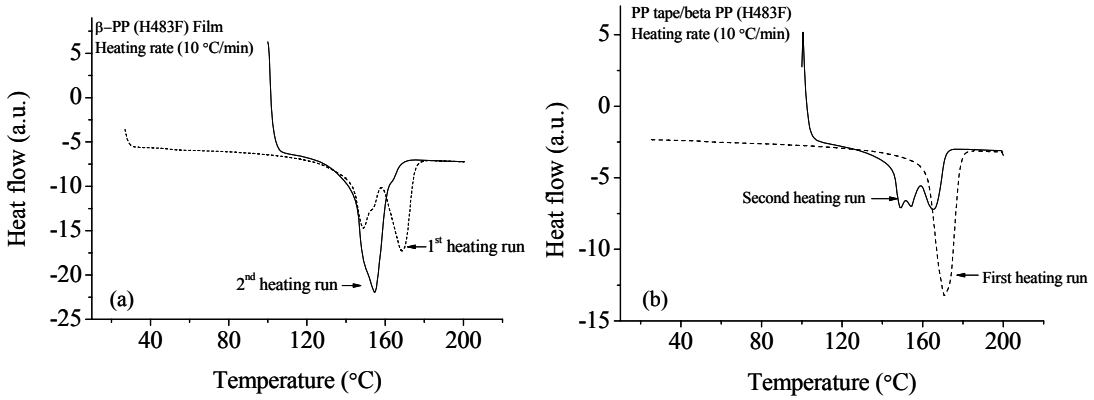

Figure 3. DSC traces of (a) β-PP matrix and (b) all-PP composite laminates (β-PP was cooled to T=100 °C prior to its second heating)

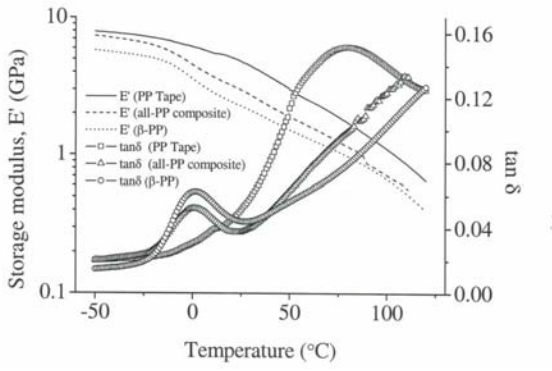

Figure 4. DMA plots of storage modulus and tanδ vs temperature for α-PP tape, all-PP composite laminates and β-PP matrix at frequency 1 Hz (note: log scale of E′)

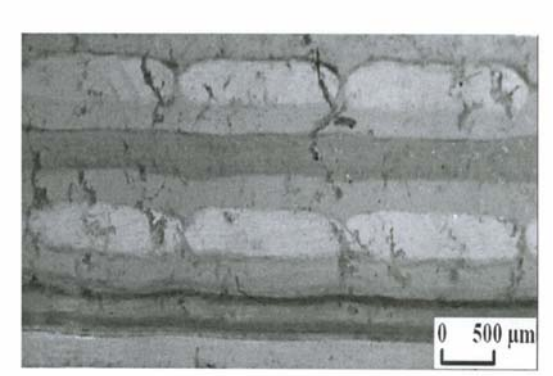

Figure 5. Optical micrograph from the cross-sections of all-PP composite laminates

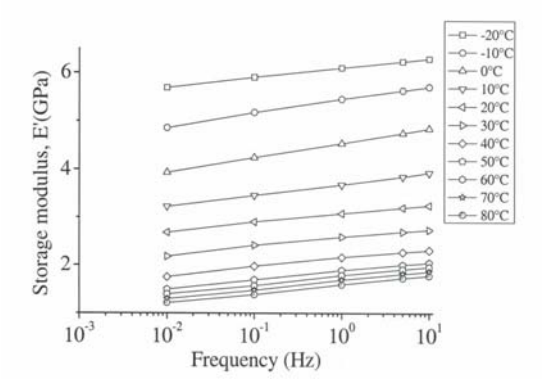

Figure 6. Storage modulus vs frequency for a range of temperatures for the all-PP composite

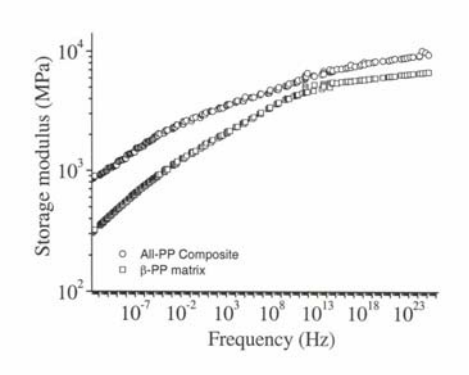

Figure 7. Storage modulus vs frequency master curves at a reference temperature of 22 °C for β-PP matrix and all-PP composite (note: log scale of y-axis)

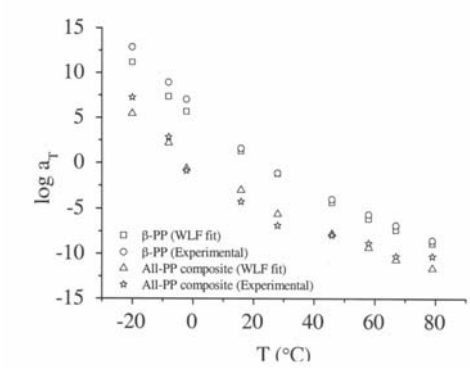

Figure 8. Experimentally determined shift factors and the WLF fits

Intercalated poly (methyl methacrylate) layered silicate nanocomposites: Effect of organoclay structure

M. Parua[1], S. Mohanty [2] and S.K. Nayak [2*]
Laboratory for Advanced Research in Polymeric Materials
1. Central Institute of Plastic Engineering and Technology, Bhubaneswar-751024, India.
2. Central Institute of Plastic Engineering and Technology, Chennai-600032, India
Email: drsknayak@gmail.com

Abstract
Poly (Methyl methacrylate)/layered silicate nanocomposites were prepared using melt intercalation technique. Commercially modified nanoclays such as Cloisite 30B, Cloisite 20A and Bentonite have been used as organoclays for the preparation of nanocomposites. Maleic anhydride (MA) has been used as a compatibilizing agent for improving the interfacial adhesion between organoclays and PMMA matrix. PMMA matrix with 5wt % of Cloisite 30B nanoclay exhibited optimum tensile properties. The tensile modulus of PMMA/Cloisite 30B 5% nanocomposite increases to about 35% as compared to virgin PMMA matrix. Thermal measurements employing differential scanning calorimetry (DSC), thermogravimetric analysis (TGA) also showed improved thermal stability and marginal increase in glass transition temperature of PMMA matrix with the incorporation of nanoclays. The morphological studies concerning wide-angle x-ray diffraction (WAXD) revealed an increase in d-spacing from 18.5 A^0 in C30B nanoclay to 39.4 A^0 in PMMA/C30B (5wt%) nanocomposites, thus confirming intercalated nanomorphology. The dispersion characteristics of organoclay with in PMMA matrix was also investigated using transmission electron microscopy (TEM). Further, dynamic mechanical analysis (DMA) shows a substantial increase in storage modulus of PMMA matrix with the incorporation of organoclays.
Key words: PMMA, Cloisite 30B, Bentonite, Nanocomposites, DMA

Introduction
Poly (methyl methacrylate) (PMMA) is an amorphous, atactic and optically transparent material with high technological importance because of its high weatherability, high optical clarity & gloss, high strength, low water absorption and stiffness. PMMA nanocomposites offer the potential to reduce gas permeability improve thermal, mechanical and flammability properties. PMMA is a highly combustible material and very difficult to impart flame retardancy even with the addition of larger amounts of conventional flame retardant agents. However, use of layer silicates as flame retardant additives is not only improves the flammability properties but also results in an increase in the physical properties of the nanocomposites relative to the polymer matrix. PMMA being semi-polar polymer, various attempts have been made by modifying the matrix polymer with numerous grafting agents to improve the interface with the layered silicate. Several reports on PMMA based nanocomposites synthesized using bulk polymerization of methyl methacrylate and also by melt compounding or extrusion of Poly (methyl methacrylate) has been studied. Free radical polymerization of methyl methacrylate using sodium montmorillonite has been used investigated by Blumstein et. al [1]. Similarly Wang et. al [2] have synthesized PMMA nanocomposites using bulk ,suspension, solution and emulsion polymerisation technique [3-5]. A detailed investigation on mechanical and thermal properties have been studied by Su and Wilkie et. al.[6] using N-methyl N,N divinyl benzyl octadecyl ammonium modified montmorillonite. Exfoliated PMMA nanocomposites were obtained at relatively lower clay loadings of < 5 wt. %, where as intercalated structure have been noticed at higher clay loading. Similar existence of intercalated and partially exfoliated structures have also been reported by Lee and Jang et. al. [7] and Brittain [8] where in PMMA/clay hybrids have been synthesised using emulsion & suspension polymerisation techniques respectively. In the present investigation PMMA based nanocomposites with different organically modified montmorillonites have been reported.

#Corresponding Author:- drsknayak@gmail.com
Fax-191-44-22254787

Experimental

Materials

PMMA (876 G) having MI: 6g/10min and density1.19g/cc, obtained from M/S GSFC Ltd., India, has been used as the base polymer matrix. Cloisite 30B (C30B, CEC of 90 meq / 100g clay), Cloisite 20A(C20A, CEC of 95 meq / 100g clay) and Bentone 109 (B109, CEC of 95 meq / 100g clay) procured from M/s Southern clay products, Inc. Gonzales, Texas and Elementis UK respectively has been used as organoclays. Maleic anhydride (MA) in presence of Benzoyl peroxide as initiator has been used as grafting agent for preparing grafted samples.

Preparation of PMMA Nanocomposites:

PMMA and nanoclays were dried at 65^0C in vaccum oven for a period of 12hrs prior to processing. PMMA nanocomposites were fabricated using different weight percentage of nanoclays (1, 3 and 5%) in Haake Rheocord at 180^0C , 50 rpm for a mixing time of 30 mins. Finally, these premixes were brought to room temperature and was injection molded using mini Injection molding machine (Haake^R Minijet 557-2270) (Thermoelectron corporation GMDH, Germany) with a barrel temperature of 200 ^{0}C and mold temperature of 140^0C with 700 bar injection pressure

Wide angle-X-Ray Diffraction: (WAXD):

Wide angle X-Ray diffraction (XRD) analysis was carried out using Philips X'Pert MPD (Japan), which had a graphite monochromator and a Cu Kα radiation source operated at 40kv and 30 mA. The basal spacing or d_{001} reflection of the samples was calculated from Bragg's equation by monitoring the diffraction angle, 2θ from $2\text{-}10^0$.

Transmission Electron Microscopy:

Samples for TEM imaging were sectioned using Lieca Ultracut UCT microtome and TEM of specimens were carried out using JEOL-1200 EX electron microscope at an accelerating voltage of 80 kV.

Thermal Characterization

The melting, glass transition temperature and thermal stability of virgin PMMA and the nanocomposite samples have been studied using DSC (Perkin-Elmer Diamond DSC, USA) and TGA (Perkin –Elmer Pyris-7 TGA, USA), respectively.

Mechanical Properties:

Tensile properties were measured as per ASTM-D 638 with gauge length of 25mm, and crosshead speed of 5 mm/min by using Universal Testing Machine (LR 100K Lloyds Instruments Ltd. UK). Tests were carried out taking five specimens for each set at a standard temperature 23 ± 2^0c and 50 ± 2% RH.

Dynamic mechanical properties:

The dynamic mechanical behaviour of the samples were carried out at fixed frequency of 1Hz and heating rate of 10^0C/min in a temperature range of –150 to 200^0C using DMTA (NETZSCH DMA 242).

Results & Discussion

Wide angle X-ray diffraction:

The WAXD patterns of PMMA/Na+ MMT, PMMA/C30B, PMMA/B109 and PMMA/C20A nanocomposites and grafted PMMA-g-MA/C30B and PMMA-g-MA/B109 nanocomposites is depicted in fig.1. The d_{001} peak in all the organically modified systems were observed within the range of 2θ =1 to 10^0 indicating intercalation of PMMA chains with in the clay galleries. Comparison of diffraction patterns of each nanocomposites systems with respective organoclays, C30B, B109 and C20A reveals that basal spacing increases from 18.5 A^0 to 39.4 A^0 in PMMA/ C30B, 30.0 A^0 to 35.3 A^0 in PMMA/ B109 and 24.2A^0 to 33 A ^{0} in PMMA/C20A nanocomposites respectively. However, in case of PMMA/ Na+ MMT nanocomposites agglomeration and intercalation was observed. Since there was no evidence of peak intensity within the investigated experimental range. Nevertheless, broadening of the peak was noticed which is probably due to macroscopic interaction between Na+ MMT & PMMA that might have resulted in dispersion of clay stacks with in the PMMA matrix. As reported by Sandeep Kumar et al. (9) some level of reduction in the no. of clay platelets per stacks in the polymer matrix might have resulted between Na+ MMT & PMMA from either the processing methods used in the fabrication of the nanocomposites or due to favourable interactions between

them. The nanocomposites prepared using C20A organoclay exhibited minimum intercalation of 33 A^0 as compared to the other two modified organoclays C30B and B109 respectively. The lower amount of intercalation possibly occurs due to less favourable intercalation between the ditallow intercalant in C20A containing more no. hydrophobic $–CH_2$ groups in the clay surface, with the polymer chain segments. In case of B109, a smectite organoclay, modified with hydrogenated tallow, provides more no. of clay platelets per surface area, which might have been the primary reason for enhancement of d spacing as compared with PMMA/C20A nanocomposites. However grafting of PMMA with MA could not show any appreciable increase in the d spacing as compared with the ungrafted nanocomposites .

Transmission Electron Microscopy: (TEM)

Bright field TEM images of PMMA with and without MA are represented in the fig.2. Dark lines represent silicate layers whereas bright region corresponds to PMMA matrix. This also indicated intercalated clay layers along with some individual clay layers for untreated PMMA/C30B nanocomposites. In case of grafted nanocomposites, PMMA-g-MA/C30B hybrid the smaller amount of stack plates appear in broad and obscure region. TEM results confirmed that PMMA based grafted and ungrafted nanocomposites mainly display an intercalated nanomorphology which is in agreement to the WAXD technique.

Thermal Analysis (DSC/TGA) :

Fig.3 shows the TGA curves of PMMA, PMMA/ Na+ MMT, PMMA/C20A, PMMA/C30B, PMMA/B109 nanocomposites and PMMA-g-MA/C30B and PMMA-g-MA/B109 grafted nanocomposites respectively. It is observed that onset of temperature increased in all the cases is around 25^0C for PMMA/C30B, 6^0C for PMMA/B109 and 24^0C for PMMA/C20A as compared with virgin PMMA. The temperature at 50% mass loss ($T_{0.5}$) also increases from 365^0C in case of PMMA to 412^0C in PMMA/C20A nanocomposites. This improvement in thermal stability of PMMA nanocomposites is mainly due to the intercalation of polymer matrix into the clay galleries, which act as a barrier for thermal degradation as well as nucleating effect of organoclays. The effect of maleic anhydride did not show a considerable improvement in thermal stability of nanocomposites. However in all the nanocomposite system the confinement of polymer chains into the clay galleries delayed the degradation process & diffusion of volatile products thereby increasing the flame retardancy.

The DSC thermograms of PMMA virgin and the nanocomposites systems are illustrated in fig .4. DSC thermograms represented the presence of second order transition corresponding to the Tg of the virgin PMMA matrix around 121.90^0C. Absence of 2^{nd} order transition or Tm indicated amorphous characteristics of the matrix polymer. DSC isotherms revealed marginal decrease in the Tg of PMMA in the nanocomposites system. PMMA/C30B nanocomposites exhibited Tg around 118.83^0C with PMMA/B109 at 120.01^0C and PMMA/C20A around 114.31^0C respectively .The grafted samples also exhibited glass transition in the similar range indicating no appreciable effect of grafting on the segmental mobility of the matrix polymer. The depression Tg is probably due to reduction in density, which caused chain end localization and reduced chain entanglements as compared with the bulk matrix. PMMA/C20A nanocomposites system exhibits maximum depression in Tg to the tune of 114.31^0C which reveals less compatibility of the ditallow organic modifier with the hydrophobic matrix.

Mechanical Properties:

Mechanical properties such as Young's modulus (E), stress at break and % strain at break and tensile strength is represented in the table1. It is evident that with the increase in clay loading from 1 to 5 wt %, there is a linear increase in the young's modulus of PMMA nanocomposites system. Incorporation of organically modified nanoclays to the tune of 5wt% increases (E) of PMMA from 1980 MPa to 2681 MPa in PMMA/C30B, 2469 MPa in PMMA/B109 and 2168 MPa in PMMA/C20A nanocomposites hybrid respectively. The nanocomposites prepared using C30B nanoclay exhibited an optimum increase in E as compared with virgin matrix which is probably due to polar interactions between ester groups of PMMA with the hydroxyl group of C30B. The grafted nanocomposites exhibited a higher modulus as compared with the ungrafted hybrids in all the cases PMMA-g-MA/C30B nanocomposites exhibited a maximum increase in Youngs modulus to the tune of 38.22 % as compared with the virgin matrix. This behaviour is probably due to formation of interfacial bonds between the anhydride groups of MA with the –OH groups in C30B as well as polar interactions of the ammonium cations with the MA. The tensile strength also increases with the increase in clay

loading. Na+MMT system shows a decrease in the tensile strength and stress at break indicating brittleness characteristics predominantly due to presence of clay agglomerates which leads to microcrack formation at the interface. The nanocomposites prepared using C30B &B109 shows an increase of 21.85 %and 20.91 % respectively as compared with the matrix polymer. PMMA/C20A nanocomposites exhibit less tensile strength of 67.94 MPa confirming comparatively less compatibility with the matrix polymer. Further grafted samples in all the systems exhibits lower tensile strength as compared with ungrafted nanocomposites system revealing brittleness characteristics of PMMA with interface modification in the nanocomposites system. Strain at break decreases with the incorporation of nanoclays, PMMA/C30B nanocomposites exhibited a decrease of 62.71% with PMMA/B109 to 54.1% and PMMA/C20A to 91.6 % respectively as compared with the matrix polymer. Grafting of PMMA with MA and influence of organic modifier /intercalant type had virtually no effect on the stress as well as strain at break of the nanocomposite hybrids.

Dynamic Mechanical Analysis:

The temperature dependence plots of storage modulus E' of PMMA and its nanocomposites as measured from –150 ^{0}C to 150 ^{0}C are depicted in fig.5. As observed in the figure, the glassy state storage modulus at 25 ^{0}C increases to the tune of 9.2% in PMMA/C30B, 15.5 % PMMA/B109 and 29.3% PMMA/C20A respectively as compared with the virgin matrix. The grafted nanocomposites also demonstrated moderate increase in E' of PMMA. PMMA-g-MA/C30B exhibits maximum increase in storage modulus Above 80 ^{0}C, the E' drops with considerable fall in matrix modulus observed in the vicinity of Tg indicating that the material undergoes a glass/ rubber transition. DMTA tests indicated remarkable increase in E' in the nanocomposites system as compared with virgin matrix. The E' values display improvement in glassy regions (except deviations in PMMA/B 109 system) confirming that incorporation of nanoclay induces reinforcing effect. At high temperature regions the nanocomposites system as well as PMMA displayed similar modulus and approaches constant level of temperature beyond 130 ^{0}C

Conclusion:

PMMA nanocomposities were prepared using melt blending technique. The effect of organic modifier on the mechanical, thermal and flammability properties of nanocomposites has been investigated. Mechanical properties indicated optimum tensile modulus is PMMA/C30B 5% as compared to virgin PMMA matrix and other nanocomposites. WAXD & TEM micrographs showed evidence of exfoliation and intercalation in PMMA/C30B nancomposites. Thermal study indicates an increase in onset of decomposition temperature and marginal increase in Tg of nanocomposites. DMA studies revealed substantial increase in the E' of the nanocomposites with the incorporation of C30B nanocomposites.

References

1. Blumstein, A.J Polym sci. part A: Gen pap 1965, 3, 2653
2. Wang, D.; Zhu, J.; Yao, Q.; Wilkie, C.A. Chem mater 2002,14,3837
3. Bandyopadhyay, S.; Giannelis, E. P.; Hsieh, A. J. Polym2000, 82, 208.
4. Hsieh, A. J.; Giannelis, E. P. Presented at the American Physical Society Symposia Presentation, Atlanta, GA, March 1999.
5. Salahuddin, N.; Shehata, M. Polymer 2001, 42, 8379.
6. S.u, S.; wilkie, C.A. J.Polym Sci. Part A: polym Chem 2003, 41, 1124
7. Lee, D.C.; Jang, L.W. J Appl Polym Sci., 1996,61,1117
8. Huang, X.; Brittain, W.J. Macromolecules, 2001,34,3255
9. S.Kumar, J.P. Jog, U.P, J. Appl. Polym. Sci. 2003, 89, 1186

Table 1: Mechanical Properties of PMMA & Nanocomposites at 5 wt% nanoclay loading

Sample ID	Tensile strength (MPa)	Tensile modulus (MPa)	Strain at break(%)
PMMA	56.4	1980	3.84
PMMA/C30B	68.81	2681	1.43
PMMA/B109	68.28	2469	1.76
PMMA/C20A	67.94	2168	0.32
PMMA-g-MA/C30B	65.29	2736	1.00
PMMA-g-MA/B109	59.40	2607	0.64

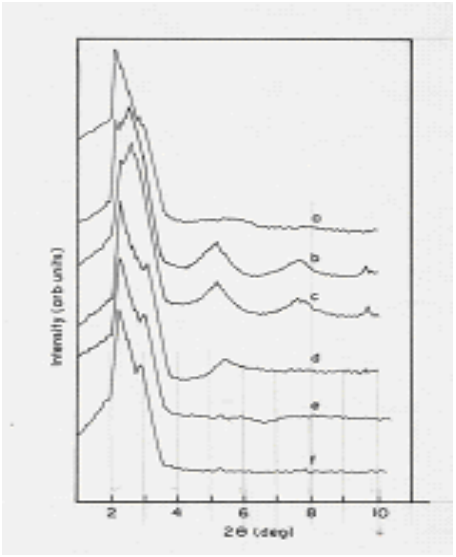

Figure.1 Wide angle X-ray Diffraction Pattern (a) PMMA/C30B, (b) PMMA/B109, (c) PMMA/C20A, (d) PMMA-g-MA/C30B, (e)PMMA-g-MA/B109,(f)PMMA-g-MA/C20A

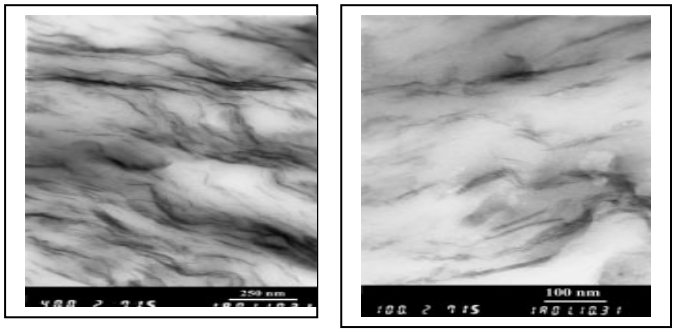

(a) (b)

Figure.2 .(a). PMMA/C30B (5%) without compatibiliser, (b), PMMA/C30B (5%) with compatibilizer

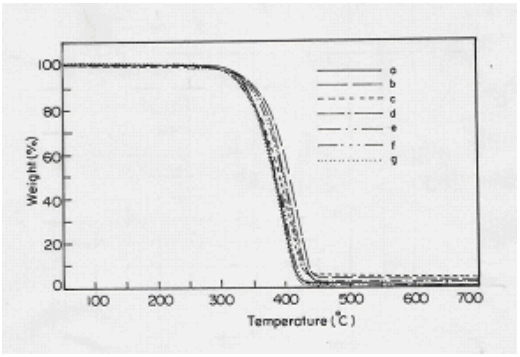

Figure.3 TGA of (a) PMMA (V), (b) PMMA/C30B, (c) PMMAB109 (d) PMMA/C20A, (e)PMMA-g-MA/C30B(f) PMMA-g-MA/B109 (g) PMMA-g-MA/C20A

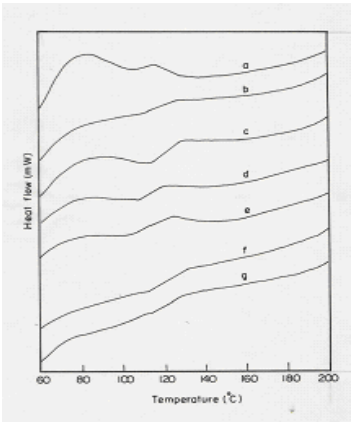

Figure.4 DSC of (a) PMMA (V), (b) PMMA/C30B (c) PMMAB109 (d) PMMA/C20A(e) PMMA-g-MA/C30B (f) PMMA-g-MA/B109 (g) PMMA-g-MA/C20A

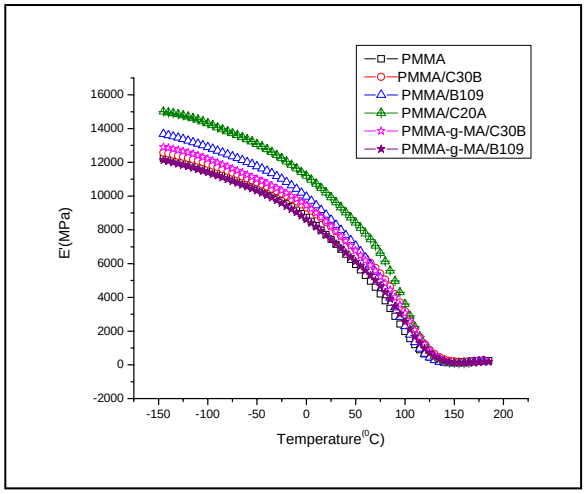

Figure.5 Variation of Storage Modulus with Temperature of PMMA and Nanocomposites

A Review on thermally stable organic modifiers for montmorillonite nanoclays

Reema Sinha* and Soumyadeb Ghosh
SABIC Innovative Plastics Program,
GE India Technology Centre – Bangalore, 560 066, India
Email: Sumanda.Bandyopadhyay@ge.com

Abstract

Among nanomaterials, polymeric nanocomposites have emerged as one of the most important class of materials and hence, a field of active research. One of the most important classes of nanocomposites is based on silicate nanoclays, modified with different ammonium cations, which have been studies most extensively for fundamental understanding as well as for commercial applications. However, the application space for polymer nanocomposites remained restricted to low temperature resins such as polyolefins and polyamides, due to relatively low thermal stability of the alkyl ammonium ions (below 250°C), used as modifiers. This restricts exploitation this technology in the arena of high performance polymers such as engineering thermoplastics, which are most often compounded at high temperatures. Hence, recently, a number of research groups have taken up the challenge of extending the applicability of nanoclays to high-temperature resins. In this presentation, recent efforts in compatibilization of nanoclays using thermally stable modifiers will be reviewed. The present status, with respect to the thermal stability reported in different classes of modified nanoclays, and the industry needs in terms of the temperature requirements for their melt-processing in different thermoplastic system, will be discussed.

Introduction

The field of nanotechnology is one of the most active areas of research in most of the technical disciplines. In recent years, polymer-layered silicate nanocomposites have attracted great interest in both in industry and in academia. This is because they show remarkable improvement in materials properties when compared with virgin polymer or conventional micro and macro-composites. These improvements include high moduli [1–3], increased strength and heat resistance [2], decreased gas permeability [4,5], flammability [6,7], and increased biodegradability of biodegradable polymers [8].

Toyota researchers [9,10] were first to show remarkable improvements in some physico-mechanical properties of polyamide-6 (PA-6) containing exfoliated organo-clay. They observed 100% improvement in modulus, 50% increase in strength and 80^{o}C enhancement in heat distortion temperature compared to neat PA-6. It is interesting that polymer-clay nanocomposites offer exceptional stiffness and strength at very low filler loading (e.g., 6.5 wt% clay), whereas ~20% of glass fibers is needed to achieve similar improvements [11]. Significant improvements in properties, albeit to lesser extent, were also demonstrated in nanocomposites based on polyolefins [12]. These advantages have benefits mainly in transportation and automotive industries, where lightweight structures and components are critical to improve the fuel economy.

The improvement in the properties are critically dependent on exfoliation of the layered silicate nanoclay particles in the nanocomposites, achieved by using appropriate modification of the negatively charged silicate layers with organic cations [12]. Nanoclay based composites of almost all classes of polymers have been evaluated for different applications and exfoliation of the

silicate layers leading to enhanced properties have been achieved in a number of systems. However, only handful of such systems has reached the market till date. One of the main reasons for this has been the thermal stability and compatibility of the organic modifier for the nanoclays. Most polymer-based products are manufactured by melt processing or require thermal treatments, whereas the commercially available nanoclays are organically modified using organic ammonium cations. Such cations are not stable at temperatures required for high rate production of nanocomposites of most polymeric systems. Hence, nanocomposites based on polyolefins and PA-6, which require comparatively lower processing temperatures, have found use in the market. In the present talk, the need for thermally stable nanoclay modifiers will be analyzed and various recent attempts for development of thermally stable modifiers for high temperature applications will be reviewed.

Thermally Stable Nanoclay Modifiers

Increasing the thermal stability of organoclay is one of the key needs in the successful industrial application of polymer-clay nanocomposites. This would enable the preparation of nanocomposites from thermoplastic polymers that require high melt-processing temperatures (PA-6,6, PC, PET, s-PS, PEI) or long residence times under high shear and from thermoset resins with high cure temperatures (cyanate esters, aromatic epoxies). To circumvent the detrimental effect of lower thermal stability of alkyl ammonium-treated montmorillonite (MMT), many cations, such as phosphonium, pyridinium, imidazolium etc. have been used to modifiy nanoclays because of their greater thermal stabilities [13,14]. Organoclays treated with these cations have thermal stability higher than 290 °C in inert atmosphere, based on the $Td_{5\%}$ data [12]. Studies on thermally stable modifiers and their application to different polymer systems have been reviewed earlier [12,15]. Here the efforts on application of different kinds of high-temperature modifiers in nanocomposites, is briefly summarized

Quaternary phosphonium modified nanoclays have been most extensively studied. Modifiers with phosphonium surfactants having either short alkyl chains, benzene ring, a long alkyl chain or a mixture of these groups have been tried. They are 50-80°C more stable than corresponding ammonium salts [16]. Besides improving mechanical properties, phosphonium clays also improves the flame retardancy and heat stabilization [17]. They have been incorporated in polymers like polyesters, syndiotactic polystyrene, epoxies, PMMA. Depending on the polymer, exfoliated, intercalated or mixed intercalated-exfoliated structures has been obtained [16,17]. Imidazolium modified nanoclay- such as trialkylimidazolium modified MMT give an organoclay, which is 100°C more stable than alkylammonium-modified MMT. The alkyl chain length affects the thermal stability of the salt, the stability decreases as the chain length is increased [18]. Studies with these clays have been done mainly in PA-6 and polystyrene to give an exfoliated PA-6 nanocomposite and a partially exfoliated polystyrene nanocomposite with improved thermal stability and reduced flammability [18,19]. Pyridinium cation modified nanoclay- Pyridinium treated nanoclays are 50-100°C more stable than ammonium modified clays. In PET, cetylpyridinium modified clay gave high level of dispersion and improved thermal stability of the nanocomposite [20].

The Need for Thermal Stability

Let us now consider the extent of thermal stability of the modified nanoclays required with respect to the present status of the technology. The typical temperature ranges required for melt-

processing of different commercial thermoplastic materials are given in figure 1 [21]. It may be observed that though many high-volume commodity thermoplastics can be processed at or below about 250°C, all the high-performance engineering thermoplastics need temperatures between 250°C – 350°C for processing, whereas some specialty polymers need up to 400°C.

To compare the state of art in nanoclay modification, some of the thermal stability indicators namely the temperature at initiation of thermal degradation and the temperatures at maximum rate of degradation, derived from the earlier works [17,22] are also presented in figure 1. It can be observed (Fig.1) that ammonium cation based modifiers, which are most commonly used for modification of nanoclays, have the lowest thermal stability among all the classes of modified presented above. While at about 250°C the phosphonium, cation based nanoclay just initiate to degrade and the other higher temperature nanoclays do not show any degradation, the ammonium based nanoclays reaches almost the point of maximum rate of degradation. According to the TGA data reported by Calderon et al., a typical ammonium nanoclay, with grade name Cloisite 10A, attains a weight-loss rate of 0.25 %/ °C. Taking the heating rate for the TGA experiment of 20°C /min [17], it can be inferred that the nanoclay degrades at a rate of about 5% per minute. For a more stable ammonium modified nanoclay, Closite 15A, the rate was about 1.5% per minute, which rapidly increases to 3.4% at 300°C and reaching the maximum of about 5.5% at 325°C.

Further, it should be noted that the TGA experiments were run under nitrogen atmosphere whereas thermoplastics are melt-processed in air and a typical thermoplastic itself may have functional groups that could be reactive to the organic modifier at the processing temperature, leading to rather severe degradation of the modifier groups on the nanoclays. This causes the loss of the alkyl long chains from the modifiers, which increases the interlayer interaction, preventing the exfoliation of nanoclays. In some cases, if the nanoclays are already exfoliated at lower temperatures (e.g. master-batching at lower temperatures using other processing methods), exposure to high temperatures in subsequent processing steps may cause collapse of the nanoclay layers on lager size particles.

In contrast to the ammonium based nanoclays, the nanoclays modified with higher temperature modifiers show negligible degradation up to 300°C. The phosphonium based nanoclay, which found to be least stable among the nanoclays studied, reaches a degradation rate of 0.15% per minute or 3% per minutes only above a temperature of 400°C, at the same experimental conditions. Similar observations may be made from figure 1 for the imidazolium and pyridinium based nanoclays too. Hence, development of organic modifiers based on these thermally stable cations should help in translating the technology to the systems of engineering thermoplastics. Since modified nanoclays has been successfully used in PA-6, which has processing temperature range that extends above 250°C, it may be hoped that some of the nanoclay modifier might survive the processing temperatures of specialty, high-temperature polymers such as Ultem*, PPS or PEEK.

* - Trademark of Sabic Innovative Plastics

Conclusion:

Though the technology of nanocomposites based on modified nanoclays has been demonstrated in a number of different polymers, it could reach the market only in cases of polymers having comparatively lower processing temperatures. Even in the market it is not very clear how well these new materials are performing. There may still be further need for the technology to achieve the right balance between the overall advantages in terms of property improvements and the cost. It may be a greater challenge to achieve this in commodity thermoplastics. On the other hand, there are strong market needs for special properties, such as thermo-mechanical stability, toughness, low flammability, chemical stability, high gas-barrier properties in polymeric materials. Nanocomposites of commodity plastics may match some of the properties (e.g. room

temperature mechanical properties, barrier properties) of the engineering polymers. However, a success in developing technology for true nanocomposites based on engineering thermoplastics would take polymers to new market arena, bettering metals with easier processibility, recyclability, design flexibility and lighter weight. Hence, development of a successful technology for exfoliation and dispersion of nanoclays in engineering or high-temperature thermoplastics, would bridge the gap between the technology and the market need with the right cost-benefit balance. In this presentation, the recent efforts in development of modified nanoclays for high temperature applications have been reviewed. A comparison of the thermal stability of the conventional, as well as, of the new high-temperature modifiers, have been made with respect to the processing temperature required for different common commercial polymers.

An effort is made to give a comprehensive picture of the field from the point of view of the present status, and the industry needs in terms temperature requirements for melt processing of different thermoplastics.

References

[1] Okada A, Kawasumi M, Usuki A, Kojima Y, Kurauchi T, Kamigaito O. Synthesis and properties of PA-6/clay hybrids. In: Schaefer DW, Mark JE, editors. Polymer based molecular composites. MRS Symposium Proceedings, Pittsburgh, vol. 171; 1990: p. 45–50.
[2] LeBaron PC, Wang Z, Pinnavaia TJ; Appl Clay Sci.1999;15: 11–29.
[3] Vaia RA, Price G, Ruth PN, Nguyen HT, Lichtenhan J.; Appl Clay Sci 1999;15:67–92.
[4] Bharadwaj RK; Macromolecules 2001; 34: 1989–92.
[5] Kojima Y, Usuki A, Kawasumi M, Fukushima Y, Okada A, Kurauchi T, Kamigaito O; J Mater Res 1993; 8:1179–84.
[6] Gilman JW; Appl Clay Sci 1999; 15:31–49.
[7] Gilman JW, Jackson CL, Morgan AB, Harris R, Manias E, Giannelis EP, Wuthenow M, Hilton D, Phillips SH; Chem Mater 2000; 12: 1866–73.
[8] Sinha Ray S, Yamada K, Okamoto M, Ueda K; Nano Lett 2002; 2:1093–6.
[9] Usuki A, Kawasumi M, Kojima Y, Okada A; J Mater Res 1993; 8:1174–8.
[10] Usuki A, Kojima Y, Kawasumi M, Ukada A, Fukushima Y, Kurauchi T, J Mater Res 1993;8:1179–84.
[11] Fornes TD, Paul DR; Polymer 2003; 44: 4993–5013.
[12] Leszczyńskaa A, Njugunab J, Pielichowskia K, Banerjee JR; Thermochim. Acta 2007; 453: 75-96.
[13] Xie W, Gao Z, Pan W, Hunte D, Singh A, Vaia R; Chem Mater 2001;13: 2979–2990.
[14] Takekoshi, T.; Khouri, F. F.; Campbell, J. R.; Jordan, T. C.; Dai, K. H. (General Electric Company). US Patent 5707439; 1998.
[15] Leszczyńskaa A, Njugunab J, Pielichowskia K, Banerjee JR; Thermochim. Acta 2007; 454: 1-22.
[16] Xie W, Xie R, Pan W, Hunter D, Koene B, Tan L, Vaia R; Chem. Mater 2002; 14: 4837–4845.
[17] Calderon JU, Lennox B, Kamal MR; Applied Clay Science 2008; 40: 90-98
[18] Awad W, Gilman J, Nyden M, Harris R, Sutto T, Callahan J, Trulove P, DeLong H, Fox D; Thermochimica Acta 2004; 409: 3–11.
[19] Gilman J, Awad W, Davis R, Shields J, Harris R, Davis C, Morgan A, Sutto T, Callahan J, Trulove P, DeLong H; Chem. Mater 2002; 14: 3776-3785.
[20] Fang Ou C, Ting Ho M, Rung Lin J; J Appl Polym Sci 2004; 91: 140–145.
[21] Injection Molding Reference Guide (4th edition), Publisher: Advanced Process Engineering, Cornvallis, Oregon; 1997: p35.
[22] Stoeffler K, Lafleur PG, Denault J; Polymer Degradation and Stability 2008; 93:1332–1350.

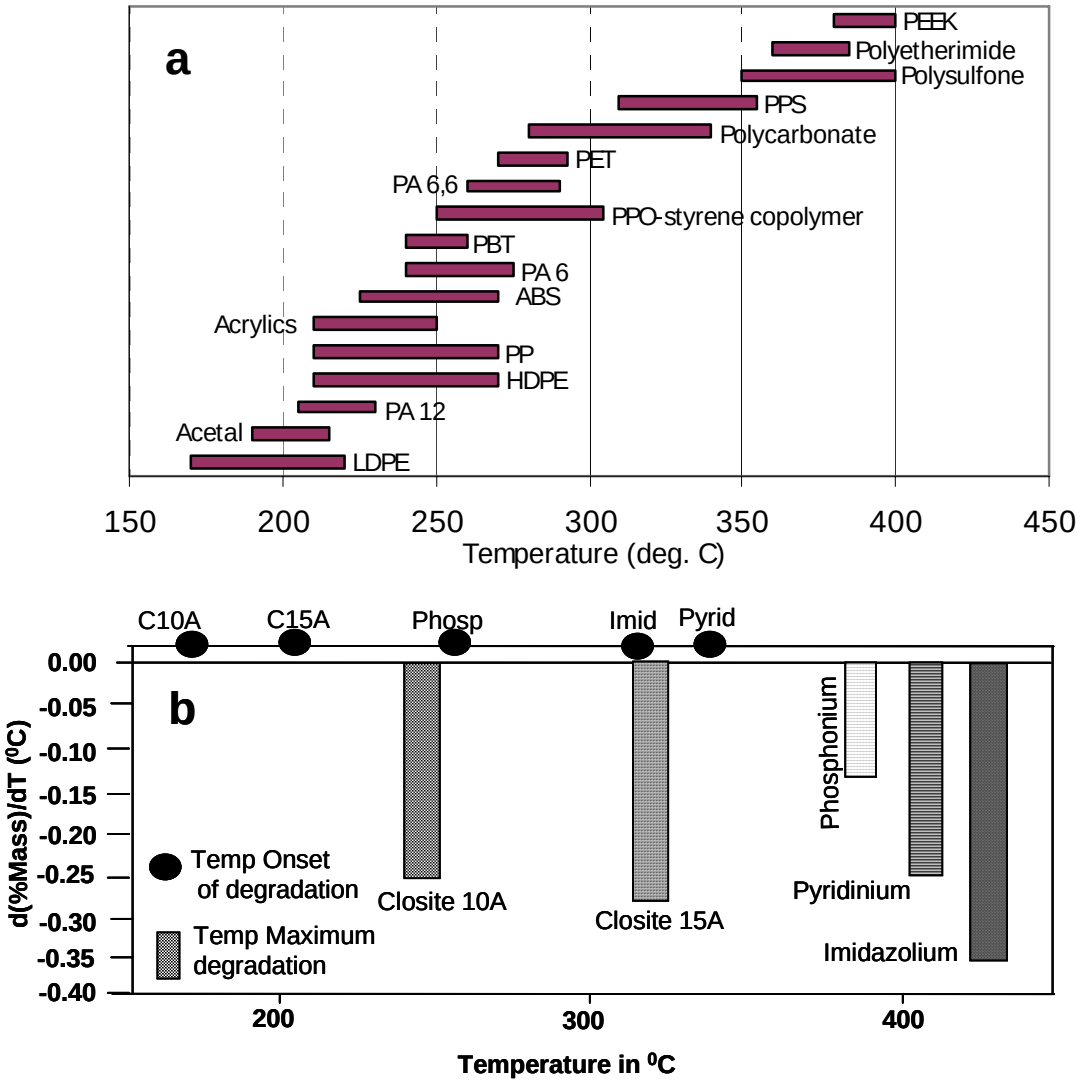

Figure 1. (a) Temperature ranges of different commercial thermoplastic polymers [21] (b) Onset temperatures and maxima of thermal degradation rates versus temperature for different nanoclays, modified different classes of organic cations (adapted from ref. 17, figure 3; ref. 22, figure 2)

Thermal and mechanical properties of poly (vinyl chloride)/ microscale and nanoscale calcium carbonate composites via melt intercalation

C. B. Patil, U. R. Kapadi, D. G. Hundiwale and P. P. Mahulikar*

School of Chemical Sciences, North Maharashtra University,
Jalgaon - 425 001 (M. S.) India
Email: mahulikarpp@rediffmail.com , dghundiwale@yahoo.com

Abstract

Calcium carbonate was synthesized by *in situ* deposition technique and its nano size (35 to 60 nm) was confirmed by Transmission Electron Microscopy (TEM). Composites of the filler $CaCO_3$ (micro and nano) and the matrix poly (vinyl chloride) (PVC) were prepared with different filler loading (0-5 wt. %) by melt intercalation. Brabender torque rheometer equipped with an internal mixer has been used for preparation of formulations for composites. The effect of filler content both nano and micro level on the nanostructure and properties is reported here. The nanostructures were studied by wide angle X-ray diffraction (WAXD). The mechanical, thermal and dynamic mechanical properties of PVC/ micro and nano $CaCO_3$ composites were characterized using Universal Testing Machine (UTM), Thermo Gravimetric Analyzer (TGA) and Dynamic Mechanical Analyzer (DMA). The results of thermal analysis indicated that the thermal stability of PVC/nano-$CaCO_3$ composites was improved as compared with corresponding microcomposites and that of pristine PVC and maximum improvement was obtained at 1 and 3 phr loadings. However, the tensile strength decreased significantly with increasing loading of both nano and micro $CaCO_3$ while storage modulus and glass transition temperature increased significantly.

Keywords: Nanoparticles, Transmission Electron Microscopy (TEM), Wide Angle X-ray Diffraction (WAXD), Tensile strength, Thermal stability.

1. Introduction:

Nanoscale calcium carbonate (nano $CaCO_3$) is one of the most common spherical nanoscale fillers used in the preparation of nanocomposites. $CaCO_3$ can be produced by a variety of methods, including precipitation, dry grinding, and wet grinding. The basic grades of $CaCO_3$ can be differentiated by changes in the size distribution, particle size, surface area, morphology, surface chemistry, and so forth [1-4].

This nanoconcept has been mostly focused on thermoplastic and thermosetting polymers including polyamides, polypropylene, epoxies and polyesters. The addition of nano-$CaCO_3$ to

composites has been reported to improve the strength, modulus, and toughness significantly. A study of polypropylene (PP)/nano-$CaCO_3$ composites revealed a dramatic toughening effect of nano-$CaCO_3$ on PP. However, the yield strength of PP slightly decreased because of the nucleating effect of nano-$CaCO_3$ [5, 6].

Relatively a little attention has been paid to polyvinyl chlorides (PVC) materials.The effects of inorganic fillers on the microstructure and mechanical properties of PVC composites depend strongly on the particle shape, particle size, aggregate size, surface characteristics, the fraction of fillers and their degree of dispersion [7-25].

2. Experimental Section:

2.1 Materials

Materials used for the synthesis of nanoparticles of calcium carbonate were $CaCl_2$, K_2CO_3 & PEG. Calcium chloride, potassium carbonate were of analytical grade and poly (ethylene glycol) (PEG; MW 6000 g) was procured from s. d. Fine Chem., Ltd. Mumbai, India. The polyvinyl chloride grade 57GERO68, was obtained from Reliance Industries Ltd., Mumbai, India.

2.2 Preparation of nanoparticles:

The nanosized calcium carbonate filler particles were synthesized using *in situ* deposition technique [7-8].

2.3 Preparation of Composites:

For preparation of composites, formulations were melt intercalated using a Brabender Plastograph EC equipped with an electrically heated mixing head (W 50 EHT mixer) having 55 cm^3 volume capacity and two non interchangeable rotors. The processing temperature, rotor speed and blending time were set at 170 ^{0}C, 60 rpm and 10 min, respectively. The sample volume of each blending was kept 90 % of the actual volume capacity of the mixer. The compounds of composites were obtained in the form of lumps. These lumps were then crushed to get the coarser particles/granules (approx. 3-4 mm size) suitable as feed for injection moulding to obtain tensile and impact specimens.

2.4 Characterization

The particle size of synthesized nano calcium carbonate particles were analysed using Transmission Electron Microscope (TEM, Philips Tecnai-20). The structure of PVC-$CaCO_3$ nanocomposites was characterized by WAXD.

A thermogravimetric analyzer was used to analyze thermal characteristics of the PVC/micro and nano $CaCO_3$ composites. The composites were heated from room temperature to 550 ^{O}C at the rate of 5 ^{O}C/min. under nitrogen stream. Tensile strength was determined by subjecting dumb-bell shaped specimens (in accordance with ASTM D – 412) to a Universal

Testing Machine. The dynamic mechanical analysis (DMA) was performed using a Gabo Eplexor dynamic mechanical analyzer at a fixed frequency rate 10 Hz in a temperature range from 30 to 120 ^{0}C, and the heating rate 2 ^{0}C/min.

3. Results and discussion

3.1 Particle Size Analysis

The particle size of the calcium carbonate was found to be in the range of 35 to 60 nm as verified from TEM micrograph of $CaCO_3$ nanoparticles [Fig.1]

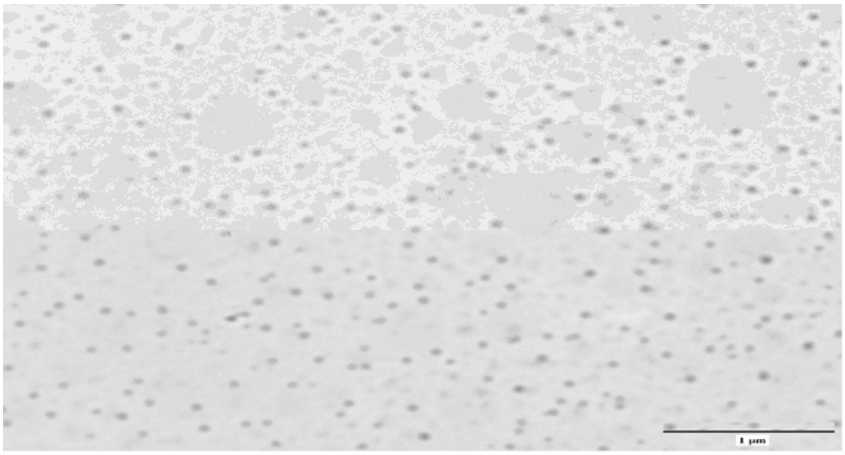

Figure 1: TEM micrograph of calcium carbonate nanoparticles prepared by *in situ* deposition technique.

3.2 Wide angle X-ray diffraction studies (WAXD)

The WAXD analysis is a very useful method to describe the extent of intercalation and exfoliation of inorganic nanofiller in the composites. Figure 2 (a) and (b) shows WAXD patterns of PVC/micro and nano-$CaCO_3$ composites of 1, 3 and 5 wt. % of filler. Figure 2 (a) shows minor peaks at 2 $\theta = 29.0^0$ while figure 2 (b) shows prominent sharp peaks at the same angle, obviously, these peaks are contributed by the filler nano-$CaCO_3$. The subsiding of peaks at 2 $\theta = 29.0^0$ in fig. 2 (a) in the case of micro-$CaCO_3$ filled composites at all wt. % (1, 3 & 5) indicates fairly good dispersion. While in the case of nano-$CaCO_3$ filled composites the peaks do not subside instead, they sharpen and the peak height at 2 $\theta = 29.0^0$ increases with increasing content of the filler (1-5 wt. %). Therefore it can be concluded that the structure of nanocomposites is intercalated and flocculated and not the exfoliated.

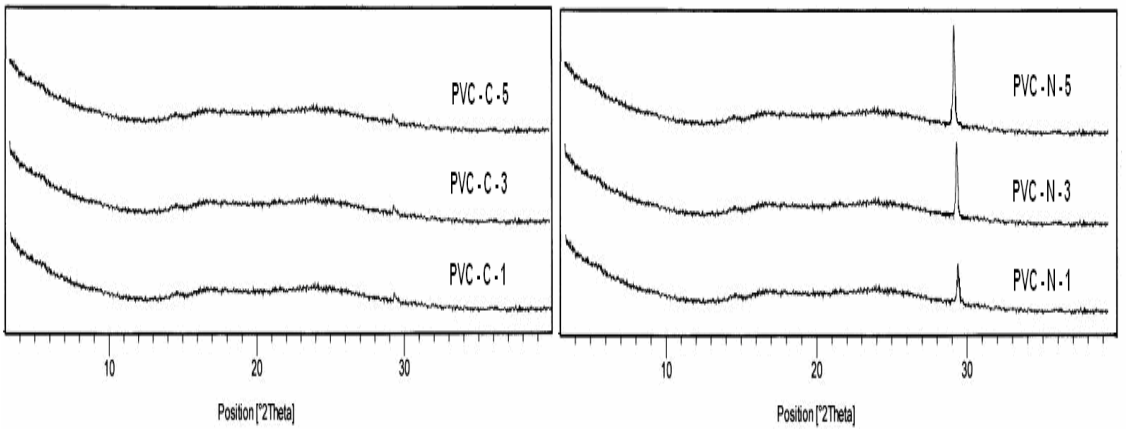

(a) **(b)**

Figure 2: WAXD of a) PVC/micro-$CaCO_3$ for composites of 1, 3 and 5 wt. % of filler and b) PVC/nano-$CaCO_3$

3.3 Tensile Behavior

Figure 4 shows the tensile behavior of PVC/micro and nano-$CaCO_3$ composites prepared by melt intercalation.

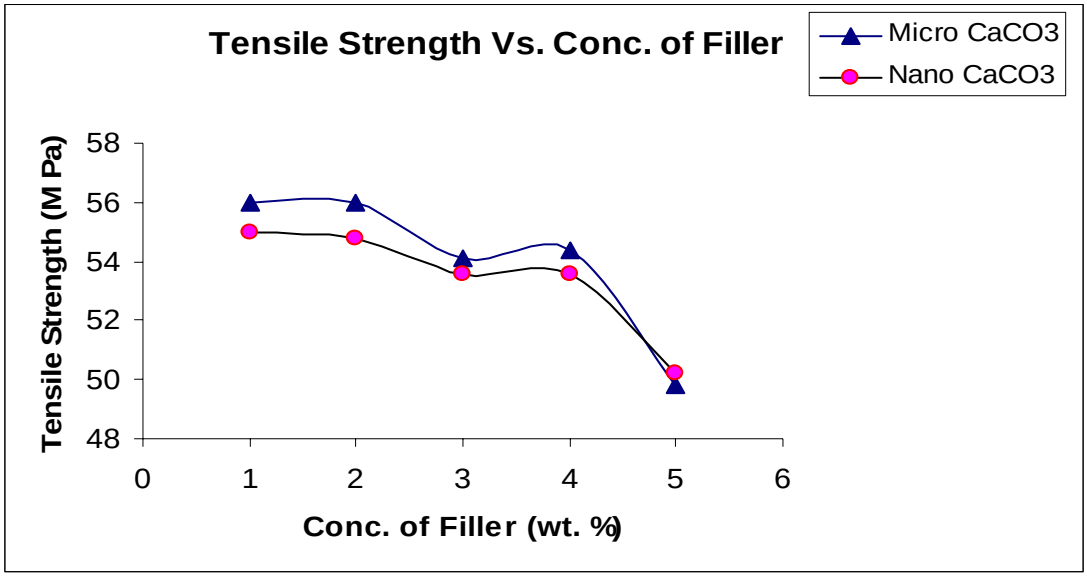

Figure 3: Tensile strength of composites (micro and nano) with the variation of filler content (1 to 5 wt. %)

With the increasing addition of the nano-$CaCO_3$ particles, due to the tendency of agglomeration of nanoparticles weak interfacial adhesion existed between the PVC matrix and the nanoparticles and hence the load bearing capacity of cross sectional area of composites decreased, and only a small amount of stress could be transferred from the matrix to inorganic particles hence tensile strength showed decrement in the magnitude; in this case agglomerated particles easily debonded from the matrix and could not bear any fraction of external load ultimately

decreasing the tensile strength. These results are inconsistent with the results of the research work carried out by Tianbin Ren et al. [16], Shuisheng Sun et al. [5], and Jie Ren et al [20].

3.4 Thermogravimetric Analysis (TGA)

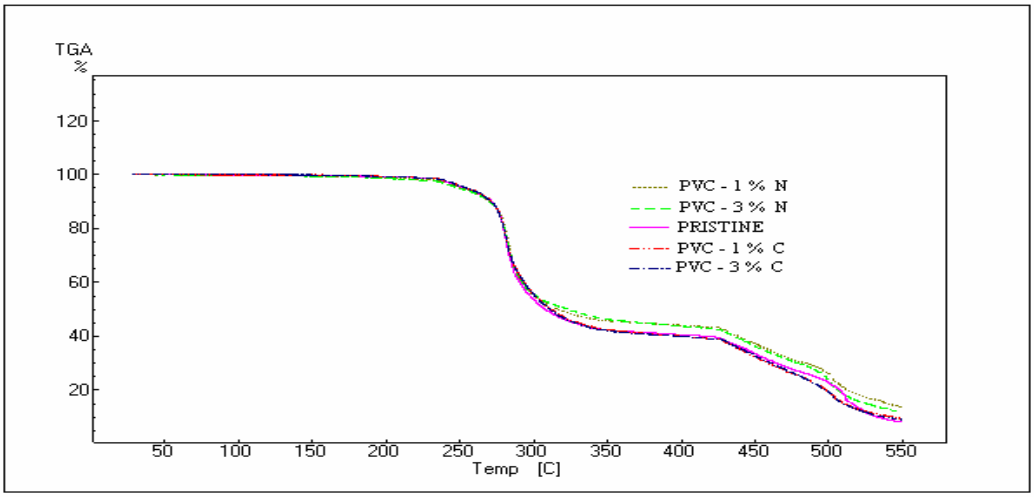

Figure 4: Representative TGA curves of PVC/micro and nano-$CaCO_3$ composites

Representative TGA curves of PVC/micro and nano-$CaCO_3$ composites are shown fig. 4 Looking at the values of T_{onset} from figure pristine PVC and PVC /micro-$CaCO_3$ composites did not show variation while those of PVC/nano-$CaCO_3$ composites showed marginal increase in the values of T_{onset}. Further, the weight residue of PVC/nano-$CaCO_3$ is higher than that of pristine PVC and their corresponding microcomposites of $CaCO_3$.

3.5 Dynamic Mechanical Analysis (DMA)

Dynamic storage modulus as a function of temperature for pristine PVC and PVC/micro and nano-$CaCO_3$ composites are ploted in fig. 5. It is observed that the storage modulus (E') of microcomposites is slightly higher than that of PVC/nanocomposites and pristine PVC in the glassy region. Moreover the magnitude of storage modulus is higher with the increasing content of micro $CaCO_3$ in the same (glassy region). A similar trend is observed in the case of glass transition temperature obtained from tan δ Vs. temperature curves. In general the nanocomposites did not show significant variation in storage modulus as well as in glass transition temperature, rather the trend is mediocre compared to pristine PVC and microcomposites this unexpected viscoelastic behavior again accounted for non uniform distribution of nanoparticles and the formation of agglomerates causing inhomogeneous interactions of organic matrix and the inorganic filler.

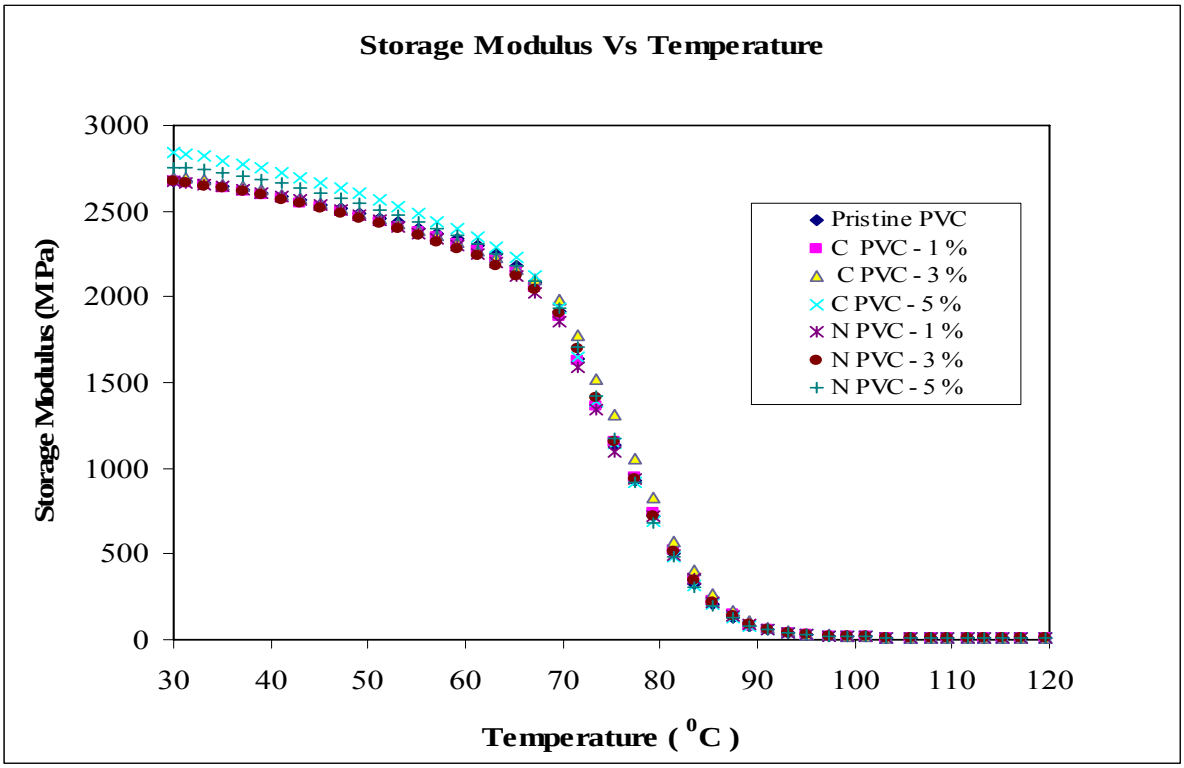

Figure 5: Variation of Storage Modulus with respect to temperature for Pristine PVC and PVC/micro and nano-$CaCO_3$ composites at 1, 3, and 5 wt. %

Table 1: T_g of PVC/ micro and nano $CaCO_3$ composites

% of Filler	T_g of PVC/micro -$CaCO_3$ composites (^{0}C)	T_g of PVC/nano-$CaCO_3$ composites (^{0}C)
0	91.2	91.2
1	91.6	92.0
3	93.3	91.4
5	93.3	91.1

Conclusions:

Nano $CaCO_3$ particles were successfully synthesized using *in situ* deposition technique and the particle size was obtained in the range of 35 to 60 nm confirmed by XRD and TEM techniques. The PVC/micro and nano-$CaCO_3$ composites were prepared by melt intercalation. The impact of nanoparticles on thermal, dynamic mechanical and tensile behavior was studied and compared with microcomposites. From the results of WAXD it was confirmed that dispersion of filler was not proper in PVC matrix and hence the structure of PVC nanocomposites was intercalated and flocculated. The tensile strength of both the micro and nanocomposites was decreased with the increasing $CaCO_3$ content. The storage modulus of both composites was found to be slightly

higher than that of pristine PVC. The glass transition temperature of both the composites was also slightly higher than pristine PVC. Further the onset degradation temperature of PVC/nano-$CaCO_3$ composites was marginally higher than microcomposites and pristine PVC. Thus this study shows that there is poor interaction between PVC and the nano-$CaCO_3$ filler. There is a need to modify interaction between PVC and nano-$CaCO_3$.

Acknowledgement

Authors thank the University Grants Commissions, New Delhi for providing financial assistance under grants of Special Assistance Programme (SAP) at Departmental Research Support (DRS) Level.

References:

1. Dezhen, W.; Xiaodong, W Yongzhi, S.; Riguang, J. J Appl Polymr Sci 2004, 92, 2714.
2. Cheng-Ho, C.; Chih-Chun, T.; Shun-Fua, S.; Wen-Chang, W.; Chien-Hsin, Y.; J Polym Sci Part B: Polym Phys 2006, 44, 451.
3. Sun, S.; Li, C.; Zhang L.; Du, HL.; Burnell- Gray, JS.; Polymer Int 2006, 55, 158.
4. Xiao-Lin, X.; Qing-Xi, L.; Robert Kwok-Yiu, L.; Xing-Ping, Z.; Qing-Xin, Z.; Zhong-Zhen, Y.; Yiu-Wing, M.; Polymer 2004, 45, 6665.
5. Ling, Z.; Xuehua, C.; Chunzhung, Li. J Mater Sci 2005, 40, 2097.
6. Chan, C.M.; Wu, J.; Li, J.X.; Cheung, Y. K.; Polymer 2002, 43, 2981.
7. Mishra, S.; Sonwane, S.H.; Singh, R.P. J Polym Sci Part B: Polym Phys 2005, 43, 107.
8. Saujanya, C.; Radhakrishan, S.; Polymer 2001, 42, 6723.
9. Cheng-Ho, C,; Chih-Chun, T,; Ming-Shyong, T,; Fu –Su, Y,; J Polym Sci Part B: Polym Phys 2006, 44, 2145.
10. Mingwang, P.; Xudong, S.; Xiucuo, L.; Haiyan, H.; Liucheng, Z. J Appl Polym Sci 2004, 94, 277.
11. Yong – Zhong, B.; Zhi-Miang, H.; Zhi-Xue, W.; J Appl Polym Sci 2006, 102, 1471.
12. Tianbin, R.; Jung, Y.; Yanxia H.; Jie, R.; Yan, L.; J Polym Comp 2006, 27, 55
13. Zhu-Mei, L.; Chao-Ying W.; Yong, Z.; Ping, W.; Jie, Y. J Appl Polym Sci 2004, 92, 567.
14. Chaoying, W.; Xiuying, Q.; Yong, Z.; Yinxi, Z. J Appl Polym Sci, 2003, 89, 2184.
15. Haiyan, Hu.; Mingwang, P.; Xiucuo Li.; Xudong, Shi.; Liucheng Z. Polymer Int 2004, 53, 225.
16. Jie, R.; Yanxia, H.; Yan, L,; Xiaozhen, T. Polym Test 2005, 24, 316.

17. Peprnicek, T.; Duchet, J.; Kovarova, L.; Malac, J.; Gerard, J. F.; Simonik, J. Polym Degrd Stab 2006, 91, 1855.
18. Gong, F. L.; Zhao, C. G.; Feng, M.; Qin, H.L.; Yang, M. S.; J Mate Sci 2004, 39, 293.
19. Peng, L.; Mingfei, Z.; Jinshan, G. J Macro Sci Part B: Phys 2006, 45, 1135.
20. Guangming, Chen. J Appl Polym Sci 2007, 106, 817.
21. Chaoying, W.; Xiuying, Q.; Yong Z.; Yinxi, Z. Polym Test 2003, 22, 453.
22. Chaoying, W.; Yong Z.; Yinxi, Z. Polym Test 2004, 23, 299.
23. Dongyan, W.; Daniel, P.; Qian, Y.; Charles A.W. J Vinyl Addit Tech 2001, 7 - 4, 203
24. Dongyan, W.; Charles, A. W, J Vinyl Addit Tech 2002, 8 - 4, 238.
25. Ismail, H.; Munusamy Y. J Rein Plast Comp 2007, 26, 1681.

In-situ generation of silica in epoxy matrix and modified epoxy matrix via sol-gel process

K.K.Iynesh Kumar and B.Kothandaraman
Department of Rubber and Plastics technology, Madras Institute of Technology, Anna University, Chennai, India.
Email: iyneshkumar@gmail.com bkraman@mitindia.edu

ABSTRACT

The precipitation of nanosilica was done through Sol-Gel process with Tetraethoxysilane (TEOS) as silica precursor at room temperature. The choice of epoxy as a matrix was made because of its polar nature which can interact with in-situ generated silica. The amine containing polydimethylsiloxane (PDMS) was used as liquid rubber modifier.

The precipitation was done directly on the organic matrix in the presence of Water, Tetraethoxysilane (TEOS) and Ethanol as mutual solvent. The nanocomposite was cured by triethylene tetramine at room temperature. To enhance bonding between organic and inorganic matrix Dichlorodimethylsilane (DDS) was used as a coupling agent.

Dispersion of silica particles was observed through Atomic force microscope (AFM). Infrared spectroscopic studies indicated the occurrence of chemical interaction within the epoxy/silica under ambient conditions. The glass transition temperature (T_g) was investigated through Differential scanning calorimeter (DSC). The thermal stability and filler content of the material were predicted through Thermogravimetricanalyser (TGA). The mechanical reinforcement within the material was demonstrated through flexural behavior of the material.

INTRODUCTION

The sol-gel process, which is mainly based on inorganic polymerization reactions, is a chemical synthesis method initially used for the preparation of inorganic materials such as glasses and ceramics. Its unique low-temperature processing characteristic also provides unique opportunities to make pure and well-controlled composition organic/inorganic hybrid materials through the incorporation of low molecular weight and oligomeric/polymeric organic molecules with appropriate inorganic moieties at temperatures under which the organics can survive. The organic/inorganic hybrid materials made in this way, which have been termed “creamers” by Wilkes [1] and “ormosils” or” ormocers” by Schmidt[2]., are normally nanocomposites and have the potential for providing unique combinations of properties which cannot be attained by other materials .

For the past decade, organic/inorganic nanocomposites prepared by the sol-gel process have attracted a great deal of attention, especially in the fields of ceramics, polymer chemistry, organic and inorganic chemistry, and physics. The preparation, characterization, and applications of organic/inorganic hybrid materials have become a fast expanding area of research in material science. The major driving forces behind the intense activities in this area are the new and different properties of the nanocomposites which the traditional macroscale composites and conventional materials don’t have. For example, unlike the traditional composite materials which have macroscale domain size of millimeter and even micrometer scale, most of the organic/inorganic hybrid materials are nanoscopic, with the physical

constraint of several nanometers, typically 1-100nm, as the minimum size of the components or phases. Therefore, they are often still optically transparent although microphase separation may exist. Through the combinations of inorganic and organic components in conjunction with appropriate processing methods, various types of primary and secondary bonding can be developed leading to materials with new properties for electrical, optical, structural, or related applications. [3]

EXPERIMENTAL

MATERIALS USED.

DGEBA liquid epoxy resin (LY556) with epoxy equivalent around 170 and viscosity of 8000 to 12000 cp at 25 degree Celsius was used as received from Araldite India Pvt. Ltd.The silicon alkoxide, TEOS was supplied by Aldrich, USA. Dimethyldichlorosilane was used as silane coupling agent supplied by M/s Merck .Organo modified polysiloxane with molecular weight around 5000 was used as liquid rubber modifier as received from Resil chemicals Pvt Ltd. Triethylene tetramine (HY 951-curing agent) was used as received from Araldite India Pvt.Ltd.

PREPARATION OF LIQUID RUBBER MODIFIED EPOXY MATRIX.

Amine containing polydimethylsiloxane was taken as liquid rubber modifier. Five phr of liquid rubber modifier was taken along with epoxy resin and the mixture was heated at 50 degree Celsius for 30 minutes with continuous stirring. Then the liquid rubber modified epoxy resin was allowed to cool in the room temperature.

PREPARATION OF SILANE COUPLING AGENT TREATED EPOXY RESIN.

Dichlorodimethylsilane was taken as silane coupling agent. The required amount of Dichlorodimethylsilane along with epoxy resin was heated at 60 degree Celsius with continuous stirring for 5 hours. The silane treated epoxy resin was left untouched for 4 to 5 hours. The same silane treatment procedure was carried out for Amine containing PDMS modified epoxy resin.

PREPARATION OF EPOXY AND MODIFIED EPOXY HYBRID MATERIALS.

The silica nano particles were prepared by hydrolysis of TEOS in ethanol medium. The reaction mixture (Water+TEOS+Ethanol) was stirred for 15 minutes in a glass beaker. Then the mixture was added to 50 ml epoxy resin and stirred continuously for 24 hours. The triethylene tetramine curing agent was added to in-situ silica precipitated epoxy resin at room temperature. Then the epoxy/silica hybrid material was cast between two polished mild steel plates and allowed to cure at room temperature for 24 hours. Then the cured material was post-cured at 150 degree Celsius for 3 hours. The above said procedure was repeated for Amine containing PDMS modified epoxy resin, silane treated epoxy resin, and silane treated Amine containing PDMS modified epoxy resin.

RESULTS AND DISCUSSIONS

FT-IR SPECTRUM STUDIES OF MODIFIED AND UNMODIFIED EPOXY –SILICA HYBRID MATERIALS

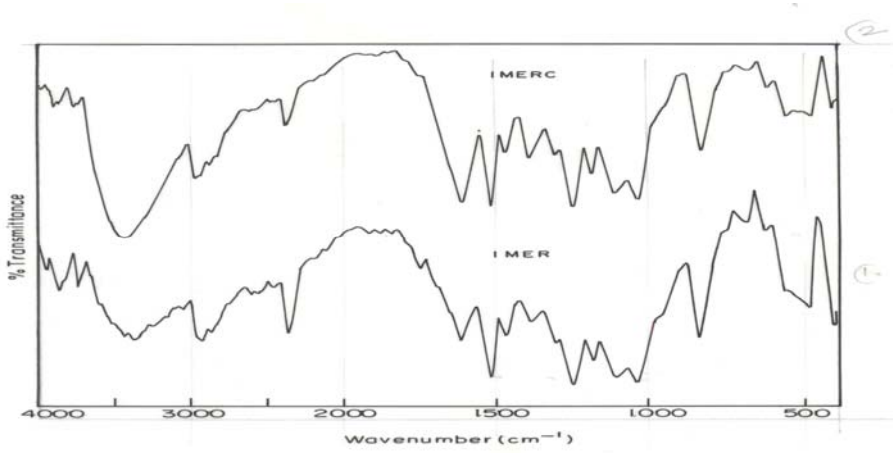

FT-IR spectrum. IMERC-in-situ silica precipitated modified epoxy resin treated with Dichlorodimethylsilane. IMER-in-situ silica precipitated modified epoxy resin.

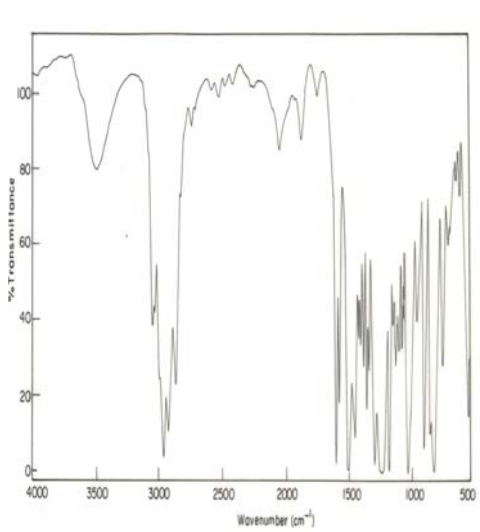

FT-IR spectrum of uncured epoxy

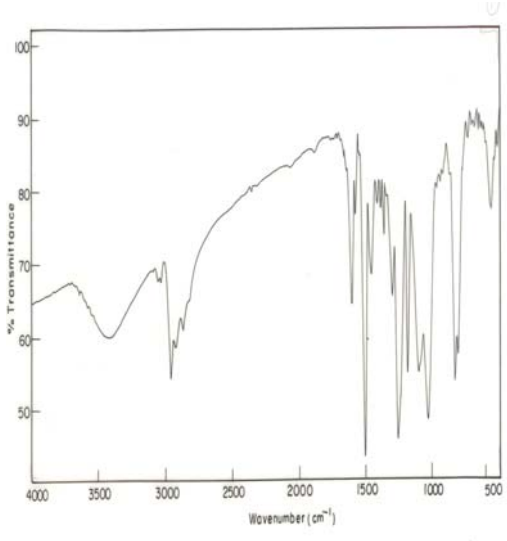

FT-IR spectrum of amine containing PDMS

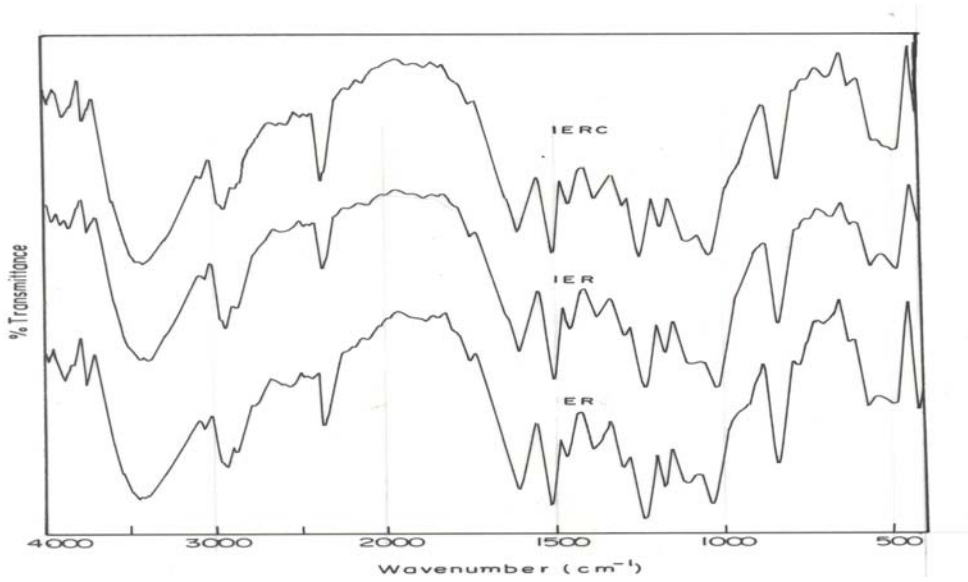

The FT-IR spectrum .ER-Epoxy resin, IER-in-situ silica precipitated epoxy resin.IERC-in-situ silica precipitated epoxy resin treated with Dichlorodimethylsilane.

The FTIR spectroscopy was done. The apparatus used was PERKIN-ELMER make.

Scanning Rate: 16 scans

Resolution: 4 cm^{-1}

IR spectroscopy is not helpful since the epoxy breathing bands as well as absorptions of the silanol groups were not clearly detected owing to a very broad band, involving the Si–O–Si network formation, ranging from 950 to 1250 cm-1[14].The Disappearance of epoxide peak at 915cm^{-1} indicates the complete curing of epoxy resin.

TGA STUDIES FOR MODIFIED AND UNMODIFIED EPOXY –SILICA HYBRID MATERIALS

TGA studies of Amine containing PDMS modified Epoxy-Silica hybrid materials

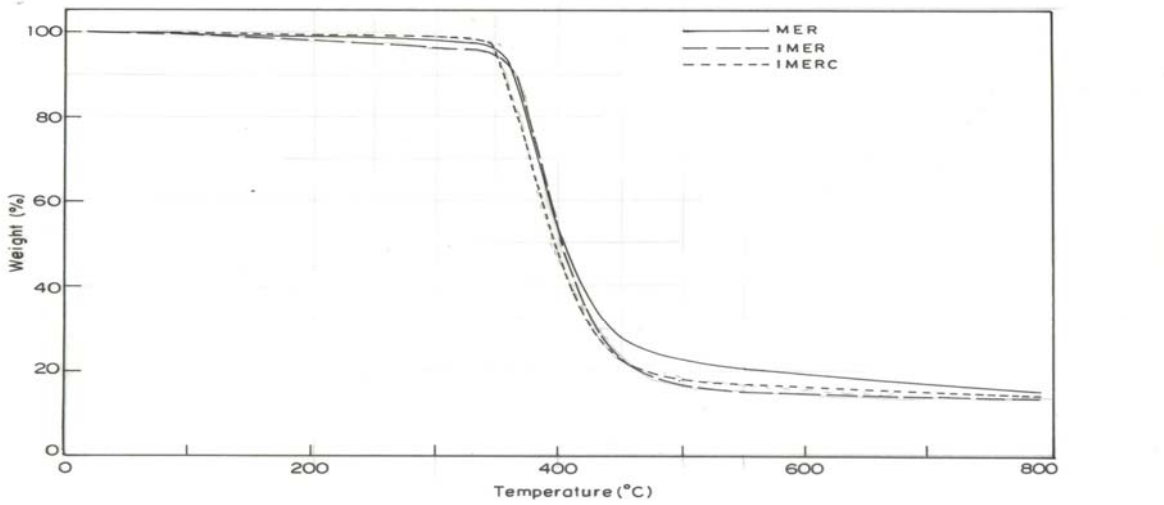

.MER-PDMS modified epoxy resin. IMER-in-situ silica precipitated PDMS modified epoxy resin. IMERC-in-situ silica precipitated PDMS modified epoxy resin.

TGA studies of Epoxy-Silica hybrid materials

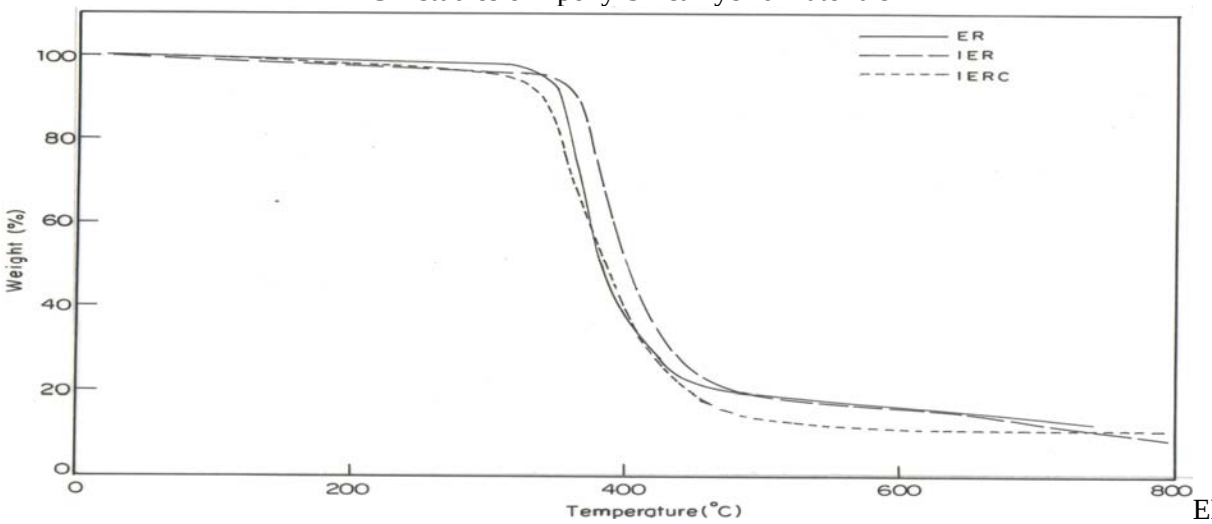

ER-ER-Epoxy resin.IER-in-situ silica precipitated epoxy resin. IERC-in-situ silica precipitated epoxy resin treated with Dichlorodimethylsilane.

The silica content and thermal stability of the materials were determined by using TA Qseries equipment at a heating rate of 20°C/min from 30°C to 800°C in the nitrogen atmosphere.

The drawback of using sol-gel process in preparing polymer-silica nanocomposites is its harm to the initial thermal stability of the resulting nanocomposites. This effect is mainly due to the residual of the silanoxy groups in the formed polymer-silica nanocomposites and the silanoxy group might perform dehydration reaction under high temperatures in the processing and the using period of nanocomposites [11]. Contradiction to this fact the initial thermal stability of the epoxy resin had improved with addition of TEOS. This shows the existence strong intermolecular hydrogen bonding between the organic and inorganic phase. The addition of DDS resulted in the decrease of initial decomposition temperature. At higher temperature Hcl liberated during the synthesize of hybrid materials resulted in the chain scission within the hybrid matrix.

The addition of Teos to Amine containing PDMS modified epoxy matrix showed improved initial decomposition temperature. The addition of Teos had reduced the free volume in the modified epoxy domains which have caused the restriction in the mobility of the chains resulted in higher initial decomposition temperature. The addition of DDS resulted in the decrease of initial decomposition temperature in the PDMS modified epoxy matrix. At higher temperature Hcl liberated during the synthesize of hybrid materials resulted in the chain scission within the hybrid matrix.

The char formation is of lesser importance as the percentage of silica loading is very low.

GLASS TRANSITION TEMPERATURE (T_g) VALUES OF MODIFIED AND UNMODIFIED EPOXY-SILICA HYBRID MATERIALS

Glass Transition temperature of Epoxy-Silica hybrid materials

S.No	Specimens	(T_g) deg Celsius
1	Neat(Without Siloxane)	106.92
2	TEOS	80
3	TEOS+DDS	106.09

Glass Transition temperature of Amine containing PDMS modified Epoxy-Silica hybrid materials

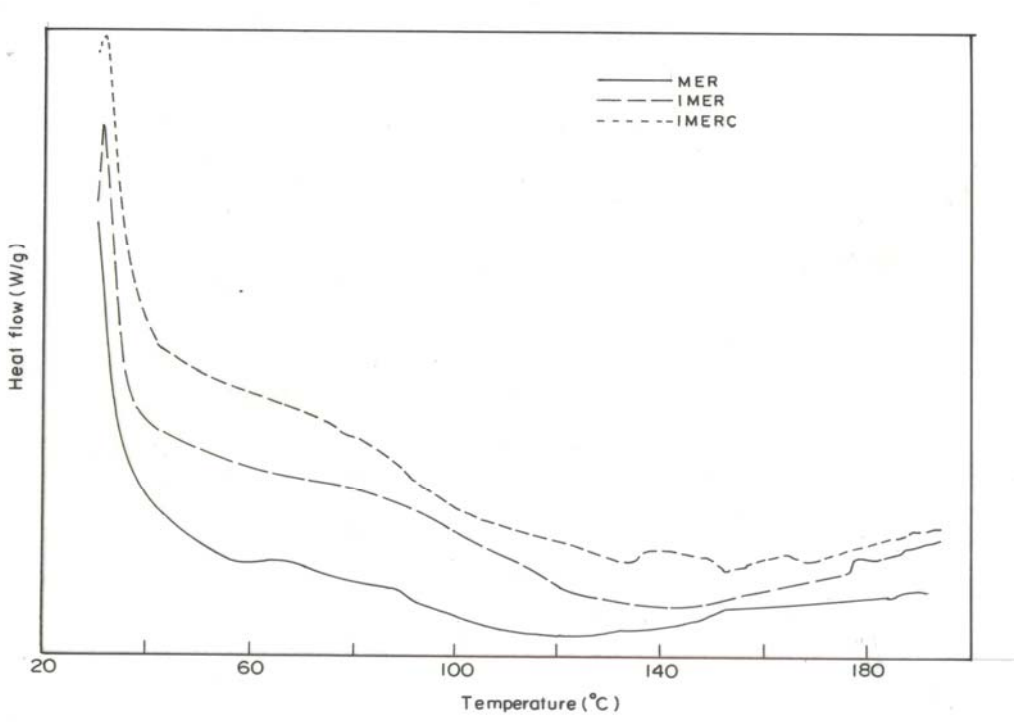

MER-PDMS modified epoxy resin. IMER-in-situ silica precipitated PDMS modified epoxy resin. IMERC-in-situ silica precipitated PDMS modified epoxy resin.

The glass transition temperature of the materials was studied by using Differential scanning calorimetry. TA Qseries equipment was used. The test was carried out with a heating rate of 20°C/min from 30°C to 200°C in the nitrogen atmosphere. The glass transition temperature

of epoxy resin was determined. It was found that, T_g of epoxy decrease with the addition of TEOS, the silica precursor. This shows the plastication effect of the silica. Introduction of silica particles might also increase the free volume of the resins to reduce their T_g. The addition of Dichlorodimethylsilane improves the additional cross-links in the organic and inorganic phase which resulted in similar T_g of neat epoxy resin.

The glass transition temperature of Amine containing PDMS modified epoxy phase was determined. The addition of Teos, the silica precursor did not decrease the T_g of epoxy phase this shows that there is limited compatibility between modified epoxy and inorganic phase. It was found that the addition of Dichlorodimethylsilane decreased the T_g of modified epoxy phase indicating the good compatibility that exists between modified epoxy and inorganic phase and the plastication effect of the silica. The Hcl liberated during the synthesize of hybrid material increases the rate of hydrolysis of TEOS.This suggest that less phase separation of PDMS and more will be incorporated in TEOS network hence good miscibility and lower T_g.

MORPHOLOGICAL PROPERTIES OF MODIFIED AND UNMODIFIED EPOXY-SILICA HYBRID MATERIALS

Here Veeco instruments AFM was used for the morphological studies of flexural fractured Modified and Unmodified Epoxy-Silica hybrid materials. Contact mode was used for morphology studies. The morphological analysis of the hybrid materials was investigated by Atomic Force Microscopy (AFM). The Atomic Force Microscopy images were taken for Modified and Unmodified Epoxy-Silica hybrid materials. The AFM images of unmodified Epoxy –Silica hybrid materials showed no phase separation and homogenous dispersion of silica particles without any aggregation. Optically transparent composite materials can be obtained if there is no macro- microphase separation during both the gel forming and drying process [3]. The resultant material was transparent. The AFM images of Amine containing PDMS modified Epoxy –Silica hybrid materials showed two phase morphology with rigid continuous phase and a dispersed rubbery phase with silica particles dispersed homogenously. The rubber particles are partly pulled out from the epoxy matrix and partially fractured. In this case, the crack developed through the rubbery particles and indicates that the interaction between the rubbery particles and matrix has occurred. The presence of cone shape in the afm images confirms the interaction of epoxy and rubbery phase.

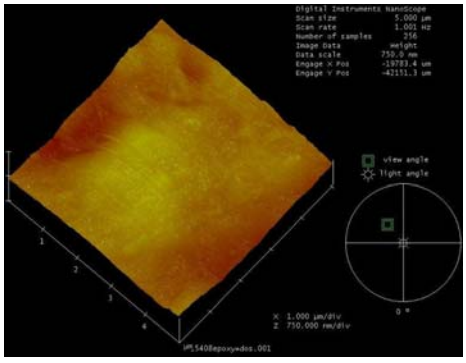

AFM image of epoxy matrix with TEOS and DDS

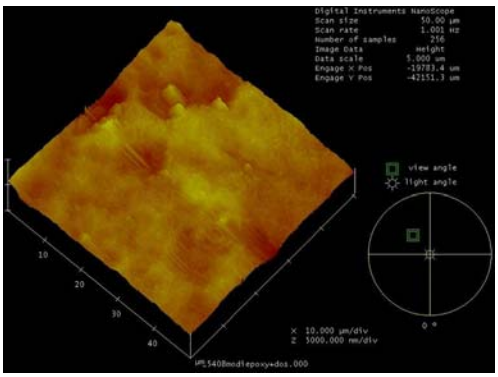

AFM image of Amine containing PDMS modified epoxy matrix with TEOS and DDS

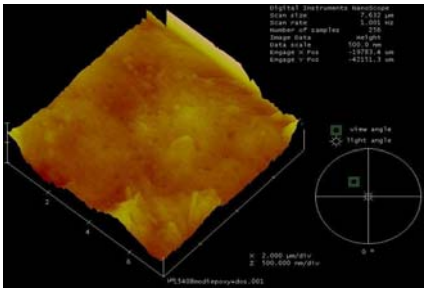

AFM image of Amine containing PDMS modified epoxy matrix with TEOS and DDS

MECHANICAL PROPERTIES OF MODIFIED AND UNMODIFIED EPOXY-SILICA HYBRID MATERIALS

The mechanical properties like flexural strength, flexural modulus and flexural strain to failure, of the modified and unmodified Epoxy-Silica hybrid materials were studied according to ASTM D790 standards. The flexural specimen dimension of 80mm × 25mm of 3mm was prepared. The flexural tests were carried at the crosshead speed of 3mm per minute. The results are tabulated below,

Flexural properties of Epoxy-silica Hybrid materials

S.No	Specimens	Flexural Strength (MPa)	Flexural Modulus (GPa)	Flexural Strain to Failure (%)
1	Neat(Without Siloxane)	97	3.8	2.5
2	TEOS	97.7	2.7	3.4
3	TEOS+DDS	122	2.8	3.9

Flexural properties of PDMS modified Epoxy-silica Hybrid materials

S.No	Specimens	Flexural Strength (MPa)	Flexural Modulus (GPa)	Flexural Strain to Failure (%)
1	Neat(With Siloxane)	75	2.6	2.8
2	TEOS	72	2.3	3.1
3	TEOS+DDS	95	2.6	3.7

The sol-gel processing of TEOS in epoxy resin decreased the flexural strength, modulus and increased the flexural strain to failure. At neutral condition, gel formation occurs at relatively low conversion and unhydrolysed TEOS can remain in the system [12, 13] those results in low modulus, and low flexural strength. The plasticizing effect of silica particles in the epoxy domains resulted in increase in the flexural strain to failure. The Dichlorodimethylsilane may act as coupling agent and it reduces gelation time. The gel formation occurs at relatively higher rate and there is a reduction in the amount of unhydrolysed TEOS in the system resulting in better flexural values.

There is a reduction in the flexural strength; modulus and increase in flexural strain to failure of Amine containing PDMS modified epoxy and TEOS system. The chemical link formation between inorganic and the amine group containing PDMS are poor, that results in incompatibility and reduction in properties. The addition of Dichlorodimethylsilane resulted with improvement in properties which are attributed to reduce in free volume which reduces chain mobility and the formation of additional cross links.

CONCLUSION

The TGA studies show the addition of Dichlorodimethylsilane decreased the thermal stability of the modified and unmodified epoxy composite and the nanosilica precipitated had not altered the thermal stability of the material. The DSC Studies showed T_g values decreased to greater extent indicating the plastication effect of silica within the matrix and slight decrease indicating the limited compatibility between organic and inorganic matrix. The AFM images confirmed no phase separation between organic and inorganic phase and fine dispersion of silica particles without any aggregation. The FT-IR spectroscopy confirmed the disappearance of epoxide peak. The flexural modulus decreased and flexural strain to failure increased indicating the plastication effect of silica .With the addition of Dichlorodimethylsilane which reduces gelation time. The gel formation occurs at relatively higher rate and there is a reduction in the amount of unhydrolysed TEOS in the system resulting in better flexural values.

REFERENCES

1. Wilkes,G.L.; Orler, B.;Huang, H.Polym.Prepr. 1985.26 pp300

2. Schmidt,H. J.Non- Cryst.Solids 1985,73,pp681.

3. Jianye Wen ., Garth L. Wilkes . Chem. Mater.1996.8,pp1667-1681

4. Sungtack Kang, Sung Il Hong, Chul Rim Choe, Min Park, Soonho Rim, JUnkyung Kim.Polymer. 2001.42, pp879

5. Suzanne Frings, Organic –inorganic coatings: based on polyester resins and in-situ formed silica,University of Eindhoven, 1999 [PhD Thesis]

6. Sanchez,C.; Ribot,F.New J. Chem. 1994, 18,1007.

7. Judeinstein,P.: Sanchez,C.J. Mater.Chem. 1996,6,511.

8. A.Al.Abrash, F.Al.Sagheer, A.A.m.Ali and Z.Ahmad, Thermal and mechanical properties of poly(hydroxyl-imide)-silica nanocomposites international journal of polymeric materials, 2006, vol.55, no-2, pp.103-120.

9. F.Al-Sagheer, A.A.M.Ali, S.Muslim, and Z.Ahmad, Thermal and mechanical properties of chemically bonded aramid-silica nanocomposite, science and technology of advanced materials, 2006, vol.7, no.1,pp.111-118

10. Gerhard Schottner, Chem.Mater.2001.13.3422-3435

11. Ying-Ling Liu, Chih-Yuan Hsu, Wen-Lung Wei, Ru-Jung Jeng, Polymer.2003.44.5159-5167

12. L.Matejka,O.Dukh and J.Kolarik,Polymer,41,(2000),1949.

13. L.Matejka.K.Dusek,J.Plestil.J.Kriz and F.Lednicky,Polymer 40(1998),171-181.

14. P. Cardianoa,*, P. Mineob, S. Sergia, R.C. Ponterioc, M. Triscari, P. Pirainoa Epoxy-silica polymers as restoration materials. Part II.Polymer 44 (2003) 4435-4441

Structure property relationship studies of melt spun carbon nanotubes filled polypropylene fiber

Pankaj B. Tambe[a*], Arup R. Bhattacharyya[a#], Srikanth Kamath[a], Ajit R. Kulkarni[a], T.V. Sreekumar[b], Kingsuk Mukhopadhyay[b] and Anurag Srivastav[b]

[a]Department of Metallurgical Engineering and Materials Science, Indian Institute of Technology Bombay, Powai, Mumbai 400076, India
[b]Defence Materials and Stores Research and Development Establishment (DMSRDE), DRDO, Kanpur 208013,India
Email: arupranjan@iitb.ac.in

Abstract

Two different types of multiwalled carbon nanotubes (MWNT) were utilized in order to understand the effect of different types of MWNT in enhancing mechanical properties of the melt spun MWNT filled polypropylene composite fibers. It was found that MWNT synthesized in DMSRDE were found to be superior over NC 3100 procured from Nanocyl, CA, Belgium in achieving high modulus and tenacity of PP/MWNT composite fibers. Herman's orientation factor of (110) PP plane and MWNT along the composite fiber axis were also calculated and it was found that MWNT prepared in DMSRDE found to exhibit higher orientation over NC 3100 MWNT.

1. Introduction

Polypropylene (PP) is one of the major polymeric fiber materials of future in view of its impressive consumption in the past decade. However, PP fiber needs reinforcement in order to achieve high stiffness and strength for engineering applications. Since the discovery of carbon nanotubes (CNT) by Iijima [1], CNT have emerged as a potential candidate as reinforcing filler in polymer based composites due to their unparallel mechanical, electrical and thermal properties. Melt spinning process is one of the most common and viable route to produce polymer fiber. The formation of fibers involves four stages: a) melting the polymer, b) extrusion of melt through spinneret, c) cooling along spin line and winding the resulting fiber on a roll and d) the resulting fiber post drawn to a maximum possible draw ratio.

Several studies have been carried out on crystallization, orientation and mechanical properties of melt-blended PP/single wall carbon nanotube (SWNT) [2] and PP/ multiwall carbon nanotube (MWNT) [3] composites fiber. In addition flourinated SWNT [4] and benzoyl per oxide initiated functionalization of SWNT [5] to PP chain were also utilized in order to improve the exfoliation and interfacial adhesion of SWNT with PP chain in order to improve the mechanical properties of composite fiber.

The aim of this work is to evaluate the effect of two different types of MWNT on the structure property of PP/MWNT composite fiber. Oriented structure of PP crystal plane and MWNT along the fiber axis are quantified as per Herman's orientation factor. The effect of orientation of PP crystal plane and MWNT are correlated with the mechanical properties of PP/MWNT composite fiber.

2. Experimental Details

Polypropylene was obtained from Reliance Industries Ltd, India (REPOL H200F, melt flow index of 20 g/10min). MWNT were obtained from Nanocyl CA Belgium (NC 3100, L/D=100-1000, purity=95%) and DMSRDE, Kanpur also subsequently utilized for our study. Various compositions of PP/MWNT composites using two different types of MWNT were prepared by melt mixing in a conical twin screw extruder (Micro 5, DSM Research, Netherlands) at optimized melt mixing condition of 260^0C with a rotational speed of 200 rpm for 15 min in which MWNT were varied from 0.5-3 wt%. Melt mixed PP/MWNT samples were dried at 80^0C under vacuum over night. PP/MWNT composite were melt-spun using a small scale spinning machine manufactured by the Bradford University Research Ltd. UK, using a single hole spinneret of 1 mm diameter. The fiber spinning was carried out at 200^0C with ram speed of 1.4 mm/min. The take up speed was kept at 20 m/min for all compositions. The melt spun fibers were further drawn at draw ratio of 8. The mechanical properties of drawn fiber were tested on a Favimat fiber tester (Textechno) with guage length of 20 mm and at a rate of 20 mm/min for 50 filaments. Raman spectroscopy was performed using Jobin Yovon (HR 800 micro-Raman) in the scanning range of 200–2000 cm^{-1} with incident laser excitation wavelength of 514 nm. Scanning electron microscopic (SEM) analysis was performed with Hitachi S3400, operated at 15 KV. Wide-angle X-ray diffraction (WAXD) studies were carried out on a Philips X-Pert Pro. The incident X-rays (λ=1.54 Å) from the Cu-target were monochromatized using a Ni filter.

3. Result and Discussion

3.1 Comparative study of Nanocyl NC 3100 and DMSRDE MWNT

TEM images of MWNT are shown in Figure (1a, 1b) shows a network of entangled MWNT. DMSRDE produced MWNT are found to be more straight, less coiled and less entangled as compared to NC 3100. Figure 1c shows the tangential Raman band for two types of MWNT. Raman peak at ~1347 cm^{-1} originates from disordered graphitic structure (D-band) and peak at ~1590 cm^{-1} originates from crystalline ordered structure of the graphene sheet (G-band); the intensity ratio, I_G/I_D provides a measure of crystalline structure in a given MWNT. The ratio of intensity of G-band and D-band (I_G/I_D) depict the order structure of MWNT. I_G/I_D value of DMSRDE MWNT (1.31) is found higher than NC 3100 MWNT (0.87) which manifests DMSRDE produced MWNT are more ordered as compared to NC 3100.

3.2 Orientation studies of PP crystal and MWNT along fiber axis

Figure 2a shows the Wide angle X-ray diffraction (WAXD) pattern for PP/MWNT composites containing 0.5 wt% MWNT. WAXD pattern of the composites show the typical α-form of PP crystals and exhibits complete absence of the β-crystal form [6, 7]. Quantification of average orientation of PP crystal plane has been carried out using WAXD by performing azimuthal scan along the specific (110) PP crystal plane (Representative Figure 2b). The detail procedure of quantification of crystal plane orientation is given below.

The crystalline orientation of the fibers has been determined quantitatively using Hermans orientation factor [8] as generalized to a set of three crystallographic axes by Stein [9]. This is defined as

$$f = \frac{3 < \cos^2 \phi > -1}{2} \qquad (1)$$

where $\left\langle \cos^2 \phi \right\rangle$ (is the averaged value of the square of the cosine of the angle ϕ between the reference direction of the sample (fiber axis) and the x-crystallographic axis. Assuming rotational symmetry about the fiber axis,

$$< \cos^2 \phi) >= \frac{\int_{-\pi/2}^{\pi/2} I(\phi) \cos^2 \phi \sin \phi d\phi}{\int_{-\pi/2}^{\pi/2} I(\phi) \sin \phi d\phi} \qquad (2)$$

where I(ϕ) is the intensity diffracted from the (hkl) planes which are normal to the x-crystallographic direction. Therefore f values can range from −0.5, when the chains are perpendicular to the x-crystallographic axis, to 1.0, when the chains are parallel to the x-crystallographic axis. When f equals zero there is random orientation in the sample.

From the X-ray diffraction pattern of drawn MWNT/P, the Herman's orientation factors for (110) PP planes are calculated, which are tabulate in Table 1. The (110) PP crystal orientation is found to be much higher in PP/MWNT composite fiber utilizing DMSRDE produced MWNT.

To calculate the Herman's orientation factor of MWNT along the fiber axis, Raman spectrum of each composition as a function of polarization angle 0, 30, 45, 60, 90^0C are considered (Representative Figure 3). From G band peak intensity at various angles, Herman's orientation factor are calculated as per equation 1 and 2. The calculated values of Herman's orientation factor are shown in Table 1, which indicates higher orientation of MWNT in PP/MWNT composite fiber while utilizing DMSRDE produced MWNT.

3.3 Mechanical Properties

Table 1 provides the details of mechanical properties data of the representative fiber compositions. Table 1 reveals composite fibers prepared by using DMSRDE MWNT show superior mechanical properties as compared to NC 3100. It is interesting to note that fiber tenacity and modulus of DMSRDE produced MWNT is higher. Fiber tenacity and modulus increases with an increase in concentration of MWNT up to 1 wt% and then decreases with an increase in MWNT concentration. The observation of superior mechanical properties in PP/MWNT composite fiber while utilizing DMSRDE produced MWNT may be related to less entangled, more straight MWNT of higher crystallinity.

3.4 Scanning electron microscopy (SEM) studies

Tensile fractured surface of PP/MWNT composite fiber are shown in Figure 4. Figure 4a shows the fibrillar structure of PP/MWNT composite fiber. The magnified micrograph of tip of fracture composite fiber (Figure 4b, c) shows that the fracture starts at PP/MWNT interface where the stress concentration was higher at the guage length of composite fiber.

4. Conclusion

Comparative study of DMSRDE produced MWNT and NC 3100 as reinforcing filler for PP/MWNT composite fiber reveal the superiority of DMSRDE produced MWNT as compared to NC 3100. The structure DMSRDE produced MWNT filled PP fiber exhibit superior orientation of PP crystal and MWNT along the fiber axis as compared to NC 3100.

5. Acknowlegements

We would like to acknowledge Microcompounder Central facility, CRNTS at IIT Bombay. We would also like to thank DMSRDE, Kanpur for financial assistance for the project.

6. References

[1] Iijima S, Nature 1991; 35:56.
[2] Bhattacharyya A R,, Sreekumar T.V, Liu T, Kumar S, Ericson L. M, Hauge R, Smalley R. E, Polymer 2003; 44:2373.
[3] Moncy V. J, Derrick D, James T, Gary P, Elijah N, Journal of Applied Polymer Science 2007; 103:3844.
[4] Daneesh M, Valery N. K, Enrique V. B, Chem. Mater., 2006; 18:4561.
[5] Daneesh M, Valery N. K, Enrique V. B, J. Phys. Chem. C 2007; 111:1592.
[6] Shaffer M. S. P., Fan X., Windle A. H., Carbon 1998; 36:1603.
[7] Kinloch I. A., Roberts S. A., Windle A. H., Polymer 2002; 43:7483.
[8] Hermans J J, Hermans P H, Vermeas D, Weidinger A. Rec Chim Trav 1946; 65:427.
[9] Stein RS. J Polym Sci, 1958; 31:327.

Table 1: Mechanical properties of melt-spun PP/MWNT composites fibers and Herman's orientation factor

Material	MWNT (wt%)	Tenacity (gpd)	Elongation (%)	Modulus (gpd)	Herman's orientation factor of (110) PP plane	Herman's orientation factor of MWNT along fiber axis
PP	------	10.02	17	114	0.6723	------
PP/MWNT DMSRDE	0.5	10.34	14	132	0.4193	0.8549
	1	11.5	14.11	153	0.4205	0.7726
	3	9.79	16	124	0.4652	0.7211
PP/MWNT Nanocyl (NC 3100)	0.5	8	21	87.5	0.3835	0.7243
	1	8.79	19.7	100	0.4246	0.7225
	3	7.2	14.8	94	0.5545	0.7181

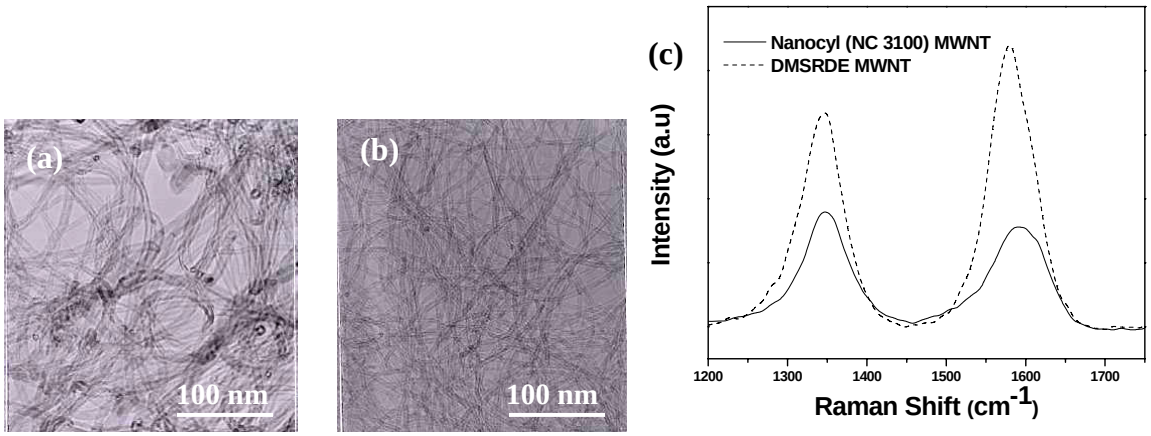

Figure 1: TEM images of MWNT (a) NC (3100) (b) DMSRDE (c) Raman spectra of DMSRE and Nanocyl (NC 3100) MWNT

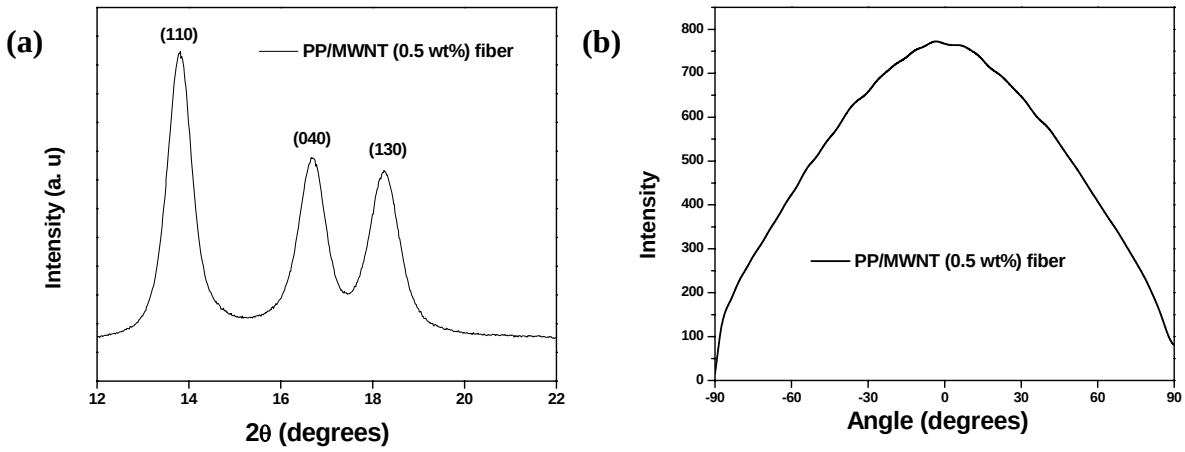

Figure 2: (a) Wide angle X-ray Diffraction (WAXD) spectra of PP/MWNT composites (b) Azimuthal scan of (110) PP plane

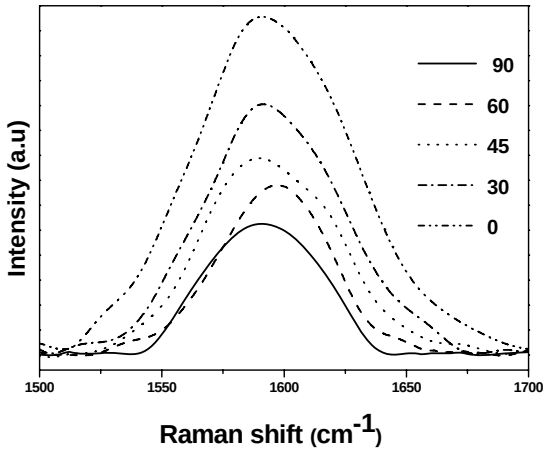

Figure 3: Tangential mode Raman spectra of PP/MWNT (0.5 wt% DMSRDE produced MWNT) composite fiber (draw ratio 8). From bottom to top, the angle between fiber axis and polarization direction is 0, 30, 45, 60, 90 degrees

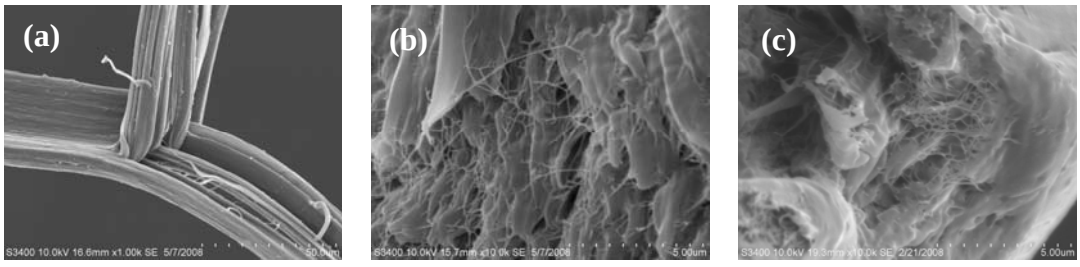

Figure 4: SEM images of PP/MWNT composite fiber

Synthesis and characterization of polypropylene/ionomer/ organoclay nanocomposites

S. R. Mallikarjuna, N. Ramesh, C. Ramesh and S. Sivaram
Divison of Polymer Science and Engineering, National Chemical Laboratory,
Pune-411 008, Maharashtra, India.
Email: c.ramesh@ncl.res.in

Abstract:
The compatibilization effects provided by ionomer-g-polypropylenes versus those of a maleated polypropylene, PPMA, for forming polypropylene-based nanocomposites were compared. We have prepared a novel compatibilizer by grafting ionic functional groups on to the PP and evaluated its efficiency as compatibilizer in the preparation of PP/clay nanocomposites. The PP/ionomer/organoclay nanocomposites were prepared by direct melt mixing and by masterbatch methods and the structure obtained were characterized by WAXD and TEM and were compared with nanocomposites prepared using PPMA as compatibilizer. Mechanical properties of the nanocomposites prepared were studied using INSTRON and the crystallization behavior was studied using Differential Scanning Calorimetry (DSC) and Polarized Optical Microscopy (POM). Thermal stabilities were characterized using TGA. The dispersion of clay was found to be dependent on the method of preparation, type of compatibilizer used and the amount of compatibilizer used. The dispersion of the organoclay was better with the ionomer than PPMA and the dispersion was better when the nanocomposites were prepared by two step masterbatch route than the single step direct mixing method. The dispersion of the organoclay improved with increase in the amount of compatibilizer. The nanocomposites obtained with ionomer as compatibilizer showed better enhancements in nucleation, thermal properties and mechanical properties as compared to the nanocomposites obtained using PPMA as compatibilizer.

Introduction:
Polypropylene (PP) is a fast growing thermoplastic and dominating the industrial applications due to its attractive combination of properties such as low density, high thermal stability, resistance to corrosion etc. and low cost. There is a strong need to improve their mechanical properties for its applications in automotive industry[1]. Researchers in the recent decade have shown that reinforcement with dispersed clay in the polymer matrix enhances the mechanical properties without much affecting the density of the polymer[2]. Therefore, various research efforts were made to disperse clay in the PP matrix. However it was very difficult to disperse clay in the PP matrix, as the polymer was highly non polar and there are no polar groups available to interact with the clay surface. The usual organo-modification of clay did not sufficiently lower the surface energy of the clay to interact with PP chains. Unmodified polyolefins lack the intrinsic thermodynamic affinity with currently available organoclays to form well dispersed nanocomposites[3]. The surface energy of PP chains was improved by introducing polar functionalities and used them for the preparation of nanocomposites[4-10]. To improve the surface energy of semi crystalline polymers in the preparation of nanocomposites, many researchers introduced ionic groups on to the polymer chains[11-19]. However compatibilizers such as amine and ammonium functionalized PP had failed to enhance the dispersion of clay in the PP matrix as compared to maleic anhydride grafted polypropylene via melt mixing[20].

Therefore in the present work, we have evaluated a novel metallic ionomer of PP as compatibilizer for preparing PP/organoclay nanocomposite by two different mixing routes. The properties of the obtained nanocomposites were compared with the nanocomposites, which are prepared using PPMA as compatibilizer.

Experimental:

The materials used in this study were polypropylene REPOL H034SG obtained from Reliance Industries (Pvt.) Ltd., maleated polypropylene (PPMA) selected for this work was FUSABOND M613-05, which contains 0.65 weight % maleic anhydride group. The organoclay, Cloisite20A provided by Southern Clay Products Inc. Potassium succinate grafted polypropylene ionomer (KPPSA) was prepared by simultaneous hydrolysis and neutralization of PPMA using methanolic KOH. All the nanocomposites were prepared by a melt mixing technique using a twin-screw extruder, DSM Micro 5 having a net barrel capacity of 5 CC with a screw speed of 100 rpm, the barrel temperature of 190 °C and a residence time of 10 min. Nanocomposites were prepared with different concentrations of compatibilizer keeping the organoclay concentration at 5 weight %. For comparison matrix polymer compositions without clay were also prepared. Nanocomposites were prepared in two different methods. In the first method, the PP, compatibilizer and the Cloisite 20A were all melt mixed directly in a single step. In the second method, the compatibilizer was mixed with the organoclay to form a masterbatch in the first step, which was then mixed with the PP in the second step. Various compositions prepared were coded in such a way that the number in the code after the compatibilizer name indicates the percentage of the respective compatibilizer, C for 5% organoclay, and the method of preparation indicated in the sample code by D for direct mixing and M for masterbatch route. Structure and morphology of all the nanocomposites prepared was studied using WAXD and TEM. Flexural moduli of the nanocomposites prepared were studied using INSTRON and the crystallization behavior was studied using Differential Scanning Calorimetry (DSC).

Results and Discussion:

Prior to evaluation of the new compatibilizer for dispersability of the organoclay in polypropylene, binary composites containing 95% compatibilizer and 5% C20A was prepared and characterized with WAXD. The WAXD pattern (figure 1a) of KPPSA/C20A showed no peak for the organoclay indicating that the organoclay was completely delaminated and exfoliated in the KPPSA matrix while PPMA/C20A showed a broad low intensity peak at a d-spacing of 38 Å indicating the presence of intercalated tactoids. The above result clearly indicates that the new compatibilizer, KPPSA containing more polar ionic functional group have better interaction with the organoclay than PPMA.

The nanocomposites were prepared by varying the concentration of the compatibilizer keeping the concentration of the organoclay, C20A, at a constant 5-wt %. Two different mixing routes such as direct mixing and masterbatch route were used to prepare the nanocomposites. The properties of the nanocomposites obtained were compared with the nanocomposites prepared using PPMA as compatibilizer under identical conditions. The WAXD patterns for the nanocomposites prepared were shown in figure1b-d. Nanocomposites prepared with KPPSA and masterbatch route showed higher d-spacing for the clay as compared the nanocomposites prepared with PPMA and direct mixing. At higher concentrations of KPPSA no peak for clay was observed indicating exfoliation. Typical TEM micrographs of the nanocomposites prepared by masterbatch route with 25% compatibilizer were shown in figure 2. It is clearly evident from the TEM pictures that the nanocomposites prepared with 25 wt % KPPSA as compatibilizer show completely exfoliated structures where the clay layers are completely delaminated and dispersed homogeneously in the polymer matrix while the nanocomposites prepared with 25% PPMA as compatibilizer showed intercalant clusters of clay layers suggesting intercalated structures.

Crystallization behaviors of various nanocomposites obtained were studied using DSC. Typical DSC thermogram curves obtained for various nanocomposites, the matrix polymers and the

pristine polypropylene during cooling from melt at 10 °C/min were shown in figure 3. Exfoliated clay nanocomposites obtained with 25 wt % KPPSA showed enhanced crystallization rates as compared to intercalated nanocomposites obtained with 25 wt % PPMA, which were evidenced with higher Tcc. In the exfoliated nanocomposite the clay layers are completely delaminated providing large surface for nucleation than the intercalated ones resulting in higher Tcc.

Flexural moduli of the nanocomposites measured were shown in Table 1. The flexural moduli of all the nanocomposites prepared showed improvements as compared to pristine PP. The improvements were highest in the case of KPPSA25C-M which contains 25% KPPSA, and was prepared by masterbatch.

Summary and Conclusions:

The nanocomposites were prepared by melt mixing of the organoclay with PP in presence of the compatibilizer in two different routes such as by single step direct mixing method and by two step method through masterbatch route. The dispersion of clay was found to be dependent on the method of preparation, type of compatibilizer used and the amount of compatibilizer used. The dispersion of the organoclay was better with KPPSA than PPMA and the dispersion was better when the nanocomposites were prepared by two step masterbatch route than the single step direct mixing method. The dispersion of the organoclay improved with increase in the amount of compatibilizer. The nanocomposites prepared using the KPPSA as compatibilizer at above critical concentrations resulted in exfoliated nanocomposites while only intercalated structures were obtained with PPMA as compatibilizer. This is further evidenced by higher crystallization rates for the exfoliated nanocomposites obtained with KPPSA than the intercalated nanocomposites obtained with PPMA as compatibilizer. The flexural modulus of the exfoliated nanocomposites prepared using novel metallic ionomer as compatibilizer showed improvements better than the intercalated nanocomposites prepared using conventional PPMA as compatibilizer. Thus we have shown that metallic ionomer such as KPPSA can act as better compatibilizer for the preparation of well-dispersed PP/organoclay nanocomposites.

References:

1. Usuki, A.; Hasegawa, N.; Koto, M. Adv. Polym. Sci. 2005, 179, 135.
2. Pinnavaia, T. J.; Beall, G. W. Polymer-Clay Nanocomposites, Wiley series in polymer science, 1997.
3. Manias, E.; Touny, A.; Wu, l.; Strawhecker, K.; Lu, B.; Chung, T. C. Chem. Mater. 2001, 13, 3516.
4. Kato, M.; Usuki, A.; Okada, A. J. Appl. Polym. Sci. 1997, 66, 1781.
5. Kawasumi, M.; Hasegawa, N.; Kato, M.; Usuki, A.; Okada, A. Macromolecules 1997, 30, 6333.
6. Hasegawa, N.; Kawasumi, M.; Kato, M.; Usuki, A.; Okada, A. J. Appl. Polym. Sci. 1998, 67, 87.
7. Reichert, P.; Nitz, H.; Klinke, S.; Brandsch, R.; Thomann, R.; Mulhaupt, R. Macromol. Mater. Engg. 2000, 275, 8.
8. Ishida, H.; Campbell, S.; Blackwell, J. Chem. Mater. 2000, 12, 1260.
9. Liu, X.; Wu, Q. Polymer 2001, 42,10013.
10. Zhang Y-Q, Lee J-H, Rhee J. M., Rhee K. Y. Composites Science and Technology 2004, 64, 1383.
11. Barber, G. D.; Calhoun, B. H.; Moore, R. B. Polymer 2005, 46, 6706.
12. Chisholm, B. J.; Moore, R. B.; Barber, G. D.; Khouri, F.; Hempstead, A.; Larsen, M.; Olson, E.; Kelley, J.; Balch, G.; Caraher, J. Macromolecules 2002, 35, 5508.

13. Wang, Z. M.; Nakajima, H.; Manias, E.; Chung, T. C. Macromolecules 2003, 36, 8919.
14. Shah, R. K.; Paul, D. R. Macromolecules 2006, 39, 3327.
15. Lee, J. A.; Kontopoulou, M.; Parent, J. S. Polymer 2005, 46, 5040.
16. Start, P. R.; Mauritz, K. A. J. Polym. Sci., Polym. Phys. 2003, 41,1563.
17. Kovarova, L.; Kalendova, A.; Malac, J.; Vaculik, J.; Malac, Z.; Simonic, J. Annu. Tech. Conf. Soc. Plast. Eng. 2002, 60, 2291.
18. Barber, G. D.; Carter, C. M.; Moore, R. B. Annu. Technol. Conf. Soc. Plast. Eng. 2000, 58, 3763.
19. Govindaiah, P.; Mallikarjuna, S. R.; and Ramesh, C. Macromolecules 2006, 39, 7199.
20. Lili C.; Paul, D. R. Polymer 2007, 48, 1632.

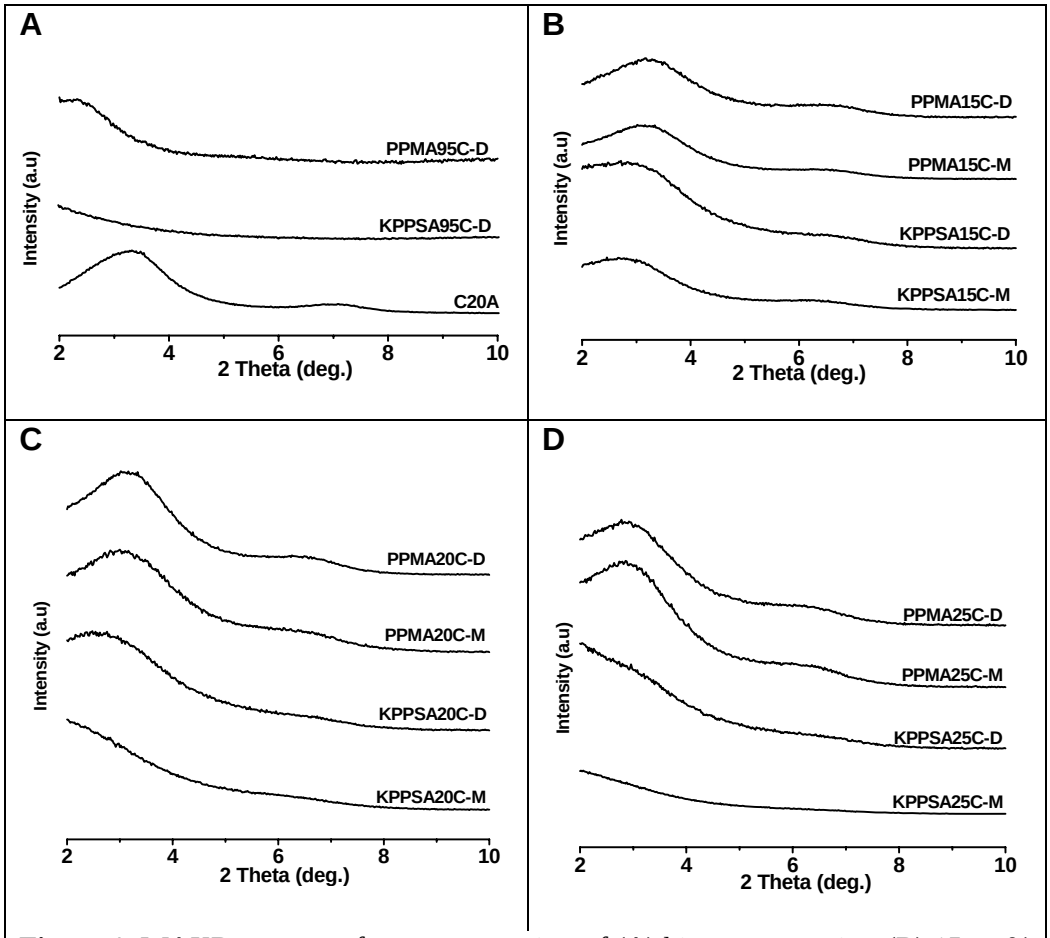

Figure 1: WAXD patterns of nanocomposites of (A) binary composites (B) 15 wt % of the compatibilizers (C) 20 wt % of the compatibilizers (D) 25 wt % of two compatibilizers; In the sample code, the number indicates wt % of the compatablizer, C indicates 5 wt % cloisite 20A, D for the samples prepared by direct mixing route and M for the samples prepared by masterbatch route.

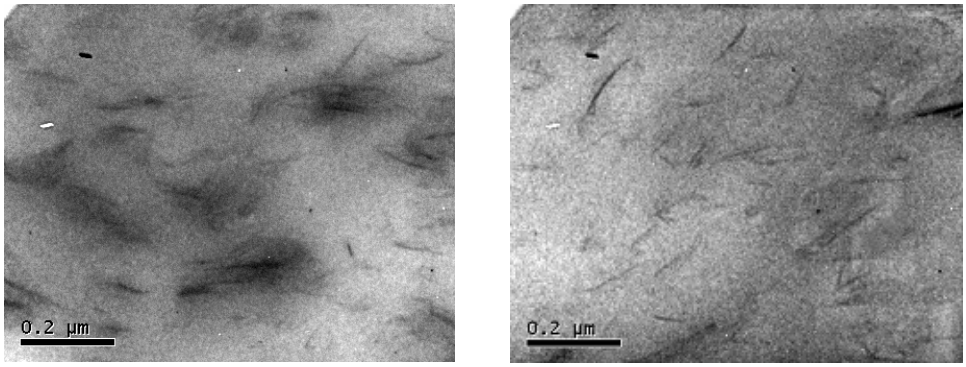

a **b**

Figure 2: Typical TEM micrographs of (a) PPMA25C-M (b) KPPSA25C-M

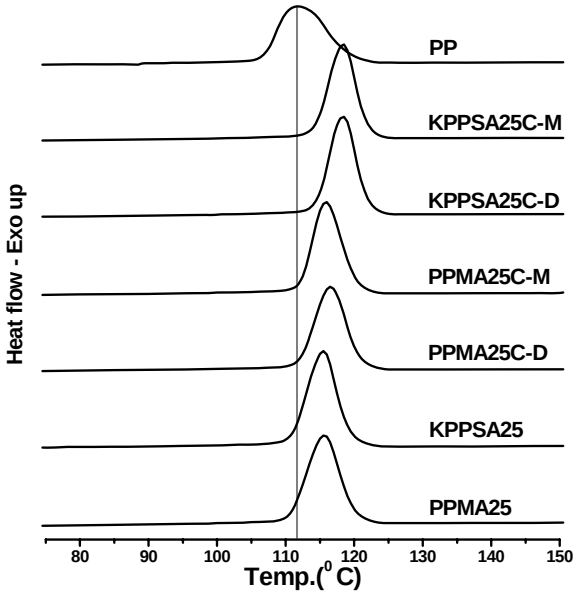

Figure 3: DSC thermogram curves of the matrix polymers and the nanocomposites during the cooling from melt at 10°C/min.

Table 1: Flexural modulus of the matrix polymer and the nanocomposites

Sample	Flexural modulus (MPa) with compatibilzer composition of		
	15 wt %	20 wt %	25 wt %
PPMA	747	710	691
KPPSA	738	759	788
PPMA-C-D	842	840	834
KPPSA-C-D	840	852	863
PPMA-C-M	862	852	845
KPPSA-C-M	888	895	937
Pristine PP	804		

A Study of mechanical properties of flax-g-poly(MA) reinforced phenol-formaldehyde composites

Susheel Kalia[1*], B.S. Kaith[2], Sanjeev Sharma[1], and Bandna Bhardwaj[1]

[1]Department of Chemistry, Singhania University, Pacheri Bari, Jhunjhunu – 333 515 (Rajasthan) India
[2]Department of Chemistry, Dr. B.R. Ambedkar National Institute of Technology (Deemed University), Jalandhar - 144 011, Panjab, India

[*]E-mail: susheel_kalia@yahoo.com, susheel.kalia@gmail.com

Abstract
In the present paper, we report the preparation of graft copolymers of flax fibers with methyl acrylate (MA) using Fenton's reagent (FAS-H_2O_2) as redox system. Synthesized flax-g-poly(MA) was characterized with FTIR, TGA/DTA, scanning electron microscopy (SEM), and X-ray diffraction (XRD) techniques. Composites were prepared using flax-g-poly(MA) as a reinforcement and phenol-formaldehyde (PF) as the binding material. Mechanical properties of phenol-formaldehyde composites were compared and it has been found that composites reinforced with flax-g-poly(MA) showed improvement in mechanical properties. Composites reinforced with flax-g-poly(MA) showed better tensile strength (235 N) and compressive strength (814 N) in comparison to composites reinforced with original flax fiber which showed lesser tensile strength (162 N) and compressive strength (372 N). Composites reinforced with flax-g-poly(MA) shows the improved MOR, MOE, and SP.

Key Words: Fiber, Flax-g-poly(MA), Composites, Mechanical Properties.

Introduction
The renewed interest in the natural fiber has resulted in a large number of modifications in order to bring it at par with and even superior to synthetic fibers. A rebirth in the application of natural fibers as reinforcing agent is occurring mainly in the automobile and packing industries. Advantage of indigenous natural fiber in their applications in the preparation of composites over synthetic fibers has been reported by Paramasivam and Kalam [1]. Flax fiber is a better reinforcing material for composites due to ecological and environmental merits and the attractive mechanical properties. Flax fiber is considered to be one of the strongest fibers among the natural fibers. Mechanical properties of polymers such as tensile strength, impact-strength, and extensibility have a direct correlation with the percentage grafting (P_g). On grafting crystal lattice of the polymer is disrupted but the strength of the material may act to reinforce the structure [2, 3]. However, if crystallinity is not disturbed on grafting, then continuous increase in strength can be obtained with increase in P_g [4]. Most of the cellulosic fibers possess both crystalline and amorphous regions. The X-ray pattern of crystalline polymers show both sharp features associated with regions of three-dimensional order and more diffused features characteristics of molecularly disordered substances like liquid. The occurrence of both types of features in the fibers indicates that ordered and disordered regions co-exist in crystalline polymers. Lower crystallinity means higher amorphous regions, which are more accessible to chemicals and water [5]. Methyl acrylate was graft copolymerized onto cellulose in alkaline aqueous solution using

potassium ditelluratoargentate (III) redox system. The evidence of grafting was obtained from IR spectra and gravimetric analysis. Thermal stability, crystallinity, and morphology of the graft copolymers were also studied [6].

Mwaikambo and Ansell [7] have prepared the hemp fiber reinforced cashew nut shell liquid composites and reported that tensile strength and modulus of untreated hemp fiber composites increase with increase in the molding pressure possibly due to reduced porosity. The properties of alkali treated hemp mat-cashew nut shell liquid composites decrease with increase in the molding pressure due to the breakage of entangled needle punched hemp fiber bundles, which have also become stiffer after alkali treatment and the hemp-cashew nut shell liquid interface is more coherent for the untreated than the alkali treated fiber. Schartel et al [8] have studied the thermal and fire behaviour of flax fiber reinforced PP composites containing ammonium polyphosphate and expandable graphite as fire retardants. The fire retardancy is a technical breakthrough for flax fiber reinforced PP composites.

Kaith et al [9-11] and Kalia et al [12-13] have reported the reinforcement of plastics with graft copolymers of flax fibers and it has been found that composites reinforced with graft copolymers of flax fibers showed better mechanical properties in comparison to original flax reinforcement. Mechanical properties of composites reinforced with acrylate grafted henequen cellulosics fibers were studied. They found that best results could be obtained with poly(MMA) grafted cellulose fibers because of better fiber-matrix adhesion [14]. Since the use of graft copolymers as reinforcing material in the preparation of composites is meagerly reported in literature, so in the present paper, we report the preparation of phenolic composites using flax-g-poly(MA) as reinforcing material.

Experimental

Materials

Natural flax fibers (*Linum usitatissimum*) were supplied by Department of Agronomy, CSK HP Agriculture University, Palampur (India). Phenolic resin (resole) was prepared by the reaction of phenol (S D Fine-Chem Ltd., India) and formaldehyde (CDH, India) in material science laboratory [11].

Flax fibers were Soxhlet extracted with acetone for 72 h. MA (Fluka) was washed with 5% sodium hydroxide followed by water and was dried over anhydrous sodium sulphate. The dried monomer was distilled and the middle fraction was used. Libror AEG-220 (Shimadzu make) electronic balance was used for weighing purpose. Graft Copolymerization of MA onto Flax was carried out as per method reported earlier [12-13]. IR spectra of the ungrafted and grafted flax fibers were taken with KBr pellets on PERKIN ELMER RXI Spectrophotometer. Scanning electron microscopic studies of flax and its graft copolymers were carried-out on Electron Microscopy Machine (LEO 435 VP). Thermogravimetric analysis and differential thermal analysis studies were carried-out in air at a heating rate of 10°C/min on a thermal analyzer (LINSEIS, L-81 11). X-ray diffraction studies were performed on X-ray diffractometer (Bruker AXS D8 Advance) as per reported methods [15-17].

Composites were prepared in Compression Molding Machine (SANTEC, India). Mechanical studies such as wear-resistance of the composites were carried-out on Wear & Friction Monitor (DUCOM, 20LE) and tensile strength, compressive strength, modulus of rupture (MOR), modulus of elasticity (MOE), and stress at the limit of proportionality (SP) of PF composites were carried on Universal Testing Machine (HOUNSFIELD, H25KS) [9-13].

Results and Discussion

C_2, C_3, and C_6 hydroxyls and the C-H groups are the active cites for grafting in cellulosics. The grafting onto flax fibers in presence of FAS-H_2O_2 as initiator is supposed to take place as per the mechanism proposed by various authors [18].

Optimization of Various Reaction Parameters

Optimized reaction conditions for getting maximum grafting were: MA (2.21 x 10^{-3} mol L^{-1}); FAS-H_2O_2 (molar ratio), 1:4; temperature (ºC), 50; time (min.), 90, and pH, 7.0.

Characterization of Graft Copolymers

FT-IR Spectra of Graft Copolymers

FT-IR spectrum of original flax showed a broad peak at 3422.8 cm^{-1} which was due to bonded –OH groups and at 2918.8, 1653.5 and 1058.7 cm^{-1} arising from –CH_2, C-C and C-O stretching, respectively. However, in case of graft copolymer, an additional peak at 1731.2 cm^{-1} because of >C=O group of MA has been observed. This suggests that MA has been graft copolymerized onto flax fiber through covalent linkages.

Thermal Analysis (TGA/DTA)

The results of TGA have been depicted in Table 1. It is shown that initial decomposition temperature (IDT) and final decomposition temperature (FDT) of original flax were 279.9 and 489.1 ºC, respectively, whereas, in case of flax-g-poly(MA), IDT and FDT were 313.7 and 478.4 ºC, respectively. Flax-g-poly(MA) showed the higher IDT than flax fiber. The results of TGA have been supported by DTA studies. DTA of original flax fiber shows the exothermic peaks at 325.3 ºC (13.8 µV) and there has been a continuous exothermic combustion of the sample at furnace temperature in presence of atmospheric oxygen. This peak shows the disturbance in H-bonded amorphous region. Another sharp exothermic peak has been observed at 455.3 ºC (38.9 µV), which indicates the complete break down of the crystalline region at this temperature. In case of flax-g-poly(MA), exothermic peaks at 322.5ºC (24.6 µV) and 380.4ºC (53.1 µV) have been observed. Thermal stability of flax-g-poly(MA) is not altered very much in comparison to original flax. This was due to undisturbed crystalline structure of the fiber. Thus, it has been found that there exists a direct correlation with percentage of grafting and crystallinity.

Table 1. TGA/DTA of flax and flax-g-poly(MA)

Sr. No.	Sample	Thermo-gravimetric analysis		Differential thermal analysis
		IDT (°C)	FDT (°C)	Exothermic peaks at temperature (μV)
1	Original flax	279.9	489.1	325.3 °C (13.8) 455.3 °C (38.9)
2	Flax-g-poly(MA)	313.7	478.4	322.5 °C (24.6) 380.4 °C (53.1)

Scanning Electron Microscopy (SEM)

A clear cut distinction between the scanning electron micrographs (SEM) of original flax and its graft copolymer reveals that there has been a sufficient deposition of poly(MA) onto flax fiber. The scans easily verify the fact that cellulosic fibers lying apart in original flax started forming bundles in the graft copolymers.

Percentage Crystallinity and Crystallinity index of Graft Copolymers

It has been observed that percentage crystallinity and crystallinity index of flax were decreased a little with grafting (Table 2). There was no comparable difference in the X-ray diffraction pattern of flax and flax-g-poly(MA). Percentage crystallinity of flax and flax-g-poly(MA) was

found to be 80.51 and 77.31, respectively. The crystalline material in the total cellulose was expressed by crystallinity index, which is an empirical measure of relative crystallinity. Crystallinity index of flax was found to be 0.7580 whereas, in case of flax-g-poly(MA), crystallinity index has been found to be 0.7065. The incorporation of monomer chains to the back-bone of flax had impaired the crystallinity of flax fiber. Therefore, grafting decreased the crystallinity of flax with reduction in its stiffness and hardness.

Table 2. Percentage crystallinity (%Cr) and crystallinity index (C.I.) of flax fiber and its graft copolymer

Sr. No.	Sample	P_g	at 2θ scale		%Cr	C.I.
			I_{22}	I_{18}		
1.	Flax fiber	–	1550	375	80.51	0.7580
2.	Flax-g-poly(MA)	86.24	3380	992	77.31	0.7065

Mechanical properties of Original flax and Graft Copolymers Reinforced Phenol-Formaldehyde Composites

Wear Test

In case of phenol-formaldehyde composites, material loss takes place by the mechanism of abrasion and frictional heat generated due to sliding. Moreover, reinforcement with graft copolymer improves the wear resistance as compared to reinforcement with original flax. Wear rate with original flax reinforced composites was much more at all loads. The wear rate was further enhanced with increase in load. In case of reinforcement of the phenol-formaldehyde matrix with graft copolymer, a reduced wear rate has been obtained. Maximum weight loss has been found in case of phenol-formaldehyde matrix followed by reinforcement with original flax. Graft copolymer reinforced PF composites showed better wear resistance in comparison to original flax reinforcement and PF matrix [9-13]. Results have been depicted in Table 3.

Tensile Strength

Composites reinforced with original flax can bear load upto 162 N and showed more extension (2.37 mm), whereas composites reinforced with graft copolymer showed 1.92 mm extension at load 235 N and PF matrix showed less extension (1.88 mm) and gets failure at load 125 N [9-13] (Table 3).

Compressive Strength

It is evident from Table 3 that pure phenol-formaldehyde matrix blocks have been observed with least compressive strength and could not withstand beyond 212 N with compression of 1.62 mm. Composites reinforced with graft copolymer showed less compression (0.78 mm) and can bear load upto 814 N, whereas composite reinforced with original flax showed 1.32 mm compression and gets failure at 372 N [9-13].

Table 3. Mechanical properties of original flax and flax-g-poly (MA) reinforced PF Composites

Sample	Tensile strength (N)	Compressive strength (N)	Wear rate (gm/m)×10^{-4}			
			1 kg	2 kg	3 kg	4 kg
PF matrix	125	212	18	34	56	77
Original flax reinforced PF composites	162	372	10	17	24	37
Flax-g-poly(MA) reinforced PF composites	235	814	09	14	19	32

Modulus of Rupture, Modulus of Elasticity and Stress at the limit of Proportionality

Table 4 shows the results of the MOR, MOE, and SP for flax fiber and its graft copolymer reinforced PF composites. MOR for phenol-formaldehyde and composites reinforced with flax fiber has been found to be 60.0 and 77.76 N/mm^2, respectively. Value of MOR was found to be 112.8 N/mm^2 for the composites reinforced with flax-g-poly(MA). Values of MOE were found to be 3404.8 N/mm^2 and 5248.0 N/mm^2 for the composites reinforced with original flax and flax-g-poly(MA), respectively. PF composites reinforced with flax-g-poly(MA) showed maximum value of SP (98.4 N/mm^2). The minimum value of SP was found in case of PF matrix [20]. Results showed that reinforcement of flax-g-poly(MA) increased the MOR. It was determined that reinforcement of PF composites with flax-g-poly(MA) increased the MOE and SP in comparison to flax fiber.

Table 4. Results of MOR, MOE, and SP for PF composites

Sr. No.	Sample	MOR (N/mm^2)	MOE (N/mm^2)	SP (N/mm^2)
1.	PF matrix	60.0	2611.2	48.9
2.	Original flax reinforcement	77.76	3404.8	63.84
3.	Flax-g-poly(MA) reinforcement	112.8	5248.0	98.4

Conclusion

Graft copolymerization is an effective method for modifying the properties of flax. Percentage crystallinity and thermal stability of flax-g-poly(MA) have been found close to that of flax fiber. Phenol-formaldehyde composites reinforced with flax-g-poly(MA) showed better mechanical properties in comparison to original flax fiber.

References

1. T. Paramasivam and A.P.J. Abdul Kalam, *Fibre. Sci. Technol.*, **7**, 85, (1974).
2. G.S. Patterson, A.S. Hoffmann, and E.W. Merill, *J. Appl. Polym. Sci.*, **4**, 159 (1960).
3. C. Sella, A. Chapiro, and A. Matsumoto, *J. Polym. Sci*., **57**, 529 (1962).
4. A. Chapiro, *J. Polym. Sci*., **23**, 377 (1957)**.**
5. S. Ishikawa, *J. Polym. Sci. Pol. Lett.*, **3**, 959 (1965).
6. Y. Liu, L. Yang, Z. Shi, and J. Li, *Polym. Int.*, **53,** 1561 (2004).
7. L.Y. Mwaikambo and M.P. Ansell, *Compos. Sci. Technol.*, **63**, 1297 (2003).
8. B. Schartel, U. Braun, U. Schwarz, and S. Reinemann, *Polymer*, **44**, 6241 (2003).
9. B.S. Kaith, Susheel Kalia, *Polym. Compos.*, **29**, 791 (2008).
10. D.K. Dwivedi, A.S. Singha, S. Kumar, and B.S. Kaith, *Int. J. Plast. Tech.*, **8**, 299 (2004).
11. A. S. Singha, Susheel Kumar, and B. S. Kaith, *Int. J. Plast. Tech*., **9**, 427 (2005).
12. B.S. Kaith, A.S. Singha, and Susheel Kalia, *Int. J. Plast. Tech*., **10**, 572 (2006).
13. B.S. Kaith, A.S. Singha, and Susheel Kalia, *Autex Res. J.*, **7**, 119 (2007).

14. G. Canche-Escamilla, J.I. Cauich-Cupul, E. Mendiza´bal, J.E. Puig, H. Va´zquez-Torres, and P. J. Herrera-Franco, *Composites: Part A*, **30**, 349 (1999).
15. N. Reddy and Y. Yang, *Polymer*, **46**, 5494 (2005).
16. A.M. Agrawal, R.V. Manek, W.M. Kolling, and S.H. Neau, *AAPS Pharm. Sci. Tech*., **4**, 1 (2003).
17. L.C. Segal, A.E. Martin, and C.M. Conrad, *Textile Res. J.*, **29**, 786 (1959).
18. A. Bhattacharya and B.N. Misra, *Prog. Polym. Sci*., **29**, 767, 2004.

Novel nanocomposite polymer electrolytes based on electrospun poly(vinylidene fluoride-co-hexafluoropropylene) for lithium batteries

Prasanth Raghavan, Xiaohui Zhao, James Manuel, Jou-Hyeon Ahn**

Department of Chemical and Biological Engineering and Engineering Research Institute, Gyeongsang National University, 900, Gajwa-dong, Jinju 660-701, Korea

Email: jhahn@gnu.ac.kr

Abstract

A series of nanocomposite polymer electrolytes (NCPE) based on poly(vinylidene fluoride-co-hexafluoropropylene) [P(VdF-HEP)] comprising nanoparticles of $BaTiO_3$, Al_2O_3 or SiO_2 were prepared by electrospinning technique. The presence of the ceramic nanoparticles has positive effect on the electrolyte uptake, relative absorption ratio and mechanical properties of the membranes. The ionic conductivity and the electrochemical stability window of the PEs were enhanced by the presence of the fillers. The prototype cell Li/$LiFePO_4$ based on the NCPE containing $BaTiO_3$ delivers a discharge capacity of 164 mAh/g, which corresponds to 96.5% utilization of the active material. In comparison, the performance of Li/$LiFePO_4$ cells with NCPEs containing Al_2O_3 and SiO_2 was observed to be lower with respective discharge capacities of 153 mAh/g and 156 mAh/g.

Keywords: Lithium batteries; Composite polymer electrolyte; Electrospinning; Fibrous membrane; Ceramic filler

1. Introduction

The high crystallinity of polymer membranes is one of the major factors of the low ionic conductivity of polymer electrolytes (PE), which limits their use in lithium batteries [1]. This problem can be addressed to a certain extent by the addition of nano-sized ceramic fillers to PEs. The addition of ceramic filler reduce the crystallinity of the host polymer. Even a small amount of these fillers can affect the mechanical strength and ionic conductivity of PEs. Apart from ionic conductivity, the ceramic filler nanoparticles also enhance interfacial stability between the PE and lithium electrode. The reduced capacity fading and improved cycling performance of the cell are other positive effects of the added nanoparticles [2].

Among many of polymers P(VdF-HFP) membranes prepared by electrospinning are suitable host polymers for preparing NCPEs due to the high affinity to the electrolyte, good electrochemical stability and desirable adhesion with the electrode.

In the present article, we report preparation, characterization and evaluation of the electrochemical properties of electrospun P(VdF-HFP) based NCPEs prepared with nanoparticles of three ceramic fillers, SiO_2, $BaTiO_3$ and Al_2O_3. The electrochemical properties of the NCPEs have been studied and the results have been compared with the PE prepared without the ceramic filler.

2. Experimental

2.1. Preparation of electrospun P(VdF-HFP) nanocomposite membranes

16% solution of P(VdF-HFP) (Kynar Flex 280) was prepared in a mixture of acetone/DMAc (7:3, w/w) at room temperature. To prepare the electrospun membranes with 6% ceramic fillers, 14% solution of P(VdF-HFP) was used. Al_2O_3, SiO_2 and $BaTiO_3$ (Aldrich), with a particle size range of 30-50 nm was used as nanoparticles. The resulting solutions were electrospun at 25 ºC as published elsewhere [3].

2.2. Characterization of electrospun P(VdF-HFP) nanocomposite membranes

The thermal properties of the membranes were evaluated by DSC (2010 TA Instruments) at a heating rate of 10 ºC/min under a nitrogen atmosphere from 50 to 200 ºC. The mechanical properties were evaluated following ASTM D638. The fiber morphology was recorded on field-emission SEM (FE-SEM: Hitachi S-4800), and the average fiber diameter (AFD) was estimated. The porosity (P) [4] and tortuosity [5] were determined as published elsewhere.

2.3. Electrochemical evaluation

PEs were prepared by soaking a circular piece of the membrane (diameter 2 cm) in the liquid electrolyte, 1 M $LiPF_6$ in EC/DMC (1:1 v/v) (Samsung Cheil Industries Inc.). The electrolyte uptake (δ) and the leakage properties of the PEs were measured following the procedure reported earlier [6].

The ionic conductivity of the PEs were measured by the AC impedance method using stainless steel (SS) Swagelok® cells with 1M6 frequency analyzer over the temperature range from 0 to 60 °C. The cell was kept at each measuring temperature for a minimum of 30 min to attain thermal equilibrium. The interfacial resistance R_f between the PE and lithium metal electrode was measured at room temperature by the impedance response of Li/PE/Li cells. Both the measurements were performed at an amplitude of 20 mV over the frequency range 10 mHz to 2 MHz. The electrochemical stability was determined by linear sweep voltammetry (LSV) of Li/PE/SS cells at a scan rate of 1 mV/s over the range of 2-5.5 V at 25 ºC. From the porosity and conductivity measurements, tortuosity of the membranes was calculated [5]:

Two-electrode lithium prototype coin cells were fabricated by placing the electrospun PE between lithium metal anode (300 μm thick, Cyprus Foote Mineral Co.) and carbon-coated lithium iron phosphate ($LiFePO_4$) cathode [7]. The electrochemical tests of the Li/PE/$LiFePO_4$ cells were conducted in an automatic galvanostatic charge-discharge unit, WBCS3000 battery cycler (WonA Tech. Co.), between 2.5 and 4.0 V at 25 ºC at a current density of 0.1 C.

3. Results and discussion

3.1. Membrane morphology

SEM images of P(VdF-HFP) membranes prepared without and with ceramic fillers reveal the presence of well interconnected interstices/pores between the fibers as shown in Fig. 1. The use of the solvent mixture of acetone/DMAc in the weight ratio of 7:3 results in membranes with lower AFD as compared to one component solvent or other solvent ratios and smaller pore size due to the formation of relatively large number of physical crosslinks. The membranes have fully interconnected pore structure. The ranges of fiber diameters obtained for different samples along with the AFDs are presented in Table 1. The membrane prepared without ceramic filler exhibits a comparatively uniform morphology with an AFD of 1.2 μm. The AFD is higher for the membranes that contain fillers. The membrane prepared with $BaTiO_3$ has more uniform fiber diameter and narrower distribution of the fiber diameters as compared to the other membranes. The larger diameter of the fiber in membranes with fillers can be attributed to the substantial increase in the viscosity that results from the blending of polymer solution with the filler particles.

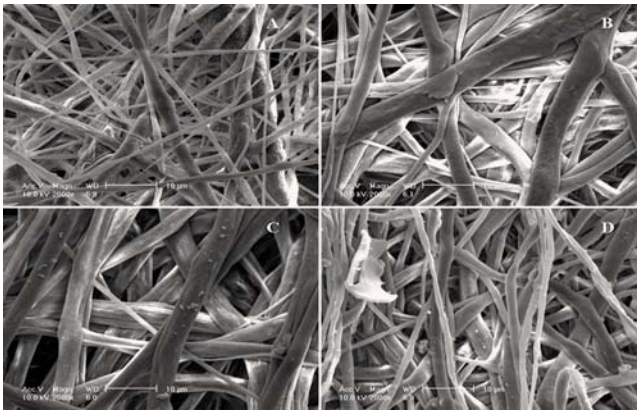

Fig. 1. SEM images of electrospun P(VdF-HFP) membranes with (A) no filler, (B) SiO_2, (C) Al_2O_3, and (D) $BaTiO_3$.

3.2. Thermal and mechanical properties

The effect of incorporation of 6% nano-sized ceramic fillers on the thermal properties of electrospun P(VdF-HFP) polymer is shown in Fig. 2. The melting temperature of pure P(VdF-HFP) is 159 ºC [8], while the electrospun

polymers with ceramic fillers have lower melting points in a close range of 153.4, 153.8 and 154.9 ºC for membranes with $BaTiO_3$, SiO_2 and Al_2O_3, respectively. The small change in the melting points of the composite membranes probably results from the orientation of the polymer chains along the fiber axis when drawn into the fibers rather than the interactions of the ceramic nanoparticles with the polymer. The % crystallinity values obtained from the DSC data follows the order $BaTiO_3$ (47.1%) < SiO_2 (47.9) < Al_2O_3 (49.2) < membrane without filler (74.5%) [8]. The mechanical properties of the membranes (based on the estimated values at the failure of the samples) are given in Table 1.

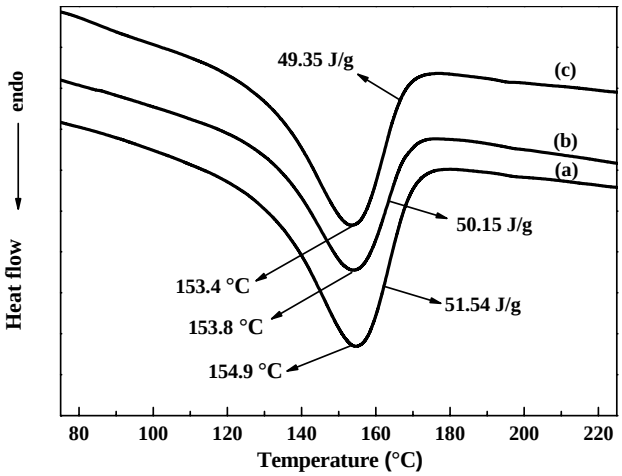

Fig. 2. Thermal properties (DSC) of electrospun P(VdF-HFP) membranes with 6% (a) Al_2O_3, (b) SiO_2 and (c) $BaTiO_3$.

3.3. Porosity, electrolyte uptake and electrolyte retention

The results of porosity determination by *n*-butanol uptake method are presented in Table 1. The porosity varies in the narrow range of 84-87% for the membranes, showing a slightly increasing trend with the filler content in the order $BaTiO_3$ > SiO_2 = Al_2O_3 > membrane without filler.

Fig. 3 presents a comparison of the electrolyte uptake (1M $LiPF_6$ in EC/DMC) of the membranes and the maximum uptake value of each membrane is also presented in Table 1. The fully interconnected pore structure of these membranes helps fast liquid penetration into the membrane, and hence the uptake process gets stabilized within a span of only 10 min. The relative absorption ratio (R) of the NCPEs and the PE without filler are presented in Fig. 3. It was seen that the electrolyte leakage reaches an equilibrium state within 1 h and all the PEs exhibit a high retention of the electrolyte with a cumulative leakage ~ 11% and ~ 14% after 1 h, respectively, in the case of the NCPEs and the PE without filler.

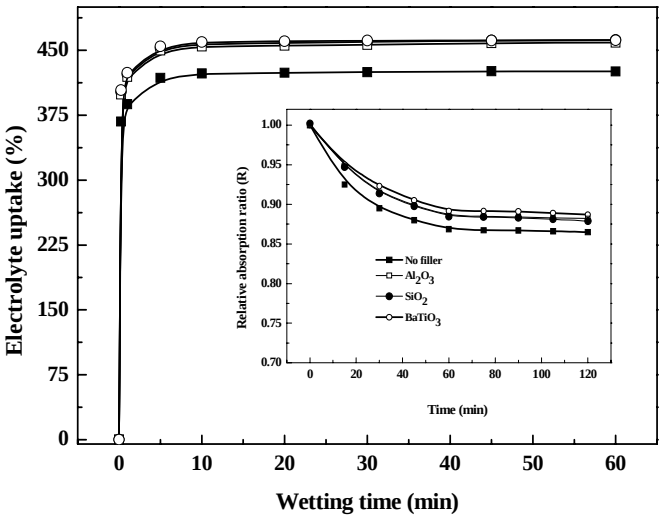

Fig. 3. Electrolyte uptake (%) of electrospun P(VdF-HFP) membranes with different ceramic fillers (liquid electrolyte: 1M $LiPF_6$ in EC/DMC).

3.4. Ionic transport properties

The ionic conductivity of the NCPEs at 25 ºC varies in the order $BaTiO_3$ > SiO_2 > Al_2O_3 > PE without filler. The higher ionic conductivity results from the interactions of O/OH groups on the filler surface and the large amorphous phase of the polymer [9]. And also the well knit porous structure of the membranes is one factor that facilitates the diffusion of the ions, hence high ionic conductivity was observed even for the PE without filler.

The tortuosity values calculated from the porosity and the ionic conductivity are listed in Table 1. As is evident from Table 1, the tortuosity of P(VdF-HFP) membranes with ceramic fillers decreases as a consequence of the nature of the filler, and follows the reverse order as is observed for the porosity of the membranes. These results are in agreement with those reported by Abraham et al. [6]. Song et al. also

reported that tortuosity decreases with the increase in the porosity of the membranes [10].

AC impedance of PEs based on electrospun P(VdF-HFP) membranes with different ceramic fillers at a temperature varies from 0 to 60 °C was determined. The bulk resistance R_b of the electrolyte at 25 °C varies between 1.6, 2.2, 3.8 and 4.8, respectively, for $BaTiO_3$, SiO_2, Al_2O_3 and PE without filler, thus, denoting a sufficiently high ionic conductivity. The temperature dependence of ionic conductivities of the NCPEs in the range of 0-60 ºC is presented in Figure 5. It can be observed that within the temperature range the Arrhenius plots are almost linear.

Properties		Filler		
		Al_2O_3	SiO_2	$BaTiO_3$
Fiber diameter range (μm)	0.4-2.2	1-4.9	0.7-4.5	0.9-3.3
Average fiber diameter (μm)	1.2	2.78	2.22	1.76
Porosity (%)	84	85	85	87
Electrolyte uptake (%)	425	459	459	462
Ionic conductivity at 25 °C (mS/cm)	4.21	5.92	6.45	7.21
Electrolyte retention ratio (R)	0.86	0.88	0.88	0.89
Tensile strength (MPa)	6.5	9.2	10.3	12.5
Modulus (MPa)	9.2	15.8	16.9	17.3
Elongation at break (%)	75	62	60	58
Tortuosity	14.81	12.56	12.04	11.52

Table 1. Properties of electrospun membranes and nanocomposite polymer electrolytes based on the membranes activated with 1M $LiPF_6$ in EC/DMC.

3.5. Electrochemical properties

The electrochemical stability window of electrospun P(VdF-HFP) based PE is shown in Fig. 6. The PE based on P(VdF-HFP) without ceramic filler exhibits an anodic stability up to 4.7 V. With the incorporation of filler particles in the polymer matrix, the electrochemical stability is enhanced. The stability order for the NCPEs follows as: 4.8 V (Al_2O_3) = 4.8 V (SiO_2) < 4.9 V ($BaTiO_3$). Thus, NCPEs have good anodic stability above 4.7 versus Li/Li^+, i.e., sufficient to be compatible with most of the common cathode materials used for lithium battery.

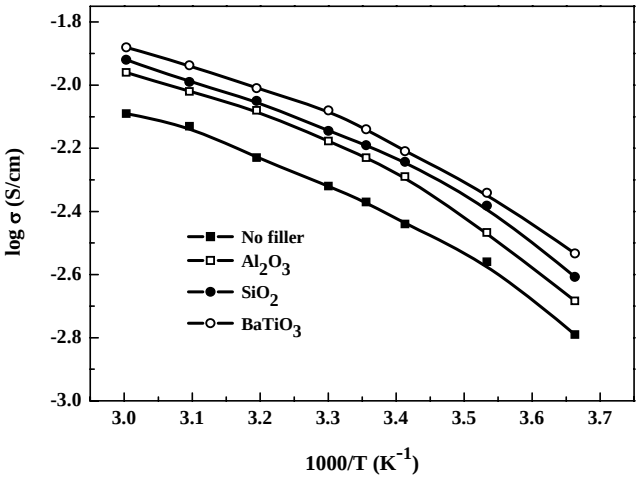

Fig. 5. Temperature effect of the ionic conductivity of PEs based on electrospun P(VdF-HFP) membranes with different ceramic fillers.

The impedance behavior of NCPEs with 1 M $LiPF_6$ in EC/DMC on lithium metal is presented in Fig. 7. R_f varies in the range 600-800 Ω with lower values recorded for the NCPEs. This indicates a good interface with the lithium electrode.

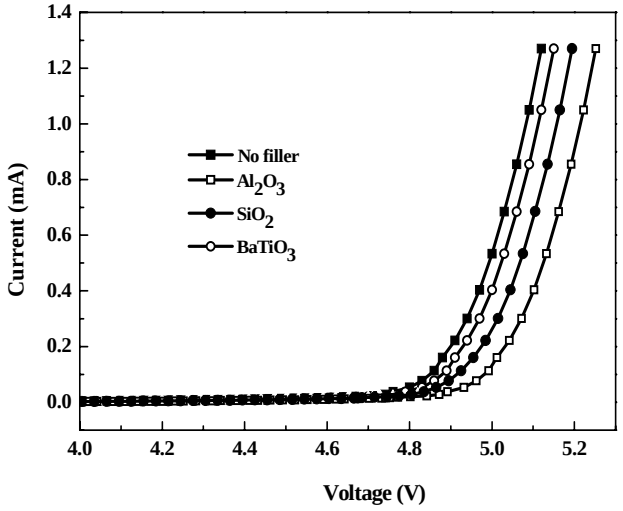

Fig. 6. Anodic stability by LSV of polymer electrolytes based on electrospun P(VdF-HFP) membranes with different ceramic fillers (Li/NCPE/SS cells, 1 mV/s, 2 to 5.5 V).

The PEs with and without filler have been evaluated for charge/discharge performance in $Li/LiFePO_4$ cells at room temperature. The first cycle charge-discharge properties at a current density corresponding to 0.1 C-rate are presented

in Fig. 8. The cell based on the PEs with $BaTiO_3$ delivers charge and discharge capacities of 164 mAh/g, which correspond to 96.5% utilization of the active material. The performance of the cell with PEs containing Al_2O_3 and SiO_2 is slightly lower as the discharge capacities of 153 and 156 mAh/g are obtained, respectively.

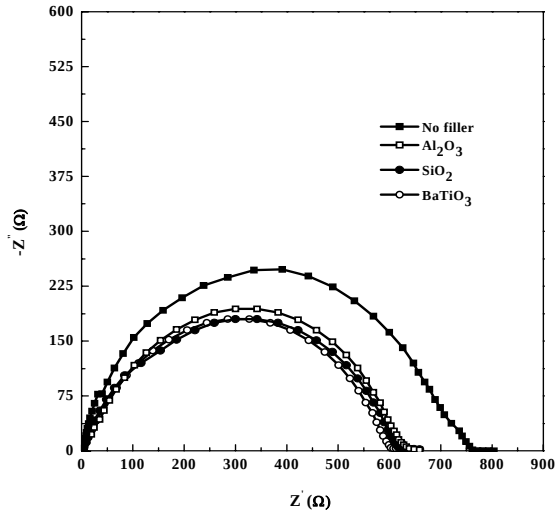

Fig. 7. AC impedance spectra of polymer electrolytes based on electrospun P(VdF-HFP) membranes with different ceramic fillers (Li/NCPE/Li cells, 10 mHz to 2 MHz).

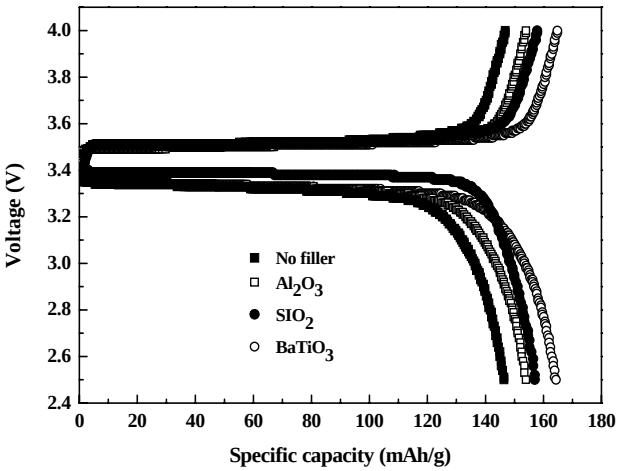

Fig. 8. Initial charge-discharge properties of Li/NCPE/$LiFePO_4$ cells with polymer electrolytes based on electrospun P(VdF-HFP) membrane containing 6% of ceramic fillers (25 °C, 0.1 C-rate, 2.5 to 4.0 V).

4. Conclusions

The nanocomposite PEs prepared by elctrospinning of P(VdF-HFP) show well interlaying of the fibers to generate a well interconnected porous membranes. The presence of the nano-scale ceramic fillers improves the mechanical properties of the membranes. The inclusion of fillers creates amorphous regions by way of the interactions between the filler surfaces and the polymer chains, which result in the reduced crystallinity of the polymer. The high electrolyte uptake by the NCPEs is attributed to the well interconnected pore structures and interactions of the fillers with the polymers as well as with the electrolyte. The nanocomposite PEs show minimum electrolyte leakage despite very high electrolyte uptake. Among the fillers $BaTiO_3$ has been observed to exhibit the highest electrolyte uptake, ionic conductivity, electrochemical stability and better compatibility with lithium metal. It also shows the maximum charge and discharge capacities. The reason for higher mechanical strength, electrolyte uptake and electrochemical performance of $BaTiO_3$ is attributed to the effective dispersion of its nanoparticles in the composite membranes during the electrospinning process that results in better interactions both with the polymer and the electrolyte.

Acknowledgements

This research was supported by Ministry of Knowledge Economy, Korea, under the Information Technology Research Center (ITRC) support program supervised by the Institute of Information Technology Assessment (IITA).

References

[1] F. Croce, S. Sacchetti, B. Scrosati, J. Power Sources 162 (2006) 685.

[2] G. Jiang, S. Maeda, H. Yang, Y. Saito, S. Tanase, T. Sakai, J. Power Sources 141 (2005) 143.

[3] X. Li, G. Cheruvally, J.K. Kim, J.W. Choi, J.H. Ahn, K.W. Kim, H.J. Ahn, J. Power Sources 167 (2007) 491.

[4] J.R. Kim, S.W. Choi, S.M. Jo, W.S. Lee, B.C. Kim, J. Electrochem. Soc. 152 (2005) A295.

[5] K.M. Abraham, M. Alamgir, D.K. Hoffman, J. Electrochem. Soc. 142 (1993) 683.

[6] J.R. Kim, S.W. Choi, S.M. Jo, W.S. Lee, B.C. Kim, Electrochim. Acta 50 (2004) 69.

[7] J.K. Kim, J.W. Choi, G. Cheruvally, J.U. Kim, J.H. Ahn, G.B. Cho, K.W. Kim, H.J. Ahn, Mater. Lett. 61 (2007) 3822.

[8] P. Raghavan, J.W. Choi, J.H. Ahn, G. Cheruvally, G.S. Chauhan, H.J. Ahn, C. Nah, J. Power Sources (doi:10.1016/j.jpowsour.2008.04.003).

[9] M.A.K.L. Dissanayake, P.A.R.D. Jayathilaka, R.S.P. Bokalawala, I. Albinsson, B.E. Mellander, J. Power Sources 119–121 (2003) 409.

[10] J.Y. Song, C.L. Cheng, Y.Y. Wang, C.C. Wan, J. Electrochem. Soc. 149 (2002) A1230.

Effect of nano TiO_2 in conducting polyaniline composites for smart corrosion prevention coatings

C.R.Siju*and S.Radhakrishnan[#]

Polymer Science and Engineering Division.
National Chemical Laboratory,
Pune 411 008, India

[#]Email: s.radhakrishnan@ncl.res.in

Abstract:

Coatings prepared from polyaniline- nanoTiO_2 particles synthesized by in situ polymerization were found to exhibit excellent corrosion resistance much superior to polyaniline in aggressive environments. The corrosion studies were carried out on steel plates coated with these formulations containing 10% polyaniline prepared with different concentrations of nanoTiO_2 by electrochemical impedance spectroscopy at periodic intervals during exposure to hot saline (65^o C) conditions for prolonged durations over a period of 90 hours. The open circuit potential (OCP) derived from Tafel plots was found to shift to more anodic side much above that of bare steel with time. The presence of nano-TiO_2 was found to be vital in prevention of corrosion and the shift of OCP to anodic side depended on the concentration of nano TiO_2 used. From these data, one could envisage more than 100 times improvement in the corrosion resistance especially for polyaniline prepared with 4.18% nano TiO_2. The exceptional improvement of performance of these coatings has been associated with the increase in barrier to diffusion as well as transport of charge by the nano sizeTiO_2, redox properties of polyaniline and very large surface area available for the liberation of dopant for the prevention of corrosion with self healing effect.

Key words: Conducting polymer, anti corrosion, nano-composite, titanium dioxide coating

1. Introduction:

Polyaniline (PANI) is one of the important conducting polymers which has been studied extensively for various applications such as sensors, transparent conductor, ESD and EMI protection, electrochromic displays etc. This polymer has been found to be an important constituent in coatings and recently that it has drawn attention as an effective material for corrosion protection. It has been reported that PANI based coatings can prevent corrosion even in scratched areas where bare steel surface is exposed to the aggressive environment. The anti corrosive coatings can be prepared from chemically synthesized PANI as dispersion coatings or PANI may be directly deposited on metal by electrochemical method as a first coat. Chemically synthesized PANI by conventional route does not dissolve in common organic solvents and hence it has to be blended with other polymers for its applicability in coatings.

The barrier properties can be enhanced if one uses appropriate fillers in the coatings. Further, it has been shown that nano-particulate fillers give much better barrier properties even at low concentrations than conventional micron size additives. As titanium dioxide (rutile or anatase) is commonly used as a pigment material for paints, it is thought worthwhile to use nano-particulate TiO_2 as a metal oxide additive in the composite which can give better dispersion of the formulation as well barrier properties in the coatings. In fact, it is anticipated that hybrid

composites containing nano additives as well as conducting PANI should improve tremendously the barrier properties of coatings as well as self healing effect giving large advantage in anticorrosion behaviour. Hence, the present studies were carried out on the preparation of nano TiO_2-PANI hybrid coating formulations using polyvinyl butyral (PVB) as the matrix and investigating their suitability for anticorrosive coatings.

2. Experimental:

2.1 Material

Aniline (ANI) (AR, Spectrochem Pvt. Ltd. India) was purified by distillation, 38% hydrochloric acid (AR,Ranbaxy), TiO_2 particles, ammonium peroxodisulphate (APS, AR, Spectrochem Pvt. Ltd, India) and methanol (E Merk) were used as such. Poly vinyl butyral (PVB) with M.W. 60,000 was obtained as granules from ABC Chemicals Exporter, Mumbai, India.

2.2 Preparation of PANI-TiO_2 composites of different PANI-TiO_2 ratio

To prepare PANI-TiO_2 composites of different ratios, the following steps were followed. 0, 0.1, 0.2, 0.3 and 0.5 g of TiO_2 nanoparticles (prepared according to procedure reported earlier) were added into a mixture of 1ml aniline and 90ml 1N HCl in a set of reaction vessels. The mixtures were stirred with magnetic stirrers in ice water baths for one hour to get a uniform suspension of TiO_2. To these mixtures, 100 ml pre-cooled 1N HCl solutions containing 2.5 g APS were added drop wise. The resulting mixtures were allowed to react in ice bath for about four hours. From these reactions we get pure PANI and TiO_2-PANI composites with compositions given in Table-1A. The products were washed with distilled water for several times and at last washed with methanol to remove low molecular weight oligomers along with other impurities. Then all samples were dried in an oven for 12 hours. These samples were characterized by UV, IR, XRD, SEM and TEM in the usual manner.

2.3 Preparation of PANI-TiO_2 dispersion formulations for coating

PVB (2g) was dissolved in methanol (20 ml) with continuous stirring for 6hr and then in a sonicator for few hours. The 10 wt % of PANI-TiO_2 powder having different compositions was crushed and slurry was made with small quantity of methanol. The slurry was added and mixed in the PVB solution and subjected to sonication for 24 Hrs. This yielded a uniform dispersion of PANI-TiO2 in the PVB solution with no settling. The stainless steel coupons (50mmx 10mmx 1mm) with rounded corners and edges were polished by C- 800 emery paper, washed with acetone and dried. The substrates were dip coated for 30 sec in PVB/PANI-TiO_2 dispersion and dried at room temperature for 30 min followed by baking in air circulating oven at 50^0 C for 4 hr. The samples were cooled and then subjected for measurement of corrosion inhibition properties..

2.4 Testing of corrosion resistance properties

Tafel plot and impedance measurements were carried out in 3.5 % NaCl solution as electrolyte. All measurements were performed on computerized electrochemical analyzer (supplied by CH instruments, USA). Stainless steel plates coated with the PANI-TiO_2 composites were used as working electrode while Pt and SCE were the counter and reference electrodes respectively. The voltammograms were measured between +1 to –1 V at a scan rate of 50 mV/s. Tafel plots was recorded at a scan rate of 10 mV/s. After initial measurements all the coupons were immersed in an external bath with hot 3.5 % NaCl solution (65 ^oC) for a period of 4 hrs so that accelerated testing could be carried out. The coupons were then again subjected to electrochemical measurements at an interval of 4 hours as described above [10, 19]. Micrographs of corroded samples were recorded on polarized optical microscope fitted with digital camera (model Leica Stereoscan 440, UK).

3. Results and Discussion :

The wide angle XRD of the PANI-nanoTiO2 powders is depicted in Figure-1 which indicates the typical PANI peaks with broad amorphous band for the samples with no TiO_2 and the characteristic reflections of anatase (JCPDS-21-1272) for the composite. The crystallite size determined from the FWHM of main 101 reflection of TiO_2 is 75 nm.

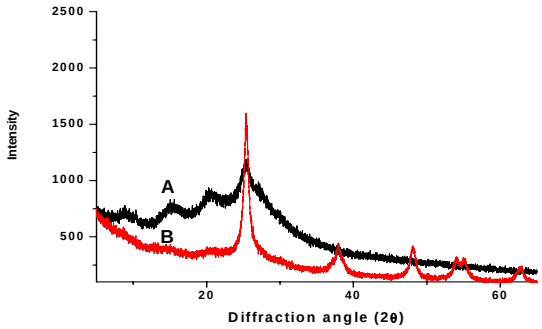

Figure:1. X-ray diffraction of (A) PANI and (B) PANI with nano-TiO_2

There is an increase in the particle size due to the formation of PANI around the particles. It is interesting to note that the polymerization yield is slightly increased for PANI-50 which indicates that polymerization is mainly initiated on the particle surface.

The PANI-nanoTiO_2 dispersed in PVB solution and studied for corrosion resistance by accelerated immersion test in 3.5% saline solution at 65^0C followed by Tafel tests. The Tafel plots of figure: 2 shows that corrosion protection of steel enhanced by the addition of increasing concentration of TiO_2.Because TiO_2 improves the barrier properties. Nano TiO_2 acts as noble metal and it may form a thin layer on the metal surface. The n-type nanoTiO_2 and p-type PANI forms p-n type junction which give potential barrier to charge transport. Also barrier to the diffusions of ions is improved due to nano-particles.

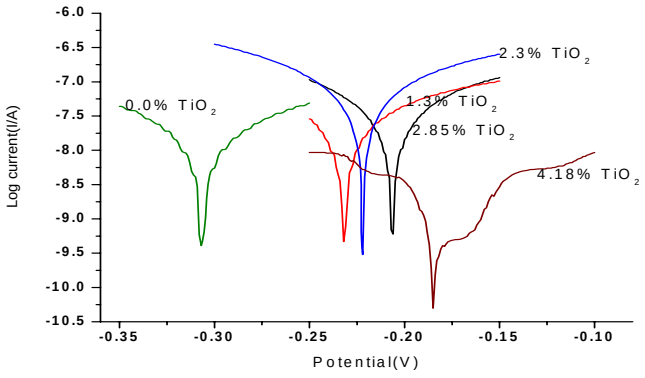

Figure:2. Tafel plots of accelerated PVB-PANI/TiO_2 coating after 40 hrs.

The open circuit potentials (OCP) determined from these plots recorded after different time of exposure to hot saline environment are indicated in Figure 3. The initial OCP of PVB is found to be on the cathodic side but more positive (-0.48) than that of bare steel (-0.6V SCE) [20] but after prolonged exposure to corrosive environment, the OCP shifts to more cathodic region. On the

other hand, the coatings containing PANI exhibit a self healing effect i.e. although there is a decrease in the OCP initially, it shifts to more anodic side after some time. This tendency to shift the OCP to potentials more nobel than the original bare steel increases with the increase in the TiO_2 content in the PANI-nano TiO_2 composite based coatings. In fact for PANI-TiO_2-4.18%, the OCP remains on the high anodic side of the other values even after 40 hr of exposure to hot saline atmosphere. High OCP value compared to that of bare substrate as well as plain PVB coated steel clearly indicates the high corrosion resistance provided by these coatings. It may also be noted that the breadth of the Tafel curve in the PANI-TiO_2-4.18% is much more than other composition.

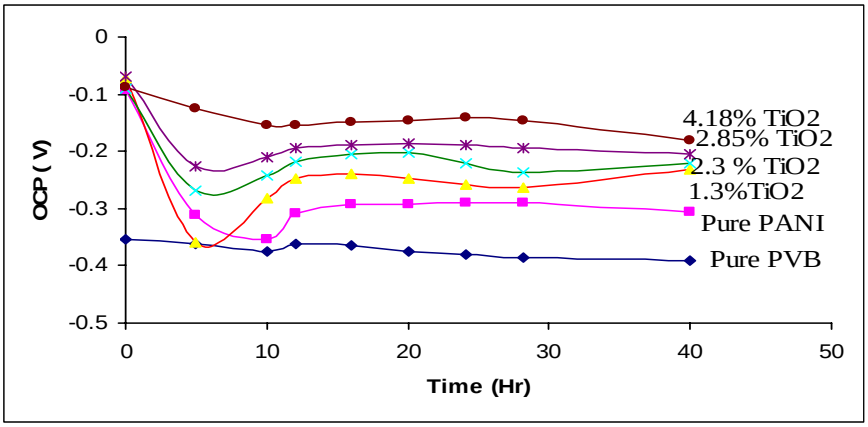

Figure: 3.OCP Vs Time graph of PVB-PANI containing different percentage of TiO_2

The corrosion rate (C_R) derived from the I_{corr} values using the equation

$$C_R = 0.129\ I_{corr}\,(EW) / (A.d)$$

Where EW is equivalent weight, A the area and d the density is shown in figure: 4 with the exposure time to hot saline conditions. It is interesting to observe that the corrosion rate initially increases but then tends to taper off above 10 hours to 20 hours. However, there is again a second region above 30 hours where the corrosion rate is seen to increase sharply. These changes can be attributed to the failure of the resin matrix, self healing due to PANI and then catastrophic failure above drastic conditions of corrosion testing. It can be noted that these changes are completely minimized in the coatings containing PANI-TiO_2-4.18% which withstand even the drastic conditions where other coatings are seen to completely give away.

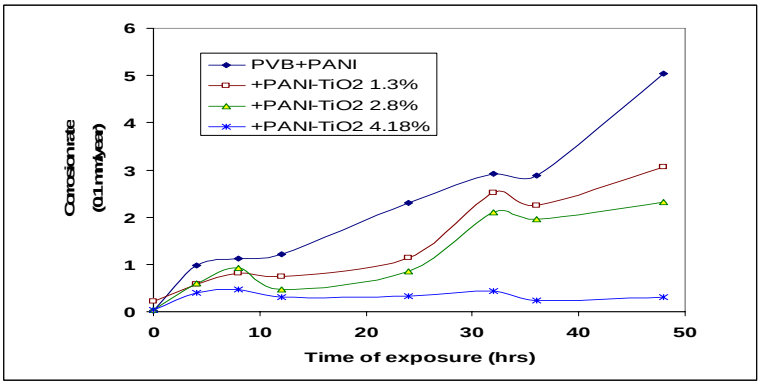

Figure: 4.Corrosion rate with respect to prolonged exposure of coatings to hot saline conditions.

This is further evidenced from the impedance plots (Bode) indicated in Figures 5 recorded after 40 hrs exposure to hot saline conditions. It can be seen from these figures that PANI-TiO_2-4.18% has higher resistance than the coatings without TiO_2 especially at low frequency which is associated with ionic transport through the film. This continues to remain high even after exposure to the corrosive environment. The accelerated testing conditions used in the present case are equivalent to testing for more than 800 hrs at room temperature which is derived using the reported logarithmic relations for corrosion rate of steel with temperature which gives about 10X as acceleration constant [21,22]. Thus, there is excellent corrosion protection obtained in these coatings especially when PANI-TiO_2 (4.18%) powder is used as an additive even at low level of loading (10wt %).

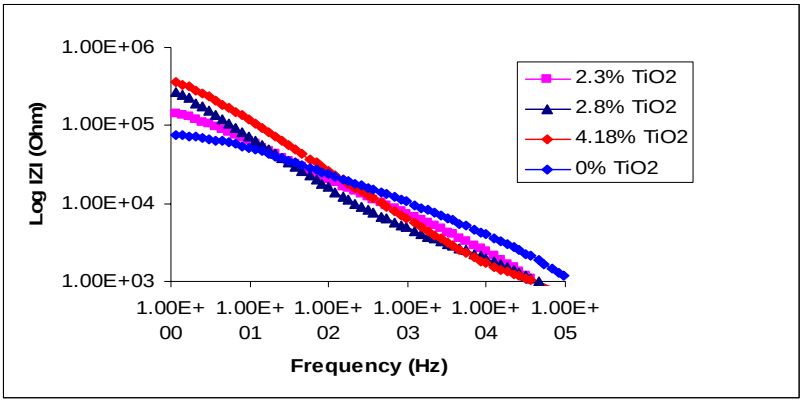

Figure: 5.Bode plots of PVB/PANI-NanoTiO_2 coatings after 40 hr immersion at 65^0C saline solution

The low frequency data in Bode plots has been associated with the diffusion processes and as mentioned above it indicates to some extent that nano-TiO_2 leads to such improvement. However, there is also an additional cause for further improvement of corrosion resistance especially when one considers that the total concentration of the additive in the formulation was same (10%) in all cases.

4. Conclusions:

The conducting PANI nano-particulate TiO_2 hybrid composites prepared by in situ polymerization were used for coating with PVB as the matrix. The effect of addition of nano TiO_2 on the improvement of has been clearly brought out The novelty of these coatings lies in generation of corrosion inhibition by three mechanisms operating simultaneously viz. improvement of barrier properties, redox behaviour of PANI and formation of p-n junctions preventing easy charge transport when coating is threatened to be destroyed due to scratch or scribble. Even if the main resin is damaged, the additives give a healing effect and prevent catastrophic failure. Apart from the prevention of corrosion, these coatings have good gloss and shiny surface, which is not easily obtained in conventional coating, prepared with commercial micron size particle additives. Such systems can be used as a primer coat or even as a single coating on steel where colour is not a very important criterion.

References :

1] L.Alcacer, Conducting Polymers, Riedel, Dordrecht, Holland, 1987

2] A.J.Dominis, G.M.Spinks, G.G.Wallace, Prog. Org. Coat. 48 (2003) 43.

3] P.J.Kinlen, J.Ding ,D.C.Silverman, Corrosion 58 (2002) 490

4] N. Ahmad, A.G. MacDiarmid, Synth. Met., 78 (1996) 103.

5] P.J.Kinlen, D.C.Silverman, C.R.Jeffreys, Synth. Met., 85 (1997) 1327.

6] T.Schauer, A.Joos, L.Dulog, C.D.Eisenbach, Prog.Org.Coat. 33 (1998) 20.

7] C.K.Tan, D.J.Blackwood, Corr. Sci., 45 (2003) 545.

8] P.Zarras, J.D.Stenge-Smith ,Y.Wei, Electroactive Polymers for Corrosion control, ACS Symposium Series 843, Washington DC,2003

9] G.G. Wallace, G.M.Spinks, L.A.P.Kane-Maguire, P.R. Teasdale, Conductive Electroactive Polymers: Intelligent Materials Systems, CRC press, New York, 2003, Chapter 1.

10] R.C.Patil , S.Radhakrishnan, Prog. Org. Coat. 57 (2006) 332

11] S.Sathiyanarayanan, S.S.Azim , G.Venkatachari, Synth.Metals 157(2007) 751

12] N.K.Lape, E.E.Nuxoll, E.L.Cussler, J.Membr.Sci. 236 (2004) 29

13] K.Yano,A.Usuki ,A.Okada, J.Polym.Sci. A: Polym.Chem. 35 (1997) 2289

14] M.Alexandre, P.Dubois, Mater.Sci.Eng. 28 (2000) 1-63

15] D.J.Chako, A.A.Leyva, Chem.Mater 17 (2005) 13

16] M.H.Priya and G.Madras J.Photochem. Photobiol. A: Chemistry 178 (2006) 1–7

17] S.Radhakrishnan , A.B.Mandale, Synth. Met. 62 (1994) 217

18] C.Saujanya ,S.Radhakrishnan , Polymer 42 (2001) 6723

19] R.G. Groseclose, C.M.Frey, F.L.Floyd, J.Coat.Technol. 56 (1984) 31

20] A.J.Bard , L.R.Faulkner, Electrochemical Methods: Fundamentals and Applications, Wiley, New York, 1980

21] J.C.Li, M.Zhao ,Q Jiang, Materials & Corrosion, 53 (2002) 269

22] P.Bruke, A.I.Sphahani ,B.S.Wright, Advances in CO2 Corrosion, Vol.2, NACE, Houston TX, 1985, p. 1-22; p.47-54

Transducer using Terfenol-D/epoxy composite

Reji John, Tusarkanta Sahoo, K A Thomas, Laly Joseph and K P B Moosad
Naval Physical and Oceanographic Laboratory
Defence Research and Development Organisation, Kochi-682021, India

Email: tsonpol@vsnl.com

Abstract:
Terfenol-D (alloy of iron, dysprosium and terbium rare-earth materials) has received considerable attention as a material for magnetostrictive transducers and actuators due to its giant magnetostriction. Nevertheless, device development using this material has always been hampered by problems related to eddy currents and high brittleness of the material. Both of these problems can be effectively addressed by developing composites of magnetostrictive materials in epoxy matrices. A study was carried out on a Terfenol-D /epoxy composite to assess its suitability as a transduction material for the application of low frequency underwater transducers. Composites with different percentages of volume filling of Terfenol-D powder having 0- 300 micron sizes were prepared and their magnetic and transduction properties were studied. The maximum attainable magnetostriction for a composite of 60% volume filling of Terfenol-D powder was found to be 450 ppm. In order to assess the suitability of the material for fabricating low frequency underwater transducer, the composite material was cast into rods (8 mm diameter X 28 mm length) and were employed in a Flextensional Transducer, as a transduction material . Underwater acoustic measurements were carried out and the results are compared with those of a similar transducer using monolithic Terfenol-D material, in the same geometries.

1.Introduction
Terfenol-D material has received considerable attention as magnetostrictive transducer and actuator material due to its giant magnetostriction. Nevertheless, device development on these materials has always been hampered by an eddy current induced bandwidth limitation to a few kilohertz and brittleness imposed challenges to produce complex shapes and designing of devices. By contrast, magnetostrictive polymer composite can be developed to alleviate the problems intrinsic in bulk material by incorporating magnetostrictive Terfenol-D particles into a passive polymer matrix. Recognizing the advantages of Terfenol-D composites, researchers began integrating these composites in sonar transducers. The motivation is partially explained from a preliminary study showing that monolithic Terfenol-D is superior to PZT in terms of power capability [1]. This idea was reinforced in a subsequent study suggesting that ‘‘composite Terfenol-D should be superior to both monolithic Terfenol-D and PZT in transducers for sonar arrays operating in the 20–30 kHz range’’ [2]. Of particular importance in sonar transducer design is the strain output and the modulus of the composite under different loading conditions. These properties dictate the work output delivered by the transducer. However, the unavailability of a comprehensive characterization of strain output, modulus, and coupling coefficient under different loading conditions and volume fractions limits the use of magnetostrictive composites. The intention of the study is to develop a Terfenol-D/ Epoxy composite having optimum modulus and large Magnetostriction to enhance the stress output for actuator applications. Also it is included in this paper, studies on the strain output of the magnetostrictive composites as a function of particulate volume fraction of Terfenol-D powder.

2. Experiments
2.1 Fabrication of magnetostrictive composite material The 1–3 composites are fabricated using a low viscosity epoxy (viscosity ~100 cps, Roto polymers, Chennai) as the matrix material and Terfenol-D powder (0-300microns, Etrema, USA) as the particulate filler. Low viscosity epoxy is

selected as matrix material due to the reason of easy removal of trapped air and wetting of the powder and further maximizing the filler loading . Composites are manufactured in an aluminum mold fabricated with a cavity of 8mm dia and 28 mm length. Appropriate volume fractions of Terfenol-D particles are mixed with epoxy resin in a beaker. The mixed slurry is placed in a vacuum for degassing. The degassed slurry is further poured into the mould just before the gelation time. The mold is then sealed and placed between two permanent magnets (field strength ~ 1000 gauss). The mould is further kept on rotation at room temperature during curing process to prevent the settling of dense Terfenol-D particles.

The magnets placed at the two ends of the mould, produce uniform horizontal magnetic field through the length of the cavity. This aligns the particulate into chains or pseudo fibers fashion, which when cured get locked in the epoxy matrix results in a 1–3 composite. A 1–3 composite produces a higher strain output than the particles are randomly aligned [3]. In addition to aligning the particles the magnetic field also further aligns the domains inside the particles, however, since Terfenol-D is a soft magnetic material the domains redistribute once the magnetic field is removed.

2.2. Magneto mechanical Characterisation

2.2 (a) compressive modulus.A universal testing machine (Zwick 1476) is employed to determine the compressive modulus of the composite.

2.2 (b) Magnetostriction The strain developed in the material is determined using a strain gauge and whetstone bridge setup.

2.2 (c) Magnetisation The saturation magnetization, remnant magnetic field and magnetic coercivity are determined using walker scientific magnetometer

2.3. Transducer Fabrication

2.3 (a) Approach: NPOL has designed and developed Flextensional Transducers (FT) using peizoceramic transduction material. The effort was to fabricate flextensional transducer using the fabricated magnetostricitve composite material. FT consists of an elliptical aluminium shell, encapsulated with neoprene rubber.

The main consideration for designing the driver using the GM material was the the space available in the shell. Composite rods of 8 mm diameter and 28 mm length were fabricated as described above. The conceptual sketch of the arrangement of the rods is shown in Fig. 1. The numbered items are (1) magentostricitve composite rods 8 mm dia, 28 mm long [6 Nos.] (2) Tablet-type 20 mm dia, 10 mm thick Samarium-Cobalt permanent magnets [12 Nos.] (3) 375 turns of 22 SWG Solenoids [6 Nos.] (4) 30 mm dia, 27.5 mm long aluminum bobbins [6 Nos.] (5) 8 mm thick brass magnetic de-coupler (6) I mm MS outer frame for magnetic flex return path (7) Aluminum shell [Elliptical cylinder]. The solenoids are connected in parallel and designed to be powered by AC current with a current limitation of 5 amp.). A compressive mechanical pre-stressing is given to the drive by elastic spring of the flextensional shell. For this the total length of the drive module taken is 0.5 mm more than the major axis of the shell. The drive module is inserted in the shell by mechanically pressing the shell in the minor axis. Once the drive module is inserted the pressing is removed and the shell is loaded against the drive and this will give sufficient pre-stress.

2.3(b) Design of magnetic circuit

Magnetic circuit was designed and analysed using a FE modeling software Vizimag^{R}. The input parameters are enlisted in table 1.On the basis of modeling a most suitable schemes is arrived at, and the plots of which is shown in Fig. 2 (a) and (b). Magnetostricitive composite material drive is shown in Fig. 3 and that of fabricated FT with is shown in Fig. 4.

2.3 (c) Transducer measurements

Measurements are made in the open water tank, keeping the transducer at a depth of 10 m. The sound projected by the transducer is picked up by a standard B& K hydrophone. A similar FT, with monolithic Terfenol-d rod drive was also subjected to measurements using the same set-up and the

results were compared. Measurements were repeated in two different methods, to confirm the results.

3. Results and discussion

The compressive modulus obtained was 1 GPa. The epoxy resin employed largely controls the modulus of the composite. Hence it is proposed to use resin having larger modulus. Upto a certain level of loading, magnetostriction of the composite increases as shown in Fig.5 with the volume fraction of the Terfenol-D powder added . The present composite having 60 % loading shows a magnetostriction of 450 ppm at a DC magnetic field of 2000 Oe. The remnant magnetic field present in the composite influences utilization of the devices for high frequency applications . As it is evident from the Fig. 6, the remnant magnetic field present in the composite is negligible. The composite exhibits saturation tendency above 4000 Oe. Fig. 3 shows a photograph of the realized drive as per the scheme in Fig.2 (a). The drive module was inserted into an elliptical Aluminum shell of a flex-tensional transducer (FT). Fig.4 shows a photograph of the assembled magnetostrictive transducer. End plates with O-rings were fastened to make the device water-worthy. As magnetostrictive transducers are current-driven devices, Transmitting Current Responses (TCRs) are used to characterize them, in place of the usual Transmitting Voltage Responses (TVRs) used in the case of transducers with piezoceramic drive.Fig. 7 shows the measured TCRs of the above FTs with monolithic Terfenol-D rods and composite rods respectively .The advantage of the composite is a slight lowering of the frequency at which the device shows peak performance. The peak performance is about 10 dB less for the FT with composite rods, compared FT with Terfenol-D rods.

5. Conclusion and suggestion for future work

Composite of Terfenol-D / epoxy resin exhibits magnetostriction. The magnetostiction values are largely depend on the percentage of Terfenol-D powder added. The magnetostrictive composite transduction material developed can drive elliptical aluminum shell. Magnetic circuit design play important role in the performance of the transducer. For improving the performance of the transducer, magneto-mechanical properties such as Young's modulus, magneto-mecahnical coupling factor etc has to be optimized.

Acknowledgement:
Authors would like to thank Prof. Markeyandalu, Dept. of physics, IIT-Madras, Chennai for the materials properties measurement. The encouragement and support of ASD(ME&MEMS) and the permission of the Director, NPOL to publish this work is greatly acknowledged.

6. Reference

[1] Moffett, M B, Porzio, R., Bernier, G L, "High Power Terfenol-D Flextensional Transducer – Revision A", NUWC Technical Document No. 10883A, 12 May 1995.
[2] M.B. Moffett, J.M. Powers, J.Acoust. Soc. Am. 90 (1991) 1184.
[3] J.H. Goldie, M.J. Gerver, J. Olesky, .P. Carman, T.A.Duenas, Proc. SPIE 3675 (1999),243.
[4] T.A. Duenas, G.P. Carman, Proc. ASME 291 (1998) 63.

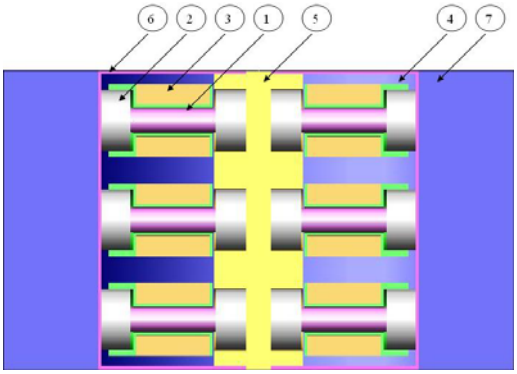

Fig.1 Conceptual sketch of Magnetostrictive composite material as driver in the aluminum shell of FT

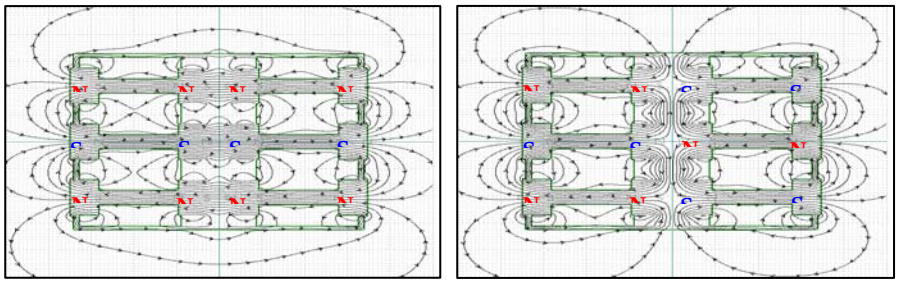

Fig. 2 (a) and (b) Field distributions in the two chosen schemes

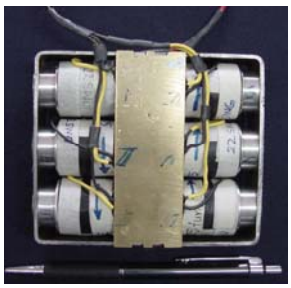

Figure 3 the Driver assembly

Fig. 4 Assembled Magnetstrictive FT

Table-1.Input parameters for modeling

Sl No.	Parameter	Value used
1	Current in the solenoid	4 Amps
2	No. of turns in the solenoid	300
3	Strength of the permanent magnets	1200 G
4	Permeability of the permanent magnets	1.2
5	Permeability of GM rod	7
6	Permeability of Mild steel frame	15
7	Permeability of Brass Magnetic decoupler	1

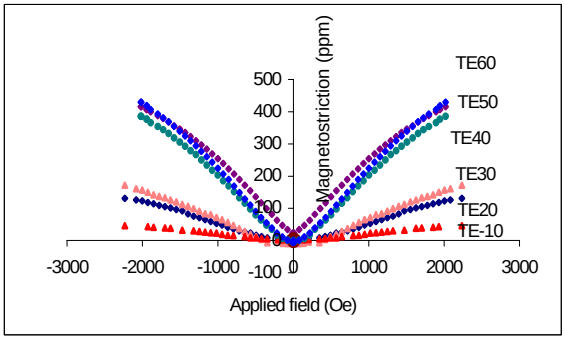

Fig.5.Magnetostriction of the composite at different volume fraction of Terfenol-D

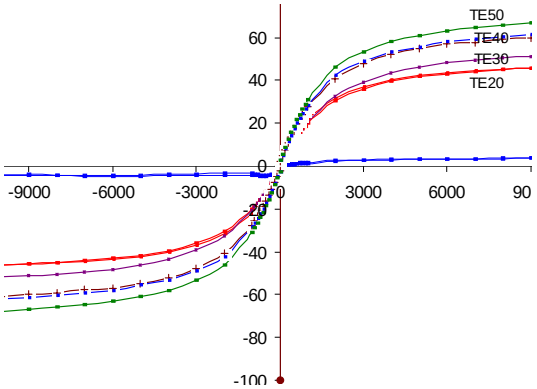

Fig. 6 Magnetisation curves of the composite for the different volume fraction

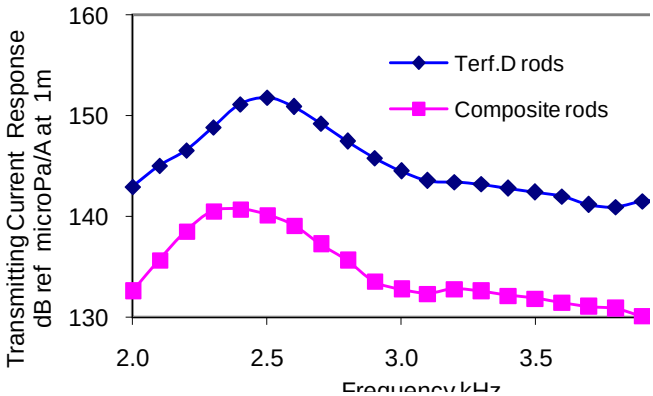

Fig. 7 TCR of a FT, driven by Terfenol D rods and Terfenol D composites

Competitive extraction of Na, K, Ba, Ca, Mg by NR/PEO-1000, NR/PEO-4000 block copolymers

Suryakala K. S. and M.R. Gopinathan Nair
School of Chemical Sciences, Mahatma Gandhi University, Kottayam 686560, Kerala, India.
Email: suryakutty@gmail.com

Abstract

A series of NR/PEO block copolymers were prepared from hydroxyl terminated liquid natural rubber and polyethylene oxide of $\bar{M}_n$=1000 (PEO-1000) and $\bar{M}_n$=4000 (PEO-4000). Complexation studies of these block copolymers with five different aqueous metal salt solutions were undertaken to find the order of competitive extraction. Selective complexation of metal cations was observed to occur with the following order of selectivity: $K^+ > Ba^{++} > Ca^{++} > Na^+ > Mg^{++}$; which parallels the results known for many crown ethers [1,2] and noncyclic polyethers [3] and is identified with the polyether portions of the block copolymers, which are thought to adopt helical conformation surrounding the complexed cation.

Introduction

In comparison with cyclic polyethers, noncyclic polyethers [3] seemed extraordinarily weak in ability of metal ion complexation [4]. A search of literature [5-7] showed that, before Pederson's discovery of macrocyclic polyethers [8], high molecular weight polyethylene oxide had been reported to form complexes with various metal salts especially alkali and alkaline earth metals [9-11].

In connection with the progress of the chemistry of macrocyclic polyethers, the interaction of open chain polyethylene oxide derivatives with metal ions has attracted special interest [12]. PEO has the structure $HO\text{-}[\text{-}CH_2\text{-}CH_2\text{-}O\text{-}]_n\text{-}H$. It differs from the crownether essentially in that the macrocyclic ring is opened and the molecule is laid out. X-ray diffraction [13,14] studies on PEO showed that the polymer in solid state is 7/2 helix. The structure is quite enough for some suggestion that every heptameric segment of PEO might behave as rudimentary crown ether. In solution, hydrodynamic evidence showed PEO chains change its helical structure into a new less ordered structure. In general the more flexible polyethylene oxide ligands are able to wrap the metal ions in a helical fashion while crown ethers, due to their rigid cavity size are found to co-ordinate in an out-of cavity fashion or are displaced to hydrogen bonded out of sphere locations if the metal cavity size fit was not compatible.

Recently, some researchers have thought that chemical modification may facilitate the enhancement of PEO complexation ability and selectivity, and have synthesized large number of PEO derivatives and related polyethers [15-25]. Based on the above reported works, it was decided to study the interaction of NR/PEO block copolymers, prepared in our laboratory with various metal salts. This was undertaken to explore the use of these block copolymers for metal ion extraction process, phase transfer catalysis, reverse osmosis and related purposes.

Experimental

Materials

Natural crumb rubber (ISNR-5): Weight average molecular weight = 8,20,000; Intrinsic viscosity in benzene at 30^0C= 4.45 dL/g; Wallace Plasticity, P_0=39 was supplied by Rubber Research Institute of India, Kottayam, Kerala.Toluene diisocyanate (TDI) (was 80/20 mixture of 2,4-and 2,6- isomers) was supplied by Aldrich, Germany and was used as received. Dibutyl tin dilaurate (DBTDL) supplied by Fluka, Switzerland, was used as catalyst without further purification. Hydrogen peroxide (30% w/v) supplied by E. Merck, India was used without further purification. Toluene (reagent grade) obtained from E. Merck; India was used as solvent without further purification. Methanol (reagent grade) supplied by E. Merck, India was used without further purification. Chloroform (laboratory reagent grade) was dried with anhydrous calcium oxide and then distilled before use. It was supplied by E. Merck, India.

Polyethylene oxide (PEO) of molecular weight ($\bar{M}_n$) 1000 and 4000 (PEO-1000 and PEO-4000 respectively) supplied by Aldrich, Germany were used as received. NaCl (Merck, India), KCl (Merck, India), $MgSO_4$ (Merck, India), $BaCl_2$ (Merck, India), $CaCl_2$ (Merck, India) were used as received. Double de-ionized water was used for the preparation of metal salt solutions.

Synthesis

Preparation of hydroxyl terminated liquid natural rubber (HTNR)

HTNR was prepared by the less vigorous but efficient method developed by Ravindran [26] et al using H_2O_2 and solar radiation.

Natural crumb rubber was masticated for 30 minutes at 40^0C, 500gm of it was dissolved in 10L toluene and the solution was charged into a flat bottomed flask made up of borosilicate glass and 500 ml of aqueous hydrogen peroxide (30%w/v) was added and thoroughly mixed with rubber solution. The mixture was then homogenized to a certain extent by the addition of 750 ml of methanol. The whole assembly with the material for irradiation was placed in sunlight under stirring. After an exposure of 60 hours a layer of water separated at the bottom with some white deposits. This was separated and the upper layer comprising liquid natural rubber in toluene was distilled to remove the toluene to recover the liquid natural rubber (HTNR). It was purified by precipitation by methanol twice from toluene solution and was dried in vacuum oven.

Synthesis of NR/PEO block copolymer

The second part of the experiment comprises the synthesis of NR/PEO block copolymer as given below [27].

HTNR (24gm) was dissolved in 68ml of chloroform (35%w/v) to get a solution. The whole solution was taken in a reaction vessel, dibutyl tin dilaurate catalyst (6% by weight of HTNR) was added and the solution brought to reflux with stirring. The stoichiometric amount of TDI (1:2.76:1 of HTNR) was added in drops, followed by the drop wise addition of 6gm of PEO-1000/24gm of PEO-4000 in chloroform (35%w/v) within a period of 1.5 hour. The reaction was allowed to continue for another 2 hours. Excess chloroform was then distilled off and the viscous polymer solution was cast in trays treated with silicone releasing agent. The sheet was removed from the tray after 24 hours, kept in a vacuum oven at 60^0C to remove traces of solvent and then cured at 70^0C for 24 hours, followed by one week ageing at room temperature in a moisture free atmosphere.

Complexation of metal ions: General procedure

A known mass of block copolymer (0.3g) was suspended in 50ml 2M metal salt solutions (NaCl, KCl, $MgSO_4$, $BaCl_2$, $CaCl_2$) at its natural pH, for 168 hours in a closed condition. The polymer was then taken out and washed the surface instantly but carefully with de-ionized water to remove any surface salt present. The metal ion intake of the block copolymer was obtained from the determination of the concentration of the metal salts solutions before and after complexation. From the decrease in concentration of metal ion solution, the amount of metal ion complexed by the polymer was calculated. The concentrations of the metal salt solutions were determined by volumetric methods-Na+ and K+ by Mohr's method [28], Mg++ and Ca++ by complexometric titrations [29], Ba++ by precipitation titration [30].

Results and discussion

Following the procedure under experimental part, sheets of polyether-natural rubber block copolymers were prepared. Polyether is hydrophilic in nature and natural rubber provides the nonpolar hydrophobic part. Series of NR/PEO-1000 and NR/PEO-4000 were synthesized by solution polymerization. The course of the reaction and the structure of the block copolymer are shown in Scheme I.

Interaction with metal salts

The interaction of NR/PEO block copolymers with various metal salts is due to the PEO content in the samples. The polyethylene oxide bearing $-[-CH_2-CH_2-O-]_n-$ units can exhibit crown ether or podand property by forming spiral or pseudo cavity of adequate size to accommodate the cations. The present study on the competitive extraction of different cations is originated from the above background. Even though the PEO part contains no crown ether like macrocycle, the long chain with $-[-CH_2-CH_2-O-]_n-$ units can adopt a ring like structure by taking a spiral shape. The salt solutions considered are NaCl, KCl, $MgSO_4$, $BaCl_2$, and $CaCl_2$.

The interaction of dried NR/PEO-1000 and NR/PEO-4000 with the above salt solutions were studied by estimating the cation impregnated in the polymer sample. The next step is to find the order of competitive extraction of these metal cations. The results have been analyzed by the overall metal complexation values [Table I]. The order of competitive extraction by these two block copolymers are the same as given below $K^+ > Ba^{++} > Ca^{++} > Na^+ > Mg^{++}$. The experiment was repeated with another concentration (0.2M) of the metal salt solutions. In that case too the extraction order was the same. From the above result it is clear that as the ionic radii increases ($Na^+=1.96A^0$, $K^+=2.66A^0$, $Ba^{++}=2.83A^0$, $Ca^{++}=2.12A^0$, $Mg^{++}=1.56A^0$) [31] complexation ability also increases, except for Ba^{++} as shown in Fig.1.

The HTNR and PEO used in the present study are made up of appreciably large number of respective monomer unit. The copolymerisation of these two using TDI makes the block copolymer system almost infinite size with alternate HTNR-PEO components. In this copolymer the NR part behaves as the soft segment and it is completely amorphous in nature. The PEO is the hard segment and in solution, not much ordering is expected from this fragment also. But when treated with metal salt solution the PEO fragments with $-[-CH_2-CH_2-O-]-$ units would tend to interact strongly with the metal ions, resulting in a high degree of ordering as shown in Fig 2. The corresponding situation with HTNR/PEO block copolymer is shown in Fig 3.

It is known that for alkali and alkaline earth metals, usually the co-ordination number is from 6-10 [32]. For the formation of a pseudohelical structure, the ligand should have 6 donor atoms. In our case, this structure is obtained using five -[-CH_2-CH_2-O-] groups along with a 6^{th} -CH_2-CH_2-O-group that forms the turn of the pseudohelix. The metal ion is accommodated in the cavity of the spiral structure, depending upon its size, i.e. either by size comparable to that of 15-crown-5 or 18-crown-6. Hence here the maximum extraction is for K^+, which shows the PEO chains prefer to take a pseudohelical structure similar to that of 18-crown-6. The cavity size of 18-crown-6 [1,2] is $2.6A^0$ which suits to K^+ ion and the extraction order is K^+>Rb^+>Cs^+>Na^+>Li^+. The situation can be diagrammatically represented in Fig 4.

The slight decrease in the affinity of block copolymer to form a strong complex with Ba^{++} can be explained as follows. Ba^{++} has a slightly greater ionic radius compared to the cavity size of 18-crown-6. Therefore the whole helical structure has to expand a little to accommodate this larger cation, which leads to lower absorption compared to K^+.

Conclusion

The work shows that NR/PEO block copolymers can be used to extract alkali and alkaline earth metals from aqueous media. The order of extractability is as follows: K^+>Ba^{++}>Ca^{++}>Na^+>Mg^{++}. The order of cation preference is nearly identical to that of 18-crown-6 derivatives and also of noncyclic polyethers. We thus believe that a helical arrangement of inwardly directed oxygen atoms forms the basis of complexation between cation and block copolymers.
Further investigation of NR/PEO extraction mechanisms is continuing in our laboratory. A number of analytical and other applications are being investigated and will be reported shortly.

References

1 Strzelbick J, Bartsch RA. Anal.Chem.1981; 53:1894-1899.
2 Strzelbick J, Bartsch RA. Anal.Chem.1981; 53: 2247-2250.
3 Awano H, Katsumichi O, Kenkichi M. Bull.Chem.Soc.Jpn. 1982; 55: 2525-2529.
4 Balasubramanian D, Chandani B. J.Chem.Educ. 1983; 60: 77-78.
5 Frensdorf HK. J.Am.Chem.Soc. 1971; 93: 600-606.
6 Timko JM, Helegeson RC, Newcomb M, Gokel GW, Cram DJ. J.Am.Chem.Soc. 1971; 96: 7097-7099.
7 Chaput G, Jeminet G, Juillard J. Can.J.Chem. 1975; 53: 2240-2246.
8 Pedersen CJ. J.Am.Chem.Soc. 1967; 89: 7017-7036.
9 Ono K, Konami H, Murakami K. Rep.Prog.Polym.Phys.Jpn. 1978; 21:17-21.
10 Barthelemy PP, Desreux JF, Marsaux J. J.Chem.Soc.Dalton.Trans. 1986; 6: 2497-2499.
11 Yanagida S, Takahshi K, Okahara M. Bull.Chem.Soc.Jpn. 1977; 50: 1386-1390.
12 Calzolari C, Favretto L, Marletta GP, Chem.Abstr. 1976; 84: 38132s.
13 Koenig JL, Angood AC. J.Polym.Sci.Part A: Polym.Chem. 1970; 8: 1787-1795.
14 Rogers RD, Bond AH, Aguinaga S, Reyes A. Pure and Appl.Chem. 1993; 65: 567-572.
15 Tummler B, Maass G, Vogtle F, Seiger H, Heimann U, Weber E. J.Am.Chem.Soc.1977; 99: 4683-4690.
16 Kang SI, Czech A, Czech BP, Stewart LE, Bartsch RA. Anal.Chem.1985; 57: 1713-1717.
17 Walkowiak W, Stewart E, Czech BP, Bartsch RA. Anal.Chem.1986; 58: 188-191.
18 McDowell WJ, Czech BP, Bartsch RA. Sovt. Extr.Ion Exch. 1986; 4: 411-419.
19 Walkowiak W, Desai DH, Lee HK, Bartsch RA. Anal.Chem.1992; 64: 1685-1690.
20 Hiratana K, Aiba S, Nakagawa T. Chem.Lett. 1980; 9: 477-480.
21 Hiratana K. Chem.Lett.1981; 1: 21-24.

22 Hiratana K. Chem.Lett.1982; 7: 1021-1024.
23 Hamon RF, Khan AS, Chow A.Talanta. 1982; 29: 313-326.
24 Okada T. Analyst. 1993; 118: 959-971.
25 Dale J, Frendrikson SB. Pur Appl.Chem.1989; 61: 1587-1592.
26 Ravindran T, Nair MRG, Francis DJ. J.Appl.Polym.Sci. 1988; 35: 1227-1239.
27 Nair, R.C., Block copolymers from liquid natural rubber and polyethers, Ph.D thesis 1998, pp 73-75.
28 Bassett J, Denney RC, Jeffery GH, Mendham J, editors, Vogel's Text book of quantitative inorganic analysis. 4th Ed.Longman group Ltd, 1978, pp-475
29 Bassett J, Denney RC, Jeffery GH, Mendham J, editors, Vogel's Text book of quantitative inorganic analysis. 4th Ed.Longman group Ltd, 1978, pp-257.
30 Bassett J, Denney RC, Jeffery GH, Mendham J, editors, Vogel's Text book of quantitative inorganic analysis. 4th Ed.Longman group Ltd, 1978, pp-452.
31 Ono K, Honda H, Murakami K. J.Macromol.Sci.Chem. 1989; A26: 567-582.
32 Truter MR, Nature 1970; 228: 648-651.

Scheme 1

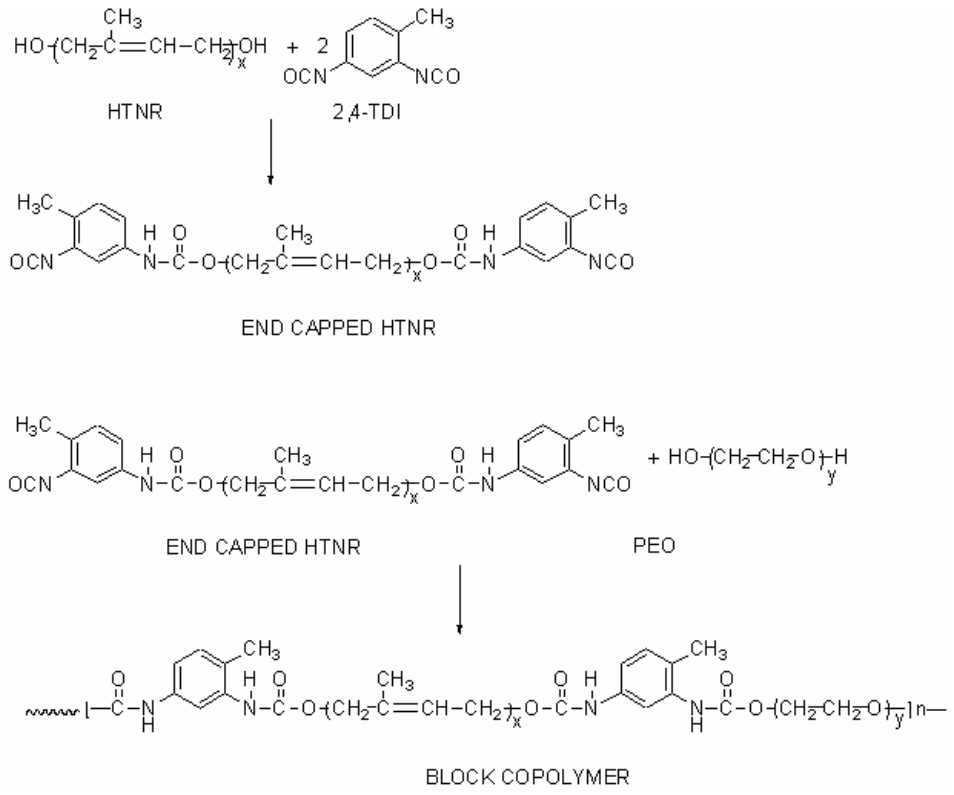

Table1. Ion uptake by the polymer samples

Polymer sample	Uptake of metal ions (mM/g)				
	Na^{+}	K^{+}	Ba^{++}	Ca^{++}	Mg^{++}
NR/PEO-1000	1.20	3.78	2.80	2.24	0.88
NR/PEO-4000	2.12	4.41	3.20	2.86	0.42

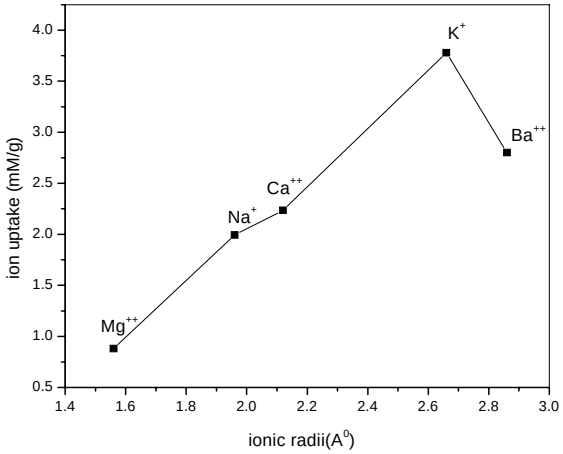

Figure 1. Plot of ion uptake versus ionic radii

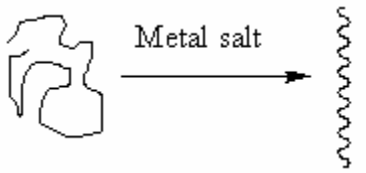

PEO before complexation

PEO after complexation

Fig.2. Complexation in polymers

Fig. 3 Complexation in NR/PEO block copolymer

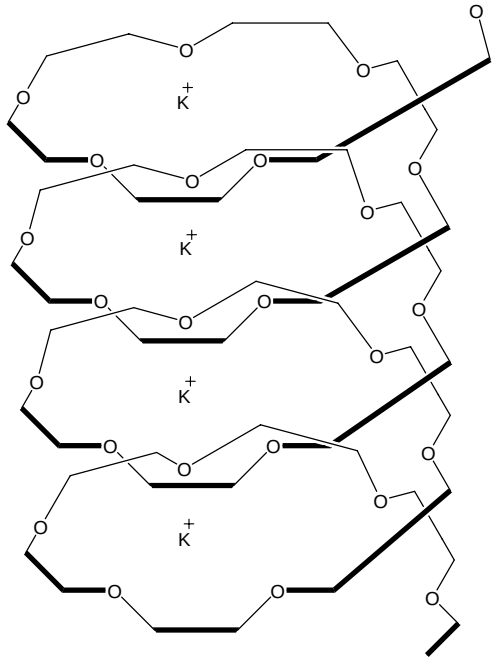

Fig. 4 Pseudocavity binding of K^+

Protein functionalized polysaccharide nano particles for novel applications

T.Emilia Abraham
Chemical Sciences & Technology Division,
National Institute for Interdisciplinary Science & Technology (NIIST), CSIR,
Thiruvananthapuram-695019
E-mail:emiliatea@gmail.com

Abstract

There has been growing interest in the use of natural polysaccharides for biomedical applications, drug delivery vehicles, as minimally invasive scaffolds for tissue engineering, because of their non toxicity, biocompatibility, biodegradability, low interfacial tension and high molecular and oxygen permeability. By exploiting these features it may be possible to mimic features of the natural extracellular matrix, and control tissue structure and cellular functions. Protein/peptide oral drug delivery is complicated process mainly due to poor intrinsic protein permeability as a result of large molecular weight, degradation by proteolytic enzymes in the stomach and in the small intestine, and chemical instability. Protein functionalized micro and nano particles are very versatile and were made to overcome this problem. Low molecular weight chitosan, guar gum, were used for the preparation of nano particles using precipitation and ionic cross linking method and was then linked to the enzyme (subtilisin) by glutaraldehyde coupling. Polysaccharides having a molecular mass of 8 to 36 KDa gave high-quality nano composite spherical particles of 100-500 nm size, with a good poly dispersity index of 0.1- 0.7. Poly saccharides having a molecular mass greater than 50 KDa gave micro particles and vesicles of more than 1 microns as indicated by Dynamic laser light scattering, SEM, and TEM studies. The optimum pH of the polysaccharide nanoparticle immobilized enzyme was shifted to 8.0 from 7.0, whereas there was no change in the optimum temperature. The immobilized enzyme shows better affinity to the substrate (casein) with a lower K_M value of 4.097×10^{-5} than the native subtilisin which is 3.30×10^{-4}. These composite catalytic nano particles are having excellent activity, pH sensitivity and stability which make them suitable for oral drug delivery, tissue scaffolds, microreactors or for cosmetic applications.

1. Introduction:

There is significant interest in the protein functionalized nanosized particles; with potential applications ranging from biosensors [1-3] enzymatic bioreactors [4] delivery of sensitive drugs [5] nano biochips and membranes for bioseparations [6], surface coatings,

adhesives, cosmetics, detergents, toothpaste, special food products and medical diagnostics. Polysaccharides possesses distinct chemical and biological properties that include biocompatibility, biodegradability to harmless products, nontoxicity, physiological inertness, remarkable affinity to proteins, hemostatic, fungistatic, antitumoral and anticholesteremic properties [19,20] Chitosan, a copolymer of β (1,4)-D-glucosamine and β(1-4)-N-acetyl-D-glucosamine, is a non toxic, biodegradable and positively charged polysaccharide widely used as a support for enzyme immobilization [8,9,10]. Galactomannas have a linear back bone of (1→4)-diequatorially linked β-D-mannose residues, some of which carry single- sugar side chains of α-L-galactose attached by (1→6) linkages. Guar gums normally have an M/G ratio of ~1.6. Low molecular weight, acid–free water-soluble polysaccharides (LMWPS), are made by depolymerization and from this nanoparticles can be made by ionic gelation technique[11, 12]. Important application of polysaccharide nanoparticles is in the controlled release of protein and peptide drugs, because they show excellent mucoadhesiveness and permeation enhancing effect across the biological surfaces. Protein/peptide oral drug delivery is complicated process mainly due to poor intrinsic protein permeability as a result of large molecular weight, degradation by proteolytic enzymes in the stomach and in the small intestine, and chemical instability [13,14]. Compared with conventional solid-phase supports, nano particulate matrices could have a higher catalyst loading capacity due to their very large surface areas [15]. Subtilisin is one of the major proteolytic enzymes having a neutral pH, which is used as a digestive aid in pancreatitis, and used for wound healing etc. The preparation and properties of subtilisin functionalized biocatalytic polysaccharide nano particles are reported here.

2. Experimental

2.1 Materials: Chitosan and Guar gum were produced from Sigma (St.Luis, USA). Subtilisin [Amano, Japan,], Gluteraldehyde and Aerosol-OT [Sigma, St.louis, USA], tripoly phosphate, solvents such as Isopropanol and all the other reagents are of analytical quality.

2.2 Preparation of polysaccharide nano particles; The polysaccharide nanoparticles were made by 3 methods such as nano precipitation and cross linking, dialysis and cross linking or by two phase separation.

2.3 Preparation of subtilisin functionalized polysaccharide nano particles(EFNP) : The sutilisin solution in phosphate buffer (pH 7.0, 0.1M) was added to a suspension having polysaccharide nano particles. The enzyme was immobilized by glutaraldehyde coupling and then glycine was added to remove any unreacted aldehyde groups. The particles were then dialyzed against fresh phosphate buffer (pH 7.0, 0.1M) for 4 hours to remove the excess cross linking agents.

2.4 Analysis of Particle size of ultra micro and nano particles of subtilisin functionalized nano particles: Particle size and polydispersity were determined by photon correlation spectroscopy (PCS) by using a Zetasizer 3000 (Malvern Instruments Ltd., UK). Mean size and polydispersity were measured three times for each batch.

2.5 Optimum pH, temperature & kinetic parameters of subtilisin functionalized chitosan nano particles : In order to determine the optimal pH of the enzyme, the enzyme assay was carried out at different pH values (6.0–10.5) at 50°C. Optimal temperature was determined by a standard activity assay in the temperature range from 30 to 80°C. The kinetic studies were done by changing the substrate (Casein) concentration from 0.25-2.5 (W/V %).

2.6 Nanoparticle morphology by Scanning Electron Microscopy; The shape and surface morphology of the subtilisin functionalized micro and nano particles were examined using electron microscope (JEOL make, model JSM 5600 LV, Tokyo, Japan). For SEM studies, lyophilized nanoparticle were mounted on metal stubs using double-sided adhesive tape and then sputtered with gold. The micrographs were taken at an accelerating voltage of 15 KV and at various magnifications.

2.7 TEM of subtilisin functionalized subtilisin functionalized chitosan nano particles: TEM pictures of polymeric nanoparticles were taken in a Hitachi H 7600 TEM instrument operating at magnification of 80 kv. A drop of aqueous solution of particle was placed on a carbon membrane coated grid surface and excess liquid was removed carefully with a filter paper (Whatman No.1). After 1 min the grid surface was dried under vacuum at room temperature before loading in the microscope.

3. Results and Discussion

Hydrogels, from naturally occurring polysaccharides which are highly stable organic compounds that swell when their environment becomes more acidic or slightly alkaline. All the methods are found to be suitable for the preparation of nano particles. The chitosans and galactomannans are essentially random coiled polysaccharides in solution. The enzyme used for the studies is a versatile serine protease, subtilisin which after purification had a specific activity of 0.012 U/mg protein**.**

3.1 Formation of chitosan nano particles: Nano composite particles were formed by the nanoprecipitation and ionic cross linking method. TPP, which is a poly anion to cross-link with the cationic amino group of chitosan through electrostatic interaction, avoiding possible toxicity. The particles are formed upon the addition of nonsolvent and tri polyphosphate and stabilized by anionic surfactant Aerosol OT. Size and size distribution of the chitosan –TPP nanoparticles

depend largely on concentration, molecular weight, additives and conditions of mixing ie, stirring or sonication. An average particle size of 310 to 490 nm was obtained with isopropanol and 347-438 nm with acetone, when chitosan of molecular mass of 8KDa was used Fig-1. The PKa of chitosan is 6.5 and below this pH, chitosan behaves as a poly cationic material, the phosphoric ions of TPP forms ionic cross linking with NH_3^+ groups of the chitosan and has a net positive charge on the surface (IEP-9.0) and the surface is comparatively hydrophobic [17].

3.2 Effect of cross linking agent on the size of nano particles of galactomannans: The cross linker used was either borate or sodium tripolyphosphate (TPP). Table 1. Two Guar gum chains cross links with borate ions -B (OH) $_4$ preferentially due to the cis diols present in the mannose ring. The reaction is favored at neutral pH conditions. TPP cross links with the hydroxyl groups of the polysaccharide forming phosphate bonds between the two polysaccharide chains

3.3 Effect of non solvent on the formation of nano particles: The production of nano particles dispersed in aqueous media by precipitation with non solvents involve the use of acetone, methanol, ethanol, isopropanol, amyl alcohol etc. The final mean particle size of NPs was clearly dependent on the nature of the non solvent used. The results showed that the use of isopropanol and acetone led to smaller particles, as measured by (DLS), where as other solvents gave larger particles (above 500 nm). Even though low log P values tend to give nano particles, there is not much correlation with the Log P values and nano particle formation. However the dielectric constants which are a measure of solvent polarity played a significant role. A slow reduction in the dielectric constant of the solution brings about nanoprecipitation. Acetone and isopropanol has similar medium dielectric constant value of 18-20, which favors the nano precipitation of chitosan molecules in water medium which is having a dielectric constant of 80

Table 1 Nano particle preparation of guar gum

Method	Z average particle size (nm)	PDI
Nano precipitation and cross linking		
Cross linker		
TPP	279.8	0.425
Boric acid	265.4	0.491
Dialysis and cross linking	128.6	0.756
Two phase separation		
Cross linker (boric acid)		
Organic	739.8	0.312
Aqueous	168	0.659
Cross linker (TPP)		
Organic	571.3	0.161
Aqueous	213.9	0.750

Table 2 Effect of non solvent on guar gum NPs

Non solvent	Dielectric Constant (ε)	log P	Zave	PI
Methanol	32.6	-0.764	300.3	0.3
Isopropanol	18.3	0.074	279.8	0.425
Acetone	20.7	-0.24	224.9	0.276
Ethanol	24.5	-0.30	320.1	0.491
Ethyl acetate	6.0	0.68	464.4	0.653

3.4 Effect of surfactants on the size of nano particles;

Nanoparticles were made using different surfactants like Triton x 100, Tween-20, Aerosol OT and Span-60. Anionic surfactant such as Aerosol OT and SPAN was useful for chitosan particle stabilization. A concentration 3mM of Aerosol OT was appropriate for the successful production of chitosan nano particles. The two non ionic surfactants found useful for the stability of the galactomannan nano particles are found to be Tween 20 and Triton X100 and the nano particle surface is thus surrounded by a thin layer of hydrated poly ethylene glycol chains. This hydrophilic shells forms a steric barrier which prevents close contact between particles and, hence, coagulation (“steric stabilization”)

(Fei Han et al.,2008) and in turn stabilizes the NPs Increase in surfactant concentration was not found suitable for nano particle preparation.

3.5 Immobilization of subtilisin on polysaccharide nano particles-EFNP

The enzyme immobilization efficiency of the nano particle was in the range of 45.38 to 70.10 % .b Immobilization of enzyme usually results in the conformational change in the enzyme resulting in a shift in the optimum pH. The effect of pH on the activity of free and immobilized protease preparations are given in (Figure 6). The optimum pH of the native enzyme was at 7.0 and was shifted to pH 8.0 after immobilization. This pH shift towards alkaline side is due to the secondary interactions between the coupling agent, enzyme and the polymeric gel matrix. The glutaraldehyde coupling of the matrix with the enzyme would have linked all the available amino groups on the surface of the enzyme, and hence the acidic groups on the enzyme surface gives a negative charge to the enzyme protein, ultimately shifting the optimum pH to the higher side. The protease activity of native enzyme increased gradually with temperature and a maximum activity was obtained at 55°C. The immobilized enzyme also showed the same temperature optima.

3.6 Reaction Kinetics of EFNPs compared with native subtilisin

The immobilized enzyme shows a lower K_m value than the native subtilisin. The higher affinity of the immobilized subtilisin towards the substrate may be due to the presence of a flexible glutaraldehyde arm, which in turn helps the enzyme to suitably orient its active site towards the substrate (casein). However the catalytic efficiency of the immobilized enzyme was found to be lower than that of the native enzyme (Table 4)

Table 4 Kinetic parameters of immobilized NPs and native subtilisin

Enzyme	K_m Moles/ml	V_{max} Moles/s/g	k_{cat} Moles/s/mole of enzyme	k_{cat}/K_m
Native	$1.07x10^{-5}$	$4.21x10^{-6}$	0.147	$1.4x10^{4}$
Immobilized	$4.097x10^{-5}$	$2.89x10^{-6}$	0.07611	$18x10^{2}$

Particle size of the nano - and micro particles is an important formulation property that influences other pharmaceutical and cellular uptake properties of the drugs.

As the particle size is reduced, surface area to volume ratio increases, resulting in a large surface area available for the buffer penetration into the particles and also for the faster escape of the polymer degradation products from the smaller sized nanoparticles. John Hopkins researchers have reported that nano particles of 200-500 nm having hydrophilic neutral polymers moves through mucus layer quickly than smaller ones which are less than 100 nm [16].

3.7 *SEM and TEM of subtilisin functionalized chitosan nano particles:* The morphological characterizations of the nanoparticles of chitosan, figure 3 and 4 shows nano particles prepared with chitosan and galactomannan functionalized with subtilisin in SEM. It was confirmed by a transmission electron microscope (Figure 5).

4. Conclusion : There is enormous interest in using ultra micro and nanoparticles for biomedical applications including enzyme encapsulation and drug delivery. Nanoparticles of chitosan and galactomannan functionalized with subtilisin in the presence of anionic surfactant, and a co solvent, with TPP and glutaraldehyde as cross linking agents was made having sizes ranging from 100 to 500 nm. The nano particles are biocompatible, non toxic and the production is cost effective and the scale-up will be easy. A therapeutic enzyme, subtilisin, a serine protease, was loaded without much inactivation. One can also load any other enzyme or any hydrophobic drug by this method and thereby the bioavailability of these drugs can be increased and more importantly may help treat previously untreatable conditions.

References

[1] G.A.Mun, Z.S.Nurkeeva, V.V.Khutoryanskiy, A.D.Sergaziyev, J.M Rosaik,. Radiat. Phys.Chem. 65 (2002) 67

[2] J.Wang, G.Liu, M.R. Jan, J.Am.Chem.Soc 126 (2004) 3010

[3]C.RMartin, P.Kohli, Nature Rev.Drug Discov 2 (2003) 29

[4] A.Star, J.C.P Gabriel, K.Bardley, G.Gruener, Nano Lett, 3 (2003) 459

[5] B.Lakshmi,C.R Martin, Nature 388 (1997)758

[6] E.S.Amalia, D.Yolanda, C. Margarita,G.Carmen, C.Sagrario,V.Ana, J.A.Maria, Invest Ophthalmol Vis Sci.,47 (2006)1416

[7] S.B.Lee, D.T.Mitchell, I.Trofin, T. K.Nevanen, H.Soderlund, C.R.Martin,,Science 296 (2002) 2198

[8] C.Walsh , Nature 409 (2001) 226

[9] F.Jinda, G.Yong, Journal of Experimental Nanoscience, 1 (2006)457

[10] R.S.Juang, F.C.Wu, R.L.Tseng, Bioresour Technol 80 (2001)187

[11] N.Duran, M.A.Rosa, A.D'Annibale, L.Gianfreda., Enzym Microb Technol 31 (2002)907

[12] R.S.Juang, F.C.Wu,Tseng, Adv. Environ. Res. 6 (2002)171

[13]. Dea, I.C.M., Morrison, A., (1975). Adv. Carbohydr.Chem. Biochem. 31, 241-312.

[14]. Doyle, J.P., Giannouli, P., Martin, E.J., Brooks, M., Morris, E.R., (2006). Carbohydr. Polym. 64, 391-401.

[15] A.P.Nicholas, J.K Nikhil, Eur J Pharm Sci.14 (2001) 201

[16] B.Savitha, F.Georg, S.Sheetal, R.Rajani, K.Collins, M.Amarnath, M.Anirba M, J Nano Biotech 5:3 (2007) 1

[17] D.R.Bhumkar, V.B.Pokharkar. AAPS PharmSci Tech. 7(2) (2006) E1-E6

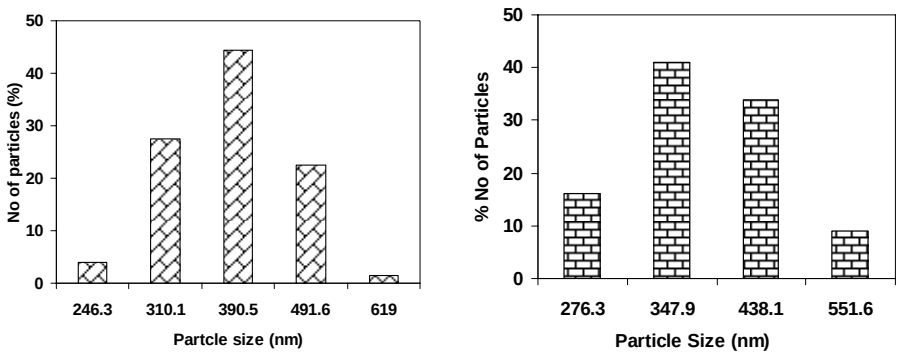

Figure 1 Nano particle distribution of chitosan enzyme composite (a, isopropanol, b acetone)

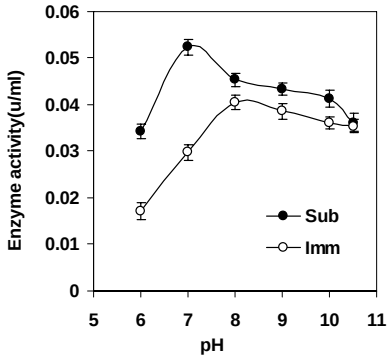

Figure 2 pH profile of immobilized & Native enzyme

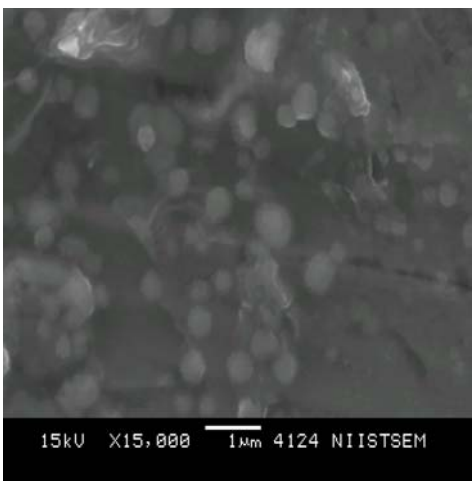

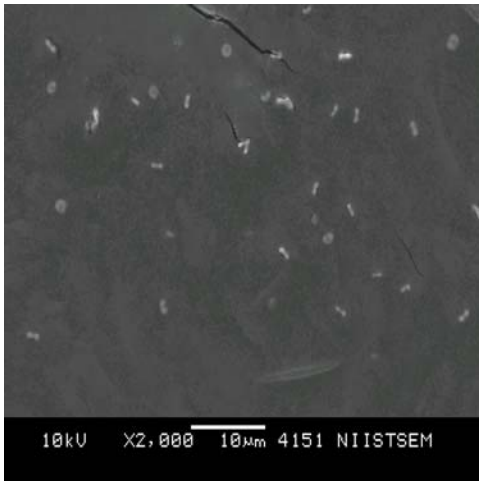

Figure- 3 SEM micrograph of EFNP of chitosan

.

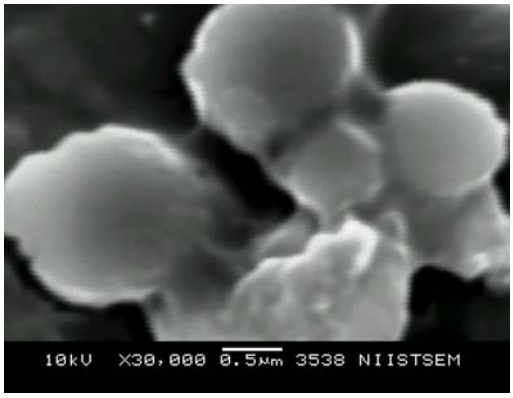

Fig-4 SEM image of EFNPs of galactomannan

Figure- 5 TEM micrograph of chitosan nano particles

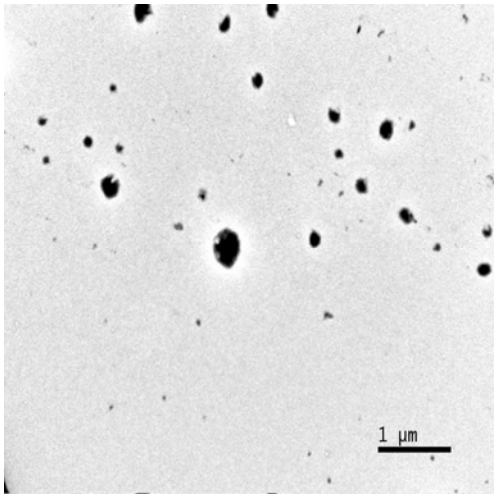

Preparation of polyvinylalcohol based thin film composite nanofiltration membranes: Application in the removal of hardness from brackish water

J.M.Gohil[*] and P.Ray[#]
Reverse Osmosis Discipline, Central Salt and Marine Chemicals Research Institute (CSIR), Bhavnagar, Gujarat, India.
E-mail: paramita022002@yahoo.co.in

Abstract
Polyvinyl alcohol (PVA) (degree of hydrolysis 86-87%), crosslinked with maleic acid (MA) has been used successfully as barrier layer of polysulphone (PSF) based thin film composite (TFC) membranes. The crosslinking of PVA and its presence in PSF matrix has been established by FTIR and contact angle study. PVA TFC membranes show dense phase morphology. The effect of variation of crosslinker (MA) dose, cure time and temperature on membrane performance (flux and rejection of inorganic salts) have been studied and the optimum membrane compositions were evaluated. Such membranes show differential rejection among the sulphate and chloride salts. On an average 65% difference exists between the rejection of $MgSO_4$ (70-90%) and NaCl (15-35%). The overall trend of rejection by such membranes is $R_{Na_2SO_4} > R_{MgSO_4} > R_{NaCl} > R_{MgCl_2} \cong R_{CaCl_2}$ (R = Rejection). The average molecular weight cutoff (MWCO) of such membranes varies between 250-450 Dalton. These membranes may be useful for the removal of dissolved sulphates (salts) and partial desalination of brackish water.

Introduction
Pressure driven membranes have acquired a significant position in the area of separation science and technology [1]. Nanofiltration (NF) membranes are relatively new class of charged pressure driven membranes. Due to preferential selectivity towards ions, lower operating pressure and higher flux, NF membranes have wide scope of applications in water and waste-water treatment [2, 3]. Hard water is probably the most common water problem found not only at home but also in the industries causing scaling in boilers, cooling towers, pipelines and other industrial equipments. Treatment of hard water with nanofiltration membranes may be a unique solution to produce soft water. Polyvinyl alcohol (PVA) being a water soluble biodegradable polymer has immense potential as a membrane material because of its high water permeation and film forming characteristics [4, 5]. Additionally presence of innumerable number of hydroxyl groups in this polymer may impart a charge effect in closer vicinity and make the membrane suitable to act as nanofiltration membranes with preferential rejection towards multivalent ions than the monovalent ones.
The main target of the work is to prepare polysulphone based thin film composite membranes with PVA as the selective barrier layer. The membrane composition has been optimized and the rejection trends of such membranes in different mono and bivalent salts have been evaluated.

Experimental
Materials:
Poly (vinyl alcohol) (PVA), with Mol. Wt. 1, 25,000, degree of hydrolysis 86-87%, Sodium chloride, Magnesium chloride, Calcium chloride, Magnesium sulfate, Sodium sulfate, Glycerol , all AR grade , supplied by SD Fine Chemicals, India.
D-Glucose Anhydride, LR grade, supplied by NICE Chemicals; Sucrose, LR grade, supplied by SRL; Raffinose pentahydrate, LR grade, supplied by Loba Chemie.

Membrane Preparation Method:
PVA solution 1% (w/w) (containing different dose of MA) was poured on PSF ultrafiltration membrane (prepared by phase inversion technique and acted as a porous support) mounted on a glass plate [6, 7].

Excess PVA solution was drained off and the membranes were dried at ambient temperature. The membranes were subsequently heated in oven at a temperature of 125±2 ºC for 30 minutes.

Characterization of Membranes:

FT-IR: The IR spectrum of PSF ultrafiltration and cross-linked PVA TFC membranes (of size 6 cm × 3 cm) were recorded in the middle infrared region using a Perkin Elmer 400 FT-IR spectrometer.

Contact angle (θ): Contact angle of resulting PVA TFC membranes was studied by Wilhelmy plate method using Dynamic Contact Angle Tensiometer (DCAT 21, Data Physics).

Scanning electron microscopy (SEM): Phase morphology (Cross-sectional and topography) of the membranes were studied using Leo microscope at 15 kV accelerating voltage.

Membranes performance testing: The salt rejection characteristics of membranes were studied in RO test cell by passing aqueous feed solutions of mono and bivalent salts separately through the membranes at different pressure (150-350 psi). Permeate flux was studied and solute rejection was calculated with the help of equation 1. The concentrations of inorganic salts in feed and permeate were determined by inductively coupled plasma spectrometry (ICP), chemical analysis and conductivity measurements.

$$Solute rejection(R)(\%) = \left[1 - \frac{Concentration\ of\ solute\ in\ permeate}{Concentration\ of\ solute\ in\ feed}\right] \times 100 \qquad (1)$$

Molecular weight cut-off (MWCO): A mixed solution containing glucose, sucrose, raffinose and glycerol each of 500 ppm was passed through the membranes. The percent organic solute in feed and permeate was analyzed by High performance liquid chromatography (HPLC) and Total organic carbon (TOC) analysis. The solute rejection was calculated by using the formula 1. The solute rejection above 85% was taken as MWCO of membranes.

Result and Discussion

The base PSF substrate was prepared from 17% PSF solution and PVA layer was coated with 1% PVA solution containing MA as curative in the concentration range from 2-50% (w/w with respect to PVA). The IR spectrum of PSF base substrate membrane is shown in figure 1(graph I). The existence of PVA at the surface of PSF TFC membranes is indicated by the peak at 3,200-3,400 cm^{-1} (Figure1, graph II), which is the characteristics of OH of PVA. The peak at 1,335 cm^{-1} is due to the ester linkages formed by the cross-linking of PVA with MA.

Contact angle reflects the hydrophilicity of any surface. PVA coating provides the hydrophilicity to hydrophobic PSF membranes. The hydrophilic nature of PVA TFC membranes are reflected by their average lower contact angle (81º) value compare to that of hydrophobic PSF membranes (89.5 º).

Cross sectional morphology of PSF membranes show a wide open pore structure (Figure 2A). However coating of PVA partially masks the polysulphone layer and overall reduction in the average pore size is observed (Figure 2B).

Effect of different process parameters on membranes performance:

Effect of variation of curative dose on membrane performance: To see the effect of MA concentration on stability of rejection layer, the flux (Figure 3) and rejection (Figure 4) profiles of the membranes (varying in the cross-link density of the rejection layer) were tested in continuous mode for a period of 24 hours using 500 ppm $MgSO_4$ solution. The membranes were cured at a temperature of 125±2 ºC for duration of 30 minutes. It is observed from Figure 3 that lowers the curative dose higher the membrane flux. However all the membranes show almost consistent flux over the studied period irrespective of the cross-linker dose. It is also observed (Figure 4) that in the rejection profiles there is a slight fall with time for membranes prepared with lower curative dose of 2 and 5% MA. However for MA dose >5% the rejection remains constant with time. Hence 5-10% concentration of MA may be considered as optimum for curing of such membranes.

Effect of cure time on membrane performance: Membranes were prepared from 17% PSF and 1% PVA-1 with MA concentration of 10% (w/w) cured by varying the cure time from 10-40 minutes at a temperature

of 125±2 ºC. Desalting performance of such membranes was studied in continuous mode for a period of 24 hours. It is observed (Figure 5) that membranes cured for all selected cure time except the lowest one (10 minutes) show almost constant flux and rejection with time. It is seen from Figure 5B that the rejection for membranes cured for 30 and 40 minutes are almost the same, whereas there is an average 15% rejection enhancement by varying the cure time from 20 to 30 minutes without much sacrifice in the flux. Hence 30 minutes cure time was selected as optimum.

Molecular weight cut off: The separation profile of different organic compounds (varying molecular weight from 90 to 600 gm/mole) with the variation of curative dose and cure time for different PVA TFC membranes are shown in Figure 6. It is seen that more the cross-link density of the barrier layer (due to higher cross-linker dose) higher the rejection of any selected organic compound. The lowest selected cross-linker dose of 2% produces membrane with no specific molecular weight cut off in the selected range i.e. 90-600 Dalton. The higher range of cross-linker doses i.e. 20-50% MA, produce membranes with MWCO in the range of 200-300 Dalton. For membranes with MA dose of 10%, MWCO values are between 350-450 Dalton.

Membranes performance with different inorganic salt solution: The desalting performances of the membranes were tested with different electrolyte solutions. The performances of the membranes (flux and rejection) varying in their curative dose are presented graphically in Figure 7. The % rejections of sulphate salts ($MgSO_4$ and Na_2SO_4) are almost same for all the selected membranes irrespective of their curative dose. The rejection of the chloride salts are much lesser than the sulfate salts, which may be due to higher repulsion of sulfate than chloride by the charged surface of the membranes. Although the variation of curative dose (2-50%) has negligible effect on the % rejection of sulphate salts but there is a gradual increase in rejection of chloride salts with increase in MA concentration which may be due to a synchronization of charge enhancement and membranes tightening.

Conclusions:

The overall trend of rejection by such membranes is $R_{Na_2SO_4} > R_{MgSO_4} > R_{NaCl} > R_{MgCl_2} \cong R_{CaCl_2}$ (R = Rejection). The average MWCO of the membranes varies between 350-450 Dalton. As for such membranes 65% difference is observed between the rejection of $MgSO_4$ (R 70-90%) and NaCl (R15-35%), hence, they may be useful for the removal of dissolved sulphate hardness and partial desalination of brackish water.

Acknowledgement: Financial assistance from CSIR, India is highly acknowledged.

References:

[1] Amjad Z. Ed.; Reverse Osmosis: Membrane Technology, Water Chemistry, and Industrial Applications, Van Nostrand Reinhold: New York, 1993.
[2] Ahn KH, Cha HY, Yeom IT, Song KG. Desalination 1998; 119(1-3):169-176.
[3] Ikeda K, Kimura S, Ueyama K. Maku 1998; 23:266-272.
[4] Krumova M, Lopez D, Benavente R, Mijangos C, Perena JM. Polymer 2000; 41(26):9265-9272.
[5] Suzuki M, Yoshida T, Koyama T, Kobayashi S, Kimura M, Hanabusa K, Shirai H. Polymer 2000; 41(12):4531-4536.
[6] Radovanovic P, Thiel SW, Hwang ST. Journal of Membrane Science 1992; 65(3):213-229.
[7] Kesting RE. A structure perspective' in: Synthetic Polymeric membranes, 2nd. ed. Wiley, 1985. Biomaterial membrane

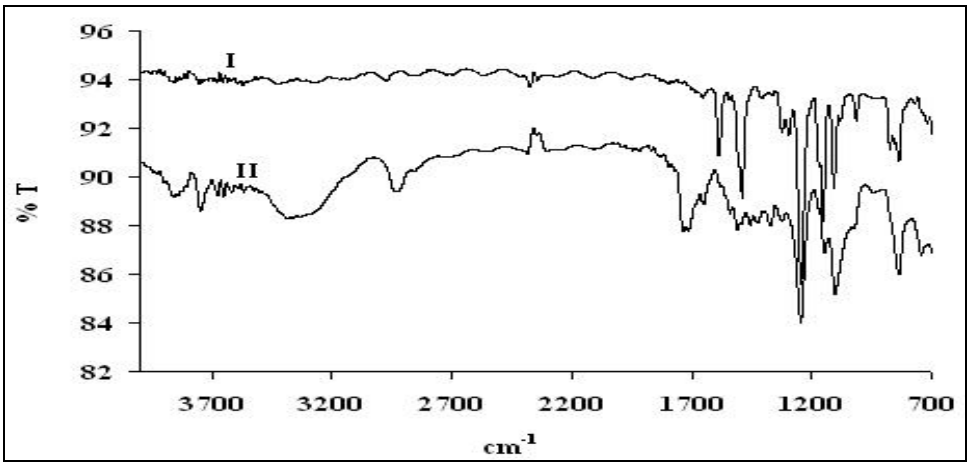

Figure 1. IR spectra of (I) PSF base membrane and (II) PVA TFC membrane

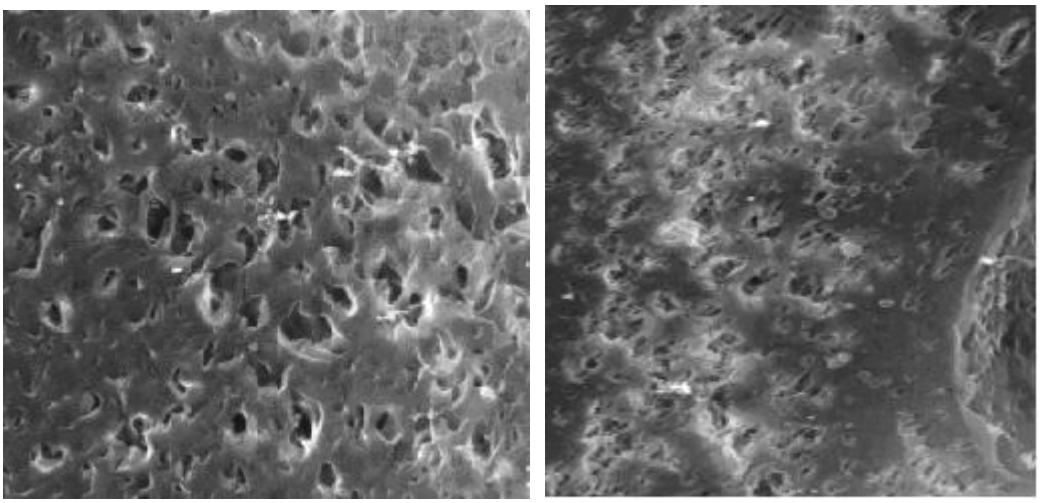

A **B**

Figure 2. SEM micrograph of A: PSF and B: PVA TFC membranes

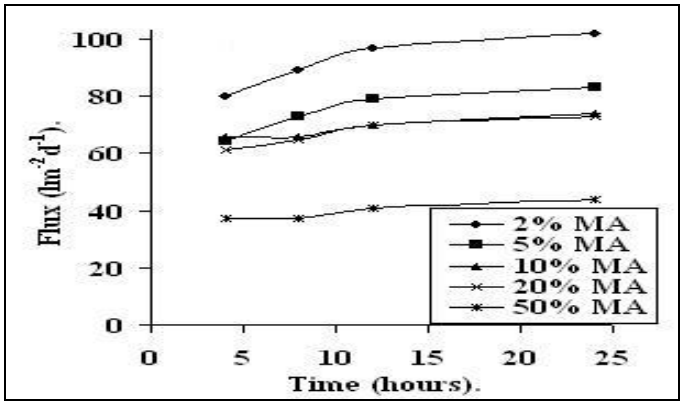

Figure 3. Time vs. Flux; for PVA TFC membranes with different cross-link densities, operating pressure 150 psi.

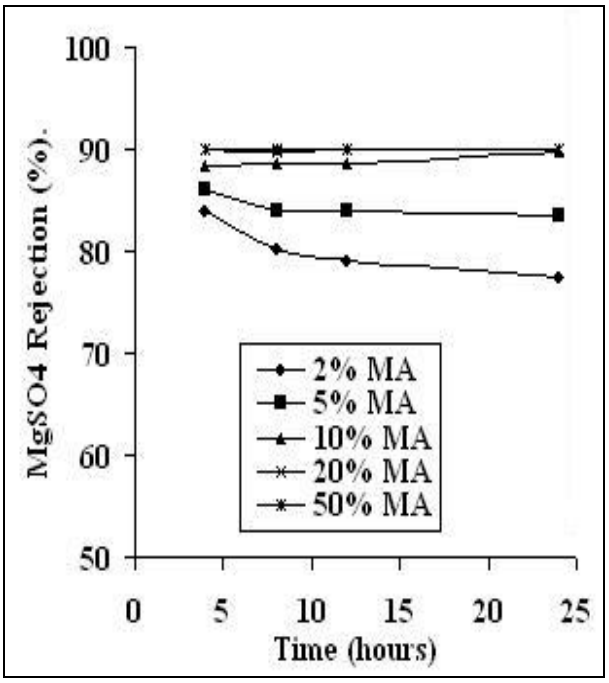

Figure 4. Time vs. % Rejection; for PVA TFC membranes with different cross-link densities, Operating pressure 150 psi.

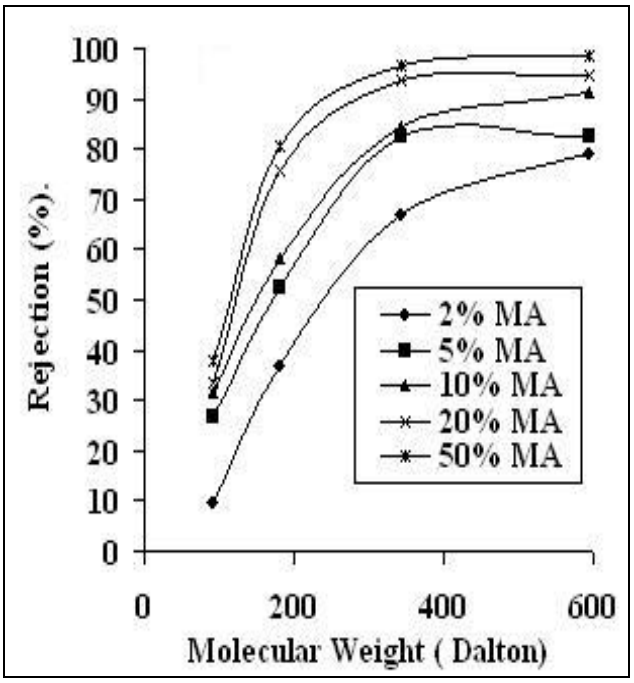

Figure 6. Molecular weight vs. % Rejection of TFC membranes with variable cross-link density of PVA layer. Operating pressure of 150 psi

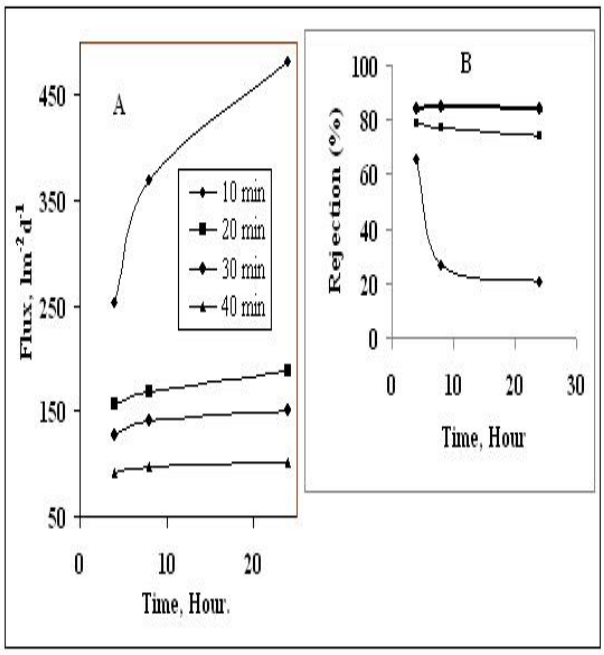

Figure 5. Variation of flux (A) and Rejection (B) with time for membranes cured for different time periods, at 125±2 ºC. MA 10%.

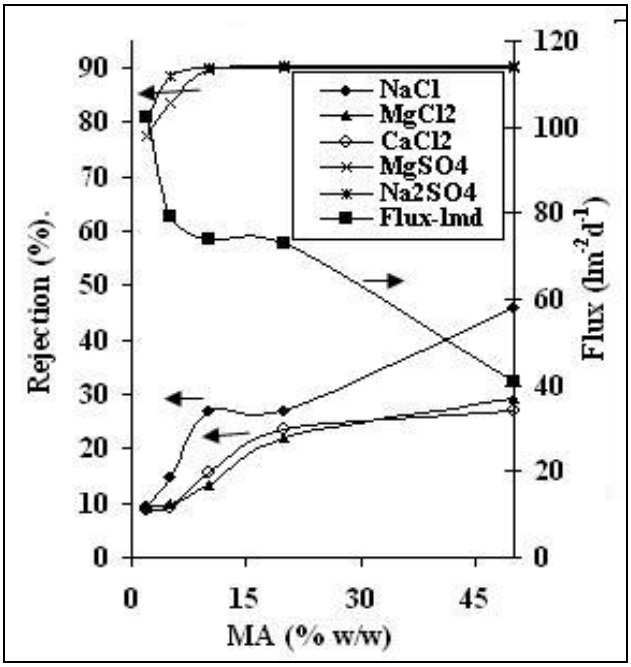

Figure 7. Variation of flux and rejection with MA concentration. Operating pressure of 150 psi

Photodegradable polypropylene film – Natural weathering studies

K. Rajakumar [a], V. Sarasvathy[a], A. Thamarai Chelvan [b], R. Chitra [c] and C. T. Vijayakumar [a,*]

[a] Department of Polymer Technology, Kamaraj College of Engineering and Technology, S. P. G. C. Nagar, K. Vellakulam Post – 625 701, Tamilnadu, India
[b] Post-graduate and Research Department of Chemistry, Thiagarajar College, P.O. Box 625 009, Madurai, India
[c] Centre for Fire, Explosive and Environment Safety, DRDO, P.O. Box 110 054, Timarpur, Delhi, India.

[*] E-mail: ctvijay22@yahoo.com

Abstract

Polypropylene (PP) is an attractive and dominating material for packaging due to its low cost, high tensile strength, gloss and versatility and hence, their consumption increases thereby littering, which leads to environmental pollution. To solve these problems, out of various technologies available, photodegradation seems to be a better choice due to the freely available sunlight. The polymers that degrade by peroxidation followed by bioassimilation of the oxidation products are more environmentally acceptable than the biodegradable polymers. In the present work, transition metal salt of stearic acid was synthesized as prodegradant (MF01) and incorporated in PP to enhance the photodegrdability. The virgin polypropylene and its blend with 0.2 % MF01 were extruded into films of 60 μm thickness. The films were naturally weathered from the period, December 2006 to March 2007 (winter season) and May 2007 to July 2007 (summer season). The photodegradation behavior was studied using Fourier Transform Infrared Spectrophotometry (FTIR), Universal Testing Machine (UTM) and Scanning Electron Microscope (SEM). A steep increase in the various indices like hydroperoxide, hydroxyl, carbonyl, lactone, ester, carboxylic acid, vinylidene and crystallinity were noted for virgin PP after 50 days of exposure whereas these values increased after 15 days of exposure for the prodegradant added PP. The sudden decrease in the elongation at break (%) for the materials signifies chain scission. PP films having higher carbonyl index values showed surface cracks in the scanning electron micrographs, indicating the degradation of the material.

Introduction

The synthetic polymers are used in vast areas based on their inertness towards outside factors like heat, radiation, chemicals and micro organism, but recently, this inertness has become a major contributor to the serious problem of solid waste disposal [1]. Increasing amounts of municipal solid waste (MSW), decreasing the landfill capacity for plastic disposal and slow degradation of plastic litter in the environment, which lead to generate intense interest in degradable plastics in the last quarter century.

According to estimates, plastic wastes represent 15-25% of municipal solid waste. To minimize this problem, there are three ways to utilize the plastic waste: landfilling, incineration with or without energy recovery and recycling. The largest amount of plastic waste is going for landfilling (65-70%), incineration and recycling amounts to about 20-25% and 10% respectively [2, 3]. Therefore, the environmental problem is still present. So, many researchers have intense interest to develop polymers that are more degradable in the natural environment after use, is desired for environmental conservation. Many authors have been investigating about degradable polymers which were reported in several research articles [4-7].

Now a days polypropylene has achieved in dominating position based on the excellent price/property relationship thereby it can be applied in various field. Also it is an attractive material

for packaging owing to their low cost of production, higher tensile strength, gloss and versatility [8]. Therefore, increase in its consumption leads to littering and causes environmental problem. So, polypropylene was taken as the material for investigation in the present study.

The degradation behaviour of PE using various photoinitiators under natural weathering condition was investigated [9, 10]. The photodegradation behaviour of polypropylene under natural weathering conditions using non-toxic transition metal carboxylate as prodegradant has not been pursued earlier. Iron stearate was taken as the prodegradant for polypropylene and the photo-degradability of polypropylene under natural weathering situations was investigated and the results are discussed.

Experimental

Materials

Stearic acid, potassium hydroxide, ferric sulphate monohydrate were used as received to synthesize ferric stearate. Iron salt of stearic acid (MF01) was synthesized by reacting ferric sulphate monohydrate with the potassium salt of the fatty acid. Polypropylene (Repol Grade H100EY) obtained from Reliance Industrial Limited, Jamnagar, India was chosen for the present study. The virgin polypropylene (4Kg) was blended with 0.2% of prepared prodegradant using a blender. The virgin PP and the prodegradant blended PP were blown into films using an extruder (Film width = 36cm and Film thickness = 60μm).

Methods

The films were naturally weathered on a suitably designed and fabricated outdoor exposure rack, which was located in the premises of Kamaraj College of Engineering and Technology, S.P.G.C. Nagar, K.Vellakulam Post - 625 701, Virudhunagar, India. The natural weathering of all PP films was carried out from December 2006 to March 2007 (winter season) and May 2007 to July 2007 (summer season). During the course of natural weathering the average temperature, pressure and humidity were about 34 °C, 748 mmHg and 40 % rel. respectively. The average visible and UV light intensity were 937 x 10^2 LUX and 998 uW/cm^2 respectively. The sampling was done at regular intervals to assess the changes occurring in the material during the natural weathering. Fourier Transform Infrared Spectrophotometry (FTIR), Universal Testing Machine (UTM) and Scanning Electron Microscopy (SEM) were utilized to follow the chemical and physical changes occurring in the material.

Results and Discussion

FTIR Studies

From the FTIR spectra of the weathered PP samples, hydroperoxide, hydroxyl, carbonyl, lactone, ester, carboxylic acid, vinylidene and crystallinity indices have been calculated. The characteristic infrared absorption frequencies for the different functional groups are listed in Table 1. In the present work, the band at 974 cm^{-1} (CH_3- rocking) was chosen as the reference peak, because it remains unchanged during photodegradation process.

Carbonyl index is the most used parameter to monitor the degree of degradation in polyolefins [11]. The carbonyl index was calculated as the ratio of the maximum absorbance at 1715 cm^{-1} to the absorbance at 974 cm^{-1}. The carbonyl index value increases with increasing exposure period only after certain days of exposure, which can be taken as the induction period for degradation. From Fig. 1, it is clear that PP weathered at winter season starts to degrade after 50 days of exposure whereas for PP weathered during summer season, the induction period for degradation was found to be 40 days. Incorporation of the prodegradant (iron stearate, MF01) in PP drastically reduces this induction period. These results confirm the fact that the added prodegradant plays an important role to induce photodegradation. Environmental conditions like temperature, UV intensity, visible light intensity, etc., also play a definite role in the photodegradation behaviour of PP. In general, carbonyl groups

were observed as a broad peak in the region of 1800 – 1700 cm^{-1} in the FTIR spectrum of weathered PP due to the overlap of different degradation products like lactone, ester, ketone, carboxylic acid, etc [12]. The carboxylic acid group concentration (Fig. 2) is higher while the lactone concentration is low because the carboxylic acid is the final stable product of degradation [13]. A similar trend was observed in the study of polypropylene natural weathering at Messina, Italy by Gallo et al.[14].

Hydroperoxide is the initial product of photooxidative degradation of PP and hence hydroperoxide group formation and its decomposition in the course of natural weathering is an important aspect, which may justify the faster degradation of materials. The hydroperoxide index was calculated as the ratio of the maximum absorbance at 3445 cm^{-1} to the absorbance at 974 cm^{-1}. From Figs. 1, 3a and 3b, the concomitant increase of the hydroperoxide groups and the carbonyl groups are explicit. It reveals that hydroperoxide formation and its decomposition take place simultaneously since the generated tertiary hydroperoxide is unstable. A similar trend has also been observed in the case of hydroxyl index variation.

In the case of photooxidation of PP, vinylidene group formation is the most probable one when compared to the vinyl group due to the presence of pendent methyl group. The vinylidene index was calculated as the ratio of absorbance at 888 cm^{-1} to the reference peak absorbance at 974 cm^{-1}. An irregular trend has been observed for this index. Certain environmental conditions lead to the consumption of this group to produce free radicals, whereas some environmental features favour the formation of this group.

In order to gather information regarding the variation of crystallinity as a function of outdoor exposure days, the ratio of absorbance at 998 cm^{-1} to the absorbance at 974 cm^{-1} was used to calculate the crystallinity index. The first band is regularity band characteristic of the crystalline PP, whereas the second band corresponds to both crystalline and amorphous phases of PP. In Figs. 1-3, it is clear that as the hydroperoxide, hydroxyl, carbonyl, lactone, ester, carboxylic acid, etc., indices increases, the crystallinity index is also increasing. This may be explained due to the formation of new low molecular weight photooxidation products capable of forming new crystalline domains.

Measurements of Tensile Properties

The elongation at break (%) can be frequently used to monitor the degradation of polymers. From Fig. 4, it is found that in the case of PP virgin, the elongation at break shows slight variation up to 45 days of exposure and then a sudden drop is seen. The value reaches near zero value soon indicating main chain scission in the polymer molecule. But, in the case of prodegradant added PP materials, the elongation properties are lost within 15 days of exposure, thereby rendering the film useless for practical applications.

Tensile strength is an important measure of product quality to certify the product and therefore its variation during weathering is one of the important parameter used to follow degradation. In almost all cases, PP films and PP containing prodegradant, tensile strength decreased considerably at the initial stages of weathering. Then a gradual decrease is noted and finally there is a sudden drop in the tensile strength values. This phenomenon may be attributed to chain reorganization and/or lower degree of orientation during natural weathering.

SEM studies

The scanning electron micrographs of weathered PP virgin (45 days) and its blend with MF01 (11 days) films are shown in Fig. 5. The SEM images clearly show the formation of cracks in the weathered material. The increase in carbonyl index, the decrease in elongation at break and the formation of cracks are enhanced at a much earlier stage when the prodegradant is added to PP.

Conclusion

A steep increase of carbonyl, hydroperoxide, hydroxyl, lactone, ester, carboxylic acid and crystallinity indices and a sudden decrease of elongation at break and tensile strength indicate the occurrence of main chain scissions in the materials investigated. Further, from the above results one can reasonably conclude that the added prodegradant (ferric stearate) plays an important role in initiating the photodegradation of polypropylene during weathering. Other weather parameters like temperature, UV intensity, visible light intensity, etc., are contribute substantially to the photooxidative degradation of the material.

References

1. Barenberg SA. In: Brash JL, Narayan R, Redpath AE, editors. Degradable Materials, Boston: CRC Press, 1990. pp. 559-583.
2. Misklczi N, Bartha L, Deak G, Jovev B. Polym Degrad Stab 2004; 86:357.
3. Aguado J, Serrano DP, Guillet JE. In: Clark JH, editor. Polymers and Ecological Problems, New York: Plenum Press, 1973.
4. Scott GJ. Polym Sci Symp 1976; 57:357.
5. Griffin JGL. In: Chemistry and technology of biodegradable polymers, London: Blackie Academic and Professional, 1994 (chapters 1-3).
6. Scott G. Degradable Polymers: Principles and Applications, London: Chapman & Hall, 1995 (chapter 9).
7. Scott G. Polymers and the Environment, Cambridge: Royal Society of Chemistry, 1999 (chapter 2).
8. Roder H, Vogl O. Prog Polym Sci 1999; 24:1205.
9. David C. Trojan M. Demarteau DA. Polym Degrad Stab 1992; 37:233.
10. Sheikh N, Akhavan A, Naiman F, Kholou F, Hasanpour S, Sohrabpour M. J Polym Env 2006; 14:103.
11. Carlsson DJ, Wiles DM. J Polym Rev 1976; 14:65.
12. Hamid SH, Prichard WH. Polym Plast Technol Eng 1988; 27:303.
13. Morlat S, Mailhot B, Gonzalez D, Gardette J. Chem Mater 2004; 16:377.
14. Gallo R, Severini F, Ipsale S, Fanti ND. Polym Degrad Stab 1997; 55:199.

Table 1. Characteristic infrared absorption frequencies

Functional Group	Frequency Range (cm^{-1})
Hydroxyl and Hydroperoxide	3600 - 3200
Carbonyl	1800 – 1700
Ketone	1725 – 1715
Carboxylic Acid	1712 – 1705
Ester	1750 – 1735
Lactone	1785 – 1760
Vinyl	909
Vinylidene	888

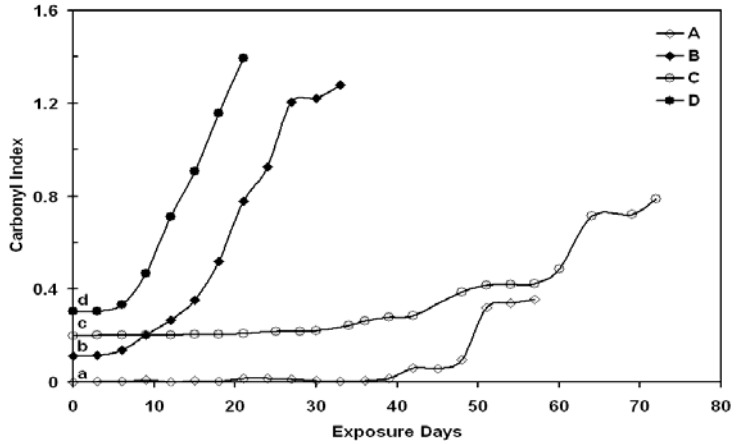

Fig. 1. Carbonyl index variation of weathered materials: Winter - (A) PP Virgin and (B) PP:MF01; Summer - (C) PP Virgin and (D) PP:MF01. The curves B, C and D are shifted along the ordinate by the distance ab, ac and ad respectively

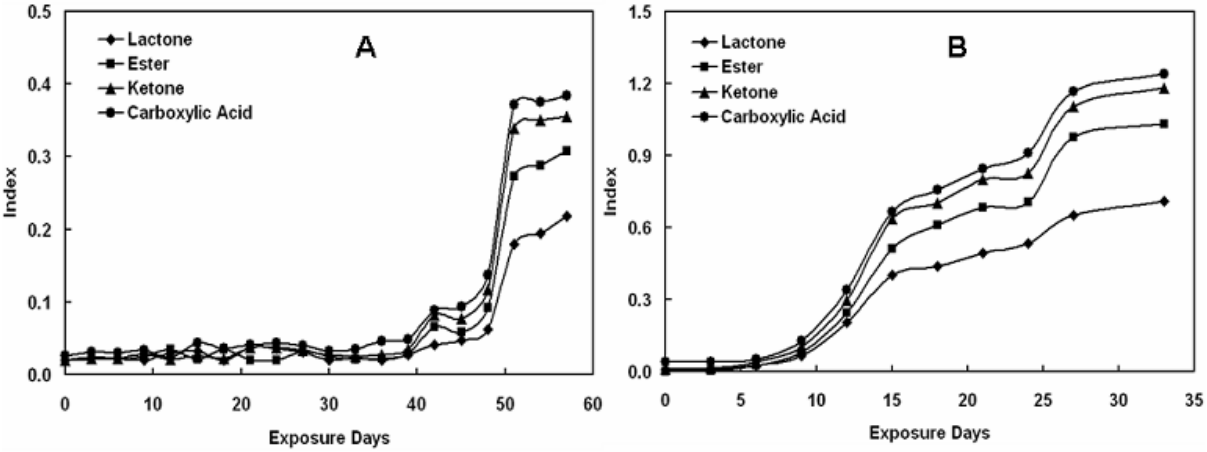

Fig. 2. Lactone, ester, ketone and carboxylic acid indices for weathered materials (A) PP Virgin; (B) PP:MF01 during winter

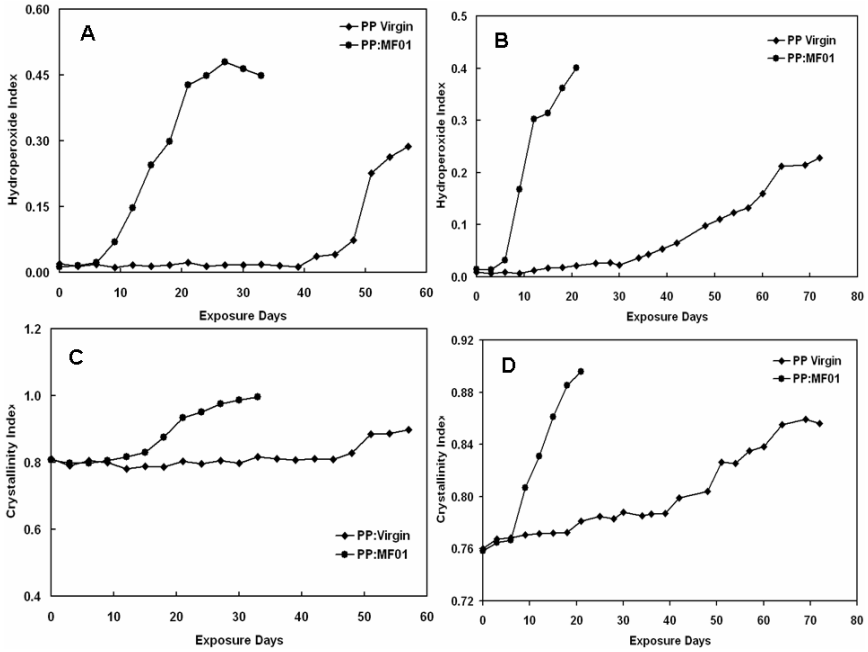

Fig. 3. Hydroperoxide and Crystallinity index variation: Winter - (A) and (C); Summer - (B) and (D)

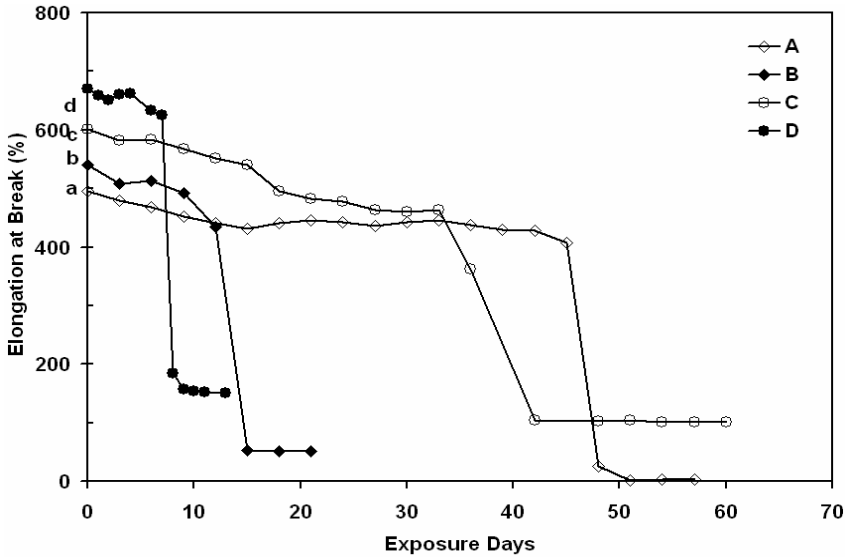

Fig. 4. Variation in the elongation at break (%) of weathered materials: Winter - (A) PP Virgin and (B) PP:MF01; Summer - (C) PP Virgin and (D) PP:MF01. The curves B, C and D are shifted along the ordinate by the distance ab, ac and ad respectively

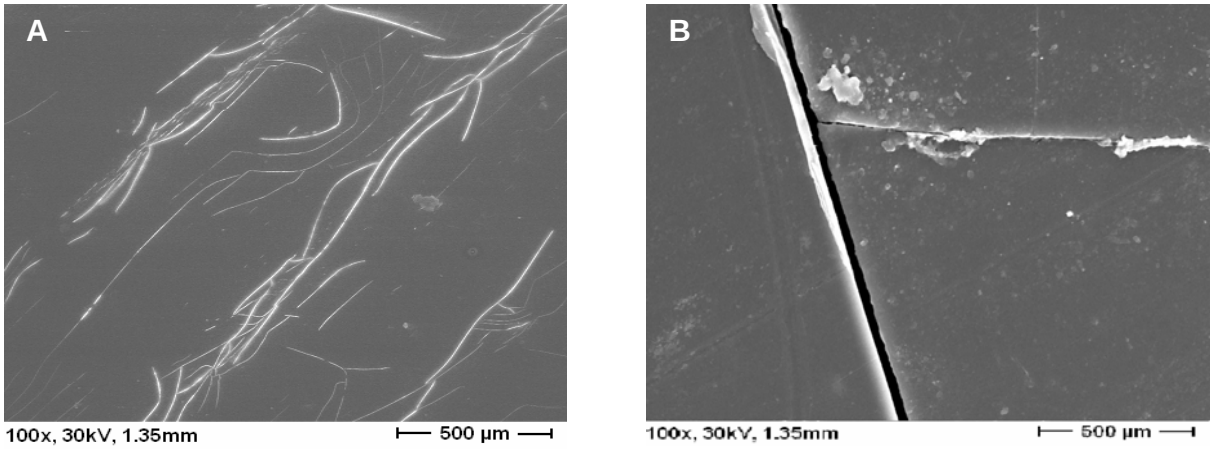

Fig. 5. SEM photographs of weathered materials: (A) PP virgin and (B) PP:MF01 blend

Swelling behaviour of hydrogels based on crosslinked NR/PEG block copolymers.

Christina George and M.R. Gopinathan Nair
School of Chemical Sciences, Mahatma Gandhi University, Priyadarshini Hills
Kottayam 686560, India.
E-mail: christeena.george@gmail.com

Abstract

A series of NR/PEG block copolymers were prepared from polyethylene glycol (PEG) and hydroxyl terminated liquid natural rubber (HTNR) by solution polymerization and dynamics of the water sorption process were studied. The effect of NCO/OH ratio and pH of the swelling medium were investigated with respect to the water sorption characteristics of the hydrogels. Results indicated that the hydrogels exhibited overshooting effect in their dynamic swelling behaviour. Mechanism of sorption, sorption kinetics and transport coefficients including diffusion coefficient, sorption coefficient and permeation coefficient were also determined. The sorption behaviour was found to vary with the variation in NCO/OH ratio of the block copolymers.

Introduction

Hydrogels are multi – component systems comprising of hydrophilic polymeric networks capable of absorbing enough water (> 20% of its dry weight) causing macroscopic changes in the sample dimension while maintaining its structural integrity. Due to the relatively high water content of these materials, they have found a plethora of applications in biomedical, pharmaceutical, food and environmental fields. Their high water content lends them high biocompatibility and makes them well tolerated when implanted in vivo. Consequently, they have emerged as promising candidates for a variety of biomedical applications such as drug delivery systems [1], wound dressings [2], contact lenses [3], artificial implants [4] etc. However, on increasing the water content, the mechanical strength of the hydrogel becomes lower and the gel transparency can decrease as a consequence of a macrophase separation between water and polymer. Hence to achieve a gel with high mechanical strength, transparency and water content, a composite molecular structure is needed. This structure will comprise of a hydrophilic component that absorbs large amounts of water and a hydrophobic component, which improves the mechanical strength [5]. It is according to this idea that for our study we synthesized amphiphilic NR/PEG block copolymers with hydrophobic natural rubber (NR) and hydrophilic polyethylene glycol (PEG).

The multitude of hydrogels available leaves numerous choices for polymeric formulations. The best approach for development of a hydrogel with desired characteristics is to correlate the macromolecular structure of the polymer with desired swelling characteristics. The swelling studies not only describes the amount of water contained within the hydrogel at equilibrium but also give ample insight into the network structure of the gels and the transport mechanisms of the water uptake process[4]. During these studies controllable volume change can be brought about in the hydrogels by changing the surrounding conditions such as pH [6], temperature [7], salt concentrations [8], chemistry [9], electric field [10], photo irradiation [11] and solvent composition [12].

Polyethylene glycol (PEG) with its desired set of properties has always been a front-runner among synthetic polymers used for designing hydrogels primarily because of its nontoxicity and biocompatibility [4]. The dynamic swelling behaviour of amphiphilic block copolymer based on polyethylene glycol (PEG) and polybutyl acrylate (PBA) was reported by Wang et al [13]. Bajpai

et al [4] reported the swelling behaviour of hydrogels prepared from polyethylene glycol (PEG) and poly (acrylamide-co-styrene) (PAMS). The water uptake of this hydrogel varied sensitively with the variation of the contents of hydrophilic polymer, crosslinking agent and temperature of the swelling medium. Karaky et al [14] synthesized a new type of pH switchable suparamolecular sliding gels based on polyrotaxanes of polyethyleneimine-block-poly (ethylene oxide)-block-polyethyleneimine block copolymer and α - cyclodextrin.

In the present work, transport behaviour of water through NR/PEG block copolymer with varying NCO/OH ratios has been investigated. The shape of diffusion profile, mechanism of sorption, sorption kinetics and the transport coefficients including diffusion coefficient, sorption coefficient and permeation coefficient are described here. Effect of NCO/OH ratio and pH on swelling behaviour of these block copolymers is also described.

Experimental

Materials

Natural crumb rubber (ISNR-5): Weight average molecular weight = 8,20,000; Intrinsic viscosity in benzene at 30^0C= 4.45 dL/g; Wallace Plasticity, P_0=39 was supplied by Rubber Research Institute of India, Kottayam, Kerala. Hydrogen peroxide (30% w/v) supplied by E. Merck, India was used without further purification. Toluene (reagent grade) obtained from E. Merck; India was used as solvent without further purification. Methanol (reagent grade) supplied by E. Merck, India was used without further purification. Toluene diisocyanate (TDI) (80/20 mixture of 2,4- and 2,6- isomers) was supplied by Aldrich, Germany and was used as received. Dibutyl tin dilaurate (DBTDL) supplied by Fluka, Switzerland, was used as catalyst without further purification. Chloroform (laboratory reagent grade) was dried with anhydrous calcium oxide and then distilled before use. It was supplied by E. Merck, India. Polyethylene glycol (PEG) of molecular weight 4000 supplied by Aldrich, Germany was used as received. Water used for the swelling studies was double distilled and deionized.

Hydroxyl terminated liquid natural rubber (HTNR) of number average molecular weight 4000 was prepared in the laboratory by the photochemical degradation of natural rubber as per reported procedure [15]. It was reprecipitated thrice from toluene using methanol and dried at 70^oC – 80^oC in vacuum.

Synthesis of the block copolymer

HTNR was dissolved in chloroform to get a 35% solution and taken in a flat-bottomed flask equipped with a magnetic stirrer, nitrogen inlet and outlet, water condenser and a dropping funnel. Dibutyl tin dilaurate (DBTDL) catalyst (6.1% by weight of HTNR) was added and the solution brought to reflux with vigorous stirring. Variation in crosslink density was brought about by varying the NCO/OH ratio. TDI was added drop wise over a period of 30 min followed by 2 h of the reaction to end cap HTNR. This was accompanied by the addition of the required amount of PEG as a solution in chloroform (35% w/v) drop wise during 1.5 h followed by 2 h of the reaction. The excess chloroform was distilled off and the viscous polymer was cast in tray treated with silicone release agent. The sheet removed from the tray after 24 h was kept in vacuum oven at 60^0C to remove traces of the solvent present and then cured at 70^0C for 24 h followed by one week ageing at room temperature in a moisture-free atmosphere [16].

Polymer designation

The block copolymer studied in this work is designated as NR/PEO (4000/4000)-1 which indicates that the sample contain HTNR and PEG where HTNR molecular weight is 4000 and PEG molecular weight is 4000. The number indicates the order of synthesis with the variation in NCO/OH ratio (Table I).

Swelling experiment

Circular shaped samples (diameter ~ 13 mm) were cut from the block copolymer sheet by means of a sharp edged steel die and thickness of the sample was measured with an accuracy of ± 0.01nm. Dry weight of the cut samples were taken before immersion into distilled water at room temperature. The samples were periodically removed from test bottles. Then the samples were weighed on an electronic balance (Shimadzu, Libor AEU-210, Japan) and immediately replaced into the test bottles. This procedure was continued until equilibrium swelling was attained in the case of each sample. The time taken for each weighing was kept constant to a minimum of 20-30s in order to avoid errors due to the escape of solvent from the samples. The results of these experiments were expressed as moles of solvent uptake by 100 g of polymer (Q_t mol %).

Results and Discussion

The swelling behaviour of the hydrogels depends on the nature of the polymer and the environmental conditions. The polymer's nature involves crosslink density, ionic content etc. The environmental conditions include pH and temperature [6,7]. A series of NR/PEG copolymeric hydrogels was investigated in terms of their swelling characteristics. The effect of NCO/OH ratio and pH on the swelling behaviour was studied.

Sorption dynamics and effect of NCO/OH ratio

The data from the sorption studies are plotted in Figure 1 with the percentage uptake of the penetrant against $t^{1/2}$, where t is the time taken to attain equilibrium. Since PEG is hydrophilic polymer and NR is hydrophobic in nature, the present block copolymer possesses these dual characteristics. In the case of a typical polar solvent like water, the interaction is restricted to only the matching hydrophilic domain in the block copolymer while the hydrophobic domain conveniently excludes it.

A remarkable feature that is observed in the sorption curves of the swelling ratio versus $t^{1/2}$ is that they are slightly sigmoidal initially and later level off. The sigmoidal shape is related to the time taken by the polymer chains to react to the swelling stress and realign themselves to accommodate the solvent molecules. Initially, due to the large concentration gradient, the swelling rate is too high. The end result of this behaviour is solvent induced stress in the polymer sample. However, as the concentration gradient decreases, the swelling ratio decreases and at equilibrium swelling the concentration differences almost vanishes [17].

In the NR/PEG hydrogels, Q_∞ mol% values varied with the variation in NCO/OH ratios (Table II). The maximum uptake was shown by the sample with NCO/OH ratio 1.1 followed by a decrease in the uptake values with the increase in NCO/OH ratios. This sort of behaviour maybe the outcome of increase in polymer mobility, free volume and better interactions existing in the sample with NCO/OH ratio 1.1.

Mechanism of sorption

The sorption data of the polymer – solvent systems for a circular geometry of the sample before the attainment of 55% equilibrium sorption have been fitted in the following empirical formula [18,19]

$$\frac{Q_t}{Q_\infty} = kt^n \qquad \text{.....(1)}$$

where Q_t and Q_∞ are the mol% increase in sorption at time t and equilibrium respectively. The type of diffusion mechanism has been analysed in terms of the empirical relation

$$\log \frac{Q_t}{Q_\infty} = \log k + n \log t \quad \ldots\ldots\ldots\ldots (2)$$

k and n have been determined from a least square fit of log Q_t / Q_∞ versus log T. Constant k depends on the structural features of the polymer system and its interaction with the solvent used [17]. The polarity and the size of the solvent along with the polar and non-polar segments in the block copolymer determine the value of k parameter. n is the diffusional exponent, which indicate the transport mechanism. If n =0.5, the mechanism of sorption is termed as Fickian, where the rate of polymer chain relaxation is higher than the diffusion rate of the penetrant. When n = 1, the mechanism is said to be non – Fickian where the chain relaxation is slower than the solvent diffusion. If the value lies between 0.5 and 1, then the mechanism follows anomalous transport where the polymer chain relaxation rates and the solvent diffusion rates are similar. By regression analysis, the values of n and k are obtained as slope and intercept and are consolidated in Table III. The correlation coefficient values are found to be 0.999. The values of n range from 0.42 to 0.61, which indicates that the mechanism of sorption follows Fickian mode in samples with lower NCO/OH ratios while the mechanism shifts to anomalous mode with a bias to non – Fickian mode in the samples with higher NCO/OH ratios. In the present study the k values do not show a regular trend.

Sorption kinetics

Sorption of liquid through polymer samples cause structural rearrangement, which induces kinetic behaviour that in turn are affected by the total free volume and its distribution in the polymer system. We have analysed the sorption data in terms of the first - order kinetic model. The first – order rate constant k_1 for the polymer – solvent system was obtained using the first – order equation [20]

$$dc/dt = k_1 (C_\infty - C_t) \quad \ldots\ldots\ldots\ldots\ldots\ldots (3)$$

where C_∞ and C_t are the concentration of the penetrant at equilibrium and time t respectively. C_∞ and C_t are equivalent to the equilibrium swelling Q_∞ and swelling at time t, which is Q_t. Integration of equation (3) gives

$$k_1 t = 2.303 \log [C_\infty / (C_\infty - C_t)] \quad \ldots\ldots\ldots (4)$$

Typical plots of log $(C_\infty - C_t)$ versus time is given in Figure 2 and the estimated rate constants for the penetrant are given in Table IV. A negative slope was observed and the values are found to range form 3.29×10^3 min^{-1} to 19.30×10^3 min^{-1}.

Transport coefficients

Diffusion in polymer is complex and depends strongly on the concentration, degree of swelling, solvent size and size of the voids in the polymer. From the slope θ of the linear portion of the sorption curve, the diffusion coefficient D has been calculated using [21]

$$D = \pi\left(\frac{h\theta}{4Q_\infty}\right)^2 \qquad \text{.....(5)}$$

where h is the thickness of the sample. Due to the swelling in a short period of time, swelling correction is necessary to get correct diffusion coefficient known as the intrinsic diffusion coefficient (D^*) [22]

$$D^* = \frac{D}{\varphi^{7/3}} \qquad \text{.....(6)}$$

where ϕ is the volume fraction of the polymer. The variation in D^* value depends on the nature of the crosslink, penetrant size and polarity. The values of D^* along with sorption and permeation coefficients are tabulated in Table V.

The D^* values varied with NCO/OH ratios, with the maximum value obtained in sample with NCO/OH ratio 1.1. With further increase in NCO/OH ratios, D^* values showed a steady decrease. This observation can be correlated to the equilibrium swelling uptake that was found to be maximum in sample with NCO/OH ratio 1.1. To sum up, D^* depends more on the molecular interaction between the penetrant and the polymer system. A better understanding of the interactions and their strengths can be obtained from the sorption coefficient S, which can be calculated as follows

$$S = \frac{M_S}{M_P} \qquad \text{.....(7)}$$

Where M_s is the mass of the solvent molecules at equilibrium swelling and M_p is the initial mass of the polymer sample [20]. The S value is high in sample showing high equilibrium swelling uptake values, i.e. the sample with NCO/OH ratio 1.1. The high S value in this system shows the better accommodation of the water molecules due to the favourable interactions with the polar region of the block copolymer. The permeability coefficient P depends on doth D and S, since permeation is a combined effect of diffusion and sorption [20].

$$P = D.S \qquad \text{.....(8)}$$

The permeation values are yet again high in sample with NCO/OH ratio 1.1. The P values reflect the net effect of diffusion and sorption. In the block copolymer studied, S values are higher compared to D^* and P, showing a larger tendency for the penetrant molecules to sorb rather than diffuse into the polymer. Thus sorption predominates over diffusion in the systems under study.

Effect of NCO/OH ratio and pH on overshooting effect

In Figure 1 and Figure 3, the dynamic swelling curves corresponding to copolymers swollen in water and at pH 9 respectively exhibit overshoot. Initially, the samples increase their swelling ratio, later on they reach a maximum and finally they deswell until an equilibrium value is reached. The sample with NCO/OH ratio 1.3, 1.4 and 1.5 exhibit overshoot in water while all the NR/PEG samples exhibit overshooting effect at pH 4, pH 7 and pH 9. We have attributed this feature to the anomalous transport with a bias to the non – Fickian mode (Table III). The primary factor contributing to overshooting effect is the difference existing between the relaxation and diffusion rates at experimental conditions. The stress generated due to the slow relaxation rate

compared to diffusion rate results in overshoot. Due to the thermodynamic interaction with macromolecular chains, water enters before these chains can relax or rearrange. Later the rearrangement of these chains result in partial exclusion of water leading to overshooting effect [23]. In short overshooting effect depends on the NCO/OH ratio and pH of the surrounding medium.

Conclusion

The water uptake of the hydrogel based on NR/PEG block copolymers varies sensitively with NCO/OH ratio. The maximum Q_∞ mol% uptake is shown by sample with NCO/OH ratio 1.1 followed by a decrease in the Q_∞ mol% values in heavily crosslinked samples. Increase in polymer mobility, free volume and better interactions existing in the sample with NCO/OH ratio 1.1 is the reason behind the high Q_∞ mol% uptake. The sorption kinetics has been studied and the experimental data suggests that the swelling process obeys first – order kinetics. Maximum D^* and S values are obtained in sample with NCO/OH ratio 1.1 which provide ample proof for the better molecular interactions existing between the polymer – water system in this sample. The S values of the block copolymers are higher compared to D^* and P values resulting in a precedence of sorption over both diffusion and permeation.
The entire block polymer samples exhibit remarkable overshoot at pH 4, pH 7 and pH 9 while in the case of samples swollen in water, the overshooting effect is limited to samples with higher NCO/OH ratios. The reason for the overshooting effect can be traced back to the swelling transport mechanism. The samples exhibiting overshooting effect follow anomalous transport with a bias to non – Fickian mode of transport. The experimental results reveal the influence of NCO/OH ratio and pH of the surrounding medium on the overshooting effect shown by the NR/PEG block copolymer samples.

References

1. Kim YH, Bae YH, Kim SW. J Control Release 1994; 28(2), 143-152.
2. Rosiak JM, Ulanski P, Pajewski LA, Yoshi F, Makuuchi K. Radiat Phys Chem 1995; 46(2): 161-168.
3. Kim J, Conway A, Chauhan A. Biomaterials 2008; 29(14): 2259-2269.
4. Bajpai AK, Shrivastava M. J Appl Polym Sci 2002; 85(7): 1419-1428.
5. Quintana JR, Valderruten NE, Katime I. Langmuir 1999; 15(14): 4728-4730.
6. Guan YL, Shao L, Liu J, Yao KD. J Appl Polym Sci 1996; 62(8): 1253-1258.
7. Hoffman AS. J Control Release 1987; 6(1): 297-305.
8. Park TG, Hoffman AS. Macromolecules 1993; 26(19): 5045-5048.
9. Ishihara K, Muramoto N, Shinohara I. J Appl Polym Sci 1984; 29(1): 211-217.
10. Eisenberg SR, Grodzinski AJ. J Membr Sci 1984; 19(2): 173-194.
11. Lee WF, Lin YH. J Appl Polym Sci 2001; 81(6): 1360-1371.
12. Katayama S, Hirokawa Y, Tanaka T. Macromolecules 1984; 17(12): 2641-2643.
13. Wang C, Zhang G, Dong Y, Chen X, Tan H. J Appl Polym Sci 2002; 86(12): 3120-3125.
14. Karaky K, Brochon C, Schlatter G, Hadziioannou G. Soft Matter 2008; 4(6): 1165-1168.
15. Ravindran T, Nayar MRG, Francis DJ. J Appl Polym Sci 1988; 35(5): 1227-1239.
16. Nair, R.C. Block copolymers from liquid natural rubber and polyethers, Ph.D thesis 1998, pp 73-75.
17. George SC, Thomas S. Polymer 1996; 37(26): 5839-5848.
18. Kim D, Caruthers JM, Peppas NA. Macromolecules 1993; 26(8): 1841-1847.
19. Johnson T, Thomas S. J Mater Sci 1999; 34(13): 3221-3239.
20. Harogoppad SB, Aminabhavi TM. Macromolecules 1991; 24(9): 2598-2605.

21. Bajsic G, Rek V. J Appl Polym Sci 2001; 79(5): 864-873.
22. Gopakumar S, Nair MRG. Polymer 2005; 46(23): 10419-10430.
23. Smith MJ, Peppas NA. Polymer 1985; 26(4): 569-574.

Table I (NR/PEG) block copolymer sample specifications

Block Copolymer	NCO/OH ratio	NR/PEG mole ratio
NR/PEG (4000/4000) – 1	1.0	1
NR/PEG (4000/4000) – 2	1.1	1
NR/PEG (4000/4000) – 3	1.2	1
NR/PEG (4000/4000) – 4	1.3	1
NR/PEG (4000/4000) – 5	1.4	1

Table II Equilibrium uptake values of the block copolymers in water

Block Copolymer	Equilibrium uptake (Q_∞ mol%) values
NR/PEG (4000/4000) – 1	9.45
NR/PEG (4000/4000) – 2	10.47
NR/PEG (4000/4000) – 3	7.78
NR/PEG (4000/4000) – 4	8.61
NR/PEG (4000/4000) – 5	4.72

Table III Swelling characteristics of NR/PEG block copolymers in water and at pH 4, pH 7 and pH 9.

Block Copolymer	Water		pH 4		pH 7		pH 9	
	n	k	n	k	n	k	n	k
NR/PEG (4000/4000) – 1	0.47	2.43	1.09	0.42	0.97	0.36	1.03	0.35
NR/PEG (4000/4000) – 2	0.42	6.63	0.74	2.78	0.74	2.43	0.60	4.79
NR/PEG (4000/4000) – 3	0.60	6.58	1.22	0.76	0.92	1.86	0.92	2.15
NR/PEG (4000/4000) – 4	0.59	4.38	0.88	1.90	0.73	3.01	0.70	3.28
NR/PEG (4000/4000) – 5	0.61	16.99	1.14	3.55	0.90	6.25	0.67	53.76

Unit: k x 10^2 gg^{-1} min^n.

Table IV Kinetic data on the solvent uptake by NR/PEG block copolymers in water.

Block Copolymer	k_1 x 10^3 (min^{-1})
NR/PEG (4000/4000) – 1	3.29
NR/PEG (4000/4000) – 2	6.33
NR/PEG (4000/4000) – 3	19.30
NR/PEG (4000/4000) – 4	33.12
NR/PEG (4000/4000) – 5	—[a]

-[a] – negative value was obtained

Table V Transport coefficients of block copolymers in water

Block Copolymer	D^* cm^2s^{-1}	S gg^{-1}	P cm^2s^{-1}
NR/PEG (4000/4000) – 1	0.96	1.70	1.63
NR/PEG (4000/4000) – 2	5.44	1.89	10.27
NR/PEG (4000/4000) – 3	0.58	1.40	0.81
NR/PEG (4000/4000) – 4	0.57	1.55	0.89
NR/PEG (4000/4000) – 5	0.43	0.85	0.37

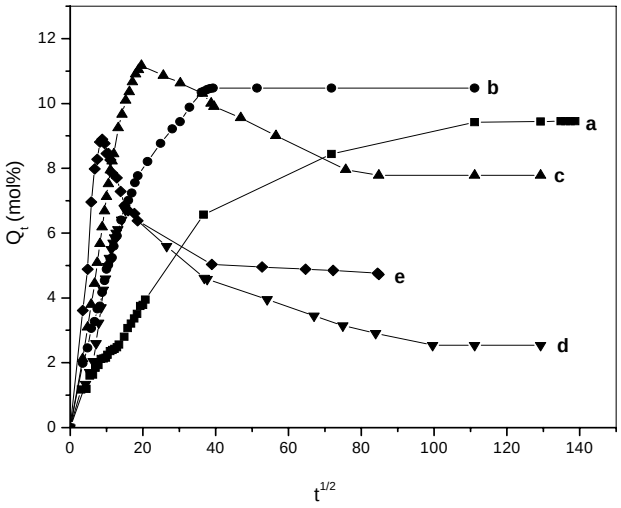

Fig.1. Percentage mass uptake for the block copolymers in water at room temperature: (a) NR/PEG (4000/4000)–1, (b) NR/PEG (4000/4000) – 2, (c) NR/PEG (4000/4000) – 3 (d) NR/PEG (4000/4000) – 4, (e) NR/PEG (4000/4000) – 5.

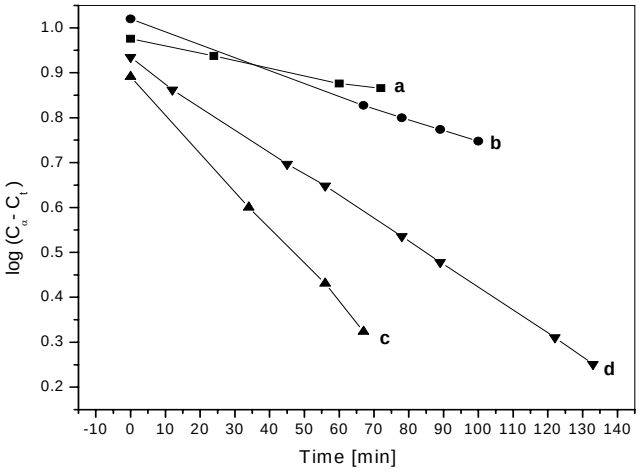

Fig.2. log (C_∞ - C_t) versus time for water uptake by block copolymers:
(a) NR/PEG (4000/4000) – 1, (b) NR/PEG (4000/4000) – 2, (c) NR/PEG (4000/4000) – 3
(d) NR/PEG (4000/4000) – 4.

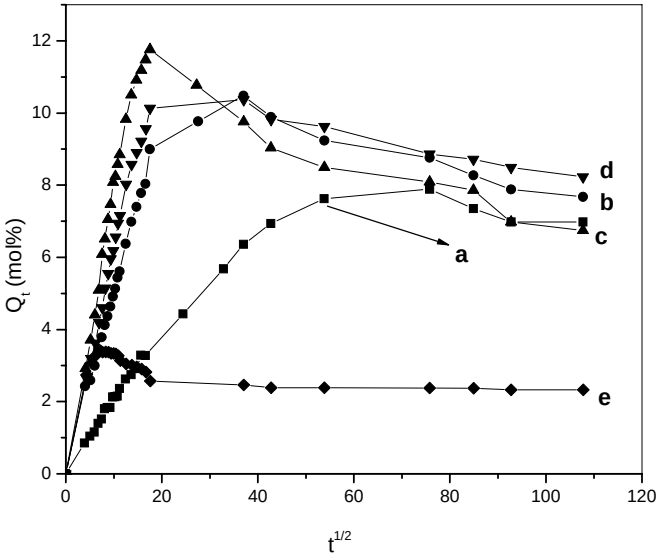

Fig.3. Percentage mass uptake for the block copolymers at pH 9:
(a) NR/PEG (4000/4000) – 1, (b) NR/PEG (4000/4000) – 2, (c) NR/PEG (4000/4000) – 3
(d) NR/PEG (4000/4000) – 4, (e) NR/PEG (4000/4000) – 5.

Studies on EPDM based compositions for underwater acoustic applications

Shajahan. K, Jayesh. P, Krishnaveni.K.P, Vasudevan.S and Reji John
Naval Physical & Oceanographic Laboratory
Defence Research & Development Organisation,
Kochi-682021
Email: tsonpol@vsnl.com

Abstract

Polymeric compositions are widely employed in various underwater acoustic applications. The major uses of these composites are for packaging underwater electronic gadgets, which cannot function if directly exposed to seawater environments. These composites have to function as acoustic windows, reflectors, absorbers or a combination of these, depending on the frequency of interest. In this paper, the acoustic properties of EPDM rubber formulations are studied for its window application. A series of compositions are made by incorporating different ingredients at various loading levels and evaluated for its acoustic parameters. All compositions are studied for its cure characteristics at various temperatures and time using MDR2000 rheometer. The compounds developed are found to be reversion resistant beyond its cure conditions. Compositions ranging from 150-250 pphr reinforcement loading are found to be transmitting acoustic energy with negligible loss. Circular discs of diameters 50mm and 200mm with 20mm thickness are used for acoustic studies. The insertion loss and echo reduction behaviour are studied in a vertical water filled pulse tube using standard acoustic projector cum receiver. Physical and mechanical properties are evaluated as per ASTM standards. Results showed that the material could be a good candidate for acoustic window application. The negligible water absorption and high underwater stability make this material suitable for sub-sea application. Studies showed that insertion loss of the material is 0.2dB in the range of 2 kHz to 15 kHz. The water absorption of the material is 0.002% when immersed in both fresh and saline for 24 hours at room temperature. The weight gain due to water absorption, when submerged in water for more than 260 days is negligible.

Keywords: encapsulants, EPDM, echo-reduction, insertion loss

Introduction

Polymeric compositions are widely employed in various underwater acoustic applications. The major uses of these composites are for packaging underwater electronic gadgets, which cannot function if directly exposed to seawater environments. These composites have to function as acoustic windows, reflectors, absorbers or a combination of these, depending on the frequency of interest [1]. In this paper, the acoustic properties of EPDM rubber formulations were studied for its window application.

Traditionally a number of polymers are used for underwater applications. Transducer encapsulation is the area where requires maximum acoustic energy transmission property , while an acoustic baffle or mount requires maximum sound energy absorption or isolation. Poly chloroprene, Halogenated Butyl, Nitrile, Styrene Butadiene rubbers and Thermoplastic elastomers are some of the candidates currently used for these applications. Each one has their merit and demerits but will operate moderately well in their functional parameters. One of the key concerns of these materials is their higher percentage of water absorption. With continuous exposure to sea environments, these materials can take considerable amount of water in and related changes in electro-acoustic parameters. These effects are become cumulative coupled with ageing factors.

In the present study, the one of the environmentally stable rubber viz. EPDM was studied for acoustic properties. EPDM has its inherent advantages of age resistance and superior water

resistance [2]. For converting it to an acoustic transparent material for using in encapsulation, we need to match the acoustic impedance (product of density and velocity of sound through the material) with seawater [3]. The present study focuses on effects of filler loading on acoustic parameters and its physico-mechanical properties.

Experimental

Materials

The materials used for this study are EPDM rubber-Nordel IP4520 procured from Dow Chemicals. Compounding ingredients like TMTD, MBT from ICI and ZnO, Stearic acid, sulphur, Silica, Precipitated $CaCO_3$, Talc, TiO_2, Naphthenic Oil etc are sourced from local market.

Compositions

To study the effect of filler loading on acoustic properties such as Insertion loss and Echo reduction, a series of compositions were made from EPDM rubber as given in Table-1. NORDEL™ IP 4520 Medium diene Hydrocarbon Rubber is an amorphous ethylene-propylene-diene terpolymer with Low molecular weight and Good low temperature properties [4]. This was selected with view to cater encapsulation by injection or transfer molding technique.
All compositions were made by mill mixing in a lab model two-roll mill. Cure characteristics were studied using rheometer MDR-2000 at 150^{o}C and 160^{o}C temperatures [5]. To study the reversion characteristics specimens were run for 60 minutes, 120 minutes and 180 minutes. The cure characteristics of optimized compositions were reported in Table-2.

Acoustic Measurements

Windows, reflectors, baffles and anechoic coatings constitute a complete set of materials insofar their function is concerned. Ideal specimens of the four materials will, respectively transmit 100%, reflect 100%, transmit 0% and reflect 0% of the sound incident on them [1]. Each of these four materials can be evaluated by measuring the percentage of sound transmitted through and reflected from the material when a sample is immersed in water. These two measurements are called “insertion loss” and “echo reduction,” are defined by

Insertion loss=20 log (Incident sound pressure / Transmitted sound pressure)

Echo reduction=20 log (Incident sound pressure/ Reflected sound pressure)

For studying Insertion loss and Echo reduction cylindrical specimens of 50mm diameter and 200mm diameter with a height of 20mm were made by compression moulding. Echo reduction behavior for 3 kHz to 15 kHz was studied using 50mm diameter specimen in vertical pulse tube with standard projectors and hydrophone at bottom. Echo reduction and Insertion loss behavior for the frequency range 1 kHz to 4 kHz was studied in vertical low frequency pulse tube using 200mm diameter specimen. For Insertion loss specimen was submerged in water in the pulse tube with projector and hydrophone located opposite sides of specimen. Mechanical properties were evaluated from standard specimens punched out from moulded test slabs of 150mm x 150mm x 2mm. For compression set study standard moulded cylinders were used. All properties were evaluated according to the relevant ASTM standards [6-7].

Short-term water absorption characteristics was studied for all specimens and reported in table-3. Long-term water absorption carried out for 260 days and the values obtained were plotted in Fig-1.

Results and Discussion

The cure characteristics of the optimised compositions are given in table-2. As filler loading increases scorch safety (ts2) decreases from 9 minutes to 2 minutes.
All the trends generally observed in the rubber compounds are also seen here. Energy dissipation capacity of the compound can alter by filler loading, as it is seen in the table. However, as the filler loading level increases the processability and mould flow characteristics seem to be decreased.

The physico-mechanical properties evaluated are presented in table-3. As observed generally with rubber compounds, higher the filler loading greater the density, hardness, compression set and tear strength etc with corresponding decrease in elongation at break. The maximum tensile strength in the talc alone series (E1-E5) was for E4 composition having 200phr filler loading. This may be due to the reinforcing effect of talc at that particular loading. For E6 the increased tensile strength was due to silica reinforcement. For E5 and E6, the elongation at break fall below 100% due excessive polymer matrix dilution. Water absorption for 24 hours was lowest for E4 (0.0247%) due to the highest level of exfoliation occurring because of optimum talc reinforcement.

Long-term water absorption characteristics of compositions are studied and plotted in figure-1. Compounds E3, E4 and E5 show the lower percentage of water absorption even after immersion for 259 days. The blank compound EB, shows a decreasing pattern due to the leaching of organic compounding ingredients [8]. Compound E6 is having higher percentage of water intake due to the presence of additional filler loading of precipitated $CaCO_3$ and Silica.

Generally all the EPDM compounds are acoustically transparent however, from the figure-2, it is seen that acoustic insertion loss of compound E4 and E5 are negligible to the extent of 0.02dB in the frequency range of 0.5 kHz to 4 kHz. These compounds can be good candidates for the developing acoustically transparent encapsulating material in the above frequency range.

The echo reduction behaviour of compounds in the frequency range of 3 kHz to 15 kHz evaluated using 50mm dia pulse tube specimens are plotted in figure-2. It is evident from the plot that all compounds except E3 and E4 are reflecting acoustic energy back to the source with almost negligible loss. This means that, compounds E2, E5 and E6 are acoustically transparent in this frequency range due to better acoustic impedance match. Compounds E3 and E4 can be used for anechoic liner application due increased echo reduction.

Echo reduction pattern of 200mm dia pulse tube specimens in the frequency range of 0.5 kHz to 4 kHz are shown in fig-4. Here similar behaviour as observed in fig-3 is obtained. Compounds E5 and E6 are less reflecting than E2, E3 and E4. Hence, E5 and E6 could be used for application where acoustic transparency is required.

Conclusions

Generally, all EPDM compositions are found to be acoustically transparent. Acoustic properties are found to be frequency dependent. However, for obtaining maximum underwater acoustic transparency, compounding with reinforcing filler like talc at 200-phr level could be a better choice with increased water resistance. The composition E4 and E5 can be used as an underwater encapsulant where acoustic transparency is required. The adhesion of EPDM compositions has to be studied and modified for better interfacing with metals and ceramics for device fabrication [9].

Acknowledgements

Authors wish to acknowledge the constant inspiration of Shri. Vishnubhatla RMR, Associate Director, NPOL. We gratefully acknowledge the Director, NPOL for granting permission to publish this work.

References

1. Bob RJ, Underwater Electro acoustic measurements, 1969
2. Blow C.M., Rubber Technology & Manufacture, Butterworth Scientific, UK
3. Thompson, Corley M, EPDM rubber as an underwater acoustic window, The Journal of the Acoustical Society of America, vol. 74, issue S1, pS50, 1983
4. Brydson J.A., Rubber Chemistry, Applied Science Publishers, UK
5. Annual Book of ASTM Standards, Section 9, Rubber, V.09.01, 1998
6. Annual Book of ASTM Standards, Section 9, Rubber, V.09.02, 1998
7. Brown, R.P, Physical Testing Rubbers,
8. Quinn, M. E. ; McGee,W. W, Analysis Technique for Determining the Levels of Organic Additives in an EPDM Rubber for Use in Underwater Acoustic Applications, Naval Research Lab, Washington DC, 1985
9. Beumel,Linda L. ; Thompson, Corley M, Development of an EPDM Elastomer with Improved Bondability for Use in Sonar Transducers, Naval Research Lab, Washington DC, 1987

Table-1. Compositions

Composition / Ingredient	**EB**	**E1**	**E2**	**E3**	**E4**	**E5**	**E6**
EPDM	100	100	100	100	100	100	100
ZnO	5	5	5	5	5	5	5
Stearic Acid	1	1	1	1	1	1	1
Sulphur	1.5	1.5	1.5	1.5	1.5	1.5	1.5
TMTD	1	1	1	1	1	1	1
MBT	0.5	0.5	0.5	0.5	0.5	0.5	0.5
Talc		50	100	150	200	250	250
TiO_2							10
Silica							75
Pptd $CaCO_3$							90
Naphthenic Oil	15	15	15	15	15	15	15
Batch weight	**124**	**174**	**224**	**274**	**324**	**374**	**549**

Table-2. Cure Characteristics @150^{o}C, 60minutes

Composition / Parameter	**EB**	**E1**	**E2**	**E3**	**E4**	**E5**	**E6**
ts1, min	7.87	7.50	5.53	4.21	3.48	2.75	2.02
ts2, min	9.29	8.88	6.47	4.89	3.98	3.13	2.37
t10, min	8.06	8.23	6.21	4.84	4.07	3.27	3.35
t50, min	12.70	14.14	10.58	9.30	8.74	8.42	17.07
t90, min	24.31	32.59	23.50	25.23	28.05	33.72	47.80
ML, dNm	0.18	0.32	0.31	0.34	0.57	0.77	21.50
mH, dNm	11.18	14.83	17.01	19.59	23.09	25.61	68.72
S”@ML	0.34	0.45	0.56	0.69	1.0	1.30	15.55
S”@MH	0.14	0.73	0.85	1.34	1.94	2.34	19.10
Tan delta @ML	1.944	1.394	1.781	2.0	1.772	1.684	0.724
Tan delta @MH	0.12	0.049	0.050	0.069	0.084	0.092	0.278

Table-3 Physico-mechanical properties

Composition / Property	EB	E1	E2	E3	E4	E5	E6
Density, g/cc	0.903	1.11	1.29	1.435	1.550	1.640	1.840
Hardness, Shore-A	45	56	65	70	75	80	92
Compression Set, %	9	11	13	14	16	19	21
Tensile Strength, MPa	1.17	2.54	3.94	4.01	4.24	3.92	6.23
M100, MPa	1.13	2.15	2.91	3.07	3.65	-	-
Elongation at Break %	108	160	214	217	174	68	32
Tear Strength, N/cm	62.83	77.40	109.43	151.80	244.66	251.70	212.17
Water absorption, (40^{o}C, 24 hrs, 3.5 % NaCl solution) %	0.1257	0.1160	0.0983	0.0270	0.0247	0.0280	0.1021

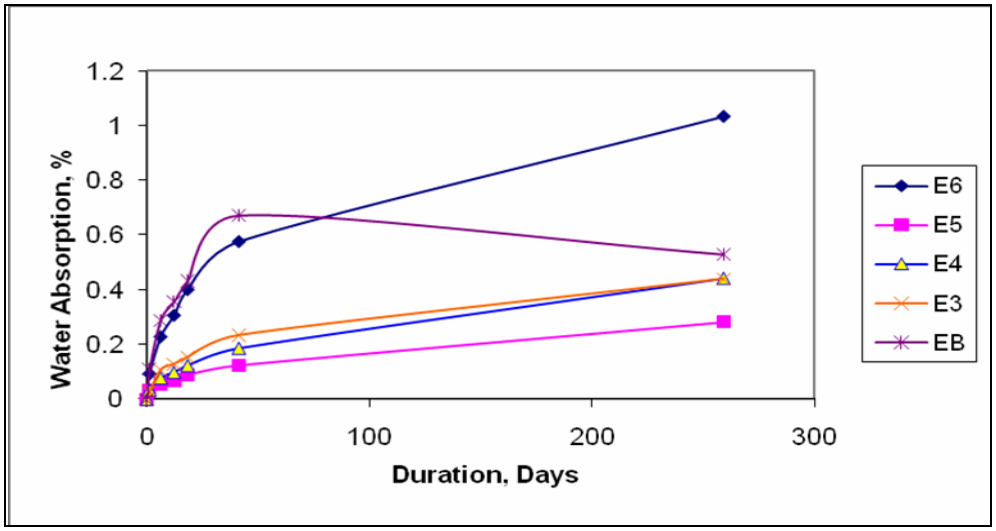

Figure-1 Long term water absorption characteristics

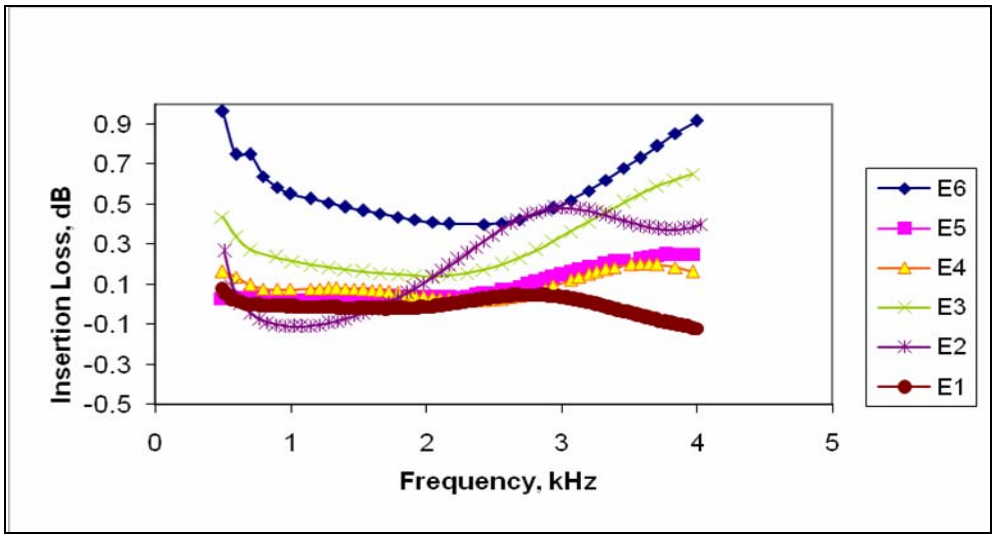

Figure-2 Insertion Loss behavior 0.5 kHz-4 kHz (200 mm dia pulse tube)

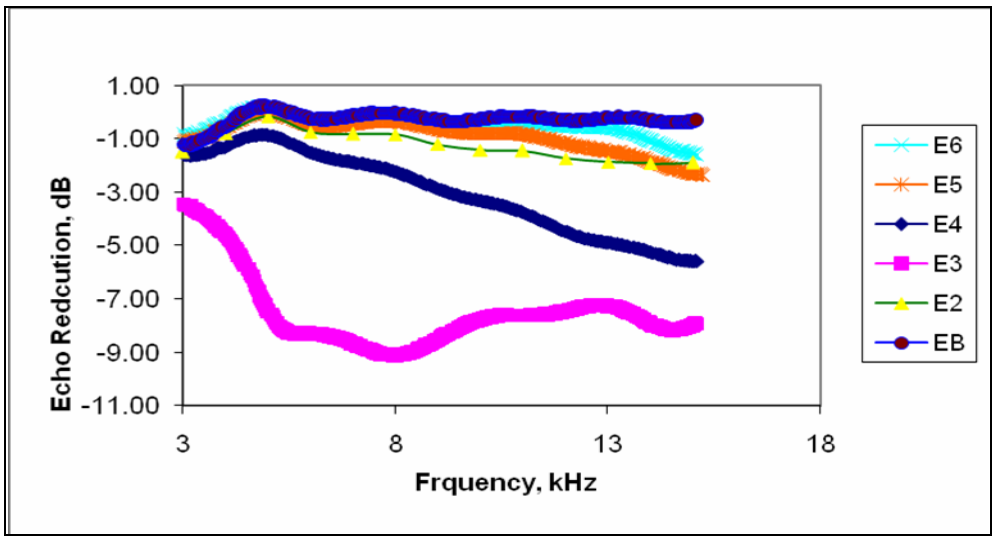

Figure-3 Echo Reduction 3kHz-15Hz (50mm dia pulse tube)

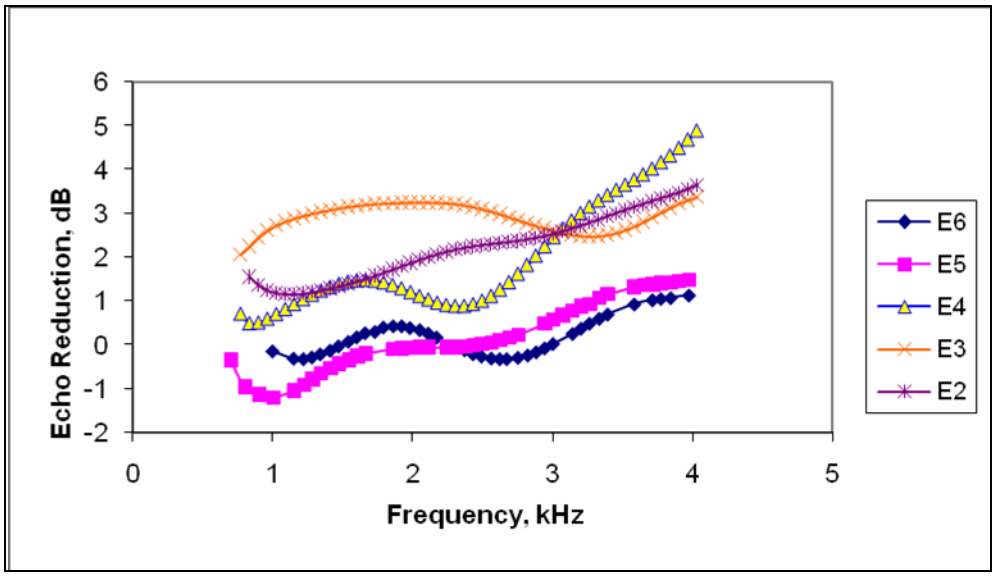

Fig-3 Echo Reduction 0.5 kHz-4 kHz (200 mm dia pulse tube)

Development of epoxy based material for rapid tooling applications

K.Elangovan*, B.Kothandaraman*, K.Kalaichelvan, Iynesh kumar***

*Department of Rubber and Plastic Technology, MIT Campus, Anna University, Chennai. India

**Department of Production Engg., MIT Campus, Anna University, Chennai,

India

Email: elango_k2000@yahoo.co.in

ABSTRACT

Development of new materials and new material processing techniques favors modern technological development. Among these composites occupy an important place in field of Aerospace, Defense, Automobiles and Biomaterials. Epoxy resin composites are frequently applied in moulds manufactured with rapid tooling technologies that are used for wax and polymer materials injection. Various percentages of Aluminum and spheriglass filled epoxy resin was prepared. Triethylene tetramine was used as room temperature curing agent. Amine containing polydimethylsiloxane was used as liquid rubber modifier. The micro structural analysis was done to examine the distribution of fillers in the matrix. The mechanical and thermal behavior of the materials was determined. Flexural, Tensile and Compressive behavior were determined by using universal testing machine. Thermal fatigue test was also done.

INTRODUCTION

Epoxy resin composites are frequently applied in moulds manufactured with rapid tooling technologies that are used for wax and polymer materials injection. With the propose of enlarging the application field of the polymer matrix systems, it is fundamental to select adequate dispersed phases and analyze their influence on the composite properties in order to reinforce the polymer matrix and tailor the properties according to the tools specifications.[1].Epoxy based sterolithography resins have been used successfully as tools for injection molding, Molds made out of these resins fail at distinct times:during the first injection of plastic; during the first part first ejection; during either injection or ejection,but after a certain number of parts have been produced.[4]

The various works was carried in this field around the world. Tri-phase materials composed by an epoxy resin, aluminum particle and milled fibers, were produced, with mechanical and thermal performances better than single materials, increasing the competitiveness of the epoxy rapid tooling process. The influence of the aluminum particles and carbon and glass fiber addition increases slightly the impact resistance of the aluminum filled composites. [2].The effects of particle size and silane treatment on the fracture toughness are experimentally evaluated for epoxy reinforced with nanometer and micrometer sized rigid particles. The fracture toughness if epoxy increases with the addition of aluminum

particles. Additionally, fractured surface are observed under an Optical metallurgical microscope to investigate both particle dispersion and evidence of extrinsic toughening mechanism. It is observed that the both improved particle dispersion and appropriated silane treatment lead to increase in toughness. [3].

Epoxy has excellent electrical, thermal and chemical resistance. Shrinkage during polymerization of epoxy resins is extremely low. Molded epoxy parts are hard, rigid, and relatively brittle and have excellent dimensional stability over a broad temperature range. Epoxy is readily machinable and can be employed over temperature range of 60 to 250° C. Aluminum has only one-third the weight of steel. Aluminium powder was used as filler material for epoxy resin to obtain good mechanical properties and high thermal capabilities and fatigue resistance.

Spheriglass solid glass spheres are microspheres with a density of 2.5g/cc. The addition of spheriglass to epoxy system does not alter viscosity of the epoxy system. These spheres are nonporous. They do not absorb resin in polymer system.

EXPERIMENTAL

MATERIALS USED.

DGEBA liquid epoxy resin (LY556) with epoxy equivalent around 170 and viscosity of 8000 to 12000 cp at 25 degree Celsius was used as received from Araldite India Pvt. Ltd.Organo modified polysiloxane with molecular weight around 5000 was used as liquid rubber modifier as received from Resil chemicals Pvt Ltd. Triethylene tetramine (HY 951-curing agent) was used as received from Araldite India Pvt.Ltd.Aluminium and spheiglass were received from Potter industries Inc.

PREPARATION OF LIQUID RUBBER MODIFIED EPOXY MATRIX.

Amine containing polydimethylsiloxane was taken as liquid rubber modifier. Five phr or ten phr of liquid rubber modifier was taken along with epoxy resin and the mixture was heated at 50 degree Celsius for 30 minutes with continuous stirring. Then the liquid rubber modified epoxy resin was allowed to cool in the room temperature.

PREPARATION OF ALUMINUM AND SPHERIGLASS FILLED EPOXY AND MODIFIED EPOXY MATRIX

The weighed amount of spheriglass was added to epoxy system and stirred for 15 min. Then weighed amount of aluminum was added to the spheriglass/epoxy system and stirred for 15 min. This tri-phase material was cured using triethylene tetramine at room temperature. The same procedure was carried out for Amine containing PDMS modified epoxy matrix. The material was cured at 100°C for 3 hrs.

Various percentages of Aluminum and spheriglass filled epoxy resin are as follows:

NOTATIONS USED

A→E-55, AL-45.S.g-27.5

B→E-50, AL-50, S.g-25

D→E-50, AL-50.S.g-50

E→E-55, Al-45, S.g-27.5, Si-10 phr

I→E-50, AL-50, S.g-50, Si-10phr

H→E-50.AL-50.S.g-50, Si-5phr

RESULTS AND DISCUSSIONS

MECHANICAL PROPERTIES OF ALUMINUM/SPHERIGLASS MATERIALS FILLED MODIFIED AND UNMODIFIED EPOXY MATRIX

The mechanical properties of the materials were studied using in SHIMAZDU universal testing machine.

The flexural specimen of dimension 80mm × 25mm with thickness of 3mm was prepared from each casting. Flexural strength, flexural modulus were studied in the universal testing machine. The flexural test was carried at the crosshead speed of 3mm/min. The flexural test was carried according to ASTM D 790 standards.

The Samples A, B, D and pure epoxy resin were prepared without post curing

S.No.	**Composition**	**Flexural strength MPa**	**Flexural Modulus GPa**
1	Pure Epoxy	53.15	3.638
2	A	46.7	6.0
3	B	36.95	6.0
4	D	37.75	6.0

The Samples E, I, H and pure epoxy resin were prepared with post curing

S.No.	Composition	Flexural strength MPa	Flexural Modulus GPa
1	Pure Epoxy	92.2	3.64
2	E	10.80	0.60
3	I	30.28	3.42
4	H	32.18	9.I5

The flexural strength reduced with addition of Amine containing PDMS which induced rubbery properties in epoxy matrix. The Modulus of the combination H increased indicating better dispersion supported by the spherical rubber precipitates and improved cross linking within the matrix.

TENSILE TEST

The flexural specimen of dimension 80mm × 10mm with thickness of 3mm was prepared from each casting. Tensile strength, Tensile modulus were studied in the universal testing machine. The tensile test was carried at the crosshead speed of 1mm/min. The flexural test was carried according to ASTM D 638 standards.

The Samples A, B, D and pure epoxy resin were prepared without post curing

S.No.	Composition	Tensile strength MPa	Tensile Modulus GPa
1	Pure Epoxy	35.32	0.947
2	A	19.26	1.343
3	B	15.76	1.212
4	D	10.51	1.659

The Samples E, I, H and pure epoxy resin were prepared with post curing

S.No.	**Composition**	**Tensile strength** **MPa**	**Tensile Modulus** **GPa**
1	Pure Epoxy	48.39	0.904
2	E	6.306	0.386
3	I	15.56	1.54
4	H	16.81	1.46

The higher phr of Amine containing PDMS reduced tensile strength to greater extent. The increase in modulus may correspond to reduce in free volume which restricts chain mobility.

COMPRESSION TESTING

Compression strength of the specimen was found out by using Universal Testing Machine (UTM). The test was carried at the crosshead speed of 1mm/min.

The Samples I, H and pure epoxy resin were prepared with post curing

S.No.	**Composition**	**Compressive strength** **MPa**	**Compressive Modulus** **GPa**
1	Pure Epoxy	115.16	1.18
3	I	124.14	1.94
4	H	124.06	2.0

The Toughening effect of Amine containing PDMS improved compressive strength and spheriglass contributed for higher modulus.

THERMAL FATIQUE TEST

The test was carried out at 250°C for measuring the thermal stability. The samples were tested for 30 cycles. Observations indicated that there is no change in dimension.

COMPOSITION	**NO.OF.CYCLES**	**TEMPERATURE AT 250°C**
Without Silicone A,B,D	30	Dimensionally stable
With Silicone E,I,H	30	Dimensionally Stable

MICROSTRUCTURAL ANALYSIS

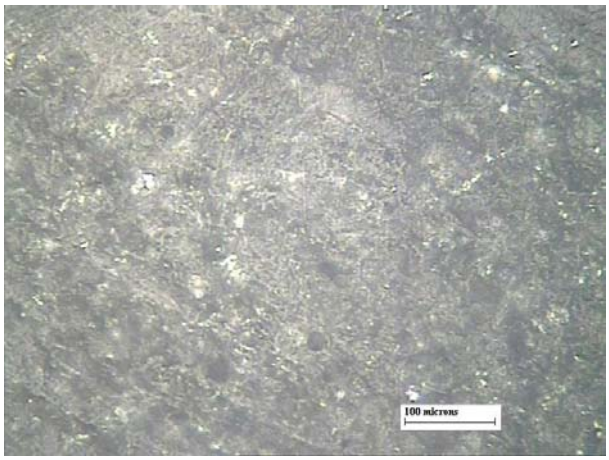

The combination A

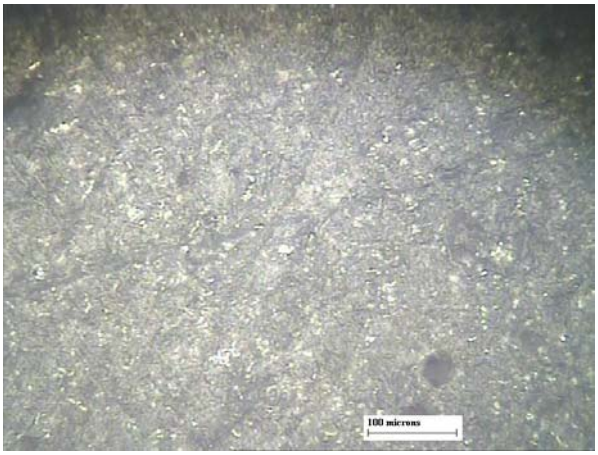

The combination E

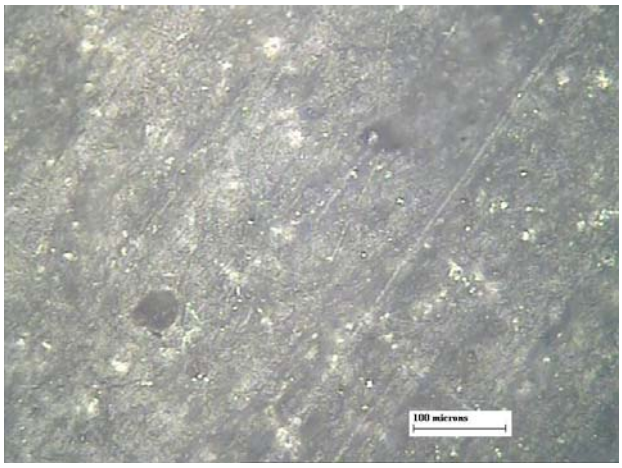

The combination B

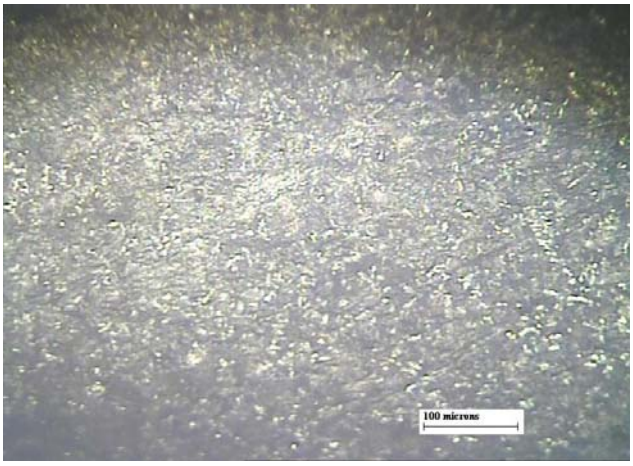

The combination I

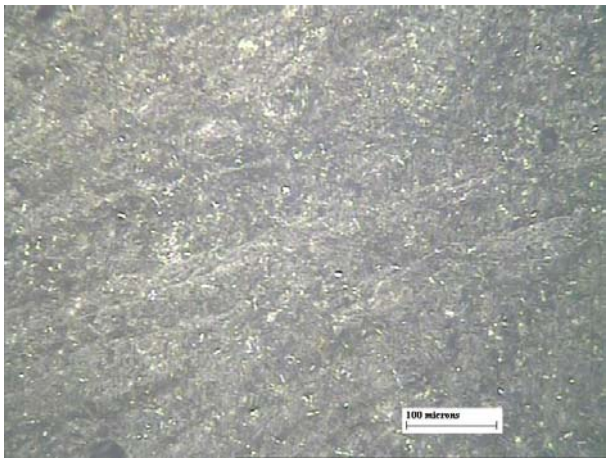

The combination D

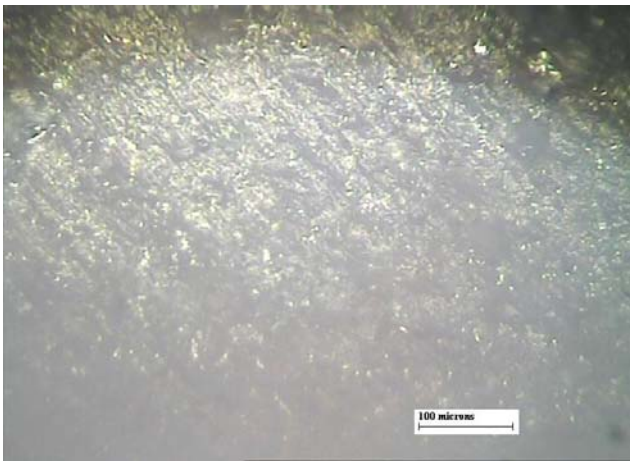

The combination H

The combination A, B, D and E shows filler aggregation with in the matrix .The combination I shows no aggregation and the combination H shows homogenous distribution of fillers without aggregation with in the Amine containing PDMS modified epoxy system. The lower phr addition of Amine containing PDMS supported homogenous distribution of fillers without any aggregation. The higher phr modification leads to decrease in free volume which resulted in agglomeration and reduced mechanical properties.

CONCLUSION

The lower phr of amine containing PDMS supported better dispersion of filler within the epoxy system. The modulus improved with addition of speriglass without changing viscosity of the material. The tri-phase composite was dimensionally stable at higher temperatures. The 5 phr of Amine containing PDMS modified epoxy resin, Aluminum, Speriglass in the ratio 1:1:1(The combination H) showed better

mechanical and thermal behaviors when compared with other materials. The combination H can be used as mould making material.

REFERENCES

1. F.Jorge lino and Co-authors Tribological behavior of epoxy based composite for rapid tooling.Wear 260(2006) 30-39
2. Vasconcelos,Lino,Magalhes,Neto Impact fracture study of epoxy-based composite with aluminum particles and milled fibers.Journal of material processing technology (2005) 277-283.
3. Suraj zunjarro, Raman singh. Characterization of the fracture behavior of epoxy reinforced with nanometer and micrometer sized aluminum particles.
4. Vincent rodet and Jonathan S.Colton ,Properties of rapid prototype injection mold tooling materials.Polymer engineering and science, January 2003,Vol.43,No.1

Graft-copolymerization of cellulose-based filter paper and its development as antibacterial food-packaging material

Rasika Tankhiwale* [#] **and S. K. Bajpai**

Polymer Research Laboratory, Dept. of Chemistry, Govt. Model Science College (Auto),

Jabalpur (M.P.)-482001, India

Email: rasika_81@rediffmail.com

Abstract

This work describes preparation of nano silver- loaded grafted filter paper. First, the filter paper was grafted with acrylamide by ceric ammonium nitrate induced free radical polymerization and then silver nanoparticles were loaded into grafted filter paper by equilibration in silver nitrate solution followed by citrate reduction. The formation of silver nanoparticles has been confirmed by TEM and SAED analysis. The particle size of nanoparticles has been determined by TEM analysis. The novel nano silver-loaded filter paper has been investigated for its antimicrobial properties against *E.coli*. This newly developed material shows strong antibacterial property and thus offers its candidature for possible use as antibacterial food- packaging material.

Keywords: grafting, hydrogel, silver nanoparticles, *E.coli*, TEM.

1. Introduction

With the growing public health awareness of disease transmissions and cross-infection caused by microorganisms, use of antimicrobial materials has increased in many application areas like protective clothing for medical and chemical works, other health related products [1-2], antibacterial packaging material that can improve product quality and keep it free from microbial adhesion [3], etc. Such antimicrobial packaging materials may be produced by introducing silver, gold or copper nanoparticles into polymer film. In particular, silver has been recognized for its broad –spectrum antimicrobial activities [4].Silver inactivates bacteria by interacting with the thiol groups of bacterial proteins and enzymes [5]. It is proposed that silver ions (Ag^{+}), released from silver nanoparticles (Ag^{o}), interact with phosphorous moieties in DNA, resulting in inactivation of DNA replication. In fact, silver nanoparticles are highly germicidal, quite harmless to humans and absolutely non-toxic. It has been reported that even the highest concentration of nano silver causes no side effects [6]. In a recent work by Wen et al [7], human fibroplasts were grown on various concentrations of silver nanoparticles during the period observation. The results of their study elucidated the non-toxicity of the interaction of nanometer- scale silver particles and the membrane surface.

Although synthetic polymeric films are frequently used as packaging material but their non-degradability has been a matter of great concern for environmentalists, and therefore attempts have been made to develop such materials which can undergo degradation and are ecofriendly. In our recent work [8], we have reported a unique approach for in situ formation of ZnO nanoparticles onto cotton fibers grafted with a copolymer. Now, utilizing this approach, we hereby report grafting of acrylamide onto filter paper, followed by incorporation of silver nanoparticles to yield antibacterial antibacterial filter paper. To the best of our belief, no such work has been reported earlier.

2. Experimental

2.1.Materials

The monomer acrylamide (AAm), crosslinker N,N'-methylene bisacrylamide (MB), and initiator ceric ammonium nitrate (CAN), nutrient broth and Nutrient m-Endo agars were obtained

from HiMedia Laboratories, Mumbai, India. The salts silver nitrate ($AgNO_3$) and tri-sodium citrate (TS) were obtained from E.Merck, Mumbai, India. Standard cultures of the organisms were provided by the department of Biotechnology, Govt. Model Science College, Jabalpur, India. The cellulose based filter paper (Whatman No.42) was received from Sameer Science Lab, Jabalpur, India. The double distilled water was used throughout the investigations.

2.2.Preparation of grafted filter paper (GFP)

The graft- co polymerization of monomer acrylamide onto filter paper was carried out using ceric ammonium nitrate as free radical initiator by following the same method as has been reported previously with cotton fabric as substrate [9].

2.3. Loading of silver nanoparticles into grafted filter paper (GFP)

The silver nanoparticles were loaded into the GFP by using a novel approach, developed in our laboratory [8]. The GFP was put in $AgNO_3$ solution (15 mg $AgNO_3$ in 40 ml distilled water) for 12 h, then was taken out and put in tri-sodium citrate solution (20 mg dissolved in 25 ml water) for next 12 h to reduce Ag^+ ions into silver nanoparticles. The material, so produced, was allowed to dry. In this way, silver nanoparticles-loaded GFP was prepared.

2.4. Water uptake analysis

Completely dry pre-weighed grafted filter paper was put in 200 ml of distilled water at 30ºC and then its mass was measured at different time- intervals. The percent mass swelling (% M_s) was calculated using the following expression [10]

$$\% M_s = \text{Swollen weight} - \text{Dry weight} \ / \ \text{Dry weight} \times 100 \qquad \ldots\ldots\ldots\ldots (5)$$

All the experiments (i.e. grafting and water uptake analysis) were done in triplicate and average values have been produced in the data.

2.4.Characterization of silver nanoparticles loaded paper

The silver nanoparticles were characterized by transmission electron microscopy (TEM). The TEM images were recorded using a Tecnai F 12 TEM instrument. X-ray photoelectron spectroscopy(XPS), Model ESCALAB Mg K α (hν = 1253.6 eV) with a resolution of 1.0×10^{-4} Pa was used to confirm formation of silver nanoparticles.

Microbial experimentation

For qualitative measurement of microbial activity, the filter paper was cut to make a circle of 7.4 cm diameter, and the antimicrobial activity was tested using modified agar diffusion assay (disc test). The plates were examined for possible clear zones after incubation at 37º C for 2 days. The presence of any clear zone that formed on the surface of the filter paper was recorded as an indication of inhibition against the microbial species.

3. Results and Discussion

Graft copolymerization of vinyl monomers onto cellulose has been studied extensively [11-15]. However, the substrates used in these studies were native cellulose, cellulose pulp or cotton linters. In our study, we have used filter paper as a substrate for graft- copolymerization. Indeed, the mechanism of grafting reaction is more or less the same and may briefly be given as below: In the presence of an acid used, HNO_3 (HA), primary radical species formation occurs as a result of the action of acid on Ce(IV):

$$Ce^{4+} + HA \rightarrow Ce^{3+} + H^+ + A^{\bullet} \qquad \ldots\ldots\ldots\ldots\ldots\ldots (1)$$

Once the free-radical species ($A^{\bullet}$) are formed, they produce cellulose macroradicals via direct abstraction of hydrogen atom cellulose molecules.

$$Cell-OH + A^{\bullet} \rightarrow Cell-O^{\bullet} + HA \quad \text{…..……..(2)}$$

where Cell – OH represents cellulose molecule. Cellulose macroradicals may also be formed by direct attack of Ce^{4+} ions on cellulose molecule via H abstraction.

$$Cell-OH + Ce^{4+} \rightarrow Cell-O^{\bullet} + Ce^{3+} + H^{+} \quad \text{……..(3)}$$

These cellulose macroradicals, so produced, combine with monomers AAm to induce graft-copolymerization.

3.1. Effect of reaction temperature

The temperature of the reaction system does influence the rate of graft polymerization and the grafting field. We varied the temperature of the monomer/crosslinker solution, in the range 10 to 15°C and determined the percent grafting. The results, as shown in the Fig.1 reveal that 30°C is the optimum reaction temperature for maximum grafting. Below 30°C, the percent grafting is poor due to insufficient formation of free radicals at lower temperatures which is commonly observed phenomenon [16-17]. However, when temperature is increased beyond 30°C, the percent grafting again shows decreasing trend. This may possibly be explained on the basis of the fact that at higher temperature, the acid catalyst may induce degradation of cellulose chains, thus lowering the number of grafting sites in substrate. It was also observed that when reaction temperature was 50°C, the filter paper became brittle and was torn to small pieces indicating enhanced breakdown of cellulose chains by HNO_3. In addition, the possibility of recombination of free of free radicals at higher temperature should also be not ruled out.

3.2. Water uptake analysis

Fig.2 depicts the water uptake behavior of grafted – filter paper (GFP) in distilled water at 30ºC. It is clear that when GFP is put in water, it begins to take up water as indicated by increasing percent mass swelling. This may simply be attributed to the fact that water enters into grafted polymer network of the filter paper, thus allowing it to absorb water which is retained within the network. After some time the water uptake attains maximum value.

3.3. Loading of Silver nanoparticles into GFP

As mentioned in the section introduction, the nano silver-loaded filter paper has been prepared by loading silver nanoparticles into the grafted filter paper, utilizing our newly developed approach [8]. The overall process of entrapment of nano silver may be explained as follows: when grafted filter paper is equilibrated in distilled water, the network swells due to hydrophilic nature of monomer and plasticization of macromolecular chains. On dipping swollen filter paper into aqueous solution of $AgNO_3$, Ag^{+} ions enter into the swollen grafted network. Later on when this Ag^{+} containing filter paper is put in the sodium citrate solution, a uniformly distributed array of Ag nanoparticles is obtained due to reduction of Ag^{+} ions. The crosslinked three dimensional network serves as stabilizer for silver nanoparticles and prevents them for aggregation.

Fig.3 clearly describes the color change observed due to reduction of Ag^{+} ions into silver nanoparticles. It is very clear that filter paper turns brown due to presence of silver nanoparticles.

3.4.Characterization

Fig.4 (A) shows the TEM image of the silver nanoparticles. The image indicates nearly uniform distribution of silver nanoparticles. In addition, a typical selected area electron diffraction (SAED) pattern of a collection of silver nanoparticles is also shown (see inset). The

pattern appears to be a little diffused due to smaller particle sizes, but three diffraction rings are clearly visible and they can be indexed to the face-centered cubic structure of silver as follows. The strongest ring and the one closest to the center is probably a combination of the (111) and (200) reflections. The second ring is likely the (222) reflection whereas the outermost and the weakest third ring are either the (420) and/or the (422) reflections. Almost similar results have also been reported elsewhere [18]. The size distributions were obtained by measuring the diameters of 35 particles in an arbitrarily chosen area of TEM image [see Fig. 4 (B)]. As can be seen, nearly 40% particles have an average diameter of 26 nm and moreover, the distribution curve appears to be almost symmetrical with all the nanoparticles falling within the narrow range of 12 to 42 nm.

Antibacterial property of nanosilver loaded GFP

Finally, we carried out antibacterial test for the prepared silver nanoparticles loaded GFP against *E.coli*. Fig.5 (A) clearly demonstrates dense population of bacterial colonies on the whole surface of the grafted filter paper which is simply due to absence of silver nanoparticles in the sample. However, in Fig 5 (B) a clear zone of inhibition can be seen on the whole surface of the nanosilver loaded grafted filter paper. This may simply be explained on the basis of the fact that as the filter paper contains silver nanoparticles, the colonization of bacteria is greatly inhibited on the nano Ag-loaded filter paper. Therefore it may be concluded that silver nanoparticles loaded grafted filter paper possesses strong antibacterial property.

4. Conclusion

From the above study it may be concluded that grafting of acrylamide onto filter paper, followed by incorporation of silver nanoparticles results in development of a novel biomaterial which demonstrates fair biocidal action against *E.coli*, and it can be used as an antibacterial packaging material to prevent food stuff from bacterial infection. As the proposed method does not involve use of toxic organic solvents or harsh conditions like high temperature, the strategy can be applied for the manufacture of antibacterial food packaging material.

Acknowledgement

I would like to owe my whole hearted gratitude to my supervisor Dr. S.K. Bajpai, Prof. of Chemistry, Govt. Model Science College, Jabalpur (M.P.) for his kind guidance.

References

1. Margaret I.P, Sau L.L, Vincent K.M.P, Ivan Lung, Andrew Bud. J.Med.Microbiology 2006;55; 59.
2. Duran N, Marcato P.D, De Souza G.I.H, Alves O.L, Esposito E. J.Biomed. Nanotech 2007;3; 203.
3. Park S.I, Zhao Y.J, Agric. Food Chem 2004 ;52 ;1933.
4. Galeano B, Korff E, Nicholson W.L. Appl.Environ.Microbial 2003;69;4329.
5. Lok C.N, Ho C.M, Chen R, He Q.Y, Yu W.Y, Sun H, Tam P.K, Chiu J.F, Che C.M. J. Proteome Res 2006;5;916.
6. Becker Robert O, Spardaro M.D, Joseph A. The Journal of Bone and Joint Surgery 1978; 60(A);871.
7. Wen Hua-Chiang Lin, Yao-Nan , Jian Sheng-Rui , Tseng Shih-Chun , Weng Ming-Xiang, Liu Yu-Pin , Lee Po-Te, Chen Pai-Yen , Hsu Ray-Quan, Wu Wen- Fa , Chou Chang-Pin. Journal of Physics: Conference Series 2007;61; 445.
8. Bajpai S.K, Mary G, Chand Navin, J. Macromol. Sci . Part. A (Pure and Appl.Chem.) 2008: 45(10).
9. Bajpai S.K, Bajpai M, Gupta Pamila. J. Macromol. Sci. Part. A (Pure and Appl.Chem.) 2008;45;1.
10. Okeowo, O.; Dorgan, J. R. Macromolecules. 2006, 39 (23), 8193.
11. Gupta, K.C.; Sahoo, S. J.Appl.Polym.Sci. 2001,79,767.
12. Zahran, M.K.; Mahmoud, R.I. J.Appl.Polym.Sci. 2003,87,1879.
13. Sabaa , M.W.; Mokhtar, S.M. Polym. Test. 2002, 71,337.
14. Salam. M.A.; J.Textile Apparel Technol. Management. 2005,4(4), 1.
15. Chen , H.; Hsieh, Y. Biotechnol. Bioeng. 2005,90(4), 405.
16. Martel,B.; Weltrowski,M.;Ruffin, D.; Morcellet, M.; J. Appl. Polym. Sci. 2002,83,1449.
17. Saihi, D.; El-Achari,A.; Vroman,I.; Caze,C.; J. Textile Apparel Technol. Management. 2004,4(1), 1
18. Andersson M, Alfredsson V, Kjellin P, Palmqvist A.E.C. Nano Lett 2002;12;1403.

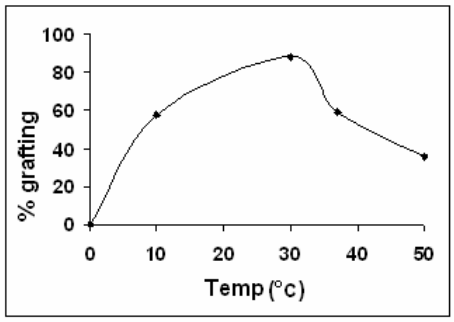

Fig.1. Effect of reaction temperature on percent grafting

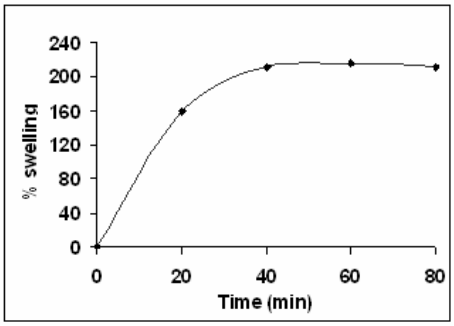

Fig.2. Dynamics of water uptake of grafted filter paper as a function of time at 30º C.

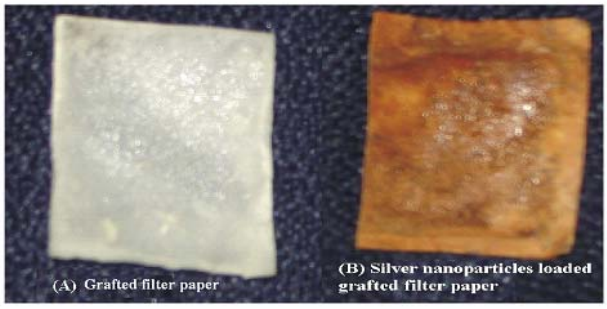

Fig 3. A comparative depiction of grafted and silver nanoparticles-loaded filter paper

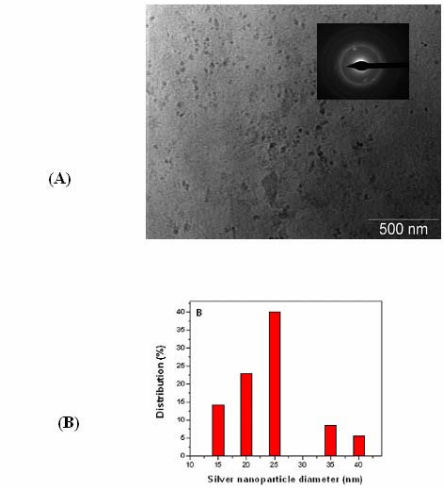

Fig.4. (A) TEM image of silver nanoparticles.
(B) Size distribution of silver nanoparticles

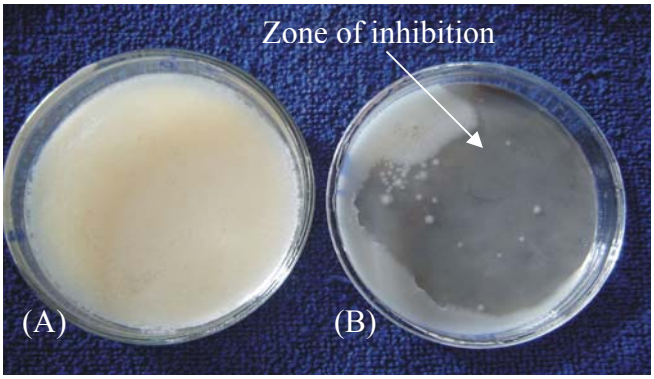

Fig.5. Photograph showing (A) growth of bacterial colonies around grafted filter paper. (B) Zone of inhibition around the silver nanoparticles loaded grafted filter paper.

Studies on processing of styrene butadiene rubber-$CaCO_3$ nanocomposites by different mixing techniques and their performance properties

A.Ahamad, C.B.Patil, P.P.Mahulikar, U.R.Kapadi, and D.G.Hundiwale*

School of Chemical Sciences, North Maharashtra University,
Umavinagar, Jalgaon - 425 001
Maharashtra, India

E-mail- dghundiwale@yahoo.com, ab_ahad@rediffmail.com

Abstract

The nano particles of $CaCO_3$ were synthesized by matrix mediated growth and controlled technique and was used as filler. The particle size of synthesized nano $CaCO_3$ (35-60 nm) was determined by XRD and confirmed by Transmission Electron Microscope (TEM). The styrene butadiene rubber (SBR) -$CaCO_3$ nanocomposites were prepared by using Brabender Plastograph. The mechanical and physical properties of SBR nanocomposites were determined .The fracture surface of SBR nanocomposites was observed by Scanning electron microscope (SEM). The results of Brabender processed SBR -$CaCO_3$ nanocomposites were compared with two roll mill processed SBR -$CaCO_3$ nanocomposites. The results showed that the reinforcement of $CaCO_3$ nano-filler in SBR polymer matrix enhanced the properties of SBR nanocomposites as compared to pristine SBR composites in both the techniques. The substantial improvement in properties was observed in case of Brabender processed SBR -$CaCO_3$ nanocomposites as compared to pristine and two roll mill processed SBR -$CaCO_3$ nanocomposites. The enhancement in properties was observed in Brabender processing technique due to the higher shear rates which resulted in proper dispersion and mixing of nano $CaCO_3$ in SBR polymer matrix and proper wettability of inorganic particles by polymer matrix.

Keywords: - Styrene butadiene rubber (SBR), Nanocomposites, Brabender Plastograph, Scanning electron microscope (SEM)

1. Introduction

Polymer nanocomposites have been intensely researched in the last decade since the addition of a small quantity of reinforcement fillers such as clays in the polymer matrix have led to improvements of mechanical, thermal, and barrier properties.[1-2]. The nano-sized fillers have dramatically increased the surface area compared with conventional-sized materials. The increased surface area of nano reinforced materials is responsible for the improvement in properties of nanocomposites compared to pure polymers or filled with conventional fillers. The nanocomposites are new class of composites that are particle filled materials in which at least one dimension of dispersed particles is in the nanometer range.

Polymer matrix must have good process properties so that the dispersed particles can result in a large improvement in composite properties.[3-4]

Normally mixing is done on two roll mill. But proper mixing (dispersion) of fillers is very important to achieve maximum level of properties. Hence in addition to two roll mill we mixed nanoparticles into SBR by using Brabender Plastograph and compared both the techniques for performance.

2. Experimental

2.1 Materials

Styrene butadiene rubber (SBR)

Rubber additives Viz. stearic acid, zinc oxide (ZnO), zinc diethyl dithiocarbamate (ZDC), mercapto benzothiozyl disulphide (MBTS), vulconex, and sulphur,

Calcium chloride (AR Grade), potassium carbonate, and poly (ethylene glycol) (PEG; molecular weight of 6000) for synthesis of nano $CaCO_3$.

2.2 Preparation of nanoparticles

The nano-sized calcium carbonate particles were synthesized in the laboratory by using-

- **Matrix mediated growth and controlled i.e. *in situ* deposition technique.** [5-10]

2.3 Preparation of Rubber nanocomposites

Two different techniques were used for preparation of styrene butadiene rubber (SBR) nanocomposites **1) Two roll mill**

2) Brabender Plastograph

2.4 Characterization

The following characterization techniques were used-

1. **Particle size determination - X-ray powder diffraction technique.**
2. **Mechanical (Tensile properties) - Universal Testing Machine**
3. **Hardness- Hardness tester Shore scale-A**

4. Swelling index – Toluene 24 hr (27 ^{0}C)

5. Surface morphology- Scanning Electron Microscope (SEM)

3 Results

1. Particle Size by X-ray diffraction (XRD) technique

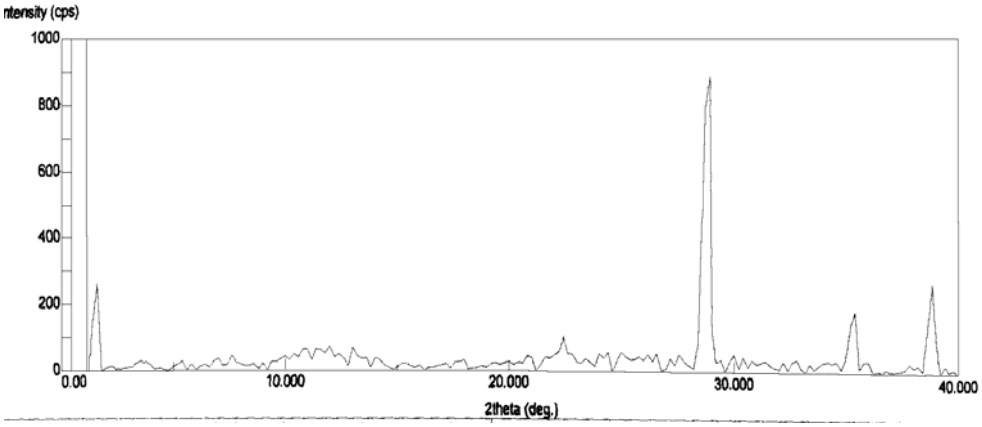

Figure 1. XRD of synthesized nano $CaCO_3$

- **Particle size determined by using Scherer's formula-**
- **$d = k \lambda / \Delta 2\theta \cos \theta$**

2. Mechanical Properties

I) Tensile strength

It is observed that the tensile strength of Brabender processed SBR nanocomposites showed better tensile strength than the two roll mill processed SBR nanocomposites.The improvement in tensile strength of samples processed on Brabender is due to the proper mixing of nano filler $CaCO_3$ in polymer matrix which results the uniform dispersion of nano filler in SBR polymer matrix.

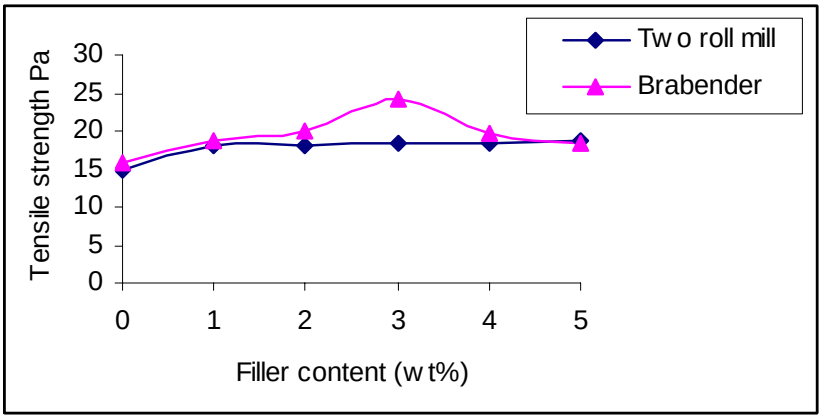

Figure 2. Tensile strength of SBR filled with nano $CaCO_3$ processed on two roll mill (TRM) and Brabender Plastograph

II) Elongation at break (% Elongation)

For all compositions, elongation at break of nanocomposites increased with increasing filler content up to 3 wt % and 4 wt % filler loading for both Brabender and two roll mill respectively. Value of elongation at break decreased after attaining the peak value, the trend was found to be similar in both the techniques. The reason may be agglomeration of nano particles as well as formation of weaker interfacial region between the filler surface and matrix where in cracks develops**.**

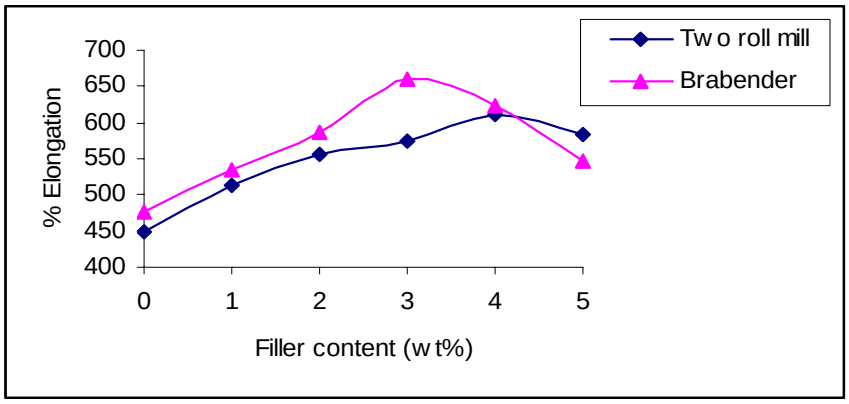

Figure 3. % elongation of SBR filled with nano $CaCO_3$ processed on two roll mill (TRM) and Brabender Plastograph

3. Hardness

Hardness of all composition increased up to 4 wt % of filler amount for both mixing technique than the pure SBR composites as shown in figure. Hardness increased due to the greater degree of crosslinkage which has been occur during vulcanization of rubber nanocomposites by uniform transfer of heat in to the rubber matrix. Also the formation of effective layer is responsible for increase in hardness of rubber nanocomposites.

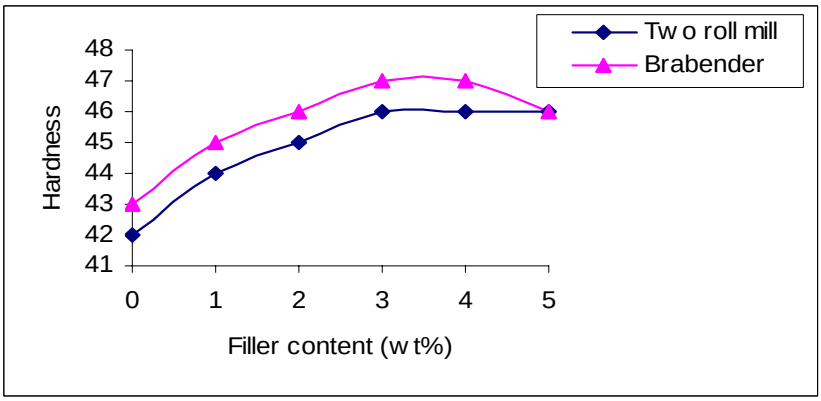

Figure 4. Hardness of SBR filled with nano $CaCO_3$ processed on two roll mill (TRM) and Brabender Plastograph

4. Swelling index

The swelling indices of different filler content of two roll mill as well as Brabender processed SBR nanocomposites are shown in Fig.-6 Lower swelling in case of Brabender processed nanocomposites is due to greater cross linking of SBR because of a uniform dispersion of nano $CaCO_3$ which brings the chains closer and keep them intact with nanofiller.

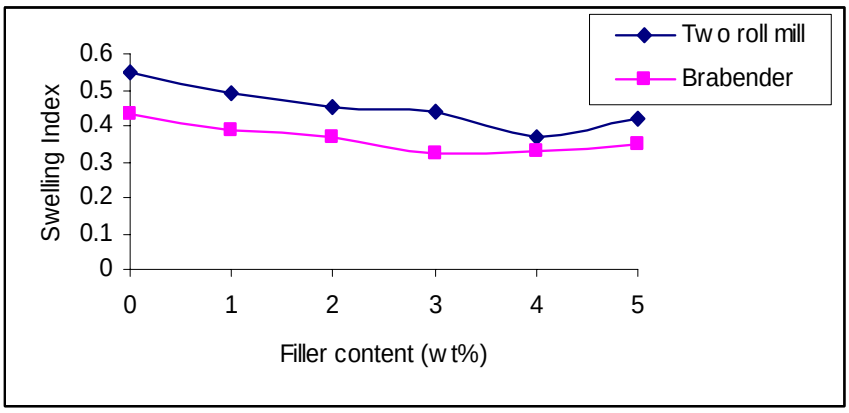

Figure 5. Swelling index of SBR filled with nano $CaCO_3$ processed on two roll mill (TRM) and Brabender Plastograph

5. Surface morphology

The surface morphology of fractured SBR nanocomposites prepared on Brabender and two roll mill mixing technique were investigated by Scanning Electron Microscope (SEM)

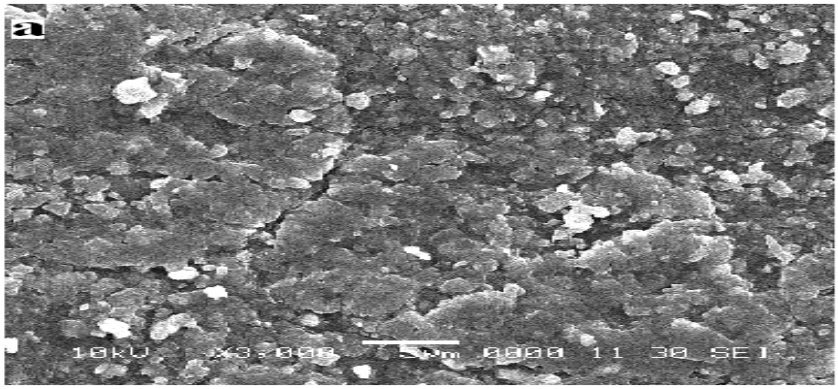

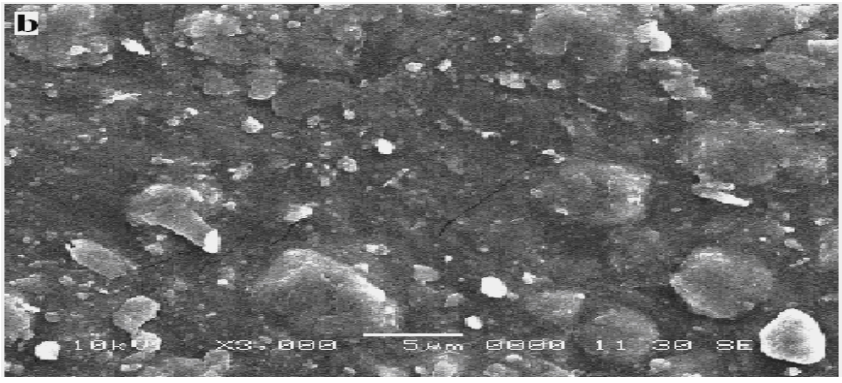

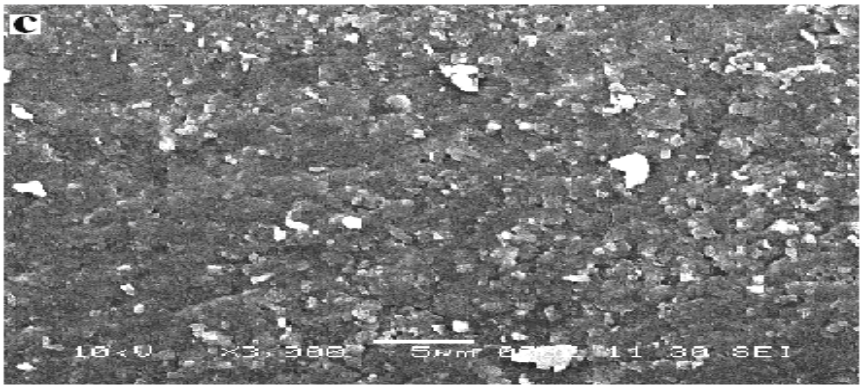
c
10.0 X3,500 5μm 0000 11 30 SEI


d
10.0 X3,000 5μm 0000 11 30 SEI

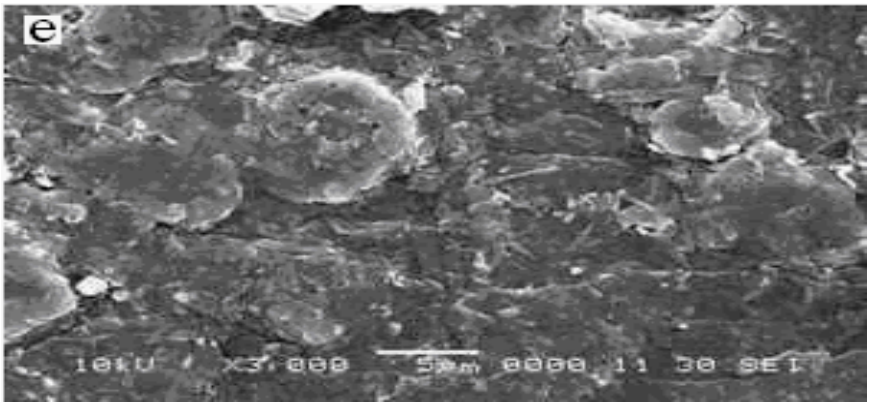
e
10kV X3,000 5μm 0000 11 30 SEI

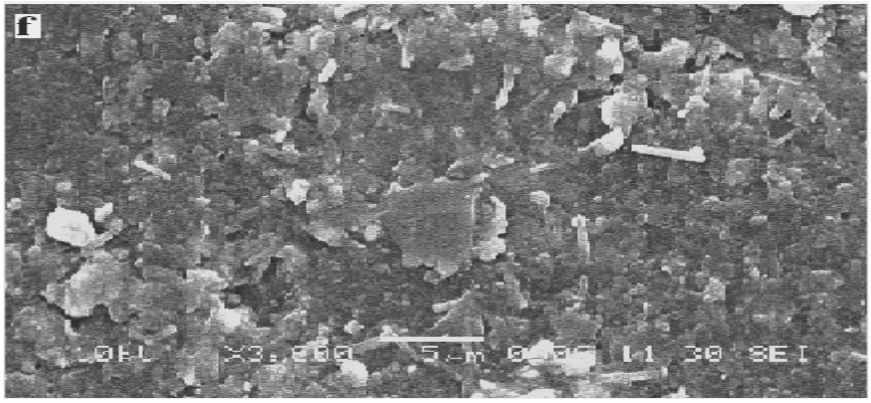
f
10kV X3,000 5μm 0000 11 30 SEI

Figure 7. Scanning Electron Micrographs of SBR -$CaCO_3$ nanocomposites a) b) & c) For 1, 3 and 5 wt% filler content processed on Two roll mill (TRM) and d) e) & f) For 1, 3 and 5 wt% filler content processed on Brabender Plastograph

Conclusion

The nano-filler $CaCO_3$ were synthesized in the laboratory. The reinforcement of nano filler $CaCO_3$ in SBR improved the mechanical as well as thermal properties of pristine SBR. The Brabender processed SBR nanocomposites as compared to two roll mill processes nanocomposites showed better improvement in properties because of more shear rate which results proper mixing of all ingredients including filler in the matrix. Therefore uniform dispersion of nano filler $CaCO_3$ in the SBR matrix was achieved by Brabender Plastograph.

References

1. Fu, X. and Qutubuddin, S., "Polymer-Clay Nanocomposites: Exfoliation of Organophilic Montmorillonite Nanolayers in Polystyrene," *Polymer*, 42, 807-813, 2001.
2. Messersmith, P.B. and Giannelis, E.P., "Synthesis and Characterization of Layer Silicate-Epoxy Nanocomposites," *Chem. Mater.*, 6, 1719-1725, 1996
3. Yano, K., Usuki, S., Okoda, A., Kurauchi, T. and Kamigatio, O. (1993).Synthesis and Properties of Polyimide-clay Hybrid, J. Polym. Science.,31(10): 2493–2498.
4. Wang, Y., Zhang, L., Tang, C. and Yu, D. (2000). Preparation and Characterization of Rubber-clay Nanocomposites, J. Applied Polymer Science., 78(11): 1879–1883.
5. Mishra, S., Shimpi, N. G. (2005). Comparision of Nano $CaCO_3$ and Flyash Filled with Styrene Butadiene Rubber on Mechanical and Thermal Properties, JSIR, Vol-64.
6. Saujanya, C., Radhakrishnan, S. (1998). Structure Development in PP/$CaSO_4$ Composites: Part-I Preparation of Filler by an *In –situ* Technique, *J Mater Sci*, 33: 1062-1068.
7. Mishra, S., Sonawane, S. H., Singh, R. P., Bendale, A. and Patil, K. (2004). Effect of Nano Mg $(OH)_2$ on the Mechanical and Flame Retarding Properties of PP Composites, *J Appl Polym Sci*, 94:116.
8. Gleiter H., *Nanostructure Mater* 1991, 1, 1.
9. Koch C C., *Nanostructure Mater*, 1991, 21:559.
10. Mishra, S., Sonawane, S. H. and Singh, R. P., (2005). Studies on Characterization of Nano $CaCO_3$ Prepared by *In-situ* Deposition Technique and Its Application in PP-nano $CaCO_3$ Composites, *J Polym. Sci Part B: Polym. Phys*, 43:107.

Effect of post drawing parameters of melt spinning of carbon nanotube filled polypropylene fiber

Srikanth S. Kamath[a]*, Arup R. Bhattacharyya[a#], Pankaj B. Tambe[a], Ajit R. Kulkarni[a], T.V. Sreekumar[b], Kingsuk Mukhopadhyay[b] and Anurag Srivastav[b]

[a]Department of Metallurgical Engineering and Materials Science, Indian Institute of Technology Bombay, Powai, Mumbai- 400076, India
[b]Defence Materials and Stores Research and Development Establishment (DMSRDE), DRDO, Kanpur 208013,India
E-mail: arupranjan@iitb.ac.in

Abstract

Melt spun multiwall carbon nanotubes (MWNT) filled polypropylene (PP) fibers were drawn at draw ratio of 8 with variation of post drawing parameters (temperature and speed of drawing the composite fibers) in order to understand the effect of post drawing parameters on mechanical properties of composite fibers. It was found that fiber drawn at high temperature and low drawing speed showed an increase in mechanical properties of PP/MWNT composite fibers than any other combination of variation of post drawing parameters.

1. Introduction

Isotactic polypropylene (PP) utilized as a commercial polymeric fiber exhibits a wide range of mechanical properties. However, PP fiber needs reinforcement in order to achieve high stiffness and strength for engineering applications. Since the discovery of carbon nanotubes (CNT) by Iijima [1], CNT have emerged as a potential candidate as reinforcing filler in polymer based composite fibers in view of their unique mechanical, electrical and thermal properties [2]. Fiber with mechanical properties suitable for advanced engineering application require orientation of polymer chains[3-7] as well as that of CNT[8, 9] during post drawing operation. It was found that the average orientation of statistical chain segments of PP within the sample was independent of the drawing temperature whereas the yield stress and elongation at break wee strongly influenced by the applied drawing temperature. A significant drop in yield stress could be observed for a fixed draw ratio with lowering the drawing temperature. At a certain temperature this drop leads to a transition from brittle to ductile failure behavior, resulting in an increase in elongation at break [3]. The effect of the postdrawing at a constant draw ratio manifests in either high stiffness in combination with superior draw ability/energy absorption (lowest possible post drawing temperature, formation of mesomorphic phase) or a high stiffness in combination with high strength (highest post drawing temperature in the affine deformation regime) [4].

The aim of this work is to understand the effect of varying post drawing parameters (temperature and speed of drawing the composite fibers) at varying multiwall carbon nanotubes (MWNT) concentration on the mechanical properties of PP/MWNT composite fibers drawn at a fixed draw ratio of 8.

2. Experimental Details

Polypropylene was obtained from Reliance Industries Ltd, India (REPOL H200F, melt flow index 20 g/10min). MWNT were obtained from DMSRDE, Kanpur. Various compositions of PP/MWNT composites were prepared by melt-mixing in which MWNT were varied from 0.5-3 wt% in a conical twin-screw microcompounder (Micro 5, DSM Research, Netherlands) at optimized melt mixing condition of 260^0C with a rotational speed of 200 rpm for 15 min. Melt compounded PP/MWNT samples were dried at 80^0C under vacuum over night. They were melt-spun using a small scale spinning machine manufactured by the Bradford University Research Ltd. UK, using a single hole spinneret of 1 mm diameter. The fiber spinning was carried out at 200^0C with ram speed of 1.4 mm/min. The take up speed was kept at 20 m/min for all compositions. The melt spun fibers were further drawn at draw ratio of 8 by varying the post drawing parameters (temperature and drawing speed). Details of variation of post drawing parameters provided in Table 1 which depicts 12 exiperments were performed for each MWNT concentration of 0.5, 1 and 3 wt% respectively. The mechanical properties of drawn fiber were tested on a Favimat fiber tester (Textechno) with gauge length of 20 mm and at a rate of 20 mm/min for 50 filaments.

3. Result and Discussion

3.1 Mechanical properties

If the composite fibers are to be obtained of high tenacity, high modulus of elasticity and low elongation at break; nanotube orientation distribution along the fiber axis should be higher. In this context, it is also reported that CNT/polymer interface influences significantly the mechanical properties of the composite fibers [10].

Figure 1 exhibits the distribution of modulus, tenacity and elongation at break of composite fibers at various post drawing parameters. It is observed that variation in post drawing parameters lead to the dramatic changes in mechanical properties of composite fibers.

Tenacity (which is a measure of fineness of fiber) and modulus increases with decreasing drawing speed and corresponding increase in temperature (Figure 1a-b). High modulus values are achieved for those combinations of post drawing parameters which exhibits less elongation. This may be due to the addition of MWNT which prevent the polymer chain from slipping past each other thereby improving modulus and reducing the elongation. In case of pure PP, failure is found to occur due to PP chains sliding past each other according to Smith Irvine model [11].

It is observed that at lowest drawing speed i.e 8 m/min modulus values are found to be higher than composite fiber drawn at higher drawing speed for all the combination of temperature and various weight fractions of MWNT. It is the orientation distribution of MWNT [10] at a definite post drawing parameter which contributes to the superior mechanical properties of composite fiber. The highest modulus and tenacity value are observed at post drawing parameters of 100^0 C, 8 m/min for 1 wt % of MWNT and 120^0 C, 8 m/min for 0.5 wt % of MWNT (Figure 1a-b).

3.2 Discussion

It is interesting to note that with an increase in temperature modulus increases at low drawing speed. At 80^0 C, drawing of fiber much above the glass transition temperature, the interaction between chains and interaction in between chain and nanotubes restrict the achievable orientation of MWNT.

Drawing the fiber at 100^0 C, which is near to the crystallization temperature result in better orientation of MWNT which manifests in an increase in overall mechanical properties than fiber drawn at 80^0 C. Drawing the fiber at 120^0 C, which is above the crystallization temperature results in even better orientation of MWNT than drawing at 100^0 C which manifests in an increase in overall mechanical properties.

However, PP/MWNT composite fibers do not exhibit any linear increase in mechanical properties with increasing MWNT concentration. The reason is due to inadequate interfacial interaction in between the PP chain and MWNT; formation of MWNT aggregates in PP matrix and due to MWNT slippage which is detrimental to the mechanical properties of composites [12, 13].

4. Conclusion

It was found that drawing speed and temperature had a profound effect on the mechanical properties of composite fiber. The favorable condition of drawing the composite fiber was drawing at higher temperature and at low drawing speed.

5. Acknowlegements

We would like to acknowledge Microcompounder Central facility, CRNTS at IIT Bombay. We would also like to thank DMSRDE, Kanpur for the financial assistance for the project (TR/0569/CARS-33).

6. References

[1] Iijima S, Nature 1991; 35:56.
[2] Baughman R. H, Zakhidov A. A, Heer W, Science 2002; 297:787.
[3] Tilo S, Ton P, Piet J, Joachim L, Macromolecules 2004; 37:1810
[4] Joachim L, Tilo S, Macromolecules 2005; 38:10678
[5] Bodaghi, H., Spruiell, J. E., and White, J. L., Int. Polym. Process 1988; 3:100
[6] Hahn, K.; Kerth, J.; Zolk, R.; Schwahn, D.; Springer, T.; Kugler,. J. Macromolecules 1988; 21:1541.
[7] Abo El Maaty M., Bassett, D., Olley R., Dobb M., Tomka J., Wang I., Polymer 1996; 37:213
[8] Bhattacharyya A R,, Sreekumar T.V, Liu T, Kumar S, Ericson L. M, Hauge R, Smalley R. E, Polymer 2003; 44:2373.
[9] Moncy V. J, Derrick D, James T, Gary P, Elijah N, Journal of Applied Polymer Science 2007; 103:3844.
[10] Bing J, Charlie L, Chuck Z, Ben W, Zhi W, Composites: Part B 2007; 38:24
[11] Irvine P, Smith Pet.al Macromolecules 1986; 19:240
[12] Ajayan P, Jonghwan S, Koratkar M, J Material Science 2006 ; 41: 7824
[13] Ajayan P, Schadler L, Giannaris C, Rubio A, Advanced Materials 2000; 12:750

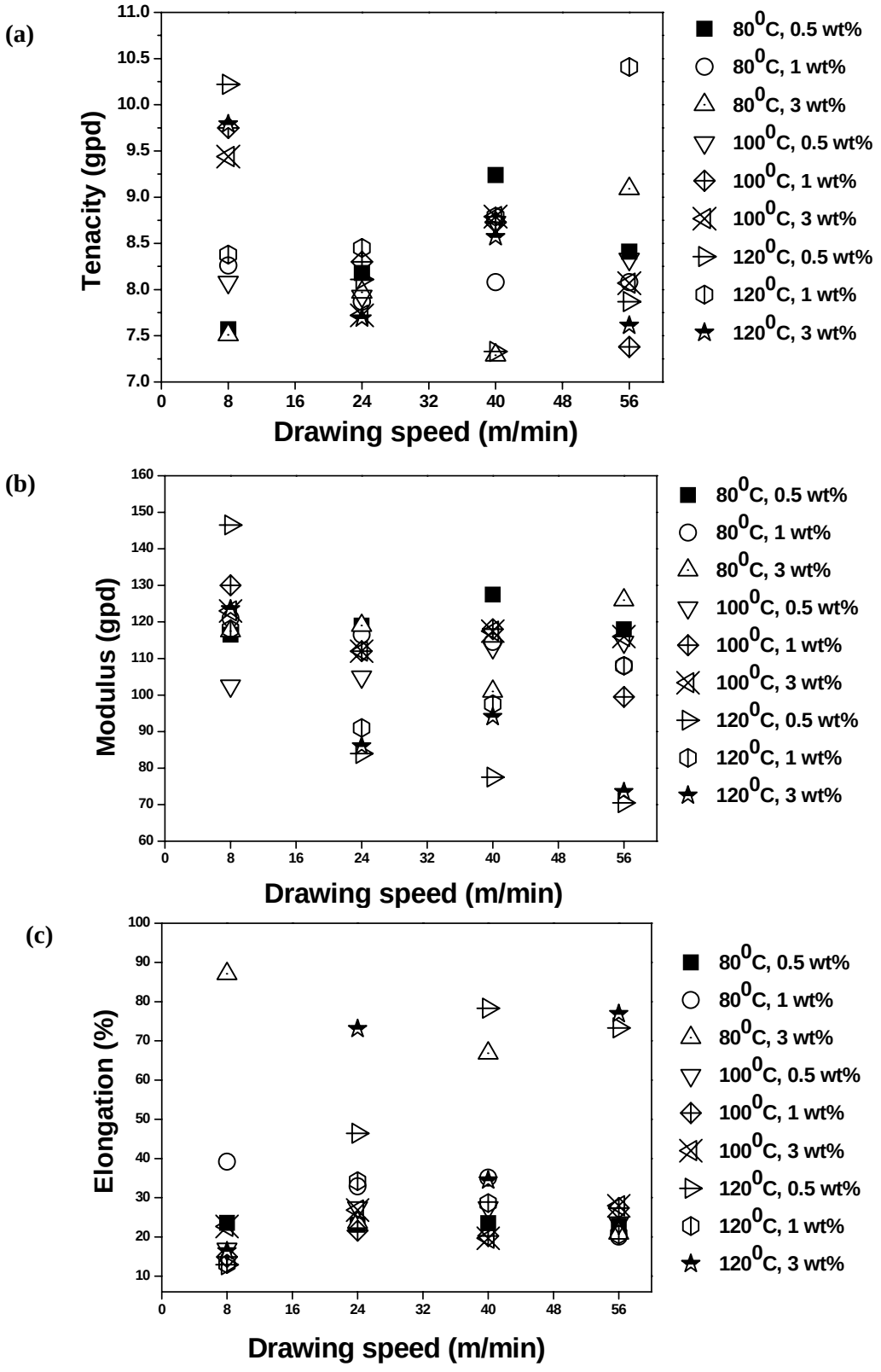

Figure 1: Effect of MWNT concentration on (a) tenacity (gpd) (b) modulus (gpd) (c) elongation at break (%)

Table 1: Experimental details of varying post drawing parameter variation

Level	Temperature (degrees)	Speed (m/min)
1	80	8
2	100	24
3	120	40
4	--	56

Finite element analysis of hyperelastic material

[1]R.Sujithra and [2]R.Dhanaraj
1. Department of Rubber Tech., 2.Department of Aerospace Engg.,
Madras Institute of Technology,
Anna University, Chennai-600044

E-mail Id: suji_forever@rediffmail.com

ABSTRACT

Due to the increasing demands of the rubber components used in the automotive and aerospace industries, the development of computational methods for elastomer analysis has attracted extensive research attention. This research work is focused on developing a finite element program code for the analysis of hyperelastic material restricted to plane stress case.

Hyperelastic refers to materials which can experience large elastic strain that is recoverable. Rubber like materials falls in this category. The behavior of hyperelastic material is described based on Mooney-Rivilin and Neo-Heokean material models. The constitutive theories for a large elastic deformation is based on the strain energy density function which is coupled with finite element method, can be used effectively to analyze and design elastomer.

Due to non-linear stress-strain relation, the hyperelastic materials will cause a structure stiffness to change at different load levels. In finite element formulation, the modeling of hyperelastic material should incorporate both geometric non-linearity due to large deformation as well as material non-linearity. Because of nonlinear relationship the finite element equations are nonlinear in terms of displacement. An iterative Newton-Raphson method was employed for the solution of non-linear governing equations. At each finite element solution step we obtained strain or strain increment, used to compute the stress which is needed to evaluate the internal force as well as the tangent stiffness matrix. The computed stress and deformation results obtained from finite element program code shows a good agreement with simple benchmark problem and as well as with FEA package (ANSYS).

I. INTRODUCTION

Hyperelastic is the capability of the material to undergo large elastic strain due to small forces, without losing its original properties. Rubber-like materials exhibit a highly non-linear behavior characterized by hyperelastic deformability and incompressibility or nearly incompressibility. But in general, all real materials are compressible to a certain degree even if the bulk modulus of the rubber-like material is larger than the shear modulus. Rubbers are widely used in tires, door seals, o-rings, conveyor belts, bearings, shock absorbers etc. An increase of applications of rubber-like materials requires better understanding of mechanical behavior which cannot be described by a simple stress-strain relation, but by the strain energy function. A hyperelastic material is also defined as a material whose stresses can be defined by a strain energy function.

Two sources of non-linearity exist in the analysis of hyperelastic materials namely, material and geometric non-linearity. The former occurs when the stress-strain behavior given by the constitutive relation is non-linear, whereas latter is important, when changes in geometry, however large or small have a significant effect on the load deformation behavior. The basic features of stress-strain behavior have been well modeled by invariant based or stretch based continuum mechanics theories. An important problem in non-linear elasticity theory is to come up with a reasonable and applicable elastic law which is the key to the development of reliable analysis tools. Many strain energy functions are proposed for rubber-like materials by Mooney (1940), Treloar (1944), Ogden (1972) etc. The simplest one parameter model is the Neo-Hookean model. In this present work, hyperelastic constitutive equations are discussed based on compressible Neo-Hookean model.

Finite element method is a procedure whereby the continuum behavior described at infinity of points is approximated in terms of finite number of points called nodes located at specific points in the continuum. These nodes are used to define regions, called finite elements over which both the geometry

and the primary variables in the governing equations are approximated. The governing equations describing the nonlinear behavior of the solid are recast in a weak integral form using principal of virtual work. The finite element approximations are then introduced into these integral equations which yields a finite set of non-linear algebraic equations in the primary variable. These equations are usually solved using Newton-Raphson iterative technique.

Based on finite element formulation, finite element program code is developed in C for the analysis of hyperelastic material for computing stresses and deformation. For simple benchmark problems, the result obtained from the coding is validated with ANSYS packages.

II. NON-LINEAR CONTINUUM MECHANICS

Continuum mechanics [1, 2] is an essential building block of nonlinear finite element analysis. We will confine our attention to the strain and stress measures which are most frequently employed in nonlinear finite element program. Two approaches are used to describe the deformation and response of a continuum. Consider a solid that is subjected to some forces and displacements such that its configuration changes from the initial to the current. In finite deformation analysis, any quantity can be described either in terms of the undeformed state or in a deformed state; the former is called material or Langrangian description while latter is called spatial or Eulerian description. In solids, the stresses generally depend on the history of deformation and an undeformed configuration must be specified to define the strain. So Langrangian descriptions are prevalent in solid mechanics.

A point is identified by a vector X in the initial configuration which moves to a new point identified by a vector x in the current configuration the mapping Θ of the motion is expressed as

$$X = \Theta(X, t) \tag{2.1}$$

In similar way, consider a line segment dx in material configuration is deformed to dX after the motion. The deformation gradient is defined by, $F = \partial x / \partial X$ (2.2)

The displacement of point is given by the vector u as a function of **X**, the differential displacement is given as $du = H\, dX$ (2.3)

The relation between deformation gradient and displacement gradient is $F = H + I$

To calculate the change in length dx after deformation using (2.2)

$$dx.dx = dX.\, F^T F\, .dX \tag{2.4}$$

At this point, we define the right Cauchy-green deformation tensor where c operates on material element and hence it is a Lagranian tensor. $c=F^T F$ (2.5)

Similarly, we define the left Cauchy-green deformation tensor b is an Eulerian tensor which operates on spatial element $dx\, b^{-1}\, dx = dX\, dX$ (2.6)

$$b = FF^T \tag{2.7}$$

.The green (or Lagragian) strain tensor is defined as $E = ½\ (c-I)$ (2.8)

And corresponding spatial spatial tensor, called Almansi strain tensor $e = ½\ (I-b^{-1})$ (2.9)

Also the volume dv and area da after deformation can be related to the initial volume dV and area dA using the deformation gradient F (det F=J) and is given as

$$dv = JdV \tag{2.10}$$

$$da = JF^{-T}.dA \tag{2.11}$$

Cauchy stress (Eulerian quantity) which relate the force dh acting on a differential area da is given as

$$dh = \sigma\, .da \tag{2.12}$$

From equ, shifting area to its initial configuration, $dh = J\, F^{-T} dA = P.dA$ (2.13)

Where P is the first piola-Kirchhoff stress defned as $P = JF^{-T}$ (2.14)

It is an unsymmetrical two point tensor and is not completely related to material configuration

The force vector dh can be related to its initial configuration in a similar manner

$$dh = F.dH \tag{2.15}$$

And rearranged as , $$dh = JF^{-1}F^{-T}.dA = S.dA \tag{2.16}$$

Where S is the second piola-kirchhoff stress tensor defined as $S=JF^{-1}F^{-1}$ (2.17)

Hyperelasticity is type of elasticity where the stress at any point can be derived from the deformation gradient and from an energy function. The behaviour of the material is said to be path independent and P is work conjugate with the rate of deformation gradient Ḟ,a stored elastic potential Ψ per unit undeformed volume can be established as the work done by the stresses form the initial to the current position as, $$\Psi = P : \dot{F} = S : \dot{E} = (\partial\Psi/\partial E)\,\dot{E} \tag{2.18}$$

Observing that ½ ċ=Ė is work conjugate to the second PK stress enables a totally lagrangian constitutive equation to be constructed in the same manner as $S = \partial\Psi/\partial E = 2\partial\Psi/\partial c$ (2.19)

Based on the isotropic assumption, the strain energy density function W is expressed as a function of the strain invariants .A better approach to modeling the response of rubbers comes from assuming existence of strain energy which is a function of deformation tensor. Strain invariants can be expressed in terms of the stretch ratios λ_1, λ_2, and λ3 as follows

$$\Psi = \Psi(I_1, I_2, I_3)$$
$$I_1 = \lambda_1^2 + \lambda_2^2 + \lambda_3^2 = \text{tr}(c)$$
$$I_2 = \lambda_1^2\lambda_2^2 + \lambda_2^2\lambda_3^2 + \lambda_3^2\lambda_1^2 = ½\,[(\text{tr}\,c)^2 - \text{tr}(c^2)]$$
$$I_3 = \lambda_1^2\lambda_2^2\lambda_3^2 = \det c \tag{2.20}$$

For incompressible material I_3=1.The strain energy function for Neo-Hookean material is given as

$$\Psi = C_1(I_1 - 3) \tag{2.21}$$

In many cases rubber is compressible to some extent and it is important to consider compressibility. This work deals with the compressible form and introduces a strain energy contribution involving the bulk modulus. For compressible form [4], the strain energy should combine both volumetric and deviatoric term.

$$\Psi = \Psi v + \Psi d$$
$$\Psi = ½\,\lambda\,(\ln(\det F))^2 - \mu \ln(\det F) + ½\,\mu\,(\text{tr}(c) - 3) \tag{2.22}$$

PK stress and Cauchy stress can be easily be computed from (2.22) and given as

$$S = \lambda(\ln(\det F))c^{-1} + ½\,\mu\,(I - c^{-1}) \tag{2.25}$$
$$\sigma = \lambda/\det t\,(\ln(\det F))\,I + (\mu/\det F)\,(b - I) \tag{2.24}$$

The components of the fourth-order elasticity tensor are obtained as follows:

$$C_{ijkl} = \lambda c_{ij}^{-1}c_{kl}^{-1} + (\mu - \lambda \ln(\det F))(cik^{-1}c_{jl}^{-1} - c_{il}^{-1}c_{kj}^{-1}) \qquad i,j,k,l = 1,2,3 \tag{2.25}$$

III. FINITE ELEMENT FORMULATION

The finite element equations are non-linear in terms of displacement because of nonlinear strain-displacement and stress-strain relationships. By the principle of virtual work, the weak form in the current configuration is given as

$$\int_V \delta e^T \sigma\, dv = \int_A \delta u^T q\, dA + \int_V \delta u^T b\, dv \tag{3.1}$$

For problems involving large displacement [6], consideration should be given to the configuration. Since the current configuration is not known, we cannot compute directly from this equ (3.1). Using the deformation gradient, the derivatives and integrals in the weak form are transformed to the initial configuration (Total Langrangian formulation).

$$\int_{V^o} S\, \delta e\, dV^o = \int_{A^o} \delta u^T q^o\, dA^o + \int_{V^o} \delta u^T b^o\, dv^o \tag{3.2}$$

The equ (3.2) is linearized and we get element tangent matrix equations as follows

$$\int_{V^o}\int\int [B\hat{S}BT + BF^T C F B^T]dV^o \Delta d = -\int_{V^o}\int\int B F^T S\, dV^o + \int_{A^o}\int N q^o dA^o + \int_{V^o}\int N b^o dV^o \quad (3.3)$$

Thus, $(K_S+K_C)\Delta d = r_i + r_q + r_b$ (3.4)

Where K_c is the current stiffness matrix, K_s is the geometric stiffness matrix, r_i , r_q , r_b are the equivalent nodal load vector due to stresses in the current known configuration, due to surface forces and due to body forces. At the current state, the linearized finite element equation is calculated for each element and assembled. The equations are assembled and solved in the usual manner to obtain the increments in the displacements. The new deformed configuration can be obtained by adding these displacements to the initial coordinates using constitutive equations, we first calculate Cauchy stresses in deformed configuration. If the computed stresses are correct, the equilibrium equations must be satisfied in the configuration

Equivalent load vector due to stresses $r_I=\iiint B_L\sigma dV$ (3.5)

The unbalance force is calculated as follows $r = r_E-r_I$ (3.6)

The load vector from each element is assembled to form global r_I vector. This vector is compared against the applied nodal load vector. If the difference between two is large, a new iteration is carried out to establish a new deformed configuration. This process is repeated until a desired level of convergence tolerance is achieved.

IV. IMPLEMENTATION OF FEM IN PROGRAMMING

A C program is written based on the above finite element formulation using Four Noded Isoparametric element for the analysis of hyperelastic material restricted to plane stress case. Flow diagram for the program is shown in Fig: 1.

A computational procedures for programming is given briefly as

1. In the first step, get the nodal datas and assume initial displacement is zero.
2. Calculate bandwidth for global stiffness matrix.
3. Begin of iteration loop
    - 3.1 compute the geometric and current stiffness matrix
    - 3.2 Assemble global stiffness matrix from individual element tangent matrix
    - 3.3 By gauss elimination, solving $\{\Delta d\} = [k_t]^{-1}\{F\}$
    - 3.4 By solving, we get incremental solution of displacement.$d_{i+1}=d_i+\Delta d$
    - 3.4 Update the coordinates
    - 3.5 Compute stress from the new deformation gradient.
    - 3.6 Compute updated thickness
    - 3.7 Calculate internal load vector
    - 3.8 Unbalance force=external load – internal load.
    - 3.9 Check for convergence parameter.
4. If no, go for next iteration step No.3 .If yes, terminate the program.

Cooks Problem [8]:

A rubber tapered panel is clamped at one end and loaded by nodal forces on the top of the other end. The material properties used are C1=0.5 and bulk modulus1500. From the material parameter we determine lames constant which is the input for coding. We consider the problem to be nearly incompressibility and the poissons ratio is taken as 0.499. The geometry is shown in Fig.2. The nodal coordinates and result obtained from coding is shown in Table: 1. The problem is solved in ANSYS using Neo-Hookean material model and deformed shape is shown in Fig: 3. The Computed results from coding shows a good agreement with ANSYS shown in Table 2.

V.CONCLUSION

The analysis of hyperelastic material behavior by finite element method has been described in this study. Rubber like materials are incompressible but still its nearly incompressibility is considered as a special feature of compressible material. The Neo-Hookean material model is discussed based on compressible strain energy function by combining both volumetric and deviatoric term. Based on this approach, a finite element program code is implemented. A simple rubber tapered panel is solved by

Programming and also with FEA packages. The output from the program code is validated with simulated results.

References:

1. Gerhard A.Holzapfel, Nonlinear solid mechanics, John Wiley & sons, New York.
2. Javier Bonet, Richard D.Wood, Nonlinear continuum mechanics for finite element analysis, Cambridge university press.
3. O.C.Zienkiewicz, R.L.Taylor, The finite element method, Vol I & II.
4. M.A.Crisfield, Non linear finite element analysis of solids and structures, Vol I &II, John Wiley &sons, New York.
5. Odgen.R.W, Nonlinear elastic deformations, Dover Publications, New York.
6. Asghar bhatti.M, Advanced topics in finite element analysis of structures, John Wiley & sons.
7. Bathe K.J & Dvorkin E.N, some practical procedures for the solution of non-linear finite element equations, comp. meth. Appl. Mech & Engng, 22, 59-85 (1980).
8. T.Estebenit, A.Guessab,E.Jankovich, An enhanced strain mixed method applied to rubber-like material, Vol 52,No.3, pp 573-579, 1994.
9. Shu.H.Peng, Wenji V.Chang, A compressible approach in finite element analysis of rubber-elastic materials, computers & structures, vol 62, No.3, pp573-593, 1997.
10. Ted belytschko, wing kam liu, Brian Moran, Nonlinear finite elements for continua and structures, John Wiley & sons.
11. A.N.Gent, Engineering with rubber, hanser publishers, 2001.

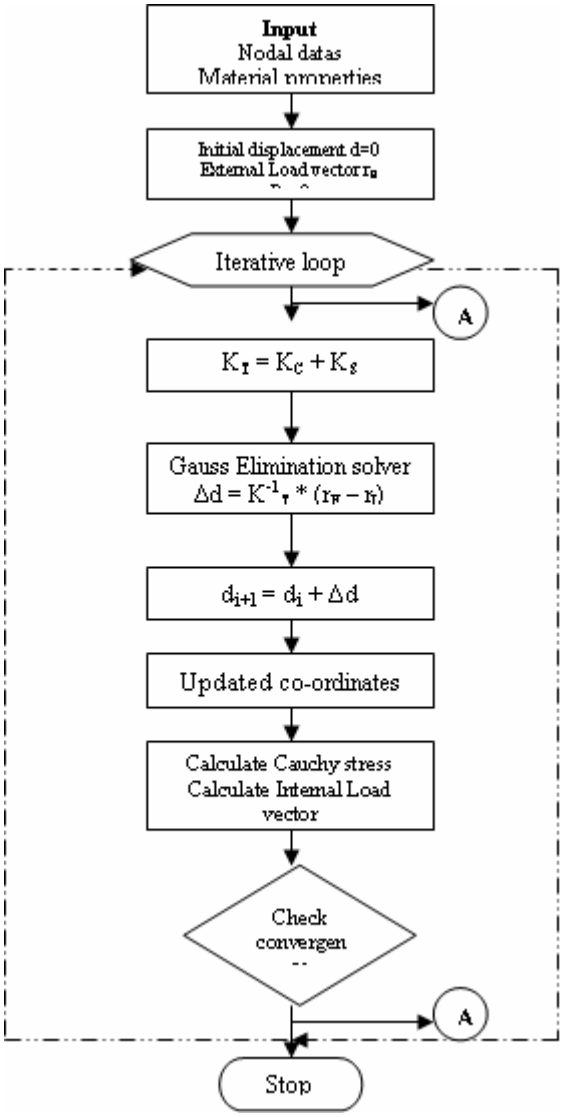

Fig: 1 Flow Diagram

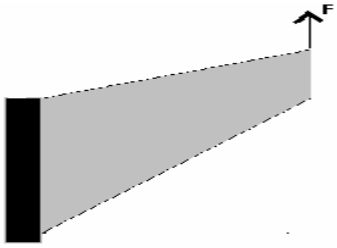

Fig: 2 Rubber panel

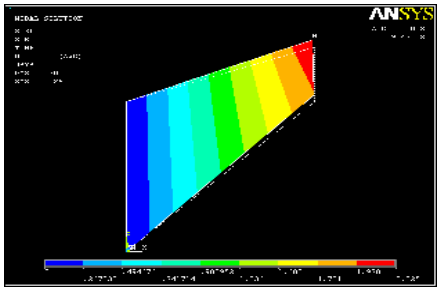

Fig: 3 Deformed shape in Ansys

Initial coordinates		Deformed coordinates	
X	Y	X	y
0	0	0	0
48	44	47.8845	45.9637
48	60	47.4028	62.2285
0	44	0	44
Convergence parameter= 0.00994			
Num of iterations =60			

Table: 1 Coding Results

Result	Program	Ansys
Max disp at top	2.2285	2.302

Table: 2

Stress analysis of air borne polymeric composite structure

Shiv Kumar, K. Shajahan, Lijo Vijayan, Reji John, R. R. Varma and M. Aravindakshan
Naval Physical & Oceanographic Laboratory,
Defence Research and Development Organisation, Kochi – 682 021
Email: tsonpol@vsnl.com

Abstract

Composite structures are extensively used in air borne applications in civilian and military field owing to inherent advantages of high strength to weight ratio, ability to withstand high loads, slow failure rates, tailorability of mechanical and chemical properties and better directional properties. The most common types of composites employed in air borne applications are carbon fibre reinforced epoxy and Glass Fibre reinforced epoxy. One of the FRP structures developed for airborne application is in the shape of 'C' with various geometrical discontinuities for weight reduction and mounting of sensors and hinges for integrating to main assembly. Presence of such deviations from regular geometries leads to build up of stress concentrations at such irregularities, which could be fatal and lead to catastrophic failures. In order to understand the actual stress distribution, predict and prevent any failure of the structure proper theoretical analysis is required

A finite element analysis software ANSYS was used to evaluate the stress response of the composite structure. As the structure is intended to operate underwater, analysis was carried out to simulate the effect of hydrostatic pressure loads. Airworthiness requirements also demands that the structure to withstand high inertial acceleration loads coming on the system during various manoeuvring. Analysis was also carried out to ensure that the structure is capable of withstanding these inertial acceleration loads. The structure is mounted with sensor elements and the effect of these sensor elements were modelled using lumped masses method. 10-node tetrahedral structural element was used to mesh the structure. As the structure is fabricated with fibre reinforce plastics having orthotropic properties, properties such as elastic modulus, shear modulus and Poison's ratio were considered for all the three directions for the analysis. The analysis was carried out for 30% glass filled polycarbonate, Glass fibre reinforced epoxy composites and Carbon fibre reinforced epoxy composites. The Von-Mises stress distribution obtained showed the maximum stress near the top hinges and the corresponding displacement distribution showed maximum displacements at the top of the structure.

Introduction

Many of the modern technological developments that have taken place in last few decades are due to new materials and new materials processing techniques. Among these materials which has come to stay, composites occupies an important place in various fields such as aerospace, defence, sports, automobile, etc. Composite structures are extensively used in air borne applications in civilian and military field owing to inherent advantages of high strength to weight ratio, ability to withstand high loads, slow failure rates, tailorability of mechanical and chemical properties and better directional properties.

A necessary prerequisite for the design and safe operation of composite structure is an accurate knowledge of their strength and stiffness properties. An assessment of these properties solely by testing of critical components or of prototype structure is feasible but is usually encumbered by punitive cost and time requirements. Therefore, analytical methods must be employed with aim of facilitating trade-off studies in early design phases, providing insight into the overall structure and identifying critical parts of the composite structures. [1]

Application of analytical methods on simple structures is feasible however, it becomes practically impossible to apply analytical solutions on complex shapes. Excessive approximations to implement analytical solutions may lead to erroneous results. Hence, it is essential to utilize other means of analysis of the structures. Various FEM tools are available to model such complex structures, however none of them specializes in FEM analysis of composite structures. Various structural analysis FEM packages however have capability to analyse complex shapes of orthotropic materials. One such software Ansys is used in analysis of current problem.

Due to inherent advantage of high strength to weight ratio and tailorable directional properties of composites, it finds extensive application in air borne systems. One such structure being developed is a 'C' channel shaped structure for housing of sensors. The structure has various grooves for mounting the sensors, discontinuities for weight reduction of overall structure and hinge holes for assembling with the main system. The details of such a 'C' channel structure is shown in figure 1.

As 'C' channel structures is non-symmetrical and has numerous discontinuities, mechanical behaviour of the structure cannot be easily predicted. Due to its irregular features, number of stress concentrations points will be present in it. Any improper fabrication or design will lead to catastrophic failure of the structure.

Analysis

The 3-D model developed was imported in FEM analysis software Ansys. Ansys was selected primarily of its excellent structural analysis capabilities and ability to support orthotropic and anisotropic materials in analysis. Von-mises stresses and Displacement Vector Sum were determined. Analysis was carried out for 3 different polymer composites viz.

1. 30 % short glass fibre filled polycarbonate,
2. 40% Unidirectional glass fibre reinforced Epoxy, and
3. 40% Unidirectional carbon fibre reinforced Epoxy.

The properties of the same are tabulated in table 1. The failure criteria were also analysed to determine whether the structure will withstand or fail while in operation.

The structure being air borne, it needs to withstand high inertial loads while in manoeuvring, take off and landing. and deployed underwater from a flying platform has to withstand high inertial loads as well as hydrostatic pressures on the system. While in analysis inertial load was taken into consideration. As the structure is to deployed underwater hydrostatic pressure was also taken in account on complete structure.

The structure is mounted with sensors of weight 180 gm at 5 different mounting point along with 2 hinge points and hydrostatic load of 4 MPa. The sensors are modelled as lumped mass for ease of modelling. A section of the boundary condition is as shown in the figure 2. The red arrows show the hydrostatic pressure acting throughout the structure while light blue arrows shows the hinge point area with zero degree of freedom. The yellow arrows represent the sensor mass acting on the structure.

The structure was modelled using 10 node tetrahedral structural element referred at SOLID 187 in Ansys. SOLID187 element is a higher order 3-D, 10-node element. SOLID187 has a quadratic displacement behaviour and is well suited to modelling irregular meshes such as those produced from various CAD/CAM systems. The element is defined by 10 nodes having three degrees of freedom at each node: translations in the nodal x, y, and z directions. The element has plasticity, hyperelasticity, creep, stress stiffening, large deflection, and large strain capabilities. It also has mixed formulation capability for simulating deformations of nearly incompressible elastoplastic materials, fully incompressible hyperelastic materials and elastic orthotropic materials. [4,5]

Results and Analysis

The analysis carried out with various materials and their results are discussed below. Von-mises stress analysis of the structure with 3 identified composites were carried out and results are shown in figure 3, 4 and 5 respectively for 30 % short glass fibre filled polycarbonate, 40% Unidirectional glass fibre reinforced Epoxy and 40% Unidirectional carbon fibre reinforced Epoxy.

The maximum stress obtained in three cases is in 320 MPa which well below the failure strength of carbon fibre based composites. Similarly, for the case of glass fibre based composite and glass fibre filled polycarbonate does satisfy the requirement of maximum breaking strength. Hence in terms of required strength, component with either of the material will withstand the operating conditions.Next, Vector displacement of the component was analysed and results are shown in the figures 6, 7 and 8.

The 30% short glass fibre filled polycarbonate shows 35 mm of deformation in the lower end of the structure. As this much variation in the location of the mounted sensor will lead to erroneous result, it is unacceptable as suitable material for fabrication of the component. Both Glass fibre and carbon fibre based epoxy composite shows much less deformation and are suitable for the application. However, it is well known from the literature that glass fibre undergo gelation when it is exposed to sea water for long period of time and hence high factor of safety is required in design of the component. [6] As the component being modelled is limited by space constraint hence only recommended material is Carbon fibre based composite for fabrication of component.

Conclusion

The modelling of a critical component used in air platform based underwater deployable system was carried out to analyse the finalize the selection of suitable material of construction of the component using FEM software ANSYS. The structure having various irregularities in the shape was modelled using solid elements and Von-mises stresses and total vector displacements were analysed. The materials selected for analysis were 30 % short glass fibre filled polycarbonate, 40% Unidirectional glass fibre reinforced Epoxy and 40% Unidirectional carbon fibre

reinforced Epoxy. It was observed that even though 30 % short glass fibre filled polycarbonate has better properties in transverse directions but maximum forces are acting along the length of the component and it undergoes large displacement and hence cannot be considered as a suitable material for fabrication of the component. Furthermore, carbon fibre based composite was selected as a suitable material for fabrication based on its better long term property retention and lesser deformation in the shape.

Acknowledgement

The authors wish to express their thanks to Director, NPOL, Kochi for granting permission to carry out this work. Authors would also like to express their gratitude to Group Head (MS & MEMS), NPOL, Kochi for their encouragement and support.

Reference

1. Course notes of "*Design and Manufacture of Composite Components*" organised by AICTE and ISTE, Coimbatore, India, June 2003
2. www.boedeker.com/polyc_p.htm
3. Quinn, JA, "*Composite Design Manual"*, James Quinn Associates, Technomics, 19999
4. Release 9.0 Documentation of Ansys
5. www.philonnet.gr/products/ansys/ed/index.html
6. Lubin & Peters, "*Handbook of Composites"*, Springer, Inc., 1997

Figure 1: Section of the 'C' channel structure showing geometrical discontinuities

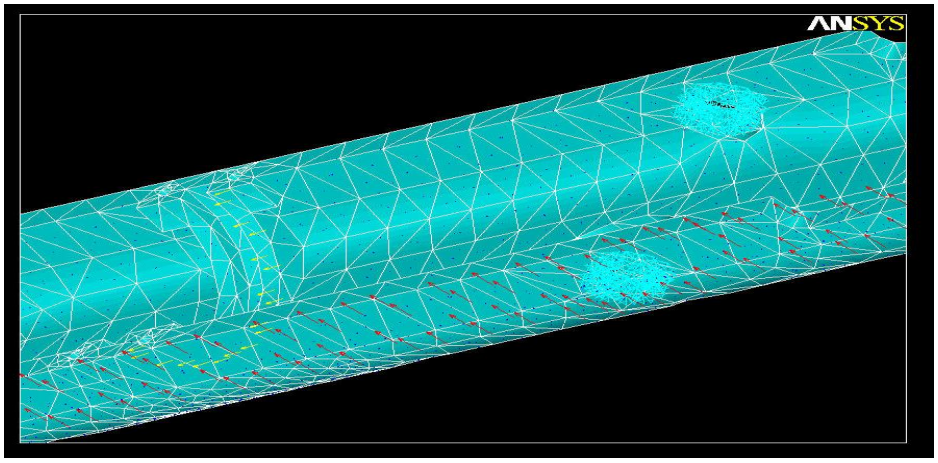

Figure 2: Section of the modelled structure showing various boundary conditions

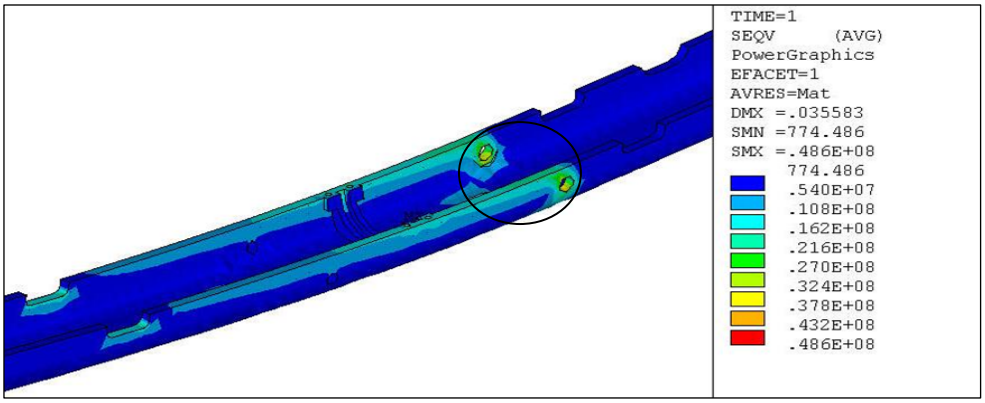

Figure 3: Von-mises stress distribution showing over a section of structure modelled with 30 % short glass fibre filled polycarbonate. Maximum stress of 48 MPa is obtained in the lower hinge section shown by the circle.

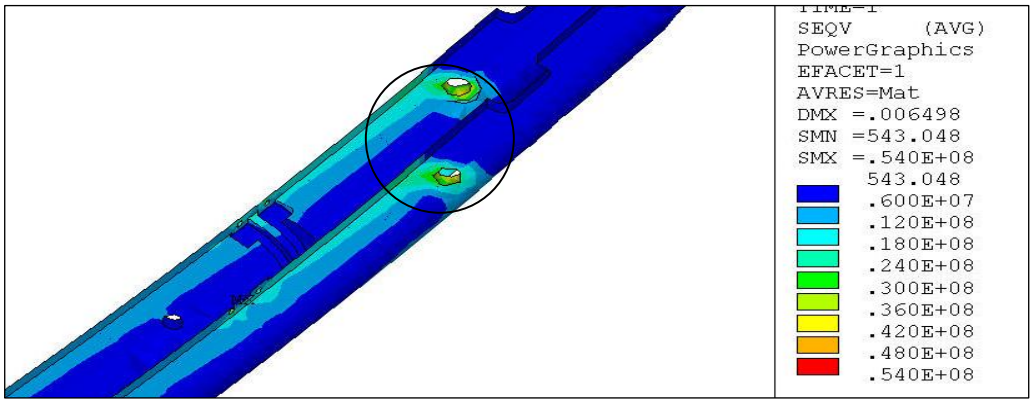

Figure 4: Von-mises stress distribution showing over a section of structure modelled with 40% Unidirectional glass fibre reinforced Epoxy. Maximum stress of 58 MPa is obtained in the lower hinge section shown by the circle.

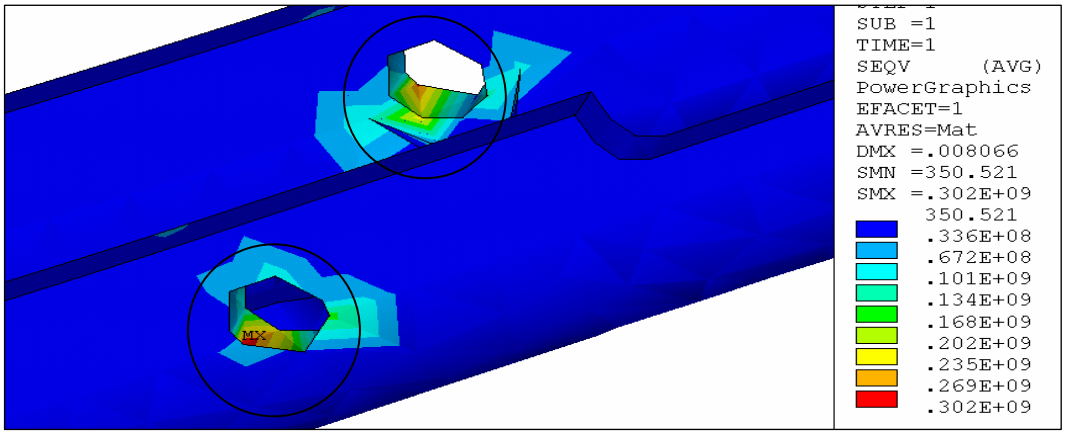

Figure 5: Von-mises stress distribution showing over a section of structure modelled with 40% Unidirectional carbon fibre reinforced Epoxy. Maximum stress of 320 MPa is obtained in the lower hinge section shown by the circle.

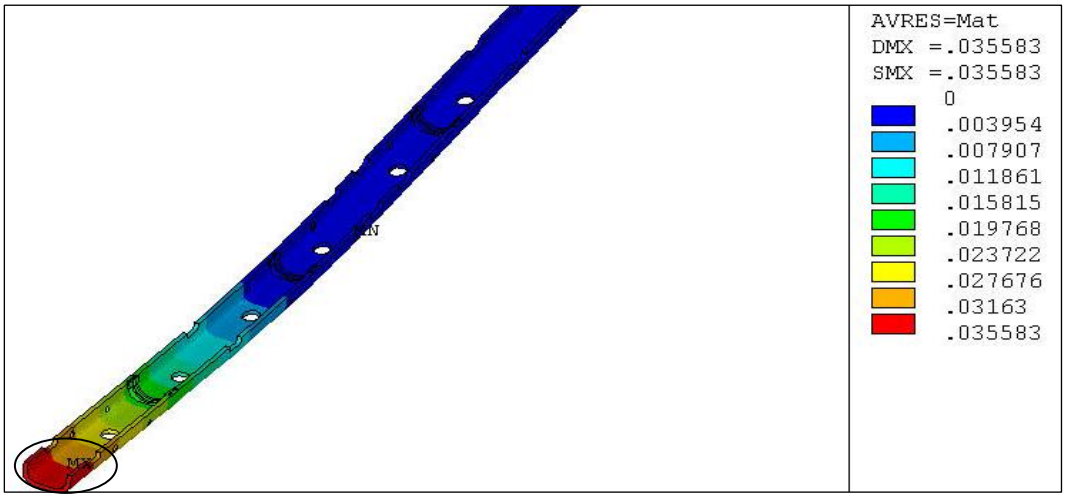

Figure 6: Total Vector displacement distribution showing over a section of structure modelled with 30 % short glass fibre filled polycarbonate . Max. displacement of 35 mm at the lower end of the component as shown by ellipse.

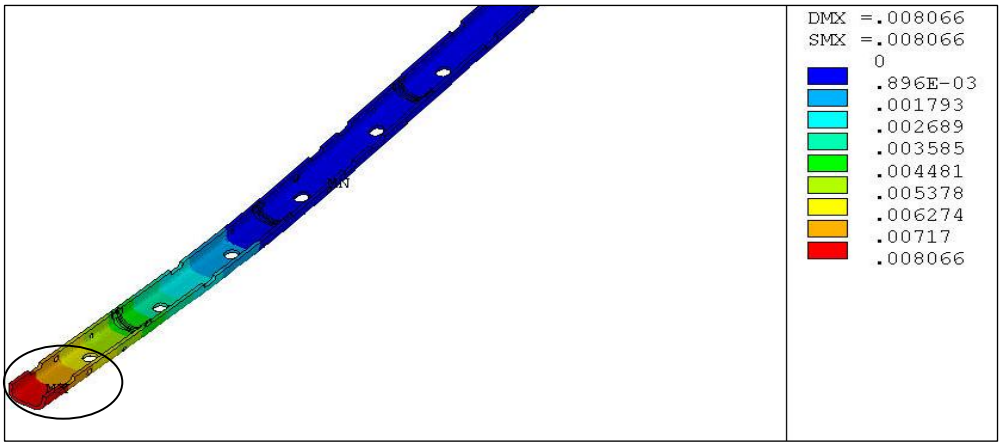

Figure 7: Total Vector displacement distribution showing over a section of structure modelled with 40% unidirectional glass fibre reinforced Epoxy. Max. displacement of 8 mm at the lower end of the component as shown by the circle.

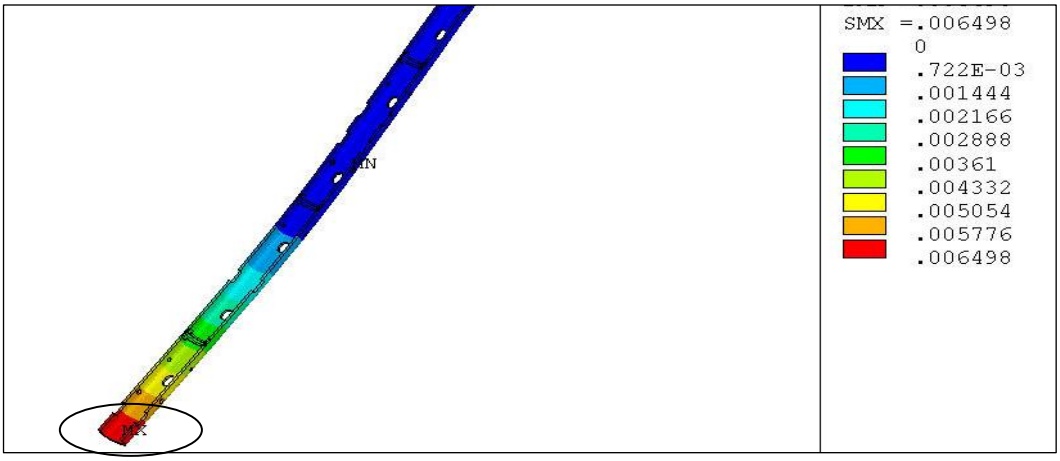

Figure 8: Total Vector displacement distribution over a section of structure modelled with 40% unidirectional carbon fibre reinforced Epoxy. Maximum displacement of 6.5 mm at the lower end of the component as shown by the circle.

Table 1: Mechanical Properties of the Composites [2,3]

Property	**30 % short glass fibre filled polycarbonate**	**40% Unidirectional glass fibre reinforced Epoxy**	**40% Unidirectional carbon fibre reinforced Epoxy**
Young's Modulus			
E_1 (Pa)	8.62 E +09	1.24 E + 10	9.96 E + 09
E_2 (Pa)	8.62 E +09	4.48 E + 10	1.45 E + 11
E_3 (Pa)	8.62 E +09	1.24 E + 10	9.96 E + 09
Poisson's Ratio			
μ_{12}	0.31	0.28	0.25
μ_{23}	0.31	0.28	0.25
μ_{13}	0.31	0.037	0.041
Shear Modulus			
G_{12} (Pa)	--	5.52 E + 09	5.86 E + 09
G_{23} (Pa)	--	5.52 E + 09	5.86 E + 09
G_{13} (Pa)	--	3.6E + 09	3.46 E + 09
Density (kg / m^3)	1430	2080	1580

Synthesis, curing and characterization of tetraglycidyl epoxy resin

D.Armstrong*, V. Agneeswaran and Dr.B.Kothandaraman[#]

Department of Rubber and Plastics Technology,
Madras Institute of Technology, Anna University Chennai

E-mail:armstrongmit@gmail.com, bkraman@mitindia.edu

Abstract:

Epoxies generally out-perform most other resin types in terms of mechanical properties and resistance to environmental degradation, which leads to their almost use in aircraft components. It has outstanding thermal and adhesion properties. Some of these resins can be cured at room temperature, but heat can be used to accelerate the cure of the epoxy. Among the high temperature epoxy resins, TetraGlycidyl Diamino Diphenyl Methane can provide high cross-linking density, so that hardened bodies obtained from the known composition exhibits both high modulus and high heat resistance which is inevitable for matrix materials for the advanced composites used in aerospace, electronics, automotive and other industries. In the present investigation, TetraGlycidyl Diamino Diphenyl Methane was synthesized through glycidation of 4, 4'-Diamino Diphenyl Methane with a large excess of Epichlorohydrin under controlled reaction conditions. Diamino Diphenyl Methane (specifically increases temperature and chemical resistance), Diamino Diphenyl Sulphone (DDS)and Triethylene Tetramine(TETA) were used for curing. The formulated curing mixture was cured as per the curing schedule described. The molecular structure of tetraglycidyl diamino diphenyl methane was confirmed by Nuclear Magnetic Resonance Spectroscopic technique. The degradation behavior of cured samples was studied by thermo gravimetric analysis. The resin was cured with the above mentioned 3 amine curatives and their properties were compared using Differential Thermal Analysis (DSC)

Introduction:

Epoxy Resins are class of thermoset materials extensively used in structural and specialty composite applications because they offer a unique combination of properties that are unbelievable with their many desirable properties, such as good adhesion, excellent chemical, thermal stabilities and electrical properties. The outstanding adhesion to various substrates makes epoxy resin, an important and efficient resin system in adhesive industries. In 1970 s, Ciba-Geigy corporation developed a series of glycidylated resins based on hydantoin and Shell Technologies introduced the glycidylated resins of hydrogenated bisphenol-A, but in both instances commercial success was limited. Epoxy adhesives can bond a wide variety of substrates with high strength particularly metals. They have been used to replace some traditional metal working methods of joining like nuts and bolts, rivets, welding, crimping, brazing and soldering. Epoxy resin adhesives are used mainly in niche applications rather than as general purpose adhesives. Good adhesion to nonporous surfaces allows them to be used in demanding situations.

In the present investigation, tetra functional epoxy resin was prepared from 4, 4'-diamino diphenyl methane and was cured with Diamino Diphenyl Methane (DDM), Diamino Di phenyl Sulphone (DDS) and triethylene tetramine (TETA). The thermal stability of cured TGDDM resins were studied by thermogravimetry in nitrogen atmosphere at a heating rate of 10° C/min, as a systematic thermal study on the selected resin system was very limited.

Experimental:

Materials:

Reagent grades of Diamino Diphenyl Methane, Epichlorohydrin, ethyl alcohol, lithium hydroxide mono hydrate, sodium hydroxide, toluene, Diamino Diphenyl Sulphone and Triethylene tetramine were obtained from E-Merck India limited, Mumbai and were used without further purification.

Synthesis of tetra glycidyl diamino diphenyl methane (TGDDM):

Diamino diphenyl methane, epichlorohydrin and 60 ml of ethyl alcohol were added with water, and the mixture was stirred at 75° C for 6 hours. Then the reaction mixture was brought to 55° C while 30% NaOH solution added over 5 hours. Excess water and epichlorohydrin were removed by distillation under reduced pressure (30 mm Hg) . The residue was dissolved in toluene and washed with water to remove salts and residual caustic.

Curing:

4,4'- diamino diphenyl methane(DDM), 4,4'- diamino diphenyl sulphone(DDS) and tri ethylene tetramine (TETA) were used as the curing agents, in which each hydrogen on an amine nitrogen will be reactive and can open one epoxide ring to form a covalent bond. The correct relative amounts of TGDDM and curing agents were determined by computing the weight of curing agent that contains one chemical equivalent of amine hydrogens and matching that with the weight of TGDDM that contains one chemical equivalent of epoxide groups.

Analytical methods:

Fourier transform infrared spectroscopy:

The FTIR of virgin Tetraglycidyl Diamino Diphenyl Methane was done. the apparatus used was PERKIN-ELMER make.

Scanning Rate: 16 scans

Resolution: 4 cm^{-1}

Nuclear magnetic resonance spectroscopy (NMR):

The proton (^{1}H) Nuclear Magnetic Resonance spectroscopic study and carbon (^{13}C) Nuclear Magnetic Resonance spectroscopic study were performed in a Bruker 500 MHz NMR spectrometer using $CDCl_3$ as the solvent.

Thermo gravimetric analyzer:

The TGA equipment used was TGA Q 50 V 20.5, from TA instruments, where the temperature range is taken from 20°C to 750°C, at a heating rate of 10°C/min in nitrogen atmosphere.

Differential scanning calorimetry:

The DSC equipment used was DSC Q 20 V 23.5, from TA instruments, where the temperature range was taken from 20°C to 300 °C, at a heating rate of 10°C/min, in nitrogen atmosphere.

Results and Discussion:

Table 4.1: FTIR Results

WAVE NUMBER (cm^{-1})	INTENSITY	FUNCTIONAL GROUP
1620	Strong & sharp	Phenyl group
838.8	Strong	p- substituted benzene
2915	Strong & Broad	Aromatic C-H stretching
699.1	Medium	Benzene ring
962.3	Strong and sharp peak	Oxirane group
1254.3	Cluster of peaks	C-N aromatic stretching
1189.8	Cluster of peaks	C-N aliphatic stretching

.

Table 4.2: Proton Magnetic Resonance Spectroscopy Results

CHEMICAL STRUCTURE	**RADIATION FREQUENCY(PPM)**
Proton in the benzene ring	7.21
Proton in the CH_2 group attached with Nitrogen	3.68
Proton in the CH group of oxirane ring	2.77
Proton in the CH_2 groups of oxirane group	2.5

Table 3: ^{13}C NMR Spectroscopy Results

CHEMICAL STRUCTURE	**RADIATION FREQUENCY(PPM)**
^{13}C in the ortho -position of phenyl ring	**127.9**
^{13}C in the meta -position of phenyl ring	**128.4**
^{13}C in the para -position of phenyl ring	**140.2**
^{13}C in the CH_2 group attached with nitrogen	**49.9**
^{13}C in the CH group of oxirane ring	**52.1**
^{13}C in the CH_2 group of oxirane ring	**44.2**

From the observed results it was confirmed that the resin synthesized was TetraGlycidyl Diamino Diphenyl Methane.

:

Table 4: TGA Results

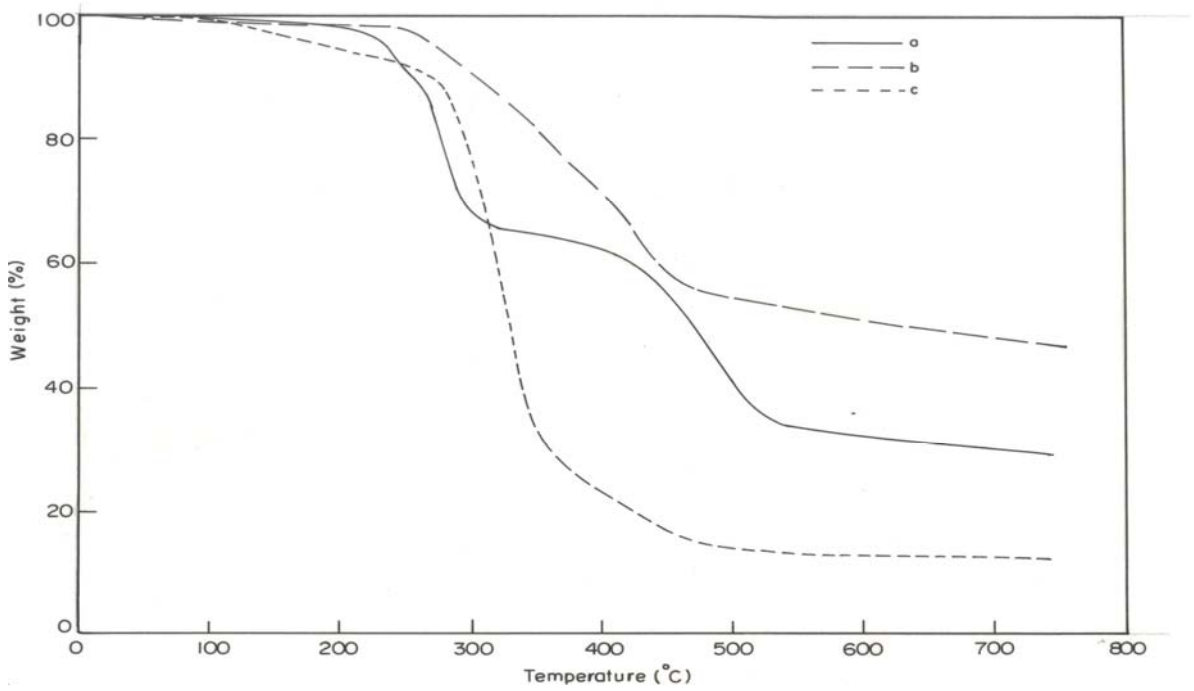

a-DDM cure b-DDS cure c-TETA cure

Sl.no	Curing system	Onset temperature(°C)				Residue (%)
		Primary transition		Secondary transition		
		T_i(°C)	T_f(°C)	T_i(°C)	T_f(°C)	
1	Uncured resin	232.47	300	426.33	518.69	22.59
2	DDM	243.67	297.55	413.52	520.69	30.85
3	DDS	258	456.92	----------	----------	48
4	TETA		491.23	----------	----------	14.33

UNCURED RESIN:

There are 2 transitions observed in TGA analysis of uncured resin. Decomposition starts at 232°C and residue obtained was 22.59 %. There are aromatic benzene groups in the backbone of the resin with aliphatic side groups. The first transition may be due to the degradation of aliphatic groups. Second transition is due to the degradation of aromatic backbone. From the TGA curve we can observe that degradation at the beginning of the curve itself this may be due to the evaporation of volatiles such as water

TGDDM/DDM SYSTEM:

There are 2 transition temperatures observed in TGDDM/DDM system. This is due to the cyclization reactions occur during curing[9]. Condensation of main chain benzene ring occurs to some extent, so the char yield is higher than the uncured resin, and from the high char yield value it is inferred that this system will have good flame resistance

TGDDM/DDS SYSTEM:

There is only one transition temperature was observed in TGDDM/DDS system and residue obtained was 48%.this is attributed to the reason that complete condensation aromatic groups upon curing and this leads to very stiff and rigid network. From the highest value of char yield depicts that the material will have excellent flame retardancy.

TGDDM/TETA SYSTEM:

In TGDDM/TETA system also has only one transition temperature is observed and the residue was 14.33%. This char yield is less than the uncured resin. Onset of degradation and it loses the maximum weight in a little interval of temperature. TETA curing system is meant for room temperature curing it is not suitable for the high temperature curing. TGDDM is a high temperature curing, so it does not yield good properties with TETA curing agent.

Table 4.5: Comparison of curing systems

Sl.no	Curing system	Temp. at 10% weight loss(°C)	Char yield (%)			
			200°C	400°C	600°C	800°C
1.	Uncured resin	157.4	83.75	46.66	26.36	20.57
2	DDM	251	98.125	62.1875	33.125	28.75
3	DDS	305.89	98.398	71.63	51.06	46.91
4	TETA	274.25	95.01	24.78	14.52	14.13

INFERENCE:

1. Temperature at 10% weight loss is 157.4°C for uncured resin. This value increases by a factor of 2 after curing. This value is comparable for both TGDDM/DDM system (251°C) and TGDDM/TETA system (274.25°C).
2. Temperature at 10% weight loss is 305.89°C for TGDDM/DDS system. This means that the cross linked network is very stiff and it has excellent flame resistance
3. Char yield at 200°C increases for the cured resin systems than the uncured resin system. The values are almost the same for both TGDDM/DDM and TGDDM/DDS system. This value is slightly less for TGDDM/TETA system
4. TGDDM/DDS system has the highest char yield at 400°C. there is drastic drop in char yield for TGDDM/TETA system at 400 °C than 200°C
5. TGDDM/DDS system has the highest char yield even at 600°C. TGDDM/DDM and TGDDM/TETA system have char yield lower than the uncured resin
6. Residues for all the above said systems were found at 750°C. TGDDM/DDS system has the highest char yield. So, it is inferred from the result that TGDDM/DDS system has very good flame resistance. If we add some flame retardants to this system we could achieve excellent flame retardancy.
7. For TGDDM/DDM and TGDDM/TETA system Char yield at 750°C is less than the uncured resin. Flame retardancy of the resin was affected by these curing agents.
8. But TGDDM/DDM system has the highest degradation temperature when compared to other systems. So this system will offer high performance even at elevated temperatures.
9. TGDDM/DDM system does not have that much crosslink density as in the case of TGDDM/DDS system. It is somewhat flexible, so this can be used for tooling applications
10. TGDDM/TETA system has first decomposition temperature at 284.78°C(Highest of all systems compared). But the final decomposition point lies at a short interval of 100°C. This system looses almost 75 % of the polymer between the primary and secondary onset temperatures. So this is not suitable for high performance

Table 4.6: DSC Results

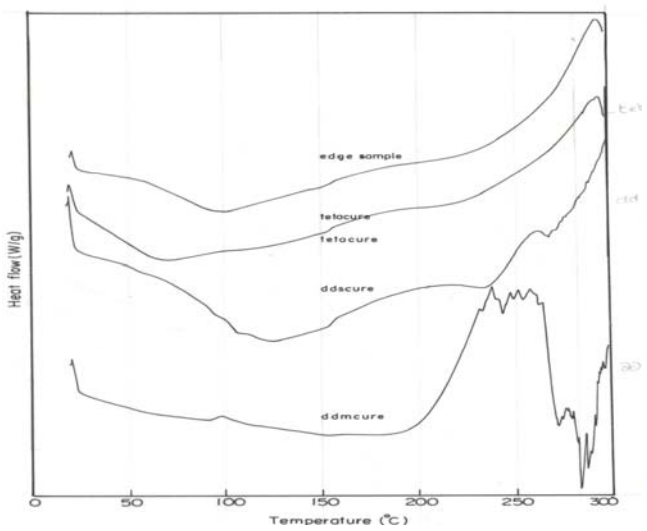

DSC thermo grams of edge sample, TETA cure, DDS cure, DDM cure.

SL. NO.	CURATIVE USED	T_g(°C)	ONSET OF EXOTHERMIC PEAK(°C)
1	DDM	145.53	235.75
2	DDS	113.71	240.49
3	TETA(MIDDLE)	53.27	229.64
4	TETA(edge)	85.97	227.04

TGDDM cured with DDM:

For TGDDM cured with DDM the T_g value was observed at 145.53°C. an exothermic peak starts at 235°C and reaches maximum exothermic heat flow at around 260°C. This indicates that post cure at 210°C is not sufficient, still higher temperature is required for post cure. That may be around 250°C because exothermic peak reaches maximum at that temperature. Maximum exothermic temperature shown in DSC curves is the temperature at which the residual cure gets completed. At 280°C there is an endothermic peak. This may be due to some impurities getting evaporated at that temperature.

The peculiarity of the DDM curing system is the cyclization reactions occur during curing. These reactions retard crosslinking. That should also be expressed by a modified behavior of physical properties during curing[9]. These cyclization reactions may be the reason for the improper cure of TGDDM/DDM system and led to the exothermic peaks.

TGDDM cured with DDS:

For TGDDM cured with DDS the T_G value was observed at 113.71°C. An exothermic peak starts at 240°C and there is no maximum peak in the temperature region analyzed (20-300°C). There is an endothermic peak at 265°C. For DDS curing system also a post curing at higher temperature is required.

TGDDM cured with TETA:

Triethylene Tetramine (TETA) is an aliphatic curative and low viscous liquid. While curing the resin was taken in a petridish and then hardener (TETA) was added to that. Due to the low viscosity the resin has moved to the edge of the sample. Curing was proper at the edges and improper cure was observed in the sample (i.e.) the sample was translucent at the center and opaque at the edges. So that 2 samples were cut out from the cured resin, one from the middle and one from the edge. They were named as TGDDM/TETA (center) and TETA (edge). Both samples were analyzed using DSC.

For the TGDDM/TETA (center) sample T_g value was observed at 53.27°C. An exothermic peak starts at 229°C and reaches maximum exothermic heat flow at around 290°C. This indicates that post cure at 100°C is not sufficient, still higher temperature is required for post cure. That may be around 250°C. Because exothermic peak reaches maximum at that temperature.

For the TGDDM/TETA (edge) sample T_g value was observed at 85.97°C. An exothermic peak starts at 227°C and reaches maximum exothermic heat flow at around 290°C.

CONCLUSION:

1. Tetraglycidyl Diamino Diphenyl Methane resin was synthesizes using 4, 4'-Diamino Diphenyl Methane (DDM) and Epichlorohydrin (ECH) as raw materials

2. Fourier Transform Infrared Spectroscopy (FTIR) was done and it was confirmed that the resin synthesized was TGDDM.

3. Proton magnetic Resonance Spectroscopy and molecular ^{13}C NMR spectroscopy was done and it was confirmed that the resin synthesized was Tetraglycidyl ether of Diamino Diphenyl Methane (TGDDM)

4. DSC curves shows exothermic peak for all the 3 systems. This may be due to the residual cure. So, post cure temperature is not sufficient. It is concluded that still higher temperature is required for post cure. From these results optimum curing procedures are proposed in this paper

5. TGA curves show that 2 transitions are there for uncured TGDDM resin and TGDDM/DDM system. But there is only one transition was observed in TGDDM/DDS system. This is attributed to the complete condensation of aromatic rings occur during DDS curing and it leads to stiff and tightly cross linked structure. It also gives the highest char yield at 750°C. So, it was inferred that TGDDM/DDS system will have the excellent flame resistance.

   TGDDM/DDM system shows 2 transitions. This is due to the cyclization occurring during curing and it retards cross linking. This system has higher char yield at 750°C, so this system also has very good flame resistance.

REFERENCES:

1. "Polymer synthesis", volume I & II,
Stanley R.Sandler, wolf karo

2. "New epoxy resins containing Hard-Soft segments: Synthesis,
Characterization and Modification studies for high temperature applications"
M. Suguna Lakshmi, M. Srividhya and B. S. R. Reddy,
CLRI, Chennai

3. "Polymer spectroscopy" - Silverstein

4. "Kinetic studies of an epoxy cure reaction
By isothermal DSC analysis"
J.Y. Leea, H.K. Choib, M.J. Shimc, S.W. Kima,*
University of Seoul, South Korea

5. Thermal library

6. "Synthesis, curing behavior and properties of siloxane
And imide-containing tetra functional epoxy"
Ming-Wei Wang & Ho-ying Wu & Mu-Shih Li

7. Rheological and thermal behaviour of DGEBA/EA and
DGEHQ/EA epoxy systems cross linked with TETA
Fanica Mustata *, Ioan Bicu

8. *"P.Poni" Institute of Macromolecular Chemistry, Aleea Grigore*
Ghica Voda, No 41A,
RO 6600, lassy

9. "The curing of epoxy resins as studied by various methods"
M.Younes, S.Wartewig and D.Lellinger,
Fachbereich Physik, Martin-Luther Universitat Halle-Wittenberg, Germany
POLYMER volume 35 November 24 1994

Studies on processing of styrene butadiene rubber-$CaCO_3$ nanocomposites by different mixing techniques and their performance properties

A.Ahamad, C.B.Patil, P.P.Mahulikar, U.R.Kapadi, and D.G.Hundiwale*

School of Chemical Sciences, North Maharashtra University,
Umavinagar, Jalgaon - 425 001
Maharashtra, India

E-mail- dghundiwale@yahoo.com, ab_ahad@rediffmail.com

Abstract

The nano particles of $CaCO_3$ were synthesized by matrix mediated growth and controlled technique and was used as filler. The particle size of synthesized nano $CaCO_3$ (35-60 nm) was determined by XRD and confirmed by Transmission Electron Microscope (TEM). The styrene butadiene rubber (SBR) -$CaCO_3$ nanocomposites were prepared by using Brabender Plastograph. The mechanical and physical properties of SBR nanocomposites were determined .The fracture surface of SBR nanocomposites was observed by Scanning electron microscope (SEM). The results of Brabender processed SBR -$CaCO_3$ nanocomposites were compared with two roll mill processed SBR -$CaCO_3$ nanocomposites. The results showed that the reinforcement of $CaCO_3$ nano-filler in SBR polymer matrix enhanced the properties of SBR nanocomposites as compared to pristine SBR composites in both the techniques. The substantial improvement in properties was observed in case of Brabender processed SBR -$CaCO_3$ nanocomposites as compared to pristine and two roll mill processed SBR -$CaCO_3$ nanocomposites. The enhancement in properties was observed in Brabender processing technique due to the higher shear rates which resulted in proper dispersion and mixing of nano $CaCO_3$ in SBR polymer matrix and proper wettability of inorganic particles by polymer matrix.

Keywords: - Styrene butadiene rubber (SBR), Nanocomposites, Brabender Plastograph, Scanning electron microscope (SEM)

1. Introduction

Polymer nanocomposites have been intensely researched in the last decade since the addition of a small quantity of reinforcement fillers such as clays in the polymer matrix have led to improvements of mechanical, thermal, and barrier properties.[1-2]. The nano-sized fillers have dramatically increased the surface area compared with conventional-sized materials. The increased surface area of nano reinforced materials is responsible for the improvement in properties of nanocomposites compared to pure polymers or filled with conventional fillers. The nanocomposites are new class of composites that are particle filled materials in which at least one dimension of dispersed particles is in the nanometer range.

Polymer matrix must have good process properties so that the dispersed particles can result in a large improvement in composite properties.[3-4]

Normally mixing is done on two roll mill. But proper mixing (dispersion) of fillers is very important to achieve maximum level of properties. Hence in addition to two roll mill we mixed nanoparticles into SBR by using Brabender Plastograph and compared both the techniques for performance.

2. Experimental

2.1 Materials

Styrene butadiene rubber (SBR)

Rubber additives Viz. stearic acid, zinc oxide (ZnO), zinc diethyl dithiocarbamate (ZDC), mercapto benzothiozyl disulphide (MBTS), vulconex, and sulphur,

Calcium chloride (AR Grade), potassium carbonate, and poly (ethylene glycol) (PEG; molecular weight of 6000) for synthesis of nano $CaCO_3$.

2.2 Preparation of nanoparticles

The nano-sized calcium carbonate particles were synthesized in the laboratory by using-

- **Matrix mediated growth and controlled i.e. *in situ* deposition technique.** [5-10]

2.3 Preparation of Rubber nanocomposites

Two different techniques were used for preparation of styrene butadiene rubber (SBR) nanocomposites **1) Two roll mill**

2) Brabender Plastograph

2.4 Characterization

The following characterization techniques were used-

1. **Particle size determination - X-ray powder diffraction technique.**
2. **Mechanical (Tensile properties) - Universal Testing Machine**
3. **Hardness- Hardness tester Shore scale-A**

4. Swelling index – Toluene 24 hr (27 ^{0}C)

5. Surface morphology- Scanning Electron Microscope (SEM)

3 Results

1. Particle Size by X-ray diffraction (XRD) technique

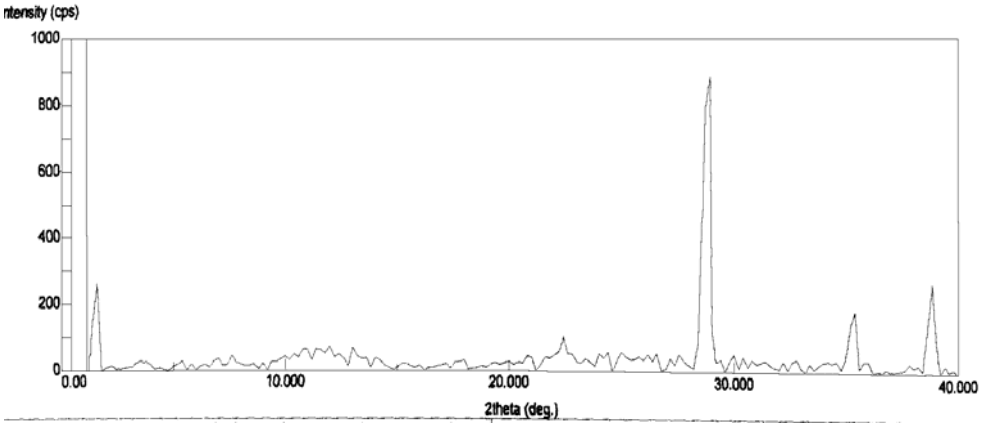

Figure 1. XRD of synthesized nano $CaCO_3$

- **Particle size determined by using Scherer's formula-**
- **$d = k \lambda / \Delta 2\theta \cos \theta$**

2. Mechanical Properties

I) Tensile strength

It is observed that the tensile strength of Brabender processed SBR nanocomposites showed better tensile strength than the two roll mill processed SBR nanocomposites.The improvement in tensile strength of samples processed on Brabender is due to the proper mixing of nano filler $CaCO_3$ in polymer matrix which results the uniform dispersion of nano filler in SBR polymer matrix.

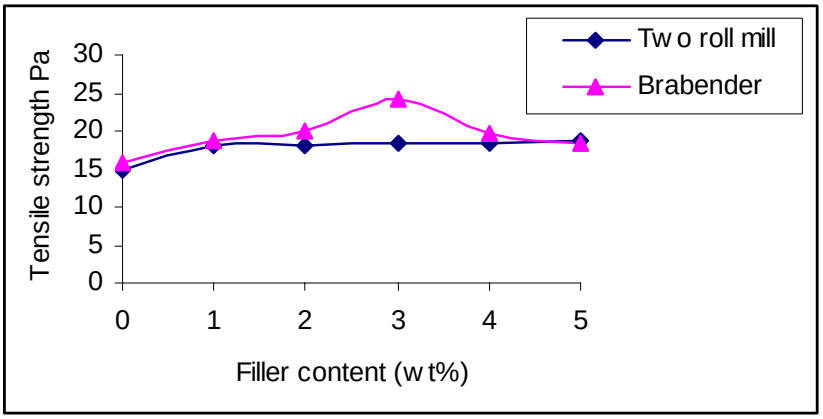

Figure 2. Tensile strength of SBR filled with nano $CaCO_3$ processed on two roll mill (TRM) and Brabender Plastograph

II) Elongation at break (% Elongation)

For all compositions, elongation at break of nanocomposites increased with increasing filler content up to 3 wt % and 4 wt % filler loading for both Brabender and two roll mill respectively. Value of elongation at break decreased after attaining the peak value, the trend was found to be similar in both the techniques. The reason may be agglomeration of nano particles as well as formation of weaker interfacial region between the filler surface and matrix where in cracks develops**.**

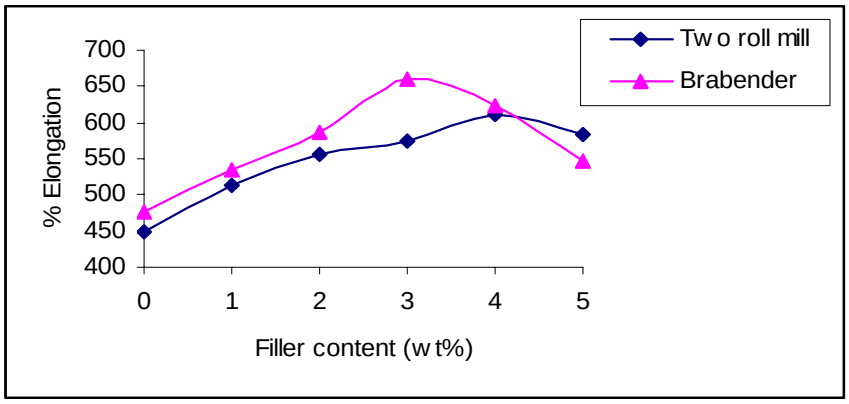

Figure 3. % elongation of SBR filled with nano $CaCO_3$ processed on two roll mill (TRM) and Brabender Plastograph

3. Hardness

Hardness of all composition increased up to 4 wt % of filler amount for both mixing technique than the pure SBR composites as shown in figure. Hardness increased due to the greater degree of crosslinkage which has been occur during vulcanization of rubber nanocomposites by uniform transfer of heat in to the rubber matrix. Also the formation of effective layer is responsible for increase in hardness of rubber nanocomposites.

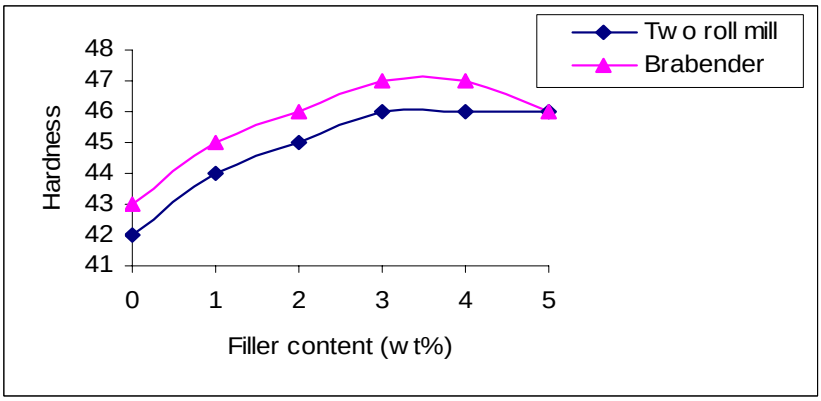

Figure 4. Hardness of SBR filled with nano $CaCO_3$ processed on two roll mill (TRM) and Brabender Plastograph

4. Swelling index

The swelling indices of different filler content of two roll mill as well as Brabender processed SBR nanocomposites are shown in Fig.-6 Lower swelling in case of Brabender processed nanocomposites is due to greater cross linking of SBR because of a uniform dispersion of nano $CaCO_3$ which brings the chains closer and keep them intact with nanofiller.

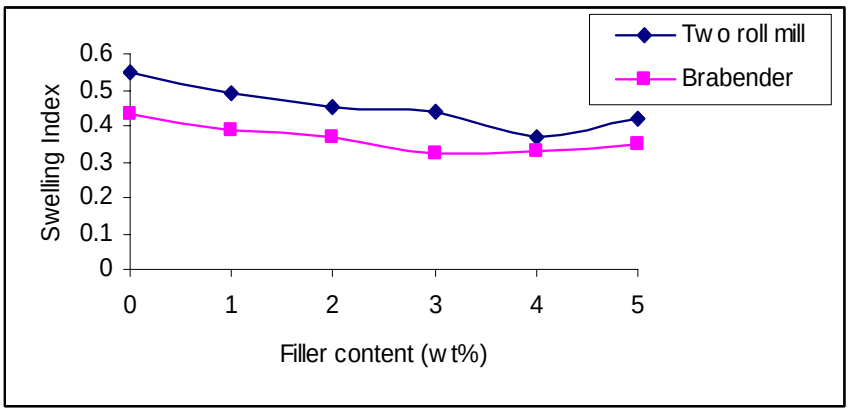

Figure 5. Swelling index of SBR filled with nano $CaCO_3$ processed on two roll mill (TRM) and Brabender Plastograph

5. Surface morphology

The surface morphology of fractured SBR nanocomposites prepared on Brabender and two roll mill mixing technique were investigated by Scanning Electron Microscope (SEM)

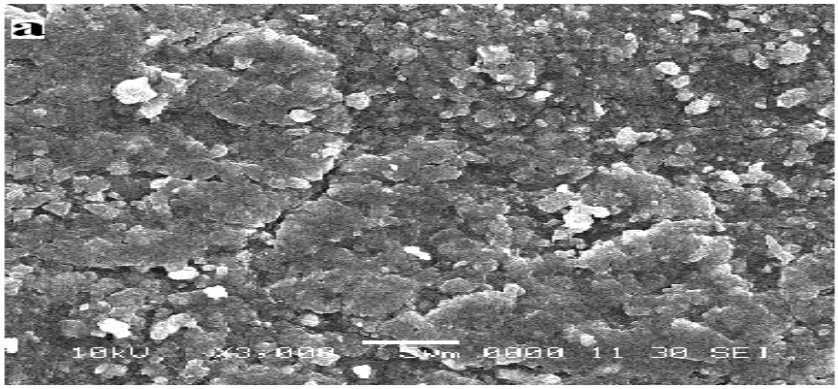

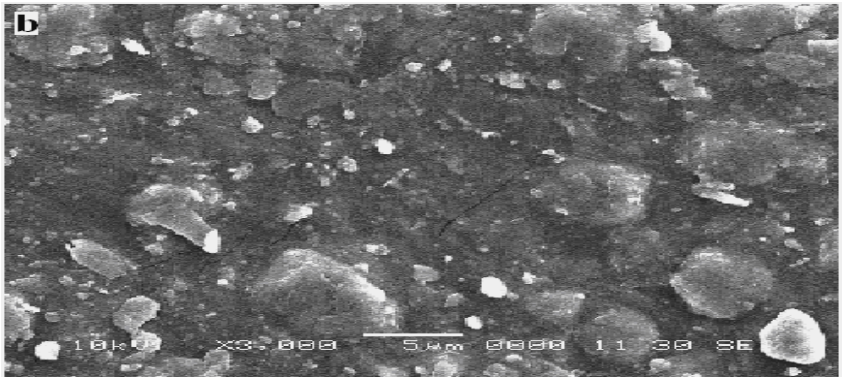

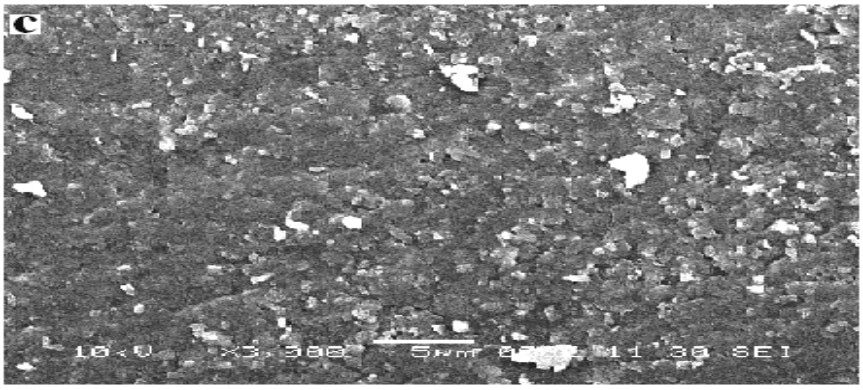
c
10.0 X3,500 5μm 0000 11 30 SEI


d
10.0 X3,000 5μm 0000 11 30 SEI

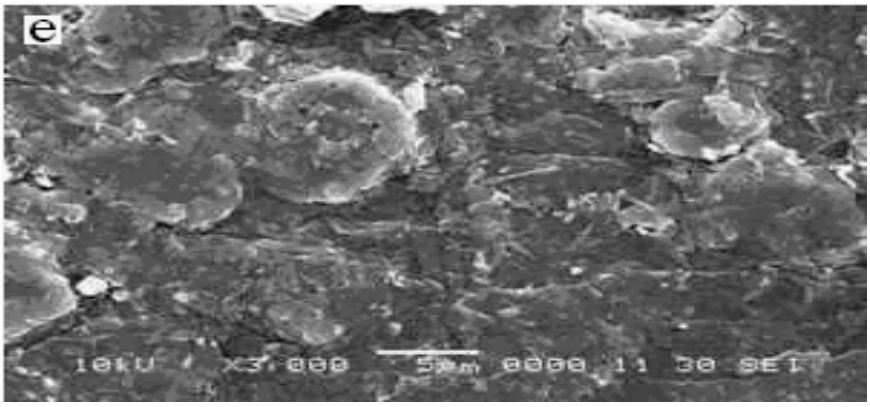
e
10kV X3,000 5μm 0000 11 30 SEI

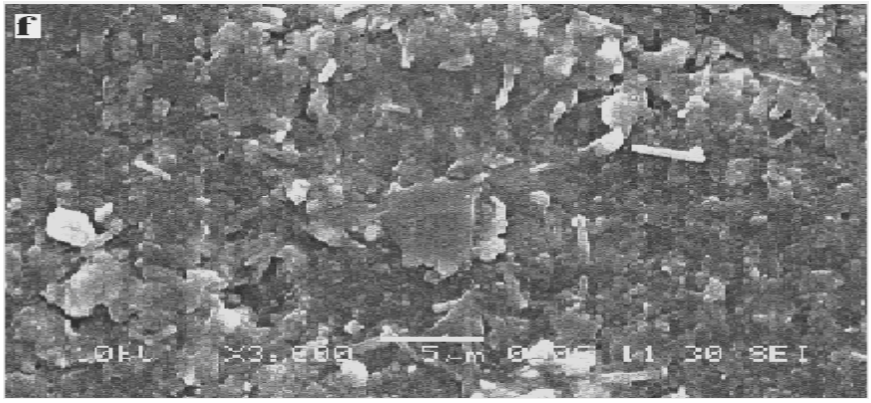
f
10kV X3,000 5μm 0000 11 30 SEI

Figure 7. Scanning Electron Micrographs of SBR -$CaCO_3$ nanocomposites a) b) & c) For 1, 3 and 5 wt% filler content processed on Two roll mill (TRM) and d) e) & f) For 1, 3 and 5 wt% filler content processed on Brabender Plastograph

Conclusion

The nano-filler $CaCO_3$ were synthesized in the laboratory. The reinforcement of nano filler $CaCO_3$ in SBR improved the mechanical as well as thermal properties of pristine SBR. The Brabender processed SBR nanocomposites as compared to two roll mill processes nanocomposites showed better improvement in properties because of more shear rate which results proper mixing of all ingredients including filler in the matrix. Therefore uniform dispersion of nano filler $CaCO_3$ in the SBR matrix was achieved by Brabender Plastograph.

References

1. Fu, X. and Qutubuddin, S., "Polymer-Clay Nanocomposites: Exfoliation of Organophilic Montmorillonite Nanolayers in Polystyrene," *Polymer*, 42, 807-813, 2001.
2. Messersmith, P.B. and Giannelis, E.P., "Synthesis and Characterization of Layer Silicate-Epoxy Nanocomposites," *Chem. Mater.*, 6, 1719-1725, 1996
3. Yano, K., Usuki, S., Okoda, A., Kurauchi, T. and Kamigatio, O. (1993).Synthesis and Properties of Polyimide-clay Hybrid, J. Polym. Science.,31(10): 2493–2498.
4. Wang, Y., Zhang, L., Tang, C. and Yu, D. (2000). Preparation and Characterization of Rubber-clay Nanocomposites, J. Applied Polymer Science., 78(11): 1879–1883.
5. Mishra, S., Shimpi, N. G. (2005). Comparision of Nano $CaCO_3$ and Flyash Filled with Styrene Butadiene Rubber on Mechanical and Thermal Properties, JSIR, Vol-64.
6. Saujanya, C., Radhakrishnan, S. (1998). Structure Development in PP/$CaSO_4$ Composites: Part-I Preparation of Filler by an *In –situ* Technique, *J Mater Sci*, 33: 1062-1068.
7. Mishra, S., Sonawane, S. H., Singh, R. P., Bendale, A. and Patil, K. (2004). Effect of Nano Mg $(OH)_2$ on the Mechanical and Flame Retarding Properties of PP Composites, *J Appl Polym Sci*, 94:116.
8. Gleiter H., *Nanostructure Mater* 1991, 1, 1.
9. Koch C C., *Nanostructure Mater*, 1991, 21:559.
10. Mishra, S., Sonawane, S. H. and Singh, R. P., (2005). Studies on Characterization of Nano $CaCO_3$ Prepared by *In-situ* Deposition Technique and Its Application in PP-nano $CaCO_3$ Composites, *J Polym. Sci Part B: Polym. Phys*, 43:107.

Effect of post drawing parameters of melt spinning of carbon nanotube filled polypropylene fiber

Srikanth S. Kamath[a]*, Arup R. Bhattacharyya[a#], Pankaj B. Tambe[a], Ajit R. Kulkarni[a], T.V. Sreekumar[b], Kingsuk Mukhopadhyay[b] and Anurag Srivastav[b]

[a]Department of Metallurgical Engineering and Materials Science, Indian Institute of Technology Bombay, Powai, Mumbai- 400076, India
[b]Defence Materials and Stores Research and Development Establishment (DMSRDE), DRDO, Kanpur 208013,India
E-mail: arupranjan@iitb.ac.in

Abstract

Melt spun multiwall carbon nanotubes (MWNT) filled polypropylene (PP) fibers were drawn at draw ratio of 8 with variation of post drawing parameters (temperature and speed of drawing the composite fibers) in order to understand the effect of post drawing parameters on mechanical properties of composite fibers. It was found that fiber drawn at high temperature and low drawing speed showed an increase in mechanical properties of PP/MWNT composite fibers than any other combination of variation of post drawing parameters.

1. Introduction

Isotactic polypropylene (PP) utilized as a commercial polymeric fiber exhibits a wide range of mechanical properties. However, PP fiber needs reinforcement in order to achieve high stiffness and strength for engineering applications. Since the discovery of carbon nanotubes (CNT) by Iijima [1], CNT have emerged as a potential candidate as reinforcing filler in polymer based composite fibers in view of their unique mechanical, electrical and thermal properties [2]. Fiber with mechanical properties suitable for advanced engineering application require orientation of polymer chains[3-7] as well as that of CNT[8, 9] during post drawing operation. It was found that the average orientation of statistical chain segments of PP within the sample was independent of the drawing temperature whereas the yield stress and elongation at break wee strongly influenced by the applied drawing temperature. A significant drop in yield stress could be observed for a fixed draw ratio with lowering the drawing temperature. At a certain temperature this drop leads to a transition from brittle to ductile failure behavior, resulting in an increase in elongation at break [3]. The effect of the postdrawing at a constant draw ratio manifests in either high stiffness in combination with superior draw ability/energy absorption (lowest possible post drawing temperature, formation of mesomorphic phase) or a high stiffness in combination with high strength (highest post drawing temperature in the affine deformation regime) [4].

The aim of this work is to understand the effect of varying post drawing parameters (temperature and speed of drawing the composite fibers) at varying multiwall carbon nanotubes (MWNT) concentration on the mechanical properties of PP/MWNT composite fibers drawn at a fixed draw ratio of 8.

2. Experimental Details

Polypropylene was obtained from Reliance Industries Ltd, India (REPOL H200F, melt flow index 20 g/10min). MWNT were obtained from DMSRDE, Kanpur. Various compositions of PP/MWNT composites were prepared by melt-mixing in which MWNT were varied from 0.5-3 wt% in a conical twin-screw microcompounder (Micro 5, DSM Research, Netherlands) at optimized melt mixing condition of 260^0C with a rotational speed of 200 rpm for 15 min. Melt compounded PP/MWNT samples were dried at 80^0C under vacuum over night. They were melt-spun using a small scale spinning machine manufactured by the Bradford University Research Ltd. UK, using a single hole spinneret of 1 mm diameter. The fiber spinning was carried out at 200^0C with ram speed of 1.4 mm/min. The take up speed was kept at 20 m/min for all compositions. The melt spun fibers were further drawn at draw ratio of 8 by varying the post drawing parameters (temperature and drawing speed). Details of variation of post drawing parameters provided in Table 1 which depicts 12 exiperments were performed for each MWNT concentration of 0.5, 1 and 3 wt% respectively. The mechanical properties of drawn fiber were tested on a Favimat fiber tester (Textechno) with gauge length of 20 mm and at a rate of 20 mm/min for 50 filaments.

3. Result and Discussion

3.1 Mechanical properties

If the composite fibers are to be obtained of high tenacity, high modulus of elasticity and low elongation at break; nanotube orientation distribution along the fiber axis should be higher. In this context, it is also reported that CNT/polymer interface influences significantly the mechanical properties of the composite fibers [10].

Figure 1 exhibits the distribution of modulus, tenacity and elongation at break of composite fibers at various post drawing parameters. It is observed that variation in post drawing parameters lead to the dramatic changes in mechanical properties of composite fibers.

Tenacity (which is a measure of fineness of fiber) and modulus increases with decreasing drawing speed and corresponding increase in temperature (Figure 1a-b). High modulus values are achieved for those combinations of post drawing parameters which exhibits less elongation. This may be due to the addition of MWNT which prevent the polymer chain from slipping past each other thereby improving modulus and reducing the elongation. In case of pure PP, failure is found to occur due to PP chains sliding past each other according to Smith Irvine model [11].

It is observed that at lowest drawing speed i.e 8 m/min modulus values are found to be higher than composite fiber drawn at higher drawing speed for all the combination of temperature and various weight fractions of MWNT. It is the orientation distribution of MWNT [10] at a definite post drawing parameter which contributes to the superior mechanical properties of composite fiber. The highest modulus and tenacity value are observed at post drawing parameters of 100^0 C, 8 m/min for 1 wt % of MWNT and 120^0 C, 8 m/min for 0.5 wt % of MWNT (Figure 1a-b).

3.2 Discussion

It is interesting to note that with an increase in temperature modulus increases at low drawing speed. At 80^0 C, drawing of fiber much above the glass transition temperature, the interaction between chains and interaction in between chain and nanotubes restrict the achievable orientation of MWNT.

Drawing the fiber at 100^0 C, which is near to the crystallization temperature result in better orientation of MWNT which manifests in an increase in overall mechanical properties than fiber drawn at 80^0 C. Drawing the fiber at 120^0 C, which is above the crystallization temperature results in even better orientation of MWNT than drawing at 100^0 C which manifests in an increase in overall mechanical properties.

However, PP/MWNT composite fibers do not exhibit any linear increase in mechanical properties with increasing MWNT concentration. The reason is due to inadequate interfacial interaction in between the PP chain and MWNT; formation of MWNT aggregates in PP matrix and due to MWNT slippage which is detrimental to the mechanical properties of composites [12, 13].

4. Conclusion

It was found that drawing speed and temperature had a profound effect on the mechanical properties of composite fiber. The favorable condition of drawing the composite fiber was drawing at higher temperature and at low drawing speed.

5. Acknowlegements

We would like to acknowledge Microcompounder Central facility, CRNTS at IIT Bombay. We would also like to thank DMSRDE, Kanpur for the financial assistance for the project (TR/0569/CARS-33).

6. References

[1] Iijima S, Nature 1991; 35:56.
[2] Baughman R. H, Zakhidov A. A, Heer W, Science 2002; 297:787.
[3] Tilo S, Ton P, Piet J, Joachim L, Macromolecules 2004; 37:1810
[4] Joachim L, Tilo S, Macromolecules 2005; 38:10678
[5] Bodaghi, H., Spruiell, J. E., and White, J. L., Int. Polym. Process 1988; 3:100
[6] Hahn, K.; Kerth, J.; Zolk, R.; Schwahn, D.; Springer, T.; Kugler,. J. Macromolecules 1988; 21:1541.
[7] Abo El Maaty M., Bassett, D., Olley R., Dobb M., Tomka J., Wang I., Polymer 1996; 37:213
[8] Bhattacharyya A R,, Sreekumar T.V, Liu T, Kumar S, Ericson L. M, Hauge R, Smalley R. E, Polymer 2003; 44:2373.
[9] Moncy V. J, Derrick D, James T, Gary P, Elijah N, Journal of Applied Polymer Science 2007; 103:3844.
[10] Bing J, Charlie L, Chuck Z, Ben W, Zhi W, Composites: Part B 2007; 38:24
[11] Irvine P, Smith Pet.al Macromolecules 1986; 19:240
[12] Ajayan P, Jonghwan S, Koratkar M, J Material Science 2006 ; 41: 7824
[13] Ajayan P, Schadler L, Giannaris C, Rubio A, Advanced Materials 2000; 12:750

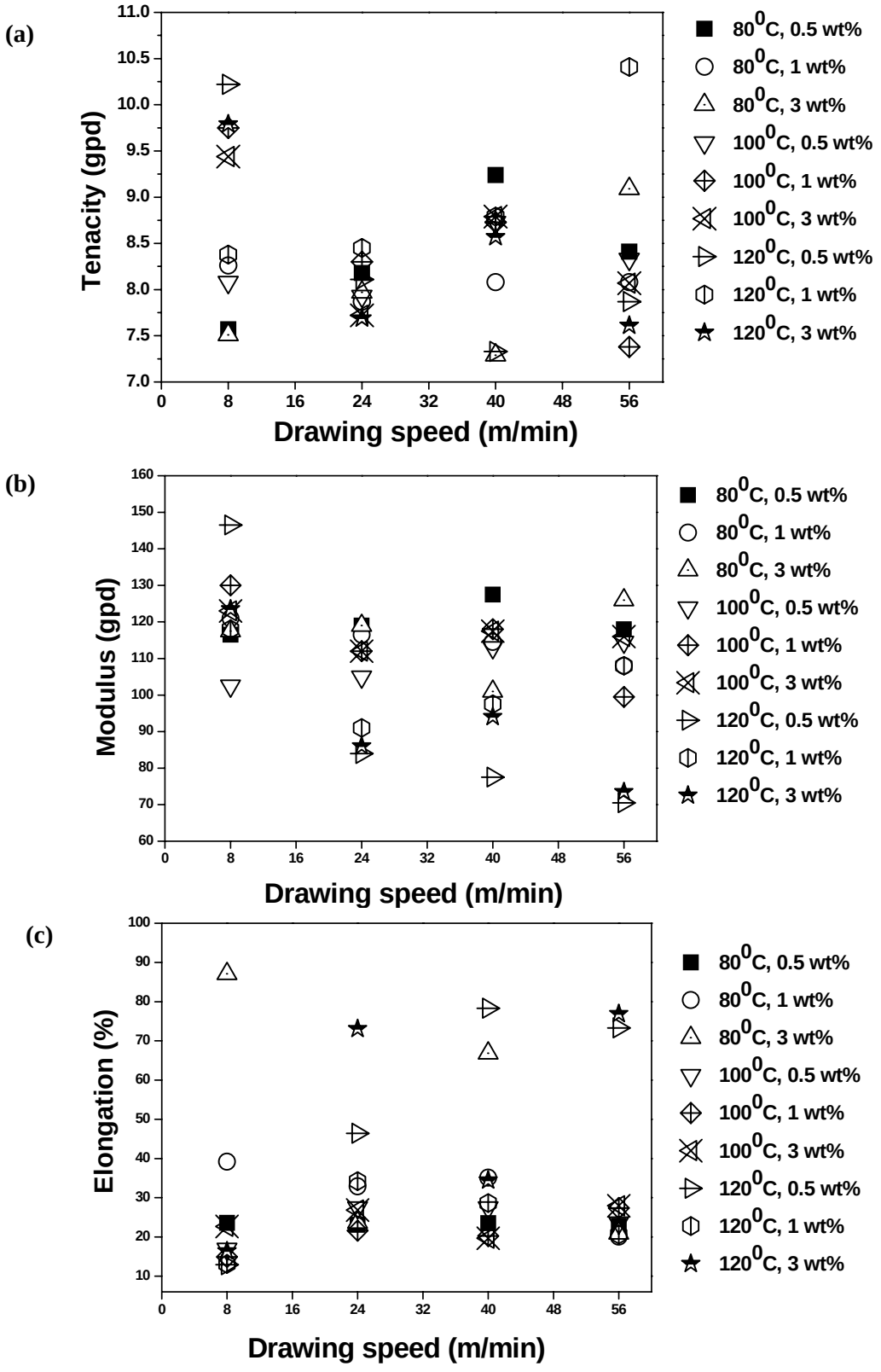

Figure 1: Effect of MWNT concentration on (a) tenacity (gpd) (b) modulus (gpd) (c) elongation at break (%)

Table 1: Experimental details of varying post drawing parameter variation

Level	Temperature (degrees)	Speed (m/min)
1	80	8
2	100	24
3	120	40
4	--	56

Finite element analysis of hyperelastic material

[1]R.Sujithra and [2]R.Dhanaraj
1. Department of Rubber Tech., 2.Department of Aerospace Engg.,
Madras Institute of Technology,
Anna University, Chennai-600044

E-mail Id: suji_forever@rediffmail.com

ABSTRACT

Due to the increasing demands of the rubber components used in the automotive and aerospace industries, the development of computational methods for elastomer analysis has attracted extensive research attention. This research work is focused on developing a finite element program code for the analysis of hyperelastic material restricted to plane stress case.

Hyperelastic refers to materials which can experience large elastic strain that is recoverable. Rubber like materials falls in this category. The behavior of hyperelastic material is described based on Mooney-Rivilin and Neo-Heokean material models. The constitutive theories for a large elastic deformation is based on the strain energy density function which is coupled with finite element method, can be used effectively to analyze and design elastomer.

Due to non-linear stress-strain relation, the hyperelastic materials will cause a structure stiffness to change at different load levels. In finite element formulation, the modeling of hyperelastic material should incorporate both geometric non-linearity due to large deformation as well as material non-linearity. Because of nonlinear relationship the finite element equations are nonlinear in terms of displacement. An iterative Newton-Raphson method was employed for the solution of non-linear governing equations. At each finite element solution step we obtained strain or strain increment, used to compute the stress which is needed to evaluate the internal force as well as the tangent stiffness matrix. The computed stress and deformation results obtained from finite element program code shows a good agreement with simple benchmark problem and as well as with FEA package (ANSYS).

I. INTRODUCTION

Hyperelastic is the capability of the material to undergo large elastic strain due to small forces, without losing its original properties. Rubber-like materials exhibit a highly non-linear behavior characterized by hyperelastic deformability and incompressibility or nearly incompressibility. But in general, all real materials are compressible to a certain degree even if the bulk modulus of the rubber-like material is larger than the shear modulus. Rubbers are widely used in tires, door seals, o-rings, conveyor belts, bearings, shock absorbers etc. An increase of applications of rubber-like materials requires better understanding of mechanical behavior which cannot be described by a simple stress-strain relation, but by the strain energy function. A hyperelastic material is also defined as a material whose stresses can be defined by a strain energy function.

Two sources of non-linearity exist in the analysis of hyperelastic materials namely, material and geometric non-linearity. The former occurs when the stress-strain behavior given by the constitutive relation is non-linear, whereas latter is important, when changes in geometry, however large or small have a significant effect on the load deformation behavior. The basic features of stress-strain behavior have been well modeled by invariant based or stretch based continuum mechanics theories. An important problem in non-linear elasticity theory is to come up with a reasonable and applicable elastic law which is the key to the development of reliable analysis tools. Many strain energy functions are proposed for rubber-like materials by Mooney (1940), Treloar (1944), Ogden (1972) etc. The simplest one parameter model is the Neo-Hookean model. In this present work, hyperelastic constitutive equations are discussed based on compressible Neo-Hookean model.

Finite element method is a procedure whereby the continuum behavior described at infinity of points is approximated in terms of finite number of points called nodes located at specific points in the continuum. These nodes are used to define regions, called finite elements over which both the geometry

and the primary variables in the governing equations are approximated. The governing equations describing the nonlinear behavior of the solid are recast in a weak integral form using principal of virtual work. The finite element approximations are then introduced into these integral equations which yields a finite set of non-linear algebraic equations in the primary variable. These equations are usually solved using Newton-Raphson iterative technique.

Based on finite element formulation, finite element program code is developed in C for the analysis of hyperelastic material for computing stresses and deformation. For simple benchmark problems, the result obtained from the coding is validated with ANSYS packages.

II. NON-LINEAR CONTINUUM MECHANICS

Continuum mechanics [1, 2] is an essential building block of nonlinear finite element analysis. We will confine our attention to the strain and stress measures which are most frequently employed in nonlinear finite element program. Two approaches are used to describe the deformation and response of a continuum. Consider a solid that is subjected to some forces and displacements such that its configuration changes from the initial to the current. In finite deformation analysis, any quantity can be described either in terms of the undeformed state or in a deformed state; the former is called material or Langrangian description while latter is called spatial or Eulerian description. In solids, the stresses generally depend on the history of deformation and an undeformed configuration must be specified to define the strain. So Langrangian descriptions are prevalent in solid mechanics.

A point is identified by a vector X in the initial configuration which moves to a new point identified by a vector x in the current configuration the mapping Θ of the motion is expressed as

$$X = \Theta(X, t) \tag{2.1}$$

In similar way, consider a line segment dx in material configuration is deformed to dX after the motion. The deformation gradient is defined by, $F = \partial x / \partial X$ (2.2)

The displacement of point is given by the vector u as a function of **X**, the differential displacement is given as $du = H\, dX$ (2.3)

The relation between deformation gradient and displacement gradient is $F = H + I$

To calculate the change in length dx after deformation using (2.2)

$$dx.dx = dX.\, F^T F\, .dX \tag{2.4}$$

At this point, we define the right Cauchy-green deformation tensor where c operates on material element and hence it is a Lagranian tensor. $c=F^T F$ (2.5)

Similarly, we define the left Cauchy-green deformation tensor b is an Eulerian tensor which operates on spatial element $dx\, b^{-1}\, dx = dX\, dX$ (2.6)

$$b = FF^T \tag{2.7}$$

.The green (or Lagragian) strain tensor is defined as $E = ½\ (c-I)$ (2.8)

And corresponding spatial spatial tensor, called Almansi strain tensor $e = ½\ (I-b^{-1})$ (2.9)

Also the volume dv and area da after deformation can be related to the initial volume dV and area dA using the deformation gradient F (det F=J) and is given as

$$dv = JdV \tag{2.10}$$

$$da = JF^{-T}.dA \tag{2.11}$$

Cauchy stress (Eulerian quantity) which relate the force dh acting on a differential area da is given as

$$dh = \sigma\, .da \tag{2.12}$$

From equ, shifting area to its initial configuration, $dh = J\, F^{-T} dA = P.dA$ (2.13)

Where P is the first piola-Kirchhoff stress defned as $P = JF^{-T}$ (2.14)

It is an unsymmetrical two point tensor and is not completely related to material configuration

The force vector dh can be related to its initial configuration in a similar manner

$$dh = F.dH \tag{2.15}$$

And rearranged as , $$dh = JF^{-1}F^{-T}.dA = S.dA \tag{2.16}$$

Where S is the second piola-kirchhoff stress tensor defined as $S=JF^{-1}F^{-1}$ (2.17)

Hyperelasticity is type of elasticity where the stress at any point can be derived from the deformation gradient and from an energy function. The behaviour of the material is said to be path independent and P is work conjugate with the rate of deformation gradient Ḟ,a stored elastic potential Ψ per unit undeformed volume can be established as the work done by the stresses form the initial to the current position as, $$\Psi = P : \dot{F} = S : \dot{E} = (\partial\Psi/\partial E)\,\dot{E} \tag{2.18}$$

Observing that ½ ċ=Ė is work conjugate to the second PK stress enables a totally lagrangian constitutive equation to be constructed in the same manner as $S = \partial\Psi/\partial E = 2\partial\Psi/\partial c$ (2.19)

Based on the isotropic assumption, the strain energy density function W is expressed as a function of the strain invariants .A better approach to modeling the response of rubbers comes from assuming existence of strain energy which is a function of deformation tensor. Strain invariants can be expressed in terms of the stretch ratios λ_1, λ_2, and λ3 as follows

$$\Psi = \Psi(I_1, I_2, I_3)$$
$$I_1 = \lambda_1^2 + \lambda_2^2 + \lambda_3^2 = \text{tr}(c)$$
$$I_2 = \lambda_1^2\lambda_2^2 + \lambda_2^2\lambda_3^2 + \lambda_3^2\lambda_1^2 = ½\,[(\text{tr}\,c)^2 - \text{tr}(c^2)]$$
$$I_3 = \lambda_1^2\lambda_2^2\lambda_3^2 = \det c \tag{2.20}$$

For incompressible material I_3=1.The strain energy function for Neo-Hookean material is given as

$$\Psi = C_1(I_1 - 3) \tag{2.21}$$

In many cases rubber is compressible to some extent and it is important to consider compressibility. This work deals with the compressible form and introduces a strain energy contribution involving the bulk modulus. For compressible form [4], the strain energy should combine both volumetric and deviatoric term.

$$\Psi = \Psi v + \Psi d$$
$$\Psi = ½\,\lambda\,(\ln(\det F))^2 - \mu \ln(\det F) + ½\,\mu\,(\text{tr}(c) - 3) \tag{2.22}$$

PK stress and Cauchy stress can be easily be computed from (2.22) and given as

$$S = \lambda(\ln(\det F))c^{-1} + ½\,\mu\,(I - c^{-1}) \tag{2.25}$$
$$\sigma = \lambda/\det t\,(\ln(\det F))\,I + (\mu/\det F)\,(b - I) \tag{2.24}$$

The components of the fourth-order elasticity tensor are obtained as follows:

$$C_{ijkl} = \lambda c_{ij}^{-1}c_{kl}^{-1} + (\mu - \lambda \ln(\det F))(cik^{-1}c_{jl}^{-1} - c_{il}^{-1}c_{kj}^{-1}) \qquad i,j,k,l = 1,2,3 \tag{2.25}$$

III. FINITE ELEMENT FORMULATION

The finite element equations are non-linear in terms of displacement because of nonlinear strain-displacement and stress-strain relationships. By the principle of virtual work, the weak form in the current configuration is given as

$$\int_V \delta e^T \sigma\, dv = \int_A \delta u^T q\, dA + \int_V \delta u^T b\, dv \tag{3.1}$$

For problems involving large displacement [6], consideration should be given to the configuration. Since the current configuration is not known, we cannot compute directly from this equ (3.1). Using the deformation gradient, the derivatives and integrals in the weak form are transformed to the initial configuration (Total Langrangian formulation).

$$\int_{V^o} S\, \delta e\, dV^o = \int_{A^o} \delta u^T q^o\, dA^o + \int_{V^o} \delta u^T b^o\, dv^o \tag{3.2}$$

The equ (3.2) is linearized and we get element tangent matrix equations as follows

$$\int_{V^o}\int\int [B\hat{S}BT + BF^T C F B^T]dV^o \Delta d = -\int_{V^o}\int\int B F^T S\, dV^o + \int_{A^o}\int N q^o dA^o + \int_{V^o}\int N b^o dV^o \quad (3.3)$$

Thus, $(K_S+K_C)\Delta d = r_i + r_q + r_b$ (3.4)

Where K_c is the current stiffness matrix, K_s is the geometric stiffness matrix, r_i , r_q , r_b are the equivalent nodal load vector due to stresses in the current known configuration, due to surface forces and due to body forces. At the current state, the linearized finite element equation is calculated for each element and assembled. The equations are assembled and solved in the usual manner to obtain the increments in the displacements. The new deformed configuration can be obtained by adding these displacements to the initial coordinates using constitutive equations, we first calculate Cauchy stresses in deformed configuration. If the computed stresses are correct, the equilibrium equations must be satisfied in the configuration

Equivalent load vector due to stresses $r_I=\iiint B_L\sigma dV$ (3.5)

The unbalance force is calculated as follows $r = r_E-r_I$ (3.6)

The load vector from each element is assembled to form global r_I vector. This vector is compared against the applied nodal load vector. If the difference between two is large, a new iteration is carried out to establish a new deformed configuration. This process is repeated until a desired level of convergence tolerance is achieved.

IV. IMPLEMENTATION OF FEM IN PROGRAMMING

A C program is written based on the above finite element formulation using Four Noded Isoparametric element for the analysis of hyperelastic material restricted to plane stress case. Flow diagram for the program is shown in Fig: 1.

A computational procedures for programming is given briefly as

1. In the first step, get the nodal datas and assume initial displacement is zero.
2. Calculate bandwidth for global stiffness matrix.
3. Begin of iteration loop
    - 3.1 compute the geometric and current stiffness matrix
    - 3.2 Assemble global stiffness matrix from individual element tangent matrix
    - 3.3 By gauss elimination, solving $\{\Delta d\} = [k_t]^{-1}\{F\}$
    - 3.4 By solving, we get incremental solution of displacement.$d_{i+1}=d_i+\Delta d$
    - 3.4 Update the coordinates
    - 3.5 Compute stress from the new deformation gradient.
    - 3.6 Compute updated thickness
    - 3.7 Calculate internal load vector
    - 3.8 Unbalance force=external load – internal load.
    - 3.9 Check for convergence parameter.
4. If no, go for next iteration step No.3 .If yes, terminate the program.

Cooks Problem [8]:

A rubber tapered panel is clamped at one end and loaded by nodal forces on the top of the other end. The material properties used are C1=0.5 and bulk modulus1500. From the material parameter we determine lames constant which is the input for coding. We consider the problem to be nearly incompressibility and the poissons ratio is taken as 0.499. The geometry is shown in Fig.2. The nodal coordinates and result obtained from coding is shown in Table: 1. The problem is solved in ANSYS using Neo-Hookean material model and deformed shape is shown in Fig: 3. The Computed results from coding shows a good agreement with ANSYS shown in Table 2.

V.CONCLUSION

The analysis of hyperelastic material behavior by finite element method has been described in this study. Rubber like materials are incompressible but still its nearly incompressibility is considered as a special feature of compressible material. The Neo-Hookean material model is discussed based on compressible strain energy function by combining both volumetric and deviatoric term. Based on this approach, a finite element program code is implemented. A simple rubber tapered panel is solved by

Programming and also with FEA packages. The output from the program code is validated with simulated results.

References:

1. Gerhard A.Holzapfel, Nonlinear solid mechanics, John Wiley & sons, New York.
2. Javier Bonet, Richard D.Wood, Nonlinear continuum mechanics for finite element analysis, Cambridge university press.
3. O.C.Zienkiewicz, R.L.Taylor, The finite element method, Vol I & II.
4. M.A.Crisfield, Non linear finite element analysis of solids and structures, Vol I &II, John Wiley &sons, New York.
5. Odgen.R.W, Nonlinear elastic deformations, Dover Publications, New York.
6. Asghar bhatti.M, Advanced topics in finite element analysis of structures, John Wiley & sons.
7. Bathe K.J & Dvorkin E.N, some practical procedures for the solution of non-linear finite element equations, comp. meth. Appl. Mech & Engng, 22, 59-85 (1980).
8. T.Estebenit, A.Guessab,E.Jankovich, An enhanced strain mixed method applied to rubber-like material, Vol 52,No.3, pp 573-579, 1994.
9. Shu.H.Peng, Wenji V.Chang, A compressible approach in finite element analysis of rubber-elastic materials, computers & structures, vol 62, No.3, pp573-593, 1997.
10. Ted belytschko, wing kam liu, Brian Moran, Nonlinear finite elements for continua and structures, John Wiley & sons.
11. A.N.Gent, Engineering with rubber, hanser publishers, 2001.

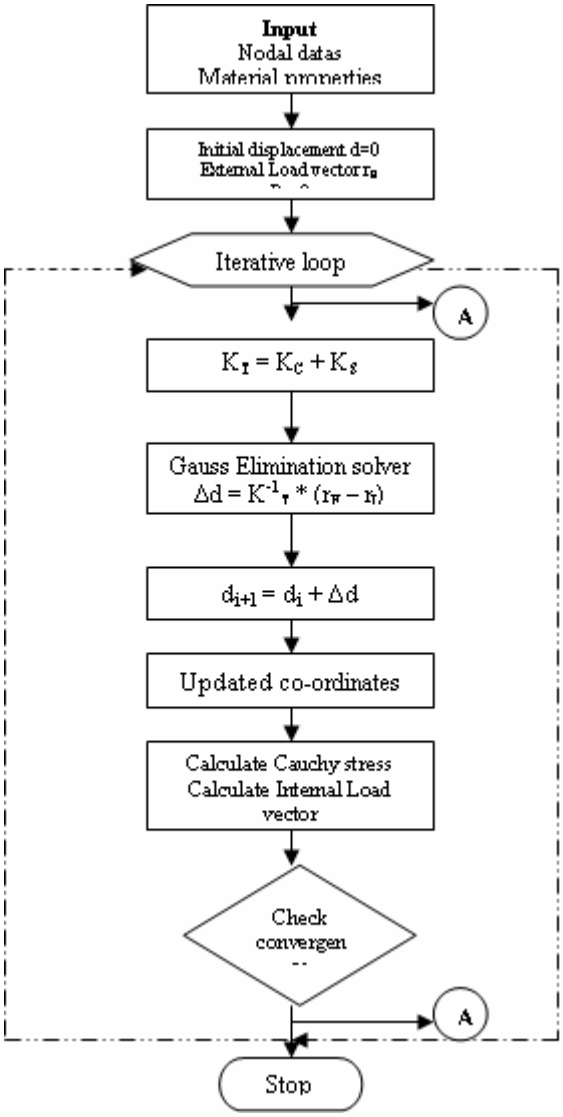

Fig: 1 Flow Diagram

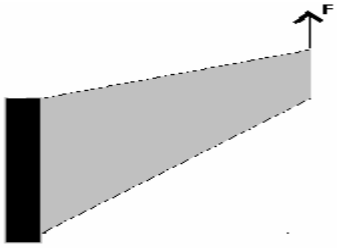

Fig: 2 Rubber panel

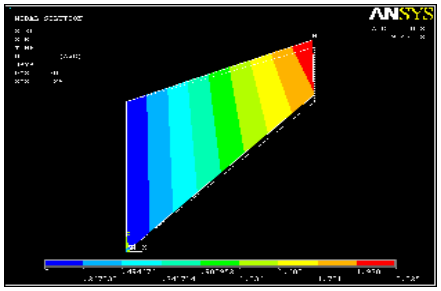

Fig: 3 Deformed shape in Ansys

Initial coordinates		Deformed coordinates	
X	Y	X	y
0	0	0	0
48	44	47.8845	45.9637
48	60	47.4028	62.2285
0	44	0	44
Convergence parameter= 0.00994			
Num of iterations =60			

Table: 1 Coding Results

Result	Program	Ansys
Max disp at top	2.2285	2.302

Table: 2

Stress analysis of air borne polymeric composite structure

Shiv Kumar, K. Shajahan, Lijo Vijayan, Reji John, R. R. Varma and M. Aravindakshan
Naval Physical & Oceanographic Laboratory,
Defence Research and Development Organisation, Kochi – 682 021
Email: tsonpol@vsnl.com

Abstract

Composite structures are extensively used in air borne applications in civilian and military field owing to inherent advantages of high strength to weight ratio, ability to withstand high loads, slow failure rates, tailorability of mechanical and chemical properties and better directional properties. The most common types of composites employed in air borne applications are carbon fibre reinforced epoxy and Glass Fibre reinforced epoxy. One of the FRP structures developed for airborne application is in the shape of 'C' with various geometrical discontinuities for weight reduction and mounting of sensors and hinges for integrating to main assembly. Presence of such deviations from regular geometries leads to build up of stress concentrations at such irregularities, which could be fatal and lead to catastrophic failures. In order to understand the actual stress distribution, predict and prevent any failure of the structure proper theoretical analysis is required

A finite element analysis software ANSYS was used to evaluate the stress response of the composite structure. As the structure is intended to operate underwater, analysis was carried out to simulate the effect of hydrostatic pressure loads. Airworthiness requirements also demands that the structure to withstand high inertial acceleration loads coming on the system during various manoeuvring. Analysis was also carried out to ensure that the structure is capable of withstanding these inertial acceleration loads. The structure is mounted with sensor elements and the effect of these sensor elements were modelled using lumped masses method. 10-node tetrahedral structural element was used to mesh the structure. As the structure is fabricated with fibre reinforce plastics having orthotropic properties, properties such as elastic modulus, shear modulus and Poison's ratio were considered for all the three directions for the analysis. The analysis was carried out for 30% glass filled polycarbonate, Glass fibre reinforced epoxy composites and Carbon fibre reinforced epoxy composites. The Von-Mises stress distribution obtained showed the maximum stress near the top hinges and the corresponding displacement distribution showed maximum displacements at the top of the structure.

Introduction

Many of the modern technological developments that have taken place in last few decades are due to new materials and new materials processing techniques. Among these materials which has come to stay, composites occupies an important place in various fields such as aerospace, defence, sports, automobile, etc. Composite structures are extensively used in air borne applications in civilian and military field owing to inherent advantages of high strength to weight ratio, ability to withstand high loads, slow failure rates, tailorability of mechanical and chemical properties and better directional properties.

A necessary prerequisite for the design and safe operation of composite structure is an accurate knowledge of their strength and stiffness properties. An assessment of these properties solely by testing of critical components or of prototype structure is feasible but is usually encumbered by punitive cost and time requirements. Therefore, analytical methods must be employed with aim of facilitating trade-off studies in early design phases, providing insight into the overall structure and identifying critical parts of the composite structures. [1]

Application of analytical methods on simple structures is feasible however, it becomes practically impossible to apply analytical solutions on complex shapes. Excessive approximations to implement analytical solutions may lead to erroneous results. Hence, it is essential to utilize other means of analysis of the structures. Various FEM tools are available to model such complex structures, however none of them specializes in FEM analysis of composite structures. Various structural analysis FEM packages however have capability to analyse complex shapes of orthotropic materials. One such software Ansys is used in analysis of current problem.

Due to inherent advantage of high strength to weight ratio and tailorable directional properties of composites, it finds extensive application in air borne systems. One such structure being developed is a 'C' channel shaped structure for housing of sensors. The structure has various grooves for mounting the sensors, discontinuities for weight reduction of overall structure and hinge holes for assembling with the main system. The details of such a 'C' channel structure is shown in figure 1.

As 'C' channel structures is non-symmetrical and has numerous discontinuities, mechanical behaviour of the structure cannot be easily predicted. Due to its irregular features, number of stress concentrations points will be present in it. Any improper fabrication or design will lead to catastrophic failure of the structure.

Analysis

The 3-D model developed was imported in FEM analysis software Ansys. Ansys was selected primarily of its excellent structural analysis capabilities and ability to support orthotropic and anisotropic materials in analysis. Von-mises stresses and Displacement Vector Sum were determined. Analysis was carried out for 3 different polymer composites viz.

1. 30 % short glass fibre filled polycarbonate,
2. 40% Unidirectional glass fibre reinforced Epoxy, and
3. 40% Unidirectional carbon fibre reinforced Epoxy.

The properties of the same are tabulated in table 1. The failure criteria were also analysed to determine whether the structure will withstand or fail while in operation.

The structure being air borne, it needs to withstand high inertial loads while in manoeuvring, take off and landing. and deployed underwater from a flying platform has to withstand high inertial loads as well as hydrostatic pressures on the system. While in analysis inertial load was taken into consideration. As the structure is to deployed underwater hydrostatic pressure was also taken in account on complete structure.

The structure is mounted with sensors of weight 180 gm at 5 different mounting point along with 2 hinge points and hydrostatic load of 4 MPa. The sensors are modelled as lumped mass for ease of modelling. A section of the boundary condition is as shown in the figure 2. The red arrows show the hydrostatic pressure acting throughout the structure while light blue arrows shows the hinge point area with zero degree of freedom. The yellow arrows represent the sensor mass acting on the structure.

The structure was modelled using 10 node tetrahedral structural element referred at SOLID 187 in Ansys. SOLID187 element is a higher order 3-D, 10-node element. SOLID187 has a quadratic displacement behaviour and is well suited to modelling irregular meshes such as those produced from various CAD/CAM systems. The element is defined by 10 nodes having three degrees of freedom at each node: translations in the nodal x, y, and z directions. The element has plasticity, hyperelasticity, creep, stress stiffening, large deflection, and large strain capabilities. It also has mixed formulation capability for simulating deformations of nearly incompressible elastoplastic materials, fully incompressible hyperelastic materials and elastic orthotropic materials. [4,5]

Results and Analysis

The analysis carried out with various materials and their results are discussed below. Von-mises stress analysis of the structure with 3 identified composites were carried out and results are shown in figure 3, 4 and 5 respectively for 30 % short glass fibre filled polycarbonate, 40% Unidirectional glass fibre reinforced Epoxy and 40% Unidirectional carbon fibre reinforced Epoxy.

The maximum stress obtained in three cases is in 320 MPa which well below the failure strength of carbon fibre based composites. Similarly, for the case of glass fibre based composite and glass fibre filled polycarbonate does satisfy the requirement of maximum breaking strength. Hence in terms of required strength, component with either of the material will withstand the operating conditions.Next, Vector displacement of the component was analysed and results are shown in the figures 6, 7 and 8.

The 30% short glass fibre filled polycarbonate shows 35 mm of deformation in the lower end of the structure. As this much variation in the location of the mounted sensor will lead to erroneous result, it is unacceptable as suitable material for fabrication of the component. Both Glass fibre and carbon fibre based epoxy composite shows much less deformation and are suitable for the application. However, it is well known from the literature that glass fibre undergo gelation when it is exposed to sea water for long period of time and hence high factor of safety is required in design of the component. [6] As the component being modelled is limited by space constraint hence only recommended material is Carbon fibre based composite for fabrication of component.

Conclusion

The modelling of a critical component used in air platform based underwater deployable system was carried out to analyse the finalize the selection of suitable material of construction of the component using FEM software ANSYS. The structure having various irregularities in the shape was modelled using solid elements and Von-mises stresses and total vector displacements were analysed. The materials selected for analysis were 30 % short glass fibre filled polycarbonate, 40% Unidirectional glass fibre reinforced Epoxy and 40% Unidirectional carbon fibre

reinforced Epoxy. It was observed that even though 30 % short glass fibre filled polycarbonate has better properties in transverse directions but maximum forces are acting along the length of the component and it undergoes large displacement and hence cannot be considered as a suitable material for fabrication of the component. Furthermore, carbon fibre based composite was selected as a suitable material for fabrication based on its better long term property retention and lesser deformation in the shape.

Acknowledgement

The authors wish to express their thanks to Director, NPOL, Kochi for granting permission to carry out this work. Authors would also like to express their gratitude to Group Head (MS & MEMS), NPOL, Kochi for their encouragement and support.

Reference

1. Course notes of "*Design and Manufacture of Composite Components*" organised by AICTE and ISTE, Coimbatore, India, June 2003
2. www.boedeker.com/polyc_p.htm
3. Quinn, JA, "*Composite Design Manual"*, James Quinn Associates, Technomics, 19999
4. Release 9.0 Documentation of Ansys
5. www.philonnet.gr/products/ansys/ed/index.html
6. Lubin & Peters, "*Handbook of Composites"*, Springer, Inc., 1997

Figure 1: Section of the 'C' channel structure showing geometrical discontinuities

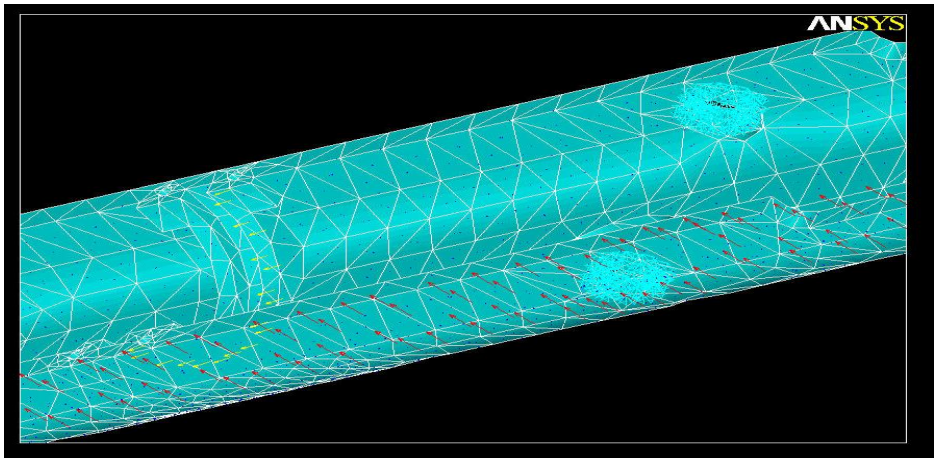

Figure 2: Section of the modelled structure showing various boundary conditions

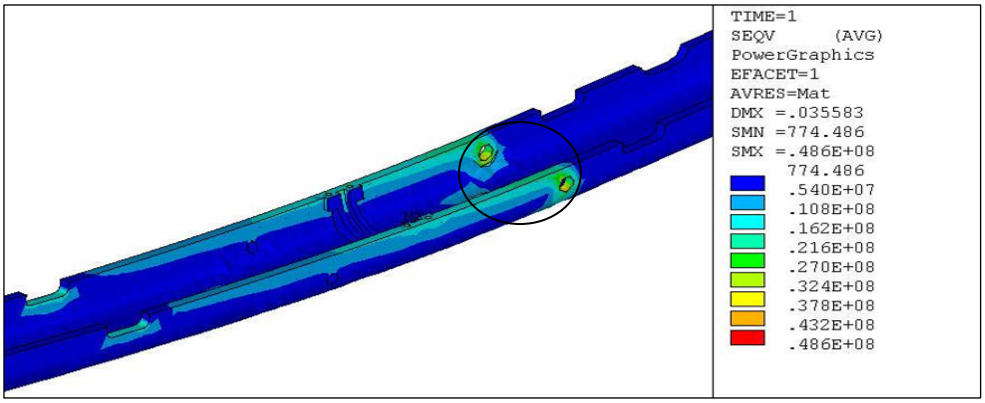

Figure 3: Von-mises stress distribution showing over a section of structure modelled with 30 % short glass fibre filled polycarbonate. Maximum stress of 48 MPa is obtained in the lower hinge section shown by the circle.

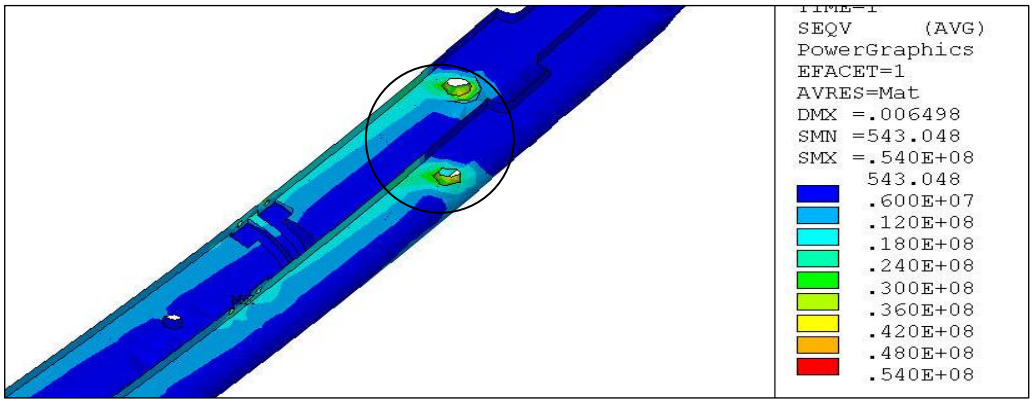

Figure 4: Von-mises stress distribution showing over a section of structure modelled with 40% Unidirectional glass fibre reinforced Epoxy. Maximum stress of 58 MPa is obtained in the lower hinge section shown by the circle.

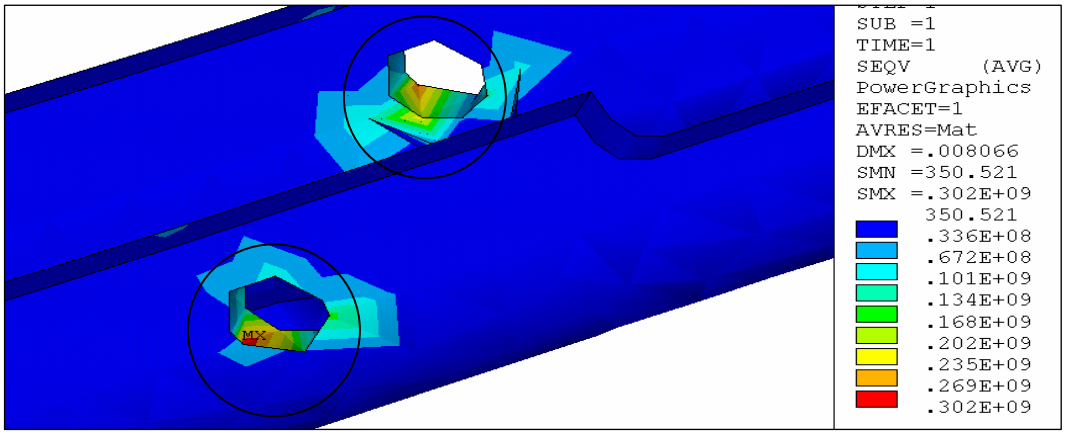

Figure 5: Von-mises stress distribution showing over a section of structure modelled with 40% Unidirectional carbon fibre reinforced Epoxy. Maximum stress of 320 MPa is obtained in the lower hinge section shown by the circle.

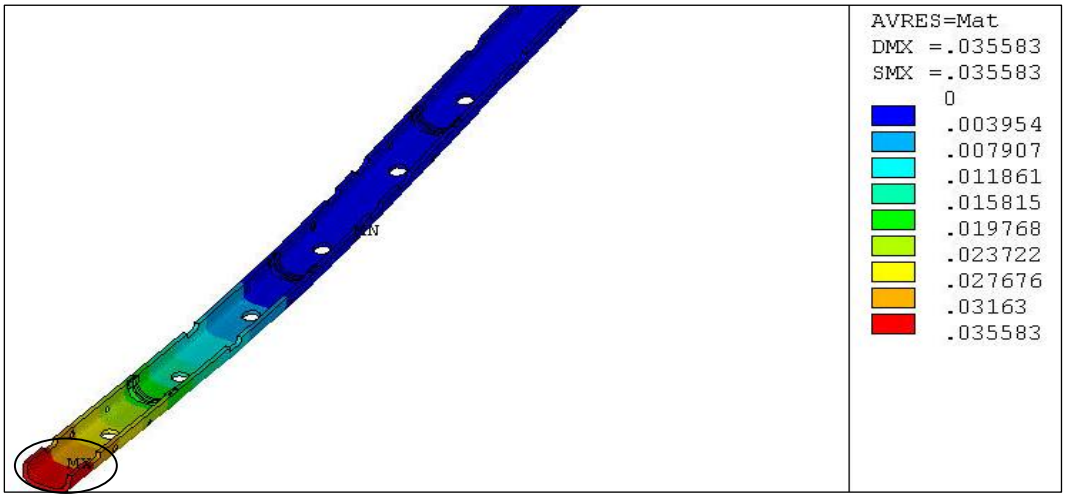

Figure 6: Total Vector displacement distribution showing over a section of structure modelled with 30 % short glass fibre filled polycarbonate . Max. displacement of 35 mm at the lower end of the component as shown by ellipse.

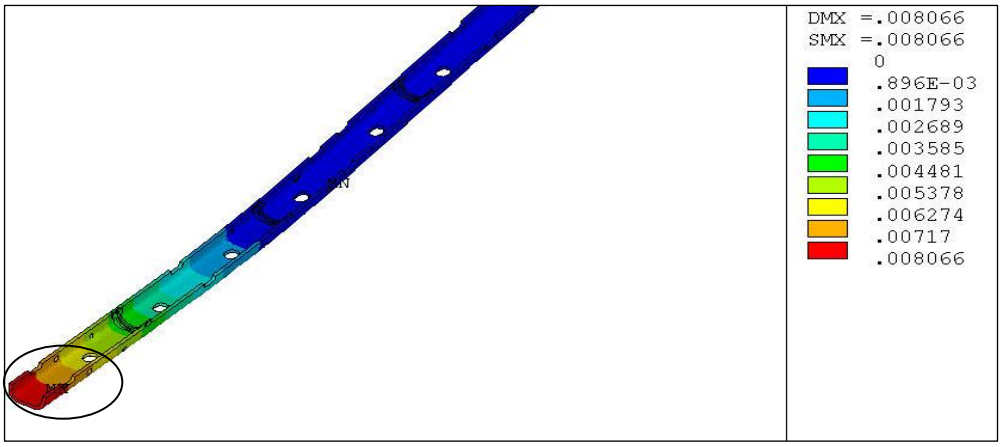

Figure 7: Total Vector displacement distribution showing over a section of structure modelled with 40% unidirectional glass fibre reinforced Epoxy. Max. displacement of 8 mm at the lower end of the component as shown by the circle.

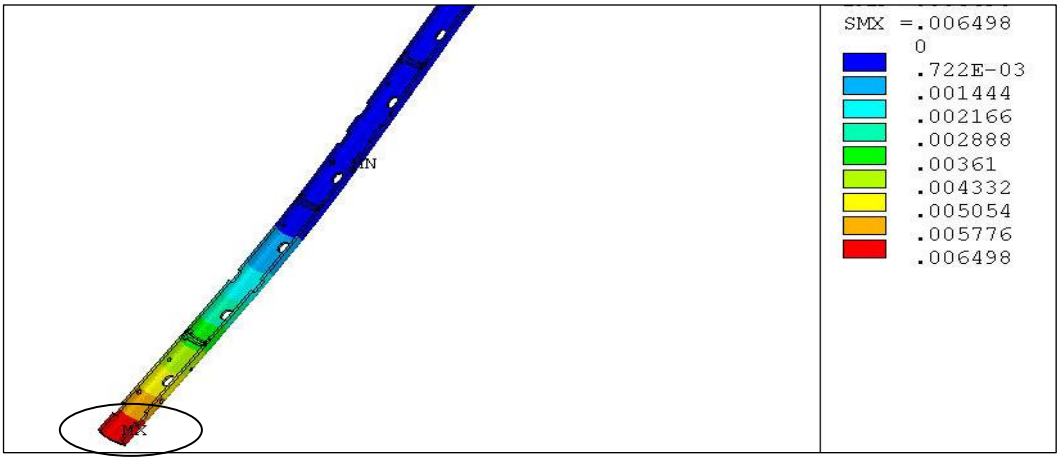

Figure 8: Total Vector displacement distribution over a section of structure modelled with 40% unidirectional carbon fibre reinforced Epoxy. Maximum displacement of 6.5 mm at the lower end of the component as shown by the circle.

Table 1: Mechanical Properties of the Composites [2,3]

Property	**30 % short glass fibre filled polycarbonate**	**40% Unidirectional glass fibre reinforced Epoxy**	**40% Unidirectional carbon fibre reinforced Epoxy**
Young's Modulus			
E_1 (Pa)	8.62 E +09	1.24 E + 10	9.96 E + 09
E_2 (Pa)	8.62 E +09	4.48 E + 10	1.45 E + 11
E_3 (Pa)	8.62 E +09	1.24 E + 10	9.96 E + 09
Poisson's Ratio			
μ_{12}	0.31	0.28	0.25
μ_{23}	0.31	0.28	0.25
μ_{13}	0.31	0.037	0.041
Shear Modulus			
G_{12} (Pa)	--	5.52 E + 09	5.86 E + 09
G_{23} (Pa)	--	5.52 E + 09	5.86 E + 09
G_{13} (Pa)	--	3.6E + 09	3.46 E + 09
Density (kg / m^3)	1430	2080	1580

Synthesis, curing and characterization of tetraglycidyl epoxy resin

D.Armstrong*, V. Agneeswaran and Dr.B.Kothandaraman[#]

Department of Rubber and Plastics Technology,
Madras Institute of Technology, Anna University Chennai

E-mail:armstrongmit@gmail.com, bkraman@mitindia.edu

Abstract:

Epoxies generally out-perform most other resin types in terms of mechanical properties and resistance to environmental degradation, which leads to their almost use in aircraft components. It has outstanding thermal and adhesion properties. Some of these resins can be cured at room temperature, but heat can be used to accelerate the cure of the epoxy. Among the high temperature epoxy resins, TetraGlycidyl Diamino Diphenyl Methane can provide high cross-linking density, so that hardened bodies obtained from the known composition exhibits both high modulus and high heat resistance which is inevitable for matrix materials for the advanced composites used in aerospace, electronics, automotive and other industries. In the present investigation, TetraGlycidyl Diamino Diphenyl Methane was synthesized through glycidation of 4, 4'-Diamino Diphenyl Methane with a large excess of Epichlorohydrin under controlled reaction conditions. Diamino Diphenyl Methane (specifically increases temperature and chemical resistance), Diamino Diphenyl Sulphone (DDS)and Triethylene Tetramine(TETA) were used for curing. The formulated curing mixture was cured as per the curing schedule described. The molecular structure of tetraglycidyl diamino diphenyl methane was confirmed by Nuclear Magnetic Resonance Spectroscopic technique. The degradation behavior of cured samples was studied by thermo gravimetric analysis. The resin was cured with the above mentioned 3 amine curatives and their properties were compared using Differential Thermal Analysis (DSC)

Introduction:

Epoxy Resins are class of thermoset materials extensively used in structural and specialty composite applications because they offer a unique combination of properties that are unbelievable with their many desirable properties, such as good adhesion, excellent chemical, thermal stabilities and electrical properties. The outstanding adhesion to various substrates makes epoxy resin, an important and efficient resin system in adhesive industries. In 1970 s, Ciba-Geigy corporation developed a series of glycidylated resins based on hydantoin and Shell Technologies introduced the glycidylated resins of hydrogenated bisphenol-A, but in both instances commercial success was limited. Epoxy adhesives can bond a wide variety of substrates with high strength particularly metals. They have been used to replace some traditional metal working methods of joining like nuts and bolts, rivets, welding, crimping, brazing and soldering. Epoxy resin adhesives are used mainly in niche applications rather than as general purpose adhesives. Good adhesion to nonporous surfaces allows them to be used in demanding situations.

In the present investigation, tetra functional epoxy resin was prepared from 4, 4'-diamino diphenyl methane and was cured with Diamino Diphenyl Methane (DDM), Diamino Di phenyl Sulphone (DDS) and triethylene tetramine (TETA). The thermal stability of cured TGDDM resins were studied by thermogravimetry in nitrogen atmosphere at a heating rate of 10° C/min, as a systematic thermal study on the selected resin system was very limited.

Experimental:

Materials:

Reagent grades of Diamino Diphenyl Methane, Epichlorohydrin, ethyl alcohol, lithium hydroxide mono hydrate, sodium hydroxide, toluene, Diamino Diphenyl Sulphone and Triethylene tetramine were obtained from E-Merck India limited, Mumbai and were used without further purification.

Synthesis of tetra glycidyl diamino diphenyl methane (TGDDM):

Diamino diphenyl methane, epichlorohydrin and 60 ml of ethyl alcohol were added with water, and the mixture was stirred at 75° C for 6 hours. Then the reaction mixture was brought to 55° C while 30% NaOH solution added over 5 hours. Excess water and epichlorohydrin were removed by distillation under reduced pressure (30 mm Hg) . The residue was dissolved in toluene and washed with water to remove salts and residual caustic.

Curing:

4,4'- diamino diphenyl methane(DDM), 4,4'- diamino diphenyl sulphone(DDS) and tri ethylene tetramine (TETA) were used as the curing agents, in which each hydrogen on an amine nitrogen will be reactive and can open one epoxide ring to form a covalent bond. The correct relative amounts of TGDDM and curing agents were determined by computing the weight of curing agent that contains one chemical equivalent of amine hydrogens and matching that with the weight of TGDDM that contains one chemical equivalent of epoxide groups.

Analytical methods:

Fourier transform infrared spectroscopy:

The FTIR of virgin Tetraglycidyl Diamino Diphenyl Methane was done. the apparatus used was PERKIN-ELMER make.

Scanning Rate: 16 scans

Resolution: 4 cm^{-1}

Nuclear magnetic resonance spectroscopy (NMR):

The proton (^{1}H) Nuclear Magnetic Resonance spectroscopic study and carbon (^{13}C) Nuclear Magnetic Resonance spectroscopic study were performed in a Bruker 500 MHz NMR spectrometer using $CDCl_3$ as the solvent.

Thermo gravimetric analyzer:

The TGA equipment used was TGA Q 50 V 20.5, from TA instruments, where the temperature range is taken from 20°C to 750°C, at a heating rate of 10°C/min in nitrogen atmosphere.

Differential scanning calorimetry:

The DSC equipment used was DSC Q 20 V 23.5, from TA instruments, where the temperature range was taken from 20°C to 300 °C, at a heating rate of 10°C/min, in nitrogen atmosphere.

Results and Discussion:

Table 4.1: FTIR Results

WAVE NUMBER (cm^{-1})	INTENSITY	FUNCTIONAL GROUP
1620	Strong & sharp	Phenyl group
838.8	Strong	p- substituted benzene
2915	Strong & Broad	Aromatic C-H stretching
699.1	Medium	Benzene ring
962.3	Strong and sharp peak	Oxirane group
1254.3	Cluster of peaks	C-N aromatic stretching
1189.8	Cluster of peaks	C-N aliphatic stretching

.

Table 4.2: Proton Magnetic Resonance Spectroscopy Results

CHEMICAL STRUCTURE	**RADIATION FREQUENCY(PPM)**
Proton in the benzene ring	7.21
Proton in the CH_2 group attached with Nitrogen	3.68
Proton in the CH group of oxirane ring	2.77
Proton in the CH_2 groups of oxirane group	2.5

Table 3: ^{13}C NMR Spectroscopy Results

CHEMICAL STRUCTURE	**RADIATION FREQUENCY(PPM)**
^{13}C in the ortho -position of phenyl ring	**127.9**
^{13}C in the meta -position of phenyl ring	**128.4**
^{13}C in the para -position of phenyl ring	**140.2**
^{13}C in the CH_2 group attached with nitrogen	**49.9**
^{13}C in the CH group of oxirane ring	**52.1**
^{13}C in the CH_2 group of oxirane ring	**44.2**

From the observed results it was confirmed that the resin synthesized was TetraGlycidyl Diamino Diphenyl Methane.

:

Table 4: TGA Results

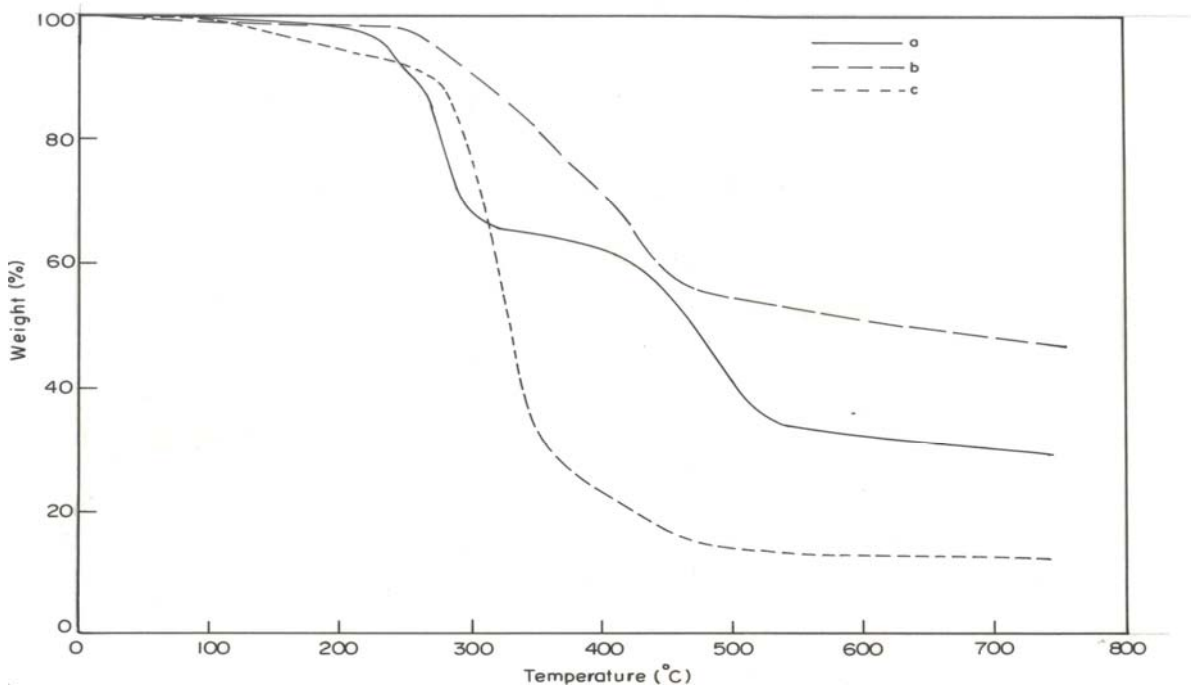

a-DDM cure b-DDS cure c-TETA cure

Sl.no	Curing system	Onset temperature(°C)				Residue (%)
		Primary transition		Secondary transition		
		T_i(°C)	T_f(°C)	T_i(°C)	T_f(°C)	
1	Uncured resin	232.47	300	426.33	518.69	22.59
2	DDM	243.67	297.55	413.52	520.69	30.85
3	DDS	258	456.92	----------	----------	48
4	TETA		491.23	----------	----------	14.33

UNCURED RESIN:

There are 2 transitions observed in TGA analysis of uncured resin. Decomposition starts at 232°C and residue obtained was 22.59 %. There are aromatic benzene groups in the backbone of the resin with aliphatic side groups. The first transition may be due to the degradation of aliphatic groups. Second transition is due to the degradation of aromatic backbone. From the TGA curve we can observe that degradation at the beginning of the curve itself this may be due to the evaporation of volatiles such as water

TGDDM/DDM SYSTEM:

There are 2 transition temperatures observed in TGDDM/DDM system. This is due to the cyclization reactions occur during curing[9]. Condensation of main chain benzene ring occurs to some extent, so the char yield is higher than the uncured resin, and from the high char yield value it is inferred that this system will have good flame resistance

TGDDM/DDS SYSTEM:

There is only one transition temperature was observed in TGDDM/DDS system and residue obtained was 48%.this is attributed to the reason that complete condensation aromatic groups upon curing and this leads to very stiff and rigid network. From the highest value of char yield depicts that the material will have excellent flame retardancy.

TGDDM/TETA SYSTEM:

In TGDDM/TETA system also has only one transition temperature is observed and the residue was 14.33%. This char yield is less than the uncured resin. Onset of degradation and it loses the maximum weight in a little interval of temperature. TETA curing system is meant for room temperature curing it is not suitable for the high temperature curing. TGDDM is a high temperature curing, so it does not yield good properties with TETA curing agent.

Table 4.5: Comparison of curing systems

Sl.no	Curing system	Temp. at 10% weight loss(°C)	Char yield (%)			
			200°C	400°C	600°C	800°C
1.	Uncured resin	157.4	83.75	46.66	26.36	20.57
2	DDM	251	98.125	62.1875	33.125	28.75
3	DDS	305.89	98.398	71.63	51.06	46.91
4	TETA	274.25	95.01	24.78	14.52	14.13

INFERENCE:

1. Temperature at 10% weight loss is 157.4°C for uncured resin. This value increases by a factor of 2 after curing. This value is comparable for both TGDDM/DDM system (251°C) and TGDDM/TETA system (274.25°C).
2. Temperature at 10% weight loss is 305.89°C for TGDDM/DDS system. This means that the cross linked network is very stiff and it has excellent flame resistance
3. Char yield at 200°C increases for the cured resin systems than the uncured resin system. The values are almost the same for both TGDDM/DDM and TGDDM/DDS system. This value is slightly less for TGDDM/TETA system
4. TGDDM/DDS system has the highest char yield at 400°C. there is drastic drop in char yield for TGDDM/TETA system at 400 °C than 200°C
5. TGDDM/DDS system has the highest char yield even at 600°C. TGDDM/DDM and TGDDM/TETA system have char yield lower than the uncured resin
6. Residues for all the above said systems were found at 750°C. TGDDM/DDS system has the highest char yield. So, it is inferred from the result that TGDDM/DDS system has very good flame resistance. If we add some flame retardants to this system we could achieve excellent flame retardancy.
7. For TGDDM/DDM and TGDDM/TETA system Char yield at 750°C is less than the uncured resin. Flame retardancy of the resin was affected by these curing agents.
8. But TGDDM/DDM system has the highest degradation temperature when compared to other systems. So this system will offer high performance even at elevated temperatures.
9. TGDDM/DDM system does not have that much crosslink density as in the case of TGDDM/DDS system. It is somewhat flexible, so this can be used for tooling applications
10. TGDDM/TETA system has first decomposition temperature at 284.78°C(Highest of all systems compared). But the final decomposition point lies at a short interval of 100°C. This system looses almost 75 % of the polymer between the primary and secondary onset temperatures. So this is not suitable for high performance

Table 4.6: DSC Results

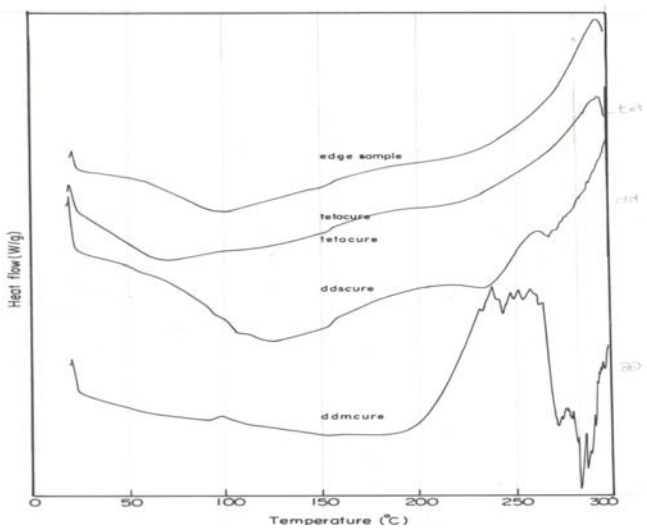

DSC thermo grams of edge sample, TETA cure, DDS cure, DDM cure.

SL. NO.	CURATIVE USED	T_g(°C)	ONSET OF EXOTHERMIC PEAK(°C)
1	DDM	145.53	235.75
2	DDS	113.71	240.49
3	TETA(MIDDLE)	53.27	229.64
4	TETA(edge)	85.97	227.04

TGDDM cured with DDM:

For TGDDM cured with DDM the T_g value was observed at 145.53°C. an exothermic peak starts at 235°C and reaches maximum exothermic heat flow at around 260°C. This indicates that post cure at 210°C is not sufficient, still higher temperature is required for post cure. That may be around 250°C because exothermic peak reaches maximum at that temperature. Maximum exothermic temperature shown in DSC curves is the temperature at which the residual cure gets completed. At 280°C there is an endothermic peak. This may be due to some impurities getting evaporated at that temperature.

The peculiarity of the DDM curing system is the cyclization reactions occur during curing. These reactions retard crosslinking. That should also be expressed by a modified behavior of physical properties during curing[9]. These cyclization reactions may be the reason for the improper cure of TGDDM/DDM system and led to the exothermic peaks.

TGDDM cured with DDS:

For TGDDM cured with DDS the T_G value was observed at 113.71°C. An exothermic peak starts at 240°C and there is no maximum peak in the temperature region analyzed (20-300°C). There is an endothermic peak at 265°C. For DDS curing system also a post curing at higher temperature is required.

TGDDM cured with TETA:

Triethylene Tetramine (TETA) is an aliphatic curative and low viscous liquid. While curing the resin was taken in a petridish and then hardener (TETA) was added to that. Due to the low viscosity the resin has moved to the edge of the sample. Curing was proper at the edges and improper cure was observed in the sample (i.e.) the sample was translucent at the center and opaque at the edges. So that 2 samples were cut out from the cured resin, one from the middle and one from the edge. They were named as TGDDM/TETA (center) and TETA (edge). Both samples were analyzed using DSC.

For the TGDDM/TETA (center) sample T_g value was observed at 53.27°C. An exothermic peak starts at 229°C and reaches maximum exothermic heat flow at around 290°C. This indicates that post cure at 100°C is not sufficient, still higher temperature is required for post cure. That may be around 250°C. Because exothermic peak reaches maximum at that temperature.

For the TGDDM/TETA (edge) sample T_g value was observed at 85.97°C. An exothermic peak starts at 227°C and reaches maximum exothermic heat flow at around 290°C.

CONCLUSION:

1. Tetraglycidyl Diamino Diphenyl Methane resin was synthesizes using 4, 4'-Diamino Diphenyl Methane (DDM) and Epichlorohydrin (ECH) as raw materials

2. Fourier Transform Infrared Spectroscopy (FTIR) was done and it was confirmed that the resin synthesized was TGDDM.

3. Proton magnetic Resonance Spectroscopy and molecular ^{13}C NMR spectroscopy was done and it was confirmed that the resin synthesized was Tetraglycidyl ether of Diamino Diphenyl Methane (TGDDM)

4. DSC curves shows exothermic peak for all the 3 systems. This may be due to the residual cure. So, post cure temperature is not sufficient. It is concluded that still higher temperature is required for post cure. From these results optimum curing procedures are proposed in this paper

5. TGA curves show that 2 transitions are there for uncured TGDDM resin and TGDDM/DDM system. But there is only one transition was observed in TGDDM/DDS system. This is attributed to the complete condensation of aromatic rings occur during DDS curing and it leads to stiff and tightly cross linked structure. It also gives the highest char yield at 750°C. So, it was inferred that TGDDM/DDS system will have the excellent flame resistance.

   TGDDM/DDM system shows 2 transitions. This is due to the cyclization occurring during curing and it retards cross linking. This system has higher char yield at 750°C, so this system also has very good flame resistance.

REFERENCES:

1. "Polymer synthesis", volume I & II,
Stanley R.Sandler, wolf karo

2. "New epoxy resins containing Hard-Soft segments: Synthesis,
Characterization and Modification studies for high temperature applications"
M. Suguna Lakshmi, M. Srividhya and B. S. R. Reddy,
CLRI, Chennai

3. "Polymer spectroscopy" - Silverstein

4. "Kinetic studies of an epoxy cure reaction
By isothermal DSC analysis"
J.Y. Leea, H.K. Choib, M.J. Shimc, S.W. Kima,*
University of Seoul, South Korea

5. Thermal library

6. "Synthesis, curing behavior and properties of siloxane
And imide-containing tetra functional epoxy"
Ming-Wei Wang & Ho-ying Wu & Mu-Shih Li

7. Rheological and thermal behaviour of DGEBA/EA and
DGEHQ/EA epoxy systems cross linked with TETA
Fanica Mustata *, Ioan Bicu

8. *"P.Poni" Institute of Macromolecular Chemistry, Aleea Grigore*
Ghica Voda, No 41A,
RO 6600, lassy

9. "The curing of epoxy resins as studied by various methods"
M.Younes, S.Wartewig and D.Lellinger,
Fachbereich Physik, Martin-Luther Universitat Halle-Wittenberg, Germany
POLYMER volume 35 November 24 1994